issn 0424-7116
An open-access journal by the German Quaternary Association
Editor-in-chief: Christopher Lüthgens

E&G

Quaternary Science Journal

Eiszeitalter und Gegenwart

Volume 72
No. 1 & 2
2023

An open-access journal of the German Quaternary Association

Copernicus Publications
The Innovative Open Access Publisher

E&G Quaternary Science Journal

An open-access journal of the German Quaternary Association

E&G Quaternary Science Journal (EGQSJ) is an interdisciplinary open-access journal, which publishes peer-reviewed articles and express reports, and retrospectives, as well as thesis abstracts related to Quaternary geology, paleo-environments, paleo-ecology, soil science, paleo-climatology, geomorphology, geochronology, archaeology, geoarchaeology, and now also encompassing methodological advances and aspects of the societal relevance of Quaternary research. EGQSJ is a non-profit, community-based effort: It is run by Quaternary scientists, financed by Quaternary scientists, and supporting Quaternary scientists, because any revenue generated is only used to support publications in the journal.

Copernicus Publications
The Innovative Open Access Publisher

Copernicus Publications
Bahnhofsallee 1e
37081 Göttingen
Germany

Phone: +49 551 90 03 39 0
Fax: +49 551 90 03 39 70

publications@copernicus.org
https://publications.copernicus.org

Printed in Germany.
Schaltungsdienst Lange o.H.G.

ISSN 0424-7116

Published by Copernicus GmbH (Copernicus Publications) on behalf of the German Quaternary Association (DEUQUA).

Image credit:
Caption: View of the Damo Gelila mountain in the Tigray region of northern Ethiopia, as seen from Daragá by Jacob Hardt (18 November 2019).

E&G

Quaternary Science Journal

An open-access journal of the German Quaternary Association

https://www.eg-quaternary-science-journal.net/

DEUQUA
DEUTSCHE QUARTÄRVEREINIGUNG

E&G Quaternary Science Journal
An open-access journal of the German Quaternary Association
https://www.eg-quaternary-science-journal.net/

E&G
Quaternary Science Journal
An open-access journal of the German Quaternary Association
https://www.eg-quaternary-science-journal.net/

Advisory board

Copernicus Publications
The Innovative Open Access Publisher

Editorial Support

Natascha Töpfer
editorial@copernicus.org

Publication Production

Sarah Schneemann
production@copernicus.org

E&G Quaternary Sci. J., 72, 1–21, 2023
https://doi.org/10.5194/egqsj-72-1-2023

Open Access E&G Quaternary Science Journal

Research article

Multi-method study of the Middle Pleistocene loess–palaeosol sequence of Köndringen, SW Germany

Lea Schwahn[1], **Tabea Schulze**[1], **Alexander Fülling**[1], **Christian Zeeden**[2], **Frank Preusser**[1], **and Tobias Sprafke**[3,4]

[1]Institute of Earth and Environmental Sciences, University of Freiburg, Freiburg, Germany
[2]Rock Physics and Borehole Geophysics, Leibniz Institute for Applied Geophysics, Hanover, Germany
[3]Center of Competence for Soils, BFH-HAFL, Zollikofen, Switzerland
[4]Institute of Geography, University of Bern, Bern, Switzerland

Correspondence: Frank Preusser (frank.preusser@geologie.uni-freiburg.de)

Relevant dates: Received: 25 July 2022 – Revised: 8 December 2022 – Accepted: 12 December 2022 – Published: 20 January 2023

How to cite: Schwahn, L., Schulze, T., Fülling, A., Zeeden, C., Preusser, F., and Sprafke, T.: Multi-method study of the Middle Pleistocene loess–palaeosol sequence of Köndringen, SW Germany, E&G Quaternary Sci. J., 72, 1–21, https://doi.org/10.5194/egqsj-72-1-2023, 2023.

Abstract: Loess–palaeosol sequences (LPSs) remain poorly investigated in the southern part of the Upper Rhine Graben but represent an important element to understand the environmental context controlling sediment dynamics in the area. A multi-method approach applied to the LPS at Köndringen reveals that its formation occurred during several glacial–interglacial cycles. Field observations, as well as colour, grain size, magnetic susceptibility, organic carbon, and carbonate content measured in three profiles at 5 cm resolution, provide detailed stratigraphical information. Only minor parts of the LPS are made up of loess sediment, whereas the major parts are polygenetic palaeosols and pedosediments of varying development that are partly intersected, testifying to a complex local geomorphic evolution. The geochronological framework is based on 10 cm resolution infrared-stimulated luminescence (IRSL) screening combined with 18 multi-elevated-temperature post-IR IRSL ages. The luminescence ages indicate that two polygenetic, truncated Luvisols formed during marine isotope stages (MISs) 9(–7?) and MIS 5e, whereas unaltered loess units correspond to the last glacial (MISs 5d–2) and MIS 8. The channel-like structure containing the two truncated Luvisols cuts into >2 m thick pedosediments apparently deposited during MIS 12. At the bottom of the LPS, a horizon with massive carbonate concretions (loess dolls) occurs, which may correspond to at least one older interglacial.

Kurzfassung: Löss-Paläoboden-Sequenzen (LPS) sind im südlichen Teil des Oberrheingrabens bisher nur unzureichend untersucht, obwohl sie ein wichtiges Element für das Verständnis der Umweltbedingungen darstellen, welche die Sedimentdynamik in diesem Gebiet gesteuert haben. Die Anwendung eines Multi-Methoden-Ansatzes auf die LPS in Köndringen enthüllt, dass diese während mehrerer glazial-interglazialer Zyklen entstanden ist. Die Feldansprache dreier Profile und Laboranalysen in 5 cm Auflösung (Farbe, Korngröße, magnetische Suszeptibilität, organischer Kohlenstoff- und Karbonatgehalt), geben detaillierte Informationen über deren stratigraphischen Aufbau. Nur geringe Teile des LPS bestehen aus Löß, der teilweise durch Hangabschwemmungen geschichtet ist, während der größte Teil aus polygenetischen Paläoböden und Pedosedimenten unterschiedlicher Ausprägung besteht, die sich teilweise überschneiden und von einer komplexen lokalen geomorphologischen Entwicklung zeugen. Der geochronologische Rahmen basiert auf Screening mittels Infrarot-Stimulierter Lumineszenz (IRSL) mit einer Auflösung von 10 cm in Kombination mit 18 Altern, die mit dem Multi-Elevated-Temperature post-IR IRSL Verfahren bestimmt wurden. Die Lumineszenzalter deuten darauf hin, dass die beiden polygenetischen, gekappten Luvisole während der marinen Isotopenstadien (MIS) 9(–7?) und MIS 5e entstanden sind, während die Lösseinheiten dem letzten Glazial (MIS 5d-2) und MIS 8 entsprechen. Die rinnenartige Struktur, welche die beiden gekappten Luvisole enthält, schneidet in > 2 m mächtige Pedosedimente ein, die offenbar während MIS 12 abgelagert wurden. An der Basis des LPS findet sich ein Horizont mit großen Karbonatkonkretionen (Lößkindl), die mindestens einem älteren Interglazial entsprechen könnten.

1 Introduction

While the Late Pleistocene climate and environmental history of Central Europe is reasonably well understood (e.g. Preusser, 2004; Heiri et al., 2014; Stephan, 2014; Lehmkuhl et al., 2016; Stojakowits et al., 2021), the timing and extent of Middle Pleistocene glaciations, as well as the number of and the environmental conditions during interglacial and interstadial phases, are controversially discussed (e.g. Kleinmann et al., 2011; Stebich et al., 2020; Tucci et al., 2021). This is mainly related to difficulties in establishing independent and robust chronological frameworks and applies in particular to the northern Alpine foreland (van Husen and Reitner, 2011; Preusser et al., 2011). In fact, Middle Pleistocene pollen records close to the Alps and in the Upper Rhine Graben (URG), a major sink of Alpine debris during the Quaternary, are rare and largely fragmentary (Preusser et al., 2005; Knipping, 2008; Gabriel et al., 2013).

Loess–palaeosol sequences (LPSs) are frequently found in the area between the realms of the Alpine and Scandinavian glaciations, yet most work during the past decades has focussed on the Late Pleistocene (e.g. Meszner et al., 2013; Lehmkuhl et al., 2016; Moine et al., 2017; Zens et al., 2018; Fischer et al., 2021; Rahimzadeh et al., 2021; Zöller et al., 2022; Schulze et al., 2022) with few sites covering the Middle Pleistocene (e.g. Terhorst, 2013; Sprafke, 2016). Some Middle Pleistocene sites have been dated using thermoluminescence (TL; e.g. Zöller et al., 1988; Frechen, 1992); however, this technique does not correspond to the present state of knowledge, and the reliability of the published ages remains uncertain. Relative chronostratigraphy (pedostratigraphy) is based on a priori assumptions and may give biased results. An example is the LPS Wels-Aschet, where Terhorst (2007) suggests a correlation of five fossil palaeosols with marine isotope stages (MISs) 5, 7, 9, 11, and 13–15 (cf. Lisiecki and Raymo, 2005), with the underlying assumption that Luvisols represent interglacial forest ecosystems that have occurred every ca. 100 000 years in Central Europe (Bibus, 2002). While this chronological assignment was apparently supported by palaeomagnetic excursions observed in this LPS (Scholger and Terhorst, 2013), Preusser and Fiebig (2009) discuss a correlation of three of the fossil Luvisols with the three pronounced warm peaks of MIS 7, seemingly supported by infrared-stimulated luminescence (IRSL) dating. This would result in a different correlation with the MIS record as suggested by Terhorst (2007). However, it is unclear if the IRSL ages could be underestimated due to signal instability and saturation effects.

Buylaert et al. (2009) have introduced an approach that allows the dating range of luminescence to be extended, erasing the unstable IRSL component during a first measurement, followed by collecting a more stable signal during subsequent stimulation at an elevated temperature (see review by Zhang and Li, 2020). This post-IR IRSL (pIR) approach was first applied to the LPS from Austria by Thiel et al. (2011a, b, c) and enabled the dating range to be extended back to about 300 ka. Other studies report reliable ages of up to 700 ka (Zander and Hilgers, 2013; Faershtein et al., 2019). A modified version of the pIR approach was suggested by Li and Li (2011) in which IRSL is subsequently stimulated at increasingly higher temperatures with 50 °C increments. The multi-elevated-temperature (MET) pIR (MET-pIR) approach allows signals with increasing stability at higher temperatures to be analysed but at the cost of bleachability of the signal (Kars et al., 2014). Furthermore, higher stimulation temperatures may also induce changes in sensitivity of the signal that may result in incorrect estimates (e.g. Zhang, 2018).

This article is a contribution towards a broader initiative that aims at improving the understanding of the factors controlling deposition in the URG geosystem during the Quaternary. Besides the effects of local tectonics, changes in climate had a major impact on deposition (Weidenfeller and Knipping, 2009; Gabriel et al., 2013; Preusser et al., 2021), in particular linked to the reoccurring glaciations of the Swiss Alps (Preusser et al., 2011), the Black Forest (Hofmann et al., 2020), and the Vosges (Mercier and Jeser, 2004). LPSs reflect changes in past environmental conditions by shifts between loess deposition, soil formation, and phases of erosion and reworking (Sprafke et al., 2014). In the URG, the accumulation of loess is assigned to cold periods (Hädrich, 1975), when the Rhine and its tributaries were braided rivers, with high debris supply due to increased frost weathering and glacial erosion and high transport potential due to meltwater discharge. During periods of a warm and humid climate (as today), the Rhine had an anastomosing to meandering character with limited debris transport and practically absent aeolian sediment activity due to widespread vegetation cover (e.g. Andres et al., 2001; Houben, 2003; Erkens et al., 2009; Kock et al., 2009). These two environmental modes can be termed glacial and temperate conditions (the latter including both interglacials and interstadials). Less well understood are the environmental conditions responsible for the phases of erosion and reworking that are observed in many Central European LPSs (Lehmkuhl et al., 2016; Sprafke, 2016; Zöller et al., 2022). Presumably these are related to the presence of flowing water (e.g. sheet wash), but deflation may also play an important role. In both cases, vegetation cover must be very limited.

Despite the prominent loess cover, LPSs from the southern part of the URG (Fig. 1) have seen very limited attention so far, with the most recent systematic studies reaching back to the 1980s (Bronger, 1969, 1970; Guenther, 1961, 1987; Hädrich, 1980; Hädrich and Lamparski, 1984; Zöller et al., 1988). Parallel to the present study, Schulze et al. (2022) investigated the Late Pleistocene site of Bahlingen-Schönenberg using a similar approach as applied here. The site investigated here is situated in the village of Köndringen at the foothills of the Black Forest (Fig. 1) and comprises a complicated succession of discontinuous units, including partly layered loess sediments (sensu Sprafke and Obreht, 2016), palaeosols, and pedosediments, as well as horizons of large carbonate concretions. These features indicate that several glacial–interglacial cycles are recorded in this outcrop but with a major contribution of slope processes leading to erosion and reworking. As a first step to unravel the complex Middle to Late Pleistocene history of the LPS at Köndringen, we focus on refining tools to derive robust stratigraphies and reliable chronologies in a easily accessible part of the outcrop.

Our multi-method approach combines a qualitative field description of the outcrop with high-resolution (5 cm) sediment and soil analyses (grain size, colour, magnetic susceptibility, organic matter, and carbonate content). A particular focus is on establishing a chronological framework by applying the MET-pIR dating approach. In addition, the potential of high-resolution (10 cm) IRSL screening is tested (e.g. Roberts et al., 2009; May et al., 2018), as this simplified procedure with regard to preparation and measurement may provide quick and low-cost semi-quantitative age information. Based on a discussion of the pedosedimentary evolution within the chronological framework, comparisons are drawn to Central European loess records of the Middle Pleistocene, and persistent gaps of knowledge and possible solutions are identified.

2 Study area

Loess deposits in the southern part of the URG are mainly found in hilly landscapes, mostly superimposing pre-Pleistocene layers with varying thickness (Keßler and Laiber, 1991). The LPS of Köndringen (48.13915° N, 7.813025° E; 220 m above sea level, a.s.l.) is located in the Black Forest foothills (Emmendinger Vorbergzone), which represent fault blocks along the eastern fault system of the URG (Fig. 1). The investigated site is situated next to a small triangular hill (Ottenberg), almost 1 km north-east of the river Elz and about 16 km E of the river Rhine. To the west of the main fault, several minor faults divide the foothills into two parts, the eastern "loess hill zone" mainly underlain by limestone and the western part where sandstone also is present; both regions are covered by loess sediment of varying thickness with up to 10–15 m (Hädrich, 1965; Hädrich and Stahr, 2001). According to heavy mineral analyses the source of the loess must have been the floodplain of the Upper Rhine (Keßler and Laiber, 1991), with the thickest accumulation of loess occurring on the adjacent foothills of the Black Forest and on the nearby Kaiserstuhl (hills of volcanic origin in the centre of the URG).

A comprehensive review of LPS in the study region was provided by Guenther (1987), including a schematic sketch showing the stratigraphic subdivision of key sites that all include several interstadial and interglacial palaeosols. According to this study, the most complex LPSs of the region are located in the wider surroundings of Köndringen and comprise up to seven loess units and six well-developed palaeosols. Unfortunately, the majority of outcrops are not easily accessible anymore. The only study including geochronological methods in the region until recently (Zöller et al., 1988) applied TL dating to eight samples taken from the LPS Riegel (Fig. 1b). While TL dating was at an early stage of development at that time, ages of 153 ± 14 and 183 ± 17 ka for loess from below what was interpreted as the Last Interglacial soil (MIS 5e; 115–130 ka; Lisiecki and Raymo, 2005) agree with the expected time frame. Middle Pleistocene ages of the four older palaeosols at Riegel are confirmed by TL ages of 259 ± 26, 254 ± 24, 273 ± 23, and > 390 ka for lower parts of the sequence. These findings indicate that regional LPSs cover more than four glacial–interglacial cycles, motivating an approach with state-of-the-art methods to the easily accessible but as yet unstudied LPS Köndringen.

3 Materials and methods

3.1 Profile description and sampling

The three investigated profiles are located at the north-eastern end of a 400 m long outcrop along Landecker Weg in Köndringen, where a complex succession of partly layered loess sediments of varying thickness intercalated by partly discontinuous pedocomplexes and loess doll horizons are ex-

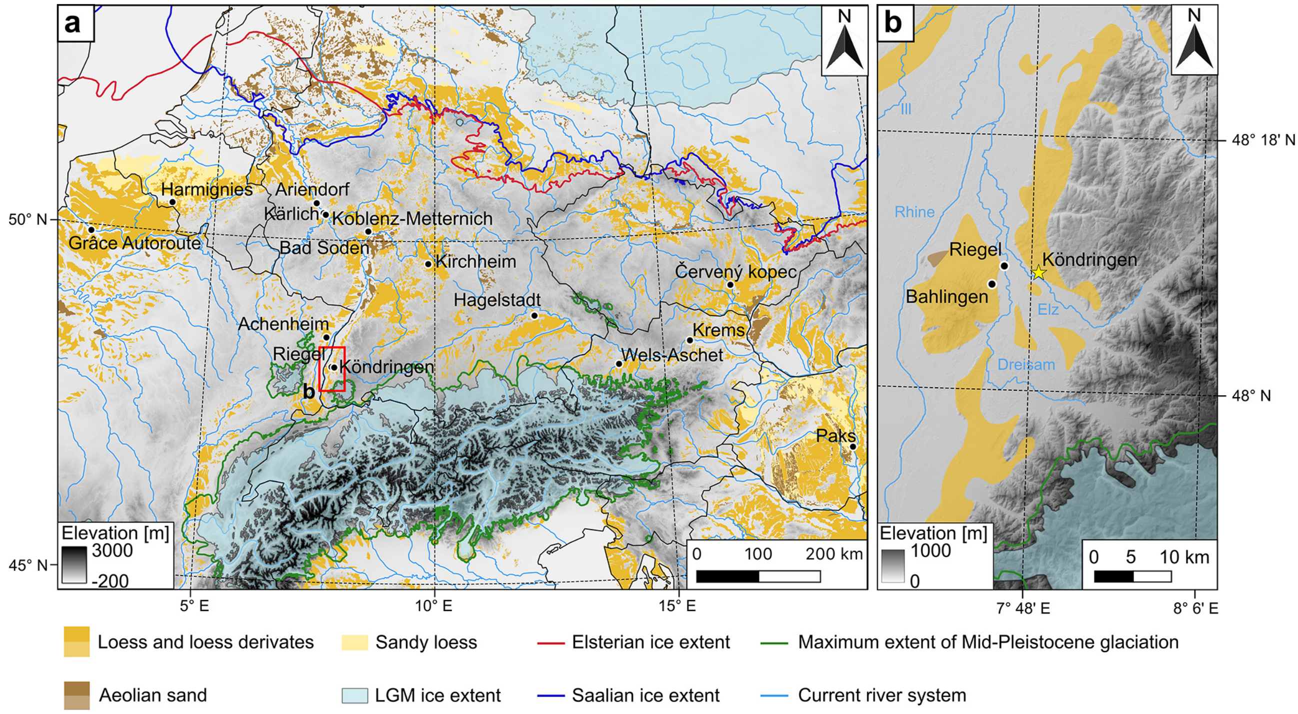

Figure 1. **(a)** Position of the study area in the Central European loess belt with the location of the mainly Middle Pleistocene LPS mentioned in the text: Grâce Autoroute (Antoine et al., 2021), Harmignies (Haesaerts et al., 2019), Ariendorf (Haesaerts et al., 2019), Kärlich (Boenigk and Frechen, 1998), Koblenz-Metternich (Boenigk and Frechen, 2001), Bad Soden (Semmel and Fromm, 1976), Kirchheim (Rösner, 1990), Achenheim (Junkmanns, 1995), Hagelstadt (Strunk, 1990), Wels-Aschet (Terhorst, 2007; Preusser and Fiebig, 2009; Scholger and Terhorst, 2013), Krems shooting range (Sprafke, 2016), Červený kopec (Kukla, 1977), and Paks (Thiel et al., 2014). **(b)** The investigated profile is situated in the foothills of the Black Forest in the village of Köndringen (yellow star). The digital elevation model data were provided by EEA (2016) and processed with QGIS 3.26. Distribution of aeolian sediments after Lehmkuhl et al. (2021), ice extent after Ehlers et al. (2011), river system from http://naturalearthdata.com (last access: 24 October 2022), and country boundary lines from http://landkartenindex.de (last access: 24 October 2022).

posed. The term loess sediments includes both loess and loess-like sediments (Sprafke and Obreht, 2016). Large parts of the outcrop are covered by a patina, vegetation, or debris, and the site remains protected from spring to autumn due to bird colonies nesting in the cliffs. To capture the main elements of stratigraphy in the most accessible part of the outcrop and to keep disturbance to the minimum, three profiles (KÖN-A, KÖN-B, KÖN-C; Fig. 2) of about 70 cm width were prepared by removing ca. 20 cm of surficial material with spades and scratchers. Colour, structural differences, and specific features were documented qualitatively for a general profile description as the basis for the interpretation of the multi-method dataset. From each profile, samples for determining organic matter and carbonate content, magnetic susceptibility, grain size analysis, and colour measurements were taken at 5 cm resolution as a continuous column (Antoine et al., 2009). Pedological horizon designations based on the qualitative field description and laboratory data (mainly colour data) follow FAO (2006) in the way suggested by Sprafke (2016). Samples for IRSL screening were taken every 10 cm using opaque plastic tubes with a length of 5 cm and a diameter of ∼ 3 cm, hammered into the freshly cleaned exposure. For luminescence dating, 18 samples were collected in metal tubes with a length of 10–15 cm, hammered into the cleaned profile.

3.2 Colour measurements

Colour measurements were done with a ColorLite sph850 spectrophotometer at the University of Bern that, which allows wavelengths from 400–700 nm to be measured with a spectral resolution of 3.5 nm (Sprafke, 2016). Samples were air-dried and sieved to fine earth (< 2 mm) and measured in a circular field with a diameter of 3.5 mm. The observer angle was 10°, and the light source (six LEDs) corresponds to D65 light. The measuring head was pushed into the loose sample material until it was completely sealed from daylight. Measurements were done at three different sample positions and the results averaged. After stirring the sample, this procedure was repeated, leading to duplicate results. The spectrophotometer was calibrated using a white standard disc after every 10th measurement. The acquired data (various colour variables, remission spectra) were analysed using Microsoft Ex-

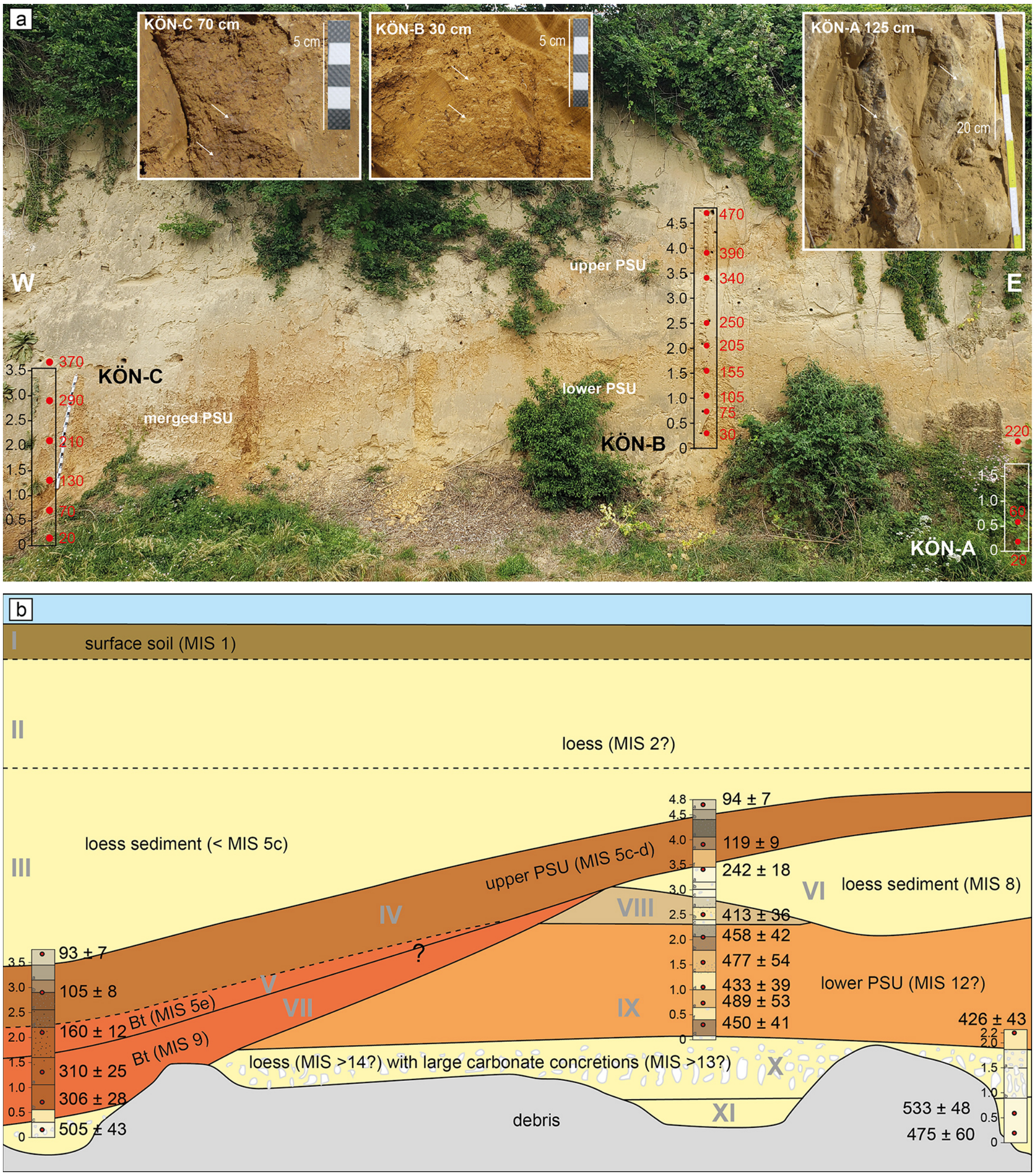

Figure 2. **(a)** Outcrop photo with the two pedosedimentary units (PSUs) merging into one towards the left hand side and location of three studied profiles KÖN-A (overgrown at moment of photography), KÖN-B, and KÖN-C, with the positions of luminescence samples and their numbers (in red). Rectangles mark the position of the sampling columns. The insets show (from left to right, marked with white arrows) clay coatings in a large crack of weakly developed subsoil of profile KÖN-C (at 70 cm), lenticular structure with silt–loam separation as a result of frost action in the lower part of KÖN-B (at 30 cm), and massive carbonate concretions exposed in profile KÖN-A (at 125 cm). **(b)** The stratigraphic units I–XI shown in the outcrop sketch consider chronostratigraphic relations (MIS after Lisiecki and Raymo, 2005) based on luminescence ages (in black, with uncertainties). Detailed profile sketches are given in Fig. 4.

cel© with the software ColorDaTra 1.0.181.5912. Mean values for each sample were calculated and visualised as real colours based on RGB variables, including two-step RGB tuning, useful to determine subtle colour variations in weakly differentiated LPSs (Sprafke et al., 2020). The L^*-value of the CIELAB colour space represents variations in lightness, whereas a^* corresponds to the intensity of red versus green (> 0 or < 0, respectively) and b^* to the intensity of yellow versus blue (> 0 or < 0, respectively) (Viscarra Rossel et al., 2006).

3.3 Sediment and soil analyses

Grain sizes distributions were measured using a Malvern Mastersizer 3000 laser diffraction spectrometry device (Malvern Panalytical). Samples were dried at 105 °C for at least 12 h and sieved through a 1 mm sieve (upper effective limit of the device), and 1–2 g was dispersed for 12 h in 50 mL sodium hexametaphosphate (33 g Na_6 P_6O_{18} and 7 g Na_2CO_3 dissolved in 1 L of distilled water). A similar protocol as used by Abdulkarim et al. (2021) was applied with a particle refractive index of 1.53, a dispersant refractive index of 1.33, an absorption index of 0.01, a stirrer speed of 1660 rpm, and with the ultrasonication off. For every sample five measurements were carried out, and average values were calculated using MATLAB R2021a. The grain size index (GSI: [%20–63 µm] / [% < 20 µm]) was calculated according to Antoine et al. (2009). Clay contents determined by laser diffraction spectrometry for samples from KÖN oscillate around 2 %, which is in disagreement to field-testing trained against classical sedimentation-based methods. Therefore, we assume that the joint clay to fine silt fraction (< 6.3 µm) roughly corresponds to the clay fraction as determined by the classical sieve–pipette analysis. This is in accordance with a large number of studies that confirm a marked difference between the laser diffraction spectrometry device and traditional sedimentation-based methods and suggest the use of alternative boundaries between 4 and 8 µm (mainly depending on soil mineralogy) to translate into "pipette clay" ($clay_p$; e.g. Konert and Vandenberghe, 1997; Antoine et al., 2009).

For the determination of organic matter (C_{org}) and carbonate contents, samples were dried at 105 °C for > 12 h and then pestled with a mortar and sieved to < 2 mm, and about 1 g was used for analyses. In the first cycle, samples were placed in a Nabertherm muffle at 550 °C for 5 h for the determination of organic carbon content (Heiri et al., 2001). Loss on ignition (LOI) was calculated by dividing the dry weight by the weight after the 550 °C burning cycle. However, this value represents double the real organic carbon content (Meyers and Lallier-Verges, 1999), and consequently all values reported have been corrected for this. As C_{org} contents of loess are usually not higher than 0.5 % (Fischer et al., 2021), we must assume that lost interlayer water of clay minerals significantly contributes to the LOI-determined signal. Carbonate contents were subsequently determined using the same material after heating for 3 h at 950 °C (Heiri et al., 2001).

For magnetic susceptibility (weight normalised; χ) measurements, carried out at the Leibniz Institute for Applied Geophysics in Grubenhagen, samples were homogenised and placed in non-magnetic plastic boxes of 6.4 cm^3 so that the material was fixed and could not move. The χ was measured in alternating fields of 505 and 5050 Hz with 400 A m^{-1} using a MAGNON VFSM, providing both low-field χ and frequency dependency of the χ. The χ is here given as weight-normalised, taking weights of samples and boxes into account. Temperature-dependent χ was measured following Zeeden et al. (2021) in an argon atmosphere for nine depth intervals (samples: KÖN-A_20–25, KÖN-A_75–80, KÖN-A_140–145, KÖN-B_85–90, KÖN-B_350–355, KÖN-C_75–80, KÖN-C_135–140, KÖN-C_225–230, KÖN-C_280–285) using an AGICO CS3 high-temperature furnace.

3.4 Luminescence screening

In the red-light laboratory, the outer ca. 1 cm of the sample material from the light-contaminated ends of the sampling tubes was discarded. Samples were then dried at 50 °C for at least 24 h and gently pestled in a mortar. Part of the material gained this way was fixed on small steel sample discs that were previously coated with a thin layer of silicon oil (6 mm stamp) so that the sample material would stick to the surface during measurement. For each sample, three subsamples were generated and measured on a Lexsyg Smart device (Freiberg Instruments; Richter et al., 2015) with the detection window centred at 410 nm. The measurement protocol comprised the IRSL stimulation of the natural signal (Ln) and that induced by laboratory irradiation (Tn, ca. 22 Gy), both after heating to 250 °C (preheat) and using a stimulation at 50 °C (Table S1 in the Supplement). The ratio Ln / Tn was calculated based on the IRSL emission recorded during the first 20 s of stimulation after subtracting the last 20 s as background.

3.5 Luminescence dating

The sediment from the outer ends of the aluminium tubes was scraped off and used for determining the activity of dose-rate-relevant elements. The remaining material was dried and subsequently treated with hydrochloric acid (20 %) and hydrogen peroxide (30 %) to remove carbonates and organic matter, respectively, each time, followed by rinsing with deionised water. Due to the low sand content of the sediment, the polymineral fine-grain fraction 4–11 µm was separated for equivalent dose (D_e) determination using Atterberg cylinders and centrifuging. The isolated fine-grain material was placed on stainless steel discs by pipetting from a sediment solution in acetone. For measuring the dose rate, samples were dried, homogenised, and subsequently transferred into flat plastic containers (7.5 × 3 cm). After storage for at least 30 d to allow for the establishment of radioactive equilibrium, the activity of uranium, thorium, and potassium were measured using high-resolution gamma ray spectrometry (Ortec high-purity germanium detector).

Measurements for the determination of D_e were carried out using a Freiberg Instruments Lexsyg Smart device (Richter et al., 2015) with an integrated beta source (max activity 7.1 GBq), delivering ca. 0.645 Gy s^{-1} to the sample material in the given geometry (calibration with Freiberg Instruments fine-grain quartz). The MET-pIR protocol originally suggested by Li and Li (2011; see review by Zhang and Li, 2020) was applied using five IRSL steps at progressively higher stimulation temperatures from 50 to 250 °C with a gradual increase of 50 °C (Table S2). The reasoning behind this procedure is that the stability of the signal increases with temperature, through this eliminating the effect of fading that may lead to the underestimation of feldspar IRSL if not corrected for. Li and Li (2011) report stable signals not affected by fading for stimulation temperatures of 200 and 250 °C. However, it is also known that the time to reset pIR signals during sediment transport requires much longer time periods compared to quartz optically stimulated luminescence (OSL). While the exact time depends on factors such as the transport mechanism and prior dose (Smedley et al., 2015), it has been shown for fluvial settings that pIR ages might significantly overestimate the known age of a sediment (Lowick et al., 2012).

Five to six aliquots were measured for each sample, and the integral 0–15 s of signal readout was used for D_e determination after subtracting the last 10 s as background (Fig. 3a). Dose response curves were fitted using the sum of two exponential growth curves (Fig. 3b). Mean D_e was calculated using the Central Age Model (CAM) of Galbraith et al. (1999; Table S3). A dose recovery test was carried out for sample KÖN-A-20, which revealed recovery ratios within 10 % of unity for all stimulation temperatures but 250 °C. For the latter, the recovery ratio was at 150 %. Problems with high-temperature pIR measurements have also been reported by Li et al. (2018) and Preusser et al. (2021) for fluvial samples from the URG, which are likely related to trap-specific changes in electron trapping probability (see Zhang, 2018; Qin et al., 2018). For some of the pIR-250 measurements aliquots had to be rejected due to saturation effects having been reached, similar to observations by Preusser et al. (2021). All other aliquots passed the usual selection criteria (recycling ratio, recuperation, signal intensity; Wintle and Murray, 2006). Dose rates (Table S4) and ages (Table 1) were calculated using ADELEv2017 software (Degering and Degering, 2020), assuming an a-value of 0.08 ± 0.02 (Rees-Jones, 1995) and an internal potassium content of 12.5 ± 0.5 % (Huntley and Baril, 1997). The water content of all samples was measured after sampling, revealing values between 1.5 % and 14 %, with the majority of values above 10 %. However, since the sediment appeared rather dried out near the surface of the exposure, it is expected that these values significantly underestimate the average sediment moisture during burial. For the dose rate calculations, an average water content of 20 ± 5 % was used. Cosmic dose rates were estimated depending on the geographic position (48.13915° N, 7.813025° E), the altitude (216 m a.s.l.), and the sampling depth following Prescott and Hutton (1994). All ages are reported as kiloyears (ka) before the year of sampling and measurement (2021 CE).

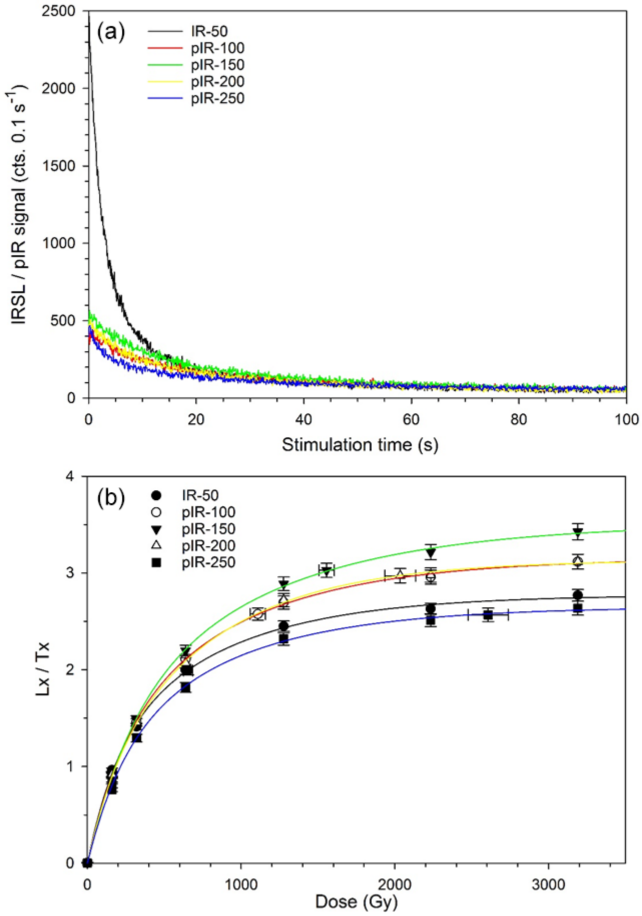

Figure 3. **(a)** Examples of IRSL decay curves (natural signal) and **(b)** dose response curves for different stimulation temperatures (sample KÖN-C-20; see panel **a** for colour codes).

4 Results

4.1 Profile description

The investigated part of the LPS Köndringen consists of loess and two intercalated brownish pedosedimentary units (PSUs). The ca. 1 m thick upper PSU is inclined to the west, cutting into the underlying loess and merging with the horizontally oriented ca. 2 m thick lower PSU (Fig. 2a). The investigated profiles complement each other to a stratigraphy of 11 units (I–XI; Fig. 2b). Designations of the units V to VIII take into account chronostratigraphic relations revealed by luminescence dating (Fig. 4). Profile KÖN-A comprises the lowermost part of the lower PSU (Unit IX) and a ca. 80 cm thick horizon with thick loess dolls (Unit X; Fig. 2), underlain by calcareous loess (Unit XI). The lower PSU (Unit IX) is exposed in KÖN-B and contains weakly aggregated brownish pedosediments, partly with visible layers and frost features (Fig. 2). In the lowermost and the uppermost parts (units IXg and IXa-c) slightly advanced pedogenic aggregation and pigmentation (pale brown) are visi-

Table 1. Ages determined at 50, 100, 150, 200, and 250 °C using the MET-pIR protocol are shown in kiloyears (ka) before the year of sampling and measurement (2021 CE).

Sample	Depth (cm)	IR-50 (ka)	pIR-100 (ka)	pIR-150 (ka)	pIR-200 (ka)	pIR-250 (ka)
KÖN-C-370	330	53 ± 4	72 ± 5	86 ± 6	93 ± 7	97 ± 7
KÖN-C-290	410	64 ± 5	83 ± 6	97 ± 8	105 ± 8	115 ± 9
KÖN-C-210	490	85 ± 6	120 ± 9	147 ± 11	160 ± 12	180 ± 14
KÖN-C-130	570	122 ± 9	206 ± 16	261 ± 20	310 ± 25	441 ± 63
KÖN-C-70	630	131 ± 9	240 ± 24	314 ± 27	306 ± 28	391 ± 56
KÖN-C-20	680	179 ± 13	310 ± 24	430 ± 34	505 ± 43	441 ± 63
KÖN-B-470	230	53 ± 4	69 ± 5	84 ± 6	94 ± 7	97 ± 7
KÖN-B-390	310	69 ± 5	91 ± 8	111 ± 8	119 ± 9	133 ± 10
KÖN-B-340	360	116 ± 8	170 ± 13	215 ± 16	242 ± 18	267 ± 21
KÖN-B-250	450	160 ± 12	265 ± 21	344 ± 28	413 ± 36	469 ± 50
KÖN-B-205	495	166 ± 13	284 ± 22	373 ± 30	458 ± 42	463 ± 50
KÖN-B-155	545	159 ± 12	294 ± 25	431 ± 40	477 ± 54	457 ± 116
KÖN-B-105	595	148 ± 11	263 ± 20	350 ± 28	433 ± 39	476 ± 57
KÖN-B-75	625	162 ± 12	291 ± 25	388 ± 33	489 ± 53	487 ± 69
KÖN-B-30	670	151 ± 11	282 ± 22	394 ± 32	450 ± 41	529 ± 111
KÖN-A-220	580	135 ± 10	293 ± 24	370 ± 30	426 ± 43	603 ± 106
KÖN-A-60	740	186 ± 14	363 ± 34	466 ± 39	533 ± 48	746 ± 87
KÖN-A-20	780	197 ± 15	353 ± 30	452 ± 38	475 ± 60	581 ± 86

ble. Superimposed is brownish loess with a weak pedogenic structure (Unit VIII) and highly calcareous loess (Unit VI). A clear boundary separates Unit VI from Unit IV, which can be subdivided into a weakly aggregated brown lower part (IVf), grading into a weakly to moderately aggregated greyish-brown upper part (IVa), with a gradual transition into overlying loess sediments (Unit III). Profile KÖN-C starts in the lowermost loess with carbonate concretions (Unit X), ends in the uppermost loess (Unit III), and contains the ca. 3 m thick merged PSU, which is well-aggregated and contains clay coatings in most parts. In Unit VII, clay coatings are mainly found along larger aggregate surfaces and in walls of larger pores, whereas the matrix is mainly yellowish-brown (Fig. 2), grading into more intense brown in the upper part (VIIa). By contrast, Unit V is reddish-brown throughout, with numerous clay coatings and some Mn oxides on ped surfaces. Contrary to KÖN-B, Unit IV in KÖN-C is more homogenous, with moderate aggregation and incipient clay coatings in the lower half (IVc–d). The transition into the overlying greyish, partly layered loess (Unit III) is sharp. Units II and I are not investigated due to accessibility problems and correspond to the uppermost, apparently homogenous loess and the present-day surface soil, respectively.

4.2 Colour

Measured colours allow for a rather robust separation of the sequence into subunits (labelled a, b, etc.) shown in Fig. 4. Colour variations in KÖN-A are minimal there is a slight increase in brownish hue in the uppermost part (Unit Xa), indicated by slightly increasing red (a^*) and yellow (b^*) colour components. The lower PSU in KÖN-B is subdivided into light brown to brown units. The incipient palaeosols in the bottom and upper part are darker (lower L^*) and more brownish (higher a^* and b^*), respectively. The uppermost unit (IXa) is again darker, with a less brownish component. From Unit VIII to VI the a^*- and b^*-values strongly decrease, along with an increase in lightness (L^*). Noticeable are a slightly dark (VIIIa) horizon and another slightly more brownish horizon (VIb). The lower half of the upper PSU has high a^*- and b^*-values, whereas in the upper part, the yellowish component decreases rapidly, and darkness stays high, resulting in a greyish-brown colour. In the merged PSU of KÖN-C L^* remains low, whereas a^* and b^* show a comparable (e.g. common increase in the lower part of VII) but partly deviating pattern. We highlight the peak of a^* in Unit V, whereas the peaks of b^* are shifted to the transition into Unit VII. In Unit IV of profile KÖN-C there are little changes in colour, different to profile KÖN-B, the unit of which is two parts.

4.3 Grain size composition

The texture of the LPS Köndringen is largely dominated by medium to coarse silt (Fig. 4). The loess between the two PSUs of KÖN-B (Unit VI) exhibits a clear mode at the medium–coarse silt boundary (20 µm). By contrast, the mode in the merged PSU (units V and VII) oscillates within the medium silt fraction and is less pronounced due to a wider distribution of grain sizes, specifically towards the finer fractions. The upper PSU in KÖN-B has a granulometry quite similar to the underlying loess, whereas the lower PSU has a

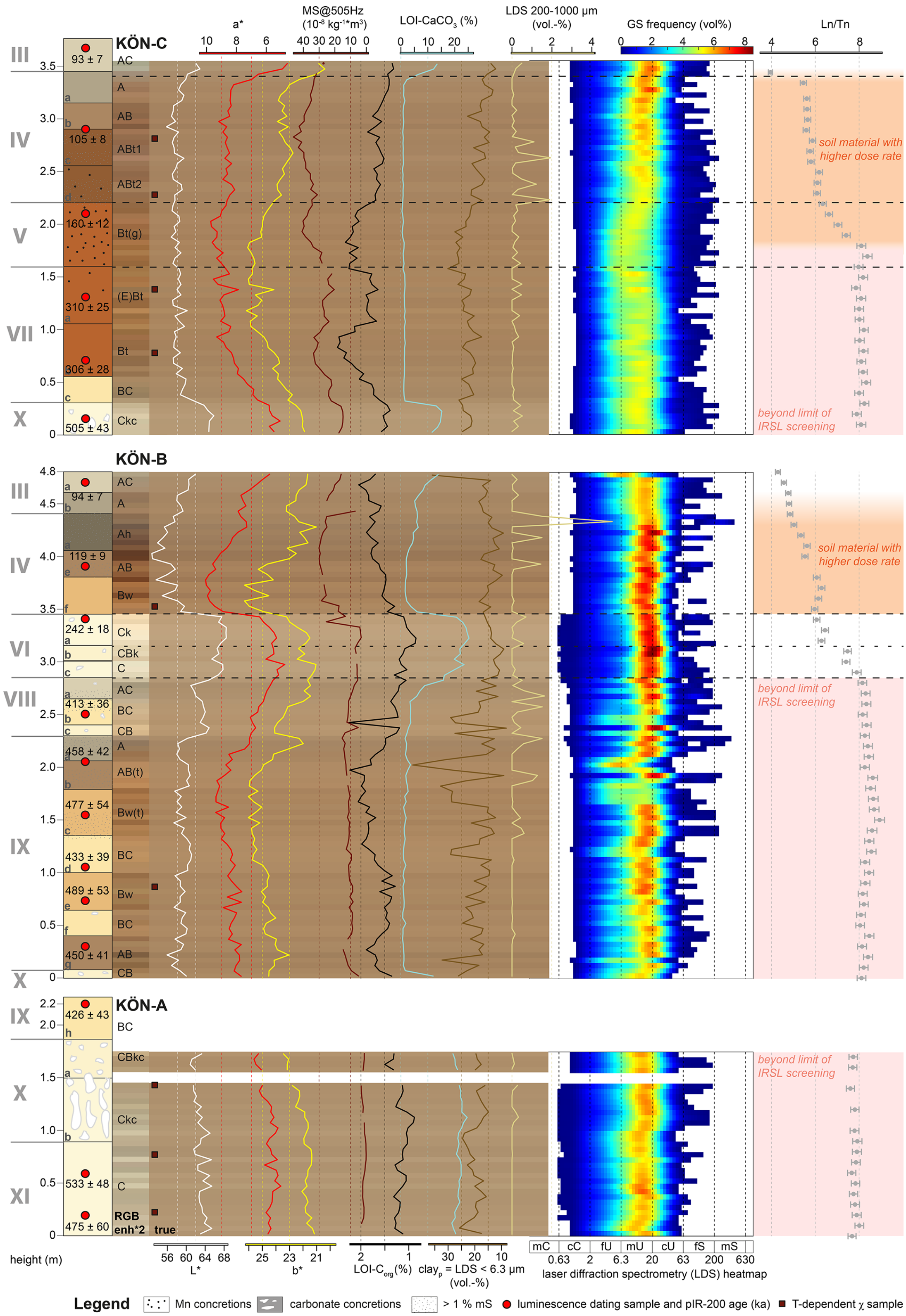

Figure 4. Stratigraphy and laboratory data of the profiles KÖN-A, KÖN-B, and KÖN-C. Real and two-times-enhanced (to the left) RGB colours of each sample are shown as background to the data plots and pedological designations, respectively. Grain size distributions are displayed as heat maps (Schulte and Lehmkuhl, 2018). Ln / Tn ratios are partly beyond the limit of this method (pale red background) or from palaeosols (pale orange background) with a higher dose rate, which is related to the enrichment of clay in such layers. Raw data are available in the Supplement.

variable pattern, with considerable oscillations in the grain size mode, especially in the upper part (VIII and IXa–b). There, more than 1 % medium to coarse sand grains are present; similar peaks are observed in the upper half of the upper PSU (units IVa–b) and the upper half of the merged PSU in KÖN C (units IVc–d).

The loess sediment (Unit VI) between the PSU of KÖN-B contains mostly less than 15 % $clay_p$, whereas the lowermost loess (Unit X–XI) has 15 %–25 % $clay_p$. The upper PSU (Unit IV) has only slightly higher $clay_p$ contents compared to the underlying loess (Fig. 4). The lower PSU (Unit IX) exhibits strong oscillations of $clay_p$ contents in the upper half (occasionally larger than 25 %), where we also noted variable grain size modes and the presence of medium to coarse sand. The merged PSU in KÖN-C has $clay_p$ contents of around 25 % in the well-developed palaeosol units V and VII and 15 %–20 % $clay_p$ in the superimposed horizons (IV).

4.4 Carbonate content, organic carbon, and magnetic susceptibility

The loess between the two PSUs in KÖN-B (Unit VI) and the lower loess (units X–XI) mostly have carbonate contents > 15 %, whereas the merged PSU is completely decalcified (Fig. 4). The upper PSU (Unit IV) contains a few percent of carbonate, which constantly increases to > 15 % in the overlying loess (Unit III). As visible in the field, the transition of Unit IV to Unit III is sharp in KÖN-CA. The lower PSU is almost free of carbonate, with minor contents in those parts with a very variable granulometry (units IXa–b and VIII). In Unit VIIIa, there is a constant increase to 15 % towards the upper unit boundary.

LOI C_{org} contents vary between 1 % in loess and 2 % in the palaeosols and likely represent a mixed signal of organic carbon and clay mineral interlayer water (see Sect. 3.3). Clear peaks in the Bt horizons of the merged PSU (units VIIb and V), high LOI C_{org} contents in the upper half of Unit IX, and some local peak in IXg, which was interpreted as weak palaeosol (Fig. 4), are present.

Mass-specific χ values vary from 10 to $46 \times 10^{-8}\,m^3\,kg^{-1}$. Generally, χ and magnetic enhancement of the frequency dependency is comparable to other loess localities in Eurasia (Fig. 5a–b; e.g. Zeeden et al., 2016; Zeeden and Hambach, 2021). The loess units at the bottom of the sequence (IX and X) and between the two PSUs (Unit VI) show distinctively lower χ, which are in a similar range as the χ from the nearby last glacial LPS Bahlingen-Schönenberg (Schulze et al., 2022). The lower PSU in profile KÖN-B shows slightly enhanced χ, with local maxima in the lowermost and uppermost parts of Unit IX and in Unit VIII. The merged PSU in KÖN-C shows the highest χ and also the highest magnetic enhancement. Distinct peaks in the Bt horizons coincide with those of LOI C_{org}. The maximum χ values occur in Unit IV and are considerably higher compared to Unit IV in KÖN-B.

The temperature-dependent magnetic susceptibility properties of nine samples are rather complex and vary considerably within the profile. The results cluster in four groups, described by their heating curves (Fig. 5c–f). All samples show an increase in χ at ca. 325 °C and a subsequent decrease towards ca. 500 °C. Furthermore, samples KÖN_A_20–25 and KÖN_A_75–80 (Fig. 5c) show a weak increase until ca. 570 °C before a sharp decrease until 600 °C. Thereafter, χ continues to decrease until ca. 700 °C. The susceptibility reaches values much higher (ca. 9-fold) during cooling than during the heating process. Samples KÖN_B_85–90 and KÖN_C_135–140 (Fig. 5d) show a further decrease in χ during heating with a steep drop at ca. 590 °C. These samples show only slightly higher χ during cooling than during heating. Samples KÖN_A_140–145, KÖN_B_350–355, and KÖN_C_75–80 (Fig. 5e) show a similar pattern as the first group (Fig. 5a) but have a much more pronounced maximum of χ at ca. 570 °C during heating. The susceptibility during cooling is only ca. 3-fold higher than during heating. Samples KÖN_C_225–230 and KÖN_C_280–285 (Fig. 5f) show a rather constant decrease in χ from ca. 300 °C until ca. 600 °C, as well as a clear further decrease in χ until ca. 700 °C.

4.5 IRSL screening

Ln / Tn values in units X and XI of KÖN-C are very consistent with an average of 7.8 ± 0.2 (Fig. 4). In the upper parts of KÖN-B (units X to VIII) and KÖN-C (units X, VIII, VII), average Ln / Tn values of 8.36 ± 0.26 and 8.08 ± 0.24, respectively, are observed. In KÖN-B, the lower part of Unit VI has an average value of 7.59 ± 0.46, whereas the upper part and that continuing into the lower part of Unit IV show a significantly lower value of 6.20 ± 0.35. In the highest part of the sequence investigated here, the mean Ln / Tn value decreases from 6.07 ± 0.14 (380 cm; Unit IVf) to 4.30 ± 0.11 (480 cm; Unit IIIa). In KÖN-C, Unit V shows a gradual decrease in values from ca. 8.14 ± 0.41 (160–180 cm) to 6.16 ± 0.16 (230 cm). These values continue in Unit IVd (mean 6.01 ± 0.26), whereas Unit IVc has a slightly lower mean value of 5.72 ± 0.24. Units IVb and IVa have similar values (mean 5.61 ± 0.10) but the uppermost sample of Unit IVa is slightly lower (5.43 ± 0.14). Significantly lower is the value of the single sample taken from Unit III (3.93 ± 0.11).

4.6 Luminescence dating

The MET-pIR results in five ages per sample (Table 1), which are expected to reflect an increasing stability of the IR-stimulated signal with increasing stimulation temperature. In fact, this trend is clearly observed for the samples investigated here, as shown in Fig. 6a. On average, the pIR-50 ages are at the ratio 0.42 ± 0.09, the pIR-100 ages at 0.69 ± 0.07, and the pIR-150 ages at 0.88 ± 0.06 of the pIR-200 ages that

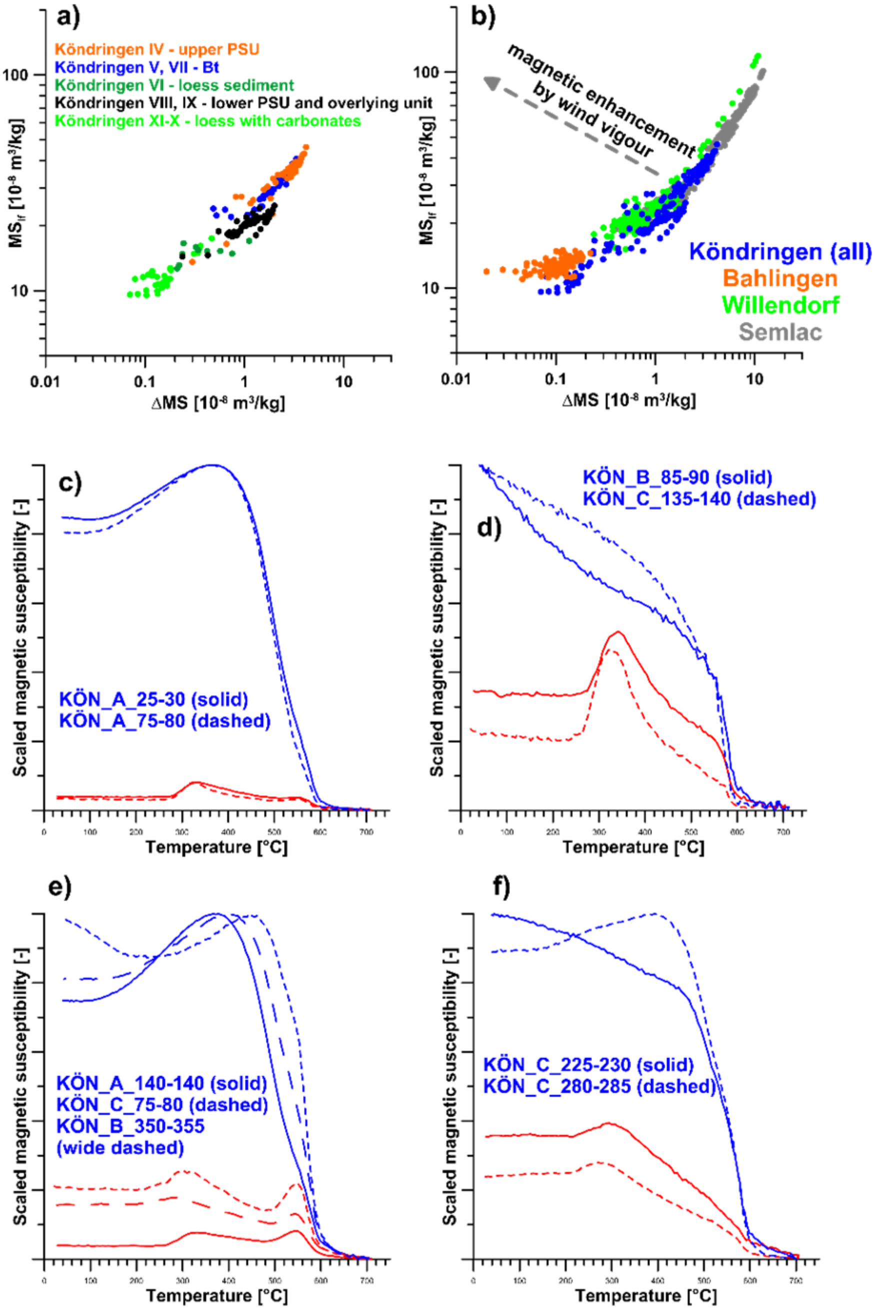

Figure 5. **(a)** Plot of the magnetic susceptibility (ordinate) and its frequency dependency (in %, abscissa) for different stratigraphic units. **(b)** Comparison of the magnetic susceptibility and its frequency dependence on Bahlingen-Schönenberg, Willendorf, and Semlac (Schulze et al., 2022; Zeeden et al., 2016; Zeeden and Hambach, 2021). This shows that the magnetic properties from Köndringen are in line with other available datasets from Eurasia. Strong indications of either wind vigour or dissolution effects are not present. **(c–f)** Temperature-dependent susceptibility during heating (red) and cooling (blue) of the samples indicated in the figure.

are used as reference. The pIR-250 ages are slightly higher (1.14 ± 0.16). The increase in stimulation temperature goes along with an increase in sensitivity change with the single aliquot regenerative dose (SAR) protocol (Fig. 6b), which is in particular strong for pIR-250 and partly leads to poor recycling ratios. Furthermore, there is a clear difference in the shape of dose response curves, with a flatter shape observed for pIR-250. The latter causes a lower saturation dose for pIR-250. In combination with the observation of highly overestimating dose recovery tests, the pIR-250 ages are considered unreliable, and the discussion of the age of the deposits will rely on the pIR-200 ages (Figs. 2 and 4).

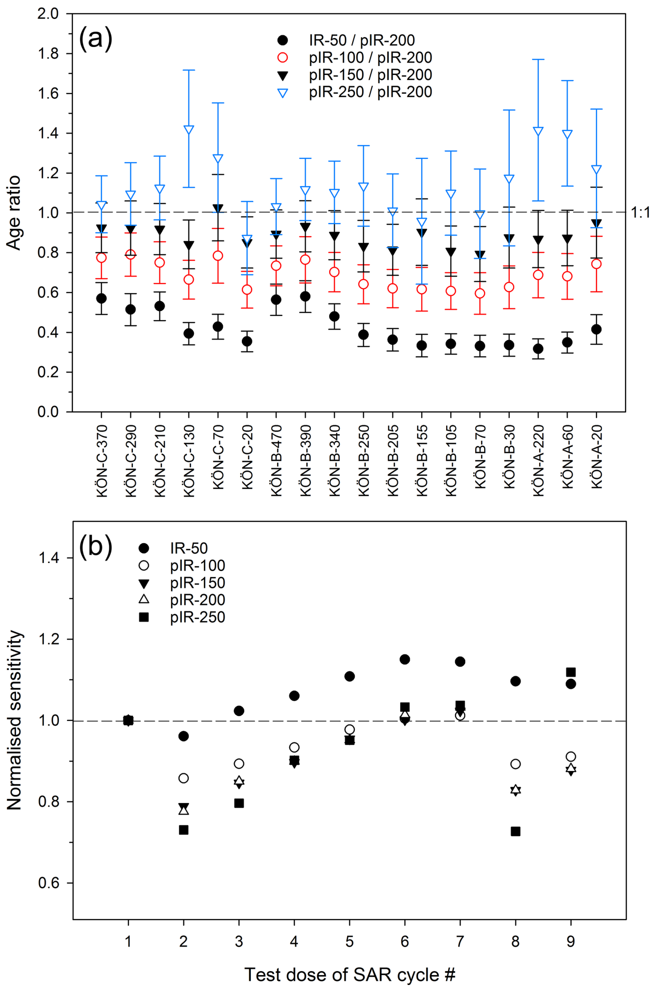

Figure 6. **(a)** The plot of IRSL and pIR ages determined for different stimulation temperatures normalised against the pIR-200 age demonstrates that ages systemically increase with stimulation temperature. **(b)** The test dose sensitivity change during the course of the SAR cycle for different stimulation temperatures normalised to the first measurement (sample KÖN-C-20) is increasingly larger for higher stimulation temperatures.

5 Discussion

5.1 LPS forming processes

The stratigraphically lowest sediment is pale yellow calcareous loess with a carbonate content of around 20 % and a clear texture mode in the medium to coarse silt fraction (ca. 20 µm; Fig. 4). With few exceptions, this mode is present throughout the LPS, which indicates that loess sediments are the parent materials of all palaeosols in the case the latter did not form from pedosediments. The high content of primary carbonate in unaltered loess reinforces earlier notions that sediment brought by the river Rhine, originating from the largely calcareous northern Swiss Alps and the Jura Mountains, must be a major source of the silt (Hädrich, 1975). Compared to last glacial loess of the nearby LPS Bahlingen (Schulze et al., 2022) and other last glacial LPSs from Central Europe, for example, Remagen, Garzweiler, and Krems-Wachtberg (Sprafke et al., 2020), which have grain size modes around 40 µm, the grain size mode at Köndringen is ca. 15–20 µm finer. Regionally distributed data on loess granulometry are not available to clarify if our data reveal deviating silt transport regimes during the Middle Pleistocene or if there is a regional differentiation in grain sizes due to transport distances and topographic barriers between the Rhine and Köndringen; it is planned to investigate this in future studies.

In last glacial LPSs with weak pedogenic differentiation, grain size variations are powerful proxies to reconstruct sedimentation dynamics, resulting from catchment geomorphic processes and wind regimes in reaction to past climate change (Antoine et al., 2009; Vandenberghe, 2013; Schulte et al., 2018; Sprafke et al., 2020). At Köndringen, the three profiles encompass mainly pedosedimentary units and well-developed palaeosols. Here, the wider grain size distribution, including increases in the clay fraction, mainly reflects the effect of post-sedimentary alteration, i.e. pedogenesis (Schulte and Lehmkuhl, 2018). Additionally, the reworking of loess and soil material by slope wash may lead to the admixture of coarse components in the case these are exposed further upslope (Sprafke et al., 2020). As the fraction above 1 mm was not determined quantitatively, we use the fraction 200–1000 µm as proxy for slope wash. Peaks are observed in the upper parts of the PSUs, which reflects a typical phenomenon in Central European LPSs, i.e. landscape degradation and slope processes at the transition of warm and moist to cold and dry environmental conditions (e.g. interglacial to glacial transitions) interrupted by phases of weak to moderate pedogenesis (Semmel, 1968; Bibus, 1974; Terhorst et al., 2002; Sprafke et al., 2014).

Landscape stability results in the alteration of loess and slope deposits by pedogenesis with weathering intensity being mainly a function of duration and humidity. Initial terrestrial (well-aerated) pedogenesis in the presence of sufficient soil moisture leads to organic matter accumulation by humification (darkening) and structural changes by bioturbation, followed by decalcification and oxidation (brownish to reddish pigmentation). In addition to pedogenic structuring (aggregation), pigmentation, and increases in χ, advanced soil development leads to increases in clay content due to silicate weathering of silicates and clay translocation, which mainly takes place in interglacials. Clay translocation in Central European loess may also occur during marked interstadials, usually in the presence of pre-weathered pedosediments (Frechen et al., 2007).

At Köndringen, we observe two major PSUs (Fig. 2; KÖN-B profile) merging into one (KÖN-C profile), with specific properties related to pedogenesis and posterior reworking. All PSUs are largely decalcified, the colours are brown, and clay contents are 5 %–15 % higher than the loess in between (Unit VI), reflecting at least moderate pedogenesis.

Clay coatings on polyhedral ped surfaces in units V and VII indicate long-term pedogenesis, likely under interglacial conditions (Semmel, 1968; Terhorst et al., 2002). The two peaks in LOI C_{org} (Fig. 4) coincide with horizons enriched in illuvial clay, as this method is sensitive to minerals with interlayer water. In the field, illuvial clay of Unit V appears to reach into the upper parts of Unit VII, which itself may be a former eluvial horizon of an older Luvisol. Superimposed on the two well-developed palaeosols is a more humic palaeosol with incipient clay coatings, which may correspond to reactivated illuvial clay from pedosediments (Unit IV). High χ values characterise the merged PSU, with peaks corresponding to the Bt horizons (units V and VII) and maxima in the humic horizons of unit IV. This suggests that χ is sensitive to subsoils of truncated to full interglacial palaeosols but even more to preserved humic topsoils, where biochemical processes occur with high intensity.

The χ values of loess at Köndringen and Bahlingen (Schulze et al., 2022) are rather low; only in units affected by advanced pedogenesis do χ values reach those of other European reference profiles (Fig. 5b). As contents of non-magnetic carbonate are similar (ca. 15 %–25 %) in loess of the URG and the Danube Basin (Sprafke, 2016; Pécsi and Richter, 1996), lower χ values of URG loess are possibly related to a higher share of coarse diamagnetic silicate minerals (e.g. quartz). The basal loess at Köndringen has the lowest χ values due to the additional contribution of (non-magnetic) secondary carbonate visible in the field. The thick carbonate concretions below and the brown colour of the lower PSU (Unit IX) give the impression of long-term pedogenesis. However, χ values of the lower PSU are rather low, indicating a weak to moderate intensity of soil formation or a mix of soil and loess material. Granulometric fluctuations in the upper part and layering, frost features, and the weak pedogenic structure in the lower part of the lower PSU (Fig. 2a) support that it consists mainly of reworked soil material. Some re-established pedogenic structure and slight increases in χ in the lowermost part (IXg) and upper part (IXa–c) of the lower PSU indicate weak to moderate pedogenesis of interstadial intensity. Specifically, Unit IXa may correspond to a humic topsoil formed during this interstadial-type pedogenesis. Unit VIII represents enhanced aeolian sedimentation, with Unit VIIIb likely representing a phase of weak pedogenesis, indicated by lower carbonate contents and a more brownish colour.

We interpret the temperature-dependent susceptibility properties (Fig. 5c–f) as indicative of relevant contributions of magnetite, maghemite, and hematite. For Eurasian loess, the increase in χ at $\sim 300\,°C$ has been related to the alteration of weakly magnetic Fe phases to maghemite or magnetite; the heating curves of the magnetic susceptibility plotted in Fig. 5e are most typical of last (inter-)glacial European palaeosols and loess sediments (see Zeeden and Hambach, 2021, and references therein). The drop in the susceptibility at $\sim 585\,°C$ likely represents the Curie temperature of magnetite. The further decrease in the χ towards 700 °C is interpreted as a contribution of hematite (Fig. 5f). While for all samples an increase in χ at $\sim 300\,°C$ is present (Fig. 5c–f), samples shown in Fig. 5c and d show this phenomenon most prominently. For the samples from units X and XI (Fig. 5c), this is not surprising as these are from typical loess, which will easily form magnetic minerals when heated. The much higher susceptibility during cooling for some samples (Fig. 5c) implies that non- or weakly magnetic iron phases are prominently present in the sediment. The susceptibilities that are not much higher during cooling for samples from Unit VIIa (merged PSU) and Unit IXe (lower PSU; Fig. 5d) are interpreted as originating from mature, likely interglacial soils. The absence of strong ferrimagnetism in the lower PSU can be explained by the removal of the very fine fraction during slope wash that led to the reworking of a previously present interglacial soil. The upper PSU in KÖN-B corresponds stratigraphically to the upper part of the merged PSU in profile KÖN-C. Yet, our data show that Unit IV has different properties in both profiles. For KÖN-C, please note the presence of a humic palaeosol with incipient clay illuviation cut sharply by overlying loess. In KÖN-B there is a clear subdivision into a brown, weakly aggregated part and a darker, moderately aggregated part, grading into overlying loess. It is likely that units IVe–f correspond to brown pedosediment which was overprinted by a humic palaeosol and successively buried by loess. The presence of carbonate in the pedosediment indicates that decalcification, allowing for clay illuviation (as in KÖN-C), was not reached in this part of the LPS, but micromorphological studies are necessary to support or neglect this hypothesis (cf. Sprafke et al., 2014). Units IVb–d instead are decalcified and have high χ values, indicating that pedogenesis was stronger. The hematite contribution, seen best in samples from the base of the upper PSU (units IVc, d; see Fig. 5f), implies that the upper PSU contains material from a mature, likely interglacial soil. As for the lower PSU, this phenomenon may be related to the incorporation of older pre-weathered material, which is typical of early glacial palaeosols in Central Europe (Frechen et al., 2007; Sprafke et al., 2014).

Overall, our colour, granulometry, magnetic susceptibility, and LOI data considerably support the subdivision and interpretation of the studied LPS (Fig. 4), although we note that the interpretation appears partly ambiguous in the absence of detailed macro- and micromorphological studies (cf. Sprafke et al., 2014; Sprafke, 2016). As the focus of this study was the testing of new methods, specifically luminescence screening and advanced dating protocols, we note a shortcoming in (micro-)structural information to precisely reconstruct the formation of this complex LPS.

5.2 Chronostratigraphy

Sections KÖN-A and KÖN-C comprise the oldest stratigraphic units (XI and X) for which consistent ages of 533 ± 48 ka (KÖN-A-20), 475 ± 60 (KÖN-A-60), and 505 ± 43 ka (KÖN-C-20) have been determined. Assuming the two units (XI and X) are quasi-synchronous allows a mean age of 505 ± 71 ka (CAM) to be calculated for the basal part of the investigated sequence. The large uncertainty does not allow an unambiguous correlation with MIS stratigraphy (Lisiecki and Raymo, 2005), but assuming the loess was deposited during a glacial period makes MIS 14 (563–533 ka) and MIS 12 (478–424 ka) the most likely candidates. However, it is at present not known if the pIR-200 ages are affected by systematic underestimation due to, for example, a low level of fading or the onset of signal saturation. The question of potential underestimation can only be answered by comparison with independent age control, which is so far not available for the region. In the absence of any evidence pointing towards age underestimation, the pIR-200 ages are considered reliable for the time being.

In Profile KÖN-A, unit X with massive loess dolls is overlain by pedosediments corresponding to the lowermost part of the lower PSU (Unit IX). The age of 426 ± 43 ka (KÖN-A-220) corresponds to late MIS 12 or early MIS 11. In section KÖN-B, Unit IX contains five superimposed pIR-200 ages overlapping within uncertainties (Table 1, Fig. 5), which represent a mean (CAM) age of 458 ± 21 ka and hence relate to MIS 12 (478–424 ka). In the Alpine region, Middle Pleistocene stratigraphies vary regionally and are fragmentary, but in northern and western Europe MIS 12 correlates with the large glaciation of the Elsterian (Cohen and Gibbard, 2019). According to our interpretation, Unit IX likely comprises soil material reworked by slope wash. Based on the susceptibility data it likely contains components of a well-developed interglacial soil, which would be pre-Elsterian (possibly Cromerian). The age of 413 ± 36 ka (KÖN-B-250) for Unit VIII on top of Unit IX may represent the MISs 12–11 boundary, as ongoing sedimentation and rather weak pedogenesis appear less likely for an interglacial (MIS 11). Based on geochronology and palaeosol morphology, there is no evidence for an MIS 11 palaeosol in the studied part of the Köndringen outcrop; it may have been eroded subsequent to its formation.

In Unit VII (profile KÖN-B), two consistent pIR-200 ages of 310 ± 25 ka (KÖN-C-130) and 306 ± 28 ka (KÖN-C-70) point towards deposition during MIS 9 (337–300 ka). Both ages are from a well-developed Bt horizon, most likely formed during interglacial conditions; therefore some rejuvenation by bioturbation or a slight age underestimation can be assumed. The highly calcareous loess of Unit VI has an age of 242 ± 18 ka (KÖN-B-340) and hence correlates with MIS 8 (300–243 ka). The age determined for the well-developed Bt horizon Unit V (160 ± 12 ka, KÖN-C-210) likely reflects the age of the parent material deposited during MIS 6 (191–130 ka), whereas soil formation presumably occurred during MIS 5e (130–115 ka), the Last Interglacial period (Eemian). Two pIR-200 ages determined for the upper PSU (Unit IV) of 119 ± 9 ka (KÖN-B-390) and 105 ± 8 ka (KÖN-C-290) fall into earlier phases of MIS 5 and likely correspond to the beginning of the last glacial period during MIS 5d (115–102 ka). The two topmost samples taken from loess above (Unit III) have ages of 94 ± 7 ka (KÖN-B-470) and 93 ± 7 ka (KÖN-C-370), indicating deposition during MIS 5c (102–92 ka) to MIS 5b (92–85 ka).

Ln / Tn values from IRSL screening determined for the lower part of section KÖN-C do not reflect the hiatus between units X and VII that is clearly observed by the pIR-200 ages (505 ± 43 ka versus 310 ± 25 ka and 306 ± 28 ka). In this context, it has to be noted that Ln / Tn values have been determined using IRSL stimulated at 50 °C, hence with a signal that will be affected by fading. In the presence of fading, the latent IRSL signal will rise to an equilibrium point at which the amount of newly produced latent signal equals the decay of the latent signal. This equilibrium point will be defined by the number of electron traps that host the latent signal, the fading rate, and the signal production rate, i.e. dose rate. The latter effect is reflected by the observation that the Ln / Tn values for the basal loess (units XI and X) are lower than those observed for the rest of the sequence. In fact, the dose rate in this part is lower (ca. 2.8 Gy kyr^{-1}) compared to other parts of the sequence (ca. 3.7–3.8 Gy kyr^{-1}), which appear to be in equilibrium. In the present setting, the IRSL screening values carry age information only up to ca. 300 ka.

In the upper part of section KÖN-B, additional chronological information is derived from IRSL screening values that is not provided by the dating itself. First, Unit VI is clearly subdivided into a lower and upper subunit, as indicated by the offset in Ln / Tn values (7.59 ± 0.46 versus 6.20 ± 0.35). Such a significant offset may represent a time of several hundreds of thousands of years; hence, the lower part may correspond to MIS 10 (374–337 ka) and the upper part to MIS 8 (300–243 ka), the latter age being confirmed by a pIR-200 age. The continuation of Ln / Tn values just above and in Unit IV reveals that this part of the sequence was likely also deposited during MIS 8 but overprinted by later soil development. The gradual decrease in values from 8.14 ± 0.41 (160–180 cm) to 6.16 ± 0.16 (230 cm) implies quasi-continuous accumulation in the upper part of the investigated sequence. Apparently, continuous deposition is also observed for the upper part of Unit V in section KÖN-C, and it is shown that the lower part of this unit developed on older material (of Unit VII?). Unit IV and its subunits in this section apparently represent episodic deposition reflected by the different mean Ln / Tn values (Unit IVd: 6.01 ± 0.26; Unit IVc: 5.72 ± 0.24; Unit IVb and lower Unit IVa: 5.61 ± 0.10; Unit IVa: 5.43 ± 0.14). However, since dosimetric effects cannot be ruled out, this statement has to be treated with caution and would require proof by full dating.

From a magnetostratigraphic perspective, we note that the magnetic signatures of the Bt horizons related to MIS 9 and MIS 5 are not as high as those typically are for full interglacial conditions, but URG loess seems to have overall lower χ values than other Central European LPSs. As noted previously (e.g. Necula et al., 2015; Marković et al., 2015), χ values of interglacial soils vary considerably in Europe. Furthermore, the type of pedogenesis and the position in the soil profile apparently influence this proxy. More geographically distributed χ data are necessary to understand the spatial pattern of the proxy intensities.

5.3 Stratigraphic context

During the past decades, research on LPSs in Central Europe has mainly focused on last glacial records, occasionally with obtained ages below Eemian palaeosols (e.g. Kadereit et al., 2013; Moine et al., 2017; Fischer et al., 2021; Lehmkuhl et al., 2016; Zens et al., 2018; Krauss et al., 2018; Rahimzadeh et al., 2021). Many Middle Pleistocene LPSs still lack state-of-the-art chronologies for individual loess and soil units, although palaeomagnetism and tephra stratigraphy are being applied where time intervals and material are present (e.g. Jordanova et al., 2022; Laag et al., 2021; Marković et al., 2015). TL ages from pre-Eemian (MIS 6 and older) loess elaborated during the 1980s to 1990s provide first approximations to the Middle Pleistocene loess chronology, though with large uncertainties (Zöller et al., 1988; Frechen et al., 1992; Frechen, 1994). IRSL ages from the late 1990s to early 2010s provide more robust estimates back to 200–250 ka (e.g. Preusser and Fiebig, 2009) at the LPS Wels-Aschet, Upper Austria. Further methodological advances are related to the application of thermally transferred (TT) OSL (Moska and Bluszcz, 2013) and pIR protocols (Schmidt et al., 2011a, b; Thiel et al., 2011a, b). Post-IR $IRSL_{290}$ dating, for example, extended the numerical age range in loess from Lower Austria (Paudorf, Göttweig-Furth and Aigen, Krems shooting range) and Hungary (Paks brickyard) to 300–350 ka (Thiel et al., 2011b, 2014; Sprafke et al., 2014; Sprafke, 2016). The MET-pIR ages determined at Köndringen reach back to 500 ka and are among the oldest luminescence ages obtained from loess in Central Europe. The opportunity to date back to pre-Holsteinian (MIS 11) times is promising from a geochronological point of view; however, pedostratigraphic relations at Köndringen are rather complicated and provide limited support to assess the reliability of our data in the absence of independent numerical age control.

A central controversy in loess research of Central Europe surrounds the questions of if Luvisols are strictly limited to full interglacial conditions and if these recurred every ca. 100 000 years, as proposed by Bibus (2002) for SW Germany and adopted by Terhorst et al. (2007, 2015) for Upper Austria. This hypothesis is apparently supported by LPSs in NW France, where Antoine et al. (2021) report seven interglacial Bt horizons between the surface soil and the Matuyama–Brunhes boundary (MBB) around 780 ka. However, at the LPS Weilbach (Hesse) it appears that MIS 7 is only represented by two humic horizons (Weilbacher Humuszonen), and the next Bt horizon below the Eemian palaeosol may rather correspond to MIS 9 (Schmidt et al., 2011b). At Harmignies in Belgium, MIS 7 may be represented by two Bt horizons of Luvisols (Haesaerts et al., 2019), similar to findings from Červený kopec (Kukla, 1977) and other localities in Central Europe (e.g. Necula et al., 2015, and references therein). At Wels-Aschet, luminescence ages point to more than one Bt horizon being equivalent to MIS 7, consistent with two prominent global warm phases separated by a cooler phase encompassing MIS 7 (Preusser and Fiebig, 2009). At Koblenz-Metternich a formation of Luvisols reportedly occurred during pronounced interstadial conditions of the early Wurmian (Boenigk and Frechen, 2001). All the mentioned LPSs lack numerical age control by state-of-the-art methods, and there are further prominent LPSs in Central Europe that contain several fossil Bt horizons but lack a robust chronological framework for the Middle Pleistocene parts, for example Kärlich (Boenigk and Frechen, 1998), Bad Soden (Semmel and Fromm, 1976), Kirchheim (Rösner, 1990), Hagelstadt (Strunk, 1990), and Achenheim (Junkmanns, 1995). In summary, considering the discrepancies in Middle Pleistocene loess stratigraphy of Central Europe, it appears mandatory to date several geographically distributed LPSs with state-of-the-art luminescence dating approaches and precisely determine pathways of palaeopedogenesis to understand the regional imprint of spatially distinct palaeoclimates to the pedosphere (Sprafke, 2016).

At Köndringen, there are too many discontinuities to support or disprove available stratigraphic models. The two well-developed Bt horizons correspond to MISs 5e and 9, which suggests that these Luvisol subsoils represent full interglacial conditions. This is in agreement with earlier assumptions of Bronger (1966) and Guenther (1987), who suggest that regional interglacials are typically represented by Luvisols yet without being backed up by numeric age control. Some clay translocation in early glacial pedosediments of Unit IV in KÖN-C is likely related to a remobilisation of illuvial clay after post-Eemian colluviation in the absence of carbonate, as reported for the LPS Schatthausen near Heidelberg (Frechen et al., 2007). Interestingly in KÖN-B, there are no signs of clay translocation in the brown early glacial pedosediments, which may relate to some admixture of carbonate during colluviation, which hampers posterior clay translocation, as suggested for the MIS 5 pedocomplex of the LPS Paudorf, Lower Austria (Sprafke et al., 2014). This underlines that palaeoclimatic inferences from polygenetic and partly reworked palaeosols are difficult and require detailed (chrono-)stratigraphic, sedimentological, and also micromorphological studies. The lack of (micro-)morphological data is obvious with respect to the lower PSU at Köndringen, which is most likely an Elsterian pedosediment (see Sect. 5.2), with incipient interstadial pedogenesis in the lowermost and upper part. Advanced interglacial pedogenesis has most likely occurred before soil reworking, which would be pre-Elsterian (MIS 12), i.e. Cromerian. Thus, a Holsteinian palaeosol in other parts of the outcrop and/or in other sites of the region may be expected. The well-developed carbonate nodules likely represent one or more Cromerian interglacials and are possibly the result of a merged soil developed during MISs 15–13, as interpreted for Central Europe (Terhorst, 2007; Bronger, 2003; Marković et al., 2015; Necula et al., 2015, and references therein).

The loess package between the upper and lower PSUs corresponds to MIS 8, which is known for rather little global ice volume compared to MISs 6, 10, and 12 (Lisiecki and Raymo, 2005). If loess volume is taken as an indicator for upstream glacier activity, the presence of a distinct MIS 8 loess package would imply a major phase of glaciation at this time. However, this period is usually not considered to represent full glacial conditions in the Alps (e.g. van Husen and Reitner, 2011), although it represents the phase of coldest sea surface temperatures of the last 1 million years at the Iberian Margin (Rodrigues et al., 2017, and references therein). Even in northern Switzerland, where one of the most complex glaciation histories has been reconstructed, there is still no unequivocal evidence for a major glaciation during MIS 8 (Preusser et al., 2011). Investigating further LPSs from the southern part of the URG, which is located downstream of the formerly glaciated areas of northern Switzerland, could give insight into aeolian sediment flux that is usually interpreted as a glacial signal in this region.

6 Conclusions

The studied section of the LPS Köndringen consists of loess sediments intercalated by two prominent pedosedimentary units (PSUs), of which the upper one is inclined to the west, cutting into the underlying loess and merging with the lower PSU. The applied high-resolution multi-method approach leads to detailed stratigraphic information and supports the reconstruction of the main phases of dust deposition, pedogenesis, and reworking of those units which were not lost by erosion. MET-pIR ages reach back to more than 500 ka and thus are among the oldest numerical ages obtained from loess in Central Europe. Massive carbonate concretions in the loess below the lower PSU point to advanced (interglacial) pedogenesis, apparently supported by the brownish colour, lack of carbonates, and higher clay contents in the lower PSU. However, the partly layered appearance, a weak pedogenic structure, and low χ values suggest at most interstadial pedogenesis. Temperature-dependent χ results support the assumption that the lower PSU contains reworked interglacial palaeosol material. Soil formation likely occurred during MIS 13 (and/or MIS 15?) and reworking during MIS 12 (Elsterian). The merged PSU in the western part of the studied outcrop comprises two well-developed interglacial Luvisol remnants (Bt horizons) dating to MIS 9 and MIS 5e (Eemian). Superimposed is a humic palaeosol with incipient clay coatings and the highest χ values likely formed during MIS 5c. As the LPS Köndringen contains several hiatuses and polygenetic units, the contribution towards refining the Central European Middle Pleistocene loess stratigraphy remains limited for the time being. However, our study motivates future studies in the region using the applied multi-method approach in combination with MET-pIR state-of-the-art dating. Future studies on loess stratigraphy and chronology in the southern URG will contribute towards a better understanding of the chronology and impact of Alpine glaciations.

Data availability. Relevant data are given either in the main text or in the Supplement.

Supplement. The supplement related to this article is available online at: https://doi.org/10.5194/egqsj-72-1-2023-supplement.

Author contributions. FP, ToS, and AF conceptualised this study. Fieldwork and most laboratory analyses were carried out by TaS and LS, under the supervision of FP, ToS, and AF. Luminescence dating was carried out by AF and magnetic susceptibility measurements by CZ. The original draft was prepared by ToS and FP, based on the master of science thesis written by LS. All authors contributed by additional writing, reviewing, and editing.

Competing interests. At least one of the (co-)authors is a member of the editorial board of *E&G Quaternary Science Journal* and co-editor of the special issue "Quaternary research from and inspired by the first virtual DEUQUA conference". The peer-review process was guided by an independent editor, and the authors also have no other competing interests to declare.

Disclaimer. Publisher's note: Copernicus Publications remains neutral with regard to jurisdictional claims in published maps and institutional affiliations.

Special issue statement. This article is part of the special issue "Quaternary research from and inspired by the first virtual DEUQUA conference". It is a result of the vDEUQUA2021 online conference in September/October 2021.

Acknowledgements. We thank Robert Petizcka (University of Vienna) for providing the spectrophotometer.

Financial support. This open-access publication was funded by the University of Freiburg.

Review statement. This paper was edited by Julia Meister and reviewed by two anonymous referees.

References

Abdulkarim, M., Grema, H. M., Adamu, I. H., Mueller, D., Schulz, M., Ulbrich, M., Miocic, J. M., and Preusser, F.: Effect of using different chemical dispersing agents in grain size analyses of fluvial sediments via laser diffraction spectrometry, Methods Protoc., 4, 44, https://doi.org/10.3390/mps4030044, 2021.

Andres, W., Bos, J. A. A., Houben, P., Kalis, A. J., Nolte, S., Rittweger, H., and Wunderlich, J.: Environmental change and fluvial activity during the Younger Dryas in central Germany, Quatern. Int., 79, 89–100, https://doi.org/10.1016/S1040-6182(00)00125-7, 2001.

Antoine, P., Rousseau, D.-D., Moine, O., Kunesch, S., Hatte, C., Lang, A., Tissoux, H., and Zöller, L.: Rapid and cyclic aeolian deposition during the Last Glacial in European loess: a high-resolution record from Nussloch, Germany, Quaternary Sci. Rev., 28, 2955–2973, https://doi.org/10.1016/j.quascirev.2009.08.001, 2009.

Antoine, P., Coutard, S., Bahain, J. J., Locht, J. L., Hérisson, D., and Goval, E.: The last 750 ka in loess–palaeosol sequences from northern France: environmental background and dating of the western European Palaeolithic, J. Quaternary Sci., 36, 1293–1310, https://doi.org/10.1002/jqs.3281, 2021.

Bibus, E.: Abtragungs- und Bodenbildungsphasen im Rißlöß, E&G Quaternary Sci. J., 25, 166–182, https://doi.org/10.3285/eg.25.1.14, 1974.

Bibus, E.: Zum Quartär im mittleren Neckarraum – Reliefentwicklung, Löß/Paläobodensequenzen, Paläoklima, Tübinger Geowissenschaftliche Arbeiten, D8, 236 pp., ISBN 3-88121-055-5, 2002.

Boenigk, W. and Frechen, M.: Zur Geologie der Deckschichten von Kärlich/Mittelrhein, E&G Quaternary Sci. J., 48, 38–49, https://doi.org/10.3285/eg.48.1.04, 1998.

Boenigk, W. and Frechen, M.: The loess record in sections at Koblenz–Metternich and Tönchesberg in the Middle Rhine Area, Quatern. Int., 76, 201–209, https://doi.org/10.1016/S1040-6182(00)00103-8, 2001.

Bronger, A.: Lösse, ihre Verbraunungszonen und fossilen Böden. Ein Beitrag zur Stratigraphie des oberen Pleistozäns in Südbaden, Schriften des Geographischen Instituts der Universität Kiel 24/2, Geographisches Institut der Universität Kiel, Kiel, 113 pp., 1966.

Bronger, A.: Zur Klimageschichte des Quartärs von Südbaden auf bodengeographischer Grundlage, Petermann. Geogr. Mitt., 113, 112–124, 1969.

Bronger, A.: Zur Mikromorphogenese und zum Tonmineralbestand quartärer Lössböden in Südbaden, Geoderma, 3, 281–320, https://doi.org/10.1016/0016-7061(70)90011-X, 1970.

Bronger, A.: Correlation of loess-paleosol sequences in East and Central Asia with SE Central Europe: towards a continental Quaternary pedostratigraphy and paleoclimatic history, Quatern. Int., 106, 11–31, https://doi.org/10.1016/S1040-6182(02)00159-3, 2003.

Buylaert, J. P., Murray, A. S., Thomsen, K. J., and Jain, M.: Testing the potential of an elevated temperature IRSL signal from K-feldspar, Radiat. Meas., 44, 560–565, https://doi.org/10.1016/j.radmeas.2009.02.007, 2009.

Cohen, K. M. and Gibbard, P. L.: Global chronostratigraphical correlation table for the last 2.7 million years, version 2019 QI-500, Quatern. Int., 500, 20–31, https://doi.org/10.1016/j.quaint.2019.03.009, 2019.

Degering, D. and Degering, A.: Change is the only constant – Time-dependent dose rates in luminescence dating, Quat. Geochronol., 58, 101074, https://doi.org/10.1016/j.quageo.2020.101074, 2020.

EEA (European Environment Agency): European Digital Elevation Model (EU-DEM), version 1.1, Copernicus Land Monitoring Service 2016, European Union, https://land.copernicus.eu/imagery-in-situ/eu-dem/eu-dem-v1.1?tab=download (last access: 20 July 2022), 2016.

Ehlers, J., Gibbard, P. L., and Hughes, P. D. (Eds.): Quaternary Glaciations – Extent and Chronology A Closer Look, Developments in Quaternary Sciences, 15, Elsevier, 1108 pp., ISBN 978-0-444-53447-7, 2011.

Erkens, G., Dambeck, R., Volleberg, K. P., Bouman, M. T. I. J., Bos, J. A. A., Cohen, K. M., Wallinga, J., and Hoek, W. Z.: Fluvial terrace formation in the northern Upper Rhine Graben during the last 20 000 years as a result of allogenic controls and autogenic evolution, Geomorphology, 103, 476–495, https://doi.org/10.1016/j.geomorph.2008.07.021, 2009.

Faershtein, G., Porat, N., and Matmon, A.: Natural saturation of OSL and TT-OSL signals of quartz grains from Nilotic origin, Quat. Geochronol., 49, 146–152, https://doi.org/10.1016/j.quageo.2018.04.002, 2019.

FAO (Food and Agriculture Organization of the United Nations): Guidelines for soil description. Food and Agriculture Organization of the United Nations, 4th edn., Roma, Italy, ISBN 92-5-105521-1, 2006.

Fischer, P., Jöris, O., Fitzsimmons, K., Vinnepand, M., Prud'homme, C., Schulte, P., Hatté, C., Hambach, U., Lindauer, S., Zeeden, C., Peric, Z., Lehmkuhl, F., Wunderlich, T., Wilken, D., Schirmer, W., and Vött, A.: Millennial-scale terrestrial ecosystem responses to Upper Pleistocene climatic changes: 4D-reconstruction of the Schwalbenberg Loess-Palaeosol- Sequence (Middle Rhine Valley, Germany), Catena, 196, 104913, https://doi.org/10.1016/j.catena.2020.104913, 2021.

Frechen, M.: Systematic Thermoluminescence Dating of 2 Loess Profiles from the Middle Rhine Area (F.R.G.), Quaternary Sci. Rev., 11, 93–101, https://doi.org/10.1016/0277-3791(92)90048-D, 1992.

Frechen, M.: Thermolumineszens-Datierungen an Lössen des Tönchesberges aus der Osteifel, E&G Quaternary Sci. J., 44, 79–93, https://doi.org/10.3285/eg.44.1.08, 1994.

Frechen, M., Brückner, H., and Radtke, U.: A comparison of different TL-techniques on loess samples from Rheindahlen (FRG), Quaternary Sci. Rev., 11, 109–113, https://doi.org/10.1016/0277-3791(92)90050-I, 1992.

Frechen, M., Terhorst, B., and Rähle, W.: The Upper Pleistocene loess/palaeosol sequence from Schatthausen in North Baden-Württemberg, E&G Quaternary Sci. J., 56, 212–227, https://doi.org/10.3285/eg.56.3.05, 2007.

Gabriel, G., Ellwanger, D., Hoselmann, C., Weidenfeller, M., Wielandt-Schuster, U., and The Heidelberg Basin Project Team: The Heidelberg Basin, Upper Rhine Graben (Germany): a unique archive of Quaternary sediments in Central Europe, Quatern. Int., 292,43–58, https://doi.org/10.1016/j.quaint.2012.10.044, 2013.

Galbraith, R. F., Roberts, R. G., Laslett, G. M., Yoshida, H., and Olley, J. M.: Optical Dating of single and multiple Grains of

Quartz from Jinmium Rock Shelter, Northern Australia: Part I, Experimental Design and Statistical Models, Archaeometry, 41, 2, 339–364, 1999.

Guenther, E. W.: Sedimentpetrographische Untersuchung von Lössen-Zur Gliederung des Eiszeitalters und zur Einordnung paläolithischer Kulturen, Teil 1 Methodische Grundlagen mit Erläuterung an Profilen, Böhlau Verlag Köln Graz, p. 10, 1961.

Guenther, E. W.: Zur Gliederung der Lösse des südlichen Oberrheintals, E&G Quaternary Sci. J., 37, 67–78, https://doi.org/10.3285/eg.37.1.07, 1987.

Hädrich, F.: Die Böden der Emmendinger Vorbergzone (Südliches Oberrheingebiet), Berichte der Naturforschenden Gesellschaft Freiburg i. Br., 56, 23–76, 1965.

Hädrich, F.: Zur Methodik der Lößdifferenzierung auf der Grundlage der Carbonatverteilung, E&G Quaternary Sci. J., 26, 95–117, https://doi.org/10.3285/eg.26.1.06, 1975.

Hädrich, F.: Paläoböden im südlichen Oberrhein Gebiet, Berichte der Naturforschenden Gesellschaft Freiburg i. Br., 70, 29–48, 1980.

Hädrich, F. and Lamparski, F.: Ein rißzeitlicher Eiskeil im Lößaufschluß von Buggingen (Südbaden) mit einem Beitrag zur Lößkindelgenese, Berichte der Naturforschenden Gesellschaft Freiburg i. Br., 74, 25–47, 1984.

Hädrich, F. and Stahr, K.: Die Böden des Breisgaus und angrenzender Gebiete, Berichte der Naturforschenden Gesellschaft Freiburg i. Br., 91., 148 pp., 2001.

Haesaerts, P., Dupuis, C., Spagna, P., Damblon, F., Balescu, S., Jadin, I., Lavachery, P., Pirson, S., and Bosquet, D.: Révision du cadre chronostratigraphique des assemblages Levallois issus des nappes alluviales du Pléistocène moyen dans le bassin de la Haine (Belgique), in: Actes du XXVIIIe Congrès Préhistorique de France, Amiens, France, 30 May–4 June 2016, Société préhistorique de France, Paris, France, 179–199, 2019.

Heiri, O., Lotter, A. F., and Lemcke, G.: Loss on ignition as a method for estimating organic and carbonate content in sediments: reproducibility and comparability of results, J. Paleolimnol., 25, 101–110, https://doi.org/10.1023/A:1008119611481, 2001.

Heiri, O., Koinig, K. A., Spötl, C., Barrett, S., Brauer, A., Drescher-Schneider, R., Gaar, D., Ivy-Ochs, S., Kerschner, H., Luetscher, M., Moran, A., Nicolussi, K., Preusser, F., Schmidt, R., Schoeneich, P., Schwörer, C., Sprafke, T., Terhorst, B., and Tinner, W.: Palaeoclimate records 60–8 ka in the Austrian and Swiss Alps and their forelands, Quaternary Sci. Rev., 106, 186–205, https://doi.org/10.1016/j.quascirev.2014.05.021, 2014.

Hofmann, F. M., Rauscher, F., McCreary, W., Bischoff, J.-P., and Preusser, F.: Revisiting Late Pleistocene glacier dynamics northwest of the Feldberg, southern Black Forest, Germany, E&G Quaternary Sci. J., 69, 61–87, https://doi.org/10.5194/egqsj-69-61-2020, 2020.

Houben, P.: Spatio-temporally variable response of fluvial systems to Late Pleistocene climate change: a case study from central Germany, Quaternary Sci. Rev., 22, 2125–2140, https://doi.org/10.1016/S0277-3791(03)00181-1, 2003.

Huntley, D. J. and Baril, M. R.: The K content of the K-feldspars being measured in optical dating or in thermoluminescence dating, Ancient TL, 15, 11–13, 1997.

Jordanova, D., Laag, C., Jordanova, N., Lagroix, F., Georgieva, B., Ishlyamski, D., and Guyodo, Y.: A detailed magnetic record of Pleistocene climate and distal ash dispersal during the last 800 kyrs – The Suhia Kladenetz quarry loess-paleosol sequence near Pleven (Bulgaria), Glob. Planet. Change, 214, 103840, https://doi.org/10.1016/j.gloplacha.2022.103840, 2022.

Junkmanns, J.: Les ensembles lithiques d'Achenheim d'apres la collection de Paul Wernert, Bull. Soc. Préhist. Fr., 92, 26–36, 1995.

Kadereit, A., Kind, C.-J., and Wagner, G. A.: The chronological position of the Lohne Soil in the Nussloch loess section – re-evaluation for a European loess-marker horizon, Quaternary Sci. Rev., 59, 67–86, https://doi.org/10.1016/j.quascirev.2012.10.026, 2013.

Kars, R. H., Reimann, T., Ankjærgaard, C., and Wallinga, J.: Bleaching of the post-IR IRSL signal: new insights for feldspar luminescence dating, Boreas, 43, 780–791, https://doi.org/10.1111/bor.12082, 2014.

Keßler, G. and Laiber, J.: Erläuterungen zu Blatt 7813 Emmendingen, Geologisches Landesamt Baden-Württemberg, Landesvermessungsamt Baden-Württemberg, Stuttgart, 1991.

Kleinmann, A., Müller, H., Lepper, J., and Waas, D.: Nachtigall: A continental sediment and pollen sequence of the Saalian Complex in NW-Germany and its relationship to the MIS-framework, Quatern. Int., 241, 97–110, https://doi.org/10.1016/j.quaint.2010.10.005, 2011.

Knipping, M.: Early and Middle Pleistocene pollen assemblages of deep core drillings in the northern Upper Rhine Graben, Germany, Neth. J. Geosci., 87, 51–65, https://doi.org/10.1017/S0016774600024045, 2008.

Kock, S., Huggenberger, P., Preusser, F., Rentzel., P., and Wetzel, A.: Formation and evolution of the Lower Terrace of the Rhine River in the area of Basel, Swiss J. Geosci. 102, 307–321, https://doi.org/10.1007/s00015-009-1325-1, 2009.

Konert, M. and Vandenberghe, J.: Comparison of laser grain size analysis with pipette and sieve analysis: a solution for the underestimation of the clay fraction, Sedimentology, 44, 523–535, https://doi.org/10.1046/j.1365-3091.1997.d01-38.x, 1997.

Krauss, L., Kappenberg, A., Zens, J., Kehl, M., Schulte, P., Zeeden, C., Eckmeier, E., and Lehmkuhl, F.: Reconstruction of Late Pleistocene paleoenvironments in southern Germany using two high-resolution loess-paleosol records, Palaeogeogr. Palaeocl., 509, 58–76, https://doi.org/10.1016/j.palaeo.2017.11.043, 2018.

Kukla G. J.: Pleistocene land-sea correlations. 1: Europe. Earth-Sci. Rev., 13, 307–374, https://doi.org/10.1016/0012-8252(77)90125-8, 1977.

Laag C., Hambach U., Zeeden C., Lagroix F., Guyodo Y., Veres V., Jovanović M., and Marković S. B.: A Detailed Paleoclimate Proxy Record for the Middle Danube Basin Over the Last 430 kyr: A Rock Magnetic and Colorimetric Study of the Zemun Loess-Paleosol Sequence, Front. Earth Sci., 9, 600086, https://doi.org/10.3389/feart.2021.600086, 2021.

Lehmkuhl, F., Zens, J., Krauß, L., Schulte, P., and Kels, H.: Loess-palaeosol sequences at the northern European loess belt in Germany: Distribution, geomorphology and stratigraphy, Quaternary Sci. Rev., 153, 11–30, https://doi.org/10.1016/j.quascirev.2016.10.008, 2016.

Lehmkuhl, F., Nett, J. J., Pötter, S., Schulte, P., Sprafke, T., Jary, Z., Antoine, P., Wacha, L., Wolf, D., Zerboni, A., Hošek, J., Marković, S. B., Obreht, I., Sümergi, P., Veres, D., Zeeden, C., Boemke, B., Schaubert, V., Viehweger, J., and Hambach, U.: Loess landscapes of Europe – Mapping, geomorphology, and zonal differentiation, Earth-Sci. Rev., 215, 103496, https://doi.org/10.1016/j.earscirev.2020.103496, 2021.

Li, B. and Li, S.-H.: Luminescence dating of K-feldspar from sediments: A protocol without anomalous fading correction, Quat. Geochronol, 6, 468–479, https://doi.org/10.1016/j.quageo.2011.05.001, 2011.

Li, Y., Tsukamoto, S., Frechen, M., and Gabriel, G.: Timing of fluvial sedimentation in the Upper Rhine Graben since the Middle Pleistocene: constraints from quartz and feldspar luminescence dating, Boreas, 47, 256–270, https://doi.org/10.1111/bor.12266, 2018.

Lisiecki, L. E. and Raymo, M. E.: A Pliocene-Pleistocene stack of 57 globally distributed benthic δ^{18}O records, Paleoceanography, 20, PA1003, https://doi.org/10.1029/2004PA001071, 2005.

Lowick, S. E., Trauerstein, M., and Preusser, F.: Testing the application of post IR-IRSL dating to fine grain waterlain sediments, Quat. Geochronol., 8, 33–40, https://doi.org/10.1016/j.quageo.2011.12.003, 2012.

Marković, S. B., Stevens, T., Kukla, G. J., Hambach, U., Fitzsimmons, K. E., Gibbard, P., Buggle, B., Zech, M., Guo, Z., Hao, Q., Wu, H., O'Hara Dhand, K., Smalley, I. J., Újvári, G., Sümegi, P., Timar-Gabor, A., Veres, D., Sirocko, F., Vasiljević, D. A., Jary, Z., Svensson, A., Jović, V., Lehmkuhl, F., Kovács, J., and Svirčev, Z.: Danube loess stratigraphy – Towards a pan-European loess stratigraphic model, Earth-Sci. Rev., 148, 228–258, https://doi.org/10.1016/j.earscirev.2015.06.005, 2015.

May, J.-H., Marx, S. K., Reynolds, W., Clark-Balzan, L., Jacobsen, G. E., and Preusser, F.: Establishing a chronological framework for a late Quaternary seasonal swamp in the Australian "Top End", Quat. Geochronol., 47, 81–92, https://doi.org/10.1016/j.quageo.2018.05.010, 2018.

Mercier, J.-L. and Jeser, N.: The glacial history of the Vosges Mountains, Developments in Quaternary Science, 2,113–118, https://doi.org/10.1016/S1571-0866(04)80061-7, 2004.

Meszner, S., Kreutzer, S., Fuchs, M., and Faust, D.: Late Pleistocene landscape dynamics in Saxony, Germany: Paleoenvironmental reconstruction using loess-paleosol sequences, Quatern. Int., 296, 94–107, https://doi.org/10.1016/j.quaint.2012.12.040, 2013.

Meyers, P. A. and Lallier-Verges, E.: Lacustrine sedimentary organic matter records of Late Quaternary paleoclimates, J. Paleolimnol., 21, 345–372, https://doi.org/10.1023/A:1008073732192, 1999.

Moine, O., Antoine, P., Hatté, C., Landais, A., Mathieu, J., Prud'homme, C., and Rousseau, D.-D.: The impact of Last Glacial climate variability in west-European loess revealed by radiocarbon dating of fossil earthworm granules, P. Natl. Acad. Sci. USA, 114, 6209–6214, https://doi.org/10.1073/pnas.1614751114, 2017.

Moska, P. and Bluszcz, A.: Luminescence dating of loess profiles in Poland, Quatern. Int., 296, 51–60, https://doi.org/10.1016/j.quaint.2012.09.004, 2013.

Necula, C., Dimofte, D., and Panaiotu, C.: Rock magnetism of a loess-palaeosol sequence from the western Black Sea shore (Romania), Geophys. J. Int., 202, 1733–1748, https://doi.org/10.1093/gji/ggv250, 2015.

Pécsi, M. and Richter, G.: Löss: Herkunft – Gliederung – Landschaften, Z. Geomorphol., N.F., Supplementband 98, Bornträger, Berlin & Stuttgart, 391 pp., ISBN 3-443-21098-8, 1996.

Prescott, J. R. and Hutton, J. T.: Cosmic ray contributions to dose rates for luminescence and ESR dating: Large depths and long-term time variations, Radiat. Meas., 23, 497–500, https://doi.org/10.1016/1350-4487(94)90086-8, 1994.

Preusser, F.: Towards a chronology of the Late Pleistocene in the northern Alpine Foreland, Boreas, 33, 195–210, https://doi.org/10.1111/j.1502-3885.2004.tb01141.x, 2004.

Preusser F. and Fiebig M.: European Middle Pleistocene loess chronostratigraphy: Some considerations based on evidence from the Wels site, Austria, Quatern. Int., 198, 37–45, https://doi.org/10.1016/j.quaint.2008.07.006, 2009.

Preusser, F., Drescher-Schneider, R., Fiebig, M., and Schlüchter, C.: Re-interpretation of the Meikirch pollen record, Swiss Alpine Foreland, and implications for Middle Pleistocene chronostratigraphy, J. Quaternary Sci., 20, 607–620, https://doi.org/10.1002/jqs.930, 2005.

Preusser, F., Graf, H. R., Keller, O., Krayss, E., and Schlüchter, C.: Quaternary glaciation history of northern Switzerland, E&G Quaternary Sci. J., 60, 21, https://doi.org/10.3285/eg.60.2-3.06, 2011.

Preusser, F., Büschelberger, M., Kemna, H. A., Miocic, J., Mueller, D., and May, J.-H.: Quaternary aggradation in the Upper Rhine Graben linked to the glaciation history of northern Switzerland, Int. J. Earth Sci., 110, 1827–1846, https://doi.org/10.1007/s00531-021-02043-7, 2021.

Qin, J., Chen, J., Li, Y., and Zhou, L.: Initial sensitivity change of K-feldspar pIRIR signals due to uncompensated decrease in electron trapping probability: evidence from radiofluorescence measurements, Radiat. Meas., 120, 131–136, https://doi.org/10.1016/j.radmeas.2018.06.017, 2018.

Rahimzadeh, N., Sprafke, T., Thiel, C., Terhorst, B., and Frechen, M.: A comparison of polymineral and K-feldspar post-infrared infrared stimulated luminescence ages of loess from Franconia, southern Germany, E&G Quaternary Sci. J., 70, 53–71, https://doi.org/10.5194/egqsj-70-53-2021, 2021.

Rees-Jones, J.: Optical Dating Of Young Sediments Using Fine-Grain Quartz, Ancient TL, 13, 9–14, 1995.

Richter, D., Richter, A., and Dornich, K.: Lexsyg smart – a luminescence detection system for dosimetry, material research and dating application, Geochronometria, 42, 202–209, https://doi.org/10.1515/geochr-2015-0022, 2015.

Roberts, H. M., Durcan, J. A., and Duller, G. A. T.: Exploring procedures for the rapid assessment of optically stimulated luminescence range-finder ages, Radiat. Meas., 44, 582–587, https://doi.org/10.1016/j.radmeas.2009.02.006, 2009.

Rodrigues, T., Alonso-García, M., Hodell, D. A., Rufino, M., Naughton, F., Grimalt, J. O., Voelker, A. H. L., and Abrantes, F.: A 1-Ma record of sea surface temperature and extreme cooling events in the North Atlantic: A perspective from the Iberian Margin, Quaternary Sci. Rev., 172, 118–130, https://doi.org/10.1016/j.quascirev.2017.07.004, 2017.

Rösner, U.: Die Mainfränkische Lößprovinz. Sedimentologische, pedologische und morphodynamische Prozesse der Lößbildung währenddes Pleistozäns in Mainfranken, Erlanger Geographische Arbeiten, 301 pp., 1990.

Schmidt, E. D., Frechen, M., Murray, A. S., Tsukamoto, S., and Bittmann, F.: Luminescence chronology of the loess record from the Tönchesberg section: A comparison of using quartz and feldspar as dosimeter to extend the age range beyond the Eemian, Quatern. Int., 234, 10–22, https://doi.org/10.1016/j.quaint.2010.07.012, 2011a.

Schmidt, E. D., Semmel, A., and Frechen, M.: Luminescence dating of the loess/palaeosol sequence at the gravel quarry Gaul/Weilbach, Southern Hesse (Germany), E&G Quaternary Sci. J., 60, 9, https://doi.org/10.3285/eg.60.1.08, 2011b.

Scholger, R. and Terhorst, B.: Magnetic excursions recorded in the Middle to Upper Pleistocene loess/palaeosol sequence Wels-Aschet (Austria), E&G Quaternary Sci. J., 62, 14–21, https://doi.org/10.3285/eg.62.1.02, 2013.

Schulte, P. and Lehmkuhl, F.: The difference of two laser diffraction patterns as an indicator for post-depositional grain size reduction in loess-paleosol sequences, Palaeogeogr. Palaeocl., 509, 126–136, https://doi.org/10.1016/j.palaeo.2017.02.022, 2018.

Schulte, P., Sprafke, T., Rodrigues, L., and Fitzsimmons, K. E.: Are fixed grain size ratios useful proxies for loess sedimentation dynamics? Experiences from Remizovka, Kazakhstan, Aeolian Res., 31, 131–140, https://doi.org/10.1016/j.aeolia.2017.09.002, 2018.

Schulze, T., Schwahn, L., Fülling, A., Zeeden, C., Preusser, F., and Sprafke, T.: Investigating the loess–palaeosol sequence of Bahlingen-Schönenberg (Kaiserstuhl), southwestern Germany, using a multi-methodological approach, E&G Quaternary Sci. J., 71, 145–162, https://doi.org/10.5194/egqsj-71-145-2022, 2022.

Semmel, A.: Studien über den Verlauf jungpleistozäner Formung in Hessen, Frankfurter geographische Hefte, 44, 1–133, 1968.

Semmel, A. and Fromm, K.: Ergebnisse paläomagnetischer Untersuchungen an quartären Sedimenten des Rhein-Main-Gebiets, E&G Quaternary Sci. J., 27, 18–25, https://doi.org/10.3285/eg.27.1.02, 1976.

Smedley, R. K., Duller, G. A. T., and Roberts, H. M.: Bleaching of the post-IR IRSL signal from individual grains of K-feldspar: Implications for single-grain dating, Radiat. Meas., 79, 33–42, https://doi.org/10.1016/j.radmeas.2015.06.003, 2015.

Sprafke, T.: Löss in Niederösterreich – Archiv quartärer Klima- und Landschaftsveränderungen, Würzburg University Press, https://doi.org/10.25972/WUP-978-3-95826-039-9, 2016.

Sprafke, T. and Obreht, I.: Loess: Rock, sediment or soil – What is missing for its definition?, Quatern. Int., 399, 198–207, https://doi.org/10.1016/j.quaint.2015.03.033, 2016.

Sprafke, T., Thiel, C., and Terhorst, B.: From micromorphology to palaeoenvironment: The MIS 10 to MIS 5 record in Paudorf (Lower Austria), Catena, 117, 60–72, https://doi.org/10.1016/j.catena.2013.06.024, 2014.

Sprafke, T., Schulte, P., Meyer-Heintze, S., Händel, M., Einwögerer, T., Simon, U., Peticka, R., Schäfer, C., Lehmkuhl, F., and Terhorst, B.: Paleoenvironments from robust loess stratigraphy using high-resolution color and grain-size data of the last glacial Krems-Wachtberg record (NE Austria), Quaternary Sci. Rev., 248, 106602, https://doi.org/10.1016/j.quascirev.2020.106602, 2020.

Stebich, M., Höfer, D., Mingram, J., Nowaczyk, N., Rohrmüller, J., Mrlina, J., and Kämpf, H.: A contribution towards the palynostratigraphical classification of the Middle Pleistocene in Central Europe: The pollen record of the Neualbenreuth Maar, northeastern Bavaria (Germany), Quaternary Sci. Rev., 250, 106681, https://doi.org/10.1016/j.quascirev.2020.106681, 2020.

Stephan, H.-J.: Climato-stratigraphic subdivision of the Pleistocene in Schleswig-Holstein, Germany and adjoining areas: status and problems, E&G Quaternary Sci. J., 63, 3–18, https://doi.org/10.3285/eg.63.1.01, 2014.

Stojakowits P., Mayr C., Ivy-Ochs S., Preusser F., Reitner J., and Spötl C.: Environments at the MIS 3/2 transition in the northern Alps and their foreland, Quatern. Int., 581/582, 99–113, https://doi.org/10.1016/j.quaint.2020.08.003, 2021.

Strunk, H.: Das Quartärprofil von Hagelstadt im Bayerischen Tertiärhügelland, E&G Quaternary Sci. J., 40, 85–96, https://doi.org/10.3285/eg.40.1.06, 1990.

Terhorst, B.: Korrelation von mittelpleistozänen Löss-/Paläobodensequenzen in Oberösterreich mit einer marinen Sauerstoffisotopenkurve, E&G Quaternary Sci. J., 56, 172–185, https://doi.org/10.3285/eg.56.3.03, 2007.

Terhorst, B.: A stratigraphic concept for Middle Pleistocene Quaternary sequences in Upper Austria , E&G Quaternary Sci. J., 62, 4–13, https://doi.org/10.3285/eg.62.1.01, 2013.

Terhorst, B., Frechen, M., and Reitner, J.: Chronostratigraphische Ergebnisse aus Lößprofilen der Inn-und Traun-Hochterrassen in Oberösterreich, Z. Geomorphol., Supplementband, 127, 213–232, 2002.

Terhorst, B., Sedov, S., Sprafke, T., Peticzka, R., Meyer-Heintze, S., Kühn, P., and Solleiro Rebolledo, E.: Austrian MIS 3/2 loess–palaeosol records – Key sites along a west–east transect, Palaeogeogr. Palaeocl., 418, 43–56, https://doi.org/10.1016/j.palaeo.2014.10.020, 2015.

Thiel, C., Buylaert, J.-P., Murray, A. S., Terhorst, B., Hofer, I., Tsukamoto, S., and Frechen, M.: Luminescence dating of the Stratzing loess profile (Austria) – testing the potential of an elevated temperature post-IR IRSL protocol, Quatern. Int., 234, 23–31, https://doi.org/10.1016/j.quaint.2010.05.018, 2011a.

Thiel, C., Buylaert, J.-P., Murray, A. S., Terhorst, B., Tsukamoto, S., Frechen, M., and Sprafke, T.: Investigating the chronostratigraphy of prominent palaeosols in Lower Austria using post-IR IRSL dating, E&G Quaternary Sci. J., 60, 11, https://doi.org/10.3285/eg.60.1.10, 2011b.

Thiel, C., Terhorst, B., Jaburová, I., Buylaert, J. P., Murray, A. S., Fladerer, F. A., Damm, B., Frechen, M., and Ottner, F.: Sedimentation and erosion processes in Middle to Late Pleistocene sequences exposed in the brickyard of Langenlois/Lower Austria, Geomorphology, 135, 295–307, https://doi.org/10.1016/j.geomorph.2011.02.011, 2011c.

Thiel, C., Horvaìth, E., and Frechen, M.: Revisiting the loess/-palaeosol sequence in Paks, Hungary: A post-IR IRSL based chronology for the “Young Loess Series”, Quatern. Int., 319, 88–98, https://doi.org/10.1016/j.quaint.2013.05.045, 2014.

Tucci, M., Krahn, K.J., Richter, D., van Kolfschoten, T., Rodríguez Álvarez, B., Verheijen, I., Serangeli, J., Lehmann, J., Degering, D., Schwalb, A., and Urban, B.: Evidence for the age and timing of environmental change associated with a Lower Palaeolithic site within the Middle Pleistocene Reinsdorf sequence of the Schöningen coal mine, Germany, Palaeogeogr. Palaeocl., 569, 110309, https://doi.org/10.1016/j.palaeo.2021.110309, 2021.

Vandenberghe, J.: Grain size of fine-grained windblown sediment: A powerful proxy for process identification, Earth-Sci. Rev., 121, 18–30, https://doi.org/10.1016/j.earscirev.2013.03.001, 2013.

Van Husen, D. and Reitner, J. M.: An Outline of the Quaternary Stratigraphy of Austria, E&G Quaternary Sci. J., 60, 24, https://doi.org/10.3285/eg.60.2-3.09, 2011.

Viscarra Rossel, R. A., Walvoort, D. J. J., McBratney, A. B., Janik, L.J., and Skjemstad, J. O.: Visible, near infrared, mid infrared or combined diffuse reflectance spectroscopy for simultaneous assessment of various soil properties, Geoderma, 131, 59–75, https://doi.org/10.1016/j.geoderma.2005.03.007, 2006.

Weidenfeller, M. and Knipping, M.: Correlation of Pleistocene sediments from boreholes in the Ludwigshafen area, western Heidelberg Basin, E&G Quaternary Sci. J., 57, 270–285, https://doi.org/10.3285/eg.57.3-4.1, 2009.

Wintle, A. G. and Murray, A. S.: A review of quartz optically stimulated luminescence characteristics and their relevance in single-aliquot regeneration dating protocols, Radiat. Meas., 41, 369–391, https://doi.org/10.1016/j.radmeas.2005.11.001, 2006.

Zander, A. and Hilgers, A.: Potential and limits of OSL, TT-OSL, IRSL and $pIRIR_{290}$ dating methods applied on a Middle Pleistocene sediment record of Lake El'gygytgyn, Russia, Clim. Past, 9, 719–733, https://doi.org/10.5194/cp-9-719-2013, 2013.

Zeeden, C. and Hambach, U.: Magnetic susceptibility properties of loess from the Willendorf archaeological site: Implications for the syn/post-depositional interpretation of magnetic fabric, Front. Earth Sci., 8, 599491, https://doi.org/10.3389/feart.2020.599491, 2021.

Zeeden, C., Kels, H., Hambach, U., Schulte, P., Protze, J., Eckmeier, E., Markovic, S. B., Klasen, N., and Lehmkuhl, F.: Three climatic cycles recorded in a loess-palaeosol sequence at Semlac (Romania) – Implications for dust accumulation in south-eastern Europe, Quaternary Sci. Rev., 154, 130–142, https://doi.org/10.1016/j.quascirev.2016.11.002, 2016.

Zeeden, C., Mir, J. A., Vinnepand, M., Laag, C., Rolf, C., and Dar, R. A.: Local mineral dust transported by varying wind intensities forms the main substrate for loess in Kashmir, E&G Quaternary Sci. J., 70, 191–195, https://doi.org/10.5194/egqsj-70-191-2021, 2021.

Zens, J., Schulte, P., Klasen, N., Krauß, L., Pirson, S., Burow, C., Brill, D., Eckmeier, E., Kels, H., Zeeden, C., Spagna, P., and Lehmkuhl, F.: OSL chronologies of paleoenvironmental dynamics recorded by loess-paleosol sequences from Europe: Case studies from the Rhine-Meuse area and the Neckar Basin, Palaeogeogr. Palaeocl, 509, 105–125, https://doi.org/10.1016/j.palaeo.2017.07.019, 2018.

Zhang, J.: Behavior of the electron trapping probability change in IRSL dating of K-feldspar: A dose recovery study, Quat. Geochronol., 44, 38–46, https://doi.org/10.1016/j.quageo.2017.12.001, 2018.

Zhang, J. and Li, S.-H.: Review of the Post-IR IRSL Dating Protocols of K-Feldspar, Methods Protoc., 3, 7, https://doi.org/10.3390/mps3010007, 2020.

Zöller, L., Stremme, H., and Wagner, G.A.: Thermolumineszenz-Datierung an Löss-Paläoboden-Sequenzen von Nieder-, Mittel- und Oberrhein/Bundesrepublik Deutschland, Chem. Geol., 73, 39–62, https://doi.org/10.1016/0168-9622(88)90020-6, 1988.

Zöller, L., Fischer, M., Jary, Z., Antoine, P., and Krawczyk, M.: Chronostratigraphic and geomorphologic challenges of last glacial loess in Poland in the light of new luminescence ages, E&G Quaternary Sci. J., 71, 59–81, https://doi.org/10.5194/egqsj-71-59-2022, 2022.

E&G Quaternary Sci. J., 72, 23–36, 2023
https://doi.org/10.5194/egqsj-72-23-2023

Open Access E&G Quaternary Science Journal

Research article

Comparison of overdeepened structures in formerly glaciated areas of the northern Alpine foreland and northern central Europe

Lukas Gegg and Frank Preusser

Institute of Earth and Environmental Sciences, University of Freiburg, Albertstraße 23b, 79104 Freiburg, Germany

Correspondence: Lukas Gegg (lukas.gegg@geologie.uni-freiburg.de)

Relevant dates: Received: 12 August 2022 – Revised: 6 December 2022 – Accepted: 21 December 2022 – Published: 20 January 2023

How to cite: Gegg, L. and Preusser, F.: Comparison of overdeepened structures in formerly glaciated areas of the northern Alpine foreland and northern central Europe, E&G Quaternary Sci. J., 72, 23–36, https://doi.org/10.5194/egqsj-72-23-2023, 2023.

Abstract: Overdeepened structures occur in formerly and presently glaciated regions around the earth and are usually referred to as overdeepenings or tunnel valleys. The existence of such troughs has been known for more than a century, and they have been attributed to similar formation processes where subglacial meltwater plays a decisive role. This comparison highlights that (foreland) overdeepenings and tunnel valleys further occur in similar dimensions and share many characteristics such as gently sinuous shapes in plan view, undulating long profiles with terminal adverse slopes, and varying cross-sectional morphologies. The best explored examples of overdeepened structures are situated in and around the European Alps and in the central European lowlands. Especially in the vicinity of the Alps, some individual troughs are well explored, allowing for a reconstruction of their infill history, whereas only a few detailed studies, notably such involving long drill core records, have been presented from northern central Europe. We suggest that more such studies could significantly further our understanding of subglacial erosion processes and the regional glaciation histories and aim to promote more intense exchange and discussion between the respective scientific communities.

Kurzfassung: In den ehemals und gegenwärtig vergletscherten Regionen der Erde finden sich übertiefte Beckenstrukturen, die üblicherweise als Übertiefungen oder Tunneltäler angesprochen werden. Die Existenz dieser Tröge ist seit mehr als einem Jahrhundert bekannt, und sie wurden ähnlichen Erosionsprozessen zugeschrieben, bei denen subglaziales Schmelzwasser eine entscheidende Rolle spielt. Mit diesem Vergleich möchten wir zeigen, dass (Vorland-)Übertiefungen und Tunneltäler in vergleichbaren Dimensionen auftreten, und eine Reihe weiterer gemeinsamer Merkmale aufweisen, zum Beispiel sanft gewundene Längsachsen, undulierende Profile mit Gegensteigungen am distalen Ende, und variable Formen im Querschnitt. Die bestuntersuchten Beispiele für übertiefte Becken befinden sich im europäischen Alpenraum, und in zentraleuropäischen Tiefländern. Vor allem im Alpenraum wurden einige übertiefte Strukturen detailliert untersucht, was eine Rekonstruktion ihrer Verfüllung erlaubt. Im Gegensatz dazu existieren nur wenige (bohrungsbasierte) Detailstudien im nördlichen Mitteleuropa. Wir betonen, dass solche Untersuchungen zu unserem Verständnis subglazialer Erosionsprozesse, aber auch regionaler Vergletscherungsgeschichten beitragen können, und möchten Austausch und Diskussion unter den entsprechenden wissenschaftlichen Lagern anregen.

1 Introduction

The repeated glaciations during the Quaternary period shaped large swathes of the earth's surface, first, by eroding and removing large rock masses from mountain areas and other regions covered by ice; glacially polished bedrock surfaces and deep valley flanks are some of the most striking features in this context. Second, the accumulation of rock debris transported by ice and meltwater led to the formation of characteristic landscape features such as moraine ridges and gravel terraces. However, a third feature that represents a combination of both erosive and aggradational processes is less well known to a broader public: geological structures deeply incised by subglacial erosion into pre-existing landscapes but hidden below the present land surface after being filled up by sediment and/or occupied by large bodies of water. First recognised within and around the European Alps as well as below the central European lowlands, these troughs are referred to as overdeepenings and tunnel valleys, respectively.

While these structures have been known since the late 19th century, for a long time they attracted relatively little scientific attention as their investigation is costly due to the fact that it requires the use of either deep drilling or geophysics – ideally a combination of both. Since the beginning of the 21st century, scientific interest in glacially eroded, and specifically overdeepened, structures increased considerably, to some extent motivated by applied aspects. On the one hand, these structures have a poorly explored potential as groundwater sources and for geothermal energy production. On the other hand, planning nuclear waste repositories requires the identification of areas that will ideally not be affected by deep glacial erosion in the near geological future (i.e. the next million years), as this may challenge the intactness of the disposal site.

Advances in geophysical techniques together with the increased interest in glacially eroded structures have triggered several projects into the subject during the past 2 decades notably in the aforementioned areas in central Europe. These can thus be regarded as the best explored regions with regard to overdeepened structures and, due to their proximity, should be subject to similar evolutionary trends over time. However, there has been very limited exchange among the communities working in and around the Alps and the northern central European lowlands, respectively. This is in contrast to the common assumption that all these structures were formed by similar erosion processes, and, hence, it should be expected they share many similarities.

The aim of this article is to summarise and compare the current knowledge about overdeepenings and tunnel valleys in general but with special regard to the northern Alpine foreland and the wider North Sea area. This comparison is done specifically in light of the question whether there are relevant differences in the morphology and/or filling history of these troughs or whether they are just different examples of basically the same type of feature. We thus touch only lightly upon the concepts of the erosion mechanisms that have been intensively discussed by others (e.g. Alley et al., 2019; Cook and Swift, 2012, and references therein).

2 History of recognition and state-of-the-art research

The term "overdeepening" is attributed to Albrecht Penck, one of the pioneers and most prominent representatives of Alpine Quaternary geology. He used it to describe intensive and deep-reaching glacial erosion focused in the main Alpine trunk valleys whose valley floors lie significantly below their off-cut tributaries (Penck and Brückner, 1909). The concept of deep-reaching subglacial erosion had been subject to intensive discussion (e.g. Heim, 1885) but was lastly confirmed in 1908 by a tragic accident during tunnel works in central Switzerland (Lötschberg), when blasting their way into an infilled overdeepening ~ 170 m below ground cost the lives of 24 workers, as the liquefied valley infill flooded the tunnel (Waltham, 2008). Over the following decades, boreholes and geophysical data revealed the existence of such deep infilled bedrock troughs below the majority of the present-day valleys not only in the Alps and the Alpine foreland (cf. Haeberli et al., 2016; Preusser et al., 2010) but also in other mountain regions on earth (e.g. Carrivick et al., 2016; Gao, 2011; James et al., 2019; Magnússon et al., 2012; Smith, 2004). First systematic compilations of these deeply incised features were provided by Van Husen (1979) and Wildi (1984), who noted that large sections of these troughs lie deeper than the bedrock at the respective valley outlet. This closed basin shape with a terminal adverse slope is today generally regarded as defining an overdeepening (Alley et al., 2019; Cook and Swift, 2012; Patton et al., 2016). Notably – but not exclusively – in Switzerland, overdeepenings have since been intensively studied based on scientific drillings (Hsü and Kelts, 1984; Preusser et al., 2005; Schlüchter, 1989; Schwenk et al., 2022), geophysical campaigns (Bandou et al., 2022; Burschil et al., 2018, 2019; Finckh et al., 1984; Nitsche et al., 2001; Reitner et al., 2010), or a combination of both (Buechi et al., 2018; Dehnert et al., 2012; Gegg et al., 2021; Pomper et al., 2017).

The recognition of tunnel valleys goes similarly far back in time, to the late 19th century, when Danish and north German scholars identified deep subsurface troughs infilled with Quaternary sediments or hosting lakes (cf. van der Vegt et al., 2012). Jentzsch (1884) already hypothesised about an origin by subglacial fluvial erosion, a concept that was refined by Ussing (1904), who attributed these troughs, characterised by internal and terminal adverse slopes, to the action of pressurised subglacial meltwater. The model of Ussing (1904) became increasingly widely accepted, and the "tunnel valleys" (Madsen, 1921) became a subject of increasing scientific interest. Systematic regional-scale mapping and investigation started in the 1960s (e.g. Kuster and Meyer, 1979) and was expanded to other regions such as Great Britain (e.g. Woodland, 1970) and North America (e.g. Wright, 1973). Soon, the widespread availability of high-resolution marine seismic data acquired for oil and gas exploration marked a breakthrough in the recognition of tunnel valleys: they were encountered in previously glaciated shelf areas all around the world and could be temporally efficiently mapped on reflection-seismic sections (Boyd et al., 1988; Destombes et al., 1975; Kunst and Deze, 1985). Tunnel valley characterisation made a second major leap forward with the establishment of 3D seismic acquisition (Praeg, 1997). Based on these datasets, the longitudinal and transverse morphology of individual structures can be imaged and analysed in high detail and free from gaps (Kirkham et al., 2021; Kristensen et al., 2008; Ottesen et al., 2020; Stewart et al., 2013). Further insights derive from electromagnetic (e.g. Bosch et al., 2009; Tezkan et al., 2009) as well as gravimetric studies (e.g. Barker and Harker, 1984; Götze et al., 2009), while only little detailed borehole information is available (e.g. Piotrowski, 1994).

3 Geological and glaciological settings

In extensively glaciated mountain ranges, such as the European Alps, large overdeepenings occur in two endmember settings: in the major intermontane trunk valleys and in the mountain forelands (Dürst Stucki and Schlunegger, 2013; Magrani et al., 2020; Preusser et al., 2010). Within the mountain range, the bedrock is generally quite resilient towards erosion (Kühni and Pfiffner, 2001), and glacial erosion occurs preferentially along zones of weakness such as faults (Dürst Stucki and Schlunegger, 2013). This is a self-promoting process: with ongoing downcutting, drainage of water and ice along the deepening valley becomes increasingly efficient, and erosion is further focused on the valley floor, the result being a spatially stable, deeply incised valley, where ice flows comparatively rapidly and under strong lateral confinement (Egholm et al., 2012; Herman et al., 2011; Ugelvig et al., 2016). Glacial erosion sensu stricto, i.e. quarrying and abrasion, probably plays an important role in this setting, aided by subglacial meltwater stripping debris off the glacier base (Alley et al., 2019). It culminates in the formation of overdeepenings, for example at confluences or valley constrictions where ice flow is accelerated (Cook and Swift, 2012; Dürst Stucki and Schlunegger, 2013; Herman et al., 2015; Preusser et al., 2010).

Foreland overdeepenings, in contrast, develop beneath the piedmont tongues of valley glaciers. There, although its large-scale pattern is defined by the locations of mountain valley outlets, the ice flow is topographically much less constrained and potentially diffluent and the ice thickness is significantly smaller (Bini et al., 2009), and as a result, glacial erosion sensu stricto should be rather limited. However, with increasing catchment area, basal water availability also increases towards the glacier termini. This subglacial water, pressurised by the englacial water column, is regarded as a driver of overdeepening erosion in the foreland setting (Alley et al., 1997; Dürst Stucki et al., 2010; Dürst Stucki and Schlunegger, 2013; Gegg et al., 2021), where the bedrock commonly consists of poorly consolidated Molasse-type sediments (Kühni and Pfiffner, 2001). As these deposits are generally readily eroded, the occurrence of faults does not appear to play a significant role facilitating their erosion (Dürst Stucki and Schlunegger, 2013; Gegg et al., 2021). With the effect of structural preconditioning being low and ice flow being largely unconfined, the focusing of subglacial erosion may shift over time, evidenced for example by branching and off-cutting overdeepened troughs (Buechi et al., 2018; Ellwanger et al., 2011).

The primary erosive agent of tunnel valleys is, by definition, inferred to be basal meltwater (Cofaigh, 1996; Kehew et al., 2012; van der Vegt et al., 2012) at the margins of continental-scale ice sheets, where topographical confinement of ice flow is significantly lower than within mountain ranges (Schoof and Hewitt, 2013). Still, discharge at ice sheet margins is concentrated along ice streams, corridors of enhanced ice flow (Margold et al., 2015; Rignot et al., 2011) that develop where basal meltwater abundance is high and facilitates tunnel valley incision (Jennings, 2006; Lelandais et al., 2018). Further, where tunnel valleys occur near highland areas, some lie distinctly in extension of fjord valleys that direct the larger-scale flow pattern of ice and water (e.g. Bradwell et al., 2008; Kearsey et al., 2019). Large tunnel valleys occur predominantly within rather soft sedimentary substrata, while troughs in more resistant lithologies tend to be smaller and narrower (Janszen et al., 2012; Jørgensen and Sandersen, 2006). In resilient crystalline bedrock, tunnel valleys are typically lacking but are replaced by large-scale esker systems that are interpreted to reflect meltwater streams cut into the basal ice instead of the substratum (Boulton et al., 2009; Clark and Walder, 1994).

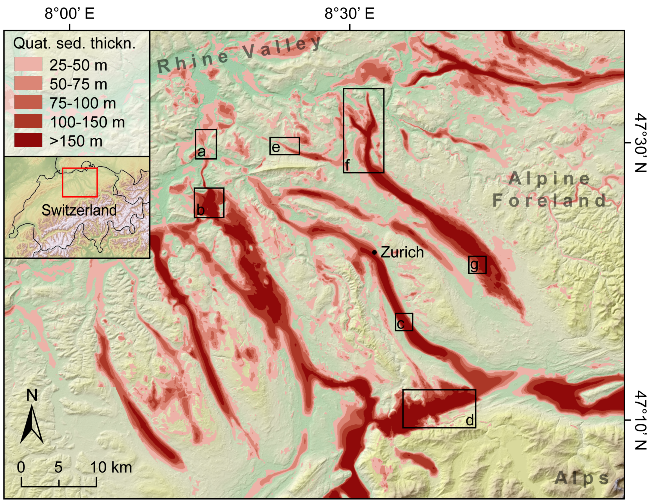

Figure 1. Foreland overdeepenings in central northern Switzerland highlighted as areas of increased Quaternary sediment thickness. Data from Pietsch and Jordan (2014), Gegg et al. (2021), and references therein. Black boxes highlight study areas mentioned in the text: (*a*) Lower Aare Valley (Gegg et al., 2021), (*b*) Birrfeld (Graf, 2009; Nitsche et al., 2001), (*c*) Lake Zurich (Lister, 1984a, b), (*d*) Richterswil (Wyssling, 2002), (*e*) Wehntal (Anselmetti et al., 2010; Dehnert et al., 2012), (*f*) Lower Glatt Valley (Buechi et al., 2018), and (*g*) Uster (Wyssling and Wyssling, 1978).

4 Morphological comparisons

4.1 Large-scale morphologies

Foreland overdeepenings are up to 15 km wide and 850 m deep bedrock incisions that reach lengths of >100 km (James et al., 2019; Magrani et al., 2020; Smith, 2004). They have been described as slightly sinuous troughs that may be arranged in seemingly anastomosing patterns (Fig. 1; Dürst Stucki and Schlunegger, 2013; Preusser et al., 2010). While some troughs have been re-excavated by multiple phases of ice advance (e.g. Birrfeld overdeepening; Nitsche et al., 2001; Lower Glatt Valley overdeepening; Buechi et al., 2018), the focus of overdeepening has in other areas laterally shifted over the course of several glaciations and produced subparallel (e.g. Reuss Valley; Jordan, 2010) or radially diverting branch basins (e.g. Lake Constance area; Ellwanger et al., 2011). The spacing between individual troughs is 5–20 km (Cummings et al., 2012; see also Jordan, 2010), and their sinuosities are around 1.05–1.10 (Gegg et al., 2021). In the longitudinal section, foreland overdeepenings often consist of several distinct sub-basins separated by abrupt bedrock swells and terminating with mostly gentle (~ 1–2°) adverse slopes (Jordan, 2010; Magrani et al., 2020; Preusser et al., 2010). While typically shifted upstream in intra-mountain overdeepenings, the deepest points in most foreland overdeepenings lie roughly at their central position (Magrani et al., 2020).

Tunnel valleys have maximum widths of ~ 12 km and maximum depths of ~ 500 m and can be over 150 km long (Cameron et al., 1987; Lutz et al., 2009; Praeg, 1997; Stewart et al., 2013). In plan view, they have straight to slightly sinuous courses and can occur in swarms or in pseudo-anastomosing (i.e. different branches of seemingly individual valleys belong to different generations of valley formation; Fig. 2; Jørgensen and Sandersen, 2006; Kristensen et al., 2008), radiating or tributary networks (Cofaigh, 1996; Kehew et al., 2012; van der Vegt et al., 2012). The lateral spacing between individual structures typically ranges between 5 (Livingstone and Clark, 2016) and 20–30 km (Kehew et al., 2012; van der Vegt et al., 2012), while Lutz et al. (2009) specifically note that tunnel valleys are not uniformly distributed and may in some areas be lacking entirely. According to data by Streuff et al. (2022), typical tunnel valley sinuosities are around 1.05. Tunnel valleys characteristically start and terminate abruptly (with terminal adverse slope angles in some cases exceeding 10°; Kristensen et al., 2008) and have undulating long courses comprising sub-basins as well as steep thresholds (Cofaigh, 1996; Kristensen et al., 2008; Lutz et al., 2009). The deepest points along the thalweg frequently lie far downstream from the valley centre (Jørgensen and Sandersen, 2006).

Based on datasets by Magrani et al. (2020) and Kristensen et al. (2008), Swiss foreland overdeepenings tend on average to be shorter, shallower, and narrower than Danish tunnel valleys, although only the difference in depth is statistically significant (unequal-variance *t* tests; Fig. 3). It should be noted, however, that the dataset by Kristensen et al. (2008) refers only to a restricted area and that other studies in the North Sea found tunnel valleys that generally tend to be shallower (Andersen et al., 2012) and narrower (Jørgensen and Sandersen, 2006; Stewart et al., 2013). The overall size of tunnel valleys as well as their form ratio appears to be influenced mainly by the erosional resistance of the substratum, whereas the valley width has been linked rather to glaciological parameters (e.g. ice thickness; van der Vegt et al., 2012). The maximum size of foreland overdeepenings on the other hand is clearly limited by the spatial extent of the respective piedmont glaciers, which were considerably smaller for example in front of the Eastern or Southern Alps (or in other mountain ranges) than in northern Switzerland (e.g. Preusser et al., 2010). Still, the comparison shows that, although the corresponding ice masses differ vastly in size, the dimensions of tunnel valleys and foreland overdeepenings are not necessarily greatly different.

4.2 Detailed cross-sectional morphologies

Cross-sections of foreland overdeepenings are frequently asymmetric and tend towards a U shape, but especially in more resistant bedrock lithologies, steep-angled (up to 60°) V-shaped valleys have been observed (Fig. 4; Dürst Stucki and Schlunegger, 2013; Jordan, 2010; Preusser et al., 2010),

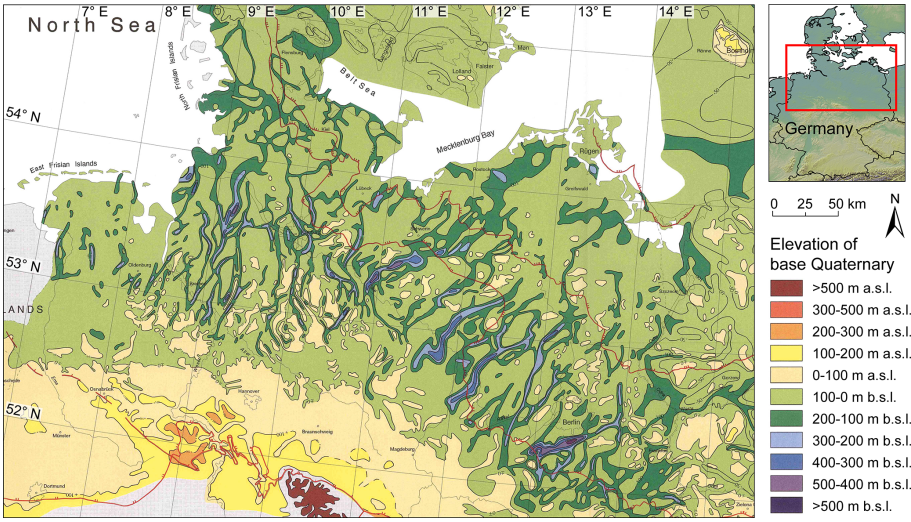

Figure 2. Buried tunnel valleys in northern Germany. Red lines mark, from NE to SW, the ice extents of the Weichselian, Saalian, and Elsterian main glacial stages. Base map (Stackebrandt et al., 2001) courtesy of the Geological Survey of Brandenburg (Landesamt für Bergbau, Geologie und Rohstoffe; LBGR), Germany (https://lbgr.brandenburg.de/lbgr/de/, last access: 5 November 2022), © LBGR 2001.

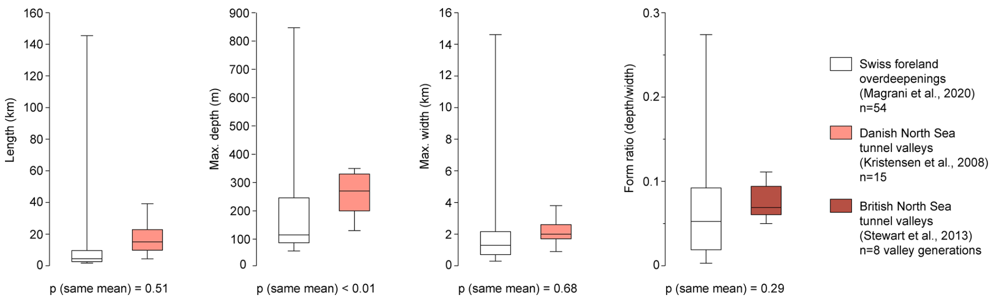

Figure 3. Comparison of lengths, depths, widths, and form ratios of Swiss foreland overdeepenings and North Sea tunnel valleys.

and both morphologies may occur within a single overdeepening (Gegg et al., 2021). Recent highly resolved geophysical studies have further revealed irregular and stepped flanks. The same morphologies are also encountered in tunnel valleys (Fig. 4). In a dataset comprising > 900 Danish tunnel valleys, Andersen et al. (2012) identified ∼ 65 % of mainly U-shaped or flat-bottomed and ∼ 35 % of V-shaped structures. Flank slopes vary between < 5° and > 55° (Cofaigh, 1996; Huuse and Lykke-Andersen, 2000), and van der Vegt et al. (2012) mention examples of overhanging valley flanks. Individual valleys exhibit downstream transitions in a cross-section, for example, from a V to a U shape (Giglio et al., 2022). In both cases, overdeepenings and tunnel valleys, U-shaped morphologies with flat valley bottoms may be linked to lithological boundaries in the substratum (Gegg et al., 2021; Janszen et al., 2012) but occur also where the bedrock is seemingly rather homogeneous (e.g. Fig. 4a, d)

5 Post-erosional history

Concrete information regarding the sedimentary fill of overdeepened structures is rather limited and is often derived from commercial or geotechnical drillings. Under such circumstances, typically no explicit sedimentological descriptions or even further reaching analyses (e.g. pollen analyses, dating) have been carried out. As a result, for the time being, detailed knowledge about the infilling history of overdeepenings is limited to a few case studies. As stated previously, a majority of detailed studies stem from central Europe. This applies especially to the Alpine realm, while fewer well-documented drillings exist for the North Sea region. There, the reconstruction of the sedimentary filling is hence often based on the interpretation of 2D or 3D seismic data that are frequently available from hydrocarbon exploration. We would like to highlight that although we focus on examples from central Europe, a variety of similar case studies on overdeepened structures in other areas exist, e.g. Iceland (Andrews et al., 2000; Gregory, 2012; Quillmann et al., 2010), North America (Atkinson et al., 2013; Smith,

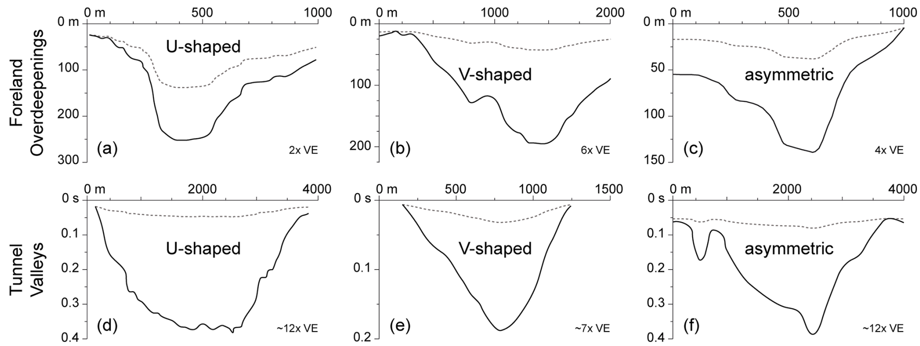

Figure 4. Comparison of overdeepening **(a–c)** and tunnel valley **(d–f)** cross-sections. x axis: horizontal distance, y axis: depth **(a–c)**/two-way travel time **(d–f)**. VE: vertical exaggeration (dotted lines plot the respective cross-sections without vertical exaggeration). **(a)** Basadingen trough, northern Switzerland (after Anselmetti et al., 2022; Brandt, 2020); **(b)** Tannwald basin, southern Germany (after Burschil et al., 2018); **(c)** Gebenstorf-Stilli Trough, northern Switzerland (after Gegg et al., 2021); **(d)** offshore tunnel valley, southern North Sea (after Benvenuti and Moscariello, 2016); **(e)** offshore tunnel valley, central North Sea (after Kirkham et al., 2021); **(f)** offshore tunnel valley, southeastern North Sea (after Lohrberg et al., 2020). Note frequently occurring stepped valley flanks.

2004; Russell et al., 2003), Patagonia (Bertrand et al., 2017; Boyd et al., 2008; Moernaut et al., 2009), and even regions glaciated during the Palaeozoic (Clerc et al., 2013; Vesely et al., 2021).

5.1 Examples from the northern Alpine foreland

A number of well-studied profiles exist in the greater Bern area/Aare Valley, Switzerland (cf. Schlüchter, 1979). The sequence of Thalgut shows a complex deposition and erosion history and is considered one of the most complete Quaternary sequences of the northern Alpine foreland (Schlüchter, 1989). The bottom part of the sequence is composed of lake deposits with pollen spectra typical of the Holsteinian Interglacial (Welten, 1982, 1988), usually attributed to Marine Isotope Stage (MIS) 11 (424–374 ka; cf. Cohen and Gibbard, 2019). Hence, the formation (or re-excavation) of the overdeepening likely occurred during MIS 12 (478–424 ka). Close to the city of Bern, the Rehhag scientific drilling targeted a tributary overdeepening feeding into the central Aare Valley and recovered a diverse, 240 m thick Quaternary succession (Schwenk et al., 2022). It is subdivided into two basin fill sequences of glacial and (glacio-)lacustrine deposits, the upper being attributed to MIS 8–7 (300–191 ka). Just north of Bern, the core of Meikirch starts with till, followed by a 70 m succession of lacustrine sediments comprising a complex vegetation history with three pronounced warm phases (Welten, 1982; Preusser et al., 2005). Based on luminescence dating, this part of the sequence was assigned to MIS 7 (243–191 ka; Preusser et al., 2005). Above the lake deposits, two successions from glaciofluvial to glacial deposits are recorded. In the overdeepened lowermost Aare Valley, at the confluence with Reuss and Limmat, the sediment filling is dominated by lacustrine sand overlying a thin layer of coarse-grained debris at the trough base (Gegg et al., 2021, and references therein). Towards the distal part of the trough, the glaciolacustrine sand interfingers with deltaic gravel. This rather unusual infill pattern is most likely related to the local confluence situation as well as the overdeepening's narrow cross-section combined with large discharge of meltwater (see also Gegg et al., 2020). The Birrfeld basin in the lower Reuss Valley contains a multiphase infill that has been attributed to up to five different ice advances (Graf, 2009; Nitsche et al., 2001).

At a water depth of 180 m, a drilling in Lake Zurich recovered a thick succession of Late Pleistocene sediments starting with coarse-grained debris interpreted as till and subglacial outwash (Lister, 1984a, b). This debris is overlain by $>$ 100 m of diamictic glaciolacustrine muds that repeatedly show traces of glaciotectonic deformation. They transition into laminated, presumably varved, basin fines and are followed by $\sim$ 30 m of postglacial lake deposits. The complex filling of the Richterswil trough, west of Lake Zurich, indicates deposition possibly related to three individual glaciations, but this evidence lacks detailed sedimentological and further analyses (Wyssling, 2002; Preusser et al., 2010; Fig. 5).

Several cores taken from the Wehntal trough (Niederweningen) show that the infill starts with glacial deposits followed by lake sediments, first containing dropstones (Anselmetti et al., 2010; Dehnert et al., 2012). Increased shear strength in the lacustrine deposits implies a second glacial advance, grounding in the lake, followed by a final lake and subsequent bog stage. According to luminescence dating, the carving of the basin occurred during early MIS 6 (around 185 ka), whereas the second ice advance is assigned to ca. 140 ka.

In the Lower Glatt Valley, Buechi et al. (2018) distinguished up to nine separate depositional sequences within the infills of the Kloten Trough and its branch basins, three of which represent episodes of overdeepened basin fill. These are characterised by successions of tills and gravel fining up-

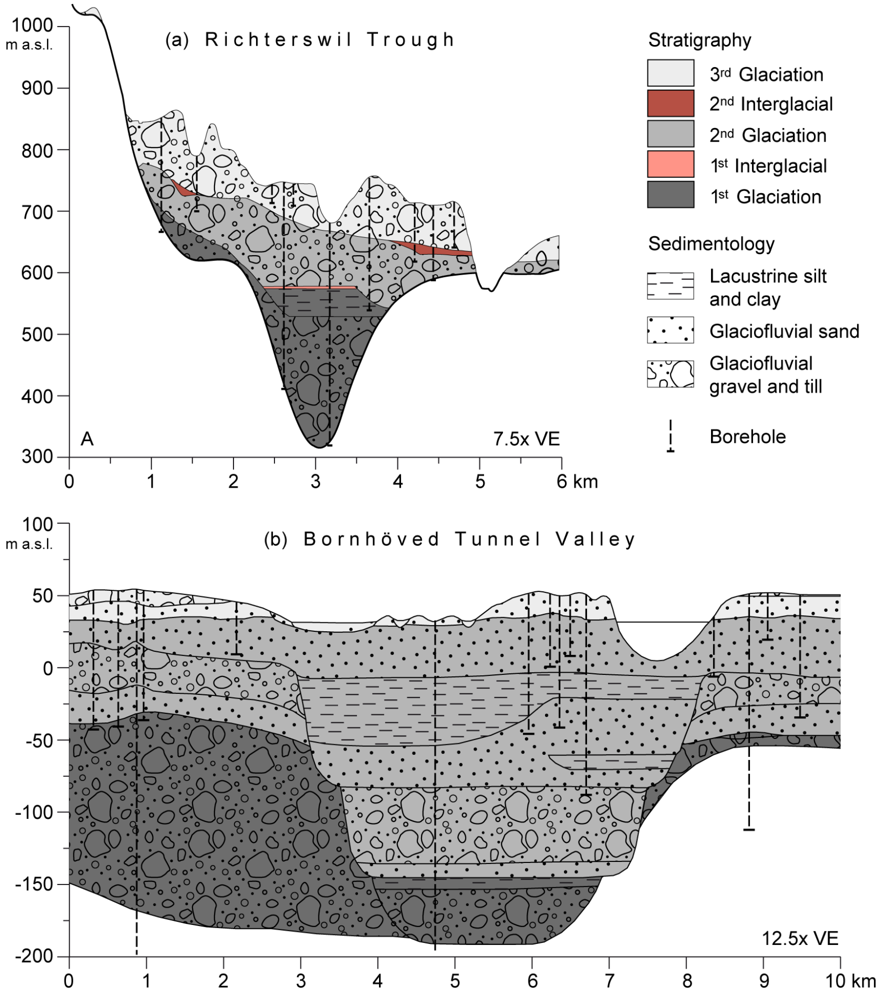

Figure 5. Examples of borehole-constrained sedimentary infills of a central Swiss foreland overdeepening (**a**: Richterswil trough; after Wyssling, 2002, in Preusser et al., 2011) and a northern German tunnel valley (**b**: Bornhöved tunnel valley; after Piotrowski, 1994). VE: vertical exaggeration.

wards into glaciodeltaic to glaciolacustrine deposits, the oldest dating back to at least MIS 8 (300–243 ka). In the middle part of the Glatt Valley, the > 200 m deep trough of Uster is filled by till and partially covered by ice decay and meltwater deposits, followed by laminated lake sediments with a thickness of 100–150 m that are interpreted to represent varved late-glacial deposits (Wyssling and Wyssling, 1978; Preusser et al., 2011). The infill of the trough is covered by the deposits of one or possibly two later glacial advances.

In the Lake Constance area, Ellwanger et al. (2011) distinguish three major generations of overdeepenings, with the drilling in the Tannwald basin being the best documented for the time being (LGRB, 2015; Burschil et al., 2018; Anselmetti et al., 2022). This basin belongs to the oldest generation recognised so far. The sequence starts with sheared allochthonous bedrock slabs on top of the bedrock contact (Upper Marine Molasse), followed by gravel with molasse components and diamictic fines. The subsequent fine-grained lacustrine deposits are correlated with a nearby sequence that contains pollen assemblages assigned to the Holsteinian (Ellwanger et al., 2011; Hahne et al., 2012). The upper part of the Tannwald core comprises evidence for further glacial advances. In Lake Constance itself, as revealed by seismic surveys, up to 150 m of sediment has accumulated, the uppermost 24 m of which was recovered by a recent drilling campaign (Schaller et al., 2022). It consists of 12 m of coarse lacustrine sands of the late-glacial period, overlain by Holocene basin fines.

The basin of Wolfratshausen in Bavaria reveals multiple basal tills and lacustrine fines, evidence for a complex erosion and infill history attributed to three individual glaciations (Jerz, 1979). Fiebig et al. (2014) report a core taken in the Salzach basin containing ∼ 90 m of lacustrine deposits, sand and fines, on top of an Alpine till. Luminescence dating of the lake deposits indicates that the initial formation and filling of the overdeepened trough date to more than 220 ka.

5.2 Examples from northern central Europe

While tunnel valleys have also been described from the British Isles (e.g. Eyles and McCabe, 1989; Coughlan et al., 2020) as well as Poland (e.g. Salamon and Mendecki, 2021), we are here concentrating on the southern North Sea region including the bordering mainland (Denmark, northern Germany, the Netherlands).

For the Bornhöved tunnel valley, Piotrowski (1994) reconstructed a polygenetic evolution based on borehole evidence (Fig. 5). This trough, situated in a peripheral sink between two Permian salt diapirs, was presumably eroded during the Elsterian Glaciation (MIS 12, 478–424 ka) and was filled by fine-grained glaciolacustrine sediments during ice retreat and marine sediments during the Holsteinian Interglacial. These sediments were reworked and redeposited in the shape of a 200 m thick glaciotectonic melange by the first Saalian advance (MIS 10?, 374–337 ka). While the second Saalian advance had little impact, the tunnel valley was reactivated as a subglacial channel during the last, Weichselian, glaciation. In Vendsyssel, northern Denmark, tunnel valleys attributed to the main Weichselian advance (ca. 23–21 ka) are infilled by glaciolacustrine sand and fines (Sandersen et al., 2009). This implies that these tunnel valleys not only have formed rapidly but were also infilled in a few hundred years, or less, before the late-glacial marine inundation (ca. 18 ka).

In the North Sea basin, over 2200 tunnel valleys attributed to up to seven generations were identified using 3D seismic and magnetic data (Stewart and Lonergan, 2011; Ottesen et al., 2020). It appears that each of the seven generations of tunnel valleys, attributed mostly to the Middle Pleistocene, has been excavated and infilled during a separate cycle of ice-sheet advance and retreat (as already suggested by others, e.g. Kristensen et al., 2008), partially reaching into the following interglacial (e.g. Hepp et al., 2012; Janszen et al., 2013; Lang et al., 2015; Steinmetz et al., 2015). Moreau and Huuse (2014) interpret the infill process of tunnel valleys off the shore of the Netherlands to be separate from the incision. Rather than filled by subglacial deposits, Moreau and Huuse (2014) expect the infill sediments were supplied from the southeast by the Rhine–Meuse systems which consistently flowed towards the North Sea basin during glacial periods. This view has been challenged by Benvenuti et al. (2018) who inferred from provenance analysis that the infill of a large Elsterian tunnel valley consists mainly of reworked glacially derived sediment. This is in line with observations by Kirkham et al. (2021) demonstrating that over 40 % of the examined tunnel valleys in the North Sea between Scotland and Norway contain buried glacial landforms such as eskers, crevasse-squeeze ridges, glaciotectonic structures, and kettle holes. Hence, grounded ice must have played an active role not only in the incision but also in the (onsetting) infilling.

5.3 Synthesis

Fillings of overdeepenings in the northern Alpine foreland are clearly dominated by glacial and proglacial deposits. The typical sedimentary succession starts with glacigenic diamicts that are frequently referred to as tills. However, only a few studies (e.g. Buechi et al., 2017) investigated these deposits in sufficient detail to clearly identify them as subglacial ice-contact deposits (cf. Evans, 2007, and references therein), and thus their palaeo-glaciological significance is often not clear. These diamicts are overlain by extensive glaciolacustrine deposits, sands or fines, that at their base frequently contain dropstones. In some basins, several such infill cycles are recorded. Interglacial sediments are in most cases lacking or occur only near the ground surface, known exceptions being the successions of Thalgut, Meikirch, Uster, and Richterswil. This suggests that overdeepened troughs are in most cases infilled and silted up under still periglacial conditions, i.e. in a brief time interval (cf. Van Husen, 1979; Pomper et al., 2017). In contrast, overdeepenings incised during the last glaciation host a number of large and deep contemporaneous, i.e. interglacial, lakes that have not yet been infilled completely (Fig. 6). Whether this is due to exceptionally large basin sizes, comparatively small sediment influxes, or other geological or climatic factors is difficult to assess.

The sediment filling of tunnel valleys and the related depositional processes in northern central Europe are less constrained and remain more poorly understood, although it appears that interglacial sediments are more frequently observed than in the Alpine realm. This could imply a longer "lifetime" of tunnel valleys before being entirely infilled. However, potential tunnel valleys of the last glaciation are completely infilled (e.g. Sandersen et al., 2009) or at least infilled to an extent that does not allow the formation of deep lakes anymore. While some large lakes also exist in the formerly glaciated areas of northern Germany and neighbouring countries, they are significantly shallower than their Alpine counterparts (Fig. 6); do not exhibit the typical elongated plan view trough morphology; and might not be products of overdeepening erosion at all but rather, for example, ice decay structures.

6 Conclusions

Foreland overdeepenings and tunnel valleys are connected to two very different types of ice masses but occur in generally similar palaeo-glaciological and topographic settings. They are formed at the termini of large ice bodies, where ice flow is little constrained, but the abundance of meltwater as well as the ice surface slope, and thus the subglacial pressure gradient towards the margin, are comparatively high. It is this pressurised meltwater that the incision of the spectacular subglacial landforms is mainly attributed to. Both foreland overdeepenings and tunnel valleys share the same morpho-

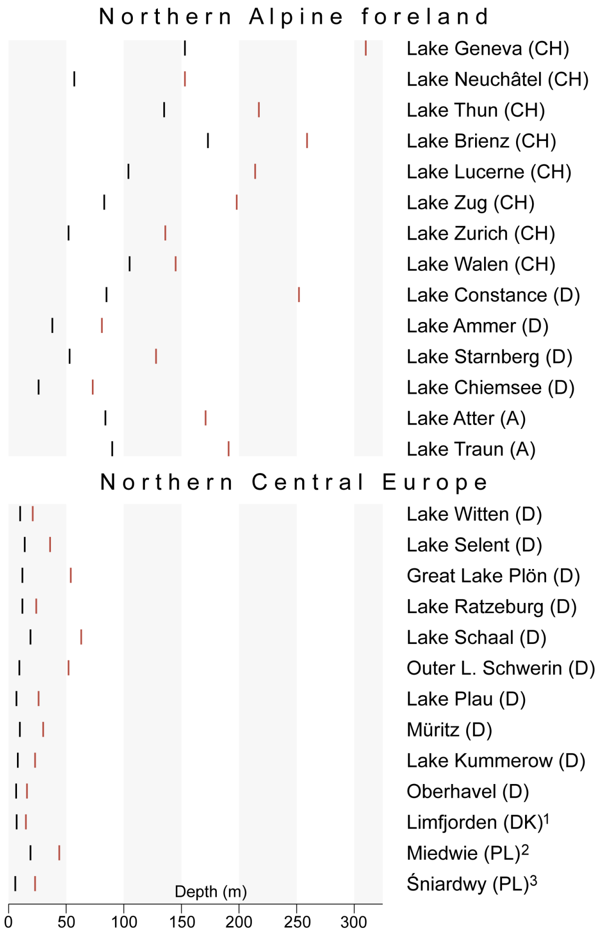

Figure 6. Comparison of mean (black) and maximum (red) depths of large contemporaneous lakes in formerly glaciated areas in the northern Alpine foreland and northern central Europe (Switzerland, CH: BAFU, 2016; Germany, D: Nixdorf et al., 2004; Austria, A: Beiwl and Mühlmann, 2008; Denmark, DK: [1]Riemann and Hoffmann, 1991; Poland, PL: [2]Czerniejewski et al., 2004; [3]Robbins and Jasinski, 1995).

logical characteristics, including anastomosing courses, undulating longitudinal profiles with swells and adverse slopes, and a variety of different cross-sectional shapes. And, perhaps surprisingly, the absolute dimensions of both groups of troughs also appear not to be significantly different from each other.

However, a review of individual troughs and their fillings in central Europe, where these structures have the longest history of recognition and exploration, reveals some notable disparities. In the northern Alpine foreland, multiple well-studied cores exist that allow the characterisation of a typical overdeepening-fill succession in the shape of glacigenic diamicts overlain by glaciolacustrine deposits. In contrast, the infills of tunnel valleys and the related processes have received only little attention and remain rather poorly understood. Further, while the Middle Pleistocene sedimentary record would imply that foreland overdeepenings are more quickly infilled and silted up than tunnel valleys (i.e. typically before interglacial conditions ensue), the characteristics of present-day lakes suggest that the exact opposite has been the case following the last glaciation.

Detailed borehole records are an important tool to better characterise the formation and infilling process of overdeepenings and tunnel valleys (e.g. by process-oriented investigations of the basal "tills"). This is the central objective of the current International Scientific Continental Drilling Program project Drilling Overdeepened Alpine Valleys (DOVE; Anselmetti et al., 2022). Similar drilling projects targeting tunnel valleys are in dire need in order to better understand the overdeepening erosion and glaciation history of northern central Europe. We would like to stress that ongoing and future work of the respective scientific communities may be significantly facilitated and improved by more intensive exchange and discussion, as stimulated for example by the "Subglaziale Rinnen" workshop. The relevance of this exchange is highlighted by the socio-economic aspects of overdeepenings and tunnel valleys, especially in the context of radioactive waste disposal.

Data availability. We utilised datasets by Magrani et al. (2020; https://www.sciencedirect.com/science/article/pii/S0277379120304455; last access: 13 January 2023) and Streuff et al. (2021; https://doi.org/10.1594/PANGAEA.937782).

Author contributions. This paper was conceptualised and the figures were prepared by LG, and the manuscript was written by LG and FP in a joint effort.

Competing interests. The contact author has declared that neither of the authors has any competing interests.

Disclaimer. Publisher's note: Copernicus Publications remains neutral with regard to jurisdictional claims in published maps and institutional affiliations.

Special issue statement. This article is part of the special issue "Subglacial erosional landforms and their relevance for the long-term safety of a radioactive waste repository". It is the result of a virtual workshop held in December 2021.

Acknowledgements. We thank the Swiss National Cooperative for the Disposal of Radioactive Waste (Nagra) for providing the base Quaternary digital elevation model (DEM) of Switzerland and the Geological Survey of Brandenburg, Germany, for permission to reproduce geological map data. We also thank editors Jörg Lang and

Christopher Lüthgens as well as Simon Cook and an anonymous reviewer for their constructive comments.

Financial support. This open-access publication was funded by the University of Freiburg.

Review statement. This paper was edited by Jörg Lang and reviewed by Simon Cook and one anonymous referee.

References

Alley, R. B., Cuffey, K. M., Evenson, E. B., Strasser, J. C., Lawson, D. E., and Larson, G. J.: How glaciers entrain and transport basal sediment: physical constraints, Quaternary Sci. Rev., 16, 1017–1038, https://doi.org/10.1016/S0277-3791(97)00034-6, 1997.

Alley, R. B., Cuffey, K. M., and Zoet, L. K.: Glacial erosion: status and outlook, Ann. Glaciol., 60, 1–13, https://doi.org/10.1017/aog.2019.38, 2019.

Andersen, T. R., Huuse, M., Jørgensen, F., and Christensen, S.: Seismic investigations of buried tunnel valleys on-and offshore Denmark, Geol. Soc. Spec. Publ., 368, 129–144, https://doi.org/10.1144/SP368.14, 2012.

Andrews, J. T., Hardardóttir, J., Helgadóttir, G., Jennings, A. E., Geirsdóttir, Á., Sveinbjörnsdóttir, Á. E., Schoolfield, S., Kristjánsdóttir, G. B., Smith, L. M., Thorse, K., and Syvitski, J. P. M.: The N and W Iceland Shelf: insights into Last Glacial Maximum ice extent and deglaciation based on acoustic stratigraphy and basal radiocarbon AMS dates, Quaternary Sci. Rev., 19, 619–631, https://doi.org/10.1016/S0277-3791(99)00036-0, 2000.

Anselmetti, F. S., Drescher-Schneider, R., Furrer, H., Graf, H. R., Lowick, S. E., Preusser, F., and Riedi, M. A.: A ∼180,000 years sedimentation history of a perialpine overdeepened glacial trough (Wehntal, N-Switzerland), Swiss J. Geosci., 103, 345–361, https://doi.org/10.1007/s00015-010-0041-1, 2010.

Anselmetti, F. S., Bavec, M., Crouzet, C., Fiebig, M., Gabriel, G., Preusser, F., Ravazzi, C., and DOVE scientific team: Drilling Overdeepened Alpine Valleys (ICDP-DOVE): quantifying the age, extent, and environmental impact of Alpine glaciations, Sci. Dril., 31, 51–70, https://doi.org/10.5194/sd-31-51-2022, 2022.

Atkinson, N., Andriashek, L. D., and Slattery, S. R.: Morphological analysis and evolution of buried tunnel valleys in northeast Alberta, Canada, Quaternary Sci. Rev., 65, 53–72, https://doi.org/10.1016/j.quascirev.2012.11.031, 2013.

BAFU: Faktenblätter Zustand bezüglich Wasserqualität, https://www.bafu.admin.ch/bafu/de/home/themen/wasser/fachinformationen/zustand-der-gewaesser/zustand-der-seen/wasserqualitaet-der-seen.html (last access: 10 November 2022), 2016.

Bandou, D., Schlunegger, F., Kissling, E., Marti, U., Schwenk, M., Schläfli, P., Douillet, G., and Mair, D.: Three-dimensional gravity modelling of a Quaternary overdeepening fill in the Bern area of Switzerland discloses two stages of glacial carving, Sci. Rep., 12, 1–14, https://doi.org/10.1038/s41598-022-04830-x, 2022.

Barker, R. D. and Harker, D.: The location of the Stour buried tunnel-valley using geophysical techniques, Q. J. Eng. Geol., 17, 103–115, https://doi.org/10.1144/GSL.QJEG.1984.017.02.03, 1984.

Beiwl, C. and Mühlmann, H.: Atlas der natürlichen Seen Österreichs mit einer Fläche ≥ 50 ha Morphometrie – Typisierung – Trophie Stand 2005, Schriftenreihe des Bundesamtes für Wasserwirtschaft, Band 29, 147 pp., ISBN: 3-901605-29-0, 2008.

Benvenuti, A. and Moscariello, A.: High-resolution seismic geomorphology and stratigraphy of a tunnel valley confined ice-margin fan (Elsterian glaciation, Southern North Sea), Interpretation, 4, T461–T483, https://doi.org/10.1190/INT-2016-0026.1, 2016.

Benvenuti, A., Šegvić, B., and Moscariello, A.: Tunnel valley deposits from the southern North Sea – material provenance and depositional processes, Boreas, 47, 625–642, https://doi.org/10.1111/bor.12292, 2018.

Bertrand, S., Lange, C. B., Pantoja, S., Hughen, K., Van Tornhout, E., and Wellner, J. S.: Postglacial fluctuations of Cordillera Darwin glaciers (southernmost Patagonia) reconstructed from Almirantazgo fjord sediments. Quaternary Sci. Rev., 177, 265–275, https://doi.org/10.1016/j.quascirev.2017.10.029, 2017.

Bini, A., Buoncristiani, J. F., Couterrand, S., Ellwanger, D., Felber, M., Florineth, D., Graf, H. R., Keller, O., Kelly, M., and Schlüchter, C.: Die Schweiz während des letzteiszeitlichen Maximums (LGM) 1:500.000, Bundesamt für Landestopographie swisstopo, Wabern, Switzerland https://opendata.swiss/de/dataset/die-schweiz-wahrend-des-letzteiszeitlichen-maximums-lgm-1-500000 (last access: 10 January 2023), 2009.

Bosch, J. A., Bakker, M. A., Gunnink, J. L., and Paap, B. F.: Airborne electromagnetic measurements as basis for a 3D geological model of an Elsterian incision, Z. Dtsch. Ges. Geowiss., 160, 249–258, https://doi.org/10.1127/1860-1804/2009/0160-0258, 2009.

Boulton, G. S., Hagdorn, M., Maillot, P. B., and Zatsepin, S.: Drainage beneath ice sheets: groundwater–channel coupling, and the origin of esker systems from former ice sheets, Quaternary Sci. Rev., 28, 621–638, https://doi.org/10.1016/j.quascirev.2008.05.009, 2009.

Boyd, B. L., Anderson, J. B., Wellner, J. S., and Fernandez, R. A.: The sedimentary record of glacial retreat, Marinelli Fjord, Patagonia: Regional correlations and climate ties, Mar. Geol., 255, 165–178, https://doi.org/10.1016/j.margeo.2008.09.001, 2008.

Boyd, R., Scott, D. B., and Douma, M.: Glacial tunnel valleys and Quaternary history of the outer Scotian shelf, Nature, 333, 61–64, https://doi.org/10.1038/333061a0, 1988.

Bradwell, T., Stoker, M. S., Golledge, N. R., Wilson, C. K., Merritt, J. W., Long, D., Everest, J. D., Hestvik, O. B., Stevenson, A. G., and Hubbard, A. L.: The northern sector of the last British Ice Sheet: maximum extent and demise, Earth-Sci. Rev., 88, 207–226, https://doi.org/10.1016/J.EARSCIREV.2008.01.008, 2008.

Brandt, A. C.: Erkundung des alpinen, glazial-übertieften Basadingen-Beckens mithilfe von P-Wellen-Seismik, Bachelor thesis, Leibniz University Hannover, 2020.

Buechi, M. W., Frank, S. M., Graf, H. R., Menzies, J., and Anselmetti, F. S.: Subglacial emplacement of tills and meltwater deposits at the base of overdeepened bedrock troughs, Sedimentology, 64, 658–685, https://doi.org/10.1111/sed.12319, 2017.

Buechi, M. W., Graf, H. R., Haldimann, P., Lowick, S. E., and Anselmetti, F. S.: Multiple Quaternary erosion and infill cycles in overdeepened basins of the northern Alpine foreland, Swiss J. Geosci., 111, 1–34, https://doi.org/10.1007/s00015-017-0289-9, 2018.

Burschil, T., Buness, H., Tanner, D. C., Wielandt-Schuster, U., Ellwanger, D., and Gabriel, G.: High-resolution reflection seismics reveal the structure and the evolution of the Quaternary glacial Tannwald Basin, Near Surf. Geophys., 16, 593–610, https://doi.org/10.1002/nsg.12011, 2018.

Burschil, T., Buness, H., Gabriel, G., Tanner, D. C., and Reitner, J. M.: Unravelling the shape and stratigraphy of a glacially-overdeepened valley with reflection seismic: the Lienz Basin (Austria), Swiss J. Geosci., 112, 341–355, https://doi.org/10.1007/s00015-019-00339-0, 2019.

Cameron, T. D. J., Stoker, M. S., and Long, D.: The history of Quaternary sedimentation in the UK sector of the North Sea Basin, J. Geol. Soc., 144, 43–58, https://doi.org/10.1144/gsjgs.144.1.0043, 1987.

Carrivick, J. L., Davies, B. J., James, W. H. M., Quincey, D. J., and Glasser, N. F.: Distributed ice thickness and glacier volume in southern South America, Global Planet. Change, 146, 122–132, https://doi.org/10.1016/j.gloplacha.2016.09.010, 2016.

Clark, P. U. and Walder, J. S.: Subglacial drainage, eskers, and deforming beds beneath the Laurentide and Eurasian ice sheets, Geol. Soc. Am. Bull., 106, 304–314, https://doi.org/10.1130/0016-7606(1994)106<0304:SDEADB>2.3.CO;2, 1994.

Clerc, S., Buoncristiani, J. F., Guiraud, M., Vennin, E., Desaubliaux, G., and Portier, E.: Subglacial to proglacial depositional environments in an Ordovician glacial tunnel valley, Alnif, Morocco, Palaeogeogr. Palaeocl., 370, 127–144, https://doi.org/10.1016/j.palaeo.2012.12.002, 2013.

Cofaigh, C. Ó.: Tunnel valley genesis, Prog. Phys. Geogr., 20, 1–19, https://doi.org/10.1177/030913339602000101, 1996.

Cohen, K. M. and Gibbard, P. L.: Global chronostratigraphical correlation table for the last 2.7 million years, version 2019 QI-500, Quatern. Int., 500, 20–31, https://doi.org/10.1016/j.quaint.2019.03.009, 2019.

Cook, S. J. and Swift, D. A.: Subglacial basins: Their origin and importance in glacial systems and landscapes, Earth-Sci. Rev., 115, 332–372, https://doi.org/10.1016/j.earscirev.2012.09.009, 2012.

Coughlan, M., Tóth, Z., Van Landeghem, K. J. J., Mccarron, S., Wheeler, A. J.: Formational history of the Wicklow Trough: a marine-transgressed tunnel valley revealing ice flow velocity and retreat rates for the largest ice stream draining the late-Devensian British–Irish Ice Sheet, J. Quateranry Sci., 35, 907–919, https://doi.org/10.1002/jqs.3234, 2020.

Cummings, D. I., Russell, H. A. J., and Sharpe, D. R.: Buried-valley aquifers in the Canadian Prairies: geology, hydrogeology, and origin, Can. J. Earth Sci., 49, 987–1004, https://doi.org/10.1139/e2012-041, 2012.

Czerniejewski, P., Filipiak, J., Poleszczuk, G., and Wawrzyniak, W.: Selected biological characteristics of the catch-available part of population of vendace, *Coregonus albula* (L.) from Lake Miedwie, Poland, Acta Ichthyologica et Piscatoria, 34, 219–233, https://doi.org/10.3750/AIP2004.34.2.09, 2004.

Dehnert, A., Lowick, S. E., Preusser, F., Anselmetti, F. S., Drescher-Schneider, R., Graf, H. R., Heller, F., Horstmeyer, H., Kemna, H. A., and Nowaczyk, N. R.: Evolution of an overdeepened trough in the northern Alpine Foreland at Niederweningen, Switzerland, Quaternary Sci. Rev., 34, 127–145, https://doi.org/10.1016/j.quascirev.2011.12.015, 2012.

Destombes, J.-P., Shephard-Thorn, E. R., Redding, J. H., and Morzadec-Kerfourn, M. T.: A buried valley system in the Strait of Dover, Philos. T. Roy. Soc. A, 279, 243–253, https://doi.org/10.1098/rsta.1975.0056, 1975.

Dürst Stucki, M. and Schlunegger, F.: Identification of erosional mechanisms during past glaciations based on a bedrock surface model of the central European Alps, Earth Planet. Sc. Lett., 384, 57–70, https://doi.org/10.1016/j.epsl.2013.10.009, 2013.

Dürst Stucki, M., Reber, R., and Schlunegger, F.: Subglacial tunnel valleys in the Alpine foreland: an example from Bern, Switzerland, Swiss J. Geosci., 103, 363–374, https://doi.org/10.1007/s00015-010-0042-0, 2010.

Egholm, D. L., Pedersen, V. K., Knudsen, M. F., and Larsen, N. K.: Coupling the flow of ice, water, and sediment in a glacial landscape evolution model, Geomorphology, 141, 47–66, https://doi.org/10.1016/j.geomorph.2011.12.019, 2012.

Ellwanger, D., Wielandt-Schuster, U., Franz, M., and Simon, T.: The Quaternary of the southwest German Alpine Foreland (Bodensee-Oberschwaben, Baden-Württemberg, Southwest Germany), E&G Quaternary Sci. J., 60, 22, https://doi.org/10.3285/eg.60.2-3.07, 2011.

Evans, D. J. A.: Glacial landforms, sediments – Tills, Encyclopedia of Quaternary Science, 959–975, https://doi.org/10.1016/B0-44-452747-8/00092-2, 2007.

Eyles, N. and McCabe, A. M.: Glaciomarine facies within subglacial tunnel valleys: the sedimentary record of glacioisostatic downwarping in the Irish Sea Basin, Sedimentology, 36, 431–448, https://doi.org/10.1111/j.1365-3091.1989.tb00618.x, 1989.

Fiebig, M., Herbst, P., Drescher-Schneider, R., Lüthgens, C., Lomax, J., and Doppler, G.: Some remarks about a new Last Glacial record from the western Salzach foreland glacier basin (Southern Germany), Quatern. Int., 328, 107–119, https://doi.org/10.1016/j.quaint.2013.12.048, 2014.

Finckh, P., Kelts, K., and Lambert, A.: Seismic stratigraphy and bedrock forms in perialpine lakes, Geol. Soc. Am. Bull., 95, 1118–1128, https://doi.org/10.1130/0016-7606(1984)95<1118:SSABFI>2.0.CO;2, 1984.

Gao, C.: Buried bedrock valleys and glacial and subglacial meltwater erosion in southern Ontario, Canada, Can. J. Earth Sci., 48, 801–818, https://doi.org/10.1139/e10-104, 2011.

Gegg, L., Buechi, M. W., Ebert, A., Deplazes, G., Madritsch, H., and Anselmetti, F. S.: Brecciation of glacially overridden palaeokarst (Lower Aare Valley, northern Switzerland): result of subglacial water-pressure peaks?, Boreas, 49, 813–827, https://doi.org/10.1111/bor.12457, 2020.

Gegg, L., Deplazes, G., Keller, L., Madritsch, H., Spillmann, T., Anselmetti, F. S., and Buechi, M. W.: 3D morphology of a glacially overdeepened trough controlled by underlying bedrock geology, Geomorphology, 394, 107950, https://doi.org/10.1016/j.geomorph.2021.107950, 2021.

Giglio, C., Benetti, S., Sacchetti, F., Lockhart, E., Hughes Clarke, J., Plets, R., van Landeghem, K., Ó Cofaigh, C., Scourse, J., and Dunlop, P.: A Late Pleistocene channelized subglacial meltwater system on the Atlantic continental shelf south of Ireland, Boreas, 51, 118–135, https://doi.org/10.1111/bor.12536, 2022.

Götze, H. J. G., Giszas, V., Hese, F., Kirsch, R. K., and Schmidt, S.: The ice age paleo-channel Ellerbeker Rinne an integrated

3D gravity study, Z. Dtsch. Ges. Geowiss., 160, 279–293, https://doi.org/10.1127/1860-1804/2009/0160-0279, 2009.

Graf, H. R.: Stratigraphie von Mittel- und Spätpleistozän in der Nordschweiz, Beiträge zur Geologischen Karte der Schweiz, NF-168, 198 pp., 2009.

Gregory, A. R.: The formation and development of proglacial overdeepenings at a contemporary Piedmont lobe glacier: Skeiðarárjökull, South East Iceland, PhD thesis, Newcastle University, http://theses.ncl.ac.uk/jspui/handle/10443/1704 (last access: 4 December 2022), 2012.

Haeberli, W., Linsbauer, A., Cochachin, A., Salazar, C., and Fischer, U.: On the morphological characteristics of overdeepenings in high-mountain glacier beds, Earth Surf. Proc. Land., 41, 1980–1990, https://doi.org/10.1002/esp.3966, 2016.

Hahne, J., Ellwanger, D., Franz, M., Stritzke, R., and Wielandt-Schuster, U.: Pollenanalytische Untersuchungsergebnisse aus dem Baden-Württembergischen Rheinsystem Oberrheingraben, Hochrhein, Oberschwaben – eine Zusammenfassung des aktuellen Kenntnisstandes, LGRB Informationen, 26, 119–154, 2012.

Heim, A.: Handbuch der Gletscherkunde, J. Engelhorn, 1885.

Hepp, D. A., Hebbeln, D., Kreiter, S., Keil, H., Bathmann, C., Ehlers, J., and Tobias Mörz, T.: An east–west-trending Quaternary tunnel valley in the south-eastern North Sea and its seismic–sedimentological interpretation, J. Quaternary Sci., 27, 844–853, https://doi.org/10.1002/jqs.2599, 2012.

Herman, F., Beaud, F., Champagnac, J.-D., Lemieux, J.-M., and Sternai, P.: Glacial hydrology and erosion patterns: a mechanism for carving glacial valleys, Earth Planet. Sc. Lett., 310, 498–508, https://doi.org/10.1016/j.epsl.2011.08.022, 2011.

Herman, F., Beyssac, O., Brughelli, M., Lane, S. N., Leprince, S., Adatte, T., Lin, J. Y. Y., Avouac, J.-P., and Cox, S. C.: Erosion by an Alpine glacier, Science, 350, 193–195, https://doi.org/10.1126/science.aab2386, 2015.

Hsü, K. J. and Kelts, K. R. (Eds.): Quaternary geology of Lake Zurich, Contributions to Sedimentary Geology, 13, 210 pp., ISBN: 978-3-510-57013-3, 1984.

Huuse, M. and Lykke-Andersen, H.: Overdeepened Quaternary valleys in the eastern Danish North Sea: morphology and origin, Quaternary Sci. Rev., 19, 1233–1253, https://doi.org/10.1016/S0277-3791(99)00103-1, 2000.

James, W. H. M., Carrivick, J. L., Quincey, D. J., and Glasser, N. F.: A geomorphology based reconstruction of ice volume distribution at the Last Glacial Maximum across the Southern Alps of New Zealand, Quaternary Sci. Rev., 219, 20–35, https://doi.org/10.1016/j.quascirev.2019.06.035, 2019.

Janszen, A., Spaak, M., and Moscariello, A.: Effects of the substratum on the formation of glacial tunnel valleys: an example from the Middle Pleistocene of the southern North Sea Basin, Boreas, 41, 629–643, https://doi.org/10.1111/j.1502-3885.2012.00260.x, 2012.

Janszen, A., Moreau, J., Moscariello, A., Ehlers, J., and Kröger, J.: Time-transgressive tunnel-valley infill revealed by a threedimensional sedimentary model, Hamburg, north-west Germany, Sedimentology, 60, 693–719, https://doi.org/10.1111/j.1365-3091.2012.01357.x, 2013.

Jennings, C. E.: Terrestrial ice streams – a view from the lobe, Geomorphology, 75, 100–124, https://doi.org/10.1016/j.geomorph.2005.05.016, 2006.

Jentzsch, A.: Über die Bildung der Preussischen Seen, Z. Dtsch. Ges. Geowiss., 36, 699–702, 1884.

Jerz, H.: Das Wolfratshausener Becken: seine glaziale Anlage und Übertiefung, E&G Quaternary Sci. J., 29, 63–70, https://doi.org/10.23689/fidgeo-1646, 1979.

Jordan, P.: Analysis of overdeepened valleys using the digital elevation model of the bedrock surface of Northern Switzerland, Swiss J. Geosci., 103, 375–384, https://doi.org/10.1007/s00015-010-0043-z, 2010.

Jørgensen, F. and Sandersen, P. B. E.: Buried and open tunnel valleys in Denmark–erosion beneath multiple ice sheets, Quaternary Sci. Rev., 25, 1339–1363, https://doi.org/10.1016/j.quascirev.2005.11.006, 2006.

Kearsey, T. I., Lee, J. R., Finlayson, A., Garcia-Bajo, M., and Irving, A. A. M.: Examining the geometry, age and genesis of buried Quaternary valley systems in the Midland Valley of Scotland, UK, Boreas, 48, 658–677, https://doi.org/10.1111/bor.12364, 2019.

Kehew, A. E., Piotrowski, J. A., and Jørgensen, F.: Tunnel valleys: Concepts and controversies – A review, Earth-Sci. Rev., 113, 33–58, https://doi.org/10.1016/j.earscirev.2012.02.002, 2012.

Kirkham, J. D., Hogan, K. A., Larter, R. D., Self, E., Games, K., Huuse, M., Stewart, M. A., Ottesen, D., Arnold, N. S., and Dowdeswell, J. A.: Tunnel valley infill and genesis revealed by high-resolution 3-D seismic data, Geology, 49, 1516–1520, https://doi.org/10.1130/G49048.1, 2021.

Kristensen, T. B., Piotrowski, J. A., Huuse, M., Clausen, O. R., and Hamberg, L.: Time-transgressive tunnel valley formation indicated by infill sediment structure, North Sea – the role of glaciohydraulic supercooling, Earth Surf. Proc. Land., 33, 546–559, https://doi.org/10.1002/esp.1668, 2008.

Kühni, A. and Pfiffner, O.-A.: The relief of the Swiss Alps and adjacent areas and its relation to lithology and structure: topographic analysis from a 250-m DEM, Geomorphology, 41, 285–307, https://doi.org/10.1016/S0169-555X(01)00060-5, 2001.

Kunst, F. and Deze, J. F.: The case history of a high-resolution seismic survey in the central North Sea, in: Offshore Tech. Conf., Houston, Texas, 6–9 May 1985, https://doi.org/10.4043/4968-MS, 1985.

Kuster, H. and Meyer, K.-D.: Glaziäre Rinnen im mittleren und nördlichen Niedersachsen, E&G Quaternary Sci. J., 29, 135–156, https://doi.org/10.3285/eg.29.1.12, 1979.

Lang, J., Böhner, U., Polom, U., Serangeli, J., and Winsemann, J.: The Middle Pleistocene tunnel valley at Schöningen as a Paleolithic archive, J. Hum. Evol., 89, 18–26, https://doi.org/10.1016/j.jhevol.2015.02.004, 2015.

Lelandais, T., Ravier, É., Pochat, S., Bourgeois, O., Clark, C., Mourgues, R., and Strzerzynski, P.: Modelled subglacial floods and tunnel valleys control the life cycle of transitory ice streams, The Cryosphere, 12, 2759–2772, https://doi.org/10.5194/tc-12-2759-2018, 2018.

LGRB: Lithostratigraphische Entwicklung des Baden-Württembergischen Rheingletschergebiets: Übertiefste Becken- und Moränen-Landschaft, LGRB-Fachbericht 2015/4, 86 pp., https://produkte.lgrb-bw.de/schriftensuche/sonstige-produkte/?aid=9 (last access: 10 January 2023), 2015.

Lister, G. S.: Lithostratigraphy of Zübo sediments, Contributions to sedimentology, 13, 31–58, 1984a.

Lister, G. S.: Deglaciation of the Lake Zurich area: a model based on the sedimentological record, Contributions to sedimentology, 13, 177–185, 1984b.

Livingstone, S. J. and Clark, C. D.: Morphological properties of tunnel valleys of the southern sector of the Laurentide Ice Sheet and implications for their formation, Earth Surf. Dynam., 4, 567–589, https://doi.org/10.5194/esurf-4-567-2016, 2016.

Lohrberg, A., Schwarzer, K., Unverricht, D., Omlin, A., and Krastel, S.: Architecture of tunnel valleys in the southeastern North Sea: new insights from high-resolution seismic imaging, J. Quaternary Sci., 35, 892–906, https://doi.org/10.1002/jqs.3244, 2020.

Lutz, R., Kalka, S., Gaedicke, C., Reinhardt, L., and Winsemann, J.: Pleistocene tunnel valleys in the German North Sea: spatial distribution and morphology, Z. Dtsch. Ges. Geowiss., 160, 225–235, https://doi.org/10.1127/1860-1804/2009/0160-0225, 2009.

Madsen, V.: Terrainformerne paa Skovbjerg Bakkeø, Danmarks Geologiske Undersøgelse, IV. Række, 1, 1–24, https://doi.org/10.34194/raekke4.v1.6971, 1921.

Magnússon, E., Pálsson, F., Björnsson, H., and Guðmundsson, S.: Removing the ice cap of Öræfajökull central volcano, SE-Iceland: mapping and interpretation of bedrock topography, ice volumes, subglacial troughs and implications for hazards assessments, Jökull, 62, 131–150, 2012.

Magrani, F., Valla, P. G., Gribenski, N., and Serra, E.: Glacial overdeepenings in the Swiss Alps and foreland: Spatial distribution and morphometrics, Quaternary Sci. Rev., 243, 106483, https://doi.org/10.1016/j.quascirev.2020.106483, 2020 (data available at: https://www.sciencedirect.com/science/article/pii/S0277379120304455, last access: 13 January 2023).

Margold, M., Stokes, C. R., and Clark, C. D.: Ice streams in the Laurentide Ice Sheet: Identification, characteristics and comparison to modern ice sheets, Earth-Sci. Rev., 143, 117–146, https://doi.org/10.1016/j.earscirev.2015.01.011, 2015.

Moernaut, J., De Batist, M., Heirman, K., Van Daele, M., Pino, M., Brümmer, R., and Urrutia, R.: Fluidization of buried mass-wasting deposits in lake sediments and its relevance for paleoseismology: results from a reflection seismic study of lakes Villarrica and Calafquén (South-Central Chile), Sediment. Geol., 213, 121–135, https://doi.org/10.1016/j.sedgeo.2008.12.002, 2009.

Moreau, J. and Huuse, M.: Infill of tunnel valleys associated with landward-flowing ice sheets: The missing Middle Pleistocene record of the NW European rivers?, Geochem. Geophy. Geosy., 15, 1–9, https://doi.org/10.1002/2013GC005007, 2014.

Nitsche, F. O., Monin, G., Marillier, F., Graf, H., and Ansorge, J.: Reflection seismic study of Cenozoic sediments in an overdeepened valley of northern Switzerland: the Birrfeld area, Eclogae Geol. Helv., 94, 363–371, https://doi.org/10.5169/seals-168901, 2001.

Nixdorf, B., Hemm, M., Hoffmann, A., and Richter, P.: Dokumentation von Zustand und Entwicklung der wichtigsten Seen Deutschlands, Umweltbundesamt Forschungsbericht 299 24 274, 274 pp., 2004.

Ottesen, D., Stewart, M., Brönner, M., and Batchelor, C. L.: Tunnel valleys of the central and northern North Sea (56° N to 62° N): Distribution and characteristics, Mar. Geol., 425, 106199, https://doi.org/10.1016/j.margeo.2020.106199, 2020.

Patton, H., Swift, D. A., Clark, C. D., Livingstone, S. J., and Cook, S. J.: Distribution and characteristics of overdeepenings beneath the Greenland and Antarctic ice sheets: Implications for overdeepening origin and evolution, Quaternary Sci. Rev., 148, 128–145, https://doi.org/10.1016/j.quascirev.2016.07.012, 2016.

Penck, A. and Brückner, E.: Die Alpen im Eiszeitalter, Tauchnitz, Leipzig, 1909.

Pietsch, J. and Jordan, P.: Digitales Höhenmodell Basis Quartär der Nordschweiz – Version 2014 und ausgewählte Auswertungen, Nagra Arbeitsbericht NAB 14-02, 69 pp., https://nagra.ch/downloads/arbeitsbericht-nab-14-02/ (last access: 10 January 2023), 2014.

Piotrowski, J. A.: Tunnel-valley formation in northwest Germany—geology, mechanisms of formation and subglacial bed conditions for the Bornhöved tunnel valley, Sediment. Geol., 89, 107–141, https://doi.org/10.1016/0037-0738(94)90086-8, 1994.

Pomper, J., Salcher, B. C., Eichkitz, C., Prasicek, G., Lang, A., Lindner, M., and Götz, J.: The glacially overdeepened trough of the Salzach Valley, Austria: Bedrock geometry and sedimentary fill of a major Alpine subglacial basin, Geomorphology, 295, 147–158, https://doi.org/10.1016/j.geomorph.2017.07.009, 2017.

Praeg, D.: Buried fluvial channels: 3D-seismic geomorphology, in: Glaciated Continental Margins, Springer, 162–163, https://doi.org/10.1007/978-94-011-5820-6_65, 1997.

Preusser, F., Drescher-Schneider, R., Fiebig, M., and Schlüchter, C.: Re-interpretation of the Meikirch pollen record, Swiss Alpine Foreland, and implications for Middle Pleistocene chrono-stratigraphy, J. Quaternary Sci., 20, 607–620, https://doi.org/10.1002/jqs.930, 2005.

Preusser, F., Reitner, J. M., and Schlüchter, C.: Distribution, geometry, age and origin of overdeepened valleys and basins in the Alps and their foreland, Swiss J. Geosci., 103, 407–426, https://doi.org/10.1007/s00015-010-0044-y, 2010.

Preusser, F., Graf, H. R., Keller, O., Krayss, E., and Schlüchter, C.: Quaternary glaciation history of northern Switzerland, E&G Quaternary Sci. J., 60, 21, https://doi.org/10.3285/eg.60.2-3.06, 2011.

Quillmann, U., Jennings, A., and Andrews, J.: Reconstructing Holocene palaeoclimate and palaeoceanography in Ìsafjarðardjúp, northwest Iceland, from two fjord records overprinted by relative sea-level and local hydrographic changes, J. Quaternary Sci., 25, 1144–1159, https://doi.org/10.1002/jqs.1395, 2010.

Reitner, J. M., Gruber, W., Römer, A., and Morawetz, R.: Alpine overdeepenings and paleo-ice flow changes: an integrated geophysical-sedimentological case study from Tyrol (Austria), Swiss J. Geosci., 103, 385–405, https://doi.org/10.1007/s00015-010-0046-9, 2010.

Riemann, B. and Hoffmann, E.: Ecological consequences of dredging and bottom trawling in the Limfjord, Denmark, Mar. Ecol. Prog. Ser., 69, 171–178, https://doi.org/10.3354/meps069171, 1991.

Rignot, E., Mouginot, J., and Scheuchl, B.: Ice flow of the Antarctic ice sheet, Science, 333, 1427–1430, https://doi.org/10.1126/science.1208336, 2011.

Robbins, J. A. and Jasinski, A. W.: Chernobyl fallout radionuclides in lake Sniardwy, Poland, J. Environ. Radioactiv., 26, 157–184, https://doi.org/10.1016/0265-931X(94)00005-H, 1995.

Russell, H. A. J., Arnott, R. W. C., and Sharpe, D. R.: Evidence for rapid sedimentation in a tunnel channel, Oak Ridges Moraine, southern Ontario, Canada, Sediment. Geol., 160, 33–55, https://doi.org/10.1016/S0037-0738(02)00335-4, 2003.

Salamon, T. and Mendecki, M.: A rare signature of subglacial outburst floods developed along structural ice weaknesses in the southern sector of the Scandinavian Ice Sheet during the Drenthian Glaciation, S Poland, Geomorphology, 378, 107593, https://doi.org/10.1016/j.geomorph.2021.107593, 2021.

Sandersen, P. B. E., Jørgensen, F., Larsen, N. K., Westergaard, J. H., and Auken, E.: Rapid tunnel valley formation beneath the receding Late Weichselian ice sheet in Vendsyssel, Denmark, Boreas, 38, 834–851, https://doi.org/10.1111/j.1502-3885.2009.00105.x, 2009.

Schaller, S., Böttcher, M. E., Buechi, M. W., Epp, L. S., Fabbri, S. C., Gribenski, N., Harms, U., Krastel, S., Liebezeit, A., Lindhorst, K., Marxen, H., Raschke, U., Schleheck, D., Schmiedinger, I., Schwalb, A., Vogel, H., Wessels, M., and Anselmetti, F. S.: Postglacial evolution of Lake Constance: sedimentological and geochemical evidence from a deep-basin sediment core, Swiss J. Geosci., 115, 7, https://doi.org/10.1186/s00015-022-00412-1, 2022.

Schlüchter, C.: Übertiefte Talabschnitte im Berner Mittelland zwischen Alpen und Jura (Schweiz), E&G Quaternary Sci. J., 29, 101—113, https://doi.org/10.23689/fidgeo-921, 1979.

Schlüchter, C.: The most complete Quaternary record of the Swiss Alpine Foreland, Palaeogeogr. Palaeocl., 72, 141–146, https://doi.org/10.1016/0031-0182(89)90138-7, 1989.

Schoof, C. and Hewitt, I.: Ice-sheet dynamics, Annu. Rev. Fluid Mech., 45, 217–239, https://doi.org/10.1146/annurev-fluid-011212-140632, 2013.

Schwenk, M. A., Schläfli, P., Bandou, D., Gribenski, N., Douillet, G. A., and Schlunegger, F.: From glacial erosion to basin overfill: a 240 m-thick overdeepening–fill sequence in Bern, Switzerland, Sci. Dril., 30, 17–42, https://doi.org/10.5194/sd-30-17-2022, 2022.

Smith, L. N.: Late Pleistocene stratigraphy and implications for deglaciation and subglacial processes of the Flathead Lobe of the Cordilleran Ice Sheet, Flathead Valley, Montana, USA, Sediment. Geol., 165, 295–332, https://doi.org/10.1016/j.sedgeo.2003.11.013, 2004.

Stackebrandt, W., Ludwig, A. O., and Ostaficzuk, S.: Base of Quaternary deposits of the Baltic Sea depression and adjacent areas (map 2), Brandenburgische Geowiss. Beitr., 8, 13–19, 2001.

Steinmetz, D., Winsemann, J., Brandes, C., Siemon, B., Ullmann, A., Wiederhold, H., and Meyer, U.: Towards an improved geological interpretation of airborne electromagnetic data: a case study from the Cuxhaven tunnel valley and its Neogene host sediments (northwest Germany), Neth. J. Geosci., 94, 201–227, https://doi.org/10.1017/njg.2014.39, 2015.

Stewart, M. A. and Lonergan, L.: Seven glacial cycles in the middle-late Pleistocene of northwest Europe: Geomorphic evidence from buried tunnel valleys, Geology, 39, 283–286, https://doi.org/10.1130/G31631.1, 2011.

Stewart, M. A., Lonergan, L., and Hampson, G.: 3D seismic analysis of buried tunnel valleys in the central North Sea: morphology, cross-cutting generations and glacial history, Quaternary Sci. Rev., 72, 1–17, https://doi.org/10.1016/j.quascirev.2013.03.016, 2013.

Streuff, K. T., Ó Cofaigh, C., and Wintersteller, P.: A GIS Database of Submarine Glacial Landforms and Sediments on Arctic Continental Shelves, PANGAEA [data set], https://doi.org/10.1594/PANGAEA.937782, 2021.

Streuff, K. T., Ó Cofaigh, C., and Wintersteller, P.: GlaciDat – a GIS database of submarine glacial landforms and sediments in the Arctic, Boreas, 51, 517–531, https://doi.org/10.1111/bor.12577, 2022.

Tezkan, B. M., Helwig, S. L., and Bergers, R.: Time domain electromagnetic (TEM) measurements on a buried subglacial valley in Northern Germany by using a large transmitter size and a high current, Z. Dtsch. Ges. Geowiss., 160, 271–278, https://doi.org/10.1127/1860-1804/2009/0160-0271, 2009.

Ugelvig, S. V., Egholm, D. L., and Iverson, N. R.: Glacial landscape evolution by subglacial quarrying: A multiscale computational approach, J. Geophys. Res.-Earth, 121, 2042–2068, https://doi.org/10.1002/2016JF003960, 2016.

Ussing, N. V.: Danmarks Geologi i almenfatteligt Omrids. Anden udgave, Danmarks Geologiske Undersøgelse III. Række, 2, 358 pp., https://doi.org/10.34194/raekke3.v2.6907, 1904.

van der Vegt, P., Janszen, A., and Moscariello, A.: Tunnel valleys: current knowledge and future perspectives, Geol. Soc. Spec. Publ., 368, 75–97, https://doi.org/10.1144/SP368.13, 2012.

Van Husen, D.: Verbreitung, Ursachen und Füllung glazial übertiefter Talabschnitte an Beispielen aus den Ostalpen, E&G Quaternary Sci. J., 29, 9–22, https://doi.org/10.3285/eg.29.1.02, 1979.

Vesely, F. F., Assine, M. L., França, A. B., Paim, P. S., and Rostirolla, S. P.: Tunnel-valley fills in the Paraná Basin and their implications for the extent of late Paleozoic glaciation in SW Gondwana, J. S. Am. Earth Sci., 106, 102969, https://doi.org/10.1016/j.jsames.2020.102969, 2021.

Waltham, T.: Lötschberg tunnel disaster, 100 years ago, Q. J. Eng. Geol. Hydroge., 41, 131–136, https://doi.org/10.1144/1470-9236/06-033, 2008.

Welten, M.: Pollenanalytische Untersuchungen im Jüngeren Quartär des nördlichen Alpenvorlandes der Schweiz, Beiträge zur Geologischen Karte der Schweiz, NF-156, 174 pp., 1982.

Welten, M.: Neue pollenanalytische Ergebnisse über das Jüngere Quartär des nördlichen Alpenvorlandes der Schweiz (Mittel- und Jungpleistozän), Beiträge zur Geologischen Karte der Schweiz, NF-162, 40 pp., 1988.

Wildi, W.: Isohypsenkarte der quartären Felstäler in der Nord-und Ostschweiz, mit kurzen Erläuterungen, Eclogae Geol. Helv., 77, 541–551, https://doi.org/10.5169/seals-165521, 1984.

Woodland, A. W.: The buried tunnel-valleys of East Anglia, P. Yorks. Geol. Soc., 37, 521–578, https://doi.org/10.1144/pygs.37.4.521, 1970.

Wright, H. E.: Tunnel valleys, glacial surges, and subglacial hydrology of the Superior Lobe, Minnesota, Geol. Soc. Mem., 136, 251–276, https://doi.org/10.1130/MEM136-p251, 1973.

Wyssling, G.: Die Ur-Sihl floss einst ins Reusstal, Zur Geologie des Sihltales zwischen Schindellegi und Sihlbrugg, Verein Pro Sihltal, 52, 1–14, 2002.

Wyssling, L. and Wyssling, G.: Interglaziale Seeablagerungen in einer Bohrung bei Uster (Kt. Zürich), Eclogae Geol. Helv., 71, 357–375, https://doi.org/10.5169/seals-164737, 1978.

E&G Quaternary Sci. J., 72, 37–55, 2023
https://doi.org/10.5194/egqsj-72-37-2023

Open Access E&G Quaternary Science Journal

Research article

Palaeoenvironmental research at Hawelti–Melazo (Tigray, northern Ethiopia) – insights from sedimentological and geomorphological analyses

Jacob Hardt[1], Nadav Nir[1], Christopher Lüthgens[2], Thomas M. Menn[3], and Brigitta Schütt[1]

[1]Physical Geography, Department of Earth Sciences, Freie Universität Berlin, Berlin, Germany
[2]Institute for Applied Geology, University of Natural Resources and Life Sciences, Vienna, Austria
[3]freelance archaeologist: Sanaa Branch, Orient Department, German Archaeological Institute (DAI), Berlin, Germany

Correspondence: Jacob Hardt (jacob.hardt@fu-berlin.de)

Relevant dates: Received: 24 June 2022 – Revised: 28 November 2022 – Accepted: 20 December 2022 – Published: 26 January 2023

How to cite: Hardt, J., Nir, N., Lüthgens, C., Menn, T. M., and Schütt, B.: Palaeoenvironmental research at Hawelti–Melazo (Tigray, northern Ethiopia) – insights from sedimentological and geomorphological analyses, E&G Quaternary Sci. J., 72, 37–55, https://doi.org/10.5194/egqsj-72-37-2023, 2023.

Abstract: The sites of Hawelti–Melazo in the Tigray region of the northern Ethiopian Highlands is an archaeological hotspot related to the D'mt kingdom (ca. 800–400 BCE). The existence of several monumental buildings, which have been excavated since the 1950s, underline the importance of this area in the Ethio-Sabaean period. We investigated the geomorphological and geological characteristics of the site and its surroundings and carried out sedimentological analyses, as well as direct (luminescence) and indirect (radiocarbon) sediment dating, to reconstruct the palaeoenvironmental conditions, which we integrated into the wider context of Tigray. Luminescence dating of feldspar grains from the May Agazin catchment indicate enhanced fluvial activity in the late Pleistocene, likely connected to the re-occurring monsoon after the Last Glacial Maximum (LGM). The abundance of trap basalt on the Melazo plateau, which provides the basis for the development of fertile soils, and the presumably higher groundwater level during the Ethio-Sabaean Period, provided favourable settlement conditions. The peninsula-like shape of the Melazo plateau was easily accessible only from the east and northeast, while relatively steep scarps enclose the other edges of the plateau. This adds a possible natural protective function to this site.

Kurzfassung: Die Stätte Hawelti–Melazo in Tigray im nördlichen Hochland von Äthiopien ist ein archäologischer hotspot, der im Zusammenhang mit dem Königreich D'mt steht (ca. 800–400 BCE). Seit den 1950er Jahren wurden dort mehrere Monumentalbauten entdeckt, die die Stellung dieses Gebiets zu äthiosabäischer Zeit unterstreichen. Wir haben die geomorphologischen und geologischen Eigenschaften des Gebiets untersucht, sedimentologische Analysen durchgeführt sowie direkte (Lumineszenz) und indirekte (Radiokohlenstoff) Sedimentdatierungsmethoden angewandt, um die Paläoumweltbedingungen zu rekonstruieren, die wir im weiteren Kontext von Tigray einordnen. Lumineszenzdatierungen an Feldspat-Körnern aus dem Einzugsgebiet des May Agazin deuten auf eine gesteigerte fluviale Aktivität im Spätpleistozän hin, die möglicherweise mit dem wiedereinsetzenden Monsun nach dem LGM in Verbindung steht. Der Trapp-Basalt des Melazo-Plateaus, der die Basis für die Bodenen-

twicklung bildet, und die wahrscheinlich höheren Grundwasserstände zur äthio-sabäischen Zeit boten gute Siedlungsbedingungen. Durch die halbinselartige Form des Melazo-Plateaus war es nur vom Osten und Nordosten einfach zugänglich, während die anderen Seiten des Plateaus durch steile Hänge begrenzt werden. Dies gab der Stätte eine zusätzliche natürliche Schutzfunktion.

1 Introduction

Located at the Horn of Africa, the northern highlands of Ethiopia are a region with a diverse and complex geological and archaeological history. The basaltic plateaus and the moderate subtropical climate with annual precipitation exceeding 600 mm at elevations around 2000 m a.s.l. (above sea level) provide the framework for the development of fertile soils and favourable living conditions not only throughout the Holocene. The abundance of natural resources, such as gold, obsidian, gums, incense, and more, led to the integration of this region in the ancient trade network between the Mediterranean and the Indian Ocean (Fattovich, 2012). In terms of archaeology, the area is probably best known for the Kingdom of Aksum (starting in the early first millennium CE), a state polity with the city of Aksum as its centre (French et al., 2009; Harrower et al., 2019). Prior to the Aksumite Period, the archaeological records show that groups related to the foreign Saba kingdom arrived during the first millennium BCE from the Arabian Peninsula (Japp et al., 2011; Fattovich, 2012, 2010). The most prominent remnants of this Ethio-Sabaean culture (ca. 800–400 BCE) in the present-day state of Tigray are several monumental buildings in the South Arabian style in Yeha, Wuqro, and Hawelti–Melazo, which give evidence for a complex hierarchical society and polity, which is named "D'mt" in literature (Fattovich, 2012). All of them are still being investigated or are still being excavated (Japp et al., 2011). D'mt disappears from the archaeological records at ca. 400 BCE, around the time of the decline of the Saba kingdom. The area did soon after witness the rise of the aforementioned, millennium-lasting Kingdom of Aksum (Fattovich, 2010).

Several studies investigated palaeoenvironmental changes and geomorphic activity phases in the northern Ethiopian Highlands (Tigray) and provided data to compare them to cultural epochs or relatively recent political upheavals in the region (Lanckriet et al., 2015; Nyssen et al., 2014, 2004, 2006b; Machado et al., 1998; Pietsch and Machado, 2014).

Here, we focus on the Daragá region of Tigray, which includes the archaeological sites of Hawelti–Melazo (de Contenson, 1961, 1963; Leclant, 1959) and lies within the basaltic Highlands (ca. 2000 m a.s.l.) about 10 km southeast of Aksum. Hawelti–Melazo are important Ethio-Sabaean and Aksumite find places (Menn, 2020). However, their direct surroundings have so far not been in the scope of palaeoenvironmental research. The aim of this study is to understand the late Pleistocene–Holocene environmental conditions of the area, which provided the base for the Ethio-Sabaean and the subsequent Aksumite occupations, using sedimentological analyses, luminescence and radiocarbon sediment dating methods, micromorphological analyses, and geomorphological mapping.

2 Study area

2.1 Archaeological overview

About 10 km southeast of Aksum, the archaeological sites of Hawelti–Melazo are to be found. In simplified terms, the most relevant sites are the hill of Hawelti and the so-called "plateaus" – most importantly Melazo – on the eastern banks of the river May Agazin, about 1.5 km southeast of Hawelti (Fig. 1).

The area first came into scientific consideration in the mid-1950s when a local farmer had accidentally discovered several (Ethio-Sabaean) finds at Goboshila (Melazo). This in turn led to the first excavations in Melazo, bringing to light a temple dedicated to the Sabaean god Almaqah (Leclant, 1959). Excavations continued in 1958 and 1959. On the Melazo plateau (specifically Inda Cherqos), two consecutive churches on top of each other were found, dating to Aksumite and probably medieval times – the older one incorporating spolia of Ethio-Sabaean heritage (de Contenson, 1961). Also, the stelae field on the hill of Hawelti was excavated revealing about 20 stelae, 2 buildings ("temples"), and some 500 finds (de Contenson, 1963). With regard to their dating, the results have to be considered as inconclusive since some of the features and finds are most probably from Ethio-Sabaean times (e.g. the stelae themselves), while others could be later additions. Furthermore, the interpretation of the stelae field's function remains uncertain.

Apart from minor surveys, no further investigations took place in Hawelti–Melazo until the still-ongoing Ethiopian–German cooperation project "Yeha and Hawelti–Melazo" took up work in 2009. Since then, the project has so far delivered one further major excavation site, as well as some 70 more find locations (Japp et al., 2011; Menn, 2020). Mostly, these sites and find locations point to Aksumite and Ethio-Sabaean heritage (Gerlach, 2018). While the former seem to be scattered all over the area, the latter appear to be concentrated on the hill of Hawelti and primarily the plateau of Melazo where also the excavation site is located about 60 m east of the church of Inda Cherqos. Here, a monumental building could be identified. With the construction method

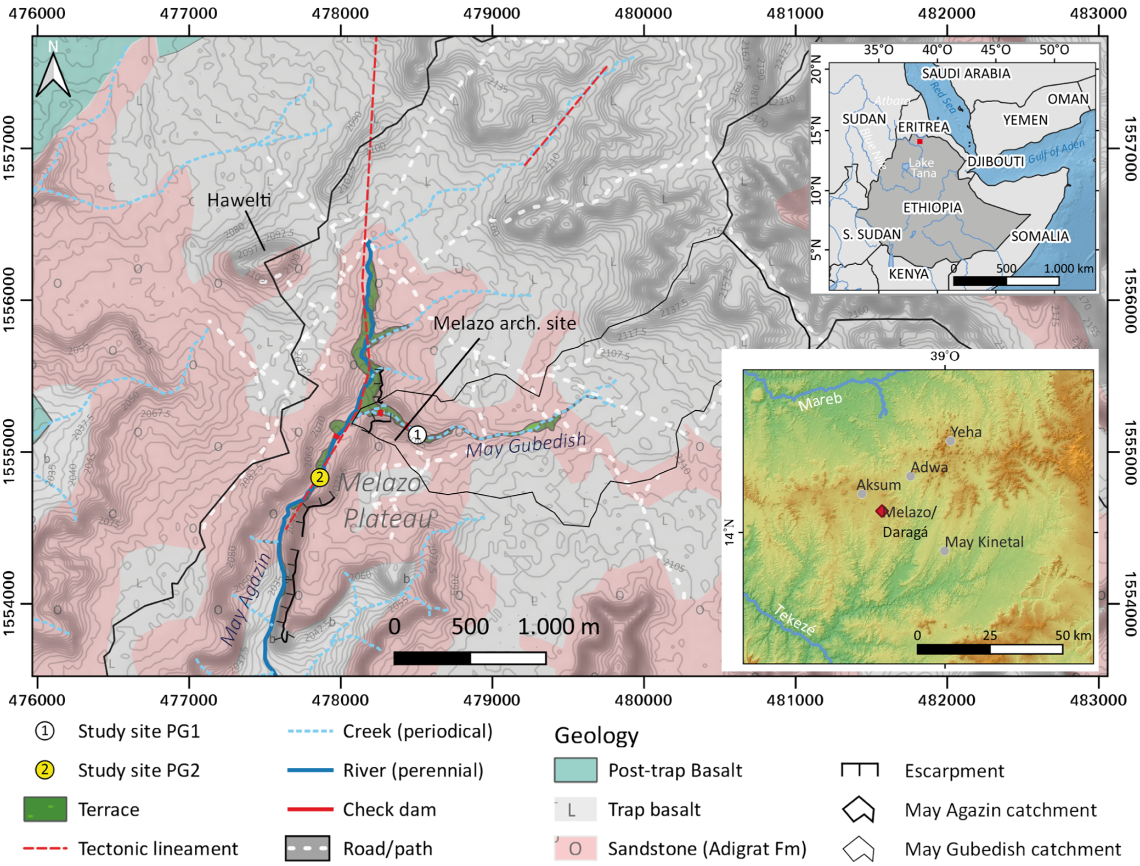

Figure 1. Geological and geomorphological map of the study area, modified from Tadesse (1999) and Hagos et al. (2010). "Melazo arch. site" refers to the location of current excavations. Several other archaeological sites were reported on the Melazo plateau to the south of the current site. Upper inset map shows the position in Ethiopia. Lower inset map shows the position in northern Ethiopia/Tigray.

similar to Yeha's Grat Be'al Gebri (Japp et al., 2011), finds corresponding to those in Yeha, and radiocarbon dating results pointing to the first half of the first millennium BCE, it can be concluded that it is of Ethio-Sabaean origin (Menn, 2020). However, several isolated finds identified during the extensive surveys also indicate the presence and possibly the settlement of people from the lithic period through to the present. Thus, the Hawelti–Melazo area has to be regarded as an archaeological hotspot.

2.2 Climate and palaeoenvironment

The study area lies in the warm and temperate subtropical highland climate zone (*Cwb* after Köppen–Geiger classification). Rainfall is mostly of monsoonal type showing a bimodal annual rainfall distribution with short rains (*belg* in Amharic) in March and long rains (*krempt* in Amharic) in June–August and a total annual precipitation of 600–700 mm (Harrower et al., 2020).

Information on late Pleistocene palaeoenvironmental conditions of the northern Ethiopian Highlands is sparse. According to Lamb et al. (2007b), Lake Tana was desiccated during the Last Glacial Maximum (LGM) due to drought caused by reduced monsoon strength (Lamb et al., 2018). A similar effect – although in a completely different environmental context – is also known for lakes in the now central Sahara (Hoelzmann et al., 2007; Umer et al., 2004). The basin of Lake Tana started to fill again at around 15 ka. In the same sense, Moeyersons et al. (2006) report increasing humidity from ca. 15 ka onwards based on numerical dating of tufa dams near Mekele (Tigray), which indicate a raised groundwater table during the late Pleistocene. Wetter conditions than today prevailed from ca. 15 ka until the mid-Holocene (ca. 5 ka; Armitage et al., 2015), owing to orbitally forced increased monsoon strength (Umer et al., 2004; Williams et al., 2006).

Climatic reconstructions for the area based on palaeopedological findings indicate that precipitation rates might have decreased in the course of the Holocene, which is in agreement with the declining monsoon strength after 5 ka (Armitage et al., 2015). Based on samples obtained close to Yeha, palaeoprecipitation rates of 870 mm a^{-1} were determined for the Early Holocene, which decreased to 780 mm a^{-1} in the first millennium BCE (Pietsch and Machado, 2014). This general trend corresponds to the findings of Dramis et al. (2003), who parallelized stratigraphic sequences in Tigray with lake level records in the Rift Valley.

Machado et al. (1998) describe three "wetter" phases during the last 4000 years with enhanced soil formation, corresponding to so-called stability phases (~ 2000–1500 BCE, 500 BCE–500 CE, 950–1000 CE), and two "drier" phases, which are represented by an increase in fluvial debris transport (1500–500 BCE, 1500–1000 CE). Lanckriet et al. (2015) compare these phases of varying morphodynamics to palaeoenvironmental studies from Lake Hayk (Lamb et al., 2007a) and Lake Ashenge (Marshall et al., 2009), as well as results from their own study site at May Tsimble (east of Mekele). This comparison confirms the general morphodynamic trends but also emphasizes several additional phases of higher and lower geomorphic activity, triggered by either climatic changes or human impact (Lanckriet et al., 2015). Human impact on the landscape in the form of land use and land cover changes comprises repeated phases of vegetation removal and intensified agriculture or livestock grazing, which have been proven throughout the last 2000–3000 years (Nyssen et al., 2004; Lanckriet et al., 2015, and references therein). Another important human imprint on the landscape are footpaths, which can incise into the land surface (Zgłobicki et al., 2021) and, for example, influence soil properties (Nir et al., 2022) and the gully erosion susceptibility (Busch et al., 2021). A footpath close to the study site was recently investigated by Nir et al. (2022) in terms of soil chemistry and micromorphology.

2.3 Geomorphological setting

The relief of the northern Ethiopian Highlands is largely structurally (tectonically and geologically) determined. Selective erosion of different rock types produced a stepped landscape, which is locally termed *amba* landscape (Coltorti et al., 2007). Several planation surfaces, the oldest being of pre-Ordovician age, once weathered and eroded at low altitudes before Cenozoic uplift of the Ethiopian Highlands, can now be found at altitudes exceeding 2000 m a.s.l. Thus, ongoing erosion not only results in stepped slopes and valleys but also exhumes relatively level palaeosurfaces (Coltorti et al., 2007; Machado, 2015).

The most typical present-day soils of the region are Vertisols and (vertic) Cambisols, which develop predominantly on the basalt surfaces and in the alluvial plains (Ferrari et al., 2015). These soils are characterized by a high content of swelling clays (montmorillonite) (Frankl et al., 2012), black colour, and relatively high fertility (Nyssen et al., 2008). Due to their high swelling potential and the seasonality of the local climate, Vertisols (locally termed *walka*; Nyssen et al., 2008) are prone to soil piping and gully erosion (Frankl et al., 2012; Nyssen et al., 2006b; Busch et al., 2021; Nir et al., 2021). Moreover, the swell-and-shrink cycles of the Vertisols trigger an upward movement of rock fragments originating from the subsurface (argillipedoturbation; Nyssen et al., 2006a).

3 Materials and methods

3.1 Fieldwork and sampling strategy

Two exposures corresponding to sections at eroded channel banks were investigated in the field and sampled for further analysis in February and November 2019. The first site in Daragá (PG1) lies on the southwestern bank of May Gubedish, a small creek flowing in a northwest direction ca. 50 m northeast of the current excavation site of Melazo. The section was chosen due to the proximity to the archaeological site, as it appeared as a potential cultural archive. The second section of Daragá (PG2) was located at the northwestern bank of May Agazin, the receiving stream of May Gubedish, ca. 300 m west of the Melazo temple and 1.5 km south of Hawelti (Table 1).

In terms of chronological control, the silty-clayey PG1 section was sampled for AMS radiocarbon dating (^{14}C), as several charcoal pieces were macroscopically visible during the sampling procedure. Oppositely, organic residue could not be found in the other sections of profile PG2, where suitable layers (sand sized, well sorted) were selected for luminescence dating. Luminescence samples were taken by driving opaque plastic cylinders (25 cm length, 5 cm diameter) into the freshly cleaned sediment, and additional samples from the bulk material were secured for radionuclide analysis.

3.2 Sedimentological analyses

The basic sedimentological analyses were performed at the physical geography laboratory of the Department of Earth Sciences, Freie Universität Berlin.

As a first preparation step, the bulk samples were dried at 105 °C, aggregates were crushed, and particles larger than 2 mm in diameter were removed by sieving. The pH values were measured with a pH meter in a solution of 10 g of dried sediment and 25 mL of 0.01 M KCl. Electrical conductivity was measured in a solution of 10 g of dried sediment in 25 mL of bi-distilled water.

The content of total carbon (TC) was determined with a Leco TruSpec CHN analyser by means of infrared CO_2 detection during sample combustion. The content of total inorganic carbon (TIC) was measured with a Woesthoff Carmhograph C-16. Total organic carbon (TOC) was subsequently calculated by the substraction of the content of TIC from the content of TC. A laser diffractometer (Beckman Coulter LS 13320) was used to determine the grain size distributions of the fractions < 1 mm. Sample preparation for grain size analysis included treatment with HCl for removal of carbonates and dispersion with sodium pyrophosphate ($Na_4P_2O_7$). Sediments from the representative units selected for dating and

Table 1. Sample overview for the studied locations.

	PG1	PG2
Location/coordinates (decimal WGS84)	May Gubedish/14.066703° N, 38.800879° E	May Agazin/14.065173° N, 38.795278° E
Bulk samples for physical and chemical analyses	27	8
Micromorphology samples	5	3
Radiocarbon samples	6 (bulk/charcoal)	/
Luminescence samples	/	2

micromorphological investigation were also mineralogically analysed by X-ray powder diffraction (XRD; Rigaku MiniFlex 600).

3.3 Micromorphological analyses

For micromorphological analyses, five sediment blocks were extracted from different sedimentary units along the profile of the main outcrop (PG1: M1–M5) and three more at sedimentary transition zones from the reference outcrop (PG2: M6_R–M8_R). Blocks were sampled using plastic boxes or jackets of gypsum bandages (plaster of Paris) depending on the sediment type and possible extraction techniques.

The micromorphological samples were dried for 4 d at room temperature (ca. 18 °C) and later heated to 50 °C for 30 h. Following this, sediments were impregnated by a 6 : 4 ($v:v$) mixture of polyester resin and acetone and a small amount of hardener (5–10 mL to 1 L of the above mixture). Due to the heavy saturation and cracking of the clay-enriched sediments, acetone removal was performed, and amounts and ratios were changed according to the reactions and impregnation of the sediments. Sampled blocks were then dried for several weeks at room temperature and cut with a slab saw to ca. 6 × 5 cm "hand-sized" units. These units were sent for 30 µm thick thin section preparation to Quality Thin Section Labs, Arizona. The analysis of the slides was performed applying a Zeiss polarizing microscope following a process performed by common micromorphological studies (Junge et al., 2018; Stoops, 2020; Verrecchia and Trombino, 2021).

3.4 Luminescence dating – sampling, preparation and experimental set-up, and radiocarbon dating

All preparation steps and luminescence measurements were carried out in the Vienna Laboratory for Luminescence Dating (VLL) at the University of Natural Resources and Life Sciences (BOKU) in Vienna, Austria. Sample preparation followed a standardized procedure at the VLL (Lüthgens et al., 2017; Rades et al., 2018), yielding extracts of potassium-rich feldspar and pure quartz. Samples for radionuclide determination were dried and subsequently stored in sealed Petri dishes (∼ 60 g dry weight) for at least a month to re-establish secondary secular radon equilibrium. Details on the radionuclide content and the overall dose rate calculations are provided in Table 3. All luminescence measurements were carried out on Risø TL/OSL DA-20 readers equipped with a $^{90}Sr/^{90}Y$ beta source (Bøtter-Jensen et al., 2000, 2003, 2010). Gamma spectrometry measurements for the calculation of the dose rate were performed using a Baltic Scientific Instruments (BSI) high-purity germanium (HPGe) p-type detector (∼ 52 % efficiency). The age calculation was done using the software ADELE (Kulig, 2005). Initial tests revealed very low sensitivity of the quartz in the samples, so all subsequent measurements were conducted using single aliquots of feldspar, which revealed good luminescence qualities in dose recovery experiments using a single aliquot regenerative dose protocol for the dating of feldspar (for details see Table 3). The resulting equivalent dose distributions were not significantly skewed, and average doses were calculated using the central age model (CAM; Galbraith et al., 1999). Unfortunately, only a few aliquots passed the rejection criteria for sample VLL-0492-L (for details see Table 3).

AMS radiocarbon dating was done at the Poznan Radiocarbon Laboratory. The C-14 dates were calibrated with the software OxCal v. 4.2.3 using the IntCal13 atmospheric curve (Reimer et al., 2013).

4 Results

4.1 Geomorphology

The Daragá area is situated at an elevation between 2000 and 2200 m a.s.l. within the Aksum plateau, which consists of the Oligocene trap basalts (Hofmann et al., 1997) and the Mesozoic Adigrat Sandstone (Tadesse, 1999; Hagos et al., 2010). Post-trap tectonic uplift of the region triggered extensive erosion of the flood basalts, resulting in several isolated table mountains (flat-topped mountains, locally named *ambas*) and larger plateau complexes. The plateaus are eroded by inward movement of the surrounding scarps. The inward erosion is promoted by weathering and mass wasting processes (Duszyński et al., 2019), possibly accelerated by human land use (Nyssen et al., 2006a). The archaeological site of Melazo is situated at the southern fringe of the Aksum plateau on a peninsula-like plateau remnant corresponding to an outlier mountain (Fig. 1). The plateau remnant measures ca. 1.6 km in southwest–northeast direction and up to 600 m in the northwest–southeast direction. Its surface is flat-topped at an altitude of 2080 m a.s.l. The surrounding valley bottoms are incised up to 60 m, resulting in steep to cliff-like scarps surrounding the plateau, which expose the various colourful (reddish) facies of the Adigrat formation. To the north, the valley of May Gubedish dissects the plateau. May Gubedish is a tributary to May Agazin, which dissects the plateau on the western side. The valley of May Agazin is up to 400 m wide, and its valley cross profile ranges from an asymmetric V shape to box-like. The valley follows a tectonic lineament (Hagos et al., 2010). Alluvial plains have developed on the wide valley floors; at profile PG2, located ca. 1 km downstream of the confluence of the tributary May Gubedish, these alluvial deposits are exposed. All hydrological regimes of nearby streams are periodical (EMA map sheet 1438 D4) and recent hydraulic constructions such as weirs and check dams were installed to control the runoff (Fig. 2).

Especially to the northeast of the Melazo plateau the soil cover is thin, resulting in frequently outcropping bedrock. The area is rural with sparse settlements; basically the whole plateau is used for arable farming while the alluvial plains of the valley bottoms are used for grazing. Stone bunds separate the fields on the plateau and the slopes, acting as erosion protection measures (Fig. 2). The widespread abundance of rock fragments covering the surface of the plateau areas can be explained by argillipedoturbation, accelerated by the use of ploughs (Nyssen et al., 2002).

The catchment of May Gubedish measures 2.27 km^2. It has a length (east–west) of roughly 3 km and a width (north-northwest–south-southeast) of up to 1 km. Ca. 30 % of the catchment is grounded in Adigrat Sandstone, while the remaining 70 % of the catchment drains trap basalt. The sandstone dominates the lower section of the catchment and is found partly also in its middle reach. The whole headwater area consists exclusively of basaltic bedrock.

While flowing through basaltic bedrock the valley profile of May Gubedish corresponds to a shallow hollow valley. To the north of the Melazo plateau, entering the Adigrat Sandstone, the May Gubedish valley is incised 10 to 20 m with a now box-like valley profile. Thus, the flanks are steeper than in the upper catchment, and slope erosion is more intense. To the northeast and north of Melazo, profile PG1 is exposed at an undercut bank where the channel of May Gubedish today incises ca. 3 m into its own sediments deposited at a local valley widening upstream of a narrow point. Downstream of the narrow point the valley profile gets box-like and is infilled by alluvial deposits. The slopes flanking the channel are covered by numerous loose blocks and stone bunds stabilize the slopes where tillage occurs; gullies can be witnessed on both valley flanks frequently stabilized by check-dams.

4.2 Sedimentology and dating results

The sediment profile PG1, located at the southwestern bank of the May Gubedish creek (Fig. 2), is built of three major lithofacies units: the overlying 160 cm sediments are formed of alternating strata each with a thickness up to 15 cm, summarized as laminated sand, silt, and mud occurring alternatively with horizontally bedded sand facies (Fl/Sh). At 160–310 cm below surface, sedimentary facies are of massive mud and silt (Fm), underlain by clast-supported, horizontally stratified gravel (Gh) 310 cm below surface. The transition between the three lithofacies units takes place gradually. In total, six different sedimentary units occurring in varying thickness and frequency could be observed in the profile (Fig. 3).

Units I and V build the major part of the outcropping sediments. Units II, III, IV, and VI are coarse-grained layers of limited thickness (2–15 cm), which separate units I and V. Unit I has a dark gray-black colour and a clayey-sandy matrix containing sharp-edged gravel. It forms the main sedimentary unit of the Fl/Sh facies of the section and can only be found until a depth of 90 cm. In its uppermost part, at 0–50 cm below surface, unit I is intersected four times by unit II, a poorly sorted stone layer with a sandy-clayey matrix and a thickness of up to 10 cm; the stones have rounded edges and a diameter of 5–10 cm. Unit III is characterized by coarse gravels in a sandy-clayey matrix occurring in thicknesses of 5–10 cm, being recorded five times between 100 and 160 cm below surface. Sedimentary unit IV was recorded in six layers of up to 12 cm thickness between 40 and 90 cm below surface. It corresponds to a red-white-grayish sand layer, occasionally containing cobbles less than 3 cm in diameter. Below 90 cm depth sedimentary unit V appears, becoming the dominating sedimentary unit 160–310 cm below surface (Fm). Unit V is a gray-green massive silty clay, which is heavily compacted. Between 90 and 160 cm below surface gravel layers of unit III are repeatedly embedded into the clayey sediments of unit V. The base of the section (Gh), below 310 cm depth, is characterized by several coarse gravel and stone layers (unit VI) intercalated by unit V. Round-edged stones 15–20 cm in diameter were recorded.

The pH values across most parts of the section are rather heterogeneous and range between pH 5.9 and pH 7.1. The lowest values were measured between 170 and 220 cm below surface (pH 5.2–5.5). The electrical conductivity of the sediments ranges between 0.06 and 0.46 mS cm^{-1}. The uppermost 70 cm of the section show very low conductivity values (0.07–0.09 mS cm^{-1}). Below 70 cm depth, from top to bottom, the electric conductivity values of the sediments increase. The contents in organic (TOC) and inorganic (TIC) carbon are at a generally low level below 0.8 wt % with only minor excursions (Fig. 3).

The radiocarbon dating resulted in ages ranging from 1432 ± 85 BP (DAT4) to 4603 ± 185 BP (DAT5; Table 2). However, the ages are not in a chronostratigraphic order.

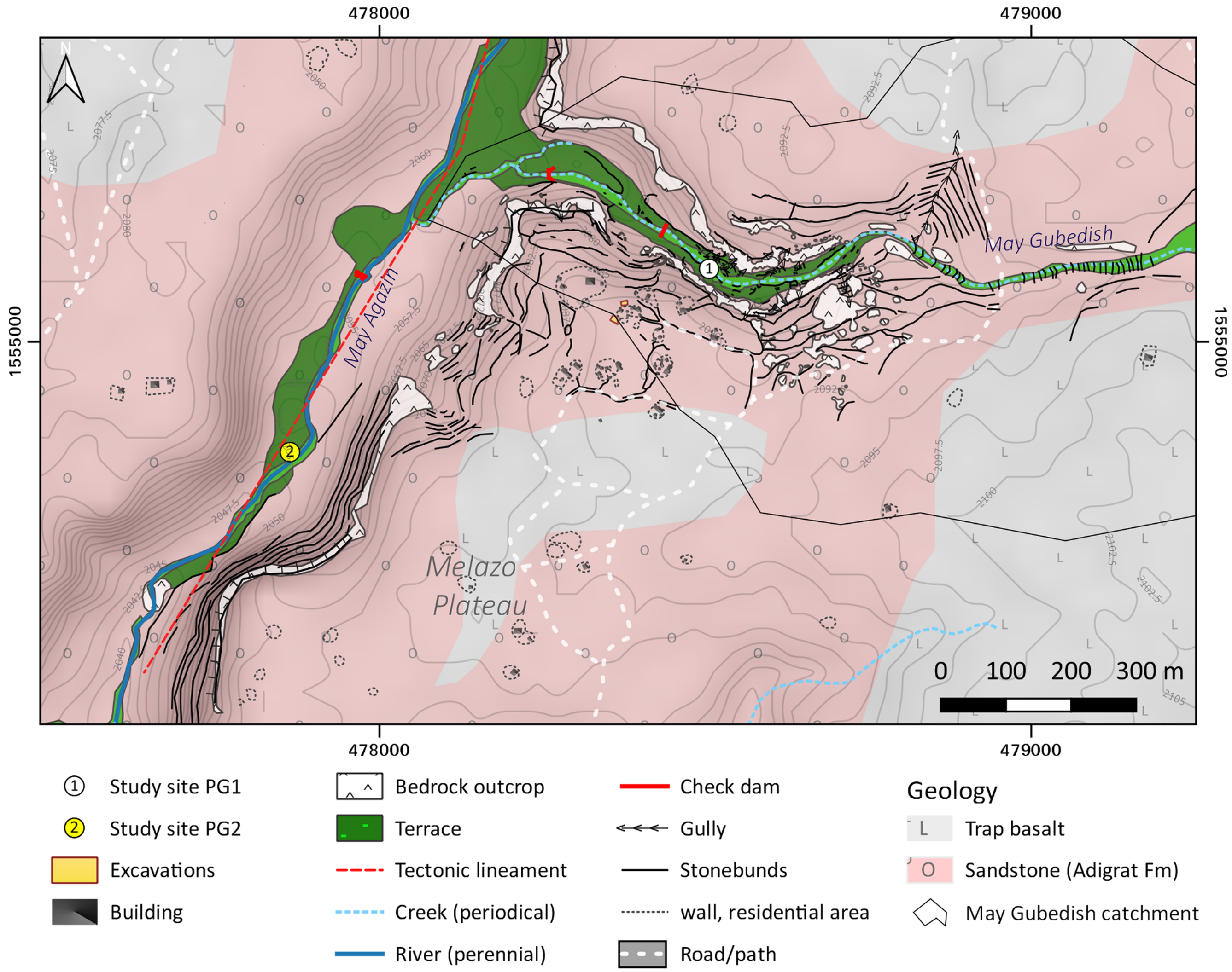

Figure 2. Geomorphological and geological map of the study area. Geology modified from Tadesse (1999) and Hagos et al. (2010). Hillshade and isolines (2.5 m spacing) based on AW3D30 digital elevation model (Jaxa, 2005).

Table 2. Overview of radiocarbon ages. All ages derived from section PG1 at May Gubedish (14.066703° N, 38.800879° E). Calibrated ages calculated using OxCal v. 4.2.3 and the IntCal13 atmospheric curve (Reimer et al., 2013). Values in bold represent the calibrated ages referred to in the text.

Lab code	Field code	Depth (cm)	Raw C-14 age BP	Calibrated age BP
POZ-126495	DAT1	65	1600 ± 30	**1470 ± 65**
POZ-114362	DAT2	70	2840 ± 360	**3021 ± 898**
POZ-123179	DAT3	100	2425 ± 30	**2525 ± 173**
POZ-123180	DAT4	180	1530 ± 30	**1432 ± 85**
POZ-126496	DAT5	365	4045 ± 35	**4603 ± 185**
POZ-122126	DAT6*	30	605 ± 30	**598 ±85**

* Sample DAT6 was taken 5 m downstream from PG1.

Sediment profile PG2, at the northwestern bank of May Agazin (Fig. 2), exposes eight strata, summarized in three different types of lithofacies: laminated sand, silt, and mud (Fl) characterize the overlying strata of the profile (0–260 cm below surface), interrupted by a layer of clast-supported, horizontally stratified gravel (Gh) 30–65 cm below surface. Below 260 cm depth lithofacies of the outcropping sediments correspond to high-energy fluvial deposits of planar-cross-bedded gravel (Gp) and planar-cross-bedded sand (Sp). The top layer (layer 1, 0–30 cm below surface) is of dark brown colour and consists of sandy silt with nested pockets filled with gravels and stones. Layer 2 (30–65 cm below surface) consists of compacted, light brown to gray silty sand with a gravelly matrix, and locally semi-angular stones are horizontally embedded. Underlying layer 3 (65–68 cm below surface) is composed of compacted brown to dark gray silt; its boundaries to the overlying layer 2 and underlying layer 4

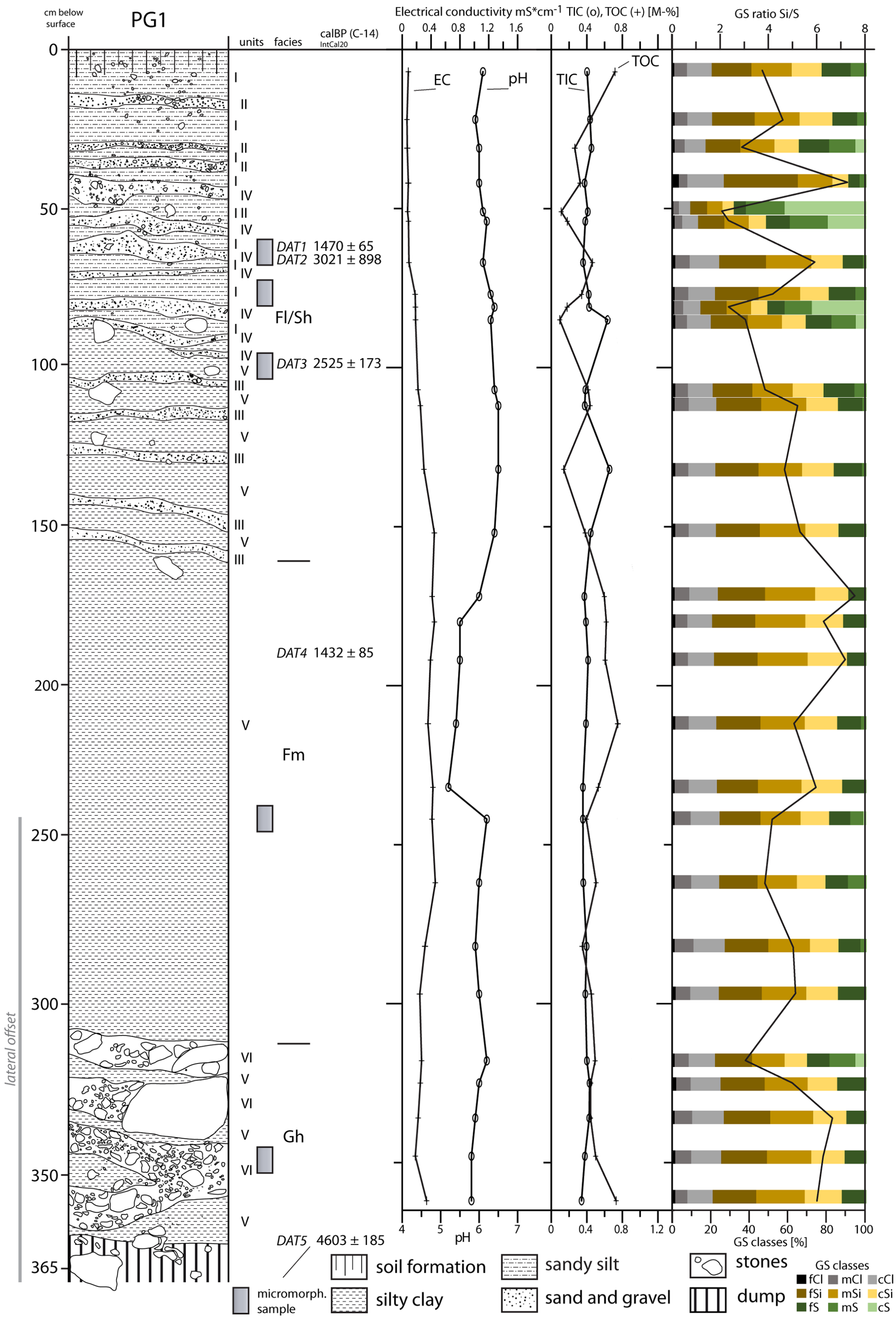

Figure 3. Sediment section PG1. Unit I: gray-black, fine roots, heavily compacted, clayey-sandy matrix with sharp-edged gravel content. Unit II: poorly sorted stone layer, 5 up to max 10 cm in diameter, rounded edges, sandy-clayey matrix. Unit III: coarse gravel layer, sandy-clayey matrix. Unit IV: red-white-grayish sand grains, occasional cobbles less than 3 cm in diameter. Unit V: gray-green massive silty clay, heavily compacted, partially embedded gravel layers (III), vertically elongated rust stains up to 1 cm length. Unit VI: gravel and stone layer. Lithofacies codes according to Miall (1996): Fm – massive mud, silt; Fl – laminated sand, silt, and mud; Sh – horizontally bedded sand; Gh – clast-supported, horizontally stratified gravel. Photographs of section PG1 can be found in the Supplement.

Table 3. Optically stimulated luminescence (OSL): results from radionuclide analysis and luminescence dating. Values in bold represent the fading corrected ages referred to in the text.

Sample lab code	Sample field code	^{238}U ($Bq\,kg^{-1}$)	^{232}Th ($Bq\,kg^{-1}$)	^{40}K ($Bq\,kg^{-1}$)	Depth (m)	Grain size (µm)	Overall dose rate Fs ($Gy\,ka^{-1}$)[a]	IR50 (n)[b]	IR50 D_e (Gy)[c]	IR50 age (ka) faded[d]	IR50 age (ka) fading corr.[e]
VLL-0491-L	PG-2-OSL5	11.18 ± 1.39	15.25 ± 1.16	200 ± 12	1.2	150–200	1.87 ± 0.15	27	23.43 ± 1.03	12.5 ± 1.1	**15.9 ± 1.5**
VLL-0492-L	PG-2-OSL6	10.80 ± 1.56	12.04 ± 0.95	127 ± 9	2.6	100–300	1.66 ± 0.13	9	25.37 ± 1.51	15.3 ± 1.5	**19.5 ± 1.5**

[a] Cosmic dose rate determined according to Prescott and Stephan (1982; Prescott and Hutton, 1994), calculated with respect to geographical position of the sampling spot (longitude, latitude, and altitude), depth below surface, and average sediment overburden density. Cosmic dose rate assigned with a 10 % error. External and internal dose rate calculated using conversion factors of Adamiec and Aitken (1998) and β attenuation factors of Mejdahl (1979), including an alpha attenuation factor of 0.08 ± 0.01, as well as an internal K content of 12.5 ± 0.5 % (Huntley and Baril, 1997) and an estimated average water content of 15 ± 5 % throughout burial time. Error was propagated to the overall dose rate calculation.

[b] Number of aliquots (4 mm diameter) passing all rejection criteria (20 % recycling ratio, 20 % recuperation in percentage of the natural signal, and 20 % test dose error, all values based on results from dose recovery experiments yielding recovery ratios in agreement with unity within error). A feldspar single-aliquot regenerative-dose (SAR) protocol using a stimulation temperature of 50 °C and a preheat temperature of 250 °C held for 60 s was used for the determination of the equivalent dose (Wallinga et al., 2000). Luminescence signals were detected through a LOT/Oriel D410/30 optical interference filter, selecting the K-feldspar emission at 410 nm (Krbetschek et al., 1997).

[c] Calculated using the CAM (Galbraith et al., 1999).

[d] Calculated using the software ADELE (Kulig, 2005).

[e] Corrected for fading according to the method of Huntley and Lamothe (2001) using the R Luminescence package (Kreutzer et al., 2012). A g value of 2.6 ± 0.3 (average value of 12 aliquots for sample VLL-0491-L) was determined using fading experiments according to Auclair et al. (2003). The fading corrected ages are used for all interpretation in this paper.

are in sharp contact. Layer 4 (68–74 cm below surface) corresponds to a light brown sandy silt in a gravelly matrix. There are several vertical cracks cutting the whole layer, which are filled with the material of layer 3. These cracks continue throughout the underlying layer 5 (74–87 cm below surface), which has a light brown colour with orange patches and consists of sandy silt with a less gravelly matrix than the above layer. It is connected with a diffuse contact to underlying layer 6 (87–97 cm below surface), a 10 cm thick layer of silt with distinct horizontal rust bands. The aforementioned cracks end in layer 6. Layer 7 (97–152 cm below surface) consists of silt and has a yellowish gray colour. Occasionally there are gravels and stones (2–4 cm in diameter) embedded. Luminescence dating of layer 7 revealed at 120 cm below surface a burial age of 15.9±1.5 ka (fading corrected; see Table 3) for this layer. The exposed basal layer 8 (below 152 cm below surface) is characterized by an intercalation of several sorted sub-layers with various grain sizes; below 220 cm depth the sub-layers become bevelled. Rust and manganese bands occur occasionally. The luminescence measurements for layer 8 (260 cm below surface) yielded a depositional age of 19.5 ± 1.5 ka (fading corrected; see Table 3).

Comparable to section PG1 the pH values of the sediments in section PG2 range between pH 6.7 and pH 7.1. The highest pH value was recognized in layer 2, at a depth of ca. 50 cm. The electrical conductivity increases from ca. 0.2 $mS\,cm^{-1}$ in layer 1 to the bottom, peaking in layer 4 (0.4 $mS\,cm^{-1}$). The TOC content is the highest in layer 1 (1.2 wt %) with two minor peaks in layers 3 (0.3 wt %) and 5 (0.23 wt %). Below 100 cm depth, the TOC decreases to values less than 0.2 wt %.

4.3 Micromorphology

At the May Agazin section (PG1), the groundmass is composed of silty to clayey weakly developed sub-angular blocky peds (Fig. 5a, c, d). The dominating colours are brown-gray-red with reduced grey more present at the bottom part, likely due to changes in groundwater level. Overall pedo-features are mostly in the form of organic and iron impregnations with some pedoturbation and little bioturbation. Little change is evident along the profile with Fe oxides, organic residues, and limpid clays detected along infilled channels. At 65–70 cm below surface (Fig. 5a), disordered interlayerings of coarse sands and gravel-sized grains with finer material are found at times along planar voids or infilled channels. They are mostly layered semi-diagonally at a 45–60° angle. These sub-rounded gravel-sized grains could be a result either of redeposition of fluvial sediments due to sheet erosion from the slopes or of a low-energy fluvial deposition. Sub-rounded sand-sized black metal oxide pseudomorphs are more dominant at this depth. The latter do not seem to be in situ pedo-features but oxidized and redeposited or pedoturbated within planes. At 110 cm below surface, the grey-gley colour decreases, and a brown-red Fe matrix dominates the micromass, indicating either more intense oxidation, most likely due to post-depositional percolation, or the groundwater not reaching up to this level (Fig. 5b). The latter process appears to be more dominant. Voids coated or infilled with limpid clay, sand-sized minerals, and hyper-coated nodules are mostly in association with planes and suggest older plane (crack) formation and therefore several cycles of pedoturbation. This process could occur either near the surface or as result of the total de- and re-hydration of the entire soil column. Some smaller voids are more rounded than the larger ones, and chambers and vesicles are common. These features indicate bioturbation occurred or is preserved over the overlying pedoturbation on the smaller scale (20–100 µm; Fig. 5, Appendix A).

Section PG2, exposing fluvial deposits of May Gubedish, exhibits silicious cementation, as well as vertical Fe oxidized cracking (Fig. 5e, f). The three micromorphological samples taken show sand- to gravel-sized volcanic minerals along with basalt rock fragments (Fig. 5e, f, g). The gravel-sized grains are coated by clay but seem to lack silt, suggesting a surface-related process of mud drying on these grains rather than a post-depositional one. The differences between the layers are related to void sizes (compaction) and to some extent to a dominance of the clayey matrix. The layers, however, exhibit large sub-angular sand- to gravel-sized grains and occasional Fe/Mn pseudomorphs. This suggests a strictly fluvial, medium-energy deposition with very minimal post-depositional activities. At 120 cm below surface (Appendix A) sand-sized grains are deposited sub-horizontally following the inclination of the present-day surface. Iron oxide nodules are mainly ordered vertically along cracks and infilled channels while some of the grains are aggregated. These observations indicate a lower-energy deposition for layer 7 (97–150 cm) than for the lowermost layer (layer 8; Fig. 5g), with some vertical voids indicating roots and/or dehydration cracks (related to the nearby surface above) infilled with oxides. A further decrease in stream energy is evident at 68–74 cm below surface (layer 4, Fig. 4), where the groundmass is compacted, matrix supported, and dominated by clays. A post-depositional silicious cementation has likely replaced biogenic features and post-dates all other features (Fig. 5e, f).

5 Discussion

Both investigated sedimentary sections and the geomorphological mapping provide insights into the late Pleistocene–Holocene palaeoenvironmental development of the Daragá area.

At the May Agazin site (PG2), the outcropping sediments are all of fluvial origin. In the basal layer 8, the sorted sands, gravels, and pebbles indicate fluvial deposition at a point bar close to the channel under varying, but generally rather high, velocities (Pazzaglia, 2013). In the overlying layer 7, laminated sands and fine gravels indicate floodplain deposition possibly related to a shift in the meandering channel in the rather wide May Agazin valley (Hooke, 2022). Accordingly, layers 6, 5, and 4 correspond to cycles fining upwards, indicating decanted floodplain deposits (Dunne and Alto, 2013; Pazzaglia, 2013). In layers 4 and 5, organic carbon contents are slightly increased. While these increased organic carbon contents could relate to redeposited organic material on the floodplain, they might also indicate soil-forming processes in a phase of reduced flood frequency (Kennedy and Woods, 2013). This interpretation agrees with the cracks infilled with fines coated by Fe oxides pervading layers 4, 5, and 6, which are signs of desiccation at the surface (Verrecchia and Trombino, 2021). Also the presence of silicified plant material observed in layer 4 (Fig. 5e) indicates that this layer formed a surface for at least some time and possibly underwent soil-forming processes. We assume that this surface was partly eroded before the accumulation of overlying layer 3 as indicated by the sharp contact between layers 3 and 4. The minor thickness of layer 3 and its sandy character indicate a single smaller flood event (Knox and Daniels, 2002). Also in layer 3, increased organic carbon contents are taken as indicators for post-sedimentary soil development and, thus, indicate a post-sedimentary phase of low flood frequency (Dixon, 2013). In contrast, in the overlying layer 2 the 50 cm thick package of unsorted sand, gravel, and sharp-edged rocks indicates strong flood activities (Benito, 2013) possibly with material contribution from the steep surrounding slopes (Nyssen et al., 2006a). However, as there is no age control for the uppermost metre of the sediment profile, a possible connection between late Holocene human impact such as deforestation (Lanckriet et al., 2015) remains highly speculative.

The deposition of layers 8 (VLL-0492-L; 19.5 ± 1.5 ka) and 7 (VLL-0491-L; 15.9 ± 1.5 ka) falls into the LGM–late Pleistocene glacial–interglacial transition period. Within 1σ error, both ages almost overlap, and within 2σ error, both ages do overlap. Given the poor luminescence properties (dim signals) of both samples, which required 4 mm aliquots each containing several hundreds of grains to be measured, signal averaging may lead to an overestimation of the ages: the luminescence signals from well-bleached grains will be masked by the much brighter luminescence signals from older feldspar grains which were not sufficiently bleached during the last sedimentary cycle (Thrasher et al., 2009; Rhodes, 2011). This is especially true for sample VLL-0492-L, which required measuring in a very broad grain size range from 100–300 µm (compared to a grain size range of only 150–200 µm for sample VLL-0491-L). This increases the averaging effect even more because a higher number of grains is measured per aliquot, which may serve as an explanation of the age offset of the two ages. In addition, the location of the PG2 section lies in the headwater area of the May Agazin catchment, roughly 4 km away from the divide. Thus, the possible transport distances of the feldspar grains

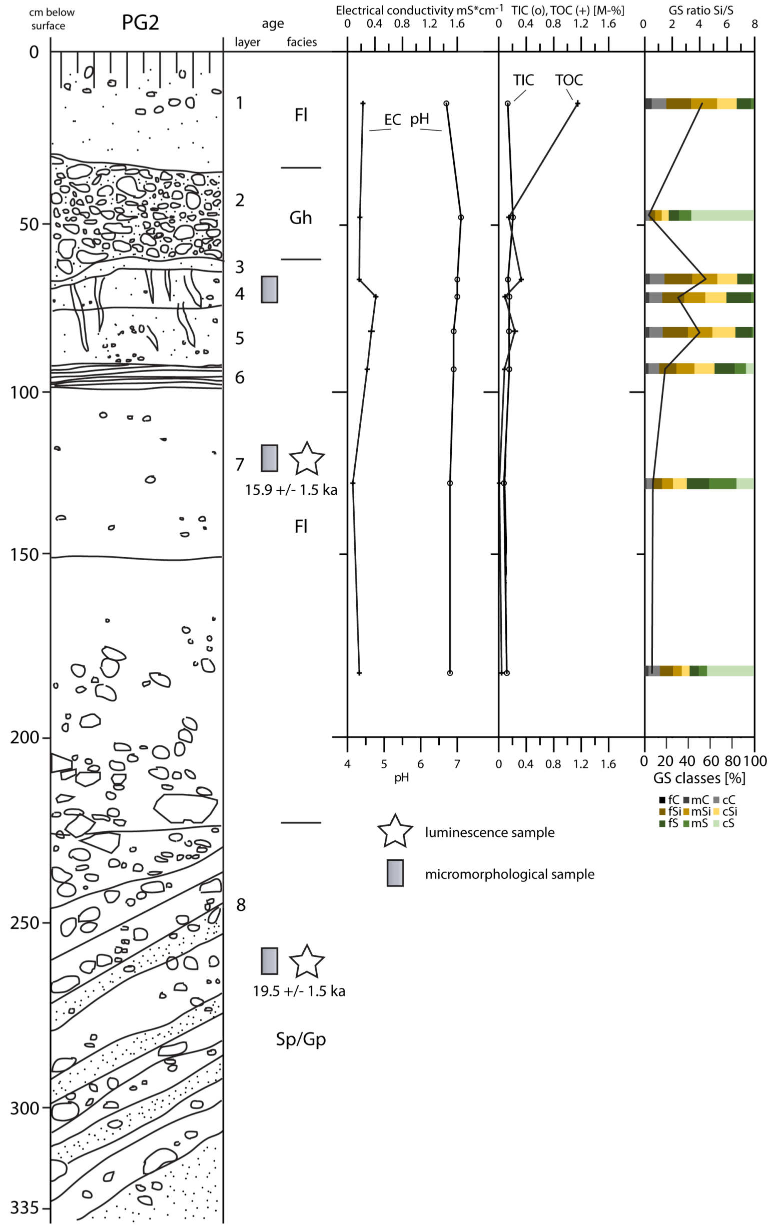

Figure 4. Sediment section PG2 (May Agazin). Layer 1: sandy silt, gravel, and stones, layered in pockets of the matrix, sub-angular small stones. Layer 2: silty sand, matrix more gravelly, rounded and semi-angular stones (2–12 cm), mostly horizontally bedded. Layer 3: sandy silt. Layer 4: sandy silt, gravels part of the matrix, sub-angular small stones. Layer 5: sandy silt with few gravels, very fine. Layer 6: silt. Layer 7: silt, occasional gravels and stones (2–4 cm), unsorted. Layer 8: intercalations of sorted layers, bedded: stones, gravels, sometimes sandy matrix. Lithofacies codes according to Miall (1996): Gp – planar-cross-bedded gravel; Sp – planar-cross-bedded sand; Gh – clast-supported, horizontally stratified gravel; Fl – laminated sand, silt, and mud. A photograph of section PG2 can be found in the Supplement.

are low, reducing the bleaching possibilities owing to only a relatively low rate of possible sedimentary cycles (Mcguire and Rhodes, 2015; Bonnet et al., 2019). Bearing in mind the possible age overestimation owing to methodological issues especially for sample VLL-0491-L, it appears more likely that both luminescence ages should be associated with the younger late Pleistocene and not with the LGM (in the case of unit 8). Consequently, both fluvial sedimentary units relate to the last glacial–interglacial transition and the abrupt onset of the summer monsoon at around ca. 15 ka (Williams et al., 2006; Gasse et al., 2008; Foerster et al., 2012). Being connected to the Nile catchment via the Tekezé and Atbara rivers, this notion is also supported by the increasing contribution of Ethiopian trap basalt components recorded in the Nile delta at the onset of the last African Humid Period (AHP) at ca. 15 ka (Revel et al., 2010; Ménot et al., 2020).

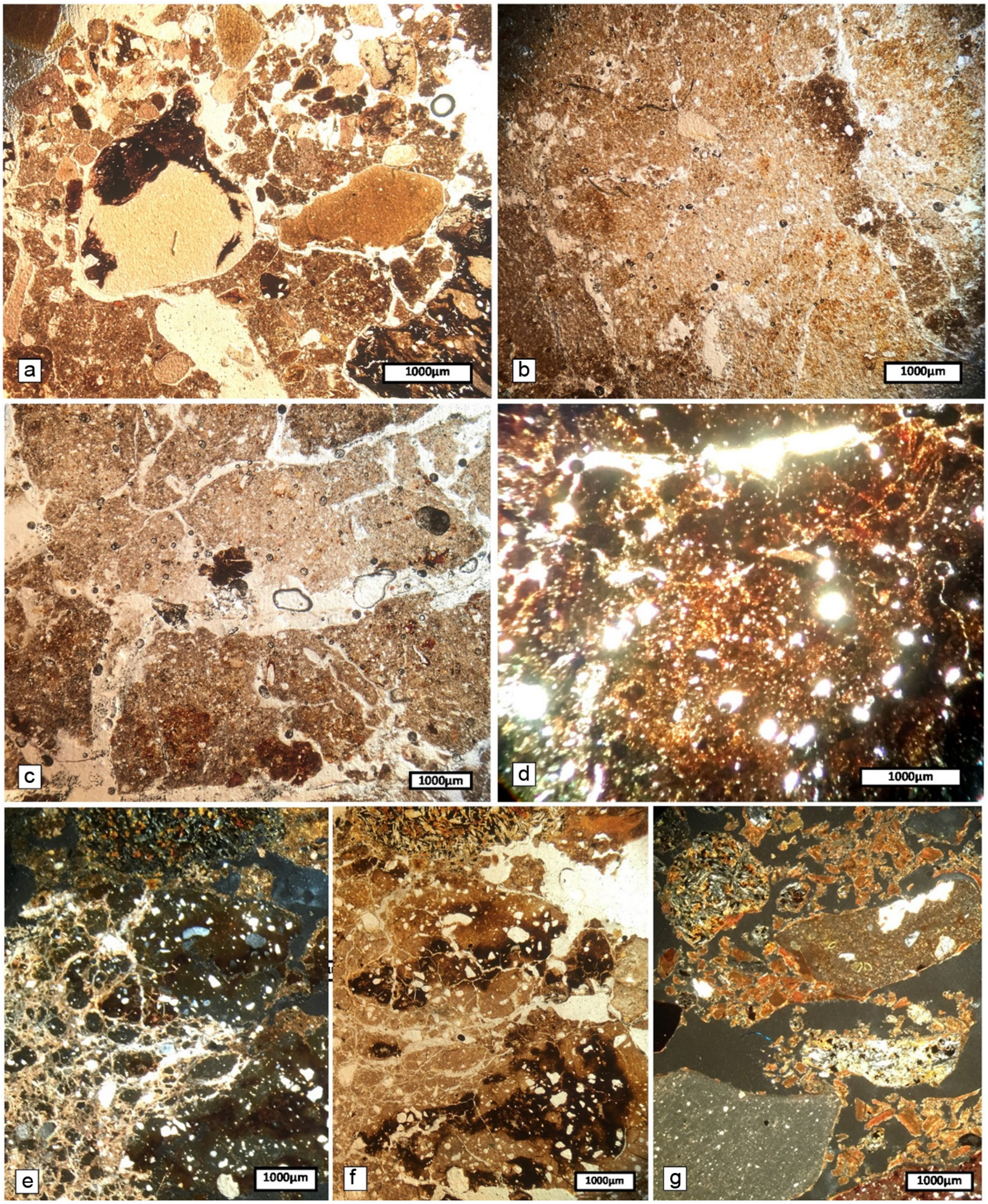

Figure 5. Thin sections of PG1 **(a–d)** and PG2 **(e–g)**. PPL = plane polarized light, and XPL = cross polarized light. **(a)** At 65–70 cm below surface (PPL) notice that the grains undergoing Mn coating are not expressed in the micromass. **(b)** At 100–110 cm below surface (PPL) clay coating and Fe–Mn oxides in a reducing and oxidizing mixed (Fe depletion) groundmass. Notice sub-vertical void along a dark brown groundmass, both typical of the matrix. **(c)** At 245–250 cm (PPL) notice that accommodating and non-accommodating planes, as well as grey and red-brown parts of the micromass, with organic impregnation and Fe–Mn oxides, are more easily differentiated. **(d)** At 365–370 cm (PPL) red-brown colour and non-accommodating planes are both more dominant. **(e)** At PG2 layer 4, 68–74 cm depth (XPL) notice that the (most likely silicious) cement is infilling voids that are cutting through the Mn–Fe oxide micromass, indicating its layer formation. **(f)** At PG2 layer 7, 115–125 cm depth: similar to panel **(e)** in PPL. **(g)** At PG2 layer 8, 255–265 cm depth (XPL) notice the basalt grain in the upper left part and limpid clay coating most of the larger grains and aggregates.

Thus, the lower parts of the PG2 section were deposited due to increased fluvial activity in response to the onset of monsoonal rainfall after a drought period during the LGM. For Lake Ashenge, Marshall et al. (2009) report increasing precipitation due to the returning monsoon already at ca. 16.2 kyr BP, which is in very close agreement with our luminescence data.

The sedimentological record from the riverbank of May Gubedish (PG1), a tributary of May Agazin, indicates completely different fluvial dynamics. The base of this section is formed by a ca. 50 cm thick package of coarse clasts (Gh facies) indicating deposition in the channel under conditions of high stream energy (Pazzaglia, 2013). The whole overlying lithostratigraphic unit (Fm facies) is dominated by silty-clayey deposits, which are in its upper layers horizontally streaked with coarser, sandy-gravelly layers (Fl/Sh facies). Either these deposits are indicative of deposition in a still water body (Reeves, 1968) or they correspond to alluvial deposits on a floodplain under very low stream energy (Pazzaglia, 2013). Deposition in a stagnant water body would require a damming situation downstream of the section, which could have been caused by a local rockfall or landslide along the river banks (Korup, 2013). The outcropping sandstone of the Adigrat Formation along the steep valley flanks and the apparent signs of ongoing gravitational mass movements at the slopes affirm this assumption (Fig. 2). Nyssen et al. (2006a) identified rockfall as an important geomorphic process in the northern Ethiopian highlands, most recently often triggered by livestock trampling. At present, however, no geomorphological evidence of a natural damming situation due to mass movements could be observed along the valley floor. The parent material of the silty-clayey deposits is the weathered trap basalt, which makes up a large part of the May Gubedish catchment (Fig. 2). The repeated occurrence of thin (few centimetres) sand and gravel layers may represent stronger rainfall events triggering slope wash and increased discharge (Cammeraat, 2013). The large clasts, which at times are embedded into the silty-clayey layers, were most likely laterally washed in from the adjacent slopes. Within the silty-clayey parts of the section signs of stratification are lacking due to pedoturbation caused by dry–wet cycles starting from the surface and influenced by a periodically alternating water table level. Consequently, Fe reduction–oxidation cycles, organic decomposition, and clay-bound swell-and-shrink processes were identified in the micromorphological analyses. The process of argillipedoturbation, which causes intense turbation of the material, has been described for Vertisols in Tigray before (Nyssen et al., 2002, 2006a). However, the sand and gravel layers above ca. 160 cm below surface have visibly not been incorporated in the pedoturbation process. Thus, we conclude that pedoturbation has not affected the larger grains and in general has mostly occurred prior to their deposition. Generally, planes and other void types are smaller than the gravels and sands in this unit and are not infilled by organic or Fe oxides as is the case for much of the lower section or even a few of the layers in this unit; i.e. gravel-sized pedomorphic organic features may have been transported within a layer in the unit but not between layers (Fig. 5).

For C-14 dating, bulk soil organic carbon was used and, thus, should be treated with caution, as soil organic carbon can be redeposited several times (e.g. old wood effect) and re-precipitate or move vertically owing to pedo- or bioturbation (Sloss et al., 2013). Our dates therefore should reflect a general time frame for the accumulation of the PG1 profile using different stratigraphic constraints to interpret the accuracy of these dates. A C-14 date from the lower part of this profile (DAT5: 4603 ± 185 BP) reveals that the early accumulation of the coarse, clast-rich Gh facies likely took place during or after the mid-Holocene. From the fines of the Fm facies, one sample was derived (DAT4: 1432 ± 85 BP), and from the layered Fl/Sh facies, three samples for C-14 dating were extracted from gravel layers (DAT1: 1470 ± 65 BP; DAT2: 3021 ± 898 BP; DAT3: 2525 ± 173 BP). Even including an age inversion due to pedoturbation, these dates indicate that sedimentation took place during the first millennium BCE and the first millennium CE; thus, it temporally corresponds to the Ethio-Sabaean and Aksumite material cultures (Phillipson, 2012). An additional date was derived from a sediment sample taken 5 m downstream of the PG 1 profile (DAT6: 598 ± 53 BP) from silty-clayey deposits (Fm facies) at a depth of 30 cm, which represents a younger re-accumulation of the May Gubedish, probably as a lower terrace segment. This age provides a frame for the incision of the May Gubedish river into its infilled valley floor, forming a river terrace that today forms the surface of PG1, which consequently took place after 598 ± 53 BP. This is in agreement with the conclusions of Lanckriet et al. (2015), who report increased channel incision especially in recent and subrecent times due to strongly increased surface runoff as a result of strong deforestation. Two C-14 outliers are likely due to syn- and post-depositional processes. Within the gravel layer DAT2 was dated 500 years older than the 50 cm deeper sample of DAT3 but with the error range of 898 years, overlapping with DAT3. However, one substantial outlier (DAT4) within the well-pedoturbated material at 1 m below this unit falls into the middle of the first millennium CE, still confirming the general age of the deposition to the late Holocene but contradicting the three ages above. This C-14 outlier is likely a result of roots activities or pedoturbation below the horizontal gravel layer. The maximum age for the deposition of the upper 180 cm of the PG1 section falls into the time of or after the decline of the Aksumite Empire (ca. 1400–1000 CE) (Phillipson, 2012), when the geomorphic activity was high due to intensified agriculture and increasing deforestation under comparably drier climatic conditions (Fig. 6; Lanckriet et al., 2015; Darbyshire et al., 2003; Machado et al., 1998).

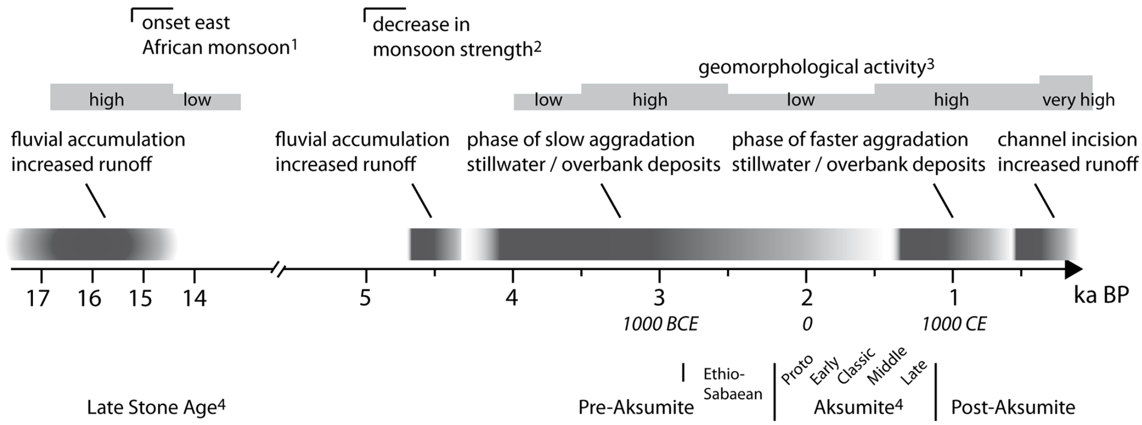

Figure 6. Integration of our results in an environmental and cultural context of northern Ethiopia. 1: Moeyersons et al. (2006), Lamb et al. (2007b), Umer et al. (2004). 2: Armitage et al. (2015). 3: this study and Lanckriet et al. (2015). 4: Bard et al. (2014), Fattovich (2012).

6 Conclusions

The environmental conditions on and around the Melazo plateau were favourable during the time of the Ethio-Sabaean settlement. This is also reflected in the findings of monumental buildings from this period. The landscape of the May Gubedish valley close to the Melazo archaeological site probably looked different during the Ethio-Sabaean period than today. The groundwater level was presumably higher, and water in the valley was probably easier to access than today due to less relief as May Gubedish was flowing at a higher level than today in its own sediments at the valley floor. Also the geological conditions appear favourable: the omnipresent Adigrat Sandstone provides building material, which is also used today for building walls and other structures. The trap basalt, found in the inner part of the Melazo plateau and the surrounding plateaus, provides fertile soils. Beyond, the peninsula-like Melazo plateau has a strong protective function as it is only easily accessible from the east–northeast, while in all other directions steep scarps enclose the plateau. The resulting large viewshed of the Melazo plateau also had tactical advantages as it allowed visitors to be recognized at an early stage. The landscape of the much wider May Agazin valley, however, was probably rather similar to most recent conditions. May Agazin like today was a hindrance for traffic, and during rainy seasons the channel could probably only be crossed at dedicated, and thus easy to control, places.

Our study provides evidence for increased fluvial activity in the May Agazin during the late Pleistocene, which is probably related to the re-occurrence of the monsoonal rainfall after the LGM. In the May Gubedish valley, being a tributary to the valley of May Agazin, coarse fluvial sediments indicating high-energy fluvial dynamics at the base of the channel were deposited around the transition from the middle to late Holocene. During the Ethio-Sabaean and probably early Aksumite period slow aggradation of the valley floor started with most likely increasing depositional rates during the late and post-Aksumite period. Since medieval or subrecent times the channel of May Gubedish incised into its own valley floor sediments – exposing the sediments of PG1 and forming a terrace which today is used for an orchard. These observations generally correlate with other studies on geomorphic activity phases in Tigray.

Appendix A

Table A1. Sedimentary analysis of selected depositional units in the PG1 and PG2 profiles. Grain sizes used are gravel (g), coarse sand (cs), medium sand (ms), fine sand (fs), silt, and clay. Sediment grain size categories are based on laser grain size analysis, while mineral occurrence is interpreted from XRD spectra. Micromass structure, mineral shapes and sizes (for those also visually identified), and pedo-features were obtained through micromorphological observation.

Site	Depth (cm)	Unit	Grain size and structure	Dominant minerals (ordered by abundance)	Pedo-features
PG1	30	Young accumulation	Clay. Weakly developed sub-angular blocky and crumble porous peds	Quartz: sub-angular (ms-fs); kaolinite, muscovite, and chlorite (silt-clay); feldspars (fs-silt); rosenhahnite	Iron mottling. Large accommodating planes and aggregates
	65–70	I/IV	Loam. Weakly developed sub-angular blocky peds, poor sorting, few sub-horizontal grain-supported layers of g-cs-sized grains	Quartz (cs-fs, sub-rounded larger grains to sub-angular smaller grains), kaolinite, muscovite, and chlorite: mostly as coating (fs-clay); plagioclase feldspar (fs); pyroxene: weathered (cs-fs) very rare	Iron mottling, organic impregnation, Mn–Fe pseudomorphs (g-ms), planes
	75–79	I/IV	Loam. Planes – ms sized in width. Moderately developed sub-angular blocky peds, poor sorting	Quartz (g-fs, sub-angular), kaolinite, muscovite, and chlorite: mostly as coating (fs-clay); plagioclase feldspar (fs); pyroxene: weathered (g-cs-fs) very rare	Some planes are infilled by the coarser material including aggregates and pseudomorphs
	95–111	V	Silty clay loam. Sub-angular blocky peds, weakly developed in a massive microstructure	Quartz mostly elliptic shaped (cs-fs); plagioclase feldspar and pyroxene: sub-angular to sub-rounded (fs); kaolinite, muscovite, and chlorite: mostly as coating (silt-clay); rosenhahnite	Iron mottling and organic impregnation, accommodating and non-accommodating planes. Voids are coated and some infilled by limpic clay and Fe–Mn oxides. Cs-sized grains are associated with planes
	345–350	V/VI	Silty loam. Weakly developed peds with poor sorting and open grain-supported structured cs-g grains at the lower part of the groundmass	Quartz: sub-angular (ms-fs), feldspar (fs-silt), kaolinite, muscovite, and chlorite (silt), possible rosenhahnite	Brown micromass with iron mottling and organic impregnation. Bioturbation is slightly more evident from the impregnation of oxides, and limpid clays feature also along infilled channels
PG2	65–68	3	Loamy sand, blocky and moderately developed peds	Quartz: sub-rounded (cs-fs); basalt: sub-angular (g-cs); clinopyroxene: sub-rounded (fs); olivine: (silt) rare; orthopyroxene: (fs) rare	Planar voids coated and filled with clays or larger grains
	68–74	4	Sandy loam, blocky in a poorly to moderately developed peds structure	Quartz: sub-rounded (ms-fs); clinopyroxene: sub-rounded (fs); basalt: sub-angular (cs) rare	Cemented by amorphous silica. Rare (g) size orthopyroxene grains with surrounding constrained minerals (corona texture) – geological feature
	97–152	7	Loamy sand with structural and planar voids. Large grains (cs-g) are crossing sub-horizontally	Basalt: sub-rounded (g-ms); pyroxene: sub-angular to sub-rounded (cs-fs); olivine: (ms-fs) rare; kaolinite, muscovite: coating (clay)	Clay coating on most of the sand-sized grains. Many of the large grains are aggregates. Mn–Fe oxide nodules (pseudomorphs) are also found along vertical lines (cracks)
	152–335	8	Sandy gravel dominant in open grain-supported structure	Quartz: sub-rounded (cs-fs); pyroxene: sub-rounded to sub-angular (ms-fs); basalts: sub-rounded (g-ms)	Three sub-units with g- and s-sized grains: 1. in large voids, 2. dominant clay-coating and 3. combination of (1) and (2) Mn–Fe oxides pseudomorphs (cs-ms) and Fe mottling. Depositional cycles

Data availability. The basic luminescence data are included in this publication. Additional data can be provided by the corresponding author upon request.

Supplement. The supplement related to this article is available online at: https://doi.org/10.5194/egqsj-72-37-2023-supplement.

Author contributions. This study was conceptualized by JH, NN, and BS, who also carried out the field work. JH and NN prepared the original draft of the manuscript. NN carried out the micromorphological analyses. CL conducted the luminescence analyses. TM provided the archaeological background. All authors discussed the results and contributed to various stages in the writing process of this paper, including reviewing and editing.

Competing interests. At least one of the (co-)authors is a member of the editorial board of *E&G Quaternary Science Journal*. The peer-review process was guided by an independent editor, and the authors also have no other competing interests to declare.

Disclaimer. Publisher's note: Copernicus Publications remains neutral with regard to jurisdictional claims in published maps and institutional affiliations.

Special issue statement. This article is part of the special issue "Quaternary research from and inspired by the first virtual DEUQUA conference". It is a result of the vDEUQUA2021 online conference in September/October 2021.

Acknowledgements. The authors wish to thank Silvan Schmieg and Robert Busch (Freie Universität Berlin) and Kristina Pfeiffer, Victoria Grünberg, Mike Schnelle, Sarah Japp, and Iris Gerlach (German Archaeological Institute (DAI), Sanaa Branch of the Orient Department). Thanks to Mareike Stahlschmidt for guidance in the analysis of the thin sections. We want to thank the two anonymous reviewers for their constructive reviews of this work.

Financial support. This research has been supported by the Deutsche Forschungsgemeinschaft (DFG) within the framework of the SPP 2143 Entangled Africa – Project Routes of Interaction (grant no. 404354728).

We acknowledge support from the Open Access Publication Initiative of Freie Universität Berlin.

Review statement. This paper was edited by Julia Meister and reviewed by two anonymous referees.

References

Adamiec, G. and Aitken, M.: Dose-rate conversion factors: update, Ancient TL, 16, 37–50, 1998.

Armitage, S. J., Bristow, C. S., and Drake, N. A.: West African monsoon dynamics inferred from abrupt fluctuations of Lake Mega-Chad, P. Natl. Acad. Sci. USA, 112, 8543–8548, https://doi.org/10.1073/pnas.1417655112, 2015.

Auclair, M., Lamothe, M., and Huot, S.: Measurement of anomalous fading for feldspar IRSL using SAR, Radiat. Meas., 37, 487–492, https://doi.org/10.1016/S1350-4487(03)00018-0, 2003.

Bard, K. A., Fattovich, R., Manzo, A., and Perlingieri, C.: The chronology of Aksum (Tigrai, Ethiopia): a view from Bieta Giyorgis, Azania, 49, 285–316, https://doi.org/10.1080/0067270X.2014.943484, 2014.

Benito, G.: 13.15 Hazardous Processes: Flooding, in: Treatise on Geomorphology, edited by: Shroder, J. F., Academic Press, San Diego, 243–261, https://doi.org/10.1016/B978-0-12-374739-6.00363-8, 2013.

Bonnet, S., Reimann, T., Wallinga, J., Lague, D., Davy, P., and Lacoste, A.: Landscape dynamics revealed by luminescence signals of feldspars from fluvial terraces, Scientific Reports, 9, 8569, https://doi.org/10.1038/s41598-019-44533-4, 2019.

Bøtter-Jensen, L., Bulur, E., Duller, G. A. T., and Murray, A. S.: Advances in luminescence instrument systems, Radiat. Meas., 32, 523–528, https://doi.org/10.1016/S1350-4487(00)00039-1, 2000.

Bøtter-Jensen, L., McKeever, S. W. S., and Wintle, A. G.: Optically Stimulated Luminescence Dosimetry, Elsevier, 355 pp., https://doi.org/10.1016/B978-0-444-50684-9.X5077-6, 2003.

Bøtter-Jensen, L., Thomsen, K. J., and Jain, M.: Review of optically stimulated luminescence (OSL) instrumental developments for retrospective dosimetry, Radiat. Meas., 45, 253–257, https://doi.org/10.1016/j.radmeas.2009.11.030, 2010.

Busch, R., Hardt, J., Nir, N., and Schütt, B.: Modeling Gully Erosion Susceptibility to Evaluate Human Impact on a Local Landscape System in Tigray, Ethiopia, Remote Sensing, 13, 2009, https://doi.org/10.3390/rs13102009, 2021.

Cammeraat, E. L. H.: 7.33 Semiarid Hillslope Processes, in: Treatise on Geomorphology, edited by: Shroder, J. F., Academic Press, San Diego, 355–362, https://doi.org/10.1016/B978-0-12-374739-6.00184-6, 2013.

Coltorti, M., Dramis, F., and Ollier, C. D.: Planation surfaces in Northern Ethiopia, Geomorphology, 89, 287–296, https://doi.org/10.1016/j.geomorph.2006.12.007, 2007.

de Contenson, H.: Les fouilles à Haoulti-Melazo en 1958, Annales d'Ethiopie, 4, 39–60, 1961.

de Contenson, H.: Les fouilles de Haoulti en 1959 – Rapport préliminaire, Annales d'Ethiopie, 5, 41–86, 1963.

Darbyshire, I., Lamb, H., and Umer, M.: Forest clearance and regrowth in northern Ethiopia during the last 3000 years, Holocene, 13, 537–546, https://doi.org/10.1191/0959683603hl644rp, 2003.

Dixon, J. C.: 4.3 Pedogenesis with Respect to Geomorphology, in: Treatise on Geomorphology, edited by: Shroder, J. F., Academic Press, San Diego, 27–43, https://doi.org/10.1016/B978-0-12-374739-6.00058-0, 2013.

Dramis, F., Umer, M., Calderoni, G., and Haile, M.: Holocene climate phases from buried soils in Tigray (northern

Ethiopia): comparison with lake level fluctuations in the Main Ethiopian Rift, Quaternary Res., 60, 274–283, https://doi.org/10.1016/j.yqres.2003.07.003, 2003.

Dunne, T. and Aalto, R. E.: 9.32 Large River Floodplains, in: Treatise on Geomorphology, edited by: Shroder, J. F., Academic Press, San Diego, 645–678, https://doi.org/10.1016/B978-0-12-374739-6.00258-X, 2013.

Duszyński, F., Migoń, P., and Strzelecki, M.C.: Escarpment retreat in sedimentary tablelands and cuesta landscapes – Landforms, mechanisms and patterns, Earth-Sci. Rev., 196, 102890, https://doi.org/10.1016/j.earscirev.2019.102890, 2019.

Fattovich, R.: The Development of Ancient States in the Northern Horn of Africa, c. 3000 BC–AD 1000: An Archaeological Outline, J. World Prehist., 23, 145–175, https://doi.org/10.1007/s10963-010-9035-1, 2010.

Fattovich, R.: The northern Horn of Africa in the first millennium BCE: local traditions and external connections, Rassegna di Studi Etiopici, 4, 1–60, 2012.

Ferrari, G., Ciampalini, R., Billi, P., and Migoń, P.: Geomorphology of the Archaeological Area of Aksum, in: Landscapes and Landforms of Ethiopia. World Geomorphological Landscapes, edited by: Billi, P., Springer, Dordrecht, 147–161, https://doi.org/10.1007/978-94-017-8026-1_7, 2015.

Foerster, V., Junginger, A., Langkamp, O., Gebru, T., Asrat, A., Umer, M., Lamb, H. F., Wennrich, V., Rethemeyer, J., Nowaczyk, N., Trauth, M. H., and Schaebitz, F.: Climatic change recorded in the sediments of the Chew Bahir basin, southern Ethiopia, during the last 45,000 years, Quatern. Int., 274, 25–37, https://doi.org/10.1016/j.quaint.2012.06.028, 2012.

Frankl, A., Poesen, J., Deckers, J., Haile, M., and Nyssen, J.: Gully head retreat rates in the semi-arid highlands of Northern Ethiopia, Geomorphology, 173–174, 185–195, https://doi.org/10.1016/j.geomorph.2012.06.011, 2012.

French, C., Sulas, F., and Madella, M.: New geoarchaeological investigations of the valley systems in the Aksum area of northern Ethiopia, CATENA, 78, 218–233, https://doi.org/10.1016/j.catena.2009.02.010, 2009.

Galbraith, R. F., Roberts, R. G., Laslett, G. M., Yoshida, H., and Olley, J. M.: Optical dating of single and multiple grains of quartz from Jinmium rock shelter, Northern Australia: Part I, experimental design and statistical models, Archaeometry, 41, 339–364, https://doi.org/10.1111/j.1475-4754.1999.tb00987.x, 1999.

Gasse, F., Chalié, F., Vincens, A., Williams, M. A. J., and Williamson, D.: Climatic patterns in equatorial and southern Africa from 30,000 to 10,000 years ago reconstructed from terrestrial and near-shore proxy data, Quaternary Sci. Rev., 27, 2316–2340, https://doi.org/10.1016/j.quascirev.2008.08.027, 2008.

Gerlach, I.: Zum äthio-sabäischen Kunsthandwerk des frühen 1. Jahrtausends v. Chr., in: Hauptsache Museum – Der alte Orient im Fokus – Festschrift für Ralf-B. Wartke, edited by: Marzahn, J. and Pedde, F., marru – Studien zur Vorderasiatischen Archäologie, 229–252, ISBN 978-3-96327-036-9, 2018.

Hagos, M., Koeberl, C., Kabeto, K., and Koller, F.: Geochemical characteristics of the alkaline basalts and phonolite-trachyte plugs of the Axum area, northern Ethiopia, Austrian J. Earth Sc., 103, 153–170, 2010.

Harrower, M. J., Dumitru, I. A., Perlingieri, C., Nathan, S., Zerue, K., Lamont, J. L., Bausi, A., Swerida, J. L., Bongers, J. L., Woldekiros, H. S., Poolman, L. A., Pohl, C. M., Brandt, S. A., and Peterson, E. A.: Beta Samati: discovery and excavation of an Aksumite town, Antiquity, 93, 1534–1552, https://doi.org/10.15184/aqy.2019.84, 2019.

Harrower, M. J., Nathan, S., Mazzariello, J. C., Zerue, K., Dumitru, I. A., Meresa, Y., Bongers, J. L., Gebreegziabher, G., Zaitchik, B. F., and Anderson, M. C.: Water, Geography, and Aksumite Civilization: The Southern Red Sea Archaeological Histories (SRSAH) Project Survey (2009–2016), Afr. Archaeol. Rev., 37, 51–67, https://doi.org/10.1007/s10437-020-09369-8, 2020.

Hoelzmann, P., Gasse, F., Dupont, L., Salzmann, U., Staubwasser, M., Leuschner, D., and Sirocko, F.: Palaeoenvironmental changes in the arid and sub arid belt (Sahara-Sahel-Arabian Peninsula) from 150 kyr to present, in: Past Climate Variability through Europe and Africa. Developments in Paleoenvironmental Research, edited by: Battarbee, R. W., Gasse, F., and Stickley, C. E., Springer, Dordrecht, 6, 219–256, https://doi.org/10.1007/978-1-4020-2121-3_12, 2007.

Hofmann, C., Courtillot, V., Féraud, G., Rochette, P., Yirgu, G., Ketefo, E., and Pik, R.: Timing of the Ethiopian flood basalt event and implications for plume birth and global change, Nature, 389, 838–841, https://doi.org/10.1038/39853, 1997.

Hooke, J. M.: 6.26 - River Meandering, in: Treatise on Geomorphology (Second Edition), edited by: Shroder, J. F., Academic Press, Oxford, 480–516, https://doi.org/10.1016/B978-0-12-409548-9.12517-5, 2022.

Huntley, D. and Baril, M.: The K content of the K-feldspars being measured in optical and thermoluminescence dating, Ancient TL, 15, 11–13, 1997.

Huntley, D. J. and Lamothe, M.: Ubiquity of anomalous fading in K-feldspars and the measurement and correction for it in optical dating, Can. J. Earth Sci., 38, 1093–1106, https://doi.org/10.1139/e01-013, 2001.

Japp, S., Gerlach, I., Hitgen, H., and Schnelle, M.: Yeha and Hawelti: cultural contacts between Saba' and D´MT – New research by the German Archaeological Institute in Ethiopia, Proc. Sem. Arab. Stud., 41, 145–160, 2011.

JAXA: ALOS Global Digital Surface Model (DSM) ALOS World 3D-30m (AW3D30) Ver. 2.2, JAXA – Japan Aerospace Exploration Agency [data set], https://www.eorc.jaxa.jp/ALOS/en/dataset/aw3d30/aw3d30_e.htm (last access: 17 January 2023), 2005.

Junge, A., Lomax, J., Shahack-Gross, R., Finkelstein, I., and Fuchs, M.: Chronology of an ancient water reservoir and the history of human activity in the Negev Highlands, Israel, Geoarchaeology, 33, 695–707, https://doi.org/10.1002/gea.21682, 2018.

Kennedy, D. M. and Woods, J. L. D.: 14.22 Determining Organic and Carbonate Content in Sediments, in: Treatise on Geomorphology, edited by: Shroder, J. F., Academic Press, San Diego, 262–273, https://doi.org/10.1016/B978-0-12-374739-6.00389-4, 2013.

Knox, J. C. and Daniels, J. M.: Watershed Scale and the Stratigraphic Record of Large Floods, in: Ancient Floods, Modern Hazards, 237–255, https://doi.org/10.1029/WS005p0237, 2002.

Korup, O.: 9.15 Landslides in the Fluvial System, in: Treatise on Geomorphology, edited by: Shroder, J. F., Academic Press, San Diego, 244–259, https://doi.org/10.1016/B978-0-12-374739-6.00240-2, 2013.

Krbetschek, M. R., Götze, J., Dietrich, A., and Trautmann, T.: Spectral information from minerals relevant for luminescence dating, Radiat. Meas., 27, 695–748, https://doi.org/10.1016/S1350-4487(97)00223-0, 1997.

Kreutzer, S., Schmidt, C., Fuchs, M. C., Dietze, M., Fischer, M., and Fuchs, M.: Introducing an R package for luminescence dating analysis, Ancient TL, 30, 1–8, 2012.

Kulig, G.: Erstellung einer Auswertesoftware zur Altersbestimmung mittels Lumineszenzverfahren unter spezieller Berücksichtigung des Einflusses radioaktiver Ungleichgewichte in der 238-U-Zerfallsreihe, Bakkalaureusarbeit Network Computing, TU Freiberg, unpublished thesis, 2005.

Lamb, H. F., Leng, M. J., Telford, R. J., Ayenew, T., and Umer, M.: Oxygen and carbon isotope composition of authigenic carbonate from an Ethiopian lake: a climate record of the last 2000 years, Holocene, 17, 517–526, https://doi.org/10.1177/0959683607076452, 2007a.

Lamb, H. F., Bates, C. R., Coombes, P. V., Marshall, M. H., Umer, M., Davies, S. J., and Dejen, E.: Late Pleistocene desiccation of Lake Tana, source of the Blue Nile, Quaternary Sci. Rev., 26, 287–299, https://doi.org/10.1016/j.quascirev.2006.11.020, 2007b.

Lamb, H. F., Bates, C. R., Bryant, C. L., Davies, S. J., Huws, D. G., Marshall, M. H., Roberts, H. M., and Toland, H.: 150,000-year palaeoclimate record from northern Ethiopia supports early, multiple dispersals of modern humans from Africa, Scientific Reports, 8, 1077, https://doi.org/10.1038/s41598-018-19601-w, 2018.

Lanckriet, S., Schwenninger, J.-L., Frankl, A., and Nyssen, J.: The Late-Holocene geomorphic history of the Ethiopian Highlands: Supportive evidence from May Tsimble, CATENA, 135, 290–303, https://doi.org/10.1016/j.catena.2015.08.011, 2015.

Leclant, J.: Haoulti-Melazo (1955–1956), Annales d'Ethiopie, 3, 43–82, 1959.

Lüthgens, C., Neuhuber, S., Grupe, S., Payer, T., Peresson, M., and Fiebig, M.: Geochronological investigations using a combination of luminescence and cosmogenic nuclide burial dating of drill cores from the Vienna Basin, Z. Dtsch. Ges. Geowiss., 168, 115–140, https://doi.org/10.1127/zdgg/2017/0081, 2017.

Machado, M.: Geomorphology of the Adwa District, in: Landscapes and Landforms of Ethiopia, World Geomorphological Landscapes, edited by: Billi, P., Springer, Dordrecht, 163–178, https://doi.org/10.1007/978-94-017-8026-1_8, 2015.

Machado, M. J., Pérez-González, A., and Benito, G.: Paleoenvironmental Changes during the Last 4000 yr in the Tigray, Northern Ethiopia, Quaternary Res., 49, 312–321, https://doi.org/10.1006/qres.1998.1965, 1998.

Marshall, M., Lamb, H., Davies, S., Leng, M., Bedaso, Z., Umer, M., and Bryant, C.: Climatic change in northern Ethiopia during the past 17,000 years: A diatom and stable isotope record from Lake Ashenge, Palaeogeogr. Palaeocl., 279, 114–127, https://doi.org/10.1016/j.palaeo.2009.05.003, 2009.

McGuire, C. and Rhodes, E. J.: Downstream MET-IRSL single-grain distributions in the Mojave River, southern California: Testing assumptions of a virtual velocity model, Quat. Geochronol., 30, 239–244, https://doi.org/10.1016/j.quageo.2015.02.004, 2015.

Mejdahl, V.: Thermoluminescence dating: beta attenuation in quartz grains, Archaeometry, 21, 61–72, https://doi.org/10.1111/j.1475-4754.1979.tb00241.x, 1979.

Menn, T. M.: Hawelti-Melazo: the French legacy and recent research – In memoriam Henri de Contenson (1926-2019), Annales d'Éthiopie, 33, 155–166, 2020.

Ménot, G., Pivot, S., Bouloubassi, I., Davtian, N., Hennekam, R., Bosch, D., Ducassou, E., Bard, E., Migeon, S., and Revel, M.: Timing and stepwise transitions of the African Humid Period from geochemical proxies in the Nile deep-sea fan sediments, Quaternary Sci. Rev., 228, 106071, https://doi.org/10.1016/j.quascirev.2019.106071, 2020.

Miall, A. D.: The geology of fluvial deposits: sedimentary facies, basin analysis, and petroleum geology, Springer, Berlin [u.a.], XVI, 582 pp., https://doi.org/10.1007/978-3-662-03237-4, 1996.

Moeyersons, J., Nyssen, J., Poesen, J., Deckers, J., and Haile, M.: Age and backfill/overfill stratigraphy of two tufa dams, Tigray Highlands, Ethiopia: Evidence for Late Pleistocene and Holocene wet conditions, Palaeogeogr. Palaeocl., 230, 165–181, https://doi.org/10.1016/j.palaeo.2005.07.013, 2006.

Nir, N., Knitter, D., Hardt, J., and Schütt, B.: Human movement and gully erosion: Investigating feedback mechanisms using Frequency Ratio and Least Cost Path analysis in Tigray, Ethiopia, PLoS ONE, 16, e0245248, https://doi.org/10.1371/journal.pone.0245248, 2021.

Nir, N., Stahlschmidt, M., Busch, R., Lüthgens, C., Schütt, B., and Hardt, J.: Footpaths: Pedogenic and geomorphological long-term effects of human trampling, CATENA, 215, 106312, https://doi.org/10.1016/j.catena.2022.106312, 2022.

Nyssen, J., Moeyersons, J., Poesen, J., Haile, M., and Deckers, J. A.: Argillipedoturbation and the development of rock fragment covers on Vertisols in the Ethiopian Highlands, BELGEO, 2, 183–194, https://doi.org/10.4000/belgeo.16184, 2002.

Nyssen, J., Poesen, J., Moeyersons, J., Deckers, J., Haile, M., and Lang, A.: Human impact on the environment in the Ethiopian and Eritrean highlands – a state of the art, Earth-Sci. Rev., 64, 273–320, https://doi.org/10.1016/S0012-8252(03)00078-3, 2004.

Nyssen, J., Poesen, J., Moeyersons, J., Deckers, J., and Haile, M.: Processes and rates of rock fragment displacement on cliffs and scree slopes in an *amba* landscape, Ethiopia, Geomorphology, 81, 265–275, https://doi.org/10.1016/j.geomorph.2006.04.021, 2006a.

Nyssen, J., Poesen, J., Veyret-Picot, M., Moeyersons, J., Haile, M., Deckers, J., Dewit, J., Naudts, J., Teka, K., and Govers, G.: Assessment of gully erosion rates through interviews and measurements: a case study from northern Ethiopia, Earth Surf. Proc. Land., 31, 167–185, https://doi.org/10.1002/esp.1317, 2006b.

Nyssen, J., Naudts, J., De Geyndt, K., Haile, M., Poesen, J., Moeyersons, J., and Deckers, J.: Soils and land use in the Tigray highlands (Northern Ethiopia), Land Degrad. Dev., 19, 257–274, https://doi.org/10.1002/ldr.840, 2008.

Nyssen, J., Frankl, A., Haile, M., Hurni, H., Descheemaeker, K., Crummey, D., Ritler, A., Portner, B., Nievergelt, B., Moeyersons, J., Munro, N., Deckers, J., Billi, P., and Poesen, J.: Environmental conditions and human drivers for changes to north Ethiopian mountain landscapes over 145 years, Sci. Total Environ., 485-486, 164–179, https://doi.org/10.1016/j.scitotenv.2014.03.052, 2014.

Pazzaglia, F. J.: 9.22 Fluvial Terraces, in: Treatise on Geomorphology, edited by: Shroder, J. F., Academic Press, San Diego, 379–412, https://doi.org/10.1016/B978-0-12-374739-6.00248-7, 2013.

Phillipson, D. W.: Foundations of an African civilisation: Aksum & the Northern Horn, 1000 BC – AD 1300, 1st edn., Eastern Africa series, Currey, Woodbridge, X, 293 pp., ISBN 9781846158735, 2012.

Pietsch, D. and Machado, M. J.: Colluvial deposits – proxies for climate change and cultural chronology. A case study from Tigray, Ethiopia, Z. Geomorphol, 58, 119–136, https://doi.org/10.1127/0372-8854/2012/S-00114, 2014.

Prescott, J. R. and Hutton, J. T.: Cosmic ray contributions to dose rates for luminescence and ESR dating: Large depths and long-term time variations, Radiat. Meas., 23, 497–500, https://doi.org/10.1016/1350-4487(94)90086-8, 1994.

Prescott, J. R. and Stephan, L. G.: The contribution of cosmic radiation to the environmental dose for thermoluminescence dating. Latitude, altitude and depth dependences, PACT, 6, 17–25, 1982.

Rades, E. F., Fiebig, M., and Lüthgens, C.: Luminescence dating of the Rissian type section in southern Germany as a base for correlation, Quatern. Int., 478, 38–50, https://doi.org/10.1016/j.quaint.2016.07.055, 2018.

Reeves, C. C. (Ed.): Chapter 6 Lacustrine Sediments: Clastic, in: Developments in Sedimentology, Elsevier, 77–85, https://doi.org/10.1016/S0070-4571(08)70829-X, 1968.

Reimer, P. J., Bard, E., Bayliss, A., Beck, J. W., Blackwell, P. G., Ramsey, C. B., Buck, C. E., Cheng, H., Edwards, R. L., Friedrich, M., Grootes, P. M., Guilderson, T. P., Haflidason, H., Hajdas, I., Hatte, C., Heaton, T. J., Hoffmann, D. L., Hogg, A. G., Hughen, K. A., Kaiser, K. F., Kromer, B., Manning, S. W., Niu, M., Reimer, R. W., Richards, D. A., Scott, E. M., Southon, J. R., Staff, R. A., Turney, C. S. M., and van der Plicht, J.: Intcal13 and Marine13 Radiocarbon Age Calibration Curves 0–50,000 Years Cal BP, Radiocarbon, 55, 1869–1887, 2013.

Revel, M., Ducassou, E., Grousset, F. E., Bernasconi, S. M., Migeon, S., Revillon, S., Mascle, J., Murat, A., Zaragosi, S., and Bosch, D.: 100,000 Years of African monsoon variability recorded in sediments of the Nile margin, Quaternary Sci. Rev., 29, 1342–1362, https://doi.org/10.1016/j.quascirev.2010.02.006, 2010.

Rhodes, E. J.: Optically Stimulated Luminescence Dating of Sediments over the Past 200,000 Years, Annu. Rev. Earth Pl. Sc., 39, 461–488, https://doi.org/10.1146/annurev-earth-040610-133425, 2011.

Sloss, C. R., Westaway, K. E., Hua, Q., and Murray-Wallace, C. V.: 14.30 An Introduction to Dating Techniques: A Guide for Geomorphologists, in: Treatise on Geomorphology, edited by: Shroder, J. F., Academic Press, San Diego, 346–369, https://doi.org/10.1016/B978-0-12-374739-6.00399-7, 2013.

Stoops, G.: Guidelines for Analysis and Description of Soil and Regolith Thin Sections, 2nd edn., Soil Science Society of America, Inc., https://doi.org/10.1002/9780891189763, 2020.

Tadesse, T.: Geological Map 1:25000 ND 37-6 Axum, Geological Survey of Ethiopia, 1999.

Thrasher, I. M., Mauz, B., Chiverrell, R. C., and Lang, A.: Luminescence dating of glaciofluvial deposits: A review, Earth-Sci. Rev., 97, 133–146, https://doi.org/10.1016/j.earscirev.2009.09.001, 2009.

Umer, M., Legesse, D., Gasse, F., Bonnefille, R., Lamb, H. F., Leng, M. J., and Lamb, A. A.: Late Quaternary climate changes in the Horn of Africa, in: Past Climate Variability through Europe and Africa, edited by: Battarbee, R. W., Gasse, F., and Stickley, C. E., Springer Netherlands, Dordrecht, 159–180, https://doi.org/10.1007/978-1-4020-2121-3_9, 2004.

Verrecchia, E. P. and Trombino, L.: Pedogenic Features, in: A Visual Atlas for Soil Micromorphologists, Springer International Publishing, Cham, 93–133, https://doi.org/10.1007/978-3-030-67806-7_4, 2021.

Wallinga, J., Murray, A., and Wintle, A.: The single-aliquot regenerative-dose (SAR) protocol applied to coarse-grain feldspar, Radiat. Meas., 32, 529–533, https://doi.org/10.1016/S1350-4487(00)00091-3, 2000.

Williams, M., Talbot, M., Aharon, P., Abdl Salaam, Y., Williams, F., and Inge Brendeland, K.: Abrupt return of the summer monsoon 15,000 years ago: new supporting evidence from the lower White Nile valley and Lake Albert, Quaternary Sci. Rev., 25, 2651–2665, https://doi.org/10.1016/j.quascirev.2005.07.019, 2006.

Zgłobicki, W., Poesen, J., De Geeter, S., Boardman, J., Gawrysiak, L., Golosov, V., Ionita, I., Niacsu, L., Rodzik, J., Stankoviansky, M., and Stolz, C.: Sunken lanes – Development and functions in landscapes, Earth-Sci. Rev., 221, 103757, https://doi.org/10.1016/j.earscirev.2021.103757, 2021.

E&G Quaternary Sci. J., 72, 57–72, 2023
https://doi.org/10.5194/egqsj-72-57-2023

Open Access E&G Quaternary Science Journal

Research article

Chronological and sedimentological investigations of the Late Pleistocene succession in Osterbylund (Schleswig-Holstein, Germany)

Christine Thiel[1], **Michael Kenzler**[2], **Hans-Jürgen Stephan**[3], **Manfred Frechen**[4], **Brigitte Urban**[5], and **Melanie Sierralta**[4]

[1]B4.3 Federal Seismological Survey and Nuclear Test Ban, Federal Institute for Geosciences and Natural Resources, Stilleweg 2, 30655 Hanover, Germany
[2]Institute of Geography and Geology, University of Greifswald, F.-L. Jahn-Straße 17a, 17487 Greifswald, Germany
[3]independent researcher: Köhlstr. 3, 24159 Kiel, Germany
[4]Section S3: Geochronology, Leibniz Institute for Applied Geophysics, Stilleweg 2, 30655 Hanover, Germany
[5]Institute of Ecology, Leuphana University Lüneburg, Universitätsallee 1, 21339 Lüneburg, Germany

Correspondence: Christine Thiel (cthiel-geo@gmx.de)

Relevant dates: Received: 26 December 2021 – Revised: 11 October 2022 – Accepted: 11 January 2023 – Published: 6 March 2023

How to cite: Thiel, C., Kenzler, M., Stephan, H.-J., Frechen, M., Urban, B., and Sierralta, M.: Chronological and sedimentological investigations of the Late Pleistocene succession in Osterbylund (Schleswig-Holstein, Germany), E&G Quaternary Sci. J., 72, 57–72, https://doi.org/10.5194/egqsj-72-57-2023, 2023.

Abstract: The age of the push moraine complex Wallsbüll-Böxlund, Schleswig-Holstein, is unclear despite investigations in this area for decades. To address the timing of formation of both the push moraine complex and the peat and soils found in its depressions, an outcrop in Osterbylund (OBL) was investigated. Optically stimulated luminescence and ^{230}Th/U dating, as well as pollen analyses, were undertaken with the aim to correlate the soils OBL 1 to OBL 4 to interglacials and interstadials. The chronological studies were accompanied by detailed sedimentological investigations. The results of the pollen analyses put the peat unambiguously to the Eemian; the peat is equivalent to OBL 1. The overlying sands and the other intercalated soils are to be placed into the early Weichselian. While for OBL 2 the assignment to the Brörup interstadial is clear, it is more difficult to clearly correlate OBL 3 and OBL 4 to an interstadial due to poor luminescence signal resetting of the sands, especially above OBL 4. Considering all data available, it is most likely that OBL 3 formed during the Odderade interstadial and OBL 4 during the Keller interstadial. From the Eemian to early Weichselian ages of the peat and soils it is evident that the push moraine complex is of Saalian age; a Weichselian ice margin further in the west, as assumed in other studies, can therefore be excluded.

Kurzfassung: Die Altersstellung des Stauchmoränenkomplexes Wallsbüll-Böxlund in Schleswig-Holstein ist trotz jahrzehntelanger Untersuchungen noch ungeklärt. Die in einem Aufschluss in Osterbylund (OBL) aufgeschlossenen Sedimente und Torfe sowie Böden wurden zur Klärung dieser Frage und auch zur Korrelation der Böden OBL 1 bis OBL 4 mit den bekannten Interglazialen und Interstadialen mittels optisch stimulierter Lumineszenz und Uran-Thorium sowie Pollenanalysen datiert. Detaillierte sedimentologische Aufnahmen ergänzten die chronologischen Arbeiten. Die Pollenanalysen ordnen den in Depressionen vorkommenden Torf dem Eem zu; der Torf ist mit OBL 1 gleichzusetzen. Die aufliegenden Sande und die übrigen eingeschalteten Böden können alle in das Frühweichsel gestellt werden. Während für OBL 2 die Stellung in das Brörup-Interstadial aufgrund der Daten belegbar ist, gestalten sich die Zuordnungen für OBL 3 und OBL 4 etwas schwieriger, da schlechte Bleichung der Lumineszenzsignale der Sande insbesondere oberhalb von OBL 4 Unsicherheiten mit sich bringen. Unter Berücksichtigung der Gesamtheit der Daten ist eine Korrelation von OBL 3 mit dem Odderade-Interstadial und von OBL 4 mit dem Keller-Interstadial am wahrscheinlichsten. Aus diesen Daten ergibt sich zudem eine saalezeitliche Entstehung des Stauchmoränenwalls; ein, wie in anderen Studien angenommen, weichselzeitlicher Eisrand noch weiter westlich als der hier untersuchte Standort kann somit ausgeschlossen werden.

1 Introduction

The extent of the Weichselian ice sheet and the environment in the southern Baltic region and bordering areas in northern Germany has received large attention (e.g. Houmark-Nielson, 2010; Kenzler et al., 2017, 2018; Rinterknecht et al., 2014). In contrast to detailed knowledge on the late Weichselian ice dynamics and its climatic implications (e.g. Hughes et al., 2016; Lüthgens et al., 2020), the early Weichselian in this area has not yet been investigated in its entirety. This period, however, is especially interesting due to the changes between cold and warm phases. While these climate variations are well preserved in ice cores (e.g. Seierstad et al., 2014), there is a lack of local terrestrial archives documenting the highly variable conditions at that time.

Among the few terrestrial sites in northern Germany where palaeosols as indicators for warm phases are preserved is the push moraine ridge in Osterbylund, northern Schleswig-Holstein, close to the Danish border (Fig. 1). However, whether the palaeosols represent the Weichselian remains controversially discussed. It has been argued that the soils got deformed by the youngest Saalian ("Warthian") glacier advance during marine isotope stage (MIS) 6 and had therefore been interpreted as "intra-Saalian", with an attribution of the lowermost and most intensively developed soil to the intra-Saalian "Treene interglacial" (e.g. Stremme, 1981, 1986; Stremme et al., 1982; Stremme and Weinhold, 1982; Zöller, 1986). In contrast, it has been claimed that the soils are of post-Saalian age, with the lowermost soil representing the Eemian interglacial, not being glacially deformed; the overlying soils represent Weichselian interstadials (Gripp et al., 1965).

To address the debate on the age of the push moraine ridge and with it on the palaeosol formation, optically stimulated luminescence (OSL) dating is the method of choice, as it can be applied to the clastic sediments underlying and covering the soils. In luminescence dating, the time elapsed since the last exposure to daylight is determined; this is in general referred to as the burial age. From that it is evident that not the soil formation itself is being dated, but that age constraints can be provided.

In our study we present detailed sedimentological investigations of the sediment succession in the push moraine complex near Osterbylund, Schleswig-Holstein, Germany, together with OSL ages from the sediment over- and underlying the palaeosols. In addition, pollen analyses from a peat underlying the clastic sediments are presented together with an attempt to date the peat using ^{230}Th/U dating. The combination of the data is then used to correlate the investigated strata and the palaeosols to MISs, with the aim to add another jigsaw piece to the glacial and intraglacial development in the western Baltic region.

2 Geological setting

For decades, several sand–gravel pits have been opened in a 9 km long, SE–NW stretching push moraine ridge between Wallsbüll and Böxlund, northern Schleswig-Holstein, close to the Danish border (Fig. 1). Two of them (Böxlund 1 and 2; Fig. 1b) have been intensely investigated over decades due to the occurrence of palaeosols (e.g. Stremme and Weinhold, 1980). Because of the presence of several organic-rich horizons, the sand–gravel pit in Osterbylund became of special interest. It is situated on the same ridge (Fig. 1) a few kilometres SW of the Danish border. The push moraine is surrounded by Weichselian sandur plains originating from meltwater streams of the Weichselian end moraines draining westwards into the North Sea. The surfaces of these plains have an elevation no higher than +25 m above present sea level (a.s.l.). The Saalian push moraine complex is 20 to 30 m higher than these plains (topographical map of Germany 1 : 25 000; sheets Medelby, 1121, and Wallsbüll, 1221), with the highest point, called Lundtop, reaching +53.8 m a.s.l.

The continuous exploitation of the pit revealed not only the complexity of the sand succession and the intercalated soils and organic-rich horizons but also various peat layers. Further, two folded palaeosols in superposition were found (see Stephan, 1988). Based on detailed sedimentary and structural studies, Stephan (1988) showed that the defor-

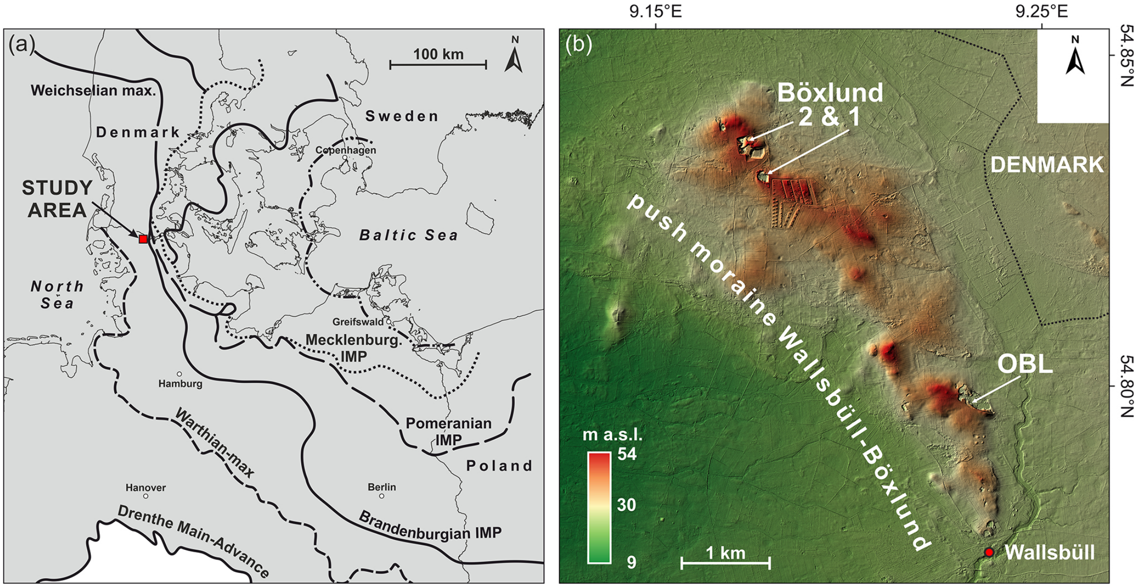

Figure 1. Overview of the Baltic region in which the study area is located, **(a)** showing the ice marginal positions of the Saalian and Weichselian glaciations and **(b)** the push moraine complex Wallsbüll-Böxlund; OBL = Osterbylund.

mation had developed by a periglacial sheet sliding downslope with thrust folding, probably initiated by an undercut of the moraine slope by Weichselian meltwater streams.

In Fig. 2, a generalised view of the sediments, structure, and deformation is given. The lower and median parts are mainly meltwater sands, in most cases strongly deformed by glacial pressure (folded and cut by thrust faults). Blocks of till and folded till beds are incorporated in the sands mostly getting smaller upwards, rarely reaching the surface. The northeastern part of the deformed sequence is covered by a thick undulating till sheet overlain by periglacial sands, which are several metres thick, not deformed, and concordantly filling push synclines, upwards with slightly undulating or increasingly even stratification. Several palaeosols (named OBL 1–4) have been observed within these sandy deposits; the lower two soils show distinct humus-rich Ah horizons (according to AG Boden, 2005). Towards the centres of the synclines the lowermost humus layer is often graded into a peat.

3 Field investigations

Different outcrop walls have been investigated over the last 2 decades, showing various sedimentological features which can be used to obtain an integrated picture. Detailed investigations and sampling for dating and pollen analyses were carried out in 2003, 2004, and 2005. The field studies in 2012 (see Stephan et al., 2017) and 2016 focussed on the sedimentological description to obtain a better understanding of the geological and geomorphological processes at the site.

3.1 Exposure and sampling in 2003

A standardised profile of the investigated exposures (54.798216° N, 9.232047° E) is given in Fig. 3 (composite profile 2003).

At the bottom, a greyish-brown till is exposed, overlain by grey sand, only 1 cm thick, upwards followed by a 1.8 m thick peat, which can be parted into a lower black and an upper blackish-brown peat (Fig. 3). The black peat is compact and has a platy structure, while the overlying peat shows an only slightly platy structure but many well-preserved fragments of plants and wood. Both peat layers were sampled for ^{230}Th/U dating (TIMS no. <700, Table S1 in the Supplement) and pollen analyses.

The peat is discordantly overlain by mainly fine- to medium-grained sand; the transition between peat and sand exhibits dislocated peat fragments. The sand appears partly weakly podsolised, and its lamination is altered by mass movements. About 1 m above the peat an OSL sample (LUM 498) was taken (Figs. 3, S1). The sand graded upwards into greyish silt, overlain by a strongly disturbed mud, which is up to 15 cm thick and interbedded with relics of an Ae horizon (Fig. 3). Above the mud, there is grey to yellowish-grey laminated sand of about 4 m in thickness. This sand was sampled some metres above the mud (LUM 469). At its top, a thin and slightly humic Ah horizon is present and overlain by a brownish sand (see composite profile 2003 in Fig. 3). One OSL sample (LUM 470) was taken from an isolated block about 60 m to the northeast below a brown clay. The sedimentary conditions at this site are slightly unclear; the material may belong to a gravity flow.

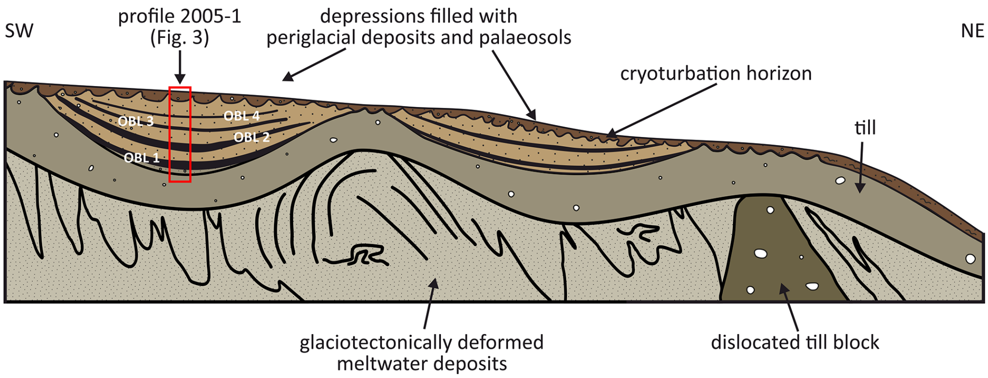

Figure 2. Generalised sketch of the push moraine in Osterbylund. In the depression, the four palaeosols OBL 1 to OBL 4 are exposed (see Figs. 3 and 4).

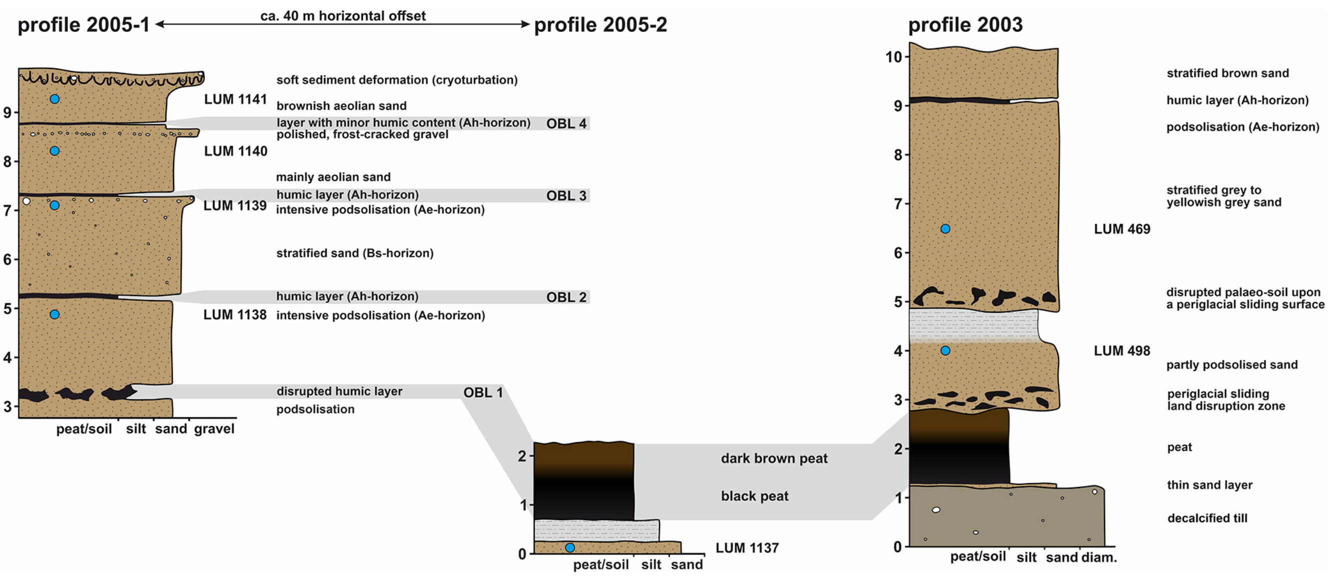

Figure 3. Profiles investigated in the years 2003 to 2005, indicating the locations where samples for luminescence dating (LUM) were taken. Sample LUM 470 originates from an isolated block, which hampers the correlation. Therefore, the sample is not marked in the profile.

3.2 Exposure and sampling in 2004 and 2005

The generalised profile of an exposure north of the site investigated in 2003 is presented in Fig. 3 (profiles 2005-1 and 2005-2). The same peat bed as found in 2003 was exposed in a small incision originating from water run-off (54.798351° N, 9.232048° E; profile 2005-2); the palaeosols were present at 54.798218° N, 9.231425° E (profile 2005-1). All four palaeosols (OBL 1–4) were present at this exposure (Fig. 4).

The bottom part (profile 2005-2) is composed of a ca. 0.2 m thick very fine-grained sand, covered by silt ca. 0.4 m in thickness. One sample for OSL dating (LUM 1137) was taken from the sand. The silt is overlain by 1.5 m thick peat; there, a series of samples for ^{230}Th/U dating was taken (TIMS no. > 700; Table S1). Above the peat, most parts of the overlying succession are dug off, with the peat forming the sole of an excavation plane (terrace). About 40 m further to the west (profile 2005-1) the peat graded into a thick humus layer with an underlying podsol (OBL 1 in profile 2005-1, Fig. 3), both periglacially disturbed and partly displaced. Above the humus layer, a 1.8 m thick mainly fine- to medium-grained, laminated sand followed, overlain by an Ah horizon (OBL 2) with intense podsolisation (distinct leached horizon and a thick yellow to rusty brown Bsh horizon). Just below OBL 2, a sample for luminescence dating was taken (LUM 1138). On top of the weak soil, there are about 2 m thick stratified sands with few gravels; these sands are distinctly podsolised and overlain by a thin humus layer (OBL 3). One sample for OSL dating (LUM 1139) was taken from the leached sand (Fig. 3; profile 2005-1, Fig. S2).

The podsol is covered by fine- to medium-grained laminated brownish sands, which are most likely of aeolian origin. One sample for OSL dating (LUM 1140) was taken

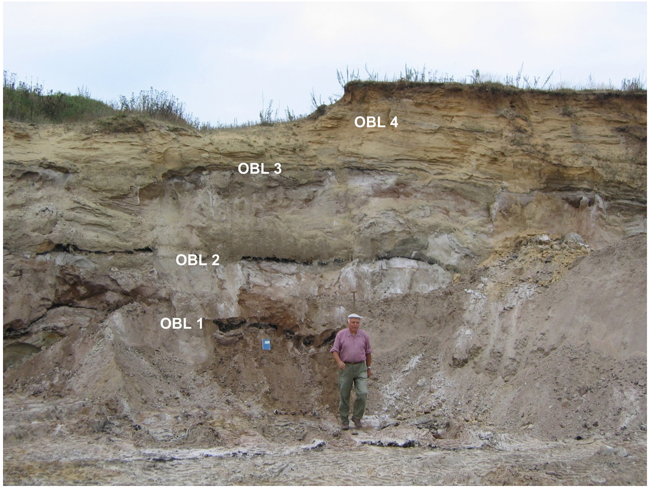

Figure 4. Photograph of the NW-facing outcrop investigated in 2005 showing OBL 1–OBL 4. This photograph corresponds to profile 2005-1 in Fig. 3.

0.75 m above the podsol from the sand. This sequence was overprinted close to the top by a thin and weak podsol with a very thin Ah layer (OBL 4); ca. 0.2 m below this Ah layer there is an intercalation with gravel. The gravels are polished and frequently split by frost. Above the Ah layer laminated brownish sands, ca. 1 m in thickness, are found. These sands are cryoturbated at the top. The cryoturbated zone has an admixture of some gravels and few stones, evidencing transport of coarse material from outcropping till further up the slope. The uppermost sample for OSL dating (LUM 1141) was taken 0.5 m above the Ah layer of OBL 4.

3.3 Exposure in 2016

The exposure investigated in 2016 (54.798162° N, 9.230141° E; Fig. 5) is located 100 m to the west of profile 2005-2.

Based on its sedimentological and pedological characteristics, profile 2016-2 has been subdivided into five lithological units (Unit I to V; Fig. 6):

Unit I comprises two superimposed diamict layers, with a total thickness of at least 1 m. The lower boundary was not visible due to slope debris. The basal part of the outcropping strata consists of a stiff, matrix-supported silty, greenish-grey diamicton with sporadic medium- to coarse-grained sand lenses. The transition to the 20–30 cm thick overlying matrix-supported sandy diamicton is gradual. Faint subhorizontally stratified domains are visible in this uppermost greenish-grey part of unit I (Fig. 6).

The 1.3 m thick unit II is composed of massive medium-grained sand intercalated with granule lenses and pebble stingers in the middle part (Figs. 6 and 7a–c). At the undulating base, a centimetre-thick faintly developed humic layer is present, which marked the transition from unit I to unit II. Isolated black humic spots at the centimetre scale are scattered across the basal 20 cm of unit II (OBL 1). The middle part shows rusty oxidation domains and patchy iron staining at the decimetre scale due to accumulation of illuvial sesquioxides and organic matter. The uppermost 20–30 cm sandy parts are better sorted with very sporadic fine-grained gravel clasts. The sands are leached due to intensive podsolisation. The uppermost 5–10 cm of unit II is formed by a humic layer (OBL 2).

The overlying 1.7 m thick unit III is characterised by medium-grained partly deformed sand layers and a basal clayey silt lens at the decimetre scale (Fig. 7a). The lower sandy part is dominated by soft sediment deformation structures recognisable by iron precipitates along lithological boundaries. Sporadic discontinuous gravel layers occur in the middle part of the unit. The upper part displays as intensive podsolisation marked by leached sand. Several outsized clasts occur in the uppermost part of this unit, some of which are broken. The top of unit III is made of a discontinuous humic layer at the millimetre to centimetre scale (OBL 3). From the base of this humic layer subvertical sand-filled cracks and fissures penetrate the underlying leached sand (Fig. 7c). From a pedological point of view, unit III can be subdivided into the following three soil horizons (Fig. 6): an up to 1.3 m thick Bsh horizon with accumulated illuvial sesquioxides and organic material, an up to 0.4 m thick intensively podsolised Ae horizon (leached sand), and an uppermost discontinuous humic Ah horizon. A hiatus represents the boundary to the overlying unit IV, which is up to 1.6 m thick and consists of massive to faintly (sub-)horizontal stratified medium-grained sand. Iron staining is present in the lower part along lithological boundaries. Several burrow-like structures identifiable by colour changes are visible in the middle part (Fig. 7b). Further features are clay bands at the millimetre scale, a faintly visible 5–10 cm thick humic layer in the lower middle part (OBL 4), and a sporadic fine-grained gravel stringer in the upper part (Figs. 5, 6, and 7b). From the top of this unit a wedge-shaped structure vertically penetrates the underlying deposits up to unit III (Figs. 6 and 7a).

The uppermost 30 cm thick unit V is dominated by non-stratified medium-grained sand and isolated fine- to medium-grained gravel clasts. A significant root penetration characterises this brownish unit, which represents the Holocene soil.

4 Age determination of the sands and peat

The chronological approach is threefold: next to absolute dating of the clastic sediments using OSL, it was attempted to date the peat using ^{230}Th/U. Additionally, pollen analyses were conducted for a qualitative allocation of the peat to possible warm phases.

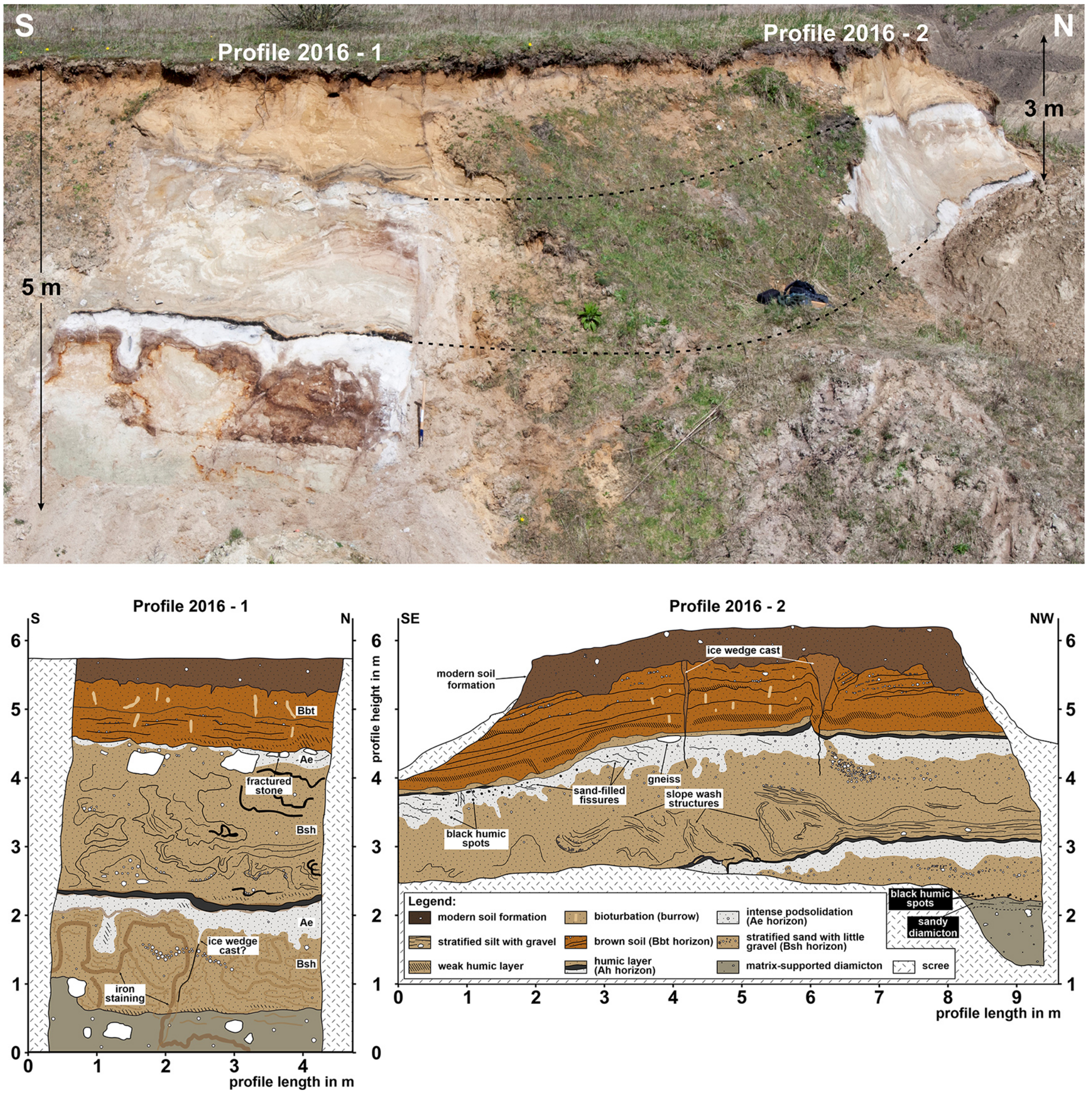

Figure 5. Photograph and sketches of the profiles investigated in 2016. A detailed lithological description is given in Fig. 6 and in the main text.

4.1 Optically stimulated luminescence dating

In total, eight samples were taken for OSL dating from three different profiles (see Table 1, Fig. 3) by hammering tubes into freshly cleaned sediment walls. After sampling, the tubes were sealed to avoid light exposure, and the material from immediately around the tubes was sampled for dose rate determination.

4.1.1 Dose rate determination

The sub-samples for dose rate determination were dried at 120 °C and then manually homogenised prior to packing in Marinelli beakers (∼ 700 g); these were tightly wrapped and stored for at least 1 month prior to counting with a high-resolution gamma spectrometer to ensure equilibrium between radon and its daughter nuclides.

The concentrations of uranium, thorium, and potassium as given in Table 1 were converted into sediment dose rates using the conversion factors given in Guérin et al. (2011) and were modified by the life-time burial water content using the expressions given in Aitken (1985). For the aeolian sands (LUM 1140 and LUM 1141) a water content of 10 ± 5 % was used. LUM 1137 originates from the sand in the depression just above the till. The sand was water-logged most of its burial time; this made us use a water content of 25 ± 5 %. Similar conditions were most likely present in the sands from which sample LUM 470 was taken so that we assumed the same water content for this sample. According to the hydromorphic features observed in the soils and sands, the other samples must have undergone changing conditions from wet to dry, with the wet phases dominating. Therefore, we assumed a water content of 17.5 ± 5 % for the remaining

Table 1. Summary of radionuclide concentrations, total dose rates (DR), and optically stimulated luminescence information. D_e = equivalent dose, n = number of aliquots, SE = standard error, and σ_{OD} = overdispersion. The water contents used for dose rate calculation are given in the text.

					Quartz OSL				
Lab ID	^{40}K ± SE (%)	U ± SE (ppm)	Th ± SE (ppm)	DR ± SE (Gy ka^{-1})	D_e ± SE (Gy)	n	σ_{OD} ± SE (%)	Age ± SE (ka)	D_epIRIR$_{290}$/ D_e OSL
LUM 469	0.75 ± 0.02	0.51 ± 0.02	1.45 ± 0.05	0.94 ± 0.07	64 ± 3	20	14.4 ± 1.1	68 ± 6	1.50 ± 0.09
LUM 470	0.80 ± 0.02	0.40 ± 0.02	1.00 ± 0.05	0.84 ± 0.07	88 ± 7	20	33.4 ± 2.2	104 ± 12[a]	7.09 ± 1.35
LUM 498	0.93 ± 0.01	0.71 ± 0.02	2.17 ± 0.04	1.16 ± 0.08	76 ± 4	20	14.2 ± 1.3	66 ± 6	1.50 ± 0.09
LUM 1137	1.13 ± 0.01	0.89 ± 0.01	3.70 ± 0.02	1.38 ± 0.08	> 100[b]	12	33.5 ± 3.0	> 70[b]	2.72 ± 0.39
LUM 1138	0.62 ± 0.01	0.75 ± 0.01	1.86 ± 0.02	0.87 ± 0.07	74 ± 3	20	4.8 ± 2.0	86 ± 8	1.73 ± 0.11
LUM 1139	0.85 ± 0.01	0.79 ± 0.01	2.08 ± 0.02	1.11 ± 0.08	76 ± 4	12	13.0 ± 1.1	69 ± 6	1.49 ± 0.07
LUM 1140	0.68 ± 0.01	0.39 ± 0.01	1.17 ± 0.01	0.93 ± 0.08	56 ± 3	20	16.3 ± 1.1	60 ± 6	1.78 ± 0.24
LUM 1141	0.67 ± 0.01	0.59 ± 0.01	1.71 ± 0.01	1.01 ± 0.08	43 ± 2	20	25.4 ± 1.8	43 ± 4[a]	2.42 ± 0.16

[a] = poorly bleached, [b] = saturated and poorly bleached.

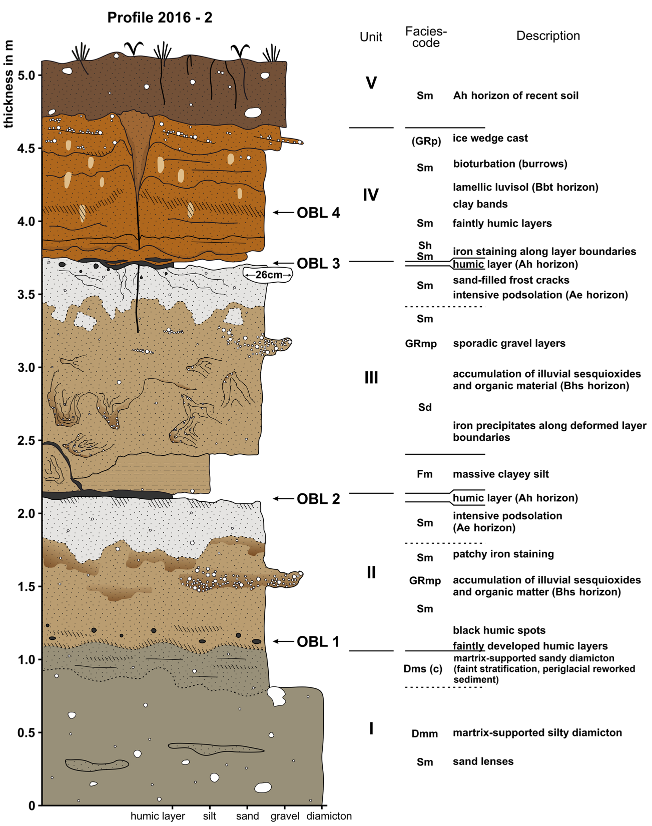

Figure 6. Detailed lithological log of profile 2016-2. The profile is subdivided into five lithological units I to V, for which a detailed description is given in the main text.

samples. The cosmic part of the dose rates was determined following Prescott and Hutton (1994) and added to the sediment dose rate, resulting in the total dose rates summarised in Table 1.

4.1.2 Equivalent dose measurements

The light-proof tubes containing the sub-sample for equivalent dose determination were opened in red light in the luminescence dating laboratory at the Leibniz Institute for Applied Geophysics, Hanover. The outer ends of each sample were discarded to ensure that any sediment exposed to light is not used.

After dry sieving, the dominating grain size fraction was chemically treated with hydrochloric acid (HCl), sodium oxalate, and hydrogen peroxide in order to remove carbonates, clay remnants, and organic matter, respectively. The samples were thoroughly washed with distilled water between each treatment step. After drying the samples at 50 °C, the quartz-rich fraction was separated from the potassium-rich feldspar (in the following called K-feldspar) fraction by heavy liquid separation using sodium polytungstate (quartz: $\rho \geq 2.62\,\mathrm{g\,cm^{-3}}$; K-feldspar: $\rho \leq 2.58\,\mathrm{g\,cm^{-3}}$). The dried quartz extracts were then purified using 40 % hydrofluoric acid for 1 h, followed by an HCl (30 %) treatment and washing with distilled water. The etched fractions were sieved again in order to avoid contamination with small particles.

The coarse-grained quartz extracts were mounted in a single layer on stainless steel discs as medium-sized (6 mm) aliquots using silicon oil as adhesive. Preference would have been given to smaller aliquots (e.g. Duller, 2008); however, the samples were not very sensitive, and we chose to increase the aliquot size for better analytical data. The luminescence measurements were made with automated Risø TL/OSL-DA-20 readers (Thomsen et al., 2006), equipped with calibrated ^{90}Sr/^{90}Y beta sources allowing for in situ beta irradiation. The quartz fractions were stimulated with an array of blue light-emitting diodes (LEDs), and the luminescence was detected through a 7.5 mm Hoya U-340 filter in the ultraviolet region.

The purity of the quartz extracts was checked by means of the IR/OSL depletion ratio (Duller, 2003); there was no

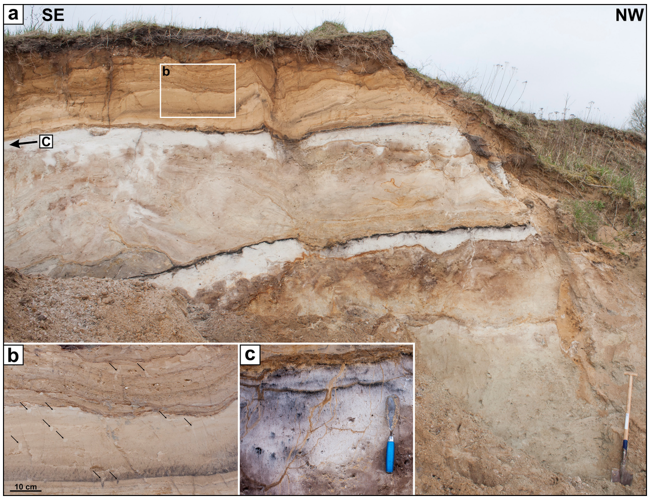

Figure 7. Detailed photographs of profile 2016-2. **(a)** Features of lithological units II and III. **(b)** Burrow-like structures identifiable by colour changes. **(c)** Base of OBL 3 with subvertical sand-filled cracks and fissures penetrating the underlying leached sands.

significant IRSL signal present, indicated by an IR depletion ratio within 5 % of unity. These initial measurements also indicated fast decay of the quartz luminescence signal; this is supported by a comparison with calibration quartz (Fig. 8a).

Preheat plateau measurements were conducted on two samples (LUM 498 and LUM 1141) to find the most appropriate temperature settings for the single-aliquot regenerative dose (SAR) procedure (Murray and Wintle, 2000). The preheat temperatures varied from 160 to 300 °C (three aliquots per sample), with the cut-heat temperature set 40 °C lower. The results of the tests are shown in Fig. 8. There is no clear plateau for either of the samples; between 240 and 260 °C there is not much variation, and the errors are small. It was chosen to set the preheat to 260 °C (10 s), and the OSL read-out was conducted at 125 °C for 40 s (Lx). After administering a fixed test dose of about 7 Gy to correct for potential sensitivity changes, the sample was heated to 220 °C, followed by another OSL read-out at 125 °C for 40 s (Tx). Each SAR cycle ended with a blue OSL clean-out at 280 °C (40 s) to minimise recuperation (Murray and Wintle, 2003). The initial 0.4 s minus a background of the subsequent 1.2 s was used to build the dose response curves, which were then fitted with a single exponential function.

Dose recovery tests were conducted on each sample. Three aliquots per quartz sample were bleached for 400 s with blue light, followed by a pause of 10 000 s and subsequently another 400 s illumination with blue light (inside the Risø TL/OSL DA-20 reader). The aliquots were then given a beta dose close to their natural dose and measured using the protocol described above.

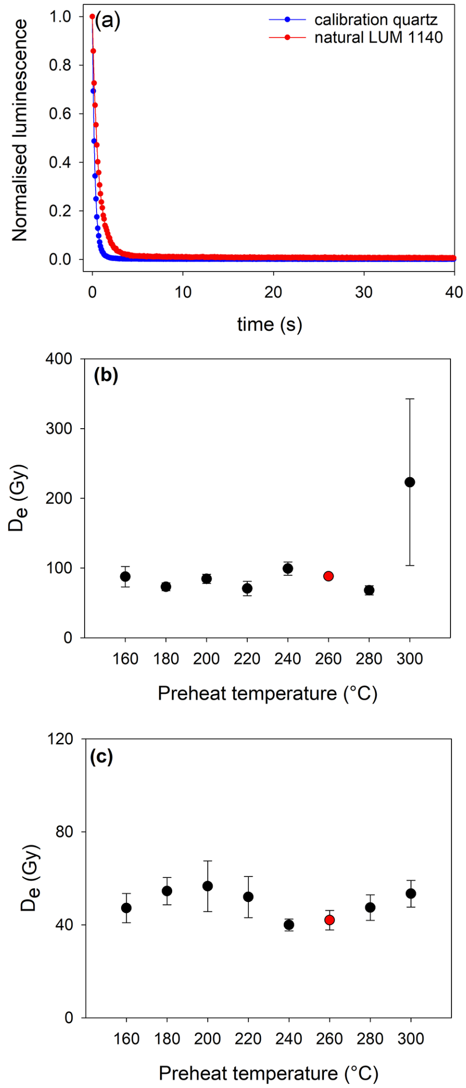

Figure 8. **(a)** Natural decay curve of one representative aliquot (sample LUM 1140) in comparison to calibration quartz (batch 30) showing that the quartz OSL signal from the Osterbylund samples is dominated by the fast component. Preheat plateaus for samples **(a)** LUM 498 and **(b)** LUM 1141. The temperatures shown in red circles are the preheat temperatures used in the D_e measurements and dose recovery experiments.

4.1.3 Testing for incomplete OSL signal resetting

In sedimentary settings in which transport and deposition are very rapid, the mineral grains might not have received sufficient daylight exposure prior to deposition. Thus, there may be a residual signal adding to the burial dose, which would result in age overestimation. While in aeolian sediments poor signal resetting is very unlikely (e.g. Roberts, 2008), there may be significant residual signals in glacial and glaciofluvial sediments (e.g. King et al., 2014).

Incomplete signal resetting can, for example, be investigated by (i) using a comparison of blue light OSL and infrared stimulated luminescence (IRSL) signals (e.g. Murray et al., 2012) as these two dosimeters show different bleaching behaviour and (ii) statistical parameters such as overdispersion (OD) (Galbraith et al., 1999).

To compare the quartz OSL results with IRSL of feldspar, the post-IR IRSL signal (Buylaert et al., 2012) on coarse-grained K-feldspar was measured on at least three aliquots per sample, prepared with a diameter of 2 mm on stainless steel discs. The aliquots were stimulated with IR LEDs, and the IRSL signals were collected through a blue filter combination (Corning 7-59 and Schott BG-39) in the blue-violet region of the light spectrum. The K-feldspar extracts were preheated at 320 °C (60 s) prior to IR (50 °C, 200 s) and post-IR IR stimulation (290 °C, 200 s). The test dose was set to about 50 % of the expected D_e (calculated from quartz D_e, taking into account the larger dose rate to feldspar). Dose response curves were fitted with a single exponential function, using the initial 2 s minus a background of the last 20 s of the decay curves. The pIRIR_{290}/OSL ratios are listed in Table 1.

The overdispersion, which expresses the amount of scatter in D_e distribution on top of the known uncertainties in measurements and analysis, was calculated for each quartz sample using Analyst version 4.57. The values are given as σ_{OD} in % and are summarised in Table 1.

4.2 ^{230}Th / U dating

For ^{230}Th/U dating all samples were prepared at the Leibniz Institute for Applied Geophysics, Hanover, for isotopic measurements following the leachate/leachate protocol of Schwarcz and Latham (1989) adopted to peat dissolution requirements (Sierralta et al., 2012; Waas et al., 2011). A double spike ^{233}U/^{236}U and a ^{229}Th spike were used for the quantification of uranium and thorium contents, respectively.

To construct the isochrons at least three sub-samples were prepared from the horizons of interest. Measurements were performed with a thermal ionisation mass spectrometer (Finnigan MAT 262 RPQ) applying the double filament technique with a peak jump routine. Mass fractionation was controlled during measurement by the double-spike ratio ^{233}U/^{236}U. All isotopic results are given in Table S1. Activities of the isotopes were calculated from the measured atomic ratios after normalisation to the double-spike ratio ^{233}U/^{236}U to correct for the thermal fractionation. The external reproducibility is 0.3 % (2σ) as determined by the measurements of the standard solution NBL U112A.

4.3 Pollen analysis

The material taken from the peat (profile 2005-2, Fig. 3) was prepared for palynological analysis in the laboratories of the Institute of Ecology of Leuphana University Lüneburg. About 1–3 g per sample was treated by standard palynological methods, which included dispersion with 10 % NaOH, carbonate removal by 10 % HCl, flotation to separate organics from the inorganic matrix using sodium metatungstate ($3Na_2 \cdot WO_4 \cdot 5WO_2 \cdot H_2O$), and acetolysis (Faegri and Iversen, 1989; Moore et al., 1991). One slide of 24 × 32 mm per sample was analysed under a transmitted-light microscope for pollen, non-pollen palynomorphs, and micro-charcoal particles at 40× magnification. Pollen and spores were identified using a reference collection of the Laboratory of the Institute of Ecology, Leuphana University Lüneburg, and the atlases of Moore et al. (1991) and Beug (2004). Percentages of all recorded taxa are based on a pollen sum composed of terrestrial taxa; pollen and spores deriving from cryptogams, aquatic plants, Ericaceae, and Cyperaceae were excluded. Due to bad pollen preservation the sum of 300 tree pollen per sample could not always be achieved; only 13 samples contained a statistically solid amount of pollen and spores. Pollen calculations for diagram construction were performed with the software packages Tilia, Tilia Graph, and Tilia View (Grimm, 1990).

5 Results

5.1 Dose rates and luminescence data

The total dose rates (Table 1) for the sands range from $0.87 \pm 0.07\,\mathrm{Gy\,ka^{-1}}$ (LUM 1138) to $1.38 \pm 0.08\,\mathrm{Gy\,ka^{-1}}$ (LUM 1137; Table 1) and are thus rather low. The low radioactivity in the sediment results in large sensitivity to water content assumptions. We did not undertake any field or laboratory water content measurements on our samples but put our observations in the field in perspective to dose rate ranges presented in the literature (Lüthgens et al., 2011; Kenzler et al., 2017; Pisarska-Jamroży et al., 2018) and from recent stationary measurements (tensiometer) from the Schuby station, run by the Landesamt für Landwirtschaft, Umwelt und ländliche Räume (LLUR), Flintbek (data from Marek Filipinski, personal communication, 2021), with absolute errors of ±5 % accounting for changes in water content over time. Nevertheless, the uncertainty of these assumptions on the final age may have an effect one must not lose sight on and may bias the results.

The satisfactory measurement performance of equivalent dose determination is shown by the good dose recovery test results. The mean measured to given doses range from 0.91 ± 0.01 (LUM 1139) to 1.09 ± 0.09 (LUM 470), with an average of 0.99 ± 0.02 ($n = 8$). In addition, recycling ratios are all within 10 % of unity, and recuperation is below 5 % for all aliquots, implying reliable D_e estimates for samples which are not in saturation (Murray and Wintle, 2003; Wintle and Murray, 2006).

The non-saturated (i.e. $< 2 \cdot D_0$; characteristic saturation limit; Wintle and Murray, 2006) D_e's range from 43 ± 2 Gy (LUM 1141) to 88 ± 7 Gy (LUM 470), resulting in ages between 43 ± 4 and 104 ± 12 ka, respectively. For the latter sample both the σ_{OD} of 33.4 ± 2.2 % and the pIRIR_{290}/OSL ratio of 7.09 ± 1.35 indicate, at first sight, very poor bleaching. In a well-bleached setting, the $\mathrm{pIRIR}_{290}/\mathrm{OSL}$ should be 1.7 or less, taking into account the about 0.7 Gy ka^{-1} larger total dose rate of feldspar due to the internal contribution of K and Rb and negligible anomalous fading for the pIRIR_{290} signal (Murray et al., 2012). Where the quartz D_e approaches saturation, the $\mathrm{pIRIR}_{290}/\mathrm{OSL}$ ratio starts to deviate and gets increasingly larger, because the OSL signal and correspondingly D_e cannot grow any larger. Therefore, for samples with quartz D_es in or close to saturation, no conclusion on the bleaching can be drawn using the $\mathrm{pIRIR}_{290}/\mathrm{OSL}$ ratio. The same holds true for overdispersion. For a well-bleached sample, it is generally assumed that the σ_{OD} is less than 20 % (e.g. Jacobs et al., 2008). Even though these assumptions are based on small aliquots and single grain measurements, these values may be used as approximations for medium aliquots. According to this, poor signal resetting may be present in sample LUM 1137, with an σ_{OD} of 33.5 ± 3.0 % (Table 1). In addition, the OSL signal is in saturation, resulting in a minimum age of > 70 ka. As mentioned above, it is difficult to judge whether the large overdispersion of this sample exclusively originates from poor bleaching. Murray et al. (2002) illustrated that the shape and width of dose distributions change significantly as the dose response curve approaches saturation. This effect may be observed here. The $\mathrm{pIRIR}_{290}/\mathrm{OSL}$ ratio of 2.72 ± 0.39 again implies insufficient signal resetting; however, with the OSL being in saturation the much larger pIRIR_{290} D_e reflected in the ratio is not necessarily due to poor resetting but may be the true dose. A conclusion on the effect of poor bleaching cannot be made for this sample. For all other samples, the σ_{OD} is well below 30 % (Table 1). The σ_{OD} of 25.4 ± 1.8 % from the top sample of profile 2004-1 (LUM 1141) evidences the admixture of older material, as observed in the field. The $\mathrm{pIRIR}_{290}/\mathrm{OSL}$ ratio for this sample is 2.42 ± 0.16 and thus supports the field observations and statistical data. The $\mathrm{pIRIR}_{290}/\mathrm{OSL}$ ratios for the other samples range from 1.49 ± 0.07 (LUM 1139) to 1.78 ± 0.24 (LUM 1140), indicating, together with the σ_{OD} values, good signal resetting for all those samples.

5.2 Dating of the peat

The uranium and thorium content range between 0.04–0.24 ppm and 0.12–0.64 ppm, respectively. The highest uranium content is found in the lowermost sample. The concentration of uranium decreases upwards and slightly increases to the top of the sampled horizons. A similar behaviour is observed for the thorium content. The activity ratios of $^{230}\mathrm{Th}/^{232}\mathrm{Th}$ are small (1.05–1.43), thus indicating a high amount of detrital material. Isochron dating is mandatory for such samples. The Rosholt-type I plot showing $^{230}\mathrm{Th}/^{232}\mathrm{Th}$ vs. $^{234}\mathrm{U}/^{232}\mathrm{Th}$ for both the black and brown peat layers is presented in Fig. S3. The scatter in data is large, and the best-fit line is highly variable. The Rosholt plot therefore provides first evidence for open-system behaviour of the two data sets.

To finally check for open-system behaviour Osmond plots were prepared and are presented in Figs. S4 and S5 (Osmond et al., 1970; Osmond and Ivanovich, 1992). The data points scatter much wider than analytical error would suggest, and the data imply open-system behaviour for the whole succession. Therefore, no age calculations can be performed (Geyh, 2008).

5.3 Palynological zonation

The zonation of the pollen diagram follows the pollen zonation of Behre (1962), Müller (1974), and Menke and Tynni (1984) for the Eemian of northern Germany (Fig. 9). For the zone description given here, we refer only to the subdivision of the Eemian of Rederstall (Menke and Tynni, 1984) due to its geographical vicinity to Osterbylund. The depths given with the zones are the sampling depths in the peat from profile 2005-2 (Fig. 3).

- Zone E IVb (1.45–1.95 m). This part of the diagram is characterised by high amounts of *Corylus* between 20 %–40 % and *Tilia* (around 20 %), whereas *Taxus* reaches values of about 10 %. *Viscum*, *Ilex*, *Hedera helix*, as well as *Buxus*, reach higher values in comparison to the preceding and following zone. *Quercus* and *Ulmus* are present with amounts below 10 %; *Picea* and *Carpinus* pollen are occurring with even smaller amounts. In the lower part of the zone Polypodiaceae spores are abundant, and Sphagnum spores occur with higher amounts during this zone compared to the rest of the investigated material. Towards the top of the zone the curves of *Picea* and particularly of *Carpinus* strongly increase, whereas *Tilia* drops below 10 %. During the entire zone *Alnus* does not reach more than 20 %. The overlap of *Tilia* and *Corylus* decreases, and *Carpinus* spread marks the upper boundary of zone E IVb.

- Zone E V (1.45–0.75 m). This zone is strongly dominated by *Carpinus* (up to 40 %), decreasing towards the top of the zone, and by *Picea* which increases parallel to the drop of *Carpinus*. The amounts of *Betula* have increased up to 20 %, whereas *Corylus* has dropped below about 5 %, disappearing entirely towards the top of the zone. *Alnus* is increasing (up to 40 %) in the lower part of the zone and decreasing towards its top. *Abies* is found to occur continuously from about the middle part of the zone. *Quercus* slightly increases again towards the top of zone. *Taxus* is found in small amounts associated with the start of the *Abies* curve. *Ilex*, *Viscum*, and *Buxus* are only present in small amounts. *Myrica* and Ericaceae, mainly *Calluna*, as well as Poaceae and further non-arboreal pollen (NAP), increase as well. Ascomycete spores and the sum of unidentified spores, probably deriving from mosses, reach rather high values. The upper boundary of Zone V is drawn at the drop

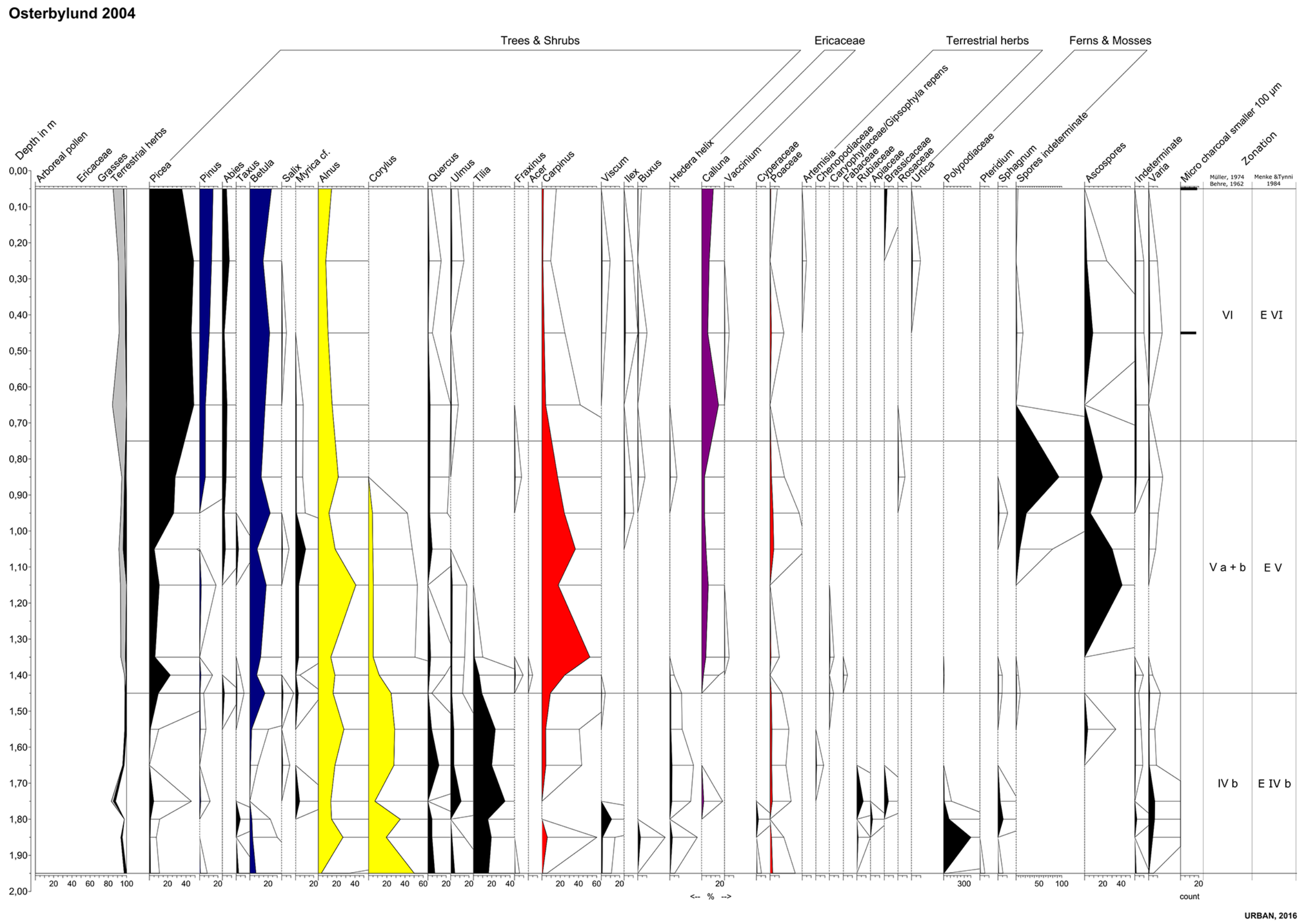

Figure 9. Pollen diagram from the brown and black peats sampled in 2004 (profile 2005-2). Pollen calculations for diagram construction were performed with the software packages Tilia, Tilia Graph, and Tilia View (Grimm, 1990).

of the *Carpinus* curve below 10 % and the increase of *Picea*, *Pinus*, and *Abies*.

- Zone E VI (0.05–0.75 m). The youngest pollen zone of the peat layer is mainly characterised by *Picea*, *Pinus*, *Abies*, and *Betula*. *Picea* reaches high amounts of about 40 %, and the *Pinus* curve is only increasing towards the top of the zone. The curves of *Ulmus*, *Quercus*, and *Carpinus* dropped down to 1 % and below 1 %. *Alnus* is still present with lower amounts of around 10 %. Within the NAP the first occurrence of *Artemisia* is as notable as a remarkable increase of *Calluna* of up to nearly 20 %.

6 Discussion

The correlation between the individual profiles is based on the humic layers representing palaeosols (OBL 1–4) and the OSL ages. The sedimentological investigations in 2016 lead to the conclusion that the lower diamicton is a subglacial traction till (Evans et al., 2006) deposited during a Saalian advance of the Scandinavian Ice Sheet. The sand lenses present (Figs. 5 and 6) could either be formed by supraglacial, englacial, or subglacial drainage systems and had been subsequently incorporated into the till. The faintly stratified upper part of unit I (Fig. 6) could either be a supraglacial melt-out till (Lukas and Rother, 2016) or the result of periglacial reworking processes after or during an ice decaying phase.

OBL 1 is to be correlated with the up to 2 m thick peat found during the excavations in profiles 2003 and 2005-2, filling a depression on the surface of the till (see Figs. 2 and 3). Due to the open-system behaviour of the peat, no $^{230}Th/U$ ages can be presented. The OSL age of 86 ± 8 ka (LUM 1138; Fig. 3) from well-bleached sediments well above OBL 1 shows that the peat is older than the Odderade interstadial (Fig. 10). The corresponding sample LUM 470 is poorly bleached and cannot add any information. Further age constraint is exclusively provided by the pollen analysis, as the OSL sample (LUM 1137) underlying the peat is

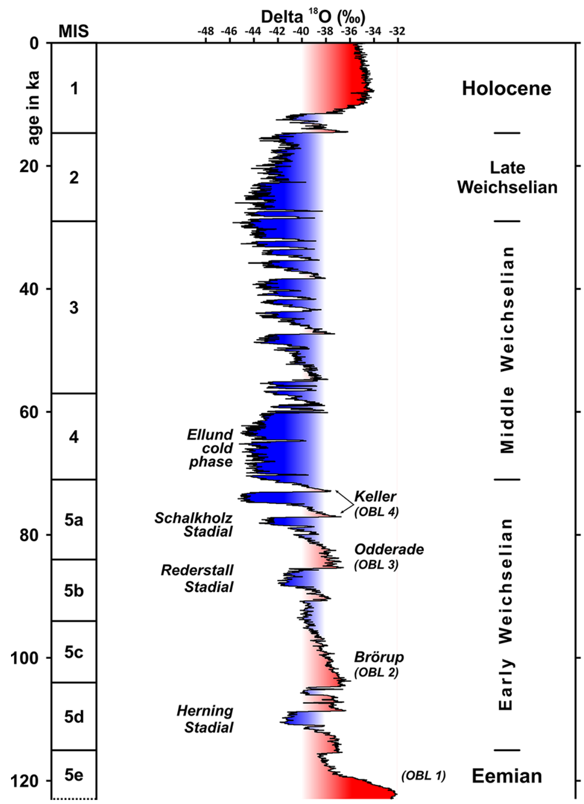

Figure 10. Oxygen isotope curve (NGRIP Community Members, 2004) showing the marine isotope stages (MIS) and Late Pleistocene subdivision. After the Eemian (5e; OBL 1) three phases warm enough for soil formation (interstadials) are present and in Osterbylund represented by palaeosols: Brörup = OBL 2, Odderade = OBL 3, and Keller = OBL 4.

both poorly bleached and saturated; no accurate age can be presented for this sample.

The onset of the *Corylus*, *Tilia*, and *Taxus* curves and the maximum distribution of *Corylus* characteristic for Eemian pollen zone E IVa (Menke and Tynni, 1984) are not recorded in the peat layer of Osterbylund. Peat growth at the investigated location started only during the second half of pollen zone IV, the *Tilia* phase of Menke and Tynni (1984) which is characterised by the dominance of *Tilia* and of *Corylus*, next to *Ulmus* and *Quercus*. *Taxus* only reaches values of about 10 % during E IVb at Osterbylund, further indicating that peat growth started only after the pronounced *Taxus* phase (Menke and Tynni, 1986) during the younger part of zone IVb. This zone corresponds to pollen zone IVb of Behre (1962) and Müller (1974), respectively. According to varve counts of Eemian deposits at Munster-Breloh and estimates of the duration of pollen zones of Müller (1974), zone IVb should have had a duration of 1100 years.

The following zone, which seems to be fully preserved, corresponds to the *Carpinus* zone E V (Menke and Tynni, 1984) and can be correlated with pollen zones Va and Vb of Müller (1974). The occurrence of *Viscum*, *Hedera helix*, and *Buxus* in this and the following zones has been recorded from other western European Eemian sites (Litt, 1994; Zagwijn, 1996; Kühl and Litt, 2007) including adjacent areas from northern Germany (Behre, 1962; Behre and Lade, 1986; Müller, 1974; Menke and Tynni, 1984; Ziemus, 1989; Behre et al., 2005) and characterises the thermal optimum of the interglacial. Müller (1974) has estimated the duration of zone E V, Va and Vb, to about 4000 years.

The youngest recorded pollen zone in Osterbylund, correlated with zone E VI (Menke and Tynni, 1984) and zone VI of Müller (1974), shows a decrease of deciduous thermophilous trees and the expansion of *Picea*, *Pinus*, *Abies*, and *Betula*, marking the beginning of the termination of the interglacial. The overrepresentation of *Picea* in the profile of Osterbylund compared to other profiles from northern Germany might be caused by local peat bog conditions favouring spruce-rich forest swamps (Menke and Tynni, 1984). This interpretation and the large occurrence of *Calluna* in the upper zone from about 0.75 m upwards are in agreement with a change in peat composition. Compared to central or southern German locations (Grüger, 1979; Urban et al., 1991; Litt, 1994; Litt et al., 1996), the relative low representation of *Abies* during this late interglacial phase at Osterbylund and at other northern German sites, e.g. Lichtenberg (Veil et al., 1994; Hein et al., 2021), is caused by the northern limit of the distribution area of *Abies* which lay in Jutland during that time (Zagwijn, 1989). The transition to pollen zone VII and the entire pollen zone VII, representing the end of the interglacial, are not recorded as the uppermost part of the peat has been eroded. Müller (1974) estimated the duration of Eemian pollen Zone VI (E VI after Menke and Tynni, 1984) to about 1000 years, whereas Kühl and Litt (2007) published a revised extrapolation of 2000 years.

According to these time estimates, the duration of the Eemian peat layer formation at Osterbylund, which comprises pollen zones E IVb, E V, and most parts of E VI (Menke and Tynni, 1984; Müller, 1974), can roughly be estimated to about 6000 years. Turner (2002) pointed out that the entire duration of the terrestrial Eemian north of the Alps or Pyrenees was less than 13 000 years, which matches the results of Urban (2007) who proposed a duration of 10 ka for pollen zones E1–E6 of the Eemian *sensu stricto* (Zagwijn, 1961) and 10 000 years for the entire interglacial. The terrestrial Eemian has been correlated with MIS5e of the deep-sea chronology (Shackleton, 1969, Mangerud et al., 1979; Fig. 10) and spans the time between about 126 to 115 ka (summarised in Urban, 2007). The age of the peat layer of Osterbylund therefore can be estimated to be about 120 ka.

The reworking of the OBL 1 palaeosol will thus have occurred after MIS5e. Due to the soil formation processes and the resulting post-depositional changes, the interpretation of the depositional environment cannot be reconstructed unambiguously. Slope movements under periglacial conditions are conceivable (Stephan et al., 2017), which filled former depressions of the landscape topography (Guerra et al., 2017). In addition, denudation processes may have partly contributed to the deposition, at least of the lower and middle part of unit II (Fig. 6). In this context, the occurrence of channel-like structures filled with granules is of importance. The better sorting of the upper sandy part of unit II might indicate that aeolian processes have also contributed to the deposition. In unit II the Ah horizon at the top (= OBL 2) illustrates a halt in sedimentation and consequently a hiatus; at least some erosion of the former Ah horizon is likely. The age of 86 ± 8 ka (LUM 1138, Fig. 3) from just below OBL 2 puts the formation of this palaeosol either into the Brörup or the Odderade interstadial (Fig. 10). Considering that there is no indication of a hiatus, it is more likely that OBL 2 is to be correlated with the Brörup interstadial.

The formation of unit III (Fig. 6), which brackets OBL 2 and OBL 3 (Figs. 3 and 4), is probably related to slope movements (Stephan et al., 2017, and their Fig. 7) under periglacial conditions (Millar, 2013). Especially soft sediment deformation structures indicate gravity-induced failures along the basin slope (Blair and McPherson, 2009). This assumption is supported by the outsized clasts within the upper part of this sand package, which have been transported downslope. Furthermore, the sand-filled cracks and fissures suggest freeze–thaw action and the existence of permafrost and thus subarctic conditions. The seasonal thawing of the active layer induced frost creeping of larger stones and boulders down the slope. Some of these boulders show fragmentation due to volume expansion of freezing water in fissures. This clearly implies cold climate conditions during the deposition of the sandy part of this unit. OBL 3 developed most likely under an interstadial climate after 69 ± 6 ka (LUM 1139), which is the age of the underlying sand. The equivalent sample LUM 469 was dated to 68 ± 6 ka, supporting the age constrain. According to these dating results, one could assign the soil formation to either the Odderade or Keller interstadial (Fig. 10).

Above the OBL 3 palaeosol there are aeolian sands, for which good OSL signal resetting had to be expected. While the age of 60 ± 6 ka (LUM 1140) just below the humic horizon of OBL 4 (Fig. 3) seems reliable according to the OSL testing and statistical parameters, the sand covering the palaeosol was poorly bleached, which results in a possibly overestimated age of 43 ± 4 ka (LUM 1141). If that age was the true depositional age, it would fall into MIS3, thus implying a significant hiatus, for which no field evidence was present. From the sedimentological observations it is not possible to reconstruct a distinct depositional environment to these sands (Fig. 6). The burrow-like structures across this unit display the occurrence of digging animals such as rodents. If true, this could indicate a tundra-steppe ecosystem in a periglacial landscape (Dupal et al., 2013). This assumption is supported by the existence of ice wedge casts. If such an ice wedge was accidentally sampled, even younger material than representative for the sandy layer could have been sampled. It is therefore not possible to finally conclude on the age of the sand overlying OBL 4.

However, there are no phases warm enough for soil formation during this period, and despite this unknown, assignment of this humic horizon to the Keller interstadial (Fig. 10) seems feasible, thereby assigning OBL 3 to the Odderade interstadial. The sandy deposits of the upper section of unit VI would therefore belong to the Ellund cold phase or even younger (Fig. 10).

Because of the unequivocal palynological assignment of the peat to the Eemian, an upper limit to the age of the palaeosols (OBL 2–4) above the peat is clear. Thus, the entire push moraine complex (Fig. 1) has to be of Saalian age. This observation makes a Weichselian glacial margin even further west unlikely, i.e. south of the Danish border, as discussed by Houmark-Nielsen (2007). All palaeosols formed during the early Weichselian (MIS 5a–d), which is in agreement with the observations of Gripp et al. (1965). While the pollen data provide a clear view on the age of OBL 1, the luminescence data cannot be interpreted unambiguously; they have to be seen in their entirety and not on their own.

7 Conclusions

The aim of this study was not only to unravel the age of the push moraine complex Wallsbüll-Böxlund, Schleswig-Holstein, but also to assign the peat and palaeosols present in depressions in Osterbylund to interglacials and interstadials in order to add another jigsaw piece to the understanding of the glacial history in the western Baltic region.

The attempt to date the peat layers using ^{230}Th/U dating failed due to the open-system behaviour of both the brown and the black peat. However, the pollen analyses allowed for clear assignment of the peat and thus of the palaeosol OBL 1 to the Eemian. This coincides with the saturated and correspondingly old age of the sands underlying the peat; the sands above the peat were dated to the early Weichselian. While for palaeosol OBL 2 the assignment to the Brörup interstadial is clear, the correlation of the palaeosols OBL 3 and OBL 4 to any interstadial is hampered due to the limited luminescence data available. Poor luminescence signal resetting especially of the sands above OBL 4 makes an assessment of an upper limit for the palaeosol formation difficult. However, from the field, as well as luminescence data, it is most likely that OBL 3 formed during the Odderade interstadial and OBL 4 during the Keller interstadial. This observation contrasts previous findings claiming that only two post-Eemian thermomers, i.e. Brörup and Odderade interstadials, are to be expected due to the insolation of the Northern Hemisphere. The weakly developed OBL 4 seems to indicate though that warm oceanic currents in the North Atlantic and correspondingly in northern Germany resulted in another – terrestrial – third weak thermomer and is thus not unique to marine settings and ice cores.

With Eemian up to early Weichselian ages of the peat and palaeosols, filling the depression it is evident that the push moraine complex is of Saalian age; a Weichselian ice margin further in the west as assumed in other studies is therefore unlikely. It is certainly worth investigating the position and ages of the Weichselian ice margins in the future as this would complement the studies from Denmark and NE Germany.

Data availability. Data are available from the authors upon request.

Sample availability. Treated and untreated material for luminescence dating, as well as dose rate samples, are stored at the Leibniz Institute for Applied Geophysics. Remaining material from the peat is stored at both Leibniz Institute for Applied Geophysics (^{230}Th/U dating) and Leuphana University Lüneburg (pollen analysis).

Supplement. The supplement related to this article is available online at: https://doi.org/10.5194/egqsj-72-57-2023-supplement.

Author contributions. HJS and MF initiated the study. HSJ, MF, MS, BU, and MK investigated the sites in the field and took samples. CT undertook the luminescence dating. MS was responsible for ^{230}Th/U dating. BU analysed and interpreted the pollen. CT and HJS prepared the manuscript with contributions from MS, BU, and MK.

Competing interests. The contact author has declared that none of the authors has any competing interests.

Disclaimer. Publisher's note: Copernicus Publications remains neutral with regard to jurisdictional claims in published maps and institutional affiliations.

Acknowledgements. The technical assistance of Sonja Riemenschneider, Gudrun Drewes, Sabine Mogwitz, and Petra Posimowski (LIAG) is very much appreciated. Margot Böse and Tony Reimann are thanked for their constructive comments, which helped to improve the manuscript. Christopher Lüthgens is thanked for the editorial handling.

Financial support. This research has been supported by the Deutsche Forschungsgemeinschaft (grant no. KE 2023/2–1).

Review statement. This paper was edited by Christopher Lüthgens and reviewed by Margot Böse and Tony Reimann.

References

Ad-hoc-Arbeitsgruppe Boden (AG Boden): Bodenkundliche Kartieranleitung, edited by: Bundesanstalt für Geowissenschaften und Rohstoffe in Zusammenarbeit mit den Staatlichen Geologischen Diensten, Hannover, 5th edn., 438 pp., ISBN 9783510959204, 2005.

Aitken, M. J.: Thermoluminescence Dating, Academic Press, London, 351 pp., 1985.

Behre, K.-E.: Pollen- und diatomeenanalytische Untersuchungen an letztinterglazialen Kieselgurlagern der Lüneburger Heide, Flora, 152, 325–370, https://doi.org/10.1016/S0367-1615(17)32595-8, 1962.

Behre, K.-E. and Lade, U.: Eine Folge von Eem und 4 Weichsel-Interstadialen in Oerel/Niedersachsen und ihr Vegetationsablauf, E&G Quaternary Sci. J., 36, 11–36, https://doi.org/10.3285/eg.36.1.02, 1986.

Behre, K.-E., Hölzer, A., and Lemdahl, G.: Botanical macroremains and insects from the Eemian and Weichselian site of Oerel (northwest Germany) and their evidence for the history of climate, Veget. Hist. Archaeobot. 14, 31–53, 2005.

Beug, H. J.: Leitfaden der Pollenbestimmung für Mitteleuropa und angrenzende Gebiete, Verlag Dr. Friedrich Pfeil, München, Germany, 542 pp., 2004.

Blair, T. C. and McPherson, J. G.: Processes and forms of alluvial fans, in: Geomorphology of desert environments, edited by: Parsons, A. J. and Abrahams, A. D., 413–467, https://doi.org/10.1007/978-1-4020-5719-9_14, 2009.

Buylaert, J.-P., Jain, M., Murray, A. S., Thomsen, K. J., Thiel, C., and Sohbati, R.: A robust feldspar luminescence dating method for Middle and Late Pleistocene sediments, Boreas, 41, 435–451, 2012.

Duller, G. A. T.: Distinguishing quartz and feldspar in single grain luminescence measurements, Rad. Measure., 37, 161–165, 2003.

Duller, G. A. T.: Single-grain optical dating of Quaternary sediments: why aliquot size matters in luminescence dating, Boreas, 37, 589–612, 2008.

Dupal, T. A., Andrenko, O. V., and Vinogradov, V. V.: Mammals of the Periglacial Hyperzone of the End of the Pleistocene and Formation of the Modern Rodent Fauna in the Mountains, Contemp. Prob. Ecol., 6, 94–104, 2013.

Evans, D. J. A., Phillips, E. R., Hiemstra, J. F., and Auton, C. A.: Subglacial till: Formation, sedimentary characteristics and classification, Earth-Sci. Rev,. 78, 115–176, 2006.

Faegri, K. and Iversen, J.: Textbook of Pollen Analysis, edited by: Faegri, K., Kaland, P. E., and Krzywinski, K., 4th Edn., John Wiley and Sons, Chichester, 328 pp., 1989.

Galbraith, R. F., Roberts, R. G., Laslett, G. M., Yoshida, H., and Olley, J. M.: Optical dating of single and multiple grains of quartz from Jinmium rock shelter, Northern Australia: Part I: experimental design and statistical models, Archaeometry, 41, 339–364, 1999.

Geyh, M. A.: 230Th/U-dating of intergarcial and interstadial fen peat and lignite: Potential limits, E&G Quaternary Sci. J., 57, 77–94, https://doi.org/10.3285/eg.57.1-2.4, 2008.

Grimm, E. C.: TILIA and TILIA. GRAPH: PC spreadsheet and graphics software for pollen data (Version 2.0.b.4), INQUA – Commission for the Study of the Holocene, Working-Group on Data-Handling Methods, Newsletter 4, 5–7, 1990.

Gripp, K., Dücker, A., and Johannsen, A.: Ekskursion til Sild, Slesvig og Øst-Holstein, Meddelelser fra Dansk Geologisk Forening, 15, 603–617, 1965.

Grüger, E.: Spätriss, Riss/Würm und Frühwürm am Samerberg in Oberbayern – ein vegetationsgeschichtlicher Beitrag zur Gliederung des Jungpleistozäns, Geol. Bavarica, 80, 5–64, 1979.

Guérin, G., Mercier, N., and Adamiec, G.: Dose-rate conversion factors: update, Ancient TL, 29, 5–8, 2011.

Guerra, A. J. T., Fullen, M. A., Jorge, M. C. O., Bezerra, J. F. R., and Shokr, M. S.: Slope Processes, Mass Movement and Soil Erosion: A Review, Pedosphere, 27, 27–41, 2017.

Hein, M., Urban, B., Tanner, D. C., Buness, A. H., Tucci, M., Hoelzmann, P., Dietel, S., Kaniecki, M., Schultz, J., Kasper, T., von Suchodoletz, H., Schwalb, A., Weiss, M., and Lauer, T.: Eemian landscape response to climatic shifts and evidence for northerly Neanderthal occupation at a palaeolake margin in Northern Germany, Earth Surf. Process. Landf., 2021, 2884–2901, https://doi.org/10.1002/esp.5219, 2021.

Houmark-Nielsen, M.: Extent and age of Middle and Late Pleistocene glaciations and periglacial episodes in southern Jylland, Denmark. DGF, B. Geol. Soc. Denmark, 50, 9–35, 2007.

Houmark-Nielsen, M.: Extent, age and dynamics of Marine Isotope Stage 3 glaciations in the southwestern Baltic Basin, Boreas, 39, 343–359, 2010.

Hughes, A. L. C., Gyllencreutz, R., Lohne, Ø. S., Mangerud, J., and Svendsen, J. I.: The last Eurasian ice sheets – a chronological database and time-slice reconstruction, DATED-1, Boreas, 45, 1–45, 2016.

Jacobs, Z., Roberts, R. G., Galbraith, R. F., Deacon, H. J., Grün, R., Mackay, A., Mitchell, P., Vogelsang, R., and Wadley, L.: Ages for the Middle Stone Age of southern Africa: implications for human behavior and dispersal, Science, 322, 733–735, 2008.

Kenzler, M., Tsukamoto, S., Meng, S., Frechen, M., and Hüneke, H.: New age constraints from the SW Baltic Sea area – implications for Scandinavian Ice Sheet dynamics and palaeoenvironmental conditions during MIS 3 and early MIS 2, Boreas, 46, 34–52, 2017.

Kenzler, M., Rother, H., Hüneke, H., Frenzel, P., Strahl, J., Tsukamoto, S., Li, Y., Meng, S., Gallas, J., and Frechen, M.: A multi-proxy palaeoenvironmental and geochronological reconstruction of the Saalian-Eemian-Weichselian succession at Klein Klütz Höved, NE Germany, Boreas, 47, 114–136, https://doi.org/10.1111/bor.12255, 2018.

King, G. E., Robinson, R. A. J., and Finch, A. A.: Towards successful OSL sampling strategies in glacial environments: deciphering the influence of depositional processes on bleaching of modern glacial sediments from Jostedalen, Southern Norway, Quaternary Sci. Rev., 89, 94–107, 2014.

Kühl, N. and Litt, T.: Quantitative Time-Series Reconstruction of Holsteinian and Eemian Temperatures Using Botanical Data, in: The Climate of Past Interglacials, edited by: Sirocko, F., Litt, T., Claussen, M., and Sanchez-Goni, M. F., 239–254, https://doi.org/10.1016/S1571-0866(07)80041-8, 2007.

Litt, T.: Paläoökologie, Paläobotanik und Stratigraphie des Jungquartärs im nordmitteleuropäischen Tiefland, Dissertationes Botanicae 227, Cramer, Berlin-Stuttgart, 185 pp., ISBN 978-3-443-64139-9, 1994.

Litt, T., Junge, F. W., and Böttger, T.: Climate during the Eemian in north-central Europe – a critical review of the palaeobotanical and stable isotope data from central Germany, Veg. Histor. Archaeob., 5, 247–256, 1996.

Lukas, S. and Rother, H.: Moränen versus Till: Empfehlungen für die Beschreibung, Interpretation und Klassifikation glazialer Landformen und Sedimente, E&G Quaternary Sci. J., 65, 95–112, https://doi.org/10.3285/eg.65.2.01, 2016.

Lüthgens, C., Böse, M., and Preusser, F.: Age of the Pomeranian ice-marginal position in northeastern Germany determined by Optically Stimulated Luminescence (OSL) dating of glaciofluvial sediments, Boreas, 40, 598–615, 2011.

Lüthgens, C., Hardt, J., and Böse, M.: Proposing a new conceptual model for the reconstruction of ice dynamics in the SW sector of the Scandinavian Ice Sheet (SIS) based on the reinterpretation of published data and new evidence from optically stimulated luminescence (OSL) dating, E&G Quaternary Sci. J., 69, 201–223, https://doi.org/10.5194/egqsj-69-201-2020, 2020.

Mangerud, J., Sonstegaard, E., and Sejrup, H. P.: Correlation of the Eemian (interglacial) stage and the deep-sea oxygen-isotope stratigraphy, Nature, 277, 189–192, 1979.

Menke, B. and Tynni, R.: Das Eeminterglazial und das Weichselfrühglazial von Rederstall/Dithmarschen und ihre Bedeutung für die mitteleuropäische Jungpleistozän-Gliederung, Geologisches Jahrbuch A, 7, 1–120, 1984.

Millar, S.: Mass movement processes in the periglacial environment, in: Treatise on Geomorphology, edited by: Shroder, J., Giardino, R., and Harbor, J., Academic Press, San Diego, CA, Vol. 8, Glacial and Periglacial Geomorphology, 374–391, https://doi.org/10.1016/B978-0-12-374739-6.00217-7, 2013.

Moore P. D., Webb J. A., and Collins, M. E.: Pollen analysis, Oxford, 216 pp., 1991.

Müller, H.: Pollenanalytische Untersuchungen und Jahresschichtenzählungen an der eem-zeitlichen Kieselgur von Bispingen/Luhe, Geologisches Jahrbuch A, 21, 149–169, 1974.

Murray, A. S. and Wintle, A. G.: Luminescence dating of quartz using an improved single-aliquot regenerative-dose protocol, Rad. Measure., 32, 57–73, 2000.

Murray, A. S. and Wintle, A. G.: The single aliquot regenerative dose protocol: potential for improvements in reliability, Rad. Measure., 37, 377–381, 2003.

Murray, A. S., Wintle, A. G., and Wallinga, J.: Dose estimation in using quartz OSL in the nonlinear region of the growth curve, Rad. Protect. Dosim., 101, 371–374, 2002.

Murray, A. S., Thomsen, K. J., Masuda, N., Buylaert, J.-P., and Jain, M.: Identifying well-bleached quartz using the different bleaching rates of quartz and feldspar luminescence signals, Rad. Measure., 47, 688–695, 2012.

NGRIP Community Members: High-resolution record of Northern Hemisphere climate extending into the last interglacial period, Nature, 431, 147–151, 2004.

Osmond, J. K. and Ivanovich, M.: Uranium-series mobilization and surface hydrology, in: Uranium-series disequilibrium, edited by: Ivanovich, M. and Harmon, R. S., 2nd ed. Oxford Science Publications, 259–289, RN:25066325, 1992.

Osmond, J. K., May, J. P., and Tanner, W. F.: Age of the Cape Kennedy barrier-and-lagoon complex, J. Geophys. Res., 75, 5459–5468, 1970.

Pisarska-Jamroży, M., Belzyt, S., Börner, A., Hoffmann, G., Hüneke, H., Kenzler, M., Obst, K., Rother, H., and Van Loon, A. T.: Evidence from seismites for glacioisostatically induced crustal faulting in front of an advancing land-ice mass (Rügen Island, SW Baltic Sea), Tectonophysics, 745, 338–348, 2018.

Prescott, J. R. and Hutton, J. T.: Cosmic ray contributions to dose rates for luminescence and ESR dating: large depths and long-term variations, Rad. Measure., 23, 497–500, https://doi.org/10.1016/1350-4487(94)90086-8, 1994.

Rinterknecht, V., Börner, A., Bourlès, D., and Braucher, R.: Cosmogenic ^{10}Be dating of ice sheet marginal belts in Mecklenburg-Vorpommern, Western Pomerania (northeast Germany), Quat. Geochronol., 19, 42–51, 2014.

Roberts, H. M.: The development and application of luminescence dating to loess deposits: a perspective on the past, present and future, Boreas, 37, 483–507, 2008.

Schwarcz, H. P. and Latham, A. G.: Dirty calcites: 1. uranium series dating of contaminated calcite using leachates alone, Chem. Geol. (Isotope Geoscience Letters), 80, 35–43, 1989.

Seierstad, I. K., Abbott, P. M., Bigler, M., Blunier, T., Bourne, A. J., Brook, E., Buchardt, S. L., Buizert, C., Clausen, H. B., Cook, E., Dahl-Jensen, D., Davies, S. M., Guillevic, M., Johnsen, S. J., Pedersen, D. S., Popp, T. J., Rasmussen, S. O., Severinghaus, J. P., and Vinther, B. M.: Consistently dated records from the Greenland GRIP, GISP2 and NGRIP ice cores for the past 104 ka reveal regional millennial-scale δ^{18}O gradients with possible Heinrich event imprint, Quaternary Sci. Rev., 106, 29–46, 2014.

Shackleton, N. J.: The last interglacial in the marine and terrestrial records, P. Roy. Soc. London 174, 134–154, 1969.

Sierralta, M., Urban, B., and Frechen, M.: ^{230}Th/U dating results from opencast mine Schöningen. Forschungen zur Urgeschichte aus dem Tagebau von Schöningen, Band 1, 143–154, https://doi.org/10.11588/propylaeum.465, 2012.

Stephan, H. J.: Osterbylund – Aufschlusskurzbericht 1121/33-I, 2 p., Flintbek (Geologisches Landesarchiv, LLUR), https://doi.org/10.1016/S1571-0866(07)80053-4, 1988.

Stephan, H.-J., Burbaum, B., Frechen, M., Kenzler, M, Krienke, K., Thiel, C., Lungershausen, U., Tummuscheit, A., Urban, B., and Sierralta, M.: Exkursion E2: Quartärgeologie und Archäologie im Norden Schleswig-Holsteins. Tagungsband und Exkursionsführer – 80. Tagung der Arbeitsgemeinschaft Norddeutscher Geologen, 6–9 June 2017, Rendsburg, 123–150, 2017.

Stremme, H. E.: Quartär-Exkursionen in Schleswig-Holstein zur 7th Session of the International Geological Correlation Programme, Project 24, Quaternary Glaciations in the Northern Hemisphere Schleswig-Holstein, Germany (21–23 September 1980), 1981.

Stremme, H. E.: Die Korrelation quartärer Paläoböden in Nordwest-Deutschland, Zeitschrift für Geomorphologie, Suppl.-Vol. 61, 89-100, ISBN 978-3-443-21061-8, 1986.

Stremme, H. E. and Weinhold, H.: Böxlund (westlich von Flensburg), fossile Böden der Treene-Warmzeit mit Stauchung durch Warthe-Gletscher und fossile Böden der Eem-Warmzeit, mit einem Beitrag von S. Christensen, in: Quartär-Exkursionen/ Quaternary-Excursions in Schleswig-Holstein, edited by: Stremme, H. E. and Menke, B., 79–89 pp., 1980.

Stremme, H. E., Felix-Henningsen, P., Weinhold, H., and Christensen, S.: Paläoböden in Schleswig-Holstein, Geologisches Jahrbuch F14, 311–361, 1982.

Thomsen, K. J., Bøtter-Jensen, L., Denby, P. M., Moska, P., and Murray, A. S.: Developments in luminescence measurement techniques, Rad. Measure., 41, 768–773, 2006.

Turner, C.: Problems of the Duration of the Eemian Interglacial in Europe North of the Alps, Quaternary Res., 58, 45–48, 2002.

Urban, B.: Interglacial pollen records from schöningen, North Germany, in: The Climate of the Past Interglacials, edited by: Sirocko, F., Litt, T., Claussen, M., and Sanchez-Goni, M. F., 417–444, 2007.

Urban, B., Elsner, H., Hölzer, A., Mania, D., and Albrecht, B.: Eine eem- und frühweichselzeitliche Abfolge im Tagebau Schöningen, Landkreis Helmstedt, Eiszeitalter und Gegenwart (E&G) 41, 85–99, 1991.

Veil, S., Breest, K., Höfle, H.-C., Meyer, H.-H., Plisson, H., Urban-Küttel, B., Wagner, G., and Zöller, L.: Ein mittelpaläolithischer Fundplatz aus der Weichsel-Kaltzeit bei Lichtenberg, Lkr. Lüchow-Dannenberg, Germania, 72, 1–66, 1994.

Waas, D., Kleinmann, A., and Lepper, J.: Uranium-series dating of fen peat horizons from pit Nachtigall in northern Germany, Quaternary Int., 241, 111–124, 2011.

Wintle, A. G. and Murray, A. S.: A review of quartz optically stimulated luminescence characteristics and their relevance in single-aliquot regeneration dating protocols, Rad. Measure., 41, 369–391, 2006.

Zagwijn, W. H.: Vegetation, climate and radiocarbon datings in the Late Pleistocene of the Netherlands, Part I,: Eemian and Early Weichselian. Mededelingen van de Geologische Stichting Nieuwe Series 14, 15–45, 1961.

Zagwijn, W. H.: Vegetation and climate during warmer intervals in the Late Pleistocene of Western and Central Europe, Quaternary Int., 3/4, 57–67, 1989.

Zagwijn, W. H.: An analysis of Eemian climate in western and central Europe, Quaternary Sci. Rev., 15, 451–469, 1996.

Ziemus, H.: Waldentwicklung der Eem-Warmzeit im südwestlichen Schleswig-Holstein am Beispiel einer Kernbohrung, Schr. Naturwiss. Ver. Schlesw.-Holst., 59, 1–17, 1989.

Zöller, L.: Zur Gliederung von Warthe-Vereisung und Treene-Warmzeit im Aufschluss Böxlund – neue Beobachtungen, Z. Geomorphol., Suppl. Vol. 61, 101–108, 1986.

E&G Quaternary Sci. J., 72, 73–76, 2023
https://doi.org/10.5194/egqsj-72-73-2023

Open Access E&G Quaternary Science Journal

Express report

Expected and deviating evolutions in representative preliminary safety assessments – a focus on glacial tunnel valleys

Paulina Müller, Eva-Maria Hoyer, Anne Bartetzko, and Wolfram Rühaak

Site Selection, Bundesgesellschaft für Endlagerung mbH, 31224 Peine, Germany

Correspondence: Paulina Müller (paulina.mueller@bge.de)

Relevant dates: Received: 30 August 2022 – Revised: 12 January 2023 – Accepted: 8 February 2023 – Published: 6 March 2023

How to cite: Müller, P., Hoyer, E.-M., Bartetzko, A., and Rühaak, W.: Expected and deviating evolutions in representative preliminary safety assessments – a focus on glacial tunnel valleys, E&G Quaternary Sci. J., 72, 73–76, https://doi.org/10.5194/egqsj-72-73-2023, 2023.

1 Introduction

Germany gave a fresh start to its site selection procedure for a repository for high-level radioactive waste with the Repository Site Selection Act (StandAG, 2017) in 2017. The procedure consists of three phases; Phase I is split into two steps. BGE published the Sub-areas Interim Report in 2020 to conclude Step 1 (BGE, 2020). Ninety areas passed the geoscientific criteria and were declared sub-areas with a generally favourable geological situation.

To select a site for a high-level radioactive waste repository, the performance of the possible sites as disposal systems that safely contain radionuclides over 1 million years has to be investigated. Hence, in Step 2 of Phase I, representative preliminary safety assessments are an important part of the regulatory toolbox for finding the most suitable areas. They are performed according to the Disposal Safety Analysis Ordinance (EndlSiAnfV, 2020; EndlSiUntV, 2020) of 2020. Their results will help in narrowing down the sub-areas, which currently cover approximately 54 % of the German land surface, to a small number of siting regions that will be subject to surface exploration in Phase II. Preliminary safety assessments are performed in each phase of the German site selection procedure. The representative preliminary safety assessments of Phase I have a limited scope compared to the assessments in Phases II and III (EndlSiAnfV, 2020). For a more detailed overview of the site selection process and the role of the preliminary safety assessments, see Hoyer et al. (2021).

2 Evolutions of the disposal system

The safety of a disposal system is not only dependent on the present-day geological situation of its site, a good repository design, and an excellent technological implementation during construction and operation of the repository but also especially on the future behaviour of the whole system. Since safety has to be achieved for 1 million years, a well-founded, circumspect estimate of the processes acting in and on the repository becomes vital. In the representative preliminary safety assessments, the focus is on future processes in the geosphere, with the challenge to estimate and attach probabilities and risks to any of these geogenic processes[1].

The range of possible evolutions of the system is the core of a safety assessment. They are ordered by likelihood (§ 3 EndlSiAnfV):

1. the expected evolution is the most likely development from the most likely initial state of the disposal system, and

[1] A term newly used in the context of nuclear waste disposal in the Site Selection Act. It is interpreted as those *geogenic* processes that would occur independently of the repository and is used to distinguish them from *technogenic* processes, which are dependent on the existence of the repository structures.

2. deviating evolutions are not expected, but they are considered as far as they cannot be ruled out from occurring in the future.

For now, the geogenic processes are the starting point for developing the evolutions (§ 7 EndlSiUntV). In later phases, all components and processes in the disposal system can be a starting point for deviating evolutions.

Any attempt at forecasting the future is likely to be wrong to some degree. The aim of a safety assessment structured around the scenario method (a particular method of thinking about the future, further explained below) is to optimise the repository in such a way that deviating unexpected developments are very unlikely to compromise the safety of the repository – as far as it is humanly possible to tell. To achieve this, it is necessary to stretch the imagination beyond extrapolating past or current trends and data observations, to examine all assumptions, and to question the sufficiency of the data used.

Sandia National Laboratories first applied the scenario methodology in the context of nuclear disposal in the USA, after the method was previously used for policy strategy development for both governments and businesses (Cranwell et al., 1990). As part of an OECD-NEA (Organisation for Economic Co-operation and Development Nuclear Energy Agency) initiative, several national nuclear waste disposal organisations started using the scenario methodology. Since then, it has become a standard instrument for the development of a safety case (IAEA, 2012).

A scenario study requires

1. a clearly defined scope (area of interest, time period, goals),
2. a compilation of knowledge about the current state (relevant actors, facts, well-known processes and trends in science and society), and
3. an understanding of which elements of the current state are least understood or least predictable in their properties or behaviour while posing the greatest risk to the goals (MacKay and McKiernan, 2018).

In a safety assessment for a potential nuclear waste disposal site, the scope is defined by national regulations. In the German site selection process, the areas of interest are the subareas identified in Step 1 of Phase I. The period of interest is 1 million years after closure of the repository; the goal is a disposal system that keeps within the limits of radionuclide mass and number of atoms transported beyond the essential barriers as given by the Disposal Safety Requirements Ordinance (EndlSiAnfV, 2020; StandAG, 2017). Dose calculations are excluded from the representative preliminary safety assessments but will be part of later assessments.

The compilation of knowledge about the current state and trends is limited to a description of the components and processes in the geosphere and the repository by the EndlSiUntV. Future human actions will not be taken into account, and at this stage, it is permitted to assume that the repository was successfully constructed and closed according to the current repository concept. Possible risks related to these aspects will be included in the preliminary safety assessments from Phase II onward.

Safety assessments for potential nuclear waste disposal sites usually build up a database called a “FEP catalogue” to document the description of the features, events, and processes studied in the safety assessment. SKB developed this highly structured system description for their safety assessments (Swedish Nuclear Fuel and Waste Management Co., 1989). Today, the OECD-NEA provides the International FEP List as a starting point or auditing instrument for new safety assessment projects (Capouet et al., 2019).

A catalogue entry of a feature, event, or process will typically include a short definition and a longer description, a statement on whether the element is relevant to the repository and why, the times at which the element is relevant, and its influence on other elements with a record of the reasoning behind the identified influence (Fig. 1).

The complete FEP catalogue holds a network of direct and indirect influences that have to be assessed for their safety relevance. This is done by analysing the performance of safety functions of different barriers in the disposal system over time.

The third part of a scenario study is an examination of knowledge, lack of knowledge, and risk. Uncertainties for all features and processes under consideration need to be mapped out and quantified wherever possible.

3 Example – subglacial tunnel valley erosion

Subglacial tunnel valley erosion is a geogenic process (occurring independently of the existence of a repository system) that has produced large-scale linear erosional features during past glaciations of what is now Germany (e.g. Weitkamp and Bebiolka, 2017). The process that leads to the development of subglacial tunnel valleys is still under debate (Weitkamp and Bebiolka, 2017). Indications that tunnel valleys are filled in quickly (most commonly with coarse material or locally reworked sediments) but can be reactivated in successive glaciations have been observed (Kuster and Meyer, 1979).

The minimum depth for a containment-providing rock zone (CRZ)[2] is 300 m below present ground surface. However, the integrity of the CRZ has to hold for 1 million years. Therefore, the depth of the repository must be below the depth reached by direct and indirect effects of exogenic processes, and there must be no reasonable doubt about the long-term integrity of the barriers in the disposal system, particularly the host rock (§ 23 StandAG). If subglacial tunnel valley erosion can be expected to occur with any glaciation, the

[2] The part of the host rock that ensures the safe containment of the radioactive waste in interaction with technical and geotechnical barriers (§ 2 Nr. 9 StandAG).

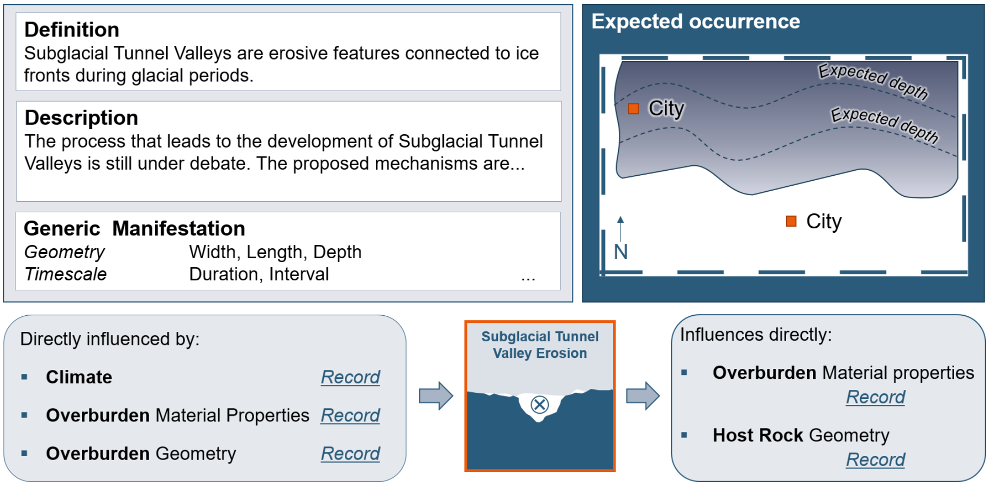

Figure 1. Sketch of FEP catalogue entry for the process of subglacial tunnel valley erosion. These are only examples of possible influences within the system. The final FEP catalogue entry in the representative preliminary safety assessments performed by BGE may look different and include different conclusions.

likely intensity of the process (erosional depth) is the key to estimating whether the siting of a repository at a certain location and depth can ensure the long-term integrity of the CRZ.

In the safety assessment, the process will first be entered into the FEP catalogue (Fig. 1). Its definition distinguishes it from other forms of erosion. The description contains a summary of the current understanding of the process in the scientific community, as well as the areas affected by the process in the past.

Next, the properties of features in the catalogue that can directly influence the manifestation of the process are identified, as are the properties of features that are in turn directly affected by the process. Tunnel valley erosion can locally reduce the thickness of the overburden of the CRZ, as well as change the permeability when the valley is filled up again. Assuming, for instance, 10 future glaciations over 1 million years, then multiple potential erosion "events" can affect a potential disposal system.

4 Consequences of expected and deviating evolutions

Uncertainty about the processes that form subglacial tunnel valleys could invite the definition of a vertical safety margin, for example 100 m. This strategy, though, has issues: to start with, increasing the depth of the repository may offer more long-term safety, but it can increase short-term risks during the operational phase, depending on the host rock, since the drilling of the mine can become more difficult.

Another issue is the problem of missing knowledge (epistemic): how can we know that we have observed the deepest possible tunnel valley? For example, in the Netherlands, a maximum erosion depth of 500 m was known. Reprocessing of existing seismic data, however, led to the discovery of "new" tunnel valleys with depths of nearly 600 m below ground surface (Ten Veen, 2015). This necessitated a re-evaluation of the risk tunnel valley erosion posits for radioactive waste disposal, increasing the maximum observed depth by approximately 100 m.

The deepest known tunnel valley in Germany is the so-called Hagenower Rinne with a depth of 584 m below present ground surface (Kuster and Meyer, 1979), but there is no way of knowing at this time whether that is the deepest valley. Tunnel valley research in the North Sea allows for the conclusion that tunnel valleys will be found when specifically (re)processing data, e.g. seismic data (e.g. Lutz et al., 2009). An absence of tunnel valleys on a thematic map does not imply that there are none present. It may just mean no appropriate study has been conducted there to gain significant data, or existing data were not analysed for this special purpose.

This leads to our understanding of the risks of tunnel valley erosion and how we assess which evolution is expected and which is deviating. It becomes hard to judge whether a safety buffer of 100 m below the deepest known tunnel valley is actually a sensible conservative measure. To account for this, Weitkamp and Bebiolka (2017) suggest zones of different representative predicted depths of erosion. Even so, this could either exclude possibly safe sites from further consideration by strongly overestimating tunnel valley erosion depths or include too many by underestimating them.

5 Conclusions

Considering the future with scenario methods should inevitably call into question the extent and certainty of our knowledge and understanding regarding both the past and the present. Particularly in high-reliability institutions such as a disposal system for high-level radioactive waste, the consequences of error need to be minimised as far as possible. A disposal system needs to be sited and conceptualised with sufficient safety reserves to accommodate a range of future evolutions beyond the expected evolution.

Data availability. No data sets were used in this article.

Author contributions. PM: conceptualisation, writing – original draft preparation. AB: writing – review and editing, supervision. EMH: conceptualisation, writing – review and editing. WR: supervision, writing – review and editing.

Competing interests. The contact author has declared that none of the authors has any competing interests.

Disclaimer. Publisher's note: Copernicus Publications remains neutral with regard to jurisdictional claims in published maps and institutional affiliations.

Special issue statement. This article is part of the special issue "Subglacial erosional landforms and their relevance for the long-term safety of a radioactive waste repository". It is the result of a virtual workshop held in December 2021.

Acknowledgements. We thank all the colleagues that have contributed and will contribute in the process of nuclear waste site selection. Their contributions are most important and valued. We especially thank the editor and reviewer for their input.

Review statement. This paper was edited by Sonja Breuer and reviewed by Axel Weitkamp.

References

BGE: Sub-areas Interim Report pursuant to Section 13 StandAG, Bundesgesellschaft für Endlagerung mbH, Peine, SG01101/16-1/2-2021#1, https://www.bge.de/fileadmin/user_upload/Standortsuche/Wesentliche_Unterlagen/Zwischenbericht_Teilgebiete/Zwischenbericht_Teilgebiete_-_Englische_Fassung_barrierefrei.pdf (last access: 1 August 2022), 2020.

Capouet, M., Carter, A., and Ciambrella, M.: International Features, Events and Processes (IFEP) List for the Deep Geological Disposal of Radioactive Waste, Version 3.0, OECD-NEA, Report No. NEA-RWM-R–2019-1, Paris, France, 166 pp., 2019.

Cranwell, R. M., Guzowski, R. W., Campbell, J. E., and Ortiz, N. R.: Risk Methodology for Geologic Disposal of Radioactive Waste: Scenario Selection Procedure, US Department of Energy, NUREG/CR-1667 SAND80-1429, Sandia National Laboratories, Albuquerque, New Mexico, USA, 1990.

EndlSiAnfV: Endlagersicherheitsanforderungsverordnung vom 6. Oktober 2020 (BGBl. I S. 2094), ISSN 0341-1095, 2020.

EndlSiUntV: Endlagersicherheitsuntersuchungsverordnung vom 6. Oktober 2020 (BGBl. I S. 2094, 2103), ISSN 0341-1095, 2020.

Hoyer, E.-M., Kreye, P., Lohser, T., and Rühaak, W.: Preliminary safety assessments in the high-level radioactive waste site selection procedure in Germany, Saf. Nucl. Waste Disposal, 1, 37–38, https://doi.org/10.5194/sand-1-37-2021, 2021.

IAEA: The Safety Case and Safety Assessment for the Disposal of Radioactive Waste: No. SSG-23, IAEA Safety Standards, International Atomic Energy Agency, Vienna, Austria, ISBN 978-92-0-128310-8, 2012.

Kuster, H. and Meyer, K.-D.: Glaziäre Rinnen im mittleren und nördlichen Niedersachsen, E&G Quaternary Sci. J., 29, 135–156, https://doi.org/10.3285/eg.29.1.12, 1979.

Lutz, R. K., Gaedicke, C., Reinhardt, L., and Winsemann, J.: Pleistocene tunnel valleys in the German North Sea: spatial distribution and morphology, Z. Dtsch. Ges. Geowiss., 160, 225–235, https://doi.org/10.1127/1860-1804/2009/0160-0225, 2009.

MacKay, R. B. and McKiernan, P.: Scenario thinking: A historical evolution of strategic foresight, Elements in business strategy, Cambridge University Press, Cambridge, 83 pp., ISBN 9781108571494, 2018.

StandAG: Standortauswahlgesetz vom 5. Mai 2017 (BGBl. I S. 1074) (das zuletzt durch Artikel 1 des Gesetzes vom 7. Dezember 2020 (BGBl. I S. 2760) geändert worden ist, ISSN 0341-1095), 2017 (updated 2020).

Swedish Nuclear Fuel and Waste Management Co.: The joint SKI/SKB scenario development project, Swedish Nuclear Fuel and Waste Management Co., Report No. SKB TR 89-35, Stockholm, Sweden, 176 pp., 1989.

ten Veen, J.: Future evolution of the geological and geohydrological properties of the geosphere: OPERA-PU-TNO412, Task 4.1.2, Centrale Organisatie foor Radioactief Avfal, Vlissingen, NL, 2015.

Weitkamp, A. and Bebiolka, A. C.: Subglaziale Rinnen – Darstellung und Bewertung des Kenntnisstandes, Bundesanstalt für Geowissenschaften und Rohstoffe, Hannover, Pleistozäne übertiefte Strukturen und ihre Bedeutung für die Langzeitsicherheit möglicher Endlagerstandorte in Süddeutschland, B3.4/B50112-44/2016-0004/002, 36 pp., 2017.

E&G Quaternary Sci. J., 72, 77–94, 2023
https://doi.org/10.5194/egqsj-72-77-2023

Open Access E&G Quaternary Science Journal

Research article

Pleniglacial dynamics in an oceanic central European loess landscape

Stephan Pötter[1,2], Katharina Seeger[3], Christiane Richter[4], Dominik Brill[3], Mathias Knaak[5], Frank Lehmkuhl[1], and Philipp Schulte[1]

[1]Department of Geography, RWTH Aachen University, 52062 Aachen, Germany
[2]Chair of Geography, University of Koblenz-Landau, 56070 Koblenz, Germany
[3]Institute of Geography, University of Cologne, 50923 Cologne, Germany
[4]Institute of Geography, Technical University Dresden, 01069 Dresden, Germany
[5]Division Applied Geosciences, Geological Survey of North Rhine-Westphalia, 47803 Krefeld, Germany

Correspondence: Stephan Pötter (stephan.poetter@geo.rwth-aachen.de)

Relevant dates: Received: 13 May 2022 – Revised: 21 December 2022 – Accepted: 23 February 2023 – Published: 24 April 2023

How to cite: Pötter, S., Seeger, K., Richter, C., Brill, D., Knaak, M., Lehmkuhl, F., and Schulte, P.: Pleniglacial dynamics in an oceanic central European loess landscape, E&G Quaternary Sci. J., 72, 77–94, https://doi.org/10.5194/egqsj-72-77-2023, 2023.

Abstract: Loess–palaeosol sequences (LPSs) of the oceanic-influenced European loess belt underwent frequent post-depositional processes induced by surface runoff or periglacial processes. The interpretation of such atypical LPSs is not straightforward, and they cannot be easily used for regional to continental correlations. Within the last few years, however, such sequences gained increased attention, as they are valuable archives for regional landscape dynamics. In this study, the Siersdorf LPS was analysed using a multi-proxy approach using sedimentological, geochemical, and spectrophotometric methods combined with luminescence dating and tentative malacological tests to unravel Pleniglacial dynamics of the Lower Rhine Embayment. A marshy wetland environment for the late Middle Pleniglacial to the early Upper Pleniglacial was shown by colour reflectance and grain size distribution. Age inversions from luminescence dating paired with geochemical and sedimentological data reveal long-lasting erosional processes during the early Upper Pleniglacial, which were constrained to a relatively small catchment with short transport ranges. The upper sequence shows typical marker horizons for the study area and indicate harsh, cold-arid conditions for the late Upper Pleniglacial. In comparison with other terrestrial archives, the Siersdorf LPS shows that the Lower Rhine Embayment was more diverse than previously assumed, regarding not only its geomorphological settings and related processes but also its ecosystems and environments.

Kurzfassung: Die Lössprofile des ozeanisch beeinflussten europäischen Lössgürtels wurden häufig durch Oberflächenabfluss oder periglaziale Prozesse umgelagert. Die Interpretation solcher atypischen LPS ist nicht einfach und sie können nicht ohne weiteres für regionale bis kontinentale Korrelationen verwendet werden. In den letzten Jahren haben solche Sequenzen jedoch zunehmend an Bedeutung gewonnen, da sie wertvolle Archive für die regionale Landschaftsdynamik darstellen. In dieser Studie wurde das Lössprofil Siersdorf mit Hilfe eines Multi-Proxy-Ansatzes analysiert, der sedimentologische, geochemische und spektrophotometrische Methoden mit Lumineszenzdatierungen und versuchsweisen malakologischen Untersuchungen kombiniert, um die pleniglaziale Dynamik der Niederrheinischen Bucht zu entschlüsseln. Die Farbadaten und die Korngrößenverteilungen zeigen, dass das Profil vom späten Mittelpleniglazial bis zum frühen Oberpleniglazial in einem sumpfigen Feuchtgebiet lag. Altersinversionen aus Lumineszenzdatierungen gepaart mit geochemischen und sedimentologischen Daten lassen auf lang anhaltende Erosionsprozesse während des frühen Oberen Pleniglazials schließen, die auf ein relativ kleines Einzugsgebiet mit kurzen Transportstrecken beschränkt waren. Die obere Abfolge zeigt typische Markerhorizonte für das Untersuchungsgebiet und weist auf raue, kalt-trockene Bedingungen für das späte Obere Pleniglazial hin. Im Vergleich zu anderen terrestrischen Archiven zeigt das Siersdorfer LPS, dass die Niederrheinische Bucht vielfältiger war als bisher angenommen, nicht nur in Bezug auf ihre geomorphologischen Gegebenheiten und die damit verbundenen Prozesse, sondern auch in Bezug auf ihre Ökosysteme und Lebensräume.

1 Introduction

Throughout the last few decades, loess–palaeosol sequences (LPSs) have been frequently analysed to reconstruct palaeoclimatic and palaeoenvironmental conditions of the terrestrial realms (Hatté et al., 2001, 2013; Marković et al., 2005; Kukla et al., 1988; Zech et al., 2013; Torre et al., 2020; Varga et al., 2011). Therefore, sequences are investigated, which are as complete and undisturbed as possible to allow interregional correlations (Marković et al., 2018; Lehmkuhl et al., 2016) or direct reconstructions of atmospheric conditions (Obreht et al., 2017; Rousseau and Hatté, 2021; Bokhorst et al., 2011). These aeolian LPSs were formed out of mineral dust, which was deposited on topographic barriers (Lehmkuhl et al., 2016; Antoine et al., 2016), biological crusts (Svirčev et al., 2013), or vegetation, typically grasses (Zech et al., 2013, 2011). The deposited dust undergoes quasi-pedogenic processes called loessification processes (Sprafke and Obreht, 2016), leading to its unique characteristics, such as its silty texture and porosity (Pécsi and Richter, 1996; Koch and Neumeister, 2005). Due to these properties, loess is prone to post-depositional reworking and erosion, especially by water (Meszner et al., 2013, p. 201), and in regions affected by permafrost, by periglacial activities and slope processes (Lehmkuhl et al., 2021, 2016). This proneness can lead to hiatuses in the stratigraphy (Obreht et al., 2015; Steup and Fuchs, 2017) or the reworking of sediments. Additionally, weathering and soil formation processes, such as decalcification, feldspar weathering, or lessivation of clay, can transform the pristine sediments on various scales and can give valuable hints on past environmental conditions (Fenn et al., 2020, 2021; Marković et al., 2018; Lehmkuhl et al., 2016).

The European loess belt (ELB; loess domain II sensu; Lehmkuhl et al., 2021), stretches from the shores of the English Channel (Antoine et al., 2003; Stevens et al., 2020) throughout Belgium (Haesaerts et al., 2016), Germany (Lehmkuhl et al., 2018), and Poland (Jary and Ciszek, 2013) towards Ukraine (Veres et al., 2018). Especially the western ELB (subdomain IIa sensu; Lehmkuhl et al., 2021), which is characterised by a humid, oceanic climate, was prone to erosional processes such as slope wash or solifluction (Lehmkuhl et al., 2016). These conditions led to frequent reorganisation processes of landscape systems due to widespread erosion throughout the ELB (Meszner et al., 2013), partially leading to relief reversals (Fischer et al., 2012; Kels, 2007; Lehmkuhl et al., 2015). The continental ice sheets to the north and the periglacially shaped central European uplands to the south dominated the Pleistocene palaeogeography of the ELB, acting as potential dust sources of Pleistocene loess deposits due to high production rates of detrital material (Baykal et al., 2021; Skurzyński et al., 2019, 2020; Vinnepand et al., 2022). Additionally, the climatic conditions and vicinity to continental and Alpine ice sheets induced periglacial conditions, especially during glacial and stadial phases (Jary, 2009; Lehmkuhl et al., 2021; Vandenberghe et al., 2014; Stadelmaier et al., 2021).

The results of these processes are, compared to other European loess regions like the Danube Basin (Marković et al., 2015), complex stratigraphic records with unconformities and polygenetic pedocomplexes in the western ELB. Therefore, complete Late Pleistocene LPSs, without any hiatuses or discordances, are scarce (Schirmer, 2002; Zens et al., 2018). Within the last few years, however, considerable attention was given to non-typical LPSs, which were either strongly reworked (Klinge et al., 2017; Steup and Fuchs, 2017; Meszner et al., 2014) or which were characterised by changing depositional milieus (Mayr et al., 2017; Sümegi et al., 2015; Hošek et al., 2017). These archives allow a detailed view of the interplay of climate, landscape development, and environment and are, therefore, a crucial addition to the vast set of Pleistocene sediment archives.

Here, we present geochronological and proxy data for a new LPS in the Lower Rhine Embayment (North Rhine-Westphalia, Germany). The Siersdorf (SID) LPS developed in a channel incised into an older Pleistocene terrace of the Meuse. It represents a high-resolution record of the transition from the late Middle (MPG) to the Upper Pleniglacial (UPG). Unlike typical LPSs from the area, the Middle Pleniglacial stadial conditions are not imprinted as a series of phases of differently intense soil formation processes but as a uniform unit of greyish-brownish silt, most likely linked to semi-terrestrial marshy conditions. In this study, we analyse the sedimentological, geochemical, and spectrophotometric data to unravel the genesis of this atypical sedimentary succession. The geomorphological and palaeoenvironmental ramifications are discussed in the framework of loess research in the Rhine catchment. The Siersdorf LPS is a crucial addition to the framework of Pleniglacial landscape reconstruction, as it is so far the first reported LPS from the Lower Rhine Embayment which records semi-terrestrial conditions during the late Middle Pleniglacial to Upper Pleniglacial. This reconstruction shows that the Pleniglacial Lower Rhine Embayment was more diverse than previously assumed, regarding not only its geomorphological settings and related processes but also its ecosystems and environments.

2 Research area and study site

2.1 The Lower Rhine Embayment

The Lower Rhine Embayment (LRE) is part of the European rift system and covers the southernmost part of the Lower Rhine catchment. It is situated on the transition of the central European uplands, namely the Rhenish Massif, and the northern German lowlands (Böse et al., 2022). As a loess region, the LRE is part of the western European maritime (Atlantic) loess subdomain of the ELB sensu (Lehmkuhl et al., 2021). This part of the ELB was dominated by North Atlantic climate conditions during the Late Pleistocene (Antoine et al., 2001, 2009; Fischer et al., 2021). Due to the oceanic climate and the accompanied high landscape dynamics (Fischer et al., 2017), the distribution and characteristics of loess deposits in the LRE are strongly site-specific, depending on geomorphological settings and related processes.

Four main geomorphological positions for LPSs can be summarised (Lehmkuhl et al., 2016). LPSs in plateau situations are often affected by erosion, both by surface runoff and by deflation (Schirmer, 2016; Antoine et al., 2016). Additionally, chemical processes such as (carbonate) solution and leaching may affect these sequences. Slope positions in the LRE are especially prone to erosional processes. Truncation, e.g. related to phases of widespread erosion, may remove previously formed LPSs in their entirety (Schirmer, 2016). Similar conditions have been reported from adjacent regions of the ELB (Meszner et al., 2013; Antoine et al., 2016). Besides fluvial relocation, processes such as solifluction play a major role in slope positions (Lehmkuhl et al., 2016). Under periglacial conditions, a slope gradient of 2° is sufficient to initiate reworking by solifluction (Lehmkuhl, 2016). Relocated material is transported downslope and deposited on the slope toe. These positions act not only as sediment traps during loess formation (Antoine et al., 2016) but also as sinks of soil sediments and other relocated material (Kappler et al., 2018; Kühn et al., 2017). This also applies to depressions and erosional channels. Within these topographic sinks, detrital material of various origins, i.e. aeolian, colluvial, or other slope sediments, accumulates, leading to complex stratigraphical archives. As the geomorphological setting and sedimentological processes are crucial in the formation of sediment sequences, their discussion is essential to understand the evolution of LPSs and for their correlation with other environmental archives (Marković et al., 2018; Lehmkuhl et al., 2016; Fischer et al., 2017).

The LRE builds the easternmost part of this maritime loess domain, which shows comparable stratigraphic records for the Late Pleistocene from northern France towards the study area (Haesaerts et al., 2011; Meijs, 2002; Schirmer, 2016; Antoine et al., 2014): the oldest sequence builds the last interglacial, i.e. Eemian, palaeosol, a truncated brown-leached soil complex. The Weichselian glacial succession starts with an early glacial (115–72 ka) complex, consisting of a grey forest soil and a steppe-like soil. The Lower Pleniglacial (LPG; 70–58 ka) is the phase with the first reported (and preserved) loess formation in central Europe (Frechen et al., 2003), accompanied by periglacial conditions. The Middle Pleniglacial (MPG; 58–32 ka) was characterised by reduced dust accumulation (Antoine et al., 2001), frequent relocation of older sediments and soils (Meszner et al., 2013), and phases of soil formation (Fischer et al., 2021; Schirmer et al., 2012). However, MPG sequences are often only preserved in geomorphologically favourable settings. The Upper Pleniglacial (UPG; 32–15 ka) was characterised by enhanced dust accretion and harsh, periglacial conditions (Lehmkuhl et al., 2021). Typical features for these periods are Gelic Gleysols (tundra gleys) and ice-wedge casts (Antoine et al., 2016). In the LRE, the UPG deposits show a typical succession encompassing inter alia the so-called Eben Zone (Schirmer, 2003).

The study site is located within the so-called Aldenhoven loess plateau as part of the Börde region of Jülich (Knaak et al., 2021). This plateau, situated between the Wurm, Inde, and Rur rivers in the foreland of the northern Eifel Mountains (Fig. 1), is slightly inclined towards the northeast (170–75 m a.s.l.). Vast loess blankets cover the palaeorelief, which is characterised by small dendritic river systems. These blankets mainly formed during the Late Pleistocene as dust was entrained from the Middle Pleistocene terraces of the Rhine, Meuse, and Rur rivers. Steps in the landscape, where loess thicknesses vary considerably within a few metres, are indicative of recent differential tectonic processes. Late Pleistocene to Holocene features approx. 1 km northwest of the studied sequence, such as solifluction layers or other stratigraphic markers, show tectonically induced offsets of approx. 1 m, indicating younger tectonic movements (Fig. S1 in the Supplement). Additionally, tectonics shaped the hydrological system, as river deflections are abundant in the study area.

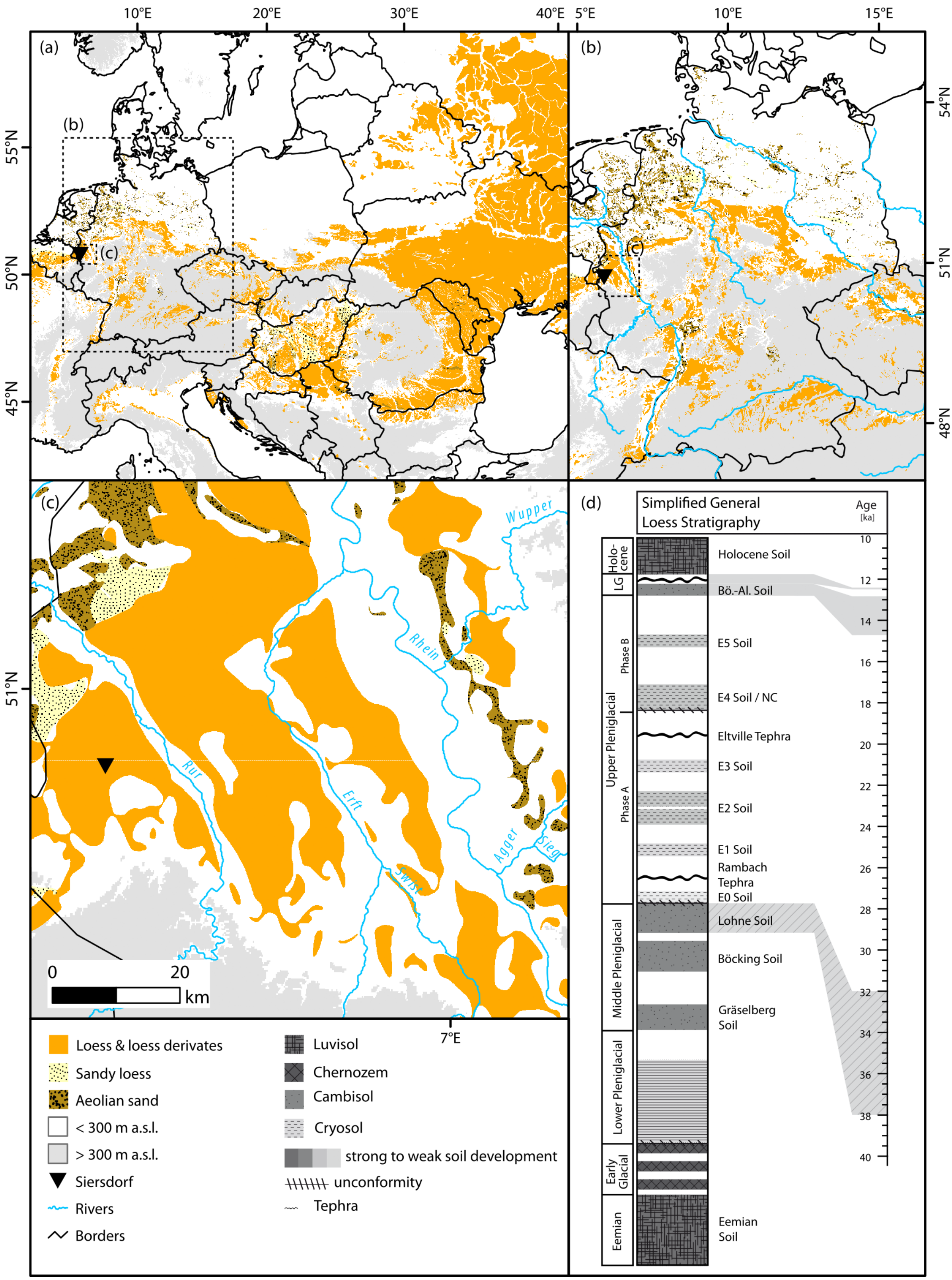

Figure 1. Location of the Siersdorf LPS (black triangle) **(a)** within the European loess belt, **(b)** in Germany, and **(c)** within the Lower Rhine Embayment. Distribution of aeolian sediment according to Lehmkuhl et al. (2021). **(d)** Simplified and generalised loess stratigraphy for central Europe, adapted from Zens et al. (2018).

2.2 The Siersdorf loess–palaeosol sequence

The Siersdorf (SID) LPS was exposed during construction works of the Zeelink natural gas pipeline in the central part of the Aldenhoven loess plateau (Fig. 1). The investigated sequence is 6 m thick (Fig. 2) and developed within a channel of a presumably Middle Pleistocene terrace of the Meuse. The deposits of the Meuse covered large parts of the central LRE during the Pleistocene (Boenigk and Frechen, 2006). The incised channel acted as a sediment trap throughout the Late Pleistocene and Holocene. Based on field observations, the sequence can be subdivided into five main units: the base, unit I, is characterised by greyish-dark-brownish silts, which change colour during drying to grey. Nearby core drillings indicate strong hydromorphic overprinting of these layers (Fig. S2). The upper part of this layer shows a high abundance of mollusc shells and shell fragments. The overlying loess (unit II) is laminated and partially characterised by cryoturbation features. At the base of this relocated loess, a thin, blackish layer occurs. The laminated layer stretches from 4.8 to 3.5 m below surface. Small ice-wedge pseudomorphs frequently disturb the layering, which shows varying contents of silt and sand. On top of the layered loess adjoins an orange, wavy layer (unit III). Greyish-brownish palaeosol layers, which show characteristics of Gelic Gleysols, built the uppermost part of unit III. Above this complex, the sequence consists of relatively unaltered loess (unit IV). This loess is also the fill material for massive ice-wedge pseudomorphs approx. 3 m left of the sampled section, which pierces the below-lying units until the top of the lowermost layer (Fig. 2). A humic, finely layered colluvial unit covers the loess (unit V). This reworked sediment contains small pebbles and charcoal flitters. The uppermost 90 cm of the sequence is anthropogenically disturbed.

3 Methods

3.1 Field work and sampling

The SID LPS was sampled in May 2021 after exposure during construction works of the Zeelink natural gas pipeline. Prior to description and sampling, several decimetres of exposed sediments were removed to avoid contamination with weathered and relocated material. The sequence was described in detail from the bottom to the top. Samples for sedimentological, geochemical, and colorimetric analyses were taken in a continuous sampling trench. Sampling was conducted using freshly cleaned tools and sterile plastic bags. The anthropogenically disturbed uppermost 90 cm was not sampled. The colluvial unit (0.9–1.7 m) was sampled in 10 cm increments, whereas the rest of the sequence was sampled every 5 cm.

For luminescence dating, six samples were taken horizontally with steel cylinders from selected units (for position of samples, see Fig. 2). Subsequently, the sediment within a 30 cm distance to the cylinders was sampled for dose rate determination.

3.2 Sedimentological, geochemical, and spectrophotometric analyses

The samples were dried at 35 °C, sieved to the fraction < 2 mm, and two subsamples of each sample (0.1 and 0.3 g) were pre-treated with 0.7 mL H_2O_2 (30 %) at 70 °C for 12 h. This process was repeated until bleaching of the material was visible (Allen and Thornley, 2004) but not longer than 3 d. To keep the particles dispersed during analysis, the samples were treated with 1.25 mL $Na_4P_2O_7 \cdot 10H_2O$ in an overhead shaker for 12 h. The grain size was determined with a Beckman Coulter LS 13 320 laser diffractometer using Mie theory (fluid refractive index (RI): 1.33, sample RI: 1.55, imaginary RI: 0.1) (Özer et al., 2010; Nottebaum et al., 2015; Schulte et al., 2016). Grain size distributions were calculated and visualised as distribution heatmaps according to Schulte and Lehmkuhl (2018, Fig. 3). To detect (neo-)formations of clay minerals, the differences between the two optical models of Mie theory and the Fraunhofer approximation were calculated and centred log transformed (Schulte and Lehmkuhl, 2018). The results are visualised as heatmaps as well (Fig. 4).

Inorganic geochemistry was analysed using energy dispersive x-ray fluorescence (EDPXRF) using a SPECTRO XEPOS. This device detects 50 elements from sodium (Na) to uranium (U), excluding erbium and ytterbium. The samples were sieved to the silt fraction (< 63 µm) and dried at 105 °C for 12 h. A subsample of 8 g for each sample was mixed with 2 g FLUXANA CEREOX wax, homogenised in a shaker. The sample was pressed to a pellet with a pressure of 19.2 MPa for 120 s. The measurements were conducted by means of a pre-calibrated method. Each sample was measured in duplicate, and the pellets were rotated by 90° between measurements to avoid matrix effects. Conspicuous samples, where the difference of both measurements was striking, were measured again in duplicate to avoid analytical artefacts. Geochemical data are visualised as depth plots and in the form of the A–CN–K ternary diagram according to Nesbitt and Young (1984). The carbonate content was defined volumetrically using a SCHEIBLER apparatus (ISO 20693, 1995; Schaller, 2000).

Spectrophotometric analysis was conducted using a Konica Minolta CM-5 spectrophotometer, following previously published methodologies (Eckmeier and Gerlach, 2012; Vlaminck et al., 2016). This device uses the diffused reflected light from a standardised source (2° Standard Observer, Illuminant C) to obtain the colour spectra of the visible light (360 to 740 nm). The results were converted to the CIELAB colour space ($L^*a^*b^*$) using the SpectraMagic NX software (Konica Minolta). The dried and homogenised samples were measured in duplicate and averaged.

Figure 2. **(a)** Simplified stratigraphic sketch of the Siersdorf loess–palaeosol sequence. **(b)** Short description of main stratigraphic units. **(c)** Photo of the sequence after sampling (photo: Stephan Pötter). **(d)** Laminated loess package and basal palaeosol (photo: Philipp Schulte). **(e)** Ice-wedge cast, approx. 3 m left of the sampled sequence, piercing the underlying layers for more than 2 m (photo: Stephan Pötter).

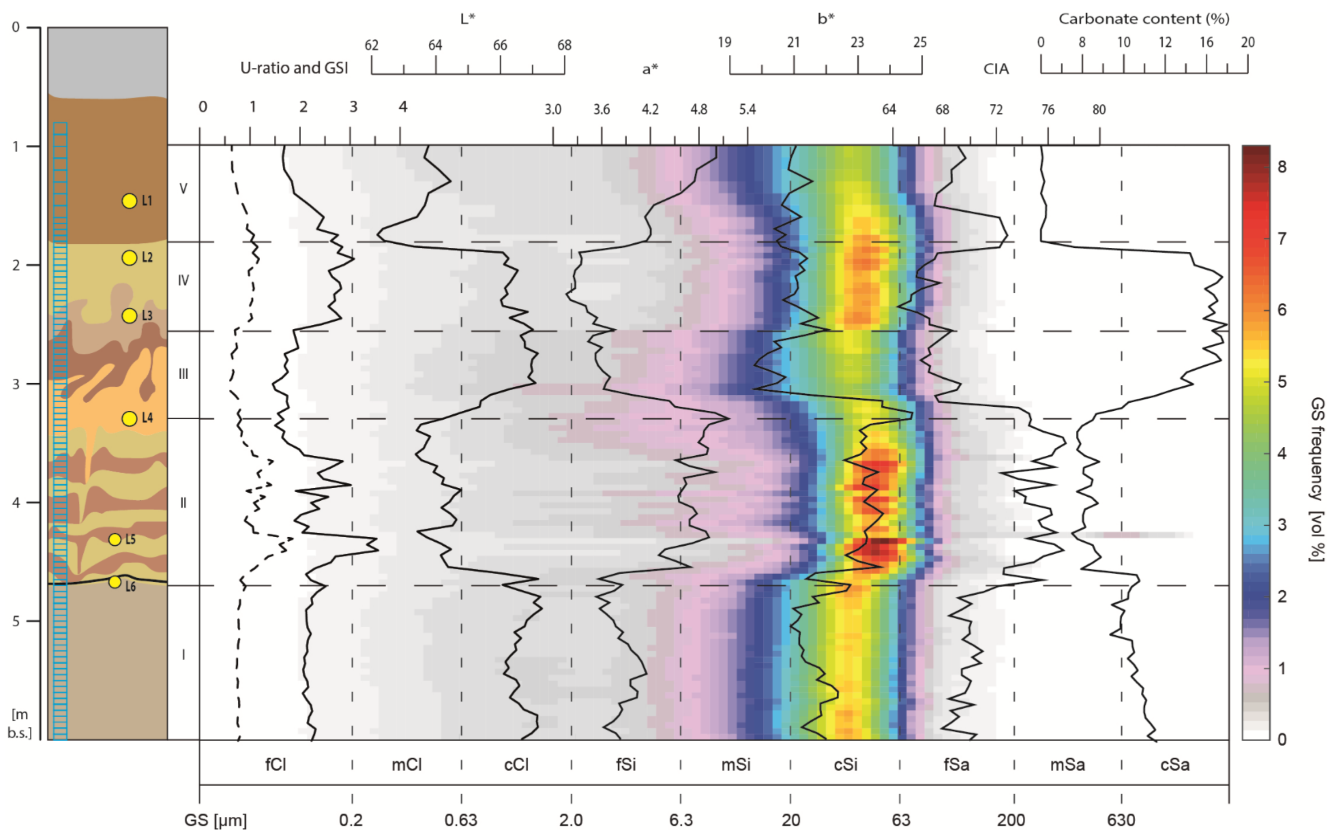

Figure 3. Heatmap visualisation of grain size distribution displayed with various sedimentological, geochemical, and spectrophotometric proxies of the Siersdorf LPS. Stratigraphic units (I–V) are shown for orientation.

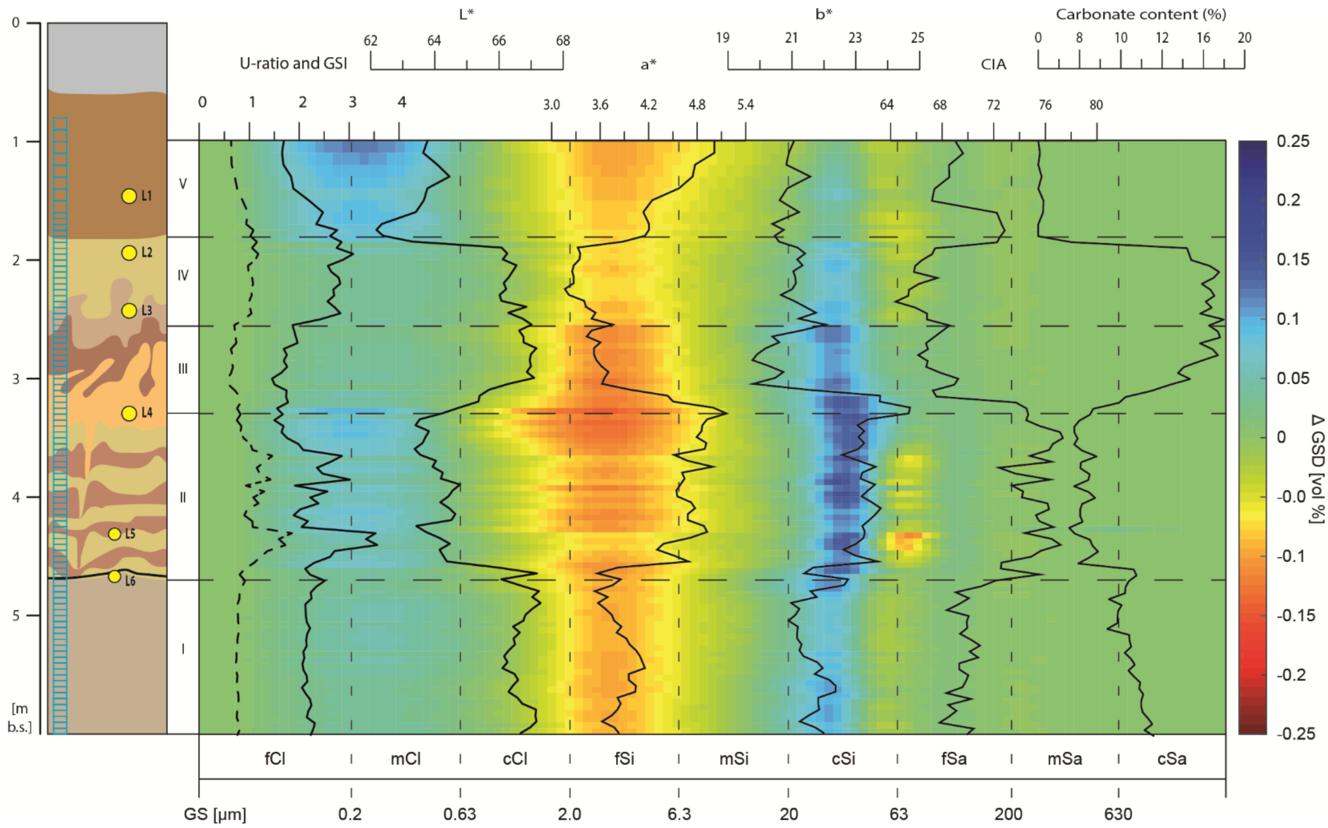

Figure 4. Heatmap visualisation of the difference between two optical models (ΔGSD) displayed with various sedimentological, geochemical, and spectrophotometric proxies of the Siersdorf LPS. Stratigraphic units (I–V) are shown for orientation.

3.3 Luminescence dating

Sample preparation and measurements were conducted in the Cologne Luminescence Laboratory (Cologne, Germany) and included pre-processing under red light conditions. Standard procedures of fine-grain preparation included chemical treatment with HCl (10 %), H_2O_2 (10 %), and $Na_2C_2O_4$ (0.01 N) to remove carbonates, organic components, and aggregates. The 4–11 µm fraction was then separated by settling due to gravitation and centrifugation following Frechen et al. (1996). To derive pure quartz, the 4–11 µm fraction was etched with HF (37 %) and finally washed with HCl (10 %).

Equivalent dose measurements were performed on an automated Risø TL/OSL DA-15 reader (DTU Nutech, Roskilde, Denmark) equipped with a calibrated $^{90}Sr\,/\,^{90}Y$ beta source. Discs were prepared by pipetting a suspension of 1 mg sediment and 0.2 mL deionised water and drying them afterwards. Polymineralic fine-grain samples were stimulated for 200 s by using infrared diodes (870 nm, FWHM = 40) and detected through an interference filter (410 nm). To obtain a feldspar signal not (or not significantly) affected by anomalous fading, a post-infrared infrared (pIRIR) stimulated luminescence protocol was applied with a second stimulation temperature of 290 °C ($pIRIR_{290}$) following Thiel et al. (2011). For quartz fine-grain samples, signals were stimulated with blue LEDs and detected through a U340 filter. Measurements followed a conventional single aliquot regenerative dose (SAR) protocol (Murray and Wintle, 2000).

The suitability of both measurement protocols for the samples of this study was tested based on preheat plateau (only for quartz samples) and dose recovery tests (for all samples). Furthermore, laboratory residual doses after solar simulator bleaching for 24 h and laboratory fading following Auclair et al. (2003) were determined for $pIRIR_{290}$ signals. For each sample, the palaeodose was calculated based on 5–12 accepted aliquots. Aliquots outside a 2σ range were excluded from further calculations. Since scatter in dose distributions of fine-grain samples is completely absent (reflected by overdispersions of around zero for all samples), the arithmetic mean plus standard deviation was chosen to calculate burial doses.

Dose rates were determined by measuring uranium, thorium, and potassium contents using high-resolution gamma spectrometry (Ortec PROFILE M-Series GEM P-type Coaxial HPGe Gamma-Ray Detector). Dosimetry and age calculation were conducted in the DRAC environment (version 1.2; Durcan et al., 2015) using typical water contents of European loess (i.e. 15 ± 5 %; Pécsi, 1990; Klasen et al., 2015) instead of in situ measured ones, as these likely underestimate the hydromorphic conditions at the SID site. Further details on the measurement procedure of dose rate and equivalent dose determination are given in the Supplement.

4 Results

4.1 Sedimentological, geochemical, and spectrophotometric analyses

The grain size distributions (GSDs) of SID show typical patterns for central European loess deposits. Figure S3 shows the distribution curves for all main units identified during fieldwork. The lowermost unit I shows a unimodal GSD with a mode in the middle-coarse silt fraction. The contents of fine particles, especially fine silt and clay, are elevated. The laminated loess unit shows high variations in GSDs. The overlying cryoturbated loess layers show less variations, with strong modes in coarse silt and varying clay and sand contents. The GSD of the brownish-greyish palaeosol also shows a unimodal shape with a mode in coarse silt. Since other fractions, especially clay, are increased, this mode does not show as high values as the other layers. The uppermost loess layer shows a strong coarse silt mode, whereas the colluvial unit is relatively clay rich.

The geochemical results (Figs. 3–5) were utilised to calculate the Chemical Index of Alteration (CIA; Nesbitt and Young, 1982) to determine phases of enhanced chemical weathering. The basal complex does not show any variations in the CIA with all values being lower than 70. The laminated loess package shows higher values of > 70, as does the orange cryoturbated layer. The uppermost loess layer again shows decreased values, with a peak on the base of the overlying colluvial unit. The A–CN–K ternary diagram shows a distribution broadly parallel to the CN join, which can be broadly divided into two clusters (Fig. 5). The lower cluster is uniformly parallel, whereas the upper cluster shows some tendencies towards a more vertical distribution. A similar pattern is reflected by spectrophotometric analyses. The lower unit shows slight variations in the L^*, a^*, and b^* values. The layered unit shows rapidly decreased L^* and increased a^* and b^* values. The orange cryoturbated layer shows the maximum values for a^* and b^*, whereas the upper loess shows decreased redness and yellowness values. The colluvial unit is characterised by dark (low L^*) and brown colours (high a^*).

4.2 Luminescence dating

The results of the luminescence experiments are presented in the Supplement. All parameters relevant for age calculation and calculated ages for the six luminescence samples are presented in Table 1. Palaeodoses were calculated based on De measurements of 5–10 aliquots that were all accepted for data analysis (the very low scatter between De values did

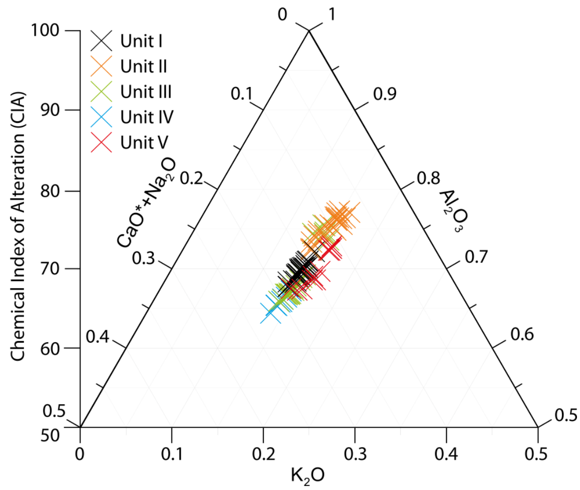

Figure 5. A–CN–K ternary diagram according to Nesbitt and Young (1984) for the Siersdorf LPS. The Chemical Index of Alteration is displayed on the y axis.

not require a larger number of aliquots). Given the absence of significant over-dispersion (Figs. S11 and S12), the arithmetic mean was chosen as the appropriate age model.

For polymineralic samples, burial doses range from 77 ± 1 Gyr (SID L1) to 177 ± 5 Gyr (SID L4). For the uppermost five samples, resulting ages are in stratigraphic order (Fig. 6). In contrast, the quartz ages are in line with the whole sedimentary sequence except for SID L1. Here, the quartz age of 34 ka significantly overestimates the feldspar age of 16 ka. Since it causes an inversion compared to the layers dated below, the quartz age of SID L1 should not be trusted. We have no explanation for this overestimation (since the pIRIR ages are significantly younger, this cannot be a bleaching issue), but this unit must be younger than at least 20 ka (SID L2). For SID L2 and L3, both quartz and feldspar ages are identical and yield ages of 18 to 23 ka. The quartz and $pIRIR_{290}$ ages calculated for samples SID L4 and L5 overlap within their uncertainties. The quartz and $pIRIR_{290}$ ages for SID L6 show an age inversion to the samples above and are therefore not stratigraphically consistent.

5 Discussion

5.1 Formation processes of an atypical loess sequence in the Lower Rhine Embayment

The Siersdorf LPS is a valuable archive for Weichselian Pleniglacial landscape dynamics. Combined sedimentological, geochemical, and spectrophotometric methods reveal distinct changes of environmental conditions and associated geomorphic processes during the formation of the investigated LPS, indicating a more heterogeneous environment in the LRE than previously assumed.

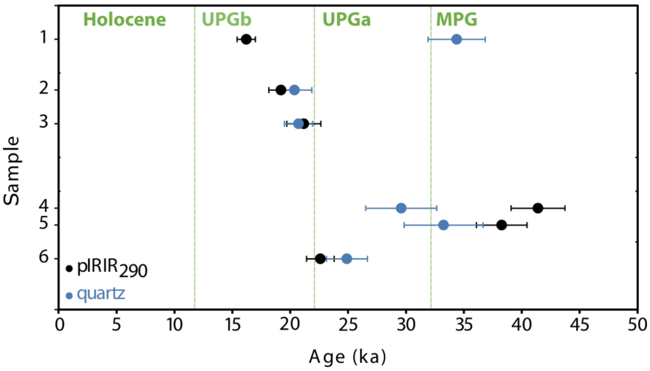

Figure 6. Age depth plot with feldspar ages and quartz ages. Age estimates for the Middle Pleniglacial (MPG), early Upper Pleniglacial (UPGa), late Upper Pleniglacial (UPGb), and the Holocene according to Zens et al. (2018).

5.1.1 Unit I

Unit I shows uniform patterns in most of the analysed proxy data. Especially the GSD and ΔGSD show almost no variations within this unit (Figs. 3 and 4). The low, uniform ΔGSD excludes this unit as a palaeosol, as pedogenic processes would favour the formation of clay minerals (Schulte and Lehmkuhl, 2018), which was observed for LPSs in the Rhine–Meuse catchment (Zens et al., 2018). The lack of large quantities of sand, as well as the uniform GSD of the unit, excludes large-scale relocation processes, pointing to an in situ formation of this unit. In-field measurements of the magnetic susceptibility in SID revealed low values for the respective lithological unit (Knaak et al., 2021), precluding biogenic formation of iron oxides. The proxy data, e.g. the low and uniform ΔGSD, indicate that unit I does not represent a typical interstadial palaeosol.

The unit's bright-greyish hues, shown by high L^* and low a^* and b^* values (Fig. 3), indicate a reductive milieu during or after deposition of the medium-coarse silt. The uniform sedimentology together with these grey shades point to a depositional milieu differing from the typical dust traps such as topographic barriers (Antoine et al., 2016; Lehmkuhl et al., 2016) or vegetation. A possible explanation for these prevailing reductive conditions would be a dust deposition in a semi-terrestrial environment. Such an environment was reported from the Bobingen LPS (BOB) in southern Germany (Mayr et al., 2017). The site was covered by a lake during the MPG, which is reflected by highly reduced blueish-greyish sediments and lacustrine faunal remains. During the late MPG, the lake silted up, and typical subaerial loess formation began. A similar situation was reported from the Ringen LPS (RGE) in the Middle Rhine Valley, where a gyttja was correlated to the MPG based on palynological evidence (Henze, 1998). This unit shows blueish-greyish hues and a silty-clayey texture and is approx. 2 m thick (Fig. S4). The colour and texture change towards the top, as the top is more oxidised and contains coarser grains. This succession reveals that the gyttja at the Ringen LPS, as a trap for both moisture and mineral dust, was continually covered by increased input of aeolian detrital material during the MPG–UPG transition, silting up the marshy environment. Similar conditions have been reported from the Bína LPS in Slovakia, although these were correlated to the Lower Pleniglacial (marine isotope stage (MIS) 4) (Hošek et al., 2017).

Besides macroscopic similarities between the two units of SID and RGE, the respective sedimentological evidence also points to similar environmental conditions. Both LPSs show unimodal GSDs, dominated by medium-coarse silt with slightly elevated clay contents (Fig. S3). These distributions indicate input of aeolian dust. Increased sand contents indicate additional but considerably less input by surface runoff. The water-saturated conditions are imprinted not only in greyish colours and sedimentology but also in wavy, flaky structures reported from field observations, indicating a micro-layering in a quiescent depositional environment. In RGE and BOB, the sediment is completely bleached and shows signs of intense reduction of ferruginous compounds, namely blueish-greyish hues. In SID, however, the lower intensity of reduction processes indicates shorter phases of semi-terrestrial conditions compared to the former sites. However, another plausible explanation is that the unit did not develop under proper lacustrine conditions comparable to BOB or RGE but in a marshy wetland situation, presumably with seasonal drying phenomena.

Within around 10 %, the carbonate content within unit I allowed the preservation of a high number of mollusc shells and shell fragments. Although no samples according to proper malacological protocols were taken, some cautious interpretation of malacofauna is feasible, always against the backdrop of the methodological issues. For this rough screening, bulk sediment samples from unit I were wet sieved (2 mm mesh) to separate the molluscs from the sediment. The tentative analyses show a poor species community with only two species comprising a high number (> 2000 individuals) of *Trochulus hispidus* and a smaller number (< 30 individuals) of *Succinella oblonga*. Both are euryoecious species, tolerating a wide range of conditions. The high number of shells that stood out visually in this layer is an indication that there was more vegetation and thus food supply and shelter compared to the rest of the sequence. However, *Trochulus hispidus* as well as *Succinella oblonga* are typical representatives of the poor snail communities found under extreme environmental conditions within Pleistocene loess ecosystems (e.g. Moine, 2008), as they are highly adaptable and able to tolerate both drought as well as temporary flooding. Their mere presence might indicate frequent wet-to-waterlogged ground conditions due to a depressed relief, permafrost-caused impermeable subsoil, and enhanced precipitation. Although caution is required due to methodological deficits, the low biodiversity and imbalance in the distribution of individuals among species equally indicate a highly stressed ecosystem and harsh conditions. Better conditions e.g. due to better-drained grounds and longer vegetation periods usually relate to a higher biodiversity within the snail communities (see Moine, 2008). For a more reliable interpretation, however, a detailed examination of the gastropod fauna is necessary, including an adequate sampling technique and analyses of the complete sequence.

From a geomorphogenetic point of view, the position of SID in an incised channel favours both sediment accumulation and moisture availability (Lehmkuhl et al., 2016). Especially during times with waterlogging, e.g. induced by permafrost conditions, moisture became concentrated in such depressions. These conditions led to the formation of wetlands, with temporary flooding within the channel caused by increased precipitation. As the Late Pleistocene was characterised by several phases of relatively enhanced dust fluxes (Zens et al., 2018; Fischer et al., 2021), and the SID site is located near potential dust sources, mainly the Pleistocene braided systems of the Meuse and the Rhine, as well as their tributaries (Lehmkuhl et al., 2018), these ponds were subjected to periodical inputs of aeolian dust. Although unit I partially shows slightly elevated sand contents (Fig. 3), the generally fine and particular unimodal GSD indicates input of aeolian dust into this marshy environment as the major sedimentological process.

5.1.2 Unit II

After the marshy environment was covered with aeolian dust, formation of unit II began. This unit's main characteristics are a distinct layering with alternating dark brown and ochre-beige bands as well as small ice-wedge pseudomorphs permeating the layers. Generally, the transition from unit I to unit II shows sharp decreases or increases in most analysed proxies (Figs. 3 and 4). Especially the GSD from a medium-coarse silt mode to a mode bordering the fine-sand fraction may indicate erosional processes during this transitional period. Layered units in LPSs are well known from the ELB (Lehmkuhl et al., 2021; Antoine et al., 2016, 2001, 2013). They are usually correlated to the Upper Pleniglacial Hesbaye loess (Haesaerts et al., 2016; Schirmer, 2016) and are explained by a shift towards colder, more humid climatic conditions, including extensive snow covers during winter. Dust sedimentation on snow covers leads to a fine lamination, which is most likely due to micro-sorting processes during snowmelt. These laminations are usually a few millimetres thick with sandy bases fining-up upwards (Antoine et al., 2001). The laminations in SID, however, are partly several centimetres thick and show distinct differences in both colour and grain size. These differences show up by the reflectance data and the grain size patterns: generally, unit II is coarser than unit I. Additionally, it shows larger GSD variations with sandier bands. These sandier bands usually show higher a^* values and a higher CIA, indicating soil sediment eroded from higher topographic positions deposited in the channel. The GSD, especially with the high fluctuations of sand contents, excludes in situ soil-forming processes in this unit, although the ΔGSD is elevated in the clay fraction compared to unit I. Usually, this proxy is an indicator for in situ soil formation, as it reflects the neo-formation of clay minerals (Schulte and Lehmkuhl, 2018). In the case of unit II, however, the high ΔGSD together with other granulometric and sedimentological features rather point to a short-range transport of eroded soil material, where clay agglomerates were not destroyed during transport, and clay particles were not removed by further outwash. The stratigraphic inconsistencies of the luminescence ages (see Fig. 6 and Sect. 4.2) also indicate relocation by surface runoff, hindering complete bleaching of the material. Relatively low contents of carbonate within unit II also point to soil sediments, as carbonates were removed by leaching prior relocation. The lighter bands are associated with higher grain size index (GSI) and U-ratio values due to increased aeolian input of mineral dust or rather increased deposition of relocated loess (Fig. 4). The slightly vertical point distribution within the upper cluster of the A–CN–K ternary diagram, a feature which indicates hydraulic sorting (Pötter et al., 2021; Ohta, 2004), also points to reworking. Unit II was frequently overprinted by harsh, periglacial conditions, as indicated by a multitude of small, centimetre-scale ice-wedge casts permeating several layers of the package. The sedimentological features of the unit are the results of fluctuating environmental conditions during the formation phase of unit II.

5.1.3 Unit III

Unit III of the SID LPS shows a characteristic succession of an orange layer and two distinct palaeosol layers (Fig. 2). The sediments of unit III generally have finer GSD modes compared to unit II, paired with a slightly decreased U ratio and GSI. The entire unit shows evidence of heavy reworking by cryoturbation, especially wavy-layer contacts and low ΔGSD values for the clay fraction. This succession strongly resembles the so-called Eben Zone (see Sect. 5.2), which is an important UPG marker horizon for the oceanic ELB (Lehmkuhl et al., 2021; Schirmer, 2003). This zone is reflected in the proxy data, e.g. by enhanced clay contents and low GSI and U-ratio values between 3 and 2.5 m depth. The reworking of the soil material is expressed in the absence of very fine particles, shown in the ΔGSD ratios (Fig. 4). Generally, unit III shows fewer signs of intensive soil formation processes and less evidence for reworking by surface runoff than the layers of unit II. The carbonate contents and L^* values are increased as opposed to the decreased CIA and a^* values (Fig. 3).

5.1.4 Unit IV

Unit IV is composed of relatively unaltered loess. The unit is well sorted and is characterised by a typical GSD for central European loess deposits, showing a strong mode in the coarse silt fraction (Fig. S3). The high carbonate contents of approx. 20 % and L^* values of approx. 66 show characteristic values for pristine Late Pleistocene deposits of the western ELB. Unit IV was, therefore, formed by the deposition of aeolian dust and subsequent loessification processes. The sharp contact to the above-lying unit V, however, both observed in the field and in proxy data (Figs. 3 and 4), points to a phase of erosion after unit IV was formed.

5.1.5 Unit V

The uppermost unit V shows a combination of no carbonate, high a^* values, and reflectance (L^*). Macroscopic features, such as the fine layering and the high abundance of charcoal flitters, together with lack of carbonate and relatively uniform GSD, point to a colluvial origin of this layer. During colluviation, (soil) sediment eroded from higher positions was transported to and deposited at the site. Additionally, the layer was influenced by post-depositional alterations, such as decalcification.

5.2 Reconstruction of Pleniglacial dynamics

In combination with the luminescence dating results (see Sect. 3.2), the formation processes of the Siersdorf LPS draw a detailed picture of regional imprints of the late MPG–UPG transition in the western ELB. The Pleniglacial dynamics of the SID site are summarised in the following conceptual model (see also Fig. 7). The correlation of unit I to the MPG–UPG transition (Fig. 7a and b) is based on one sample (SID L6) near the upper boundary of the unit. Luminescence analyses yield ages of 24.9 ± 1.8 ka (Q) and 22.6 ± 1.2 ka (KF, potassium feldspar) respectively. These ages indicate that the marshy environment at SID prevailed at least until the Upper Pleniglacial phase a (UPGa) sensu (Zens et al., 2018). Nearby core drillings, however, show that this unit is in total approx. 2 m thick, reaching a depth of around 7 m (Fig. S2). Therefore, the waterlogged environment in the incised terrace channel occurred during large parts of the UPGa and most likely also during the MPG–UPG transition. This interpretation, however, is based on the SID L6 sample and stratigraphic evidence. Further and more detailed reconstructions of fluctuations within the MPG require a denser chronological framework, e.g. by radiocarbon dating of mollusc shells. Nonetheless, the here-presented data allow a tentative correlation of unit I to the MPG–UPG transition.

The MPG, closely correlated with the MIS 3, was a phase of severe environmental fluctuations in the ELB. Periods of climatic ameliorations and pedogenesis, due to higher moisture availability (Fischer et al., 2021; Antoine et al., 2013; Schirmer et al., 2012; Hošek et al., 2017; Vinnepand et al., 2020), alternated with periods of erosion and (re-)deposition of soils and sediment (Meszner et al., 2011, 2013). Phases of soil formations can be traced in proxy data, as the ΔGSD signals (Zens et al., 2018), organic carbon contents (Fischer et al., 2021), or the a^* values increase in palaeosols (Krauß et al., 2016), whereas relocation can be reconstructed e.g. using grain size data (Meszner et al., 2014). In SID, the late MPG and early UPG are characterised by marshy conditions (see Sect. 5.1). These conditions were favoured by waterlogging

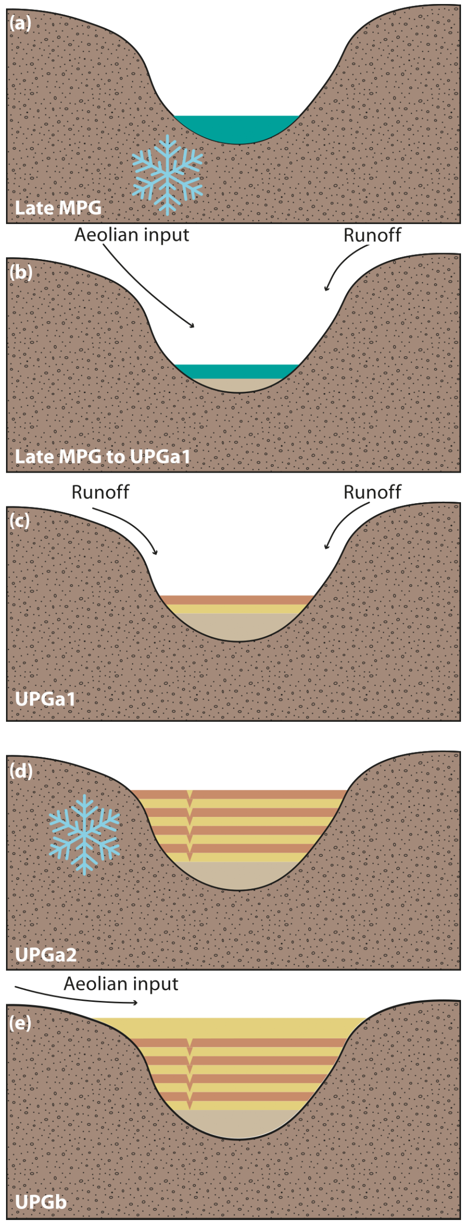

Figure 7. Schematic model of the Middle and early Upper Pleniglacial site formation of the Siersdorf LPS. **(a)** Marshy wetland conditions during the late MPG. **(b)** Silting up by aeolian input and surface runoff during the late MPG to early UPG. **(c)** Formation of layered unit by relocation of silty and sandy material by surface runoff in the early UPG (UPGa$_1$). **(d)** Periglacial overprinting and deformation of the layered unit during the LGM (UPGa$_2$). **(e)** Typical, subaerial loess formation during the UPGb.

due to permafrost (Fig. 7a), which was observed for other regions of the ELB (Sedov et al., 2016). These conditions are also reflected in the tentative malacological results, which show a potentially wet environment where the faunal assemblages were subjected to environmental stress.

The silting up of the marshy environment lasted during the MPG–UPG transitions until the early UPG (UPGa sensu; Zens et al., 2018). This phase of rapid climatic deterioration is in European loess landscapes coupled with a strong increase in dust production and subsequent loess formation (Meszner et al., 2013; Meyer-Heintze et al., 2018; Lehmkuhl et al., 2016; Antoine et al., 2013, 2009). This period is considered the phase with the highest dust accumulation rates in Europe (Zens et al., 2018; Frechen et al., 2003). In the LRE and other oceanic-influenced loess regions, the loess deposits of the beginning UPG, the so-called UPGa (Lehmkuhl et al., 2016; Zens et al., 2018, 2017), are named Hesbaye loess, (Schirmer, 2016) after the Belgian loess region (Haesaerts et al., 1997, 1981). The layered Hesbaye loess is often characterised by fluvial reworking or by dust deposition and loess formation under snow-influenced conditions. This feature is typical for the ELB and can be found from France towards the East European Plain (Antoine et al., 2009; Zens et al., 2018; Lehmkuhl et al., 2021). In SID, the layered unit II is dated by the quartz ages of samples SID L4 and L5 to 36.7–26.5 ka (Fig. 6). These calculated ages are stratigraphically inconsistent compared to SID L6, indicating deposition of older material after the formation of unit I. The inherited older ages of L4 and L5 as well as slightly older feldspar ages point to incomplete bleaching due to the relocation of the sediment, which points to a short transport range during sediment transport by surface runoff. The erosional processes during the MPG–UPG transition and the early UPG are widespread phenomena within the ELB (Meszner et al., 2013), often removing large parts or even entire MPG successions. The proxy data of unit II, in combination with the luminescence properties, allow for a reconstruction of short-scale transport of Middle Pleniglacial soil material during the UPGa, particularly to the steppe phase (Zens et al., 2018; Sirocko et al., 2016). The relocated material was frequently subjected to harsh, periglacial conditions, as indicated by a multitude of small ice-wedge casts (Fig. 2). Based on these geomorphological features, the periglacial overprinting is correlated to the tundra stage of the UPGa (Zens et al., 2018; Sirocko et al., 2016) where cold, dry conditions prevailed.

The later UPG succession (UPGb; Lehmkuhl et al., 2016; Zens et al., 2018, 2017) is also known as the Brabant member in the regional stratigraphy and mostly reflects loess formation during fully glacial conditions (Schirmer, 2016, 2000). Samples L4 and L3 bracket the orange and brownish-greyish complex of unit III, with ages between 30 and 21 ka. The ages, especially derived from quartz minerals (L4: 29.6 ± 3.1 ka; L3: 20.7 ± 1.2 ka), as well as the characteristics of this unit, allow a correlation with the so-called Eben Zone, composed of the orange Kesselt layer and the brownish-greyish Belmen and Elfgen soils (Schirmer, 2003). The high overlap of quartz- and feldspar-derived luminescence ages can be explained by the aeolian origin of this layer, which was indeed overprinted by periglacial processes but not by relocation. This characteristic zone is restricted to the Lower Rhine area and is a key marker layer for the UPG (Zens et al., 2018; Lehmkuhl et al., 2016, 2021). Samples L3 and L2 reflect the MIS 2 age of the Brabant loess. Their partial overlap within uncertainties allows a tentative, semi-quantitative reconstruction of accumulation rates, which were the highest during the LGM. This is in accordance with the general aeolian setting of the ELB (Rousseau et al., 2021). The typical subaerial characteristics of the upper units of SID indicate drier conditions compared to unit I, which can be related to the ongoing filling of the channel and lower moisture availability.

As the geomorphological setting is crucial not only for dust accumulation but also for preservation of LPSs especially (Lehmkuhl et al., 2016; Antoine et al., 2016; Marković et al., 2018), the favourable position of SID in a channel incised into an old Meuse River terrace led to a relatively thick accumulation of most likely Middle but especially Upper Pleniglacial sediments. Although LPSs in other extraordinary geomorphological situations such as loess dunes, so-called *gredas* (Antoine et al., 2001, 2009), or near watersheds (Henze, 1998; Zens et al., 2018) allow even thicker Pleniglacial loess deposits, the UPG record of SID exceeds those of many other regions in adjacent areas (Krauß et al., 2021; Antoine et al., 2016; Rahimzadeh et al., 2021; Krauß et al., 2016). Unit IV preserved 1 m of unaltered loess. Although loess formation generally continued throughout the late glacial in the Rhenish loess realm (Zens et al., 2018; Fischer et al., 2021), the SID sequence does not show any signs of late MIS 2 loess formation. The uppermost sample SID L2 within the Brabant loess yields quartz ages of 20.4 ± 1.5 ka (feldspar: 19.2 ± 1.1 ka), indicating late UPG ages for loess formation of the youngest preserved loess. Late glacial loess formation cannot be excluded for SID. However, these deposits were most likely eroded during the Pleistocene–Holocene transition. Extremely harsh and cold periglacial conditions during the UPG have influenced the sequence, as a large approx. 2 m deep ice-wedge pseudomorph pierced almost the entire sequence 3 m from the sampling spot (Fig. 2). As this cast is filled with material very similar to unit IV and pierces all underlying units, the age can be constrained to the UPG, although no direct timing was possible.

The LRE was strongly affected by anthropogenically induced soil erosion since the Early to Middle Holocene (Gerlach, 2006; Gerlach et al., 2006; Protze, 2014; Schulz, 2007; Gerz, 2017). However, the feldspar age calculated from the sample SID L1, taken from the base of the colluvial unit, yields a late glacial age (16.2 ± 0.8 ka). The quartz age (34.4 ± 2.5 ka) was excluded from the discussion, as it cannot be explained e.g. by partial bleaching possibly during extreme precipitation events. As the widespread and intensive colluviation in the area only occurred in the Middle to Late Holocene (Schulz, 2007; Protze, 2014), it appears that the material was not fully bleached during relocation. Therefore, an exact timing of these erosional processes is not possible. Stratigraphical evidence of nearby exposures, however, indicates tectonic activities during the Late Pleistocene and Holocene, as features such as the decalcification boundary were affected by tectonic displacement. Therefore, the colluviation in SID could be the result of a landscape reorganisation due to tectonic movements in a highly active region (Fernández-Steeger et al., 2011; Reicherter et al., 2011; Grützner et al., 2016).

The sedimentary sequence of SID shows a complex interplay of various depositional milieus together with proposed active tectonic setting. It is a valuable archive for landscape dynamics in the LRE and suggests that the area was highly diverse during the Late Pleistocene. The high-resolution sedimentological, geochemical, and spectrophotometric analyses reveal a change from wetter conditions with ephemeral ponds and wetlands to a silting up of these wetlands and highly erosive conditions towards typical subaerial loess formation. The SID sequence, therefore, is a crucial addition to the framework of the landscape analyses of the Pleniglacial western ELB.

6 Conclusions

The Siersdorf LPS is an important site for Late Pleistocene dynamics of the Lower Rhine Embayment, indicating changing depositional environments during the period covered. The combination of sedimentological, geochemical, and spectrophotometric data with luminescence dating and tentative malacological tests shows that the sequence was under the influence of a marshy wetland environment during the late MPG and early UPGa, a unique feature for the LRE. Observed permafrost-induced conditions show the strong influence of the geomorphological setting and related processes on characteristics of sedimentary sequences. The UPGb was influenced by long-lasting erosional processes, which, however, were constrained to short-range transport mechanisms. The typical subaerial formation processes of the upper part of the sequence correlated to the UPGa, with typical regional marker horizons such as the Eben Zone, point to cold-arid conditions during this time, as observed for large parts of the European loess belt. Overall, this study stresses the importance of the geomorphological setting and related sedimentological and post-depositional processes in relation to the formation, preservation, and resulting characteristics of LPSs. Our results show not only that the LRE was subjected to fluctuating climate during the Pleniglacial but also that the area was more fragmented than previously thought, especially regarding the environmental setting.

Data availability. Data are available upon request to the corresponding author.

Supplement. The supplement related to this article is available online at: https://doi.org/10.5194/egqsj-72-77-2023-supplement.

Author contributions. SP designed the study together with FL and PS. PS, MK, FL, and SP took the analysed samples during two separate fieldwork campaigns in 2020. KS and DB performed luminescence dating and laboratory tests and compiled and discussed the results within the scientific framework. CR analysed the mollusc shells and fragments, which were provided by MK, and discussed their interpretability. SP wrote the initial draft of the manuscript with helpful comments and suggestions from the other authors. All authors discussed the data and participated in its interpretation.

Competing interests. The contact author has declared that none of the authors has any competing interests.

Special issue statement. This article is part of the special issue "Quaternary research from and inspired by the first virtual DEUQUA conference". It is a result of the vDEUQUA2021 online conference in September/October 2021.

Acknowledgements. We thank Marianne Dohms, Renate Erdweg, and their team for the laboratory framework and Klaus Reicherter for his helpful comments on the tectonic evolution of the Lower Rhine Embayment in the field. We also thank the three anonymous reviewers for their constructive comments and remarks, which substantially improved this manuscript, and the editorial team for the uncomplicated handling of the manuscript.

Financial support. The investigations were carried out in the frame of the CRC 806 Our way to Europe – funded by the Deutsche Forschungsgemeinschaft (DFG, German Research Foundation, grant no. 57444011-SFB 806).

This open-access publication was funded
by the RWTH Aachen University.

Review statement. This paper was edited by Julia Meister and reviewed by three anonymous referees.

References

Allen, J. R. L. and Thornley, D. M.: Laser granulometry of Holocene estuarine silts: effects of hydrogen peroxide treatment, Holocene, 14, 290–295, https://doi.org/10.1191/0959683604hl681rr, 2004.

Antoine, P., Rousseau, D.-D., Zöller, L., Lang, A., Munaut, A.-V., Hatté, C., and Fontugne, M.: High-resolution record of the last Interglacial–glacial cycle in the Nussloch loess–palaeosol sequences, Upper Rhine Area, Germany, Quatern. Int., 76–77, 211–229, https://doi.org/10.1016/S1040-6182(00)00104-X, 2001.

Antoine, P., Catt, J., Lautridou, J.-P., and Sommé, J.: The loess and coversands of northern France and southern England, J. Quaternary Sci., 18, 309–318, https://doi.org/10.1002/jqs.750, 2003.

Antoine, P., Rousseau, D.-D., Moine, O., Kunesch, S., Hatté, C., Lang, A., Tissoux, H., and Zöller, L.: Rapid and cyclic aeolian deposition during the Last Glacial in European loess: a high-resolution record from Nussloch, Germany, Quaternary Sci. Rev., 28, 2955–2973, https://doi.org/10.1016/j.quascirev.2009.08.001, 2009.

Antoine, P., Rousseau, D.-D., Degeai, J.-P., Moine, O., Lagroix, F., Kreutzer, S., Fuchs, M., Hatté, C., Gauthier, C., Svoboda, J., and Lisá, L.: High-resolution record of the environmental response to climatic variations during the Last Interglacial–Glacial cycle in Central Europe: the loess-palaeosol sequence of Dolní Věstonice (Czech Republic), Quaternary Sci. Rev., 67, 17–38, https://doi.org/10.1016/j.quascirev.2013.01.014, 2013.

Antoine, P., Goval, E., Jamet, G., Coutard, S., Moine, O., Hérisson, D., Auguste, P., Guérin, G., Lagroix, F., Schmidt, E., Robert, V., Debenham, N., Meszner, S., and Bahain, J.-J.: Les séquences loessiques pléistocène supérieur d'Havrincourt (Pas-de-Calais, France): stratigraphie, paléoenvironnements, géochronologie et occupations paléolithiques, Quaternaire, 25, 321–368, https://doi.org/10.4000/quaternaire.7278, 2014.

Antoine, P., Coutard, S., Guerin, G., Deschodt, L., Goval, E., Locht, J.-L., and Paris, C.: Upper Pleistocene loess-palaeosol records from Northern France in the European context: Environmental background and dating of the Middle Palaeolithic, Quatern. Int., 411, 4–24, https://doi.org/10.1016/j.quaint.2015.11.036, 2016.

Auclair, M., Lamothe, M., and Huot, S.: Measurement of anomalous fading for feldspar IRSL using SAR, Radiat. Meas., 37, 487–492, https://doi.org/10.1016/S1350-4487(03)00018-0, 2003.

Baykal, Y., Stevens, T., Engström-Johansson, A., Skurzyński, J., Zhang, H., He, J., Lu, H., Adamiec, G., Költringer, C., and Jary, Z.: Detrital zircon U–Pb age analysis of last glacial loess sources and proglacial sediment dynamics in the Northern European Plain, Quaternary Sci. Rev., 274, 107265, https://doi.org/10.1016/j.quascirev.2021.107265, 2021.

Boenigk, W. and Frechen, M.: The Pliocene and Quaternary fluvial archives of the Rhine system, Quaternary Sci. Rev., 25, 550–574, https://doi.org/10.1016/j.quascirev.2005.01.018, 2006.

Bokhorst, M. P., Vandenberghe, J., Sümegi, P., Łanczont, M., Gerasimenko, N. P., Matviishina, Z. N., Marković, S. B., and Frechen, M.: Atmospheric circulation patterns in central and eastern Europe during the Weichselian Pleniglacial inferred from loess grain-size records, Quatern. Int., 234, 62–74, https://doi.org/10.1016/j.quaint.2010.07.018, 2011.

Böse, M., Ehlers, J., and Lehmkuhl, F.: Der Mittelgebirgsrand, in: Deutschlands Norden, Springer, Berlin, Heidelberg, 63–87, https://doi.org/10.1007/978-3-662-64361-7_4, 2022.

Durcan, J. A., King, G., and Duller, G. A. T.: DRAC: Dose Rate and Age Calculator for trapped charge dating, Quat. Geochronol., 28, 54–61, https://doi.org/10.1016/j.quageo.2015.03.012, 2015.

Eckmeier, E. and Gerlach, R.: Characterization of Archaeological Soils and Sediments Using VIS Spectroscopy, eTopoi – Journal for Ancient Studies, 3, 285–290, https://doi.org/10.17169/refubium-21739, 2012.

Fenn, K., Durcan, J. A., Thomas, D. S. G., Millar, I. L., and Marković, S. B.: Re-analysis of late Quaternary dust mass accumulation rates in Serbia using new luminescence chronology for loess–palaeosol sequence at Surduk, Boreas, 49, 634–652, https://doi.org/10.1111/bor.12445, 2020.

Fenn, K., Thomas, D. S. G., Durcan, J. A., Millar, I. L., Veres, D., Piermattei, A., and Lane, C. S.: A tale of two signals: Global and local influences on the Late Pleistocene loess sequences in Bulgarian Lower Danube, Quaternary Sci. Rev., 274, 107264, https://doi.org/10.1016/j.quascirev.2021.107264, 2021.

Fernández-Steeger, T., Grützner, C., Reicherter, K., and Schaub, A.: Aquisgrani terrae motus factus est (part 1): The Aachen cathedral (Germany) built on weak ground?, Quatern. Int., 242, 138–148, https://doi.org/10.1016/j.quaint.2011.05.004, 2011.

Fischer, P., Hilgers, A., Protze, J., Kels, H., Lehmkuhl, F., and Gerlach, R.: Formation and geochronology of Last Interglacial to Lower Weichselian loess/palaeosol sequences – case studies from the Lower Rhine Embayment, Germany, E&G Quaternary Sci. J., 61, 48–63, https://doi.org/10.3285/eg.61.1.04, 2012.

Fischer, P., Hambach, U., Klasen, N., Schulte, P., Zeeden, C., Steininger, F., Lehmkuhl, F., Gerlach, R., and Radtke, U.: Landscape instability at the end of MIS 3 in western Central Europe: evidence from a multi proxy study on a Loess-Palaeosol-Sequence from the eastern Lower Rhine Embayment, Germany, Quatern. Int., 502, 119–136, https://doi.org/10.1016/j.quaint.2017.09.008, 2017.

Fischer, P., Jöris, O., Fitzsimmons, K. E., Vinnepand, M., Prud'homme, C., Schulte, P., Hatté, C., Hambach, U., Lindauer, S., Zeeden, C., Peric, Z., Lehmkuhl, F., Wunderlich, T., Wilken, D., Schirmer, W., and Vött, A.: Millennial-scale terrestrial ecosystem responses to Upper Pleistocene climatic changes: 4D-reconstruction of the Schwalbenberg Loess-Palaeosol-Sequence (Middle Rhine Valley, Germany), CATENA, 196, 104913, https://doi.org/10.1016/j.catena.2020.104913, 2021.

Frechen, M., Schweitzer, U., and Zander, A.: Improvements in sample preparation for the fine grain technique, Anc. TL, 14, 15–17, 1996.

Frechen, M., Oches, E. A., and Kohfeld, K. E.: Loess in Europe – mass accumulation rates during the Last Glacial Period, Quaternary Sci. Rev., 22, 1835–1857, https://doi.org/10.1016/S0277-3791(03)00183-5, 2003.

Gerlach, R.: Holozän: Die Umgestaltung der Landschaft durch den Menschen seit dem Neolithikum, in: Urgeschichte im Rheinland, edited by: Kunow, J. and Wegner, H., Verlag des Rheinischen Vereins für Denkmalpflege und Landschaftsschutz, Köln, 87–98, ISBN 9783880948143, 2006.

Gerlach, R., Baumewerd-Schmidt, H., van den Borg, K., Eckmeier, E., and Schmidt, M. W. I.: Prehistoric alteration of soil in the Lower Rhine Basin, Northwest Germany – archaeological, 14C and geochemical evidence, Geoderma, 136, 38–50, https://doi.org/10.1016/j.geoderma.2006.01.011, 2006.

Gerz, J.: Prähistorische Mensch-Umwelt-Interaktionen im Spiegel von Kolluvien und Befundböden in zwei Löss-Altsiedellandschaften mit unterschiedlicher Boden- und Kulturgeschichte (Schwarzerderegion bei Halle/Saale und Parabraunerderegion Niederrheinische Bucht), Universitäts- und Stadtbibliothek Köln, Köln, URN urn:nbn:de:hbz:38-75297, 2017.

Grützner, C., Fischer, P., and Reicherter, K.: Holocene surface ruptures of the Rurrand Fault, Germany – insights from palaeoseismology, remote sensing and shallow geophysics, Geophys. J. Int., 204, 1662–1677, https://doi.org/10.1093/gji/ggv558, 2016.

Haesaerts, P., Juvigne, E., Kuyl, O., Mucher, H., and Roebroeks, W.: An account of the excursion of June, 13, 1981 in the Hesbaye area and to Dutch Limbourg, devoted to the chronostratigraphy of Upper Pleistocene loess, Ann.-Soc. Geol. Belg., 104, 223–240, 1981.

Haesaerts, P., Mestdagh, H., and Bosquet, D.: La séquence loessique de Remicourt (Hesbaye, Belgique), Notae Praehistoricae, 17, 45–52, 1997.

Haesaerts, P., Pirson, S., and Meijs, E.: Revised Lithostratigraphy of the aeolian loess deposits. Addendum to F. Gullentops et al. 2001. "Quaternary lithostratigraphic units (Belgium)", Geol. Belg., 4, 153–164, 2011.

Haesaerts, P., Damblon, F., Gerasimenko, N., Spagna, P., and Pirson, S.: The Late Pleistocene loess-palaeosol sequence of Middle Belgium, Quatern. Int., 411, 25–43, https://doi.org/10.1016/j.quaint.2016.02.012, 2016.

Hatté, C., Antoine, P., Fontugne, M., Lang, A., Rousseau, D.-D., and Zöller, L.: δ^{13}C of Loess Organic Matter as a Potential Proxy for Paleoprecipitation, Quaternary Res., 55, 33–38, https://doi.org/10.1006/qres.2000.2191, 2001.

Hatté, C., Gauthier, C., Rousseau, D.-D., Antoine, P., Fuchs, M., Lagroix, F., Marković, S. B., Moine, O., and Sima, A.: Excursions to C4 vegetation recorded in the Upper Pleistocene loess of Surduk (Northern Serbia): an organic isotope geochemistry study, Clim. Past, 9, 1001–1014, https://doi.org/10.5194/cp-9-1001-2013, 2013.

Henze, N.: Kennzeichnung des Oberwürmlösses der Niederrheinischen Bucht, Geologisches Institut der Universität zu Köln, Dissertation, Köln, 212 pp., ISBN 978-3-934027-00-8, 1998.

Hošek, J., Lisá, L., Hambach, U., Petr, L., Vejrostová, L., Bajer, A., Grygar, T. M., Moska, P., Gottvald, Z., and Horsák, M.: Middle Pleniglacial pedogenesis on the northwestern edge of the Carpathian basin: A multidisciplinary investigation of the Bíňa pedo-sedimentary section, SW Slovakia, Palaeogeogr. Palaeoclimatol. Palaeoecol., 487, 321–339, https://doi.org/10.1016/j.palaeo.2017.09.017, 2017.

ISO 20693: Soil quality – Determination of carbonate content – Volumetric method, International Organization for Standardization, Geneva, 1995.

Jary, Z.: Periglacial markers within the Late Pleistocene loess–palaeosol sequences in Poland and Western Ukraine, Quatern. Int., 198, 124–135, https://doi.org/10.1016/j.quaint.2008.01.008, 2009.

Jary, Z. and Ciszek, D.: Late Pleistocene loess–palaeosol sequences in Poland and western Ukraine, Quatern. Int., 296, 37–50, https://doi.org/10.1016/j.quaint.2012.07.009, 2013.

Kappler, C., Kaiser, K., Tanski, P., Klos, F., Fülling, A., Mrotzek, A., Sommer, M., and Bens, O.: Stratigraphy and age of colluvial deposits indicating Late Holocene soil erosion in northeastern Germany, CATENA, 170, 224–245, https://doi.org/10.1016/j.catena.2018.06.010, 2018.

Kels, H.: Bau und Bilanzierung der Lössdecke am westlichen Niederrhein, Heinrich-Heine-Universität Düsseldorf, URN urn:nbn:de:hbz:061-20070220-084835-4, 2007.

Klasen, N., Fischer, P., Lehmkuhl, F., and Hilgers, A.: Luminescence dating of loess deposits from the Remagen-Schwalbenberg site, Western Germany, Geochronometria, 42, https://doi.org/10.1515/geochr-2015-0008, 2015.

Klinge, M., Lehmkuhl, F., Schulte, P., Hülle, D., and Nottebaum, V.: Implications of (reworked) aeolian sediments and paleosols for Holocene environmental change in Western Mongolia, Geomorphology, 292, 59–71, https://doi.org/10.1016/j.geomorph.2017.04.027, 2017.

Knaak, M., Becker, S., Steffens, W., Mustereit, B., Hartkopf-Fröder, C., Prinz, L., Stichling, S., Schulte, P., and Lehmkuhl, F.: Boden des Jahres 2021 – ein Lössprofil auf der Aldenhovener Lössplatte, in: Archäologie im Rheinland 2020, Nünnerich-Asmus, Oppenheim, ISBN 978-3-96176-162-3, 2021.

Koch, R. and Neumeister, H.: Zur Klassifikation von Lösssedimenten nach genetischen Kriterien (About the classification of loess sediments using genetic criteria), Z. Geomorphol. NF, 49, 183–203, 2005.

Krauß, L., Zens, J., Zeeden, C., Schulte, P., Eckmeier, E., and Lehmkuhl, F.: A multi-proxy analysis of two loess-paleosol sequences in the northern Harz foreland, Germany, Palaeogeogr. Palaeoclimatol. Palaeoecol., 461, 401–417, https://doi.org/10.1016/j.palaeo.2016.09.001, 2016.

Krauß, L., Klasen, N., Schulte, P., and Lehmkuhl, F.: New results concerning the pedo- and chronostratigraphy of the loess–palaeosol sequence Attenfeld (Bavaria, Germany) derived from a multi-methodological approach, J. Quaternary Sci., 36, 1382–1396, https://doi.org/10.1002/jqs.3298, 2021.

Kühn, P., Lehndorff, E., and Fuchs, M.: Lateglacial to Holocene pedogenesis and formation of colluvial deposits in a loess landscape of Central Europe (Wetterau, Germany), CATENA, 154, 118–135, https://doi.org/10.1016/j.catena.2017.02.015, 2017.

Kukla, G., Heller, F., Ming, L. X., Chun, X. T., Sheng, L. T., and Sheng, A. Z.: Pleistocene climates in China dated by magnetic susceptibility, Geology, 16, 811–814, https://doi.org/10.1130/0091-7613(1988)016<0811:PCICDB>2.3.CO;2, 1988.

Lehmkuhl, F.: Modern and past periglacial features in Central Asia and their implication for paleoclimate reconstructions, Prog. Phys. Geogr. Earth Environ., 40, 369–391, https://doi.org/10.1177/0309133315615778, 2016.

Lehmkuhl, F., Wirtz, S., Falk, D., and Kels, H.: Geowissenschaftliche Untersuchungen zur Landschaftsentwicklung im Tagebau Garzweiler – LANU-Projekt 2012–2014, in: Archäologie im Rheinland 2014, edited by: Kunow, J. and Trier, M., Theiss Verlag, Stuttgart, 64–66, ISBN 978-3-8062-3214-1, 2015.

Lehmkuhl, F., Zens, J., Krauß, L., Schulte, P., and Kels, H.: Loess-paleosol sequences at the northern European loess belt in Germany: Distribution, geomorphology and stratigraphy, Quaternary Sci. Rev., 153, 11–30, https://doi.org/10.1016/j.quascirev.2016.10.008, 2016.

Lehmkuhl, F., Pötter, S., Pauligk, A., and Bösken, J.: Loess and other Quaternary sediments in Germany, J. Maps, 14, 330–340, https://doi.org/10.1080/17445647.2018.1473817, 2018.

Lehmkuhl, F., Nett, J. J., Pötter, S., Schulte, P., Sprafke, T., Jary, Z., Antoine, P., Wacha, L., Wolf, D., Zerboni, A., Hošek, J., Marković, S. B., Obreht, I., Sümegi, P., Veres, D., Zeeden, C., Boemke, B. J., Schaubert, V., Viehweger, J., and Hambach, U.: Loess landscapes of Europe – mapping, geomorphology, and zonal differentiation, Earth-Sci. Rev., 215, 103496, https://doi.org/10.1016/j.earscirev.2020.103496, 2021.

Marković, S. B., McCoy, W. D., Oches, E. A., Savic, S., Gaudenyi, T., Jovanovic, M., Stevens, T., Walther, R., Ivanisevic, P., and Galic, Z.: Paleoclimate record in the Upper Pleistocene loess-paleosol sequence at Petrovaradin brickyard (Vojvodina, Serbia), Geol. Carpathica, 56, 545–552, 2005.

Marković, S. B., Stevens, T., Kukla, G. J., Hambach, U., Fitzsimmons, K. E., Gibbard, P., Buggle, B., Zech, M., Guo, Z., Hao, Q., Wu, H., O'Hara Dhand, K., Smalley, I. J., Újvári, G., Sümegi, P., Timar-Gabor, A., Veres, D., Sirocko, F., Vasiljević, D. A., Jary, Z., Svensson, A., Jović, V., Lehmkuhl, F., Kovács, J., and Svirčev, Z.: Danube loess stratigraphy – Towards a pan-European loess stratigraphic model, Earth-Sci. Rev., 148, 228–258, https://doi.org/10.1016/j.earscirev.2015.06.005, 2015.

Marković, S. B., Stevens, T., Mason, J., Vandenberghe, J., Yang, S., Veres, D., Újvári, G., Timar-Gabor, A., Zeeden, C., Guo, Z., Hao, Q., Obreht, I., Hambach, U., Wu, H., Gavrilov, M. B., Rolf, C., Tomić, N., and Lehmkuhl, F.: Loess correlations – Between myth and reality, Palaeogeogr. Palaeoclimatol. Palaeoecol., 509, 4–23, https://doi.org/10.1016/j.palaeo.2018.04.018, 2018.

Mayr, C., Matzke-Karasz, R., Stojakowits, P., Lowick, S. E., Zolitschka, B., Heigl, T., Mollath, R., Theuerkauf, M., Weckend, M.-O., Bäumler, R., and Gregor, H.-J.: Palaeoenvironments during MIS 3 and MIS 2 inferred from lacustrine intercalations in the loess–palaeosol sequence at Bobingen (southern Germany), E&G Quaternary Sci. J., 66, 73–89, https://doi.org/10.5194/egqsj-66-73-2017, 2017.

Meijs, E. P. M.: Loess stratigraphy in Dutch and Belgian Limburg, E&G Quaternary Sci. J., 51, 115–131, https://doi.org/10.3285/eg.51.1.08, 2002.

Meszner, S., Fuchs, M., and Faust, D.: Loess-Palaeosol-Sequences from the loess area of Saxony (Germany), E&G Quaternary Sci. J., 60, 4, https://doi.org/10.3285/eg.60.1.03, 2011.

Meszner, S., Kreutzer, S., Fuchs, M., and Faust, D.: Late Pleistocene landscape dynamics in Saxony, Germany: Paleoenvironmental reconstruction using loess-paleosol sequences, Quatern. Int., 296, 94–107, https://doi.org/10.1016/j.quaint.2012.12.040, 2013.

Meszner, S., Kreutzer, S., Fuchs, M., and Faust, D.: Identifying depositional and pedogenetic controls of Late Pleistocene loess-paleosol sequences (Saxony, Germany) by combined grain size and microscopic analyses, Z. Geomorphol., 58, 63–90, https://doi.org/10.1127/0372-8854/2014/S-00169, 2014.

Meyer-Heintze, S., Sprafke, T., Schulte, P., Terhorst, B., Lomax, J., Fuchs, M., Lehmkuhl, F., Neugebauer-Maresch, C., Einwögerer, T., Händel, M., Simon, U., and Solís Castillo, B.: The MIS 3/2 transition in a new loess profile at Krems-Wachtberg East – A multi-methodological approach, Quatern. Int., 464, 370–385, https://doi.org/10.1016/j.quaint.2017.11.048, 2018.

Moine, O.: West-european malacofauna from loess deposits of the weichselian upper pleniglacial: Compilation and preliminary analysis of the database, Quaternaire, 19, 11–29, https://doi.org/10.4000/quaternaire.1532, 2008.

Murray, A. S. and Wintle, A. G.: Luminescence dating of quartz using an improved single-aliquot regenerative-dose protocol, Radiat. Meas., 32, 57–73, https://doi.org/10.1016/S1350-4487(99)00253-X, 2000.

Nesbitt, H. W. and Young, G. M.: Early Proterozoic climates and plate motions inferred from major element chemistry of lutites, Nature, 299, 715–717, https://doi.org/10.1038/299715a0, 1982.

Nesbitt, H. W. and Young, G. M.: Prediction of some weathering trends of plutonic and volcanic rocks based on thermodynamic and kinetic considerations, Geochim. Cosmochim. Ac., 48, 1523–1534, https://doi.org/10.1016/0016-7037(84)90408-3, 1984.

Nottebaum, V., Stauch, G., Hartmann, K., Zhang, J., and Lehmkuhl, F.: Unmixed loess grain size populations along the northern Qilian Shan (China): Relationships between geomorphologic, sedimentologic and climatic controls, Quatern. Int., 372, 151–166, https://doi.org/10.1016/j.quaint.2014.12.071, 2015.

Obreht, I., Zeeden, C., Schulte, P., Hambach, U., Eckmeier, E., Timar-Gabor, A., and Lehmkuhl, F.: Aeolian dynamics at the Orlovat loess–paleosol sequence, northern Serbia, based on detailed textural and geochemical evidence, Aeolian Res., 18, 69–81, https://doi.org/10.1016/j.aeolia.2015.06.004, 2015.

Obreht, I., Hambach, U., Veres, D., Zeeden, C., Bösken, J., Stevens, T., Marković, S. B., Klasen, N., Brill, D., Burow, C., and Lehmkuhl, F.: Shift of large-scale atmospheric systems over Europe during late MIS 3 and implications for Modern Human dispersal, Sci. Rep., 7, 5848, https://doi.org/10.1038/s41598-017-06285-x, 2017.

Ohta, T.: Geochemistry of Jurassic to earliest Cretaceous deposits in the Nagato Basin, SW Japan: implication of factor analysis to sorting effects and provenance signatures, Sediment. Geol., 171, 159–180, https://doi.org/10.1016/j.sedgeo.2004.05.014, 2004.

Özer, M., Orhan, M., and Işik, N. S.: Effect of particle optical properties on size distribution of soils obtained by laser diffraction, Environ. Eng. Geosci., 16, 163–173, 2010.

Pécsi, M.: Loess is not just the accumulation of dust, Quatern. Int., 7–8, 1–21, https://doi.org/10.1016/1040-6182(90)90034-2, 1990.

Pécsi, M. and Richter, G.: Löß: Herkunft – Gliederung – Landschaften, Borntraeger, Berlin, 391 pp., ISBN 978-3-443-21098-4, 1996.

Pötter, S., Veres, D., Baykal, Y., Nett, J. J., Schulte, P., Hambach, U., and Lehmkuhl, F.: Disentangling sedimentary pathways for the Pleniglacial Lower Danube loess based on geochemical signatures, Front. Earth Sci., 9, 1–25, https://doi.org/10.3389/feart.2021.600010, 2021.

Protze, J.: Eine "Mensch gemachte Landschaft" – Diachrone, geochemische und sedimentologische Untersuchungen an anthropogen beeinflussten Sedimenten und Böden der Niederrheinischen Lössbörde, Hochschulbibliothek der Rheinisch-Westfälischen Technischen Hochschule Aachen, Aachen, URN urn:nbn:de:hbz:82-opus-49066, 2014.

Rahimzadeh, N., Sprafke, T., Thiel, C., Terhorst, B., and Frechen, M.: A comparison of polymineral and K-feldspar post-infrared infrared stimulated luminescence ages of loess from Franconia, southern Germany, E&G Quaternary Sci. J., 70, 53–71, https://doi.org/10.5194/egqsj-70-53-2021, 2021.

Reicherter, K., Schaub, A., Fernández-Steeger, T., Grützner, C., and Kohlberger-Schaub, T.: Aquisgrani terrae motus factus est (part 2): Evidence for medieval earthquake damage in the Aachen Cathedral (Germany), Quatern. Int., 242, 149–157, https://doi.org/10.1016/j.quaint.2011.05.006, 2011.

Rousseau, D.-D. and Hatté, C.: Ground-Air Interface: The Loess Sequences, Markers of Atmospheric Circulation, in: Paleoclimatology, edited by: Ramstein, G., Landais, A., Bouttes, N., Sepulchre, P., and Govin, A., Springer International Publishing, Cham, 157–167, https://doi.org/10.1007/978-3-030-24982-3_13, 2021.

Rousseau, D.-D., Antoine, P., and Sun, Y.: How dusty was the last glacial maximum over Europe?, Quaternary Sci. Rev., 254, 106775, https://doi.org/10.1016/j.quascirev.2020.106775, 2021.

Schaller, K.: Praktikum Zur Bodenkunde Und Pflanzenernährung, 8th edn., Forschungsanstalt Geisenheim, Geisenheim, ISBN 978-3980187213, 2000.

Schirmer, W.: Eine Klimakurve des Oberpleistozäns aus dem rheinischen Löss, E&G Quaternary Sci. J., 50, 25–49, https://doi.org/10.3285/eg.50.1.02, 2000.

Schirmer, W.: Compendium of the Rhein loess sequence, Terra Nostra, 10, 8–23, 2002.

Schirmer, W.: Die Eben-Zone im Oberwürmlöss zwischen Maas und Rhein, in: Landschaftsgeschichte im Europäischen Rheinland, vol. 4, edited by: Schirmer, W., LIT Verlag, Münster, 351–416, ISBN 978-3-825-86009-7, 2003.

Schirmer, W.: Late Pleistocene loess of the Lower Rhine, Quatern. Int., 411, 44–61, https://doi.org/10.1016/j.quaint.2016.01.034, 2016.

Schirmer, W., Ikinger, A., and Nehring, F.: Die terrestrischen Böden im Profil Schwalbenberg/Mittelrhein (Terrestrial soils of the Schwalbenberg profile/Middle Rhine), Mainzer Geowissenschaftliche Mitteilungen, 40, 53–78, 2012.

Schulte, P. and Lehmkuhl, F.: The difference of two laser diffraction patterns as an indicator for post-depositional grain size reduction in loess-paleosol sequences, Palaeogeogr. Palaeoclimatol. Palaeoecol., 509, 126–136, https://doi.org/10.1016/j.palaeo.2017.02.022, 2018.

Schulte, P., Lehmkuhl, F., Steininger, F., Loibl, D., Lockot, G., Protze, J., Fischer, P., and Stauch, G.: Influence of HCl pretreatment and organo-mineral complexes on laser diffraction measurement of loess–paleosol-sequences, CATENA, 137, 392–405, https://doi.org/10.1016/j.catena.2015.10.015, 2016.

Schulz, W.: Die Kolluvien der westlichen Kölner Bucht – Gliederung, Entstehungszeit und geomorphologische Bedeutung, Universitäts- und Stadtbibliothek Köln, Cologne, Germany, URN urn:nbn:de:hbz:38-19656, 2007.

Sedov, S., Rusakov, A., Sheinkman, V., and Korkka, M.: MIS3 paleosols in the center-north of Eastern Europe and Western Siberia: Reductomorphic pedogenesis conditioned by permafrost?, CATENA, 146, 38–47, https://doi.org/10.1016/j.catena.2016.03.022, 2016.

Sirocko, F., Knapp, H., Dreher, F., Förster, M. W., Albert, J., Brunck, H., Veres, D., Dietrich, S., Zech, M., Hambach, U., Röhner, M., Rudert, S., Schwibus, K., Adams, C., and Sigl, P.: The ELSA-Vegetation-Stack: Reconstruction of Landscape Evolution Zones (LEZ) from laminated Eifel maar sediments of the last 60 000 years, Glob. Planet. Change, 142, 108–135, https://doi.org/10.1016/j.gloplacha.2016.03.005, 2016.

Skurzyński, J., Jary, Z., Raczyk, J., Moska, P., Korabiewski, B., Ryzner, K., and Krawczyk, M.: Geochemical characterization of the Late Pleistocene loess-palaeosol sequence in Tyszowce (Sokal Plateau-Ridge, SE Poland), Quatern. Int., 502, 108–118, https://doi.org/10.1016/j.quaint.2018.04.023, 2019.

Skurzyński, J., Jary, Z., Kenis, P., Kubik, R., Moska, P., Raczyk, J., and Seul, C.: Geochemistry and mineralogy of the Late Pleistocene loess-palaeosol sequence in Złota (near Sandomierz, Poland): Implications for weathering, sedimentary recycling and provenance, Geoderma, 375, 114459, https://doi.org/10.1016/j.geoderma.2020.114459, 2020.

Sprafke, T. and Obreht, I.: Loess: Rock, sediment or soil – What is missing for its definition?, Quatern. Int., 399, 198–207, https://doi.org/10.1016/j.quaint.2015.03.033, 2016.

Stadelmaier, K. H., Ludwig, P., Bertran, P., Antoine, P., Shi, X., Lohmann, G., and Pinto, J. G.: A new perspective on permafrost boundaries in France during the Last Glacial Maximum, Clim. Past, 17, 2559–2576, https://doi.org/10.5194/cp-17-2559-2021, 2021.

Steup, R. and Fuchs, M.: The loess sequence at Münzenberg (Wetterau/Germany): A reinterpretation based on new luminescence dating results, Z. Geomorphol., 61, 101–120, https://doi.org/10.1127/zfg_suppl/2016/0408, 2017.

Stevens, T., Sechi, D., Bradák, B., Orbe, R., Baykal, Y., Cossu, G., Tziavaras, C., Andreucci, S., and Pascucci, V.: Abrupt last glacial dust fall over southeast England associated with dynamics of the British-Irish ice sheet, Quaternary Sci. Rev., 250, 106641, https://doi.org/10.1016/j.quascirev.2020.106641, 2020.

Sümegi, P., Náfrádi, K., Molnár, D., and Sávai, S.: Results of paleoecological studies in the loess region of Szeged-Öthalom (SE Hungary), Quatern. Int., 372, 66–78, https://doi.org/10.1016/j.quaint.2014.09.003, 2015.

Svirčev, Z., Marković, S. B., Stevens, T., Codd, G. A., Smalley, I., Simeunović, J., Obreht, I., Dulić, T., Pantelić, D., and Hambach, U.: Importance of biological loess crusts for loess formation in semi-arid environments, Quatern. Int., 296, 206–215, https://doi.org/10.1016/j.quaint.2012.10.048, 2013.

Thiel, C., Buylaert, J.-P., Murray, A., Terhorst, B., Hofer, I., Tsukamoto, S., and Frechen, M.: Luminescence dating of the Stratzing loess profile (Austria) – Testing the potential of an elevated temperature post-IR IRSL protocol, Quatern. Int., 234, 23–31, https://doi.org/10.1016/j.quaint.2010.05.018, 2011.

Torre, G., Gaiero, D. M., Cosentino, N. J., and Coppo, R.: The paleoclimatic message from the polymodal grain-size distribution of late Pleistocene-early Holocene Pampean loess (Argentina), Aeolian Res., 42, 100563, https://doi.org/10.1016/j.aeolia.2019.100563, 2020.

Vandenberghe, J., French, H. M., Gorbunov, A., Marchenko, S., Velichko, A. A., Jin, H., Cui, Z., Zhang, T., and Wan, X.: The Last Permafrost Maximum (LPM) map of the Northern Hemisphere: permafrost extent and mean annual air temperatures, 25–17 ka BP: The Last Permafrost Maximum (LPM) map of the Northern Hemisphere, Boreas, 43, 652–666, https://doi.org/10.1111/bor.12070, 2014.

Varga, A., Újvári, G., and Raucsik, B.: Tectonic versus climatic control on the evolution of a loess–paleosol sequence at Beremend, Hungary: an integrated approach based on paleoecological, clay mineralogical, and geochemical data, Quatern. Int., 240, 71–86, https://doi.org/10.1016/j.quaint.2010.10.032, 2011.

Veres, D., Tecsa, V., Gerasimenko, N., Zeeden, C., Hambach, U., and Timar-Gabor, A.: Short-term soil formation events in last glacial east European loess, evidence from multi-method luminescence dating, Quaternary Sci. Rev., 200, 34–51, https://doi.org/10.1016/j.quascirev.2018.09.037, 2018.

Vinnepand, M., Fischer, P., Fitzsimmons, K., Thornton, B., Fiedler, S., and Vött, A.: Combining Inorganic and Organic Carbon Stable Isotope Signatures in the Schwalbenberg Loess-Palaeosol-Sequence Near Remagen (Middle Rhine Valley, Germany), Front. Earth Sci., 8, 276, https://doi.org/10.3389/feart.2020.00276, 2020.

Vinnepand, M., Fischer, P., Jöris, O., Hambach, U., Zeeden, C., Schulte, P., Fitzsimmons, K. E., Prud'homme, C., Perić, Z., Schirmer, W., Lehmkuhl, F., Fiedler, S., and Vött, A.: Decoding geochemical signals of the Schwalbenberg Loess-Palaeosol-Sequences – A key to Upper Pleistocene ecosystem responses to climate changes in western Central Europe, CATENA, 212, 106076, https://doi.org/10.1016/j.catena.2022.106076, 2022.

Vlaminck, S., Kehl, M., Lauer, T., Shahriari, A., Sharifi, J., Eckmeier, E., Lehndorff, E., Khormali, F., and Frechen, M.: Loess-soil sequence at Toshan (Northern Iran): Insights into late Pleistocene climate change, Quatern. Int., 399, 122–135, https://doi.org/10.1016/j.quaint.2015.04.028, 2016.

Zech, M., Zech, R., Buggle, B., and Zöller, L.: Novel methodological approaches in loess research – interrogating biomarkers and compound-specific stable isotopes, E&G Quaternary Sci. J., 60, 13, https://doi.org/10.3285/eg.60.1.12, 2011.

Zech, R., Zech, M., Marković, S., Hambach, U., and Huang, Y.: Humid glacials, arid interglacials? Critical thoughts on pedogenesis and paleoclimate based on multi-proxy analyses of the loess–paleosol sequence Crvenka, Northern Serbia, Palaeogeogr. Palaeoclimatol. Palaeoecol., 387, 165–175, https://doi.org/10.1016/j.palaeo.2013.07.023, 2013.

Zens, J., Zeeden, C., Römer, W., Fuchs, M., Klasen, N., and Lehmkuhl, F.: The Eltville Tephra (Western Europe) age revised: Integrating stratigraphic and dating information from different Last Glacial loess localities, Palaeogeogr. Palaeoclimatol. Palaeoecol., 466, 240–251, https://doi.org/10.1016/j.palaeo.2016.11.033, 2017.

Zens, J., Schulte, P., Klasen, N., Krauß, L., Pirson, S., Burow, C., Brill, D., Eckmeier, E., Kels, H., Zeeden, C., Spagna, P., and Lehmkuhl, F.: OSL chronologies of paleoenvironmental dynamics recorded by loess-paleosol sequences from Europe: Case studies from the Rhine-Meuse area and the Neckar Basin, Palaeogeogr. Palaeoclimatol. Palaeoecol., 509, 105–125, https://doi.org/10.1016/j.palaeo.2017.07.019, 2018.

E&G Quaternary Sci. J., 72, 95–111, 2023
https://doi.org/10.5194/egqsj-72-95-2023

Open Access E&G Quaternary Science Journal

Research article

Late Weichselian–Holocene valley development of the Elbe valley near Dresden – linking sedimentation, soil formation and archaeology

Christian Tinapp[1,2], Johannes Selzer[2], Norman Döhlert-Albani[1], Birgit Fischer[1], Susann Heinrich[3], Christoph Herbig[4], Frauke Kreienbrink[1], Tobias Lauer[3,5], Birgit Schneider[2], and Harald Stäuble[1]

[1]Saxonian Archaeological Heritage Office, Zur Wetterwarte 7, 01109 Dresden, Germany
[2]Institute of Geography, Leipzig University, Johannisallee 19a, 04103 Leipzig, Germany
[3]Max Planck Institute for Evolutionary Anthropology, Deutscher Platz 6, 04103 Leipzig, Germany
[4]independent researcher: Am Dorf 12, 63517 Rodenbach, Germany
[5]Department of Geosciences, University of Tübingen, Schnarrenbergerstrasse 94–96, 72076 Tübingen, Germany

Correspondence: Christian Tinapp (christian.tinapp@lfa.sachsen.de) and Johannes Selzer (johannes.selzer@bodengeo.de)

Relevant dates: Received: 21 July 2022 – Revised: 13 March 2023 – Accepted: 22 March 2023 – Published: 16 May 2023

How to cite: Tinapp, C., Selzer, J., Döhlert-Albani, N., Fischer, B., Heinrich, S., Herbig, C., Kreienbrink, F., Lauer, T., Schneider, B., and Stäuble, H.: Late Weichselian–Holocene valley development of the Elbe valley near Dresden – linking sedimentation, soil formation and archaeology, E&G Quaternary Sci. J., 72, 95–111, https://doi.org/10.5194/egqsj-72-95-2023, 2023.

Abstract: Valley infills are essential for understanding changes in hydrology and landscape. Anthropogenic activities are proven by prehistoric settlement remains, which mark distinct sediments and soils as usable land during certain time periods. In 2009 and 2018/19, excavations by the Saxonian Archaeological Heritage Office were conducted in the Elbe valley between Meißen and Dresden, preceding the construction of two natural gas pipelines. As a result, two important multicultural prehistoric sites were discovered on the Lower Weichselian Terrace (LWT) in different sediments and on varying stratigraphic levels.

During this study sediments and soils at the excavation sites and throughout the pipe trench have been documented. Micromorphological, sedimentological and geochemical investigations and analyses of archaeobotanical and archaeological finds, complemented by ^{14}C and optically stimulated luminescence (OSL) dating, enabled deciphering the structure of sediments and soils. Two major sites were the focus. At the Clieben site, an early Neolithic settlement and former topsoil, developed in a Weichselian valley loam above gravels and sands, are covered by younger overbank fines. At the Brockwitz site, shallow incision channels in the LWT were filled with clayey overbank fines during the Preboreal. An overprinting humic soil horizon was later anthropogenically overprinted during the early and middle Neolithic period. An omnipresent layer of Subboreal or younger overbank fines, covering the majority of the LWT in combination with the spatially confined Preboreal overbank fines, mirrors the ever-growing risk of flooding in a formerly attractive settlement area.

Kurzfassung: Talsedimente erlauben wichtige Einblicke in Veränderungen der Landschaft und der Hydrologie. Prähistorische anthropogene Aktivitäten hinterlassen Spuren in Sediment und Boden, die für bestimmte Phasen die Nutzbarkeit belegen. In den Jahren 2009 und 2018/19 führte der Bau von zwei Erdgasleitungen zu Ausgrabungen des Landesamtes für Archäologie Sachsen im Elbetal zwischen Meißen und Dresden. Zwei mehrphasige Siedlungsplätze wurden auf der Tieferen Niederterrasse (Lower Weichselian Terrace, LWT) entdeckt. Die Funde lagen in unterschiedlichen Sedimenten auf verschiedenen stratigraphischen Niveaus. Im Rahmen der Arbeiten wurden Sedimente und Böden im Bereich der Ausgrabungsplätze und im Bereich des Rohrgrabens aufgenommen. Mikromorphologische, sedimentologische, geochemische Untersuchungen, archäobotanische und archäologische Funde sowie ^{14}C- und OSL-Datierungen ermöglichen die zeitliche Einordnung der Sedimente und Böden. Dabei stehen zwei größere Areale im Fokus. Im Cliebener Untersuchungsareal liegen frühneolithische Siedlungsreste im Bereich eines begrabenen Bodens aus weichselzeitlichem Tallehm über Kiesen und Sanden, die von jüngeren Auenlehmen überdeckt werden. Im Brockwitzer Untersuchungsareal befinden sich flach eingeschnittene Rinnen in der LWT, die bereits im Präboreal mit tonigem Lehm verfüllt wurden. Ein in diesen Sedimenten entstandener humoser Oberbodenhorizont wurde durch anthropogene Aktivitäten während des Früh- und Mittelneolithikums überprägt. Nahezu die gesamte LWT wird von jüngeren Auenlehmen überdeckt, die seit dem Subboreal abgelagert wurden. Dies belegt die zunehmende Gefahr von Überschwemmungen auf einer ehemals siedlungsgünstigen Terrassenfläche.

1 Introduction

Archaeological sites in river valleys are important sources to reconstruct the Late Pleistocene–Holocene landscape development. This is due to the fact that prehistoric settlements or activities on the surfaces of different sediment and soil types demonstrate their accessibility for at least temporal site usage and that this accessibility strongly interacted with the river dynamics controlled by different external factors – tectonic activity, climate change, base level change and anthropogenic activity (Kaiser et al., 2012; Houben et al., 2013; Notebaert et al., 2018; Tinapp et al., 2019; Khoravichenar et al., 2020; von Suchodoletz et al., 2018, 2022).

The Elbe is the largest river in northeastern Germany. However, compared with other important central European river systems, such as the Rhine (Schirmer 1995), Vistula (Starkel et al., 2006) or Danube (Schellmann, 2018), late Weichselian–Holocene river and valley development is only fragmentarily understood (Kaiser et al., 2012). This is also caused by the fact that many archaeological sites within the Elbe valley still lack precise allocations to distinct sedimentary units (Ullrich and Ender, 2014; Conrad and Ender, 2016; Meller and Friederich, 2018). During the last years two pipeline construction projects have facilitated valuable transects across the sediments of the upper Elbe valley between the cities of Dresden and Meißen, allowing for studying the late Weichselian–Holocene evolution.

In the course of the archaeological excavations during the construction of the OPAL (Ostsee-Pipeline-Anbindungsleitung) natural gas pipeline in 2009, performed by the Saxonian Archaeological Heritage Office, an early Neolithic, middle Neolithic, late Bronze Age and medieval Slavic settlement were discovered (Steinmann, 2010). Later on, the construction of the EUGAL (Europäische Gas-Anbindungsleitung) pipeline parallel to the OPAL in 2019 allowed for further excavations, resulting in the expansion of already known and the discovery of new archaeological sites such as an early Mesolithic camp site and a middle Neolithic palisade/ditch enclosure (Kreienbrink et al., 2020; Döhlert-Albani et al., 2022; Stäuble et al., 2022).

Nearly all those archaeological sites were subsequently covered by overbank fines, whereas their archaeological features cut different older sediment units mostly belonging to the Lower Weichselian Terrace (LWT; "Tiefere weichselzeitliche Niederterrasse") of the Elbe River. Former geologic references indicate the sediments of the LWT to be sand and gravels with a younger cover of sandy loam or loamy sand called "valley loam" (*Tallehm*; Alexowsky, 2005). However, the discovery of not yet described clayey sediments with an overprinting palaeosol covering the LWT at the Brockwitz study site made further studies necessary.

Hence, this study aims to reconstruct the late Weichselian–Holocene evolution of the Elbe valley between the cities of Dresden and Meißen. This will allow for valid conclusions about former human occupation and its geomorphic–palaeoenvironmental context in the river valley and a comparison with the fluvial histories of other central European river systems. During our study we applied a comprehensive geoarchaeological approach that closely combined geoscientific methods with the archaeological excavations, an approach that is necessary to precisely study human–environmental interactions but that has been not very often systematically applied so far (von Suchodoletz et al., 2020). Our geoscientific set of methods encompassed stratigraph-

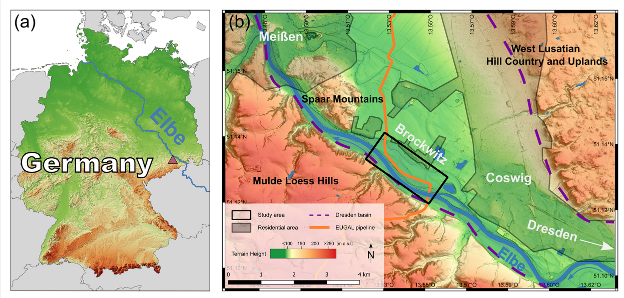

Figure 1. **(a)** The location of the study site with the Elbe River course and **(b)** the EUGAL pipeline in the Elbe valley with the study site (© GeoBasis-DE/BKG 2020, DGM1-GeoSN, OpenStreetMap contributors 2020 under the Open Data Commons Open Database License (ODbL) v1.0).

ical, micromorphological, sedimentological–geochemical and archaeobotanical methods as well as radiocarbon and luminescence dating and enabled the analysis of the formerly and newly detected fluvial sediments and palaeosols and their precise relations with former human activities.

2 Regional setting

The study area is situated in the northwestern Dresden basin ("Dresdner Elbtalweitung"), between the cities of Coswig and Meißen on the right Elbe banks (Figs. 1 and 2). Here, the about 3–8 km wide Dresden basin is framed by the West Lusatian Hill Country and Uplands ("Westlausitzer Hügel- und Bergland") granite massif to the east and northeast, the Mulde Loess Hills ("Mulde-Lösshügelland") to the west and the hilly "Großenhainer Pflege" to the north (Mannsfeld and Bernhardt, 2008; Tinapp, 2022).

Being one of central Europe's largest rivers (river length of 1094 km, catchment of 148 000 km^2) (Pusch et al., 2009), the Elbe originates from the southern Giant Mountains ("Krkonoše") in the Czech Republic at 1386 m a.s.l. From there, the upper Elbe flows in an arc through Bohemia, heads north and after crossing the German border passes over into the middle Elbe valley when entering the North German Plain north of the city of Meißen. Finally, the river meets the North Sea west of Hamburg (Hantke, 1993; Pusch et al., 2009).

Between the cities of Dresden and Meißen the Elbe valley's course has been predefined by the Variscan Elbe Fault System (EFS), one of the major crustal shear zones in Europe (Scheck et al., 2002). Up to 650 m of Cretaceous shallow marine and alluvial sand- and limestone reflect a manifold landscape history in and around this sedimentary basin (Tröger 2008). Simultaneously to the formation of the North Atlantic, the EFS shear zone reactivated during a late Cretaceous–early Cenozoic compression phase, when western Lusatia

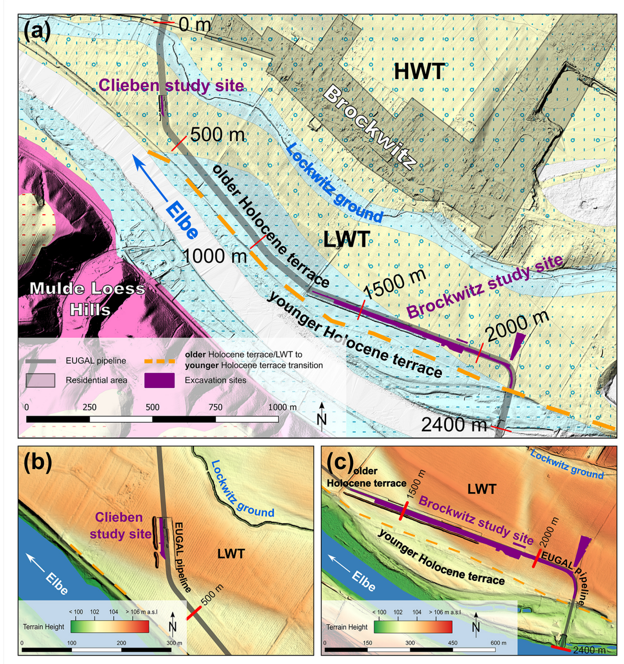

Figure 2. **(a)** Detailed view of the study area around the EUGAL pipeline with close-ups on the **(b)** Clieben and **(c)** Brockwitz study sites (© DGM1-GeoSN, OpenStreetMap contributors 2020 under the Open Data Commons Open Database License (ODbL) v1.0: Geologische Karte der eiszeitlich bedeckten Gebiete Sachsen 1 : 50 000 – LfULG Sachsen).

was moved southwestwards and thrusted over the EFS and its Cretaceous sediments (Krentz, 2008).

Until the Pliocene, a levelled landscape with shallow river valleys and a higher altitude than the current highlands had established. Throughout the Quaternary strong fluvial incision took place, resulting in the formation of multiple sets of river terraces (Wolf et al., 2008). In the study area, the current Elbe valley was initially used by several smaller streams, and only strong meltwater erosion caused by a lowered erosional base following the Elster 2 glaciation enabled the Elbe River to flow along its quasi-current course in the Dresden basin.

During the Drenthe stage of the Saalian glaciation the glaciers maximally advanced just south of the city of Meißen (Eissmann, 2002). Subsequently, up to 20 m thick sands were deposited in the Elbe valley by melting water. During the following Warthe stage strong river erosion occurred, forming several deep channels southeast of the Spaar Mountains, which represent the Quaternary base in this part of the Elbe valley (Huhle, 2015) (Fig. 1b).

During the Weichselian glaciation, a gravely Higher Weichselian Terrace (HWT) and Lower Weichselian Terrace (LWT) were aggraded under periglacial conditions (Wolf et al., 1994; Eissmann, 2002). Most likely during the Last Glacial Maximum were the gravely LWT sediments subsequently covered by a so-called valley loam (Tallehm; Alexowsky, 2005). Due to erosional processes during the Weichselian deglaciation, full LWT sequences including the covering valley loam are only rarely preserved (Eissmann, 1997).

During the Late Pleistocene and Holocene two additional fluvial terraces were aggraded (Wolf et al., 2008). The older and morphologically higher terrace is dated from the Late Pleistocene to Middle Holocene (Wolf et al., 1994, 2008), and the younger one had formed since the late Subboreal (Wolf et al., 2008; Lange et al., 2016). Holocene overbank fines cover both Holocene terraces and the LWT.

The Elbe valley between the cities of Dresden and Meißen has been occupied by sedentary humans for the last ca. 7500 years (Brestrich, 1998; Stäuble, 2010, 2016). Accordingly, during archaeological excavations in 2009 and 2018/19 at our Clieben study site, features of an early Neolithic village were discovered within the valley loam in the uppermost part of the LWT fines that was covered by younger overbank fines (Fig. 4; Steinmann, 2010; Kreienbrink et al., 2020; Kreienbrink, 2022). Here, about 10 LPC (Linear Pottery culture) houses were detected, and a large-scale geophysical survey gave evidence that these belong to a major early Neolithic settlement. Also a few late Bronze Age features were found between the early Neolithic pits on the same stratigraphical level (Kreienbrink, 2022).

Further to the south, at our Brockwitz study site, early Mesolithic, early and middle Neolithic, early and late Bronze Age, Iron Age, and medieval Slavic archaeological remains have been uncovered at different levels within different deposits during archaeological excavations in 2009 and 2018/19 (Steinmann, 2010; Kreienbrink et al., 2020; Döhlert-Albani et al., 2022). Most sites were situated on the LWT, and only early medieval Slavic features were predominantly situated on the older Holocene terrace (Tinapp et al., 2022).

3 Methods

3.1 Fieldwork

Parallel to the EUGAL pipeline construction in 2019, a 2400 m long stretch of the pipe trench with a depth of about 3 m, locally 6 m, has been examined. As a result, 42 profiles were logged, and the strata's courses were recorded and paralleled. The distinct strata were characterized in the field for grain size; sediment/soil colour; humus and moisture content; and pedogenetic and further features such as archaeological finds, plant material, sediment features or anomalies. Furthermore, plant and/or wood material was taken for radiocarbon dating.

At the Clieben and Brockwitz study sites profiles have been recorded in detail during the excavations. Their description followed the FAO (Food and Agriculture Organization of the United Nations) classification (IUSS Working Group WRB, 2014; soil colour was determined using the Munsell soil colour chart). Furthermore, samples were taken for sedimentological, micromorphological and palaeoecological analyses, as well as for optically stimulated luminescence (OSL) dating.

3.2 Sedimentological analyses

- First, bulk sediment samples were air-dried and sieved to obtain the fine fraction of < 2 mm that was used for the analyses. A portion of this material was subsequently ground in a planetary ball mill (PM 200) for 10 min to obtain a grain size of < 30 µm that is needed for X-ray fluorescence (XRF) and elemental analysis (CNS). Grain-size analyses were conducted on organic-free (pretreated with 35 % H_2O_2) material. The sand fraction was analysed by sieve analysis, and the clay silt fraction was analysed by X-ray granulometry (XRG; Micromeritics SediGraph III 5120).

- pH values were measured in a 0.01 M $CaCl_2$ suspension following DIN ISO 10390 with a ratio of 1 : 2.5 (soil / water).

- Carbonate contents were measured with the volumetric method referring to Scheibler by using an Eijkelkamp calcimeter.

- Total organic carbon (TOC) was determined by measuring C_{total} with a vario EL cube elemental analyser (Elementar) and subsequently subtracting inorganic carbon (taken from the carbonate measurements) from C_{total}. Total nitrogen and sulfur contents were measured with the vario EL cube elemental analyser in parallel with C_{total}.

- Element concentrations were measured using non-destructive X-ray fluorescence spectrometry (XRF). For this purpose, bulk samples were mixed with a wax binder (CEREOX Licowax) and pressed into 32 mm pellets. The measurements were performed with an energy-dispersive polarization XRF (EDPXRF) SPECTRO XEPOS (SPECTRO Analytical Instruments Ltd.) analyser in a helium gas atmosphere. All elements from Na to U were determined simultaneously and adjusted to the sample weight.

Pedogenesis depends not only on the properties of the parent material, the climatic conditions and human activity but also significantly on time. Weathering indices are multicomponent ratios of lithogeochemical compositional element and are commonly used to estimate weathering intensity, since they depict structural and mineralogical changes of the sediments during weathering. Over the past decades, very different indices and element ratios have been developed for different sediments in various climates (Pandarinath, 2022). Generally, the applied ratios usually expressed as oxidic proportions in moles determined by means of XRF are included in the calculation. Ideally, the applied ratios should only have been altered by pedogenetic processes.

During weathering, soluble cations with a low ion potential of < 3 (e.g. K^+, Na^+, Ca^{2+}, Mg^{2+}) are washed out relatively easily, whereas e.g. Al^{3+} with a high ion potential of 5.9 is bound in clay minerals and forms relatively insoluble hydroxides between a pH value of 4 and 10. Thus, the Al_2O_3 content changes very little during weathering and can hence be assumed to be constant (Bowen, 1979; Kausch, 2009). Consequently we selected the weathering index (VWI, visual weathering index) of Birkeland (1999), whereof low ratios indicate intensive weathering:

$$\mathrm{VWI} = (\mathrm{K_2O} + \mathrm{Na_2O} + \mathrm{CaO} + \mathrm{MgO})/\mathrm{Al_{2O_3}}.$$

In general, ion mobility decreases and the tendency of adsorption to fine-grain sediment or soil particles increases with a rising ion radius (Smykatz-Kloss et al., 2004). Hence, the larger Rb^+ ion is better adsorbed compared with the smaller K^+ ion so that the K_2O/Rb_2O ratio normally decreases during in situ soil formation. However, it is also assumed that high values in loess/palaeosol sequences could also reflect secondary potassium enrichment, possibly caused by clay accumulation due to the input of preweathered material (Fischer et al., 2012).

Also the ratios Rb/Sr and K_2O/Na_2O can be interpreted using differences in ionic radii. The respective smaller ions in the denominator ($Sr^{2''+}$ and Na^+) are more easily discharged as a result of weathering than the larger ions in the numerator (Rb^+ and K^+). Hence, high ratios represent strong weathering (Smykatz-Kloss, 2003; Reitner and Ottner, 2011).

3.3 Numerical dating

Luminescence (OSL) dating

Six luminescence samples were taken at the Brockwitz study site using light-tight steel tubes, which were hammered into the freshly cleaned outcrop walls (for sampling positions, see Fig. 7).

Preparation of the coarse-grain quartz fraction (180–250 µm) was done under subdued red light in the Department of Human Evolution, Max Planck Institute for Evolutionary Anthropology (Leipzig). Sample preparation started with drying and sieving, and subsequent chemical preparation included a treatment with 10 % HCl and 30 % H_2O_2 to remove carbonates and organic material, respectively. Following this, quartz was separated from the other mineral fractions by density separation using sodium polytungstate solutions (2.62 and 2.70 g cm^{-3}). Finally, the quartz-rich material was etched with 40 % hydrofluoric acid (HF) for 60 min and subsequently resieved.

Equivalent dose (De) measurements using a single-grain regeneration (SAR) approach (Murray and Wintle, 2003) were performed on a Risø TL/OSL (thermoluminescence) DA-20 reader equipped with blue and IR-emitting diodes. The blue stimulated quartz signal was measured at 125 °C for 40 s, and the 340 nm emission was filtered through a Hoya U340 filter. Irradiation was conducted with a calibrated $^{90}Sr/^{90}Y$ beta source (dose rate of 0.1 Gy s^{-1}). The preheat and cutheat temperatures were set to 170 °C, respectively, as this combination yielded satisfying results of the dose recovery test with a ratio of the measured to the given dose of 1.08 ± 0.09.

Between 24 and 48 aliquots with 2 mm size were measured of each sample. This aliquot size was chosen to obtain a sufficient high signal-to-noise ratio. The dose response curve was built with four regenerative doses, and for a quality check IR depletion and recycling ratios were determined. For final De estimation, only aliquots with deviations of < 20 % from unity (IR depletion and recycling ratio) were accepted.

Material for dosimetry was taken from the sampling spots and their nearby surroundings. Concentrations of the radioactive elements U, Th and K were determined using high-resolution gamma spectrometry at the Felsenkeller laboratory (VKTA) in Dresden, Germany, using a N-type detector.

Radiocarbon dating

Five radiocarbon samples were analysed in the Curt-Engelhorn-Zentrum Archäometrie in Mannheim (CEZ) using accelerator mass spectrometry (AMS) radiocarbon dating and were calibrated using IntCal20 and SwissCal 1.0.

3.4 Micromorphology

Micromorphological samples were taken from the Brockwitz study site in 2018 to characterize the different sediment layers and soil horizons. Thin sections were prepared from oriented and undisturbed blocks that were impregnated with resin. The thin sections were analysed using a petrographic microscope under plane-polarized light (ppl), cross-polarized light (xpl) and oblique incident light (oil). The microscopic description mainly followed the terminology after Bullock et al. (1985) and Stoops (2003).

3.5 Palaeobotanical analyses

Plant macroremains were extracted by flotation and wet sieving (mesh widths of 2, 0.5 and 0.25 mm) and determined under magnification from 6.3× to 40× using standard literature (e.g. Cappers et al., 2012) and the reference collection at the Laboratory of Archaeobotany, Institute of Prehistoric Archaeology, Goethe University. Attribution of the taxa to ecological units followed Oberdorfer (2001).

4 Results

The pipe trench and especially the uncovered sediments and soils at the two study sites during the excavations (Clieben and Brockwitz) allowed for detailed examinations of the late Weichselian and Holocene deposits in the Elbe valley.

Table 1. Stratigraphical positions (also see Fig. 7), dosimetric data, equivalent doses (De) and quartz OSL ages of the luminescence samples taken from profile 17 at the Brockwitz study site. The De values are based on the weighted mean of all accepted single De's.

Sample ID (L-Eva)	Unit	U [ppm]	Th [ppm]	K [%]	Cosmic Dose [mGy a^{-1}]	Total dose rate [mGy a^{-1}]	De (weighted mean) [Gy]	Age [ka]
1867	Overbank fines	3.9 ± 0.4	13.3 ± 0.8	1.87 ± 0.1	0.21 ± 0.02	3.09 ± 0.2	13.1 ± 3.7	4.24 ± 1.23
1868	Neolithic ditch	5.4 ± 0.6	14.6 ± 1.0	2.0 ± 0.1	0.19 ± 0.02	3.49 ± 0.2	28.2 ± 1.4	8.07 ± 0.64
1869	Clayey loam	4.1 ± 0.5	13.4 ± 0.9	1.92 ± 0.1	0.18 ± 0.02	3.15 ± 0.2	32.3 ± 3.7	10.27 ± 1.36
1870	Neolithic ditch	5.5 ± 0.6	14.4 ± 0.9	1.97 ± 0.1	0.18 ± 0.02	3.47 ± 0.2	27.2 ± 1.1	7.84 ± 0.58
1871	LWT sands	1.07 ± 0.2	2.98 ± 0.2	1.36 ± 0.1	0.17 ± 0.02	1.60 ± 0.2	25.1 ± 1.9	15.65 ± 2.15
1872	LWT sands	0.77 ± 0.2	2.32 ± 0.2	1.42 ± 0.1	0.16 ± 0.02	1.56 ± 0.2	22.9 ± 3.0	14.72 ± 2.60

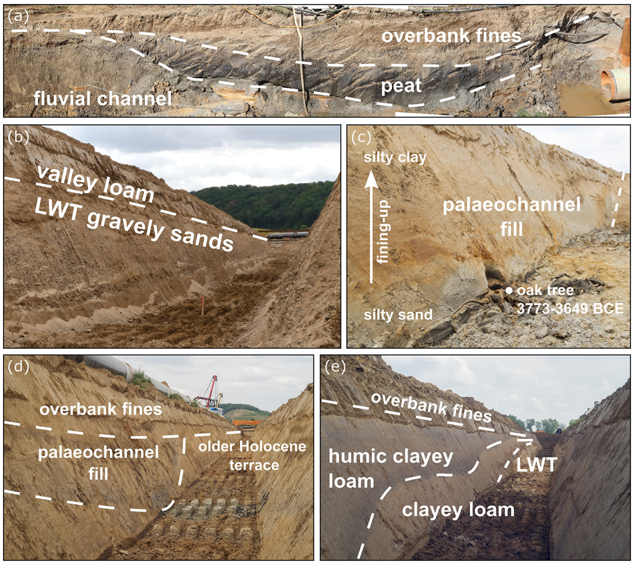

Figure 3. Several locations along the pipeline trench. **(a)** West-oriented profile in the Lockwitz ground, exposing peat covered by overbank fines surrounded by fluvial channel sediments (at 35 m). **(b)** South-oriented profile exposing LWT gravels with valley loam and Holocene overbank fines (at 350 m). **(c)** West-oriented profile south of the Clieben study site, exposing a palaeochannel at the transition of the LWT to the older Holocene terrace (at 430 m). **(d)** Southeast-oriented profile showing sediments of the older Holocene terrace with a palaeochannel and overlying overbank fines (at 870 m). **(e)** Southeast-oriented profile exposing clayey loam with a humic topsoil and arising LWT sediments in the background (at 1780 m).

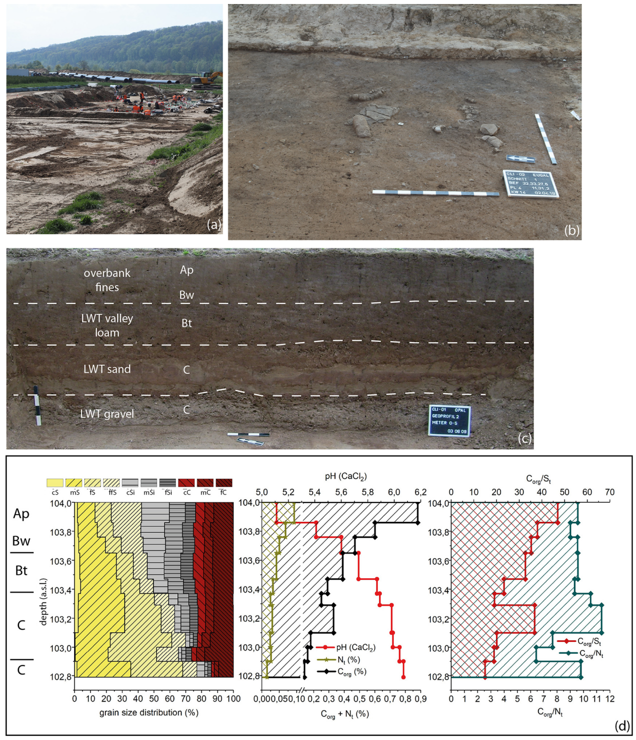

Figure 4. Clieben study site. **(a)** Overview of the archaeological excavations in 2019. **(b)** A section of the Neolithic surface with a broken rubbing stone. **(c)** Photo of profile 2 documented in 2008: the uppermost part of the LWT is formed by a valley loam that is covered by younger Holocene overbank fines. **(d)** Analytical values of profile 2 with particle size distribution and pH values, as well as organic carbon, sulfur and nitrogen contents and ratios.

4.1 Trench

Based on the examination of about 2.4 km of the EUGAL pipeline trench, several distinct sedimentary units could be identified. However, due to time and security constraints during pipeline construction, sediment description and sampling could not always be carried out at the same qualitative level along the trench.

4.1.1 LWT

LWT sediments were mainly found in two areas along the trench: in the northwestern part of the Clieben study site (Fig. 2, 150–420 m) and the southeastern part of the Brockwitz study site (Fig. 2, 2075–2175 m). LWT sandy gravels were superimposed by valley loam, which was covered by Holocene overbank fines (Fig. 3b). Remains of an early Neolithic settlement and linked archaeological findings at the Clieben study site stratigraphically reach from the surface of the valley loam into the underlying gravels and sands (Fig. 4). The terrain rises to > 104 m a.s.l. in the former settlement area at the Clieben study site (at 340 m), roughly 1 m higher compared with the surroundings (Fig. 2b). Similarly, in the southeastern part of the Brockwitz study site, a terrain height of 105 m a.s.l. (at ∼ 2125 m) after a steady ascent to the southeast marks a local maximum that surpasses its surrounding terrain height by ca. 1 m (Fig. 2c).

4.1.2 LWT and clayey loam

Along approximately 500 m of the pipe trench (1575–2075 m), i.e. a major part of the Brockwitz study site, a sequence of basal LWT gravely sands were cropped out. Upwards, these concordantly pass over into a 1–2 m thick layer of clayey loam that is overlain by Holocene overbank fines (Fig. 3e). OSL dating indicates a late Weichselian formation of the upper LWT deposits around 15 ka (Table 1, Fig. 7). In agreement with the OSL ages, an early Mesolithic camp site (at 1870 m) at the base of the clayey loam indicates a predominantly early Holocene deposition of the clayey loam. To the southeastern part of the Brockwitz study site, the clayey loam crosses out in gradually arising LWT sediments (at 2075 m).

One distinct palaeochannel was discovered in this part of the pipe trench (at 1950 m), cutting the clayey loam and the underlying LWT sands and gravels. The channel filling was similar to the clayey loam. These sediments are covered by older and younger Holocene overbank fines that are separated from each other by another palaeosol.

4.1.3 Holocene sediments

Gravely and sandy sediments of the older Holocene terrace with overlying overbank fines dominated the pipe trench for approximately 1.1 km between the Clieben and Brockwitz study sites (Fig. 3d, 420–1525 m). The base of the older Holocene terrace was formed by an about 1 m thick layer of gravely sands with some loamy strata showing a general decrease in gravels upwards. These were covered by ca. 2.5 m sandy overbank fines with a fining-upward trend. Here, strata thicknesses vary widely along the trench. Repeatedly, the base of the overbank fines reached deeper than the pipe trench, implying a vertical extension of > 4 m at these sections. Wood samples were taken from an oak tree that was found at the transition from the terrace gravels to the overlying overbank fines (635 m), which were 4.3 m thick at this particular location. Radiocarbon dating of this material gave a terminus post quem for the onset of the fine overbank sedimentation between 3962 and 3802 BCE (MAMS-45651, Table 2). Partly observed palaeosols divide the overbank into an older and younger sedimentation phase.

South of the Brockwitz study site (at 2240 m) the transition of the LWT with its covering overbank fines towards the current Elbe floodplain is marked by a ca. 2 m drop in terrain height. Within the latter the stratigraphy is dominated by sands and gravels of the younger Holocene terrace with covering younger Holocene overbank fines. With closer proximity to the river, the overbank fines' thickness gradually decreases. Additionally, a former river island with a thick gravel body, surpassing its vicinity by ca. 1 m, was observed close to the current bank of the Elbe River between 2300 and 2350 m (Fig. 2).

4.1.4 Holocene channels

The northwesternmost section of the pipe trench was dominated by non-LWT gravely sands. These stretched for approximately 150 m southward along the trench and subsequently thinned out into LWT sediments north of the Clieben study site around 150 m. Within these non-LWT gravely sands, an up to 3.3 m thick trough-shaped layer of dark-brown organic sediments with plant remains such as roots and stalks was embedded, showing a maximum lateral extent of ca. 25 m (Fig. 3a). Archaeobotanical analyses of the excavated organic material from the profile base classified these as sedge peat derived from a large variety of plant taxa, giving insight into the former local vegetation during the Boreal. The sedge peat/reed is represented by *Carex* spp., *Alisma plantago-aquatica* agg., *Lycopus europaeus*, *Scirpus lacustris*, *Typha* or *Oenanthe aquatica*, and several taxa suggest nutrient-rich conditions with a herbaceous vegetation in some parts of the banks (*Rumex maritimus*, *Ranunculus sceleratus*, *Polygonum lapathifolium*, *Polygonum minus* and *Chenopodium polyspermum*). Remains of *Betula pendula*, *Quercus*, *Polygonum dumetorum*, *Thalictrum flavum* and *Urtica dioica* mirror the adjacent alluvial forest, whereas aquatic plants such as *Nymphaea alba* or *Ceratophyllum demersum* show a standing waterbody without strong currents or waves.

The archaeobotanical analyses of the overlying layers dating to the Atlantic period merely confirmed the Boreal taxa spectrum with only minor alterations. The more abundant annuals *Atriplex* and *Chenopodium album* could have been distributed along the riverbanks or hint to nearby human activities. Especially seeds of the bladder cherry *Physalis alkekengi* are of special interest, since its natural distribution is on riverbanks in southeastern Europe. Hence, it must have been brought to the study area most probably with LPC settlers as a cultivated plant (Herbig 2012, p. 153).

The radiocarbon ages of three peat samples were 7776–7595 BCE (MAMS-44467), 6742–6573 BCE (MAMS-47072) and 3961–3800 BCE (MAMS-47071) (see Table 2). Hence, peat formation extended from the Boreal until the Atlantic period. Subsequently, the peat was covered by about 3 m thick overbank fines (loamy sands), into which the bed of the "Lockwitzbach" current creek is embedded.

Within an eastward bend of the trench south of the Clieben study site (Fig. 3c), the terrain height suddenly drops by about 1 m. Here, a diagonal, ca. 25 m wide palaeochannel marks the transition between the LWT to the north and the

Table 2. Results of the ^{14}C analyses.

MAMS	Unit	Material	^{14}C age [years]	±	$\delta^{13}C$ [‰]	Cal 1σ cal BCE [years]	Cal 2σ cal BCE [years]	C [%]
44 467	Peat, Lockwitz ground	Wood	8693	30	−27.9	7720–7613	7780–7600	57.8
44 468	Older Holocene terrace	Wood	4943	25	−27.5	3761–3664	3773–3657	50.1
45 651	Older Holocene terrace	Wood	5093	22	−28.4	3955–3813	3962–3802	53.4
47 071	Peat, Lockwitz ground	Seed	5090	23	−23.6	3953–3809	3961–3800	54.8
47 072	Peat, Lockwitz ground	Seed	7817	28	−26.7	6683–6600	6739–6576	46.9

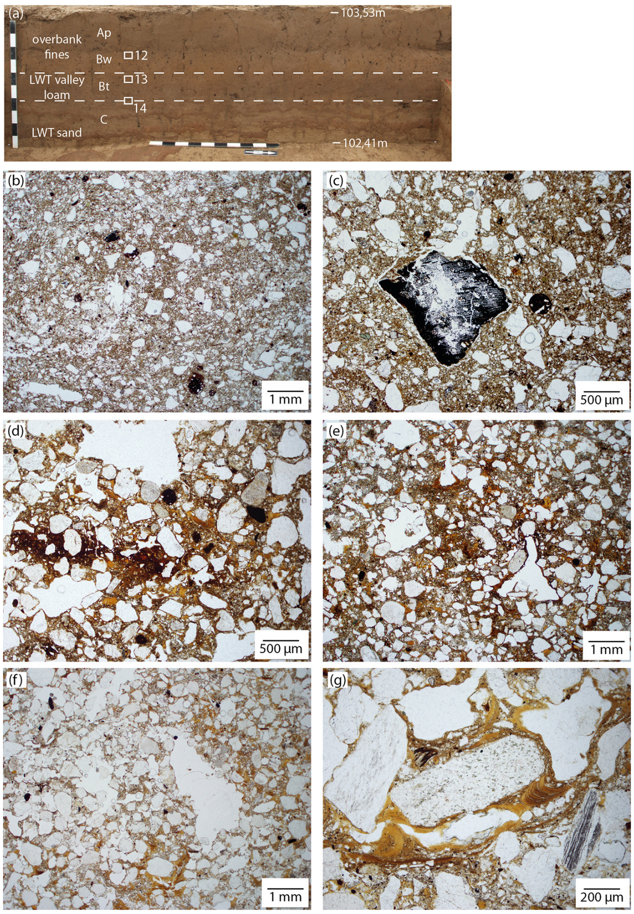

Figure 5. Clieben study site. **(a)** Photo of profile 3 which was studied in 2019 with locations of the thin-section samples (12: overbank fines, 13: LWT valley loam, 14: transition LWT valley loam to LWT sands). Microphotos of the thin sections (all in ppl): **(b)** sandy and silty overbank fines with disorthic iron oxide nodules, **(c)** overbank fines with charcoal pieces, **(d)** valley loam with disorthic iron oxide nodules and matrix impregnation, **(e)** valley loam with clay infillings and coatings of voids, **(f)** sandy material of the LWT, and **(g)** LWT material with clay infillings and coating of a void.

older Holocene terrace to the south and southeast (Fig. 2a). At the trench base at ca. 3 m depth, the channel is filled with organic-rich loamy sands, which contained one oak tree trunk. This oak tree has been radiocarbon-dated to 3773–3649 BCE (MAMS-44468, Table 2), i.e. to the late Atlantic period. The loamy sands are superimposed by grey sands, then followed by a fining-upward loam layer with a thickness of ca. 1 m that contained small proportions of sand and charcoal. The top of the profile was formed by 1.9 m thick clayey overbank fines (Fig. 3c). In addition to this a palaeochannel, three further palaeochannels with equal or smaller dimensions and similar sedimentary fillings were observed that were also incised into the sediments of the older Holocene terrace.

4.2 Clieben study site

Post holes and pits found between 0.5 and 1 m below the surface after removal of the covering overbank fines prove an early Neolithic settlement on the LWT (Fig. 4a and b; Steinmann, 2010; Kreienbrink, 2022). Furthermore also some features originating from the late Bronze Age were recorded on the same level. The northern boundary of the settlement is represented by the remnants of an old channel used by a small creek (Lockwitzbach) in recent times (Figs. 2 and 3a). In the south, the LWT is limited by the older Holocene terrace.

In the central part of the early Neolithic settlement the stratigraphical base is formed by LWT sands that merge upwards into the valley loam without clear boundaries (Fig. 4c). Soil development – weathering and lessivage – overprinted these Weichselian sediments. The Neolithic surface is found at an altitude of 103.6 m a.s.l. on the topographically highest part of the valley loam, and the LWT including the archaeological surface is covered by younger Holocene overbank fines. The latter consist of brown loamy sands that contain charcoal, fired clay and younger potsherds.

According to the analytical values of profile 2, the valley loam contains ∼ 0.3 % organic carbon, and the highest values of 0.9 % are found in the recent plough horizon (Ap) at the top of the overbank fines. However, the Neolithic surface with archaeological features and findings (upper part of the Bt horizon) does not show a peak of organic carbon. This is consistent with nearly the same colour of the valley loam and the Holocene overbank fines (dark yellowish brown, 10YR4/4).

The micromorphological analyses of samples taken from profile 3 prove that the upper overbank fines contain dis-

Figure 6. Brockwitz study site. **(a)** Aerial photo of the archaeological excavation with the Neolithic palisade in 2018 (1850–1940 m). **(b)** The early Mesolithic chipping floor during excavations. **(c)** Microliths (at 1870 m).

orthic (reworked) iron oxide nodules and charcoal pieces (Fig. 5b, c).

Pedogenic transformation of the Holocene overbank fines is rather weak, as only few small clay infillings and coatings of voids could be detected. Also the underlying Weichselian valley loam contains reworked iron oxides (disorthic nodules). In addition, in situ formed ferruginous matrix impregnations and an increasing number of clay coatings and infillings (Fig. 5d, e) are detectable in the valley loam. The latter features are undisturbed, indicating a stable period of postsedimentary soil formation during the late Weichselian to Holocene. The transition to the underlying LWT sands is clear, and these show downwards decreasing features of soil formation with the exception of clay illuviation features like infillings and coatings of voids that were even found in greater profile depth (Fig. 5f, g).

4.3 Brockwitz study site

The geological structure at the Brockwitz study site is less homogeneous compared to Clieben. A small area in the southeastern part belongs to the topographically highest peaks of the LWT, showing heights around 105 m a.s.l. (2075–2175 m). Here, some late Bronze Age features were dug into the valley loam and the underlying gravels and sands, and overbank fines are missing here. Compared to the elevated terrain in the southeast, the height of the remaining LWT surface is 1–3 m lower in most other parts of the study site. However, nowadays this altitudinal difference is levelled by Holocene overbank fines. Several sediment profiles were recorded here, and a combined sampling approach was applied to the sediments, soils and Neolithic features of profile 17 (Figs. 6, 7).

The base of that profile is formed by LWT sands that were dated by OSL to around 15 ka (Table 1, Fig. 7) and show only minor pedogenetic features. Thin sections show that parts of the sands are free of finer components, while clay illuviation, bridging the individual grains, is visible in other parts (Fig. 8e, f). Upwards the sands merge into clayey loam with up to 1 m thickness. Soil development overprinted parts of the latter material, and a 0.4 m thick Ahb horizon had established at its surface. The OSL date from the lowest part of the clayey loam shows an early Holocene age of 10.27 ± 1.36 ka (Table 1). In this layer clay percentages reach > 40 %, while sand remains around 20 %. Micromorphological samples were taken from both the undisturbed clayey loam and a Neolithic ditch filled with relocated clayey loam. The infilling is dark greyish brown and thus seems to be rich in organic matter and contains numerous undisturbed clay infillings and coatings of voids (Fig. 8b–d). Charcoal pieces prove anthropogenic activities (Fig. 8c). Deep cracks in the Ahb horizon caused by shrinking of the clayey material were filled with brown-coloured, younger overbank fines. Also macroscopic analysis shows strong aggregation features, while under the microscope vertic properties such as slickensides are absent. Despite the dark colour of the Ahb horizon (very dark greyish brown, 10YR3/2) organic carbon values reach only 0.6 % (Fig. 7).

The small VWI ratios in the upper, clay-rich C horizon show obvious preweathering of the substrate (Fig. 9). This tendency becomes even clearer in the K_2O/Rb_2O ratios. In the clay-rich Ahb and C horizons (103.4–102.55 m a.s.l.), the K_2O/Rb_2O ratio is < 400 and clearly demarcated from the other horizons, indicating in situ soil formation. Despite very high clay contents, it cannot be assumed that preweathered material was introduced.

The commonly used Rb/Sr ratio is based on different ion radii, since the much smaller Sr^{2+} ion is more easily leached during weathering, whereas Rb is fixed to clay (McLennan et al., 1993; Reitner and Ottner, 2011). Hence, high Rb/Sr ratios indicate intense weathering.

Similarly, due to partial adsorption of K^+ on clay minerals and organic substances, less K^+ is removed compared with the smaller Na^+ ion during chemical weathering so that increasing K_2O/Na_2O ratios indicate chemical weathering (Smykatz-Kloss, 2003). When comparing the soluble alkali cations K^+ and Na^+, a clear enrichment of the larger and therefore less mobile K^+ compared to the Na^+ ion can be detected during soil formation. Although both cations are dissolved during chemical weathering, some of the K^+ ions (radius of 138 pm) can subsequently be adsorbed again by fine-grain particles such as clay minerals or organic matter and thus be partially retained in the soil, while the smaller Na^+ ion (102 pm) is discharged into the soil solution. Given

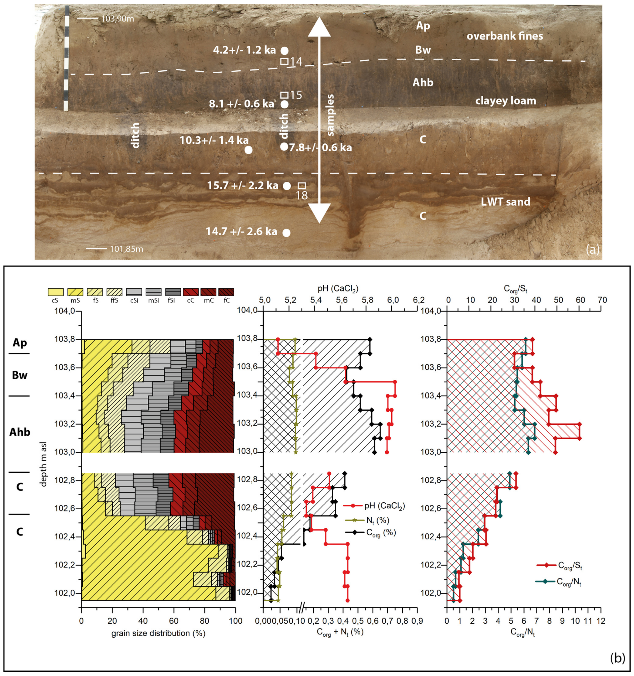

Figure 7. Brockwitz study site. **(a)** Photo of profile 17 (at 1860 m) that was studied in 2018 with two ditches from the Neolithic palisade, OSL ages and the positions of micromorphological samples (14: overbank fines, 15: clayey loam/Neolithic ditch, 18: LWT sands). **(b)** Analytical values of this profile with the particle size distribution and pH values, as well as organic carbon, sulfur and nitrogen contents and ratios.

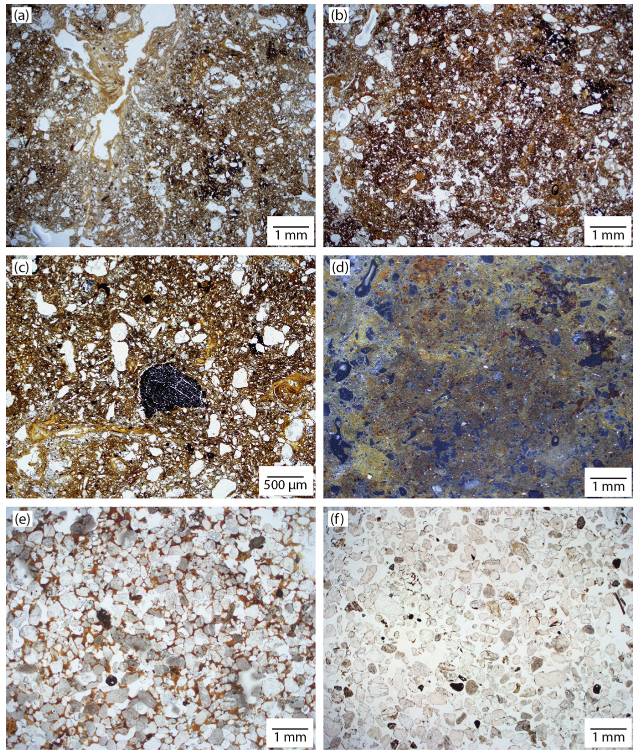

Figure 8. Brockwitz study site. Microphotos of profile 17 (A–C and E–F in ppl, D in oil). Sample 14 (overbank fines): **(a)** loamy cover sediment with iron oxides and clay coating of a void. Sample 15 (clayey loam from Neolithic ditch): **(b)** clayey loam rich in clay infillings and coatings of voids, **(c)** clayey loam with charcoal pieces, and **(d)** dark greyish brown of the clayey loam due to organic matter. Sample 18 (LWT sands): **(e)** sandy material of the LWT with clay bridging the sand grains and **(f)** sandy material of the LWT without fines.

that both the Rb/Sr and K_2O/Na_2O ratio are increased in the Ahb and C horizon, this clearly indicates their intensive weathering.

Just a few centimetres above the base of the clayey loam, an early Mesolithic campsite for hafting and retooling was discovered and excavated near profile 17 (Fig. 6). It consists of silex artefacts, destroyed by fire; quartzite pebbles; and pieces of burnt animal bone (Fischer in Döhlert-Albani et al., 2022). This demonstrates short human activity during the middle Preboreal causing the accumulation of a great number of artefacts and leftovers from meals (Fig. 6). Afterwards, clay-rich overbank sedimentation covered these artefacts relatively contemporaneously largely without replacing them, since $> 50\,\%$ of the silex inventory are chips of < 1 cm in length. The next verified human activities took place during the early and middle Neolithic leaving many pits, with up to six parallel ditches belonging to former palisades (Figs. 6, 7). Two OSL samples taken from the archaeosediments in one of these ditches gave early Neolithic ages of 7.8 ± 0.6 and 8.1 ± 0.6 ka (Table 1). Despite these numerical ages, a younger age (middle Neolithic: 6.4–4.8 ka; Miera et al., 2022) is assumed here for archaeological reasons; i.e. the luminescence ages must be overestimated (Stäuble et al., 2022). Later, these archaeosediments and the overprinting Ahb soil horizon were covered by younger overbank fines. The latter deposition started at the end of the Neolithic or the beginning of the Bronze Age during the Subboreal period, which is proved by the OSL age of 4.2 ± 1.2 ka and archaeological features of the late Bronze Age, which were partly dug into these younger overbank fines.

The younger overbank fines covering the clayey loam are more sandy and less clayey compared with the latter. Similar to the overbank fines in Clieben, their colour is dark yellowish brown (10YR4/4) and they contain charcoal pieces and reworked iron oxides (Fig. 8a).

5 Discussion

5.1 Late Weichselian–Holocene transition

During the late Weichselian cold period, the LWT showed a surface with a diverse morphology (Fig. 10): around 15 ka older gravels, supposedly deposited between the Denekamp Interstadial and the Last Glacial Maximum (LGM) (30 000–20 000 ka) (Alexowsky, 2005; Litt et al., 2007), nearly

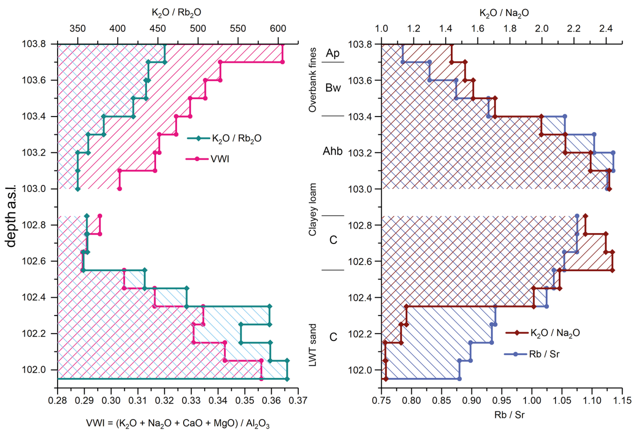

Figure 9. Brockwitz study site. Profile 17 with the alteration index (VWI) and the element ratios of K_2O, Rb_2O / Sr and K_2O / Na_2O.

reached an altitude of 105 m a.s.l., while sands were deposited in a 3 m deep channel at the Brockwitz study site. During that time the large gravel plain of the LWT, belonging to the braided Elbe River system (Kaiser et al., 2012), was dissected by several shallowly incised channels. Subsequently, fluvial sands were deposited during the initial warmer phases of the final glacial period. The channels on the LWT had been preserved and remained visible until the transition to the Holocene, quite similar to other late Weichselian terraces of the Rhine River or Danube River systems (Schirmer, 1995; Schellmann, 2018).

Sedimentation and erosion in the study area and especially during the formation of the LWT were closely connected to the larger-scale development of the Elbe River system. Seemingly, intense incision occurred in the central European river systems during the Early Holocene. However, in the Elbe valley this switch apparently occurred later (Brose and Präger, 1983) compared with other central European river systems (Kaiser et al., 2012). Here, a late Weichselian–Early Holocene anastomosing channel pattern is assumed. During that time the “Lockwitz ground” at the northern valley margin of our study area also formed part of the Elbe floodplain (Figs. 2, 3a). According to our ^{14}C dates, this channel was abandoned only after a middle–late Preboreal incision phase of the Elbe system, and its organic sediments demonstrate boggy conditions from the Boreal until the Atlantic period. Here, the location of the channel near the transition to the HWT intensified water influx, supporting organic-rich sedimentation regardless of the deep incision of the main Elbe channel. Hence, the location of the Lockwitz ground at the transition from the LWT towards the HWT defines it as a seam channel (*Nahtrinne*). This channel type marks the border between different terraces and hence aids as their distinction and was described e.g. at the Rhine, Main and Danube terraces (Schirmer, 1995; Schellmann, 2018).

The clayey loam was deposited in abandoned channels on the LWT during the Early Holocene. Whereas the covering younger Late Holocene overbank sediments were explained by increasing river discharge caused by anthropogenic impact on the catchment, the cause of the deposition of these Early Holocene deposits has not been addressed so far. Similar observations were reported from the lower Weser valley (Schellmann, 1994; Schirmer, 1995). It is located in the low mountain ranges of southern northern Germany, i.e. some kilometres south of the North German Plain. There, a dark soil (*Feuchtschwarzerde*) had developed in overbank fines, which were deposited in palaeochannels (*Aurinnen*) incised in Weichselian gravels. According to Schellmann (1994) these soils had developed in the Allerød period as well as in the Early Holocene. Similar conditions are also found for the Elbe valley between Dresden and Riesa. Here the valley bottom still consists of Palaeozoic rocks, whereas in the North German Plain near Riesa some kilometres to the north, glacial sediments dominate the valley bottom. Hence, we suggest that gravel accumulation in the narrow parts of the valley, especially upstream of the Spaar Mountains, decelerated the Early Holocene incision (Fig. 2). Consequently the lower parts of the LWT were submerged during Early Holocene flood events so that the clayey loam could be deposited. After the middle–late Preboreal incision, floods no longer reached the LWT, so clayey loam deposition ended. This scenario is also reflected by the early Mesolithic camp site. The microliths were embedded in the basal clayey loam and remained predominately undisturbed as a result of ongoing sedimentation during the early Preboreal. After deposition ended, a humic A horizon developed during the late Preboreal and the Boreal, which did not reach the level of the early Mesolithic finds.

Different weathering indices and element ratios gave clear evidence for soil formation in the course of chemical weathering within the clay-rich Ahb and C horizon (Fig. 9). It can be clearly seen that the lowest VWI values could be detected at the sediment base of the clayey loam between 102.6 and 102.8 m a.s.l. This is clear evidence of weathering and thus soil formation, which is also validated by the K_2O/Rb_2O ratio because there is greater retention and thus slower release of heavier alkali metal ions (Rb^+) from clay minerals compared to the lighter alkali metal ion (K^+) (Bosq et al., 2020; Matys Grygar et al., 2020). In comparison to Na and Ca, a possible resorption of K to clay minerals and its stronger binding through sorptive complexes in the soil are considered to be more likely. These conditions can lead to K enrichment when weathering processes are weak or, conversely, K depletion under stronger weathering conditions (Buggle et al., 2011). Although the highest organic carbon values only reach 0.6 %, the low values for VWI are an indication of soil formation that has taken place within these deposits. Additionally, also the Rb/Sr ratio proved to be very meaningful in investigations of the intensity of weathering of loess palaeosols (Reitner and Ottner, 2011). Accordingly, at our study site the highest Rb/Sr ratios were found in the clay-rich Ahb and C horizon, proving their high weathering intensity.

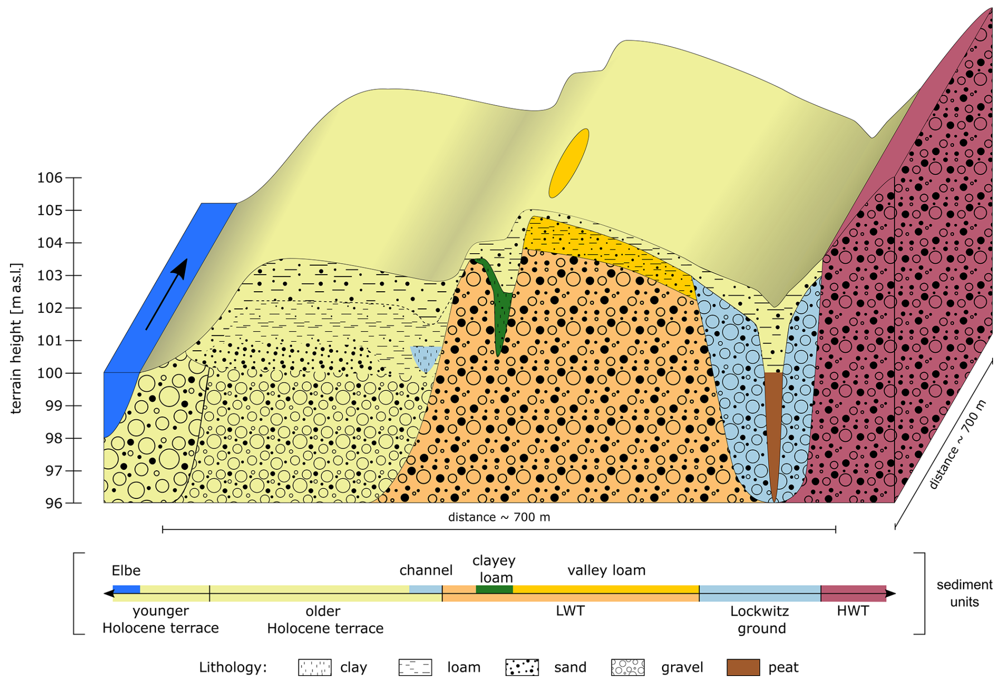

Figure 10. Schematic transect through the right bank of the Elbe valley in the study area in the northwestern Dresden basin between the Spaar Mountains and the city of Coswig, south of Meißen (see Fig. 1b for the location). HWT: Higher Weichselian Terrace, LWT: Lower Weichselian Terrace.

Most of the oldest detected Holocene floodplain sediments in several central European river systems are peats (Hiller et al., 1991; Tinapp, 2002; Notebaert et al., 2018; Tinapp et al., 2019). These were usually covered by humic fine-grain material with relatively constant vertical contents of organic matter, and its formation is suggested to have occurred during long-lasting periods with high groundwater levels and reduced composition of organic material. This material was referred to as "black floodplain soil" in the Ohm (Rittweger, 2000) or "black clay" in the Pleiße River (Tinapp et al., 2019) and was dated to between the Boreal and Atlantic periods. Similar formations were also described from various other river systems in central Europe (Schirmer, 1983; Bork, 1983; Brosche, 1984; Pretzsch, 1994; Schellmann, 1994; Hilgart, 1995; Bos et al., 2008; Brown et al., 2018; von Suchodoletz et al., 2022). Their stratigraphical position and properties, however, differ greatly from those of the Early Holocene clayey loam on the Elbe LWT. In the latter, the low content of organic carbon of 0.6 % (Fig. 7), mainly derived from in situ soil formation, slightly decreases downwards to 0.2 % (Fig. 7) in the lower part just above the LWT sands and gravels. This indicates only minor input of organic material during sedimentation. Furthermore, the sand content of the clayey loam reaches $> 20\,\%$, indicating the temporal influence of flowing water during its deposition. In contrast, low sand values of $< 2\,\%$ in the black floodplain soil (Rittweger, 2000) and the black clay (Tinapp et al., 2019) demonstrate different sedimentation conditions for these layers.

Consequently, given that there are no signs of long-lasting periods with high groundwater and reduced decomposition of organic material, as well as higher sand contents, despite visual similarities with the black-coloured fine-grain Holocene sediments known from many other central European river valleys, the fine-grain Early Holocene material on the LWT in Brockwitz must have had a different genesis.

During the early Holocene, early Mesolithic hunters and gatherers occupied a former LWT river channel for several days and left their remains in the basal clayey loam. Hence, sedimentation of the latter had apparently started before. After this short human occupation, nearly 0.8 m of clayey loam has been deposited. Its low content of organic carbon, originating from soil development, suggests a merely sparse vegetation cover. Therefore, a relatively short sedimentation process at the transition from the Younger Dryas to the Preboreal is assumed, when the vegetation cover on the LWT was thinner than during subsequent periods. Afterwards, long-lasting development of the overprinting dark-coloured humic topsoil horizon began.

5.2 Holocene overbank deposits

The first human settlers appeared in the study area around 7500 BCE, colonized the LWT surface, and left their traces in the form of pits that were dug into the upper sediments and the overprinting topsoil. The lack of overbank sediments in the prehistoric pits at both the Clieben and Brockwitz study sites evidences that floods did not reach these locations during the Atlantic period.

Later, during the end of the Subboreal, floods must have reached the higher parts of the LWT surface again, since overbank fines were deposited at both study sites, Clieben and Brockwitz. Accordingly, parts of the late Bronze Age settlement are situated around the topographically highest part of the LWT, which is not reached by floods even today. Furthermore, in topographically lower positions of the settlement, some archaeological features were found within the younger overbank fines that are connected to a scattered intercalated humic horizon (Tinapp et al., 2022). Also, medieval Slavic features were found in the same stratigraphic position. Therefore, the younger Holocene overbank fines can be divided into a lower Bronze Age–medieval period and an overlying younger part.

The early Neolithic archaeological finds and features represent the best parameters to distinguish between the valley loam and the overlying younger Holocene overbank fines, since these finds are found at the surface and in the upper part of the former. In contrast, the sedimentological proxies are rather diffuse to some extent so that neither organic carbon nor the particle size distribution could help to differentiate both units from each other (Figs. 4, 5). Accordingly, also the assumed former topsoil horizon of the Atlantic period, overprinting the Weichselian valley loam, could not properly be detected by these proxies. The archaeological finds in the upper part of the valley loam are distributed over the whole excavated area, regardless of whether archaeological features were documented below those finds. This find distribution, as well as some special find situations (Fig. 4b) and the mostly remarkably deeply preserved postholes and pits, clearly evidences only minor erosion processes after settlement abandonment, leading to the predominant preservation of the occupation layer of the settlement. Some of the archaeological finds were used at the surface of the settlement (rubbing stones; Fig. 4b). According to observations, pottery fragments within the occupation layer are generally heavily fragmented and weathered and their edges are rounded. This suggests their long-term atmospheric exposition and possibly also human activity at or near the surface, before they were covered by younger floodplain fines.

Large sections of the pipe trench in the current floodplain were cut through the older Holocene terrace. A buried oak tree from > 6 ka at the transition of the lower sandy gravels to the overlying overbank fines confirms that coarse fluvial sedimentation stopped at the end of the Atlantic period and that since then only younger overbank fines have been deposited (Wolf et al., 2008). In contrast to other central European river valleys (Schirmer, 1995), there is no evidence for more than two Holocene terraces in the Elbe valley between Dresden and Meißen.

5.3 Valley development and prehistory

Many studies demonstrate the spatial link between fluvial terraces and (pre)historic sites (Torke, 2012; Brown et al., 2018; Tinapp et al., 2020), since fertile land facilitating settlement founding was available in close vicinity to rivers. Accordingly, also in the Elbe valley many prehistoric settlements were formerly detected (Brestrich, 1998; Torke, 2012; Ullrich and Ender, 2014; Conrad and Ender, 2016; Meller and Friederich, 2018). Whereas late Bronze Age–medieval archaeological features were regularly found within the current floodplains (Hiller et al., 1991), older prehistoric sites were often found on fluvial terraces below a cover of younger overbank fines (Tinapp et al., 2020). Hitherto, most LPC settlements between Dresden and Meißen have been discovered on the left banks of the Elbe River (Brestrich, 1998; Stäuble, 2010). Hence, given its location on the right riverbank, the geographic location of the early Neolithic village at the Clieben study site was under discussion in archaeology after its discovery in 2008 (Steinmann, 2010). Given that the channel at the Lockwitz ground had been abandoned already during the Preboreal and subsequently developed into a peat swamp, its active phase is much older than the LPC settlement. Hence, an active Elbe channel north of the Clieben study site can clearly be excluded for that time, confirming that the LPC settlement must actually have been located on the right bank of the Elbe River. This forms an important finding with respect to the reconstruction of the spread of the initial LPC in central Europe (Brestrich, 1998; Stäuble, 2010).

Generally, data about the late Weichselian–Holocene development of the Elbe River system are still rather patchy (Kaiser et al., 2012). This also leads to difficulties in linking the fluvial sediments and hence the local geomorphic–palaeoenvironmental conditions – strongly influencing human behaviour – of the upper with those of the middle Elbe valley. Accordingly, also our detailed geoarchaeological approach applied to a rather unstudied area in the northern Dresden basin strongly stresses the need for further research regarding the late Weichselian–Holocene Elbe valley development to better understand former regional patterns of human settlement.

6 Conclusions

Our geoarchaeological investigations during the OPAL and the EUGAL pipeline constructions in the northern Dresden basin between Meißen and Dresden gave new insights into the fluvial sediments that were deposited since 15 ka in this part of the Elbe valley. Overall, one phase of clayey sedimentation during the Early Holocene and two subsequent periods of fine overbank sedimentation have been deciphered on the LWT, separated from each other by a long-lasting period without fluvial sedimentation during the Atlantic period. Preboreal clayey sedimentation on the LWT is quite unique in central Europe, suggesting a later incision of the Elbe River compared with other central European rivers.

Sedimentation processes and soil development in this part of the Elbe valley were connected to former human occupation. While the palaeochannels on the LWT were temporarily reached by floods during the Preboreal, only allowing a short occupation by Mesolithic humans, the early Neolithic findings were found below the following fine-grain younger Holocene overbanks. Hence, during a longer period between the Atlantic and Subboreal, the LWT was no longer flooded, allowing for LPC settlements on the LWT. The following late Bronze Age features were mainly concentrated around the topographic peaks of the LWT, and subsequent temporary flooding of most parts of the LWT obviously stopped the intensive anthropogenic occupation.

Only multidisciplinary approaches allow for reconstructing the interdependence between humans and nature in fluvial environments, since accurately recorded archaeological excavations have to be combined with geoarchaeological investigations to identify distinct sediment units and soils and their relation with human finds.

Data availability. The archaeological data in the "Results" section can be found in Döhlert-Albani et al. (2022) (Sect. 4.1 and 4.3), Kreienbrink et al. (2022) (Sect. 4.1 and 4.2) and Stäuble et al. (2022) (Sect. 4.1 and 4.3). The palaeobotanical data can be found in Tinapp et al. (2022) (Sect. 4.1).

Supplement. The supplement related to this article is available online at: https://doi.org/10.5194/egqsj-72-95-2023-supplement.

Author contributions. HS, FK and CT organized the project. CT, JS, FK, NDA and TL carried out the fieldwork. The concept and structure of the paper were organized by CT and JS. The laboratory work was done by CH (plant macro remains), BS (geochemistry, particle size distribution) and TL (OSL). Thin-section analysis was carried out by SH. Archaeological investigations were performed by FK, NDA and BF. CT and JS took the lead in writing the manuscript, with input from BF, SH, CH, BS, TL, FK, NDA and HS. All authors discussed the results and contributed to the final manuscript.

Competing interests. The contact author has declared that none of the authors has any competing interests.

Special issue statement. This article is part of the special issue "Quaternary research from and inspired by the first virtual DEUQUA conference". It is a result of the vDEUQUA2021 online conference in September/October 2021.

Disclaimer. Publisher's note: Copernicus Publications remains neutral with regard to jurisdictional claims in published maps and institutional affiliations.

Review statement. This paper was edited by Christian Zeeden and reviewed by Philipp Schulte and two anonymous referees.

References

Alexowsky, W.: Geologische Karte des Freistaates Sachsen, Erläuterungen zu Blatt 4947 Wilsdruff, Dresden, ISBN 3896793985, 2005.

Birkeland, P. W.: Soils and Geomorphology. Oxford University Press, New York, Oxford, ISBN 9780195078862, 448 pp., 1999.

Bork, H.-R.: Die holozäne Relief- und Bodenentwicklung in Lössgebieten, Catena, supplementary volume, 1–93, ISBN 3923381026, 1983.

Bosq, M., Bertranan, P., Degeai, J.-P., Queffelec, A., and Moine, O.: Geochemical signature of sources, recycling and weathering in the Last Glacial loess from the Rhône Valley (southeast France) and comparison with other European regions, Aeolia Res., 42, 100561, https://doi.org/10.1016/j.aeolia.2019.100561, 2020.

Bowen, H. J. M.: Environmental Chemistry of the Elements, London, ISBN 978-0121204501, 333 pp., 1979.

Brestrich, W.: Gedanken zur archäologischen Kulturlandschaft des oberen Elbtals, in: Archäologische Forschungen in frühgeschichtlichen Siedlungslandschaften, Festschrift für Georg Kossack zum 75. Geburtstag, edited by: Küster, H., Lang, A., and Schauer, P., Regensburger Beitr. Prähist. Arch. 5, Regensburg, 67–91, ISBN 3930480247, 1998.

Brosche, K. H.: Zur jungpleistozänen und holozänen Entwicklung des Werratales zwischen Hannoversch Münden und Phillipsthal (östl. Bad Hersfeld), Eiszeitalter u. Gegenwart, 34, 105–129, https://doi.org/10.3285/eg.34.1.06, 1984.

Brose, F. and Präger, F.: Regionale Zusammenhänge und Differenzierungen der holozänen Flussgenese im nordmitteleuropäischen Vergletscherungsgebiet, in: Das Jungquartär und seine Nutzung im Küsten- und Binnentiefland der DDR und der VR Polen, Vorträge und Erörterungen von der 4. Bilateralen Arbeitstagung 1979 in Greifswald, edited by: Kliewe, H., Galon, R., Jäger, K.-D., and Niewiarowski, Petermanns Geogr. Mitt. supplementary issue, 282, Gotha, 164–175, 1983.

Brown, A. G., Lespez, L., Sear, D. A., Macaire, J.-J., Houben, P., Klimek, K., Brazier, R. E., Van Oost, K., and Pears, B.: Natural vs anthropogenic streams in Europe: History, ecology and implications for restoration, river-rewilding and riverine ecosystem services, Earth-Sci. Rev., 180, 185–205, https://doi.org/10.1016/j.earscirev.2018.02.001, 2018.

Buggle, B., Glaser, B., Hambach, U., Gerasimenko, N., and Marković, S.: An evaluation of geochemical weathering indices in loess–paleosol studies, Quaternart Int., 240, 12–21, https://doi.org/10.1016/j.quaint.2010.07.019, 2011.

Bullock, P., Fedoroff, N., Jongerius, A., Stoops, G., and Tursina, T. (Eds.): Handbook for soil thin section description, Waine Research Publications, Albrighton, Wolverhampton, 152 pp., ISBN 9780905184098, 152 pp., 1985.

Cappers, R. T. J., Bekker, R. M., and Jans, J. E. A.: Digitale zadenatlas van Nederland – Digital seed atlas of the Netherlands. Groningen Archaeological Studies 4, 2nd Edn., Barkhuis Publishing, Eelde, ISBN 9077922113, 2012.

Conrad, S. and Ender, W.: Ein Tell bei Rosenfeld. Siedlungsspuren des Früh- und Mittelneolithikums, der vorrömischen Eisen- und Römischen Kaiserzeit sowie des Mittelalters am Elbufer nördlich von Torgau, in: Ausgrabungen in Sachsen 5, edited by: Smolnik, R., Arbeits- und Forschungsberichte zur sächsischen. Bodendenkmalpflege, supplement, 31, Dresden, 217-232, ISBN 9783943770261, 2016.

Döhlert-Albani, N., Conrad, M., Fischer, B., Kreienbrink, F., Oehlert, M., and Stäuble, H.: Ein polykultureller Siedlungsplatz bei Brockwitz an der Elbe, in: Steinzeitjägerin trifft auf Bergknappen. Trassenarchäologie an EUGAL und OPAL in Sachsen, edited by: Smolnik, R., Arbeits- und Forschungsberichte zur sächsischen Bodendenkmalpflege, supplement, 35, Dresden, 231–303, ISBN 9783943770759, 2022.

Eissmann, L.: Das quartäre Eiszeitalter in Sachsen und Nordostthüringen, Altenburger Naturwiss. Forsch. 8, Altenburg, 98 pp., ISSN 02325381, 1997.

Eissmann, L.: Quaternary geology of eastern Germany (Saxony, Saxon-Anhalt, South Brandenburg, Thüringia), type area of the Elsterian and Saalian stages in Europe, Quaternary Sci. Rev., 21, 1275–1346, https://doi.org/10.1016/S0277-3791(01)00075-0, 2002.

Fischer, P., Hilgers, A., Protze, J., Kels, H., Lehmkuhl, F., and Gerlach, R.: Formation and geochronology of Last Interglacial to Lower Weichselian loess/palaeosol sequences – case studies from the Lower Rhine Embayment, Germany, E&G – Quaternary Sci. J., 61, 48–63, https://doi.org/10.3285/eg.61.1.04, 2012.

Hantke, R.: Flußgeschichte Mitteleuropas: Skizzen zu einer Erd-, Vegetations-, und Klimageschichte der letzten 40 Millionen Jahre, Ferdinand Enke Verlag, Stuttgart, ISBN 3432997817, 459 pp., 1993.

Herbig, C.: Unkraut oder in Gärten kultivierte Heilpflanze? Die Rolle des Schwarzen Bilsenkrauts (Hyoscyamus niger L.) im Neolithikum. Neue archäobotanische Nachweise in linienbandkeramischen Brunnenbefunden in Sachsen, in: Verzweigungen. Eine Würdigung für A.J. Kalis u. J. Meurers-Balke, edited by: Stobbe, A. and Tegtmeier, U., Frankfurter Archäol. Schr. 18, Bonn, 147–157, ISBN 9783774937680, 2012.

Hilgart, M.: Die geomorphologische Entwicklung des Altmühl- und Donautales im Raum Dietfurt-Kelheim-Regensburg im jüngeren Quartär, Forschungen zur deutschen Landeskunde, 242, Trier, ISBN 9783881430548, 336pp., 1995.

Hiller, A., Litt, T., and Eissmann, L.: Zur Entwicklung der jungquartären Tieflandstäler im Elbe-Saale-Gebiet unter besonderer Berücksichtigung von 14C-Daten, Eiszeitalter u. Gegenwart, 41, 26–46, https://doi.org/10.3285/eg.41.1.03, 1991.

Houben, P., Schmidt, M., Mauz, B., Stobbe, A., and Lang, A.: Asynchronous Holocene colluvial and alluvial aggradation: A matter of hydrosedimentary connectivity, Holocene, 23, 544–555, https://doi.org/10.1177/0959683612463105, 2013.

Huhle, K.: Lithostratigrafie einiger Bohrungen in der Dresdner Elbtalwanne, Geologica Saxonica, 60, 461–488, ISBN 9783910005651, 2015.

IUSS Working Group WRB: World Reference Base for Soil Resources 2014, in: World Soil Resources Reports No. 106 FAO, Rome, 192, ISBN 9789251083697, 2014.

Kaiser, K., Lorenz, S., Germer, S., Juschus, O., Küster, M., Libra, J., Bens, O., and Hüttl, R. F.: Late Quaternary evolution of rivers, lakes and peatlands in northeast Germany reflecting past climatic and human impact – an overview, Quaternary Sci. J., 61, 103–132, https://doi.org/10.3285/eg.61.2.01, 2012.

Kausch, B.: Geoarchäologische Untersuchungen an Schwemmfächern als korrelate Sedimentkörper holozäner Bodenerosion zur Erfassung morphodynamischer Prozessphasen in der Region Trier, Geographische Gesellschaft Trier, ISBN 978-3-921599-61-7, 272 pp., 2009.

Khoravichenar, A., Fattahi, M., Amini, H., and von Suchodoletz, H.: The potential of small mountain river systems for paleoenvironmental reconstructions in drylands – an example from the Binaloud Mountains in northeastern Iran, Geosciences, 10, 448, https://doi.org/10.3390/geosciences10110448, 2020.

Kreienbrink, F.: Eine linienbandkeramische Siedlung bei Clieben in der nordwestlichen Dresdner Elbtalweitung, in: Steinzeitjägerin trifft auf Bergknappen. Trassenarchäologie an EUGAL und OPAL in Sachsen, edited by: Smolnik, R., Arbeits- und Forschungsberichte zur sächsischen Bodendenkmalpflege, supplement, 35, Dresden, 217–230, ISBN 9783943770759, 2022.

Kreienbrink, F., Döhlert-Albani, N., Conrad, M., Herbig, C., Martin, I., Schuber, M., Tinapp, C., Hößler, R., Johl, S., Krämer, U., Mauksch, K., Priske, C., and Stäuble, H.: Von der Großenhainer Pflege übers Elbetal ins Erzgebirge. Die Ausgrabungen an der EUGAL, in: Ausgrabungen in Sachsen 7, edited by: Smolnik, R., Arbeits- und Forschungsberichte zur sächsischen Bodendenkmalpflege, supplement, 34, 134–149, ISBN 9783943770537, 2020.

Krentz, O.: Postvariszische tektonische Entwicklung. in: Geologie von Sachsen, edited by: Pälchen, W. and Walter, H., E. Schweizerbart'sche Verlagsbuchhandlung, Stuttgart, 472–478, ISBN 9783510652709, 2008.

Lange, J.-M., Alexowsky, W., and Haubold, F.: Die Entwicklung der Elbe und ihr Einfluss auf die quartäre Landschaftsformung in der Umgebung von Dresden, in: Erkundungen in Sachsen und Schlesien. Quartäre Sedimente im landschaftsgenetischen Kontext, edited by: Faust, D. and Heller, K., conference volume, 25–30 September 2016, Dresden, Berlin, 13–30, https://doi.org/10.3285/g.00015, 2016.

Litt, T., Behre, K.-E., Meyer, K.-D., Stephan, H.-J., und Wansa, S.: Stratigraphical terms for the Quaternary of the North German Glaciation Area, E & G – Quaternary Sci. J., 56, 1–2, 7–65, 2007.

Mannsfeld, K. and Bernhardt, A.: Dresdner Elbtalweitung, in: Naturräume in Sachsen. Forschungen zur deutschen Landeskunde, edited by: Mannsfeld, K. and Syrbe, R.-U., Deutsche Akademie für Landeskunde, Leipzig, 148–154, ISBN 9783881430784, 2008.

Matys Grygar, T., Mach, K., Hron, K., Fačevicová, K., Martinez, M., Zeeden, C., and Schnabl, P.: Lithological correction of chemical weathering proxies based on K, Rb, and Mg contents for isolation of orbital signals in clastic sedimentary archives, Sediment. Geol., 406, 105758, https://doi.org/10.1016/j.sedgeo.2020.105717, 2020.

McLennan, S. M., Hemming, S., McDaniel, D. K., and Hanson, G. N.: Geochemical approaches to sedimentation, provenance and tectonics, Geological Society of America, Special Papers, 285, 21–40, 1993.

Meller, H. and Friederich, S. (Eds.): Archäologie in der Flussaue – 20 Jahre Hochwasserschutz und Ortsumgehung Eutzsch, Archäologie in Sachsen-Anhalt, 27, Halle, ISBN 9783944507804, 2018.

Miera, J. J., Schmidt, K., von Suchodoletz, H., Ulrich, M., Werther, L., Zielhofer, C., Ettel, P., and Veit, U.: Large-scale investigations on Neolithic settlement dynamics in Central Germany based on machine learning analysis: a case study from the Weiße Elster river catchment, PLoS ONE 17, e0265835, https://doi.org/10.1371/journal.pone.0265835, 2022.

Murray, A. S. and Wintle, A. G.: The single aliquot regenerative dose protocol: Potential for improvements in reliability, Radiat. Meas., 37, 377–381, https://doi.org/10.1016/S1350-4487(03)00053-2, 2003.

Notebaert, B., Broothaerts, N., and Verstraeten, G.: Evidence of anthropogenic tipping points in fluvial dynamics in Europe, Global Planet. Change, 164, 27–38, https://doi.org/10.1016/S1350-4487(03)00053-2, 2018.

Oberdorfer, E.: Pflanzensoziologische Exkursionsflora, Ulmer, Stuttgart, ISBN 9783800131310, 2001.

Pandarinath, K.: Application potential of chemical weathering indices in the identification of hydrothermally altered surface volcanic rocks from geothermal fields, Geosci. J., 26, 415–442 https://doi.org/10.1007/s12303-021-0042-2, 2022.

Pretzsch, K.: Spätpleistozäne und holozäne Ablagerungen als Indikatoren der fluvialen Morphodynamik im Bereich der mittleren Leine, Göttinger Geogr. Abh., 99, Göttingen, ISBN 9783884520994, 105 pp., 1994.

Pusch, M., Behrendt, H., Gancarczyk, A., Kronvang, B., Sandin, L., Stendera, S., Wolter, C., Andersen, H. E., Fischer, H., Hoffmann, C. C., Nowacki, F., Schöll, F., Svendsen, L. M., Bäthe, J., Friberg, N., Hachol, J., Pedersen, M. L., Scholten, M., and Wnuk-Glawdel, E.: Rivers of the Central European Highlands and Plains, in: Rivers of Europe, edited by: Tockner, K., Uehlinger, U., and Robinson, C. T., London, 525–576, ISBN 9780123694492, 2009.

Reitner, J. M. and Ottner, F.: Geochemische Charakterisierung der Verwitterungsintensität der Löss-Paläoboden-Sequenz von Wels/Aschet, in: Die Löss-Sequenz Wels/Aschet (ehemalige Lehmgrube Würzburger), Mitteilungen der Kommission für Quartärforschung der Österreichischen Akademie der Wissenschaften 19, edited by: Van Husen, D. and Reitner, J. M., Verlag der Österreichischen Akademie der Wissenschaften, Wien, ISBN 978-3-7001-6992-5, 2011.

Rittweger, H.: The Black Floodplain Soil“ in the Amöneburger Becken, Germany: a lower Holocene marker horizon and indicator of an upper Atlantic to Subboreal dry period in Central Europe?, Catena, 41, 143–164, https://doi.org/10.1016/S0341-8162(00)00113-2, 2000.

Scheck, M., Bayer, U., Otto, V., Lamarche, J., Banka, D., and Pharaoh, T.: The Elbe Fault System in North Central Europe – a basement controlled zone of crustal weakness, Tectonophysics, 360, 281–299, https://doi.org/10.1016/S0040-1951(02)00357-8, 2002.

Schellmann, G.: Die Talentwicklung der unteren Oberweser im jüngeren Quartär, Düsseldorfer Geographische Schriften, 34, 11–43, 1994.

Schellmann, G.: Quartärgeologische Karte 1:25.000 des Donautals auf Blatt 7039 Mintraching mit Erläuterungen. Kartierungsergebnisse aus den Jahren 2008 und 2009, Bamberger Geographische Schriften, SF 14, 105–162, 2018.

Schirmer, W.: Die Talentwicklung an Main und Regnitz seit dem Hochwürm, Geol. Jahrb., A 71, 11–43, 1983.

Schirmer, W.: Valley bottoms in the Late Quaternary, Z. für Geomorphologie N.F., Suppl.-Bd, 100, 27–51, 1995.

Smykatz-Kloss, B.: Die Lößvorkommen des Pleiser Hügellandes bei Bonn und von Neustadt/Wied sowie der Picardie: Mineralogisch-geochemische und geomorphologische Charakterisierung, Verwitterungs-Beeinflussung und Herkunft der Lösse. Dissertation Universität Bonn, Bonn, 343 pp., http://hss.ulb.uni-bonn.de:90/2003/0308/0308.htm (last access: 2 March 2023), 2003.

Smykatz-Kloss, W., Smykatz-Kloss, B., Naguib, N., and Zöller, L.: The reconstruction of paleoclimatological changes from mineralogical and geochemical compositions of loess and alluvial loess profiles, edited by: Smykatz-Kloss, W. and Felix-Henningsen, P., Palaeoecology of Quaternary Drylands. Lecture Notes in Earth Sciences, 102, Springer-Verlag, Heidelberg, 101–118, ISBN 3540403450, 2004.

Starkel, L., Soja, R., and Michczynska, D. J.: Past hydrological events reflected in Holocene history of Polish rivers, Catena, 66, 24–33, 2006.

Stäuble, H.: Linienband- und Stichbandkeramische Kulturen, in: Ur- und Frühgeschichte Sachsens. Atlas zur Geschichte und Landeskunde von Sachsen. supplement map B I 1.1–1.5, edited by: Heynowski, R. and Reiß, R., Leipzig, Dresden, 24–42, ISBN 9783896799234, 2010.

Stäuble, H.: Neues zur Bandkeramik in Sachsen: Die letzten 25 Jahre, in: Centenary of Jaroslav Palliardi's Neolithic and Aeneolithic relative chronology (1914–2014), edited by: Kovárník, J., Ústí nad Orlicí, 67–106, ISBN 9788074053962, 2016.

Stäuble, H., Döhlert-Albani, N., and Kreienbrink, F.: Eine neolithische Palisaden-/Grabenanlage mit Elbblick, in: Steinzeitjägerin trifft auf Bergknappen. Trassenarchäologie an EUGAL und OPAL in Sachsen, edited by: Smolnik, R., Arbeits- und Forschungsberichte zur sächsischen Bodendenkmalpflege, supplement, 35, Dresden, 245–266, ISBN 9783943770759, 2022.

Steinmann, C.: Die OPAL-Trasse als archäologisches Großprojekt, in: Ausgrabungen in Sachsen 2, edited by: Smolnik, R., Arbeits- und Forschungsberichte zur sächsischen Bodendenkmalpflege, supplement 21, Dresden, 227–230, ISBN 9783910008915, 2010.

Stoops, G.: Guidelines for analysis and description of soil and regolith thin sections, Soil Science Society of America, Inc., Madison, ISBN 9780891188421, 2003.

Tinapp, C.: Geoarchäologische Untersuchungen zur holozänen Landschaftsentwicklung der südlichen Leipziger Tieflandsbucht, Trierer Geographische Studien, 26, Trier, 275 pp., ISBN 3921599377, 2002.

Tinapp, C.: Geoarchäologische Untersuchungen an der OPAL- und EUGAL-Trasse, in: Steinzeitjägerin trifft auf Bergknappen. Trassenarchäologie an EUGAL und OPAL in Sachsen, edited by: Smolnik, R., Arbeits- und Forschungsberichte zur sächsischen Bodendenkmalpflege, supplement, 35, Dresden, 21–29, ISBN 9783943770759, 2022.

Tinapp, C., Heinrich, S., Herbig, C., Schneider, B., Stäuble, H., Miera, J., and von Suchodoletz, H.: Holocene floodplain evolution in a Central European loess landscape – Geoarchaeological investigations of the lower Pleiße valley in NW-Saxony, E & G – Quaternary Sci. J., 68, 95–105, https://doi.org/10.5194/egqsj-68-95-2019, 2019.

Tinapp, C., Heine, Y., Heinrich, S., Herbig, C., Schneider, B., Stäuble, H., and von Suchodoletz, H.: Die Pleißeaue südlich von Leipzig. Geoarchäologische Erkenntnisse zur stratigraphischen Position archäologischer Fundstellen im unteren Pleißetal, in: Ausgrabungen in Sachsen 7, edited by: Smolnik, R., Arbeits- und Forschungsberichte zur sächsischen Bodendenkmalpflege, supplement, 34, Dresden, 7–19, ISBN 9783943770537, 2020.

Tinapp, C., Selzer, J., Heinrich, S., Herbig, C., Lauer, T., and Schneider, B.: Das Elbtal bei Coswig. Geoarchäologische Erkenntnisse zur holozänen Entwicklung eines früh besiedelten Landschaftsraums, in: Steinzeitjägerin trifft auf Bergknappen. Trassenarchäologie an EUGAL und OPAL in Sachsen, edited by: Smolnik, R., Arbeits- und Forschungsberichte zur sächsischen Bodendenkmalpflege, supplement, 35, Dresden, 193–206, ISBN 9783943770759, 2022.

Torke, M.: Siedeln am Strom: Risiko oder Chance? Zu Urrelief, präurbaner Topographie und Hochwasserexposition Pirnas vor der Stadtwerdung, edited by Smolnik, R., Arbeits- und Forschungsberichte zur sächsischen Bodendenkmalpflege 53/54, Dresden, 359-410, ISBN 9783943770056, 2012.

Tröger, K.-A.: Kreide – Oberkreide, in: Geologie von Sachsen, edited by: Pälchen, W. and Walter, H., E. Schweizerbart'sche Verlagsbuchandlung, Stuttgart, 311–358, ISBN 9783510652709, 2008.

Ullrich, O. and Ender, W.: Siedlungsbefunde und ein Brunnen aus der Elbaue im Kieswerk Liebersee (Gem. Staritz, Lkr. Nordsachsen, in: Ausgrabungen in Sachsen 4, edited by: Smolnik, R., Arbeits- und Forschungsberichte zur sächsischen Bodendenkmalpflege, supplement 27, Dresden, 160–170, ISBN 9783943770131, 2014.

von Suchodoletz, H., Gärtner, A., Zielhofer, C., and Faust, D.: Eemian and post-Eemian fluvial dynamics in the Lesser Caucasus, Quaternary Sci. Rev. 191, 189–203, https://doi.org/10.1016/j.quascirev.2018.05.012, 2018.

von Suchodoletz, H., Berg, S., Eckmeier, E., Werther, L., and Zielhofer, C.: Preface: Special Issue "Geoarchaeology and past human–environment interactions", E & G – Quaternary Sci. J., 68, 237–240, https://doi.org/10.5194/egqsj-68-237-2020, 2020.

von Suchodoletz, H., Pohle, M., Khosravichenar, A., Ulrich, M., Hein, M., Tinapp, C., Schultz, J., Ballasus, H., Veit, U., Ettel, P., Werther, L., Zielhofer, C., and Werban, U.: The fluvial architecture of buried floodplain sediments of the Weiße Elster River (Germany) revealed by a novel method combination of drill cores with two-dimensional and spatially resolved geophysical measurements, Earth Surf. Process. Landf., 47, 955–976, https://doi.org/10.1002/esp.5296, 2022.

Wolf, L., Alexowsky, W., Dietze, W., Hiller, A., Krbetschek, M., Lange, J.-M., Seifert, M., Tröger, K.-A., Voigt, T., and Walther, H.: Fluviatile und glaziäre Ablagerungen am äußersten Rand der Elster- und Saale-Vereisung; die spättertiäre und quartäre Geschichte des sächsischen Elbegebietes (Exkursion A2), in: Das Quartär Mitteldeutschlands, edited by: Eissmann, L. and Litt, T., Altenburger naturwissenschaftliche Forschungen, Altenburg, 190–232, ISSN 02325381, 1994.

Wolf, L., Alexowsky, W., Heilmann, H. and Symanngk, R.: Quartär, in: Geologie von Sachsen, edited by: Pälchen, W. and Walter, H., E. Schweizerbart'sche Verlagsbuchandlung, Stuttgart, 419–472, ISBN 9783510652709, 2008.

E&G Quaternary Sci. J., 72, 113–125, 2023
https://doi.org/10.5194/egqsj-72-113-2023

Open Access E&G Quaternary Science Journal

Research article

The past is the key to the future – considering Pleistocene subglacial erosion for the minimum depth of a radioactive waste repository

Sonja Breuer[1], **Anke Bebiolka**[2], **Vera Noack**[2], **and Jörg Lang**[1]

[1]Bundesanstalt für Geowissenschaften und Rohstoffe (BGR), Stilleweg 2, 30655 Hanover, Germany
[2]Bundesanstalt für Geowissenschaften und Rohstoffe (BGR), Wilhelmstr. 25–30, 13593 Berlin, Germany

Correspondence: Sonja Breuer (sonja.breuer@bgr.de)

Relevant dates: Received: 19 October 2022 – Revised: 6 March 2023 – Accepted: 5 April 2023 – Published: 17 May 2023

How to cite: Breuer, S., Bebiolka, A., Noack, V., and Lang, J.: The past is the key to the future – considering Pleistocene subglacial erosion for the minimum depth of a radioactive waste repository, E&G Quaternary Sci. J., 72, 113–125, https://doi.org/10.5194/egqsj-72-113-2023, 2023.

Abstract: Erosion during potential future glaciations, especially the incision of deep tunnel valleys, is a major challenge for the long-term safety of a radioactive waste repository. Tunnel valleys are a common feature of formerly glaciated sedimentary basins and were incised by pressurised subglacial meltwater. Besides glaciological conditions, tunnel-valley formation depends strongly on the erodibility and hydraulic conductivity of the substratum. In northern Germany, tunnel valleys formed during the Pleistocene glaciations are widespread and may attain depths of almost 600 m. The Pleistocene record may provide an indication for the potential regional distribution and maximum depth of future glaciogenic erosion. We present a new overview map of the maximum depth of Pleistocene erosion in northern Germany. Depth zones were extracted from the existing data and maps provided by the state geological surveys. Based on the mapped depth zones, the potential for future tunnel-valley formation can be assessed. The map may serve as a base to define a spatially variable additional depth that should be added to the minimum depth of a repository required by legislation.

Kurzfassung: Erosion während möglicher zukünftiger Eiszeiten, insbesondere das Einschneiden tiefer subglazialer Rinnen, ist eine große Herausforderung für die Langzeitsicherheit eines Endlagers für hochradioaktive Abfälle. Subglaziale Rinnen sind in ehemals vergletscherten Sedimentbecken weit verbreitet und wurden durch subglaziales Schmelzwasser unter hohem Druck eingeschnitten. Außer durch glaziologische Faktoren wird die Bildung subglazialer Rinnen stark durch die Erodierbarkeit und die hydraulische Durchlässigkeit des Untergrundes bestimmt. In Norddeutschland sind pleistozäne subglaziale Rinnen weit verbreitet und erreichen Tiefen von fast 600 m. Die pleistozäne Überlieferung kann Hinweise auf die potenzielle regionale Verbreitung und maximale Tiefe zukünftiger glazigener Erosion liefern. Wir stellen eine neue Übersichtskarte der maximalen pleistozänen Erosionstiefe in Norddeutschland vor. Tiefenzonen wurden aus den existierenden Daten und Karten, die von den Staatlichen geologischen Diensten zur Verfügung gestellt wurden, extrahiert. Anhand der kartierten Tiefenzonen kann das Potenzial einer zukünftigen Bildung subglazialer Rinnen abgeschätzt werden.

Die Karte kann als Grundlage zur Festlegung eines räumlich variablen Aufschlags zur gesetzlich vorgeschriebenen Mindesttiefe eines Endlagers dienen.

1 Introduction

Tunnel valleys, although commonly no longer directly perceptible at the surface, are among the most impressive landforms related to former glaciations. Tunnel valleys are incised by pressurised meltwater beneath ice sheets and are an important component of the subglacial hydrological system (Kehew et al., 2012; van der Vegt et al., 2012). As overdeepened erosional landforms, tunnel valleys form independently of the regional base level and commonly reach depths of several hundreds of metres. The deepest Pleistocene tunnel valley in northern Germany, for example, has a depth of 554 m below sea level (b.s.l.; Schulz, 2002; Müller and Obst, 2008).

Subglacial erosion during potential future glaciations is a major challenge for the long-term safety of a repository for radioactive waste in deep geological formations. Future tunnel-valley incision is indirectly referred to as "intense erosion caused by an ice age" in the German Site Selection Act (StandAG, 2017). According to German legislation, the safety of a repository for high-level radioactive waste must be assessed for the next 1 million years (StandAG, 2017). Within this period, up to 10 glaciations could occur that may reach similar maximum extents as the Pleistocene glaciations (Fischer et al., 2021). Therefore, the impact of potential future glaciations on the safety of a repository must be considered. The Site Selection Act requires a minimum depth of the upper boundary of the effective containment zone (ECZ) of 300 m b.s.l. (StandAG, 2017). However, 300 m may be insufficient to safeguard the effective containment zone against the impact of deep subglacial erosion.

Assessing the potential for future tunnel-valley formation and its impact on a repository requires a thorough understanding of the processes and controlling factors of tunnel-valley formation. As the formation of tunnel valleys is controlled not only by geological but also by glaciological and climatic factors (Kehew et al., 2012; van der Vegt et al., 2012; Kirkham et al., 2022), predicting future incision is a major challenge. The dimensions and distribution of Pleistocene tunnel valleys may provide indications for future glaciogenic erosion. In this study, we describe a new approach to assessing the potential for future tunnel-valley formation based on the Pleistocene record. Our new approach is based on the assessment of the zones of maximum depth of the tunnel valleys and aims to recommend a minimum depth of the upper boundary of the effective containment zone (300 m or deeper), considering potential future tunnel-valley formation.

2 Processes of tunnel-valley formation

Tunnel valleys are characterised by undulating basal profiles, abrupt terminations, steep flanks and infills dominated by meltwater deposits (e.g. Kehew et al., 2012; van der Vegt et al., 2012). Various processes have been invoked for tunnel-valley formation, including erosion by meltwater, rivers or glaciers in subglacial or proglacial environments. Erosion by pressurised subglacial meltwater is now generally accepted as being responsible for tunnel-valley formation (Wingfield, 1990; Ó Cofaigh, 1996; Huuse and Lykke-Andersen, 2000b; Kehew et al., 2012; van der Vegt et al., 2012; Kirkham et al., 2022).

Subglacial meltwater conduits are crucial features in the drainage network of ice sheets, as the meltwater volumes are too large to be evacuated by groundwater flow (Piotrowski, 1997; Kehew et al., 2012). According to Clayton et al. (1999), tunnel channels can be defined as subglacial meltwater conduits with dimensions (width and depth) adapted to bankfull discharge. Tunnel channels are characterised by uniform dimensions along their course, lack tributaries and can commonly be linked to specific palaeo-ice-margin positions (Clayton et al., 1999). In contrast, tunnel valleys are higher-order, polyphase features, typically comprising multiple tunnel channels and their infills (Kehew et al., 2012). However, due to the wide variety of tunnel valleys and their infills, there is no single model that can explain all observations. Current models of tunnel-valley formation broadly fall into two groups: (i) erosion by steady-state meltwater discharge or (ii) erosion by sudden outbursts from meltwater reservoirs (cf. Kehew et al., 2012; van der Vegt et al., 2012; Kirkham et al., 2022).

- (i) Tunnel-valley formation by steady-state meltwater discharge is a gradual process that requires the substratum of the ice sheet to be permeable, erodible and poorly lithified (Boulton and Hindmarsh, 1987; Boulton et al., 2009; Kehew et al., 2012; van der Vegt et al., 2012; Kirkham et al., 2022). Incision is caused by downcutting of subglacial tunnel channels that switch laterally in space and time, forming an anastomosing or anabranching pattern near the base of the evolving tunnel valley (Catania and Paola, 2001; Ravier et al., 2015; Kirkham et al., 2022). Modelling results by Kirkham et al. (2022) imply that the meltwater responsible for tunnel-valley formation is mainly derived from melting at the surface of the ice sheet. Tunnel-valley formation is furthermore impacted by the interplay between subglacial channelised meltwater discharge, groundwater flow and remobilisation of the bed (Boulton and Hindmarsh, 1987; Piotrowski et al., 1999; Janszen et al., 2013; Ravier et al., 2015). If the water pressure in the subglacial conduits remains lower than in the substratum, the pressure gradient causes a flow from the substratum into the conduits (Boulton et al., 2009). Creeping of soft sediment into the evolving tunnel valley enlarges incipient subglacial channels (Boulton and Hindmarsh, 1987). If the pressure gradient becomes sufficiently high, fluidisation of the substratum may occur that strongly enhances erosion (Boulton et al., 2009; Janszen et al., 2013). Vice versa, pressurised meltwater within a subglacial conduit may trigger hydrofracturing in the substratum that also leads to sediment remobilisation (Ravier et al., 2015). The water pressure beneath a warm-based ice sheet is highly variable in both space and time (Piotrowski et al., 2004), and zones of increased water pressure are prone to brecciation, liquefaction and fluidisation, allowing for a remobilisation of the subglacial bed and the gradual incision of tunnel valleys (Janszen et al., 2013; Ravier et al., 2014, 2015).

- (ii) Outbursts of large volumes of stored meltwater with high flow velocities and discharge rates are another possible mechanism of tunnel-valley formation. Incision by meltwater outbursts is mainly related to retrograde erosion, causing the rapid enlargement of an initial meltwater pathway (Wingfield, 1990; Hooke and Jennings, 2006). Different models exist on the magnitudes, trigger mechanisms and recurrences of such subglacial outburst floods. Outburst floods may be responsible for the formation of individual tunnel channels (Hooke and Jennings, 2006; Sandersen et al., 2009) or tunnel valleys (Ehlers and Linke, 1989; Wingfield, 1990; Jørgensen and Sandersen, 2006). Meltwater storage in subglacial lakes is controlled by the hydraulic gradient, subglacial topography and the permeability of the substratum (Shreve, 1972; Piotrowski, 1994). The presence of permafrost, which lowers the permeability of the substratum and allows for the accumulation of meltwater reservoirs, is often considered a prerequisite for subglacial meltwater-reservoir formation (Piotrowski, 1994; Hooke and Jennings, 2006). Outbursts of stored meltwater occur if the pressure in the meltwater reservoir exceeds the strength of the impermeable substratum that forms the seal (Hooke and Jennings, 2006). Tunnel channels or valleys formed by meltwater outbursts afterwards serve as low-pressure meltwater conduits (Kehew et al., 2012). Episodic outbursts along the same pathway will eventually form larger tunnel valleys comprising multiple cut-and-fill sequences (Jørgensen and Sandersen, 2006).

Strong arguments exist both supporting and refuting the different models of tunnel-valley formation (cf. Ó Cofaigh, 1996; Kehew et al., 2012; van der Vegt et al., 2012; Kirkham et al., 2022). The widespread occurrence of tunnel valleys, however, suggests the existence of a common mechanism for their formation. In most instances, a formative model comprising quasi-steady-state meltwater discharge in combination with small outbursts is applicable to explain tunnel-valley formation (van der Vegt et al., 2012). In addition to erosion by meltwater, tunnel-valley evolution may be affected by erosion of the moving ice sheet and mass-wasting processes, which may enlarge tunnel valleys or modify their cross-sectional geometries and infills (Prins et al., 2020; Kirkham et al., 2021, 2022).

Tunnel-valley fills may indicate repeated episodes of erosion and deposition, which may relate to a single ice advance or multiple ice advances or extend across multiple glaciations (Piotrowski, 1994; Sandersen et al., 2009; Kirkham et al., 2022). The incision of tunnel valleys by meltwater is reflected by their infills, which are commonly dominated by meltwater deposits. Typically, tunnel-valley fills may be subdivided into synglacial and postglacial deposits (e.g. Piotrowski, 1994; Huuse and Lykke-Andersen, 2000b; Lang et al., 2012; van der Vegt et al., 2012; Janszen et al., 2013). Synglacial deposits comprise subglacial and ice-contact deposits formed during or immediately after incision and proglacial successions deposited during ice-sheet retreat. Meltwater deposits typically display fining-upward trends due to deposition at an increasing distance from the ice margin, with fine-grained glaciomarine or glaciolacustrine deposits forming the uppermost part of the synglacial successions. After deglaciation, remnant tunnel valleys commonly form local depocentres for postglacial marine, lacustrine or fluvial deposition (Ehlers and Linke, 1989; Piotrowski, 1994; Lang et al., 2012; Janszen et al., 2013; Lang et al., 2015; Steinmetz et al., 2015).

3 Controlling factors of tunnel-valley formation

Tunnel-valley formation is controlled by glaciological and geological factors. Glaciological factors include the thickness and temperature of the ice sheet, which control the availability and pressure of the meltwater. Furthermore, tunnel valleys develop broadly parallel to the ice-flow direction. The geological control on tunnel-valley formation is mainly exerted by the erodibility and hydraulic conductivity of the substratum (Ó Cofaigh, 1996; Huuse and Lykke-Andersen, 2000b; Kehew et al., 2012; van der Vegt et al., 2012).

3.1 Substratum control

Tunnel valleys are generally restricted to areas with an easily erodible substratum as the infill of sedimentary basins. In areas characterised by resistant (e.g. crystalline) bedrock, eskers form instead of tunnel valleys (Boulton et al., 2009; Kehew et al., 2012).

In northern central Europe, the highest density of Pleistocene tunnel valleys and the deepest incisions occur in areas with thick, largely unlithified Cenozoic deposits (Hinsch, 1979; Kuster and Meyer, 1979; Ehlers and Linke, 1989; Stackebrandt et al., 2001; Stackebrandt, 2009; Lohrberg et al., 2020; Ottesen et al., 2020). Tunnel valleys, which were incised into more resistant (Mesozoic) rocks, are generally relatively shallow (Stackebrandt, 2009; Sandersen and Jørgensen, 2012). According to Stackebrandt (2009), Pleistocene tunnel valleys in northern Germany are concentrated in the area of the subsiding basin axis of the North German Basin, which was oriented approximately normal to the main ice-advance directions.

Tunnel-valley formation also depends on the hydraulic conductivity of the substratum. Initial subglacial incision commonly occurs if the substratum is unable to drain meltwater by groundwater flow, e.g. in areas of high meltwater production or low-permeability substrata (Piotrowski, 1997; Huuse and Lykke-Andersen, 2000b; Boulton et al., 2009; Kehew et al., 2012; Sandersen and Jørgensen, 2012). A layer-cake stratigraphy of high- and low-permeability strata favours the build-up of high pressures in subglacial aquifers, allowing for remobilisation of the sediment at the margins of tunnel valleys (Janszen et al., 2013; Ravier et al., 2014; Ravier et al., 2015).

3.2 Structural control

Faulting modifies the hydraulic conductivity and resistance to erosion of the affected rocks, thus creating structural weaknesses, which may act as preferential pathways of tunnel-valley incision (Wenau and Alves, 2020; Sandersen and Jørgensen, 2022). Sandersen and Jørgensen (2022) demonstrated a close correlation between the orientations of faults and tunnel valleys in Denmark, suggesting that the locations of many tunnel valleys are fault controlled. However, there are few studies showing a clear connection between faults and the incision of tunnel valleys (e.g. Al Hseinat et al., 2016; Wenau and Alves, 2020; Brandes et al., 2022). Furthermore, Stackebrandt (2009) suggested that also the terminations of tunnel valleys might be controlled by (neotectonically active) faults based on the observation of the simultaneous beginning and ending of parallel tunnel valleys.

Different interpretations exist on the impact of salt structures on tunnel-valley formation, based on observations that tunnel valleys may cross-cut, be parallel to or evade salt structures. Some tunnel valleys cut across salt structures, crestal faults and rim synclines without any perceptible interrelation (Grube, 1983; Ehlers and Linke, 1989; Sonntag and Lippstreu, 2010). In other cases, tunnel-valley incision is interpreted as having exploited pre-existing weaknesses related to salt structures, such as crestal faults or depressions related to the subsurface dissolution of evaporites (Kuster and Meyer, 1979; Ehlers and Linke, 1989; Huuse and Lykke-Andersen, 2000b; Lang et al., 2014; Wenau and Alves, 2020). Based on the interpretation of 3D seismic data from the southern North Sea, Wenau and Alves (2020) demonstrated that some tunnel valleys follow the trend of underlying salt structures and their crestal graben faults. In contrast, Kristensen et al. (2007) mapped tunnel valleys that circle around salt diapirs. Such changes in tunnel-valley trends may be explained by the uplift of more resistant sedimentary rocks at the flanks of salt structures (Kuster and Meyer, 1979) or by hydrogeological changes near salt structures (Piotrowski, 1997).

4 Pleistocene tunnel valleys in northern Germany

Northern Germany is one of the classic areas for tunnel-valley research, and tunnel valleys are a common feature in the areas that were covered by the Pleistocene ice sheets. Three major glaciations referred to as the Middle Pleistocene Elsterian and Saalian and the Late Pleistocene Weichselian glaciations are well documented (e.g. Litt et al., 2007; Ehlers et al., 2011). Pleistocene tunnel valleys in northern Germany are several hundred metres deep; are several hundred metres to a few kilometres, in extreme cases 8–12 km, wide; and can be longer than 100 km (e.g. Kuster and Meyer, 1979; Ehlers and Linke, 1989; Smed, 1998; Stackebrandt, 2009; Gegg and Preusser, 2023, and references therein).

Deep tunnel valleys characterise the base of the Quaternary across northern Germany and are generally interpreted as having formed during the Elsterian glaciation (Grube, 1979; Hinsch, 1979; Kuster and Meyer, 1979; Ehlers and Linke, 1989; Stackebrandt, 2009). The major trend of the tunnel valleys is north–south in northwestern Germany and northeast–southwest in northeastern Germany, which is generally interpreted as pointing to different ice-advance directions and probably a temporal change in the ice-advance directions (Ehlers and Linke, 1989; Stackebrandt, 2009). However, the tunnel valleys form a complex net-like anastomosing pattern and the controls on tunnel-valley orientations may be more complex. Major tunnel valleys display a regular spacing of 25 to 30 km (Stackebrandt, 2009). The deepest mapped Elsterian tunnel valley has a maximum depth of 554 m b.s.l. (Schulz, 2002; Müller and Obst, 2008). The deep ($>$ 200 m) Elsterian tunnel valleys were formed at a distance of at least 100 km inside the former ice margin. Shallower ($<$ 100 m) Elsterian tunnel valleys are known from areas close to the former ice-marginal position (e.g. Eissmann, 2002; Lang et al., 2012).

In contrast to the many and deep Elsterian tunnel valleys, Saalian tunnel valleys are generally considered rare (Passchier et al., 2010). The few tunnel valleys that have been attributed to the Saalian glaciation are commonly isolated and shallow ($<$ 100 m) features (e.g. Grube, 1979; Piotrowski, 1994; Piotrowski et al., 1999). Passchier et al. (2010) suggested that the lack of Saalian tunnel valleys may be related to different glaciological and hydrogeological conditions compared with the Elsterian glaciation. However, the attribution of the majority of tunnel valleys to the Elsterian glaciation is almost entirely based on lithostratigraphy.

The Weichselian glaciation had a lesser maximum extent than the Middle Pleistocene glaciations, covering only parts of northern Germany (Ehlers et al., 2011). Weichselian tunnel valleys are shallower (< 100 m), shorter and narrower than their Elsterian counterparts (Smed, 1998; Stackebrandt, 2009). Weichselian tunnel valleys are visible in the present-day landscape as narrow depressions, commonly leading to the formation of lakes. In some instances, Weichselian tunnel valleys can be linked to palaeo-ice-marginal positions and outwash fans (Smed, 1998; Jørgensen and Sandersen, 2006).

5 Data

As a database for this study, maps and models showing the base of the Quaternary provided by the state geological surveys of Schleswig-Holstein, Hamburg, Bremen, Lower Saxony, Saxony-Anhalt, Mecklenburg-Western Pomerania, Brandenburg and Berlin were used (Table 1). Most of the maps showing the base of the Quaternary were provided as line shapefiles by the state geological surveys.

Currently, all northern German state geological surveys are in the process of revising their base Quaternary maps or creating 3D models of the medium-depth subsurface. The results of new boreholes and geophysical investigations and their interpretations will be used to update the maps of the base Quaternary and adapt them to the current state of research. However, the progress and planned completion dates of the individual federal states vary, so it was decided to work with the data that were available at the starting point of this project.

The base Quaternary maps were used as the main input data sets. The base of the Quaternary actually represents a diachronous basal surface of glaciogenic erosion, which can mostly be attributed to the Middle Pleistocene ice advances. As the focus of this project is on the areas with the deepest erosion, the investigations concentrate on the mapped tunnel valleys. For this purpose, the tunnel valleys were extracted from the respective base Quaternary maps of the federal states.

For data preparation, ArcMap (version 10.8.1) and ArcGIS Pro (version 2.9.1) were used. Merging the depth-contour maps of the individual federal states into a common map proved a major challenge. The use of different data sets, resolutions and mapping approaches led to major discontinuities at the state borders. Without data harmonisation and/or reinterpretation of the border areas, the maps could not be merged. However, such a reinterpretation was not possible within the time frame of our project. Therefore, the data for each federal state were considered individually in the first step.

6 Methods

The focus of this study was on the evaluation of areas with deep tunnel valleys. Therefore, the areas without clearly defined tunnel valleys and with an erosion depth of less than 100 m were removed from the data sets. After this manual processing, only the deep tunnel valleys remain visible on the map (Fig. 1).

To further reduce the complexity of the base Quaternary maps, a geographic information system (GIS) workflow was developed to extract the thalweg lines of the tunnel valleys. The GIS workflow made it possible to extract the deepest points along the tunnel valleys. Details on the GIS workflow are provided in the Supplement (Figs. S1 and S2). Based on the map of the tunnel-valley thalwegs and their depths, zones of similar maximum tunnel-valley depths were defined.

7 Results

Removing the areas from the base Quaternary maps that are shallower than 100 m b.s.l. provides a comprehensive overview of the Pleistocene tunnel-valley network (Fig. 1). The deepest parts and southern terminations of the tunnel valleys are both aligned in an approximately northwest–southeast-trending zone.

The extracted thalweg map allows for an easier recognition of individual tunnel valleys and their respective depths (Fig. 2). As each wide tunnel valley is now represented by a line of defined depth (Fig. 2), it becomes easier to identify zones of similar maximum depth (Fig. 3). Furthermore, the thalweg lines will be intersected with other geological structures and units to analyse their relationships and potential impact on the formation of the tunnel valleys in a subsequent step of our project. The visual analysis of the data showed that the tunnel valleys could be divided into five depth zones: no tunnel valley deeper than 100 m, up to 200 m, up to 300 m, up to 400 m and up to 600 m (Fig. 3), with the zone "no tunnel valley deeper than 100 m" extending to the maximum ice margin. The transitions between the depth zones are always placed at the terminations of the respective tunnel-valley sections and therefore occur abruptly. The depth zones of the tunnel valleys display a clear northwest–southeast-trending pattern. The deepest zone occurs in an area approximately between Hamburg and Berlin (Fig. 3). Towards the northeast and southwest, the maximum depths decrease successively.

8 Discussion

We developed an effective and timesaving method to extract an overview map of the Pleistocene tunnel-valley network from the available data sets. The focus of the new map is on the distribution of the maximum depths rather than on individual tunnel valleys and their geometries.

Table 1. The input data (maps and models of the base of the Quaternary) for each federal state, with data type, scale, year of publication and reference, as far as this information is known. "/" denotes no scale.

	Data type	Scale	Publication date	Reference
Schleswig-Holstein (SH)	line shapefile	1 : 200 000	2016	provided by the geological survey
Hamburg (HH)	surface (.ts)	/	2018	provided by the geological survey
Bremen (HB)	surface (.ts)	/	2016	provided by the geological survey
Lower Saxony (NDS)	line shapefile	1 : 500 000	2011	provided by the geological survey
Mecklenburg-Western Pomerania (MVP)	line shapefile	unknown	2002	Brückner-Röhling et al. (2002)
Saxony-Anhalt (SA)	line shapefile	1 : 50 000	1993–2014	provided by the geological survey
Berlin and Brandenburg (BB)	point shapefile	1 : 1 000 000	2010	Noack et al. (2010)

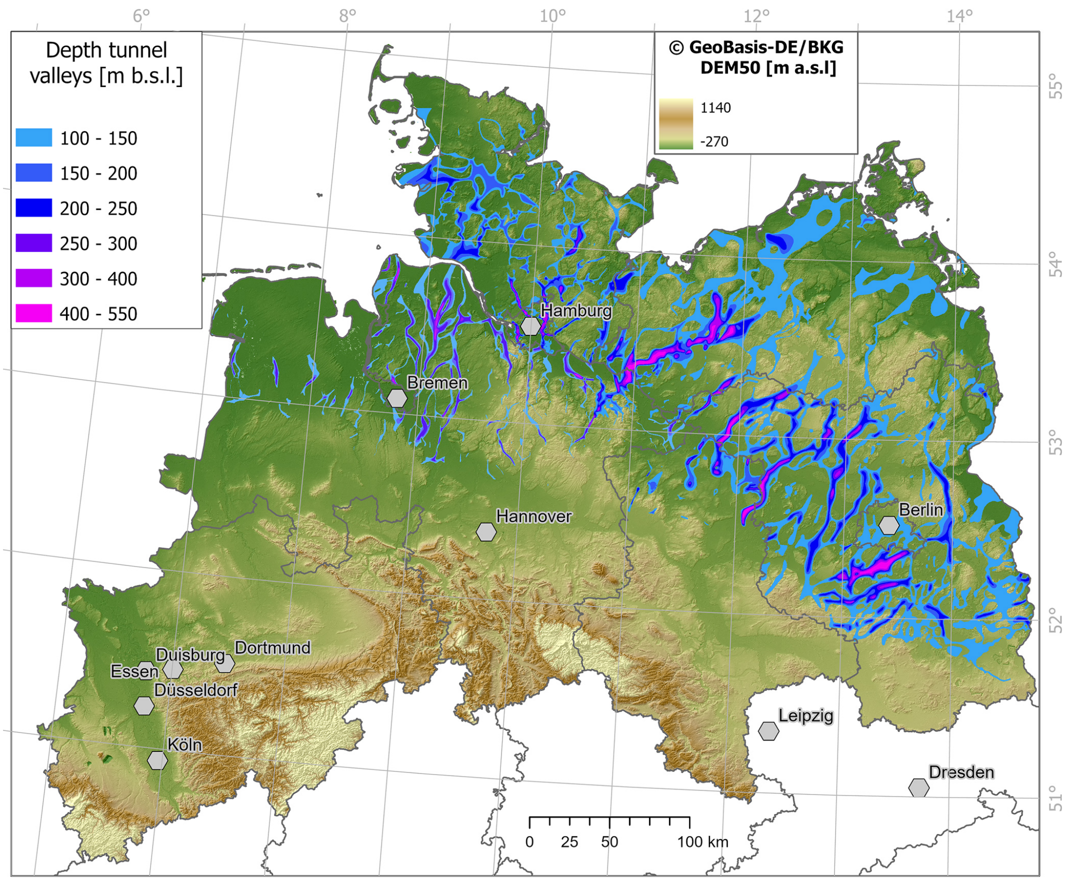

Figure 1. Map showing the digital elevation model (DEM) of northern Germany with a cell size of 50 m (© GeoBasis-DE/BKG) and a raster of the tunnel valleys with a cell size of 100 m extracted from the base Quaternary data sets.

By calculating the thalweg lines, the map of the distribution and maximum depths of the tunnel valleys becomes much clearer and focussed on the major incisions (Fig. 2). When interpreting the course of the thalweg lines, however, it is important to bear in mind that the "Flow Accumulation" tool is a hydrological tool that always searches for connections downslope. Although tunnel valleys represent former drainage pathways, the tunnel-valley floors display undulating morphologies. This undulating morphology is characteristic of tunnel valleys and caused by the flow of pressurised water below an ice sheet (Kehew et al., 2012; van der Vegt et al., 2012). The derived thalweg maps represent a simplification of the complex tunnel-valley network. Therefore, the map of the thalweg lines should always be considered in combination with contoured depth maps, as otherwise the continuity of the tunnel valleys is underestimated.

The ultimate aim of our research is to assess the long-term safety of a repository for highly radioactive waste and, in particular, effects on the integrity of the effective containment zone (ECZ). The deepest tunnel valleys attain depths

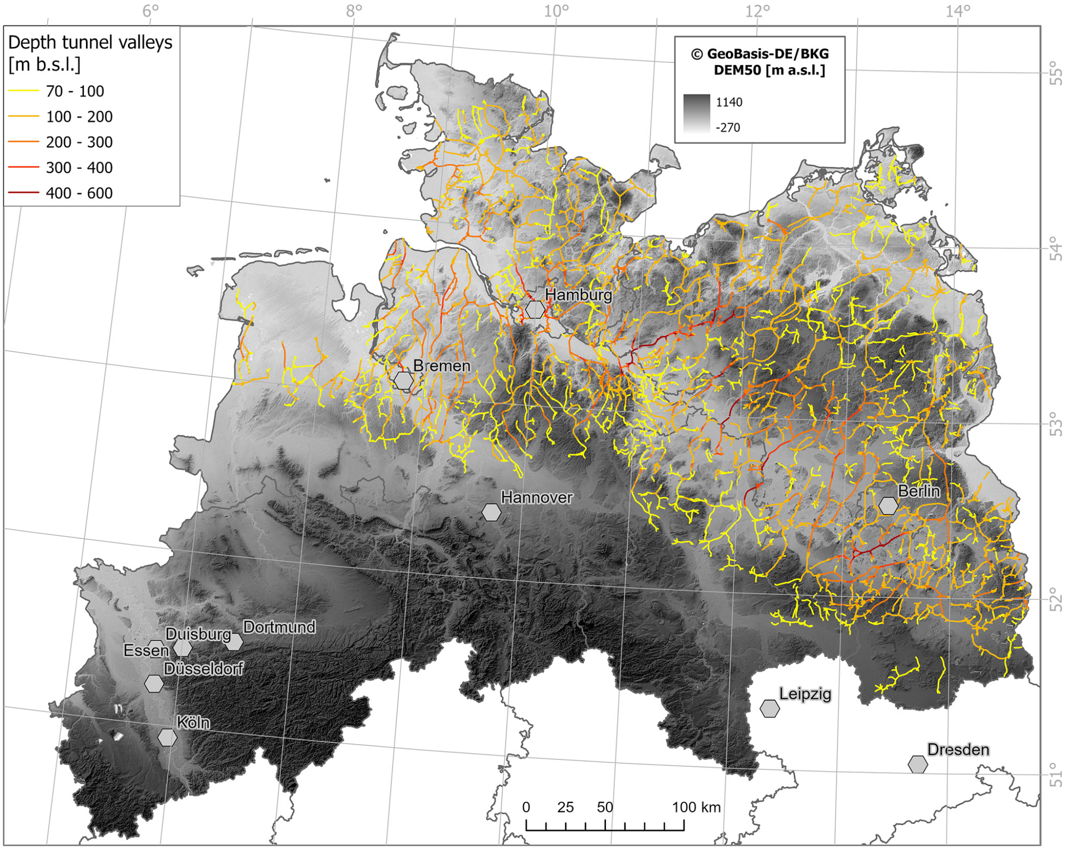

Figure 2. Map showing the digital elevation model (DEM) of northern Germany with a cell size of 50 m (© GeoBasis-DE/BKG) and the result of the thalweg extraction. The depths of the thalweg lines are colour-coded.

of more than 500 m (Fig. 3). Potential future erosion with similar depths may thus pose a risk to the ECZ. However, legislation only stipulates a required minimum depth of the top of the ECZ of 300 m b.s.l. (StandAG, 2017).

The depths of Pleistocene tunnel valleys clearly exceed the legally required minimum depth of 300 m. To minimise the risk posed by future tunnel-valley formation, an additional depth might be added to the minimum depth requirement. The mapped depth zones can be used to guide the definition of such an additional depth (Figs. 4 and 5).

The block diagram (Fig. 4) represents a schematic cross section across the Pleistocene tunnel valleys of northern Germany. Within the block diagram the geological bedrock is not further divided and therefore consists only of preglacial rocks and syn- and postglacial deposits. A dashed black line indicates the legally required minimum depth (A) of the repository (300 m). The dashed red line represents the envelope of the tunnel-valley bases. Deep tunnel valleys (> 100 m) only occur near the maximum extent of the Pleistocene ice sheets. The greater the distance from the maximum ice-sheet extent, the greater the number and depth of the tunnel valleys. The calculated depth zones of the tunnel valleys (Fig. 3) are shown in the block diagram. Since the deepest tunnel valleys in northern Germany have only been formed in a spatially limited area, it is postulated that this will also be the case in the future. In the central area with the greatest tunnel-valley depths (up to 600 m), the final depth of the repository must be significantly below the depth of the tunnel valleys.

It has long been observed that tunnel valleys tend to form in certain areas that provide favourable conditions (e.g. Boulton et al., 2009; Stackebrandt, 2009; Kehew et al., 2012). Considering the depth and distribution of the tunnel valleys together with the pre-Quaternary subcrop map (i.e. a map without the Quaternary deposits; Fig. 5), it becomes clear that the majority of, and deepest, tunnel valleys occur in the central area of the basin, where poorly lithified and easily erodible Neogene sediments of the Pliocene and Miocene underlie the Quaternary deposits. In northeastern Mecklenburg-Western Pomerania, where more resistant Jurassic and Cretaceous rocks underlie the Quaternary deposits, significantly fewer and shallower tunnel valleys (Fig. 5) are present. Figure 6 shows the depth to near the base of the Cenozoic succession (top Danian Chalk Group; Doornenbal and Stevenson, 2010) together with the tunnel-valley thalwegs. For clarity, only thalweg depths greater than 200 m are shown. The

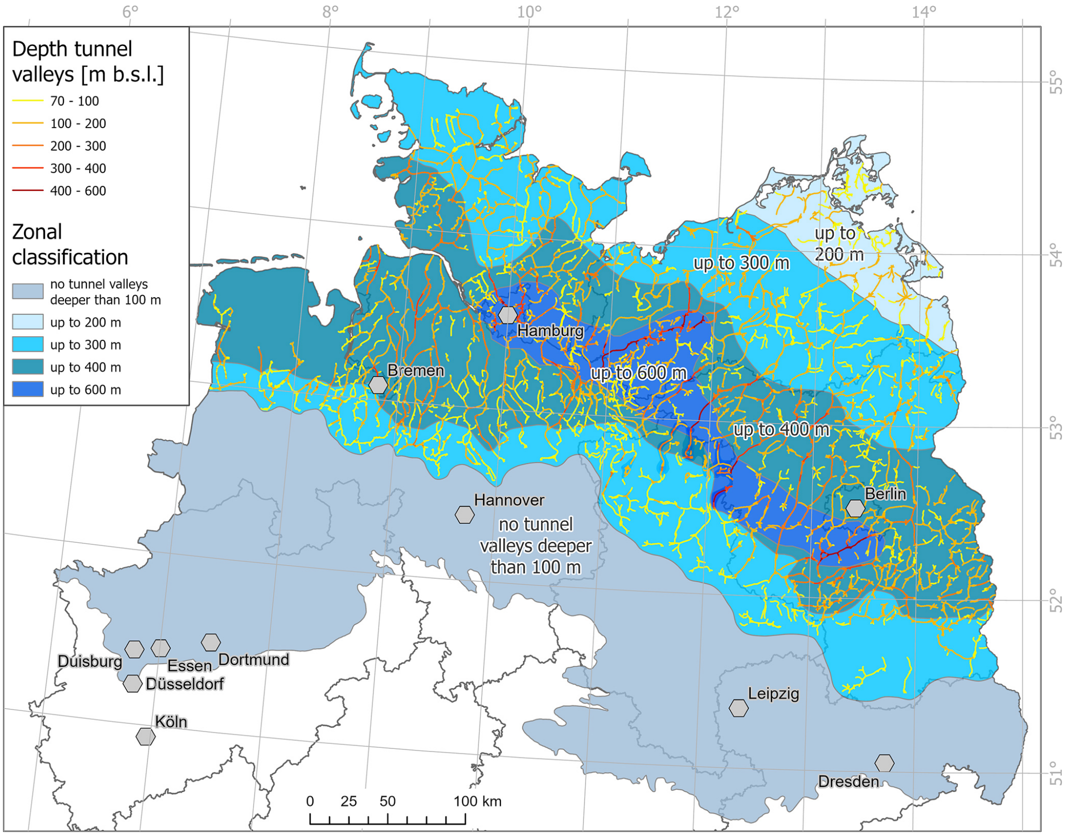

Figure 3. Map showing the analysed depth zones of the tunnel valleys defined from the spatial distribution of the thalweg depths. Five different depth zones were defined.

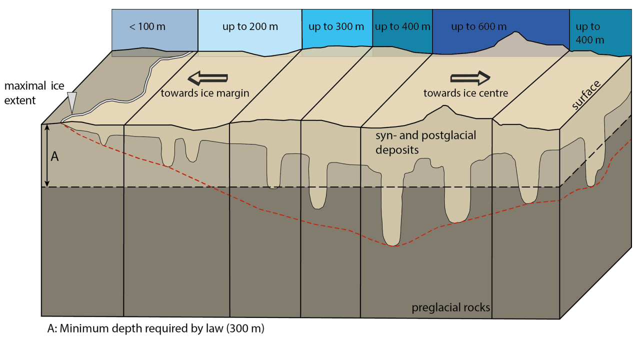

Figure 4. Block diagram showing a schematic section across the five zones of tunnel-valley depths.

map can be regarded as an approximate thickness map of the Cenozoic succession.

The greatest depths of the tunnel-valley thalwegs are reached in the central basin area where the thickness of the Cenozoic sediments is highest. The location of the basin centre correlates with the majority of the deep tunnel valleys between 200 and 558 m b.s.l. (Fig. 6). The Palaeogene and Neogene units consist mainly of poorly lithified sands, silts and clays (Doornenbal and Stevenson, 2010). The greater erodibility of the poorly lithified sediments most likely favoured deep tunnel-valley incision (cf. Stackebrandt, 2009; Kehew et al., 2012).

Deep glaciogenic erosion is also caused by the formation of basins associated with glaciotectonic thrust complexes. Basins are formed beneath the ice sheet where thrust sheets are removed and transported to the ice margin to form glaciotectonic ridges (van der Wateren, 1995; Huuse and Lykke-Andersen, 2000a; Aber and Ber, 2007). Individual thrust sheets can be up to 250 m thick and can be transported for several kilometres (Kupetz, 1997; Huuse and Lykke-Andersen, 2000a; Winsemann et al., 2020). The depth of the basins and the thickness of the thrust sheets are controlled by the depth of the detachment, which typically consists of mechanically weak beds of clay, chalk or organic-rich sediments (Huuse and Lykke-Andersen, 2000a; Andersen et al., 2005; Aber and Ber, 2007). Detachments may occur in depths of up to 350 m (Huuse and Lykke-Andersen, 2000a; Aber and Ber, 2007). In northern Germany, glaciotectonic complexes with associated basins have formed during all major ice advances (Meyer, 1987; Van Der Wateren, 1995; Kupetz, 1997; Winsemann et al., 2020; Gehrmann et al., 2022). Glaciotectonic basins attain maximum depths between 120 and 290 m (Kupetz, 1997; Winsemann et al., 2020). However, as these

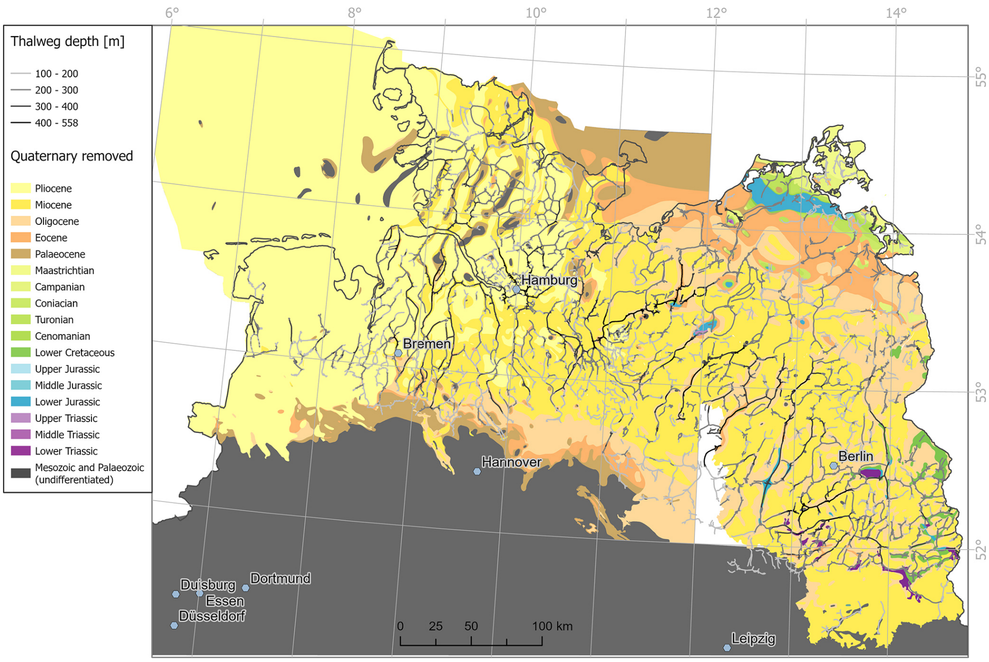

Figure 5. Pre-Quaternary subcrop map (i.e. a map without the Quaternary deposits), which is a combination of the pre-Quaternary subcrop map of the Gorleben project (Brückner-Röhling et al., 2002) and the pre-Quaternary subcrop map of Mecklenburg-Western Pomerania at 1 : 500 000 (Schütze, 2006) and the pre-Quaternary subcrop map of Brandenburg from the *Atlas zur Geologie von Brandenburg* (Stackebrandt et al., 2010) at 1 : 1 000 000.

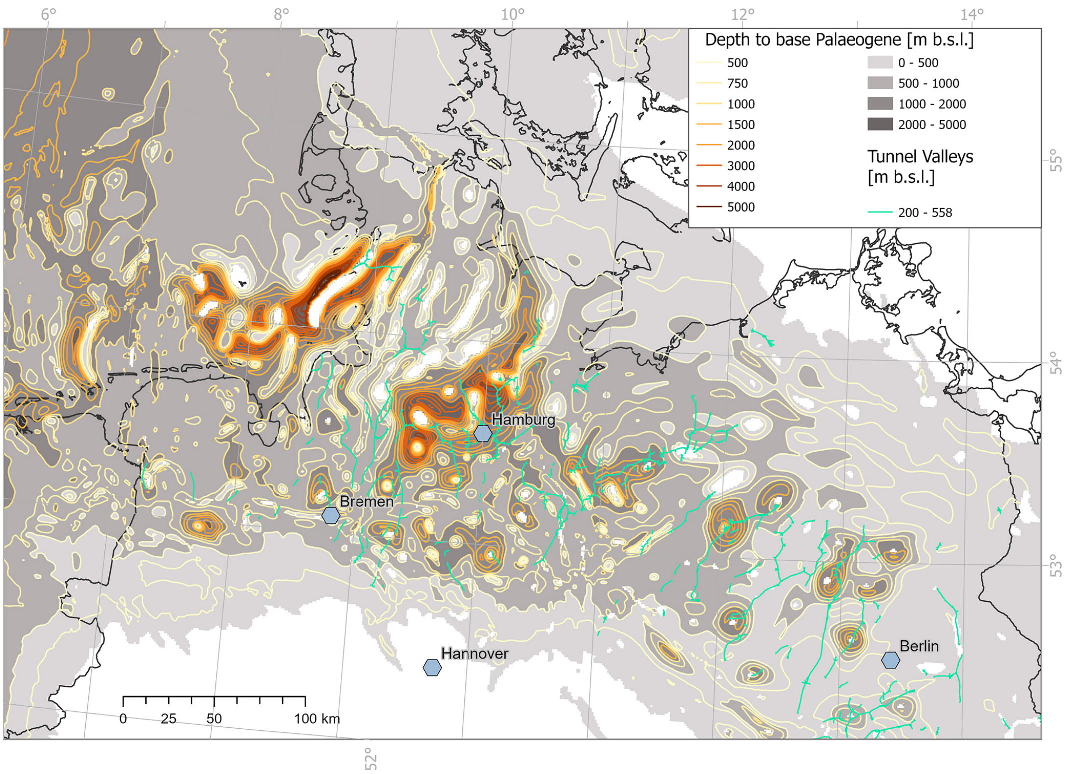

Figure 6. Map showing the near base of the Cenozoic (top Danian Chalk Group) derived from the Southern Permian Basin Atlas (Doornenbal and Stevenson, 2010). The green lines show the thalweg lines of the tunnel valleys with depths ranging from 200 to 558 m.

basins are shallower than many tunnel valleys, they are not clearly visible on most maps of the base Quaternary.

Predicting future tunnel-valley formation is extremely challenging due to the complex glaciological and geological factors controlling tunnel-valley formation. The analysis of the Pleistocene record provides valuable insights into the patterns of tunnel-valley formation that will apply to the future processes. It seems plausible that areas where deep incision occurred during the Pleistocene glaciations may also be affected by future glaciogenic erosion. The favourable conditions for tunnel-valley formation are related to the overall regional geological setting, e.g. the setting in a sedimentary basin filled by poorly lithified and erodible deposits. The overall geological setting is unlikely to undergo major changes in the next 100 000 to 1 000 000 years. However, glaciations will strongly modify the morphology and near-surface geology. Therefore, in the case of multiple future glaciations, an assessment of potential tunnel-valley formation becomes even more challenging. Furthermore, multiple occupations of tunnel valleys may occur (e.g. Piotrowski, 1994; Jørgensen and Sandersen, 2006) and a reactivation of tunnel valleys during future glaciations cannot be ruled out.

For the recommendation of the depth zones, several assumptions need to be made with regard to (i) the available data of the study area, (ii) maximum tunnel-valley depths and (iii) the extent of future glaciations. The study area is sufficiently well explored, and maps of the existing tunnel valleys are available from the state geological surveys and other publications. The source data are very heterogeneous, with regional and local variations, as the published maps of the base Quaternary have been under constant revision since the 1970s. The overall density of data in the study area is very high, and we can assume that no major structures have been overlooked that would change the observed broad trends. However, new details of the Pleistocene tunnel-valley network are still being revealed by ongoing mapping (e.g. Hese et al., 2021; Bruns et al., 2022; Lohrberg et al., 2022a, b). With maximum depths of 554 m b.s.l., the tunnel valleys in northern Germany are among the deepest known tunnel valleys (Schulz, 2002; Müller and Obst, 2008; Stackebrandt, 2009). Similar extreme depths are known from the Netherlands (ten Veen, 2015) and the continental shelf off the east coast of North America (Macrae and Christians, 2013). However, the vast majority of tunnel valleys are shallower than 400 m (Kehew et al., 2012; van der Vegt et al., 2012; Ottesen et al., 2020). Therefore, very deep tunnel valleys can be considered extreme examples formed under favourable conditions. Future research should investigate these favourable conditions in more detail. A similar assumption applies to the potential extent of future glaciations, where the well-studied Pleistocene ice-sheet extents (e.g. Ehlers et al., 2011; Batchelor et al., 2019) serve as analogues for probable future glacial limits.

9 Conclusions

Subglacial tunnel valleys are among the deepest erosional landforms and are ubiquitous features of formerly glaciated sedimentary basins. Tunnel valleys are incised by pressurised meltwater and are thus formed independently of any regional base level. In addition to glaciological factors, tunnel-valley formation is strongly controlled by the geology of the substratum. The main geological controls are the resistance to erosion and the hydraulic conductivity.

Tunnel-valley formation during potential future glaciations needs to be included in the long-term safety assessment of radioactive waste repositories. As prediction of the location of future tunnel valleys is a major challenge, the new depth-zonation map provides a straightforward approach to assessing the potential for tunnel-valley formation based on the Pleistocene record. When recommending the minimum depth for a repository, the geology of the substratum should also be considered and its potential impact on tunnel-valley formation assessed.

Data availability. The data that support the findings of this study are available from the corresponding author upon reasonable request.

Supplement. The supplement related to this article is available online at: https://doi.org/10.5194/egqsj-72-113-2023-supplement.

Author contributions. Concept and design of the study: SB and JL; data compilation and analysis: SB; interpretation and discussion of the results: SB, AB, VN and JL; first draft of manuscript and figures: SB and JL. All authors approved the submitted version.

Competing interests. The contact author has declared that none of the authors has any competing interests.

Special issue statement. This article is part of the special issue "Subglacial erosional landforms and their relevance for the long-term safety of a radioactive waste repository". It is the result of a virtual workshop held in December 2021.

Acknowledgements. We thank Mads Huuse, the anonymous reviewer and editor Sven Lukas for constructive comments, which greatly helped to improve the manuscript. The state geological surveys of Schleswig-Holstein, Hamburg, Bremen, Lower Saxony, Saxony-Anhalt, Mecklenburg-Western Pomerania, Brandenburg and Berlin are acknowledged for providing maps and data for this study. Discussions with Steffen Jahn, Nils-Peter Nilius, Maximilian Pfaff and Nadine Schöner helped to sharpen our ideas.

Review statement. This paper was edited by Sven Lukas and reviewed by Mads Huuse and one anonymous referee.

References

Aber, J. S. and Ber, A.: Glaciotectonism, Developments in Quaternary Sciences, Elsevier, 256 pp., ISBN 9780444529435, 2007.

Al Hseinat, M., Hübscher, C., Lang, J., Lüdmann, T., Ott, I., and Polom, U.: Triassic to recent tectonic evolution of a crestal collapse graben above a salt-cored anticline in the Glückstadt Graben/North German Basin, Tectonophysics, 680, 50–66, https://doi.org/10.1016/j.tecto.2016.05.008, 2016.

Andersen, L. T., Hansen, D. L., and Huuse, M.: Numerical modelling of thrust structures in unconsolidated sediments: implications for glaciotectonic deformation, J. Struct. Geol., 27, 587–596, https://doi.org/10.1016/j.jsg.2005.01.005, 2005.

Batchelor, C. L., Margold, M., Krapp, M., Murton, D. K., Dalton, A. S., Gibbard, P. L., Stokes, C. R., Murton, J. B., and Manica, A.: The configuration of Northern Hemisphere ice sheets through the Quaternary, Nat. Commun., 10, 3713, https://doi.org/10.1038/s41467-019-11601-2, 2019.

Boulton, G. S. and Hindmarsh, R. C. A.: Sediment deformation beneath glaciers: Rheology and geological consequences, J. Geophys. Res.-Solid Earth, 92, 9059–9082, https://doi.org/10.1029/JB092iB09p09059, 1987.

Boulton, G. S., Hagdorn, M., Maillot, P. B., and Zatsepin, S.: Drainage beneath ice sheets: groundwater–channel coupling, and the origin of esker systems from former ice sheets, Quaternary Sci. Rev., 28, 621–638, https://doi.org/10.1016/j.quascirev.2008.05.009, 2009.

Brandes, C., Polom, U., Winsemann, J., and Sandersen, P. B. E.: The near-surface structure in the area of the Børglum fault, Sorgenfrei-Tornquist Zone, northern Denmark: Implications for fault kinematics, timing of fault activity and fault control on tunnel valley formation, Quaternary Sci. Rev., 289, 107619, https://doi.org/10.1016/j.quascirev.2022.107619, 2022.

Brückner-Röhling, S., Espig, M., Fischer, M., Fleig, S., Forsbach, H., Kockel, F., Krull, P., Stiewe, H., and Wirth, H.: Standsicherheitsnachweise Nachbetriebsphase: Seismische Gefährdung – Teil 1: Strukturgeologie, Bundesanstalt für Geowissenschaften und Rohstoffe (BGR), Hannover, BGR-Bericht, 253, 2002.

Bruns, I., Fischer, K., Meinsen, J., and Wangenheim, C.: Eine aktualisierte Quartärbasis für Niedersachsen – Erste Einblicke in die Modellierung, DEUQUA "Connecting Geoarchives, Potsdam, 1 p., https://doi.org/10.48440/GFZ.b103-22024, 2022.

Catania, G. and Paola, C.: Braiding under glass, Geology, 29, 259–262, https://doi.org/10.1130/0091-7613(2001)029%3C0259:BUG%3E2.0.CO;2, 2001.

Clayton, L., Attig, J. W., and Mickelson, D. M.: Tunnel channels formed in Wisconsin during the last glaciation, in: Glacial Processes Past and Present, edited by: Mickelson, D. M. and Attig, J. W., Geological Society of America, https://doi.org/10.1130/0-8137-2337-x.69, 1999.

Doornenbal, H. and Stevenson, A.: Petroleum Geological Atlas of the Southern Permian Basin Area, EAGE Publications b.v. (Houten), ISBN 978-90-73781-61-0, 2010.

Ehlers, J. and Linke, G.: The origin of deep buried channels of Elsterian age in Northwest Germany, J. Quaternary Sci., 4, 255–265, https://doi.org/10.1002/jqs.3390040306, 1989.

Ehlers, J., Grube, A., Stephan, H.-J., and Wansa, S.: Pleistocene Glaciations of North Germany – New Results, in: Developments in Quaternary Sciences, edited by: Ehlers, J., Gibbard, P. L., and Hughes, P. D., Elsevier, 149–162, https://doi.org/10.1016/B978-0-444-53447-7.00013-1, 2011.

Eissmann, L.: Quaternary geology of eastern Germany (Saxony, Saxon–Anhalt, South Brandenburg, Thüringia), type area of the Elsterian and Saalian Stages in Europe, Quaternary Sci. Rev., 21, 1275–1346, https://doi.org/10.1016/S0277-3791(01)00075-0, 2002.

Fischer, U. H., Bebiolka, A., Brandefelt, J., Cohen, D., Harper, J., Hirschorn, S., Jensen, M., Kennell, L., Liakka, J., Näslund, J.-O., Normani, S., Stück, H., and Weitkamp, A.: Radioactive waste under conditions of future ice ages, in: Snow and Ice-Related Hazards, Risks, and Disasters (Second Edition), edited by: Haeberli, W. and Whiteman, C., Elsevier, 323–375, https://doi.org/10.1016/B978-0-12-817129-5.00005-6, 2021.

Gegg, L. and Preusser, F.: Comparison of overdeepened structures in formerly glaciated areas of the northern Alpine foreland and northern central Europe, E&G Quaternary Sci. J., 72, 23–36, https://doi.org/10.5194/egqsj-72-23-2023, 2023.

Gehrmann, A., Pedersen, S. A. S., and Meschede, M.: New insights into the structural development and shortening of the southern Jasmund Glacitectonic Complex (Rügen, Germany) based on balanced cross sections, Int. J. Earth Sci., 111, 1697–1715, https://doi.org/10.1007/s00531-022-02216-y, 2022.

Grube, F.: Übertiefte Rinnen im Hamburger Raum, E&G Quaternary Sci. J., 29, 157–172, https://doi.org/10.3285/eg.29.1.13, 1979.

Grube, F.: Tunnel Valleys, in: Glacial Deposits in North-West Europe, edited by: Ehlers, J., A. A. Balkema, Rotterdam, 257–258, 1983.

Hese, F., Ahlers, P., Krienke, K., and Neumann, T.: Neubearbeitung der Quartärbasis in Schleswig-Holstein, Subglaziale Rinnen Workshop 2021, Poster, 10 December 2021, Hannover, 2021.

Hinsch, W.: Rinnen an der Basis des glaziären Pleistozäns in Schleswig-Holstein, E&G Quaternary Sci. J., 29, 173–178, https://doi.org/10.3285/eg.29.1.14, 1979.

Hooke, R. L. and Jennings, C. E.: On the formation of the tunnel valleys of the southern Laurentide ice sheet, Quaternary Sci. Rev., 25, 1364–1372, https://doi.org/10.1016/j.quascirev.2006.01.018, 2006.

Huuse, M. and Lykke-Andersen, H.: Large-scale glaciotectonic thrust structures in the eastern Danish North Sea, Geological Society, London, Special Publications, 176, 293–305, https://doi.org/10.1144/GSL.SP.2000.176.01.22, 2000a.

Huuse, M. and Lykke-Andersen, H.: Overdeepened Quaternary valleys in the eastern Danish North Sea: morphology and origin, Quaternary Sci. Rev., 19, 1233–1253, https://doi.org/10.1016/S0277-3791(99)00103-1, 2000b.

Janszen, A., Moreau, J., Moscariello, A., Ehlers, J., and Kröger, J.: Time-transgressive tunnel-valley infill revealed by a three-dimensional sedimentary model, Hamburg, north-west Germany, Sedimentology, 60, 693–719, https://doi.org/10.1111/j.1365-3091.2012.01357.x, 2013.

Jørgensen, F. and Sandersen, P. B. E.: Buried and open tunnel valleys in Denmark – erosion beneath multiple ice sheets, Quaternary Sci. Rev.,, 25, 1339–1363, https://doi.org/10.1016/j.quascirev.2005.11.006, 2006.

Kehew, A., Piotrowski, J., and Jørgensen, F.: Tunnel valleys: Concepts and controversies – A review, Earth-Sci. Rev., 113, 33–58, https://doi.org/10.1016/j.earscirev.2012.02.002, 2012.

Kirkham, J. D., Hogan, K. A., Larter, R. D., Self, E., Games, K., Huuse, M., Stewart, M. A., Ottesen, D., Arnold, N. S., and Dowdeswell, J. A.: Tunnel valley infill and genesis revealed by high-resolution 3-D seismic data, Geology, 49, 1516–1520, https://doi.org/10.1130/g49048.1, 2021.

Kirkham, J. D., Hogan, K. A., Larter, R. D., Arnold, N. S., Ely, J. C., Clark, C. D., Self, E., Games, K., Huuse, M., Stewart, M. A., Ottesen, D., and Dowdeswell, J. A.: Tunnel valley formation beneath deglaciating mid-latitude ice sheets: Observations and modelling, Quaternary Sci. Rev., 107680, https://doi.org/10.1016/j.quascirev.2022.107680, 2022.

Kristensen, T. B., Huuse, M., Piotrowski, J. A., and Clausen, O. R.: A morphometric analysis of tunnel valleys in the eastern North Sea based on 3D seismic data, J. Quaternary Sci., 22, 801–815, https://doi.org/10.1002/jqs.1123, 2007.

Kupetz, M.: Geologischer Bau und Genese der Stauchendmoräne Muskauer Faltenbogen, Brandenburgische Geowissenschaftliche Beiträge, 4, 1–20, http://www.schweizerbart.de//publications/detail/isbn/9783510652952/Stackebrandt_Franke_Geologie_von_Brande (last access: 17 May 2023), 1997.

Kuster, H. and Meyer, K. D.: Glaziäre Rinnen im mittleren und nördlichen Niedersachsen, E&G Quaternary Sci. J., 29, 135–156, https://doi.org/10.3285/eg.29.1.12, 1979.

Lang, J., Winsemann, J., Steinmetz, D., Polom, U., Pollok, L., Böhner, U., Serangeli, J., Brandes, C., Hampel, A., and Winghart, S.: The Pleistocene of Schöningen, Germany: a complex tunnel valley fill revealed from 3D subsurface modelling and shear wave seismics, Quaternary Sci. Rev., 39, 86–105, https://doi.org/10.1016/j.quascirev.2012.02.009, 2012.

Lang, J., Hampel, A., Brandes, C., and Winsemann, J.: Response of salt structures to ice-sheet loading: implications for ice-marginal and subglacial processes, Quaternary Sci. Rev., 101, 217–233, https://doi.org/10.1016/j.quascirev.2014.07.022, 2014.

Lang, J., Böhner, U., Polom, U., Serangeli, J., and Winsemann, J.: The Middle Pleistocene tunnel valley at Schöningen as a Paleolithic archive, J. Human Evolut., 89, 18–26, https://doi.org/10.1016/j.jhevol.2015.02.004, 2015.

Litt, T., Behre, K.-E., Meyer, K.-D., Stephan, H.-J., and Wansa, S.: Stratigraphische Begriffe für das Quartär des norddeutschen Vereisungsgebietes, E&G Quaternary Sci. J., 56, 7–65, https://doi.org/10.3285/eg.56.1-2.02, 2007.

Lohrberg, A., Schwarzer, K., Unverricht, D., Omlin, A., and Krastel, S.: Architecture of tunnel valleys in the southeastern North Sea: new insights from high-resolution seismic imaging, J. Quatern. Sci., 35, 892–906, https://doi.org/10.1002/jqs.3244, 2020.

Lohrberg, A., Krastel, S., Unverricht, D., and Schwarzer, K.: The Heligoland Glacitectonic Complex in the southeastern North Sea: indicators of a pre- or early-Elsterian ice margin, Boreas, 51, 100–117, https://doi.org/10.1111/bor.12551, 2022a.

Lohrberg, A., Schneider von Deimling, J., Grob, H., Lenz, K.-F., and Krastel, S.: Tunnel valleys in the southeastern North Sea: more data, more complexity, E&G Quaternary Sci. J., 71, 267–274, https://doi.org/10.5194/egqsj-71-267-2022, 2022b.

MacRae, R. A. and Christians, A. R.: A reexamination of Pleistocene tunnel valley distribution on the central Scotian Shelf, Can. J. Earth Sci., 50, 535–544, https://doi.org/10.1139/cjes-2012-0057, 2013.

Meyer, K. D.: Ground and end moraines in Lower Saxony, in: Tills and Glaciotectonics, edited by: van der Meer, J. J. M., Balkema, Rotterdam, 197–204, ISBN 0317650114, 1987.

Müller, U. and Obst, K.: Junge halokinetische Bewegungen im Bereich der Salzkissen Schlieven und Marnitz in Südwest-Mecklenburg, Brandenburg. geowiss. Beitr., 15, 147–145, https://www.schweizerbart.de/publications/detail/isbn/9783510652952/Stackebrandt/_Franke/_Geologie_von_Brande (last access: 17 May 2023), 2008.

Noack, V., Cherubini, Y., Scheck-Wenderoth, M., Lewerenz, B., Höding, T., Simon, A., and Moeck, I. S.: Assessment of the present-day thermal field (NE German Basin) – Inferences from 3D modelling, Geochemistry, 70, 47–62, https://doi.org/10.1016/j.chemer.2010.05.008, 2010.

Ó Cofaigh, C.: Tunnel valley genesis, Prog. Phys. Geog.-Earth Environ., 20, 1–19, https://doi.org/10.1177/030913339602000101, 1996.

Ottesen, D., Stewart, M., Brönner, M., and Batchelor, C. L.: Tunnel valleys of the central and northern North Sea (56° N to 62° N): Distribution and characteristics, Mar. Geol., 425, 106199, https://doi.org/10.1016/j.margeo.2020.106199, 2020.

Passchier, S., Laban, C., Mesdag, C. S., and Rijsdijk, K. F.: Subglacial bed conditions during Late Pleistocene glaciations and their impact on ice dynamics in the southern North Sea, Boreas, 39, 633–647, https://doi.org/10.1111/j.1502-3885.2009.00138.x, 2010.

Piotrowski, J. A.: Tunnel-valley formation in northwest Germany – geology, mechanisms of formation and subglacial bed conditions for the Bornhöved tunnel valley, Sediment. Geol., 89, 107–141, https://doi.org/10.1016/0037-0738(94)90086-8, 1994.

Piotrowski, J. A.: Subglacial hydrology in north-western Germany during the last glaciation: groundwater flow, tunnel valleys and hydrological cycles, Quaternary Sci. Rev., 16, 169–185, https://doi.org/10.1016/S0277-3791(96)00046-7, 1997.

Piotrowski, J. A., Geletneky, J., and Vater, R.: Soft-bedded subglacial meltwater channel from Welzow-Süd open-cast lignite mine, Lower Lusatia, eastern Germany, Boreas, 28, 363–374, https://doi.org/10.1111/j.1502-3885.1999.tb00226.x, 1999.

Piotrowski, J. A., Larsen, N. K., and Junge, F. W.: Reflections on soft subglacial beds as a mosaic of deforming and stable spots, Quaternary Sci. Rev., 23, 993–1000, https://doi.org/10.1016/j.quascirev.2004.01.006, 2004.

Prins, L. T., Andresen, K. J., Clausen, O. R., and Piotrowski, J. A.: Formation and widening of a North Sea tunnel valley – The impact of slope processes on valley morphology, Geomorphology, 368, 107347, https://doi.org/10.1016/j.geomorph.2020.107347, 2020.

Ravier, E., Buoncristiani, J.-F., Guiraud, M., Menzies, J., Clerc, S., Goupy, B., and Portier, E.: Porewater pressure control on subglacial soft sediment remobilization and tunnel valley formation: A case study from the Alnif tunnel valley (Morocco), Sediment. Geol., 304, 71–95, https://doi.org/10.1016/j.sedgeo.2014.02.005, 2014.

Ravier, E., Buoncristiani, J.-F., Menzies, J., Guiraud, M., Clerc, S., and Portier, E.: Does porewater or meltwater control tunnel valley genesis? Case studies from the Hirnantian of Morocco, Palaeogeogr. Palaeocl., 418, 359–376, https://doi.org/10.1016/j.palaeo.2014.12.003, 2015.

Sandersen, P. B. E. and Jørgensen, F.: Substratum control on tunnel-valley formation in Denmark, in: Glaciogenic Reservoirs and Hydrocarbon Systems, edited by: Huuse, M., Redfern, J., Le Heron, D. P., Dixon, R. J., Moscariello, A., and Craig, A., Geological Society Special Publications, 1, Geological Society of London, London/UK, 145–157, https://doi.org/10.1144/SP368.12, 2012.

Sandersen, P. B. E. and Jørgensen, F.: Tectonic impact on Pleistocene and Holocene erosional patterns in a formerly glaciated intra-plate area, Quaternary Sci. Rev., 293, 107681, https://doi.org/10.1016/j.quascirev.2022.107681, 2022.

Sandersen, P. B. E., Jørgensen, F., Larsen, N. K., Westergaard, J. H., and Auken, E.: Rapid tunnel-valley formation beneath the receding Late Weichselian ice sheet in Vendsyssel, Denmark, Boreas, 38, 834–851, https://doi.org/10.1111/j.1502-3885.2009.00105.x, 2009.

Schulz, R.: Forschungsbohrungen des GGA-Instituts, Zeitschrift für angewandte Geologie, 48, 3–8, ISSN 0044-2259, 2002.

Schütze, K.: Übersichtskarte Präquartär und Quartärbasis, Landesamt für Umwelt, Naturschutz und Geologie Mecklenburg-Vorpommern (LUNG), Geologische Karte von Mecklenburg-Vorpommern 1:500.000, 2006.

Shreve, R. L.: Movement of Water in Glaciers, J. Glaciol., 11, 205–214, https://doi.org/10.3189/S002214300002219X, 1972.

Smed, P.: Die Entstehung der dänischen und norddeutschen Rinnentäler (Tunneltäler) – Glaziologische Gesichtspunkte, E&G Quaternary Sci. J., 48, 1–18, https://doi.org/10.3285/eg.48.1.01, 1998.

Sonntag, A. and Lippstreu, L.: Tiefenlage der Quartärbasisfläche, in: Atlas zur Geologie von Brandenburg, 4. aktualisierte Auflage ed., edited by: Stackebrandt, W. and Manhenke, V., Landesamt für Bergbau, Geologie und Rohstoffe Brandenburg (LBGR), Cottbus, 54–55, ISBN 978-3-9808157-4-1, 2010.

Stackebrandt, W.: Subglacial channels of Northern Germany – a brief review, Zeitschrift der Deutschen Gesellschaft für Geowissenschaften, 160, 203–210, https://doi.org/10.1127/1860-1804/2009/0160-0203, 2009.

Stackebrandt, W., Ludwig, A. O., and Ostaficzuk, S.: Base of Quaternary deposits of the Baltic Sea depression and adjacent areas (Map 2), Brandenburgische geowissenschaftliche Beiträge, 8, 13–19, https://lbgr.brandenburg.de/lbgr/de/geologischer-dienst/brandenburgische-geowissenschaftliche-beitraege/ (last access: 17 May 2023), 2001.

Stackebrandt, W., Manhenke, V., Stackebrandt, W., Andreae, A., and Strahl, J. (Eds.): Atlas zur Geologie von Brandenburg, 4. aktualisierte Auflage, Landesamt für Bergbau, Geologie und Rohstoffe Brandenburg (LBGR), Cottbus, 157 pp., ISBN 978-3-9808157-4-1, 2010.

StandAG: Gesetz zur Suche und Auswahl eines Standortes für ein Endlager für hochradioaktive Abfälle (Standortauswahlgesetz – StandAG) vom 5. Mai 2017 (BGBl. I 2017, Nr. 26, S. 1074) zuletzt geändert durch Artikel 3 des Gesetzes vom 12. Dezember 2019 (BGBl. I 2019, Nr. 48, S. 2510), Stand 01/20, Deutscher Bundestag, 2017.

Steinmetz, D., Winsemann, J., Brandes, C., Siemon, B., Ullmann, A., Wiederhold, H., and Meyer, U.: Towards an improved geological interpretation of airborne electromagnetic data: a case study from the Cuxhaven tunnel valley and its Neogene host sediments (northwest Germany), Netherlands J. Geosci., 94, 201–227, https://doi.org/10.1017/njg.2014.39, 2015.

ten Veen, J.: Future evolution of the geological and geohydrological properties of the geosphere, TNO, Utrecht, OPERA-PU-TNO412, 121, Utrecht, OPERA, 2015.

van der Vegt, P., Janszen, A., and Moscariello, A.: Tunnel valleys: current knowledge and future perspectives, Geological Society, London, Special Publications, 368, 75–97, https://doi.org/10.1144/sp368.13, 2012.

van der Wateren, F. M.: Structural geology and sedimentology of push moraines: processes of soft sediment deformation in a glacial environment and the distribution of glaciotectonic styles, Mededelingen Rijks Geologische Dienst, 54, 167 pp., ISSN 90-72869-44-3, 1995.

Wenau, S. and Alves, T. M.: Salt-induced crestal faults control the formation of Quaternary tunnel valleys in the southern North Sea, Boreas, 49, 799–812, https://doi.org/10.1111/bor.12461, 2020.

Wingfield, R.: The origin of major incisions within the Pleistocene deposits of the North Sea, Mar. Geol., 91, 31–52, https://doi.org/10.1016/0025-3227(90)90131-3, 1990.

Winsemann, J., Koopmann, H., Tanner, D. C., Lutz, R., Lang, J., Brandes, C., and Gaedicke, C.: Seismic interpretation and structural restoration of the Heligoland glaciotectonic thrust-fault complex: Implications for multiple deformation during (pre-)Elsterian to Warthian ice advances into the southern North Sea Basin, Quaternary Sci. Rev., 227, 106068, https://doi.org/10.1016/j.quascirev.2019.106068, 2020.

E&G Quaternary Sci. J., 72, 127–161, 2023
https://doi.org/10.5194/egqsj-72-127-2023

Open Access E&G Quaternary Science Journal

Research article

Holocene forest and land-use history of the Erzgebirge, central Europe: a review of palynological data

Knut Kaiser[1], **Martin Theuerkauf**[2], **and Falk Hieke**[3]

[1]GFZ German Research Centre for Geosciences, Telegrafenberg, 14473 Potsdam, Germany
[2]Institute of Botany and Landscape Ecology, University of Greifswald, Soldmannstrasse 15, 17487 Greifswald, Germany
[3]Büro für Bodenwissenschaft, Nonnengasse 28, 09599 Freiberg, Germany

Correspondence: Knut Kaiser (kaiserk@gfz-potsdam.de)

Relevant dates: Received: 5 January 2023 – Revised: 16 May 2023 – Accepted: 6 June 2023 – Published: 11 July 2023

How to cite: Kaiser, K., Theuerkauf, M., and Hieke, F.: Holocene forest and land-use history of the Erzgebirge, central Europe: a review of palynological data, E&G Quaternary Sci. J., 72, 127–161, https://doi.org/10.5194/egqsj-72-127-2023, 2023.

Abstract: The ongoing ecological conversion of mountain forests in central Europe from widespread *Picea* monocultures to mixed stands conceptually also requires a historical perspective on the very long-term, i.e. Holocene, vegetation and land-use dynamics. Detailed sources of information for this are palynological data. The Erzgebirge in focus here, with a maximum height of 1244 m a.s.l., represents an extreme case of extensive historical deforestation since the Middle Ages due to mining, metallurgy, and other industrial activities, as well as rural and urban colonisation. For this regional review we collected and evaluated 121 pollen diagrams of different stratigraphic, taxonomic, and chronological resolution. This number makes this region an upland area in central Europe with an exceptionally high density of palynological data. Using well-dated diagrams going back to the early Holocene, main regional vegetation phases were derived: the *Betula–Pinus* phase (ca. 11 600–10 200 cal yr BP), the *Corylus* phase (ca. 10 200–9000 cal yr BP), the *Picea* phase (ca. 9000–6000 cal yr BP), the *Fagus–Picea* phase (ca. 6000–4500 cal yr BP), the *Abies–Fagus–Picea* phase (ca. 4000–1000 cal yr BP), and the anthropogenic vegetation phase (ca. 1000–0 cal yr BP). Some diagrams show the presence or even continuous curves of potential pasture and meadow indicators from around 2000 cal BCE at the earliest. Even cereal pollen grains occur sporadically already before the High Medieval. These palynological indications of a local prehistoric human impact also in the higher altitudes find parallels in the (geo-)archaeologically proven Bronze Age tin placer mining and in the geochemically proven Iron Age metallurgy in the Erzgebirge. The pollen data show that immediately before the medieval clearing, i.e. beginning at the end of the 12th century CE, forests were mainly dominated by *Fagus* and *Abies* and complemented by *Picea* with increasing share towards the highest altitudes. According to historical data, the minimum of the regional forest cover was reached during the 17th–18th centuries CE. The dominance of *Picea* in modern pollen spectra is caused by anthropogenic afforestation in the form of monocultures since that time. Future palynological investigations, preferably within the framework of altitudinal transect studies, should aim for chronologically and taxonomically high-resolution and radiometrically well-dated pollen diagrams from the larger peatlands.

Kurzfassung: Der ökologische Umbau der Gebirgswälder in Mitteleuropa von vorherrschenden *Picea*-Monokulturen zu gemischten Beständen erfordert konzeptionell auch eine historische Perspektive auf die sehr langfristige, das heißt holozäne Vegetations- und Landnutzungsdynamik. Eine detailreiche Informationsquelle dafür sind palynologische Daten. Das hier im Fokus stehende, maximal 1244 m NN hohe Erzgebirge repräsentiert einen Extremfall flächendeckender historischer Entwaldung seit dem Mittelalter durch Bergbau, Metallurgie, weitere industrielle Aktivitäten sowie bäuerliche und städtische Kolonisation. Für dieses regionale Review wurden durch uns 121 Pollendiagramme unterschiedlicher stratigraphischer, taxonomischer und chronologischer Auflösung gesammelt und evaluiert. Diese Anzahl macht diese Region zu einem Gebirgsareal in Mitteleuropa mit einer besonders hohen Dichte an palynologischen Daten. Anhand zeitlich bis in das Frühholozän zurückreichender, gut datierter Diagramme wurden regionale Hauptvegetationsphasen abgeleitet: *Betula–Pinus*-Phase (ca. 11 600–10 200 cal yr BP), *Corylus*-Phase (ca. 10 200–9000 cal yr BP), *Picea*-Phase (ca. 9000–6000 cal yr BP), *Fagus–Picea*-Phase (ca. 6000–4500 cal yr BP), *Abies–Fagus–Picea*-Phase (ca. 4000–1000 cal yr BP) und anthropogene Phase (ca. 1000–0 cal yr BP). Einige Diagramme zeigen das Vorhandensein oder sogar kontinuierliche Kurven potenzieller Weide- und Wiesenindikatoren ab frühestens etwa 2000 cal BCE. Auch Getreidepollen kommen vereinzelt schon vor dem Hochmittelalter vor. Diese palynologischen Hinweise auf einen lokalen prähistorischen menschlichen Einfluss auch in den höheren Gebirgslagen finden Parallelen in dem (geo-)archäologisch nachgewiesenen bronzezeitlichen Zinn-Seifenbergbau und in der geochemisch nachgewiesenen eisenzeitlichen Metallurgie im Erzgebirge. Die Pollendaten zeigen, dass unmittelbar vor der mittelalterlichen Rodung, das heißt beginnend am Ende des 12. Jahrhunderts, in allen Höhenzonen des Gebirges die Wälder durch *Fagus* und *Abies* dominiert waren, ergänzt durch einen zunehmenden Anteil von *Picea* in den Hochlagen. Das Minimum der regionalen Waldbedeckung wurde nach historischen Daten im 17.–18. Jahrhundert erreicht. Die Dominanz von *Picea* in modernen Pollenspektren wurde durch anthropogene Aufforstungen in Form von Monokulturen seit dieser Zeit verursacht. Künftige palynologische Untersuchungen, bevorzugt im Rahmen von Höhentransekt-Studien, sollten auf chronologisch und taxonomisch hoch aufgelöste sowie radiometrisch gut datierte Pollendiagramme aus größeren Mooren zielen.

1 Introduction: an extreme mountain forest landscape

With regard to their forests, the Erzgebirge (Czech: Krušne hoří, English: Ore Mountains; Fig. 1) represent a historical extreme in central Europe, both in environmental and scientific–academic terms. Against the background of harsh but not at all extreme natural conditions in this up to 1244 m a.s.l. high mountain range, extremely intensive mining and other industrial as well as agricultural activities from the 12th to the 18th centuries CE temporarily led to almost complete deforestation (Thomasius, 1994; Hempel, 2009). The extent of clearing is certainly unique in the central European uplands, even though similar medieval to early modern mountain forest and mining areas, such as Harz, Schwarzwald, Sudetes, Böhmerwald/Šumava, or Českomoravská vrchovina, were also affected by intensive overexploitation of its wood resources (Segers-Glocke and Witthöft, 2000; Hrubý et al., 2014; Rösch, 2015; Cembrzyński, 2019; Piekalski, 2020; Kozáková et al., 2022).

After the re-establishment of now highly artificial (spruce) forests in the 18th and 19th centuries CE (Thomasius, 1994), two further anthropogenically triggered extremes followed in the 20th century CE: first, large parts of the Bohemian Erzgebirge were depopulated by the expatriation of the Germans after World War II. An open, intensively used landscape for centuries widely became a fallow or forested landscape here again (Bičík and Štěpánek, 1994; Zelinka et al., 2021). Second, from the 1960s to the 1990s large parts of the forests died back (German: *Waldsterben*) due to heavy industrial air pollution basically by sulfur dioxide emissions (Zimmermann et al., 2003; Grunewald and Bastian, 2015; Kupková et al., 2018). Together with the nearby Jizera/Izera Mountains, the Erzgebirge represented a part of the so-called "Black Triangle region", which was an industrial pollution hotspot caused by lignite combustion for energy generation in the border area between east Germany, the Czech Republic, and Poland. Nowhere else in central Europe was the extent of forest dieback and other environmental effects of industrial air pollution so extreme as here (Kubíková, 1991; Schmidt, 1993; Scheithauer and Grunewald, 2007).

But the Erzgebirge and its forest also came up with – this time positively connoted – extremes from a scientific–academic point of view: the humanistic scholar Georgius Agricola (1494–1555) developed the mining sciences in the Erzgebirge. Various geoscientific disciplines were estab-

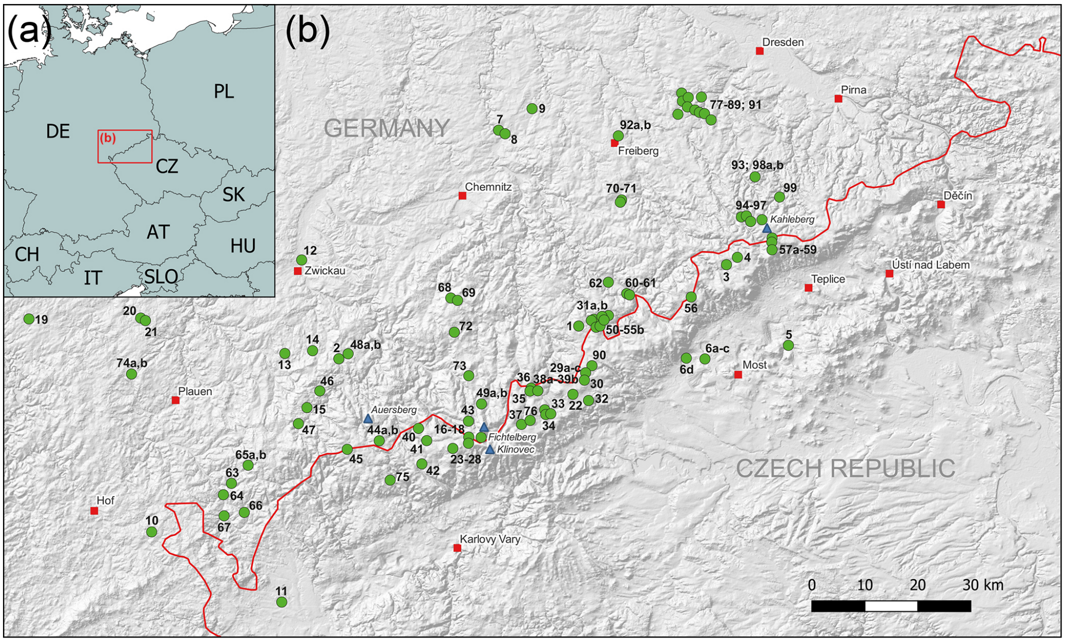

Figure 1. Distribution map of pollen diagrams in the Erzgebirge. **(a)** Situation of the study area in central Europe. **(b)** Pollen diagrams collected from the study area (green dots are the pollen diagrams with IDs, blue triangles are prominent mountain tops, red squares are towns, and the red line is the state border). For decoding and referencing of the IDs see Table 1. The steep southern escarpment of Erzgebirge to the Ohře/Eger Graben and the North Bohemian Basin is clearly visible in the underlying digital elevation model, forming a diagonal, SW–NE trending structure. The digital elevation data are funded under the GMES preparatory action 2009 on Reference Data Access by the European Commission, DG Enterprise and Industry (https://sdi.eea.europa.eu/, last access: 13 June 2022).

lished at the Mining Academy founded in Freiberg in 1765, one of the oldest in the world. In 1713, the Saxon mining official Hans Carl von Carlowitz (1645–1714) developed the principle of sustainability in forestry due to the pressing regional timber shortage (Grober, 2012; von Carlowitz and von Rohr, 2012). Today sustainability, although more comprehensively defined, is the increasingly influential guiding principle of a meaningful global development. A little later, in 1811–1816, one of the oldest forest faculties in the world was founded in nearby Tharandt, which still influences the forest practice and the regional forest structure to this day.

Finally, at the beginning of the 20th century CE, the Bohemian and Saxon Erzgebirge became the subject of systematic, large-scale palynological investigations into the postglacial forest history (Rudolph and Firbas, 1924): in the early days of palynology and for the first time with such intensity in a central European low mountain range, with astonishing modernity to this day. In general, it can be said for the Erzgebirge that in the past extreme forest resource problems resulted in extreme forest scientific and academic innovation forces!

Now at the beginning of the 21st century CE, after around 200 years of relative climatic stability and after around 30 years of ecological restoration, the Erzgebirge is once again affected by a rapid change in its environment in general and especially in its forests: recent climate change with its extreme weather events, such as storms and droughts, but also initially rather unspectacular, long-term phenomena, such as the increase in temperatures and decrease in snow precipitation (Bednářová et al., 2014; Vlach et al., 2021), predictably lead to a more or less "catastrophic end" to the previous forest management system dominantly comprising spruce monoculture age class forests. The new forest crisis is expressed by large areas severely damaged (12 200 ha) and completely cleared (2600 ha) of mainly spruce forest between 2017 and 2020 by abiotic (drought, storm) and biotic factors (bark beetles; Gdulová et al., 2021). In general, the severe bark beetle infestation in spruces that occurred during the last few years has led to an unheard-of amount of damaged forests since the beginning of regulated forestry in Saxony some 200 years ago (SMEKUL, 2020). Although alternative forest management concepts, such as the principle of natural forest or permanent (mixed) forest, have a long local tradition in the region and beyond (Möller, 1922; Krutzsch, 1952), they could not prevail against the industrial engineering forest mainstream in the 20th century CE (Knapp et al., 2021). Only in the last two to three decades have the forests in the Erzgebirge been increasingly "rebuilt" from an ecological point of view; that is, a mixed mountain forest mainly consisting of beech, fir, and spruce has been replanted at the sites of previous spruce monocultures (Eisenhauer and Sonnemann, 2009; Staatsbetrieb Sachsenforst, 2017).

The underlying theoretical concept is based on both forest ecological observations and ecological–theoretical considerations in the region and beyond (e.g. Ellenberg, 1996; Küssner and Mosandl, 2002), as well as, but to a very limited extent, on forest historical analyses for the past few centuries (Thomasius, 1994; Hempel, 2009). However, the region also has a not yet fully exploited potential for very long-term analyses of forest dynamics depending on natural and anthropogenic processes: more than 120 pollen diagrams have been produced from the Erzgebirge since the 1920s (see Sects. 3 and 4). This number makes this region an upland area in central Europe with an exceptionally high density of palynological data on forest and land-use history.

Initiated by current research on the medieval and early modern mining and environmental history in the Erzgebirge (e.g. Derner, 2018; Hemker, 2018; Tolksdorf, 2018; Cappenberg et al., 2020; Kaiser et al., 2021), the opportunity arose to systematically compile the palynological data available from the region, make it accessible for further research, and carry out overview analyses on it. This review paper therefore focuses on data presentation and certain data reflection, especially in methodical terms, as well as on selected research questions about regional forest and land-use dynamics in the Holocene.

(1) What were the general trends in Holocene forest development in the Erzgebirge? (2) What were the distributional patterns of the main tree taxa (e.g. with respect to altitude and soil) in certain forest vegetation phases? (3) Are there any palynological signals that indicate an already pre-medieval anthropogenic influence on the mountain forests? (4) How were forests composed at different altitudes before extensive clearings in the High Middle Ages (12th–13th centuries CE)? (5) How is the deforestation and the subsequent replacement vegetation reflected palynologically? (6) Are there sediment sequences in the Erzgebirge that could reveal the vegetation development of the recent past, i.e. the last ca. 300 years?

2 Study area

Identified in early medieval sources as *Miriquidi* (also *Mircwidu*; old Low German for "dark forest"), the area was referred to as Böhmerwald, Böhmischer Wald, or Böhmisches Gebirge in the high and late Middle Ages up to the Early Modern Period (Hengst, 2006). It was not until the end of the 16th century CE that the name Erzgebirge came up, referring to the character of this area by ore mining (Peschel and Wetzel, 2010). The mountain range has formed a natural border between the territories of Saxony (Germany) and Bohemia (Czech Republic) for around 800 years (Thomasius, 1994; Lauterbach, 2018). For centuries the Erzgebirge played an outstanding role in the mining and other industries in central Europe and made important contributions to ores, metallurgical and other products as well as to technical and academic innovations. Parts of the Erzgebirge were therefore assigned as a UNESCO world heritage site Erzgebirge/Krušnohoří mining region in 2019 (ICOMOS, 2019; Hansell, 2022).

The Erzgebirge has a larger German/Saxon and a smaller Czech/Bohemian part with a total area of ca. 5300 km^2. The around 130 km long and 40 km wide Erzgebirge extends from the Elbsandsteingebirge in the northeast to the Elstergebirge (Vogtland) in the southwest (Bramer et al., 1991; Fig. 1). In the north the Erzgebirge Basin and the Mulde-Lösshügelland (loess hills) and in the south the Eger/Ohře Graben and the North Bohemian Basin/Mostecká pánev limit the mountains. The transition from the foothills to the mountains is around 300 m a.s.l. The Erzgebirge is divided into an eastern, central, and western part with different characteristics, especially in terms of geology, geomorphology, and climate.

The Erzgebirge is a Hercynian fault-block mountain range with a steep and high escarpment in the southeast and a gentle slope in the northwest, forming a half-horst (German: *Pultscholle*) as a whole. As a basement unit, similar to Schwarzwald and Harz, it was folded by the Variscan mountain formation in the Carboniferous, eroded in the Permian, and raised in the Tertiary (Sebastian, 2013; Vilímek and Raška, 2016). In addition to the dominant metamorphic rocks (mainly gneiss but also phyllite, clay, and mica schist), there are plutonites (granite, rhyolite), locally also Cretaceous sediments (mainly sandstone), and tertiary volcanites (basalt, phonolite). Plateaus with deeply incised and terraced valleys that follow the northern slope of the mountains characterise the area. The crest region in particular has wide flat or only flat sloping areas, which formed the topographical prerequisite of Holocene peatland formation. The highest summits are the Klínovec/Keilberg (1244 m a.s.l.) and the Fichtelberg (1215 m a.s.l.) in the central Erzgebirge (Fig. 1). The Pleistocene inland ice reached the edge of the Erzgebirge from the north in the Elsterian glaciation (ca. 500–300 ka) around Freiberg and Chemnitz (Sebastian, 2013). A possible, very local glaciation of the higher elevations of the mountains remains uncertain (Käubler, 1969).

Periglacial debris layers (cover beds) with a high proportion of loess cover almost the entire Erzgebirge and are predominantly the substrates for Holocene soil formation (Kleber et al., 2013). Cambisols and Podzol–Cambisols dominate, supplemented by Podzols, Stagnosols, Gleysols, Fluvisols, and Anthrosols (Sebastian, 2013). Characteristic of the higher elevations of the Erzgebirge are mires, which are mainly formed as raised bogs (i.e. rain-fed mires) and swamp mires (fens; Fig. 2g, h). They are mostly found at watershed positions and in spring basins. In terms of the ecological type, mesotrophic and oligotrophic acidic mires dominate. The area of the peat deposits that existed in the Saxon Erzgebirge up to the end of the 19th century CE is estimated to be 60 km^2 (today 42 km^2; Zinke, 2002). The original mire area for the entire Erzgebirge is estimated to be 100 km^2 (Firbas, 1952). All of the mires in the area were drained, and many were used for peat extraction. For about 30 years, the mires have been the focus of restoration measures in both Saxony and Bohemia (Sächsische Landesstiftung Natur und Umwelt, 2007).

The Erzgebirge belongs entirely to the Elbe/Labe Catchment, with the mountain crest separating the Mulde from the Eger/Ohře sub-catchments. Zwickauer Mulde and Freiberger Mulde are the main rivers, while Schwarzwasser, Chemnitz, and Zschopau are the most important tributaries. Characteristic of these rivers are deeply incised and steep valleys (Bramer et al., 1991). Since the Middle Ages, the hydrological system in the region has been intensively reshaped through anthropogenic measures, following the energetic needs of mining, metallurgy, and other purposes. The result is a large number of ponds, weirs, ditches, aqueducts, and water pipe tunnels (Wagenbreth and Wächtler, 1988). The Erzgebirge has a number of larger dam lakes, most of which were built in the 20th century CE for flood protection and drinking water production (Landestalsperrenverwaltung des Freistaates Sachsen, 2017).

The Erzgebirge shows a climatic differentiation between a wetter western and a drier eastern part. The average annual precipitation also declines from 1000–1200 mm in the crest area to about 750 mm at the mountain foot (Bramer et al., 1991). Average January and July temperatures show a strong vertical gradient from the mountain foot to the crest at only a short horizontal distance (Chemnitz, 420 m a.s.l.: annual average 7.9 °C, July 16.6 °C, January −1.2 °C; Fichtelberg, 1215 m a.s.l.: annual average 2.9 °C, July 11.2 °C, January −5.1 °C; https://www.dwd.de/DE/Home/home_node.html, last access: 15 April 2022). The Erzgebirge shows a number of impressive weather extremes. These include over the last 100 years a snow depth of 335 cm on 24 March 1944 and a wind peak of 216 km h^{-1} on 3 January 1976 on the Fichtelberg (1215 m a.s.l.), a temperature minimum of −33.5 °C on 1 February 1998 in Kühnhaide (723 m a.s.l.), and an extreme rain event with 312 mm on 12–13 August 2002 in Zinnwald (877 m a.s.l.; https://www.dwd.de/DE/Home/home_node.html, last access: 15 April 2022).

The Erzgebirge contributes to three ecological altitude levels (Ellenberg, 1996), whose original forest vegetation was reconstructed for the High Middle Ages by Hempel (2009) and whose potentially natural vegetation (PNV) was characterised by Schmidt et al. (2002; Fig. 3). In view of the PNV on dry, i.e. zonal locations, oak–beech forests dominate on the submontane level (ca. 300–500 m a.s.l.), fir–spruce–beech forests dominate on the montane level (ca. 500–900 m a.s.l.), and first beech–spruce forests then spruce forests with a high proportion of mountain ash/rowan dominate in the high-montane level (ca. 900–1200 m a.s.l.; Fig. 2a–f). Some substantial differences between original forest vegetation and PNV are discussed in Sect. 6.6. In the central Erzgebirge, the tree line is at ca. 1200 m a.s.l. on the summits of Fichtelberg and Klínovec/Keilberg (Fig. 2e, f), which were in historical times anthropogenically deforested

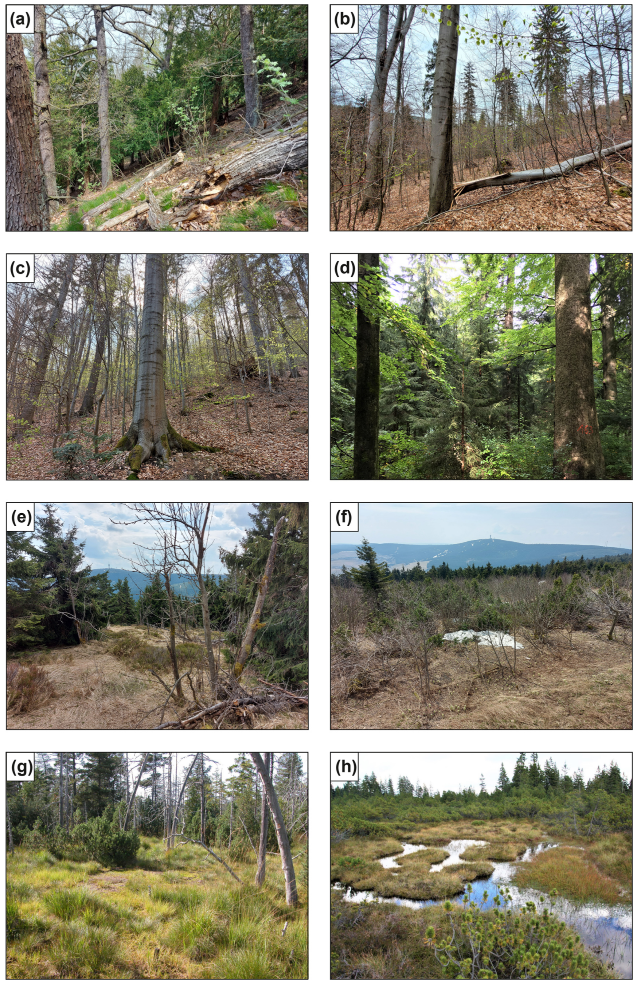

Figure 2. Photographs of typical near-natural forest communities and mires in the Erzgebirge. **(a)** West-exposed slope covered with oak, beech, and yew in the nature reserve Müglitzhang bei Schlottwitz, eastern Erzgebirge, ca. 300 m a.s.l. (photo: K. Kaiser). **(b)** West-exposed slope covered with beech, maple, fir, and spruce in the nature reserve Weißtannenbestand Pöbeltal, eastern Erzgebirge, ca. 570 m a.s.l. (photo: K. Kaiser). **(c)** East-exposed slope covered with beech, maple, fir, and spruce in the nature reserve Hofehübel Bärenfels, eastern Erzgebirge, ca. 660 m a.s.l. (photo: K. Kaiser). **(d)** North-exposed slope covered with beech, spruce, and fir in the nature reserve Riedert, western Erzgebirge, ca. 720 m a.s.l. (photo: F. Jacob). **(e)** South-exposed slope covered with a patchy stand of spruce and mountain ash/rowan in the nature reserve Fichtelberg, central Erzgebirge, ca. 1170 m a.s.l. (photo: K. Kaiser). **(f)**: Summit plateau of Fichtelberg covered with mountain ash/rowan, dwarf mountain pine, and low individuals of spruce, central Erzgebirge, ca. 1210 m a.s.l. (photo: K. Kaiser). The view is directed towards the highest mountain top of Erzgebirge, the Klínovec/Keilberg (1244 m a.s.l.). **(g)** Mothäuser Heide mire, central Erzgebirge, ca. 770 m a.s.l. (photo: Wikimedia/K. Keßler). **(h)** Kleiner Kranichsee mire, western Erzgebirge, ca. 930 m a.s.l. (photo: Wikimedia/K. Keßler).

and later reforested (Heynert, 1964). Thus, the highest mountain peaks in the region protrude just a few metres above this assumed tree line. At particular locations such as block heaps, wind lanes, or cold-air-collecting basins, the tree line can very locally drop to ca. 900 m a.s.l. (Heynert, 1964). Damp and wet, i.e. azonal, sites are characterised by different tree species such as ash, black alder, downy birch, and bog pine (Fig. 2g, h). These general orographic–geobotanical features are confronted with special local deviations. Beech, for example, locally reaches altitudes of ca. 1000 m a.s.l., larger (natural) spruce stands come down to ca. 700 m a.s.l., and very deep fir occurrences can also be found well below 300 m a.s.l. Currently, vegetation of the Saxon Erzgebirge is predominantly open (ca. 60 % of open land), the largest area being intensively used for agriculture and forestry, and densely populated and industrialised, especially in the stream and river valleys. Agriculture is characterised in the lower altitudes by cultivation of cereals, oilseeds, and fodder crops. Livestock farming dominates in the upper elevations. Forest has been preserved along steep valley flanks and partly in the watershed areas. With respect to forest structure, planted spruce monocultures dominate (ca. 80 %). The immediate vicinity of Erzgebirge is characterised by climatically very advantageous and settlement-favourable areas such as the Saxon Elbe Valley and the North Bohemian Basin landscapes, both since the Middle Ages even with cultivation of thermophilic crops such as grapes and hops.

Detailed information on the prehistoric and historic settlement and land-use history of the Erzgebirge is given in Sect. 6.4 to 6.6.

3 History of regional palynological research

Research on regional forest history using palynology began in the Erzgebirge in the 1920s with the investigation of several peatlands along the mountain crest, such as Großer Kranichsee, Gottesgab/Boží Dar, Sebastiansberg/Hora Svatého Šebestiána, and Georgenfeld near Zinnwald/Cínovec (Fig. 1, Table 1). This work was carried out by the botanists Karl Rudolph and Franz Firbas at the German Charles-Ferdinand University in Prague and is considered a pioneer study of palynology in central Europe (Rudolph and Firbas, 1922, 1924; Rudolph, 1928; Firbas, 1952; Beug, 1965, 2003; Tolksdorf et al., 2018). Inspired by this, a short time later further palynological work was carried out in the peat bogs of the Saxon and Bohemian Erzgebirge (Frenzel, 1930; Schmeidl, 1940).

In the 1950s to 1970s, some pollen analyses with a geobotanical, geological, and archaeological focus in the eastern and western Erzgebirge and in the neighbouring Vogtland followed (Jacob, 1956; Gross, 1958; Heynert, 1961, 1964; Heinrich and Lange, 1969; Lange and Heinrich, 1970). On the southern foothills of the Erzgebirge around Most/Brüx, extensive palynological investigations have been carried out since the 1970s in the former lake Komořanské jezero/Kommerner See, which has now been completely devastated by lignite mining (see overviews in Jankovská and Pokorný, 2013; Houfková et al., 2017).

With the political changes in 1989–1990, a strong revival of palynological research began on both the German and the Czech side of the Erzgebirge, which was primarily aimed at questions on the history of the environment, mires, mining, and settlements. In addition to some radiocarbon-dated pollen diagrams, such as from the raised bogs Georgenfeld (Stebich and Litt, 1997), Fláje/Fleyh (Jankovská et al., 2007), Boží Dar/Gottesgab (Veron et al., 2014), and Kovářská/Schmiedeberg (Bohdálková et al., 2018), as well as the deserted villages Spindelbach (Houfková et al., 2019) and Ullersdorf (Tolksdorf et al., 2020a), further diagrams are available but without radiocarbon data (e.g. Großer et al., 2006; Schwabenicky, 2009; Schlöffel, 2011). The Mothäuser Heide pollen diagram presented in detail below (Lange et al., 2005; Theuerkauf et al., 2007; Edom et al., 2011) is also a result of this research period. In addition, there are 20 pollen profiles that were only published in 2016 (Seifert-Eulen, 2016), which were mainly obtained from raised bogs between the 1960s and 2000s.

Comprehensive palynological data were finally produced in the course of the interdisciplinary ArchaeoMontan project, which was dedicated to research into medieval mining history in the Erzgebirge from 2012 to 2018 (Derner, 2018; Hemker, 2018; Tolksdorf, 2018). From this project context, there are now several pollen diagrams and a large number of individual samples that come from alluvial sediment sequences and fens in stream valleys. These diagrams are radiocarbon dated, mostly combined with macro-botanical and anthracological, as well as often also with geochemical–sedimentological data, and above all illuminate the medieval to modern development of vegetation and land use in the central and eastern Erzgebirge. The follow-up project ArchaeoForest (2019–2023) is aimed at the forest history of the last millennium in the Erzgebirge and combines new palynological results, anthracological data from charcoal kilns, dendrochronological material from an archaeological context, and historical sources (Cappenberg et al., 2020).

To sum up, the Erzgebirge can be called a "cradle" of palynological vegetation history in central Europe. With currently more than 120 pollen diagrams, this area has now been examined rather in depth with 100 years of research by means of palynological analyses (Fig. 1, Table 1). While the early palynological work had its starting point primarily in the academic sphere, later project-related investigations by various non-academic institutions prevailed. Recently, however, there has been a revival of academic palynological interest in the region, particularly on the Czech side (e.g. Abraham, 2014; Abraham et al., 2016; Bobek et al., 2019; Marešová, 2022). It shall be noted, however, that most of the existing pollen diagrams cover only (short) sections of the Holocene,

Table 1. Pollen diagrams from the Erzgebirge. Further metadata per pollen diagram are given in Table S1 in the Supplement.

ID	Diagram name	Country	Northing	Easting	Altitude (m a.s.l.)	Depositional environment	Reference
1	Mothäuser Heide	DE	50.598684	13.217411	768	Peat bog	Lange et al. (2005)
2	Jahnsgrün	DE	50.558812	12.575594	565	Peat bog	Großer et al. (2006)
3	Fláje-Kiefern/Fleyh	CZ	50.690833	13.619722	751	Peat bog	Jankovská et al. (2007)
4	Grünwalder Heide bei Moldau (Moldava)	CZ	50.702394	13.649808	852	Peat bog	Rudolph and Firbas (1924)
5	Most, Profile PK-2-A	CZ	50.548543	13.773620	204	River	Jankovská (1995)
6a	Komořanské jezero, PK-1-B	CZ	50.533313	13.550022	230	Lake	Jankovská and Pokorný (2013)
6b	Komořanské jezero, PK-1-D	CZ	50.533313	13.550022	230	Lake	Jankovská and Pokorný (2013)
6c	Komořanské jezero, PK-1-E	CZ	50.533313	13.550022	230	Lake	Jankovská and Pokorný (2013)
6d	Komořanské jezero, PK-1-CH	CZ	50.535550	13.500727	230	Lake	Jankovská and Pokorný (2013)
7	Treppenhauer	DE	50.936512	13.025150	335	Fen	Schwabenicky (2009)
8	Frankenberg-Saugrund	DE	50.929750	13.042861	296	Fen	Lange and Heinrich (1970)
9	Hainichen	DE	50.970959	13.117486	320	Fen	Gross (1958)
10	Rehauer Forst Sauborst	DE	50.275573	12.063246	571	Fen	Hahne (1992)
11	Soos 1	CZ	50.149444	12.401667	436	Lake	Suda (2012)
12	Zwickau, Pestalozzischule	DE	50.728920	12.484829	261	Lake	Frenzel (1930)
13	Röthenbach-Stangengrün	DE	50.571103	12.432164	510	Peat bog	Heynert (1961)
14	Moosheide bei Bärenwalde	DE	50.574297	12.505806	495	Peat bog	Heynert (1961)
15	Grünheide bei Beerheide	DE	50.478250	12.485556	695	Peat bog	Heynert (1961)
16	N-Hang Großer Fichtelberg	DE	50.424514	12.948819	1170	Fen	Heynert (1964)
17	SO-Hang Kleiner Fichtelberg	DE	50.424469	12.953172	1120	Fen	Heynert (1964)
18	SW-Hang Kleiner Fichtelberg	DE	50.424514	12.948819	1125	Fen	Heynert (1964)
19	Moosteich bei Plothen Profile V	DE	50.642244	11.752075	475	Fen	Heinrich and Lange (1969)
20	Pöllwitzer Forst Profile IIb	DE	50.638028	12.051431	452	Fen	Heinrich and Lange (1969)
21	Pöllwitzer Forst Profile I Abt. 95	DE	50.634461	12.061203	447	Fen	Heinrich and Lange (1969)
22	Spindelbach SP-1	CZ	50.482933	13.194167	854	Stream	Houfková et al. (2019)
23	Boží Dar	CZ	50.399436	12.869797	1015	Peat bog	Brízová (1995)
24a	Gottesgab, Torfstich A, Reißzeche, Profile I	CZ	50.407497	12.907792	1000	Peat bog	Rudolph and Firbas (1924)
24b	Gottesgab, Torfstich A, Reißzeche, Profile II	CZ	50.407497	12.907792	1000	Peat bog	Rudolph and Firbas (1924)
24c	Gottesgab, Torfstich A, Reißzeche, Profile III	CZ	50.407497	12.907792	1000	Peat bog	Rudolph and Firbas (1924)
24d	Gottesgab, Torfstich A, Reißzeche, Profile IV	CZ	50.407497	12.907792	1000	Peat bog	Rudolph and Firbas (1924)
25	Gottesgab, Torfstich B, Profile V	CZ	50.407194	12.915036	1001	Peat bog	Rudolph and Firbas (1924)
26	Gottesgab, Torfstich C, Mongolei, Ostprofil	CZ	50.411733	12.913692	997	Peat bog	Rudolph and Firbas (1924)
27	Gottesgab, Torfstich D, Pechhütte, Ostprofil	CZ	50.417086	12.912150	996	Peat bog	Rudolph and Firbas (1924)
28	Gottesgab, Torfstich E, Zuflucht, Ostprofil	CZ	50.411139	12.909278	989	Peat bog	Rudolph and Firbas (1924)
29a	Sebastiansberger Heide, Profile I	CZ	50.518478	13.229619	842	Peat bog	Rudolph and Firbas (1924)
29b	Sebastiansberger Heide, Profile II	CZ	50.518478	13.229619	842	Peat bog	Rudolph and Firbas (1924)
29c	Sebastiansberger Hochmoor, Profile 5	CZ	50.518478	13.229619	842	Peat bog	Schmeidl (1940)
30	Neudorfer Heide	CZ	50.506549	13.226509	853	Peat bog	Rudolph and Firbas (1924)
31a	Ullersdorf, OH-12, Profile 2	DE	50.608056	13.258056	728	Stream	Tolksdorf et al. (2020a)
31b	Ullersdorf, OH-12, Profile 3	DE	50.608844	13.259726	728	Stream	Tolksdorf et al. (2020a)
32	Výsluní	CZ	50.471207	13.235584	754	Stream	Kočár et al. (2018)

Table 1. Continued.

ID	Diagram name	Country	Northing	Easting	Altitude (m a.s.l.)	Depositional environment	Reference
33	Dolina 1	CZ	50.451796	13.129818	740	Stream	Kočár et al. (2018)
34	Dolina 2	CZ	50.451178	13.121950	745	Stream	Kočár et al. (2018)
35	Přísečnice, Profile 2016	CZ	50.458309	13.117877	752	Stream	Kočár et al. (2018)
36	Černý Potok, Profile 2016	CZ	50.492521	13.080784	738	Stream	Kočár et al. (2018)
37	Kovářská	CZ	50.435715	13.054742	810	Stream	Kočár et al. (2018)
38a	Černý Potok, Profile 1/2019	CZ	50.496996	13.083778	704	Stream	L. Petr, Brno (unpublished data)
38b	Černý Potok, Profile 2/2019	CZ	50.496864	13.083648	704	Stream	L. Petr, Brno (unpublished data)
39a	Přísečnice, Kremsiger 1/2019	CZ	50.491372	13.101919	815	Slope	L. Petr, Brno (unpublished data)
39b	Přísečnice, Kremsiger 2/2019	CZ	50.491372	13.101919	815	Slope	L. Petr, Brno (unpublished data)
40	E2 – Streitberg	CZ	50.436048	12.780404	842	Stream	L. Petr, Brno (unpublished data)
41	E3 – Zwittermühl	CZ	50.414602	12.800985	877	Stream	L. Petr, Brno (unpublished data)
42	E4 – Pernink	CZ	50.375338	12.785298	871	Stream	L. Petr, Brno (unpublished data)
43	Pfahlbergmoor	DE	50.444850	12.913946	1017	Peat bog	Seifert-Eulen (2016)
44a	Kleiner Kranichsee	DE	50.417435	12.674855	927	Peat bog	Seifert-Eulen (2016)
44b	Kleiner Kranichsee	DE	50.417435	12.674855	928	Peat bog	Frenzel (1930)
45	Großer Kranichsee	CZ	50.404886	12.58905	930	Peat bog	Rudolph and Firbas (1924)
46	Ober-Schönheide	DE	50.506131	12.521578	687	Peat bog	Frenzel (1930)
47	Jägersgrün	DE	50.451283	12.461019	628	Peat bog	Frenzel (1930)
48a	Filzteich Ia+b	DE	50.566733	12.599628	568	Peat bog	Frenzel (1930)
48b	Filzteich II	DE	50.566733	12.599628	568	Peat bog	Frenzel (1930)
49a	Siebensäure	DE	50.473192	12.950203	830	Peat bog	Seifert-Eulen (2016)
49b	Siebensäure	DE	50.473192	12.950203	830	Peat bog	Frenzel (1930)
50	Rübenau I	DE	50.610686	13.279661	761	Peat bog	Frenzel (1930)
51	Rübenau II	DE	50.596042	13.264764	755	Peat bog	Frenzel (1930)
52	Hühnerheide, Hüh-S-3	DE	50.596372	13.273293	753	Peat bog	Seifert-Eulen (2016)
53	Schwarze Heide, Sh-1	DE	50.612427	13.292942	758	Peat bog	Seifert-Eulen (2016)
54	Lehmheide, LNE-1b	DE	50.611640	13.282818	770	Peat bog	Seifert-Eulen (2016)
55a	Lehmheide, LNW-3a	DE	50.610156	13.282877	774	Peat bog	Seifert-Eulen (2016)
55b	Lehmheide, LNW-3	DE	50.609974	13.283055	774	Peat bog	Seifert-Eulen (2016)
56	Deutsch-Einsiedel	DE	50.639010	13.521595	725	Peat bog	Frenzel (1930)
57a	Georgenfelder Hochmoor	DE	50.729162	13.743231	867	Peat bog	Seifert-Eulen (2016)
57b	Georgenfelder Hochmoor	DE	50.729162	13.743231	867	Peat bog	Stebich and Litt (1997)
58	Seeheide bei Georgenfeld-Zinnwald	CZ	50.727092	13.743069	870	Peat bog	Rudolph and Firbas (1924)
59	Große Auerhahnbalz	CZ	50.712814	13.743614	856	Peat bog	Rudolph and Firbas (1924)
60	Stadtgebiet Olbernhau, Olb 1-47	DE	50.650181	13.352660	462	River	Seifert-Eulen (2016)
61	Stadtgebiet Olbernhau, Olb 1-50	DE	50.649714	13.355729	462	River	Seifert-Eulen (2016)
62	Blumenau bei Olbernhau	DE	50.671042	13.302336	435	Peat bog	Frenzel (1930)
63	Mtbl. Adorf-Saaliger Bach, Sa 1/65	DE	50.354053	12.278436	487	Stream	Seifert-Eulen (2016)
64	Mtbl. Adorf-Elstertal bei Adorf, Ad 1/65	DE	50.334543	12.255990	443	River	Seifert-Eulen (2016)
65a	Mtbl. Adorf-Schöneck/Bockmühle, P Schö I	DE	50.383593	12.324094	600	Stream	Seifert-Eulen (2016)
65b	Mtbl. Adorf-Schöneck/Bockmühle, P Schö II	DE	50.383474	12.324712	597	Stream	Seifert-Eulen (2016)

Table 1. Continued.

ID	Diagram name	Country	Northing	Easting	Altitude (m a.s.l.)	Depositional environment	Reference
66	Mtbl. Adorf-Schurf Markneukirchen, S 3/67	DE	50.303224	12.310199	564	Fen	Seifert-Eulen (2016)
67	Mtbl. Adorf-Schurf Mühlhausen, S 5/67	DE	50.299103	12.256473	454	Stream	Seifert-Eulen (2016)
68	Geyerscher Wald-Hormersdorfer Moor	DE	50.655437	12.878925	673	Peat bog	Seifert-Eulen (2016)
69	Geyerscher Wald-Rotes Wasser	DE	50.650350	12.897637	640	Stream	Seifert-Eulen (2016)
70	Großhartmannsdorfer Großteich, Gh II/75	DE	50.808755	13.346324	491	Peat bog	Seifert-Eulen (2016)
71	Groß-Hartmannsdorf	DE	50.805200	13.344167	492	Peat bog	Frenzel (1930)
72	Magdloch bei Geyer	DE	50.596769	12.886236	630	Peat bog	Frenzel (1930)
73	Heide bei Crottendorf	DE	50.522308	12.919742	670	Peat bog	Frenzel (1930)
74a	Oberpirk I	DE	50.544494	12.021333	482	Fen	Frenzel (1930)
74b	Oberpirk II	DE	50.544494	12.021333	482	Fen	Frenzel (1930)
75	Ocean Bog	CZ	50.350000	12.700000	900	Peat bog	Novak et al. (2008)
76	Kovářská Bog, peat core KV1	CZ	50.442222	13.077500	870	Peat bog	Bohdálková et al. (2018)
77	Profile 1 Moor, Abteilung 17	DE	50.961506	13.533403	350	Stream	Jacob (1956)
78	Profile 2 Hertha Moor IV	DE	50.971881	13.523186	360	Fen	Jacob (1956)
79	Profile 3 Moor Harthaer Luftbad	DE	50.985547	13.522236	365	Fen	Jacob (1956)
80	Profile 4 Moor in der Paulsdorfer Heide	DE	50.918117	13.630594	370	Fen	Jacob (1956)
81	Profile 5 Rohhumus (anmoorig) aus Abteilung 21	DE	50.976736	13.537428	407	Humus layer	Jacob (1956)
82	Profile 6 Rohhumus, Mauerhammer Abt. 9	DE	50.977175	13.573803	360	Humus layer	Jacob (1956)
83	Profile 7 Trockentorf, Warnsdorfer Quelle	DE	50.955536	13.553050	370	Fen	Jacob (1956)
84	Profile 8 Rohhumus, Abteilung 29	DE	50.955839	13.557892	400	Humus layer	Jacob (1956)
85	Profile 9 Humusprobe, Abteilung 104	DE	50.949050	13.580031	360	Humus layer	Jacob (1956)
86	Profile 10 Rohhumus, Markgrafenweg I	DE	50.951811	13.568081	390	Humus layer	Jacob (1956)
87	Profile 11 Rohhumus, Markgrafenweg II	DE	50.950044	13.570506	385	Humus layer	Jacob (1956)
88	Profile 12 Rohhumus, Nasser Weg	DE	50.950067	13.566008	380	Humus layer	Jacob (1956)
89	Profile 13 Rohhumus, Faule Pfütze	DE	50.942194	13.494542	400	Humus layer	Jacob (1956)
90	Hora Svatého Šebestiána, HSŠ	CZ	50.530389	13.248356	832	Peat bog	Břízová (2014a)
91	Warnsdorf, TRD-04	DE	50.962348	13.536060	350	Fen	Kaiser et al. (2020a)
92a	Freiberg, Münzbachtal, FG-317, Bohrkern 3	DE	50.917611	13.346484	386	Stream	Tolksdorf (2018)
92b	Freiberg, Münzbachtal, FG-323, Bohrkern 1	DE	50.918817	13.346562	385	Stream	Tolksdorf (2018)
93	Faule Pfütze, OFD-01, Profile 1	DE	50.837533	13.707494	555	Stream	Tolksdorf (2018)
94	Oberpöbel-Vorderer Grünwald, SNF-01, Profile 9	DE	50.770482	13.666810	629	Stream	Tolksdorf (2018)
95a	Schellerhau, ABG-01, Profile 8	DE	50.764375	13.720894	744	Stream	Tolksdorf (2018)
95b	Schellerhau, ABG-01, Profile 6	DE	50.764375	13.720894	744	Stream	Tolksdorf (2018)
95c	Schellerhau, ABG-01, Profile 12	DE	50.764375	13.720894	744	Stream	Tolksdorf (2018)
96	Pöbelbachtal, SHL-02, Profile Zinnbrücke	DE	50.762275	13.689131	694	Stream	K. Korzeń, Kraków (unpublished data)
97	Pöbelbachtal, SNF-02, Profile Magdalena-Erbstolln	DE	50.771186	13.677644	660	Stream	K. Korzeń, Kraków (unpublished data)
98a	Faule Pfütze, Profile OFD-03a	DE	50.837533	13.707494	555	Stream	K. Korzeń, Kraków (unpublished data)
98b	Faule Pfütze, Profile OFD-03b	DE	50.837533	13.707494	555	Stream	K. Korzeń, Kraków (unpublished data)
99	Bielatal, Profile BRS-05	DE	50.801039	13.771116	486	Stream	K. Korzeń, Kraków (unpublished data)

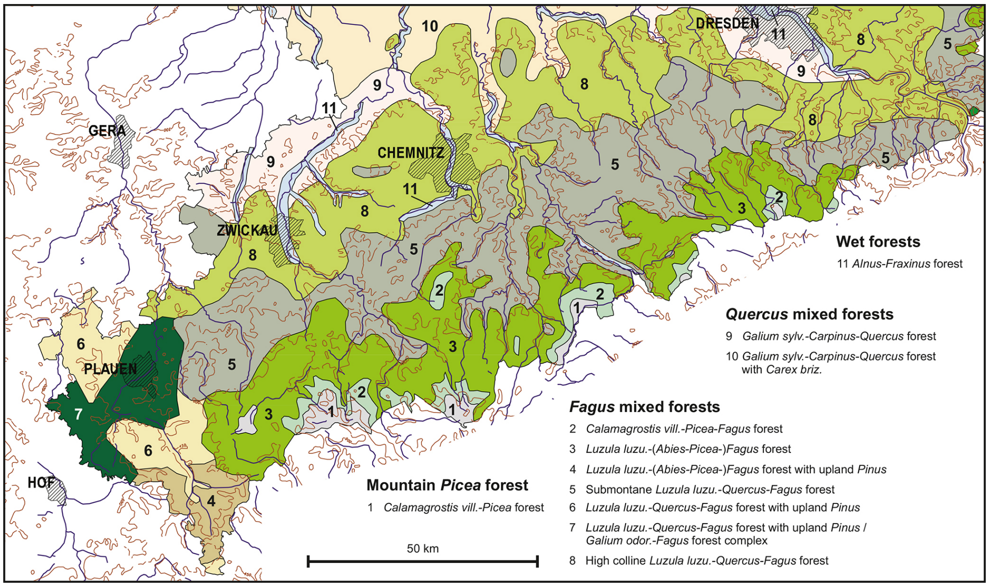

Figure 3. Potentially natural vegetation of the Erzgebirge (Saxon part) and surroundings (Sächsisches Landesamt für Umwelt und Geologie 2006, adapted, following Schmidt et al., 2002).

usually with low sample resolution and no or only very few independent dating control by radiocarbon ages.

4 Available data

4.1 Pollen diagrams and their metadata

At present, i.e. the end of 2022, a total of 121 pollen diagrams from the Erzgebirge, its immediate foothills, and the Vogtland are available. We here include the Vogtland mountain area, adjoining to the west, because it is difficult to separate from the Erzgebirge in terms of nature and landscape history. Two-thirds of the diagrams are located in Saxony ($n = 80$) and one third in Bohemia ($n = 41$; Fig. 1, Table 1, Table S1 in the Supplement). This compilation includes all palynological records with at least three vertically superimposed pollen spectra. Thus, in addition to classic pollen diagrams, which often comprise several-metre-thick (mostly peat) and in some cases several tens of pollen spectra, very short pollen diagrams of a few centimetres to decimetres are also available from the region and will be considered for this review. However, the number of the latter with 17 diagrams (14 %) is quite small compared to the classic diagrams ($n = 104$, 86 %).

The taxonomic resolution of the older pollen diagrams prepared before about 1950 is limited; i.e. mostly only tree pollen types are included. Only younger records also include herbal pollen. However, published versions even of many recent records often include only selected arboreal and non-arboreal taxa. Only very few records (ca. 10) have been stored in digital repositories.

Of all diagrams, 27 % were published from 1924 to 1940; only 20 % between the 1950s and 1980s; and 53 % after 1989–1990, many of them (35 %) between 2010 and 2020 (Fig. 4a).

The majority of the pollen diagrams, i.e. 35 %, originates from sites between 700 and 900 m a.s.l., 33 % from 300–500 m a.s.l., 18 % from 500–700 m a.s.l., and only 14 % from above 900 m a.s.l. (Fig. 4b). The highest pollen diagrams (IDs 16–18) come from the slope of the Fichtelberg at 1125–1170 m a.s.l. (Heynert, 1964), while the immediate summit positions on this mountain and on the neighbouring Klínovec/Keilberg have not been studied yet.

With regard to the palynologically examined depositional environment, two types dominate: peat bogs (42 %), i.e. rainfed mires at various topographic positions (Slobodda, 1998; Böhm, 2006; Wendel, 2010) and, with increasing importance in the last decade, river and stream valleys (31 %; Fig. 4c). The latter is mainly represented by flood loam stratigraphies. The rest of the sites (27 %) are distributed among (palaeo-)lakes; fens; slopes (colluvial deposits); and organic soil surfaces, i.e. raw humus layers.

The depth of most pollen diagrams is very small with a value between 50 and 100 cm (24 %), followed by the depth ranges 100–200 cm (23 %) and 200–300 cm (18 %; Fig. 4d). The longest pollen diagram so far, at 790 cm, comes from the peat bog Mothäuser Heide in the central Erzgebirge (Lange et al., 2005; Theuerkauf et al., 2007; ID 1 in Fig. 1). The largest peat thickness is reported from the raised bog Pod novoveským vrchem near Hora Svatého Šebestiána/Sebastiansberg with 10.5 m. This is also the largest known peat thickness in the Czech Republic (https://www.kr-ustecky.cz/, last access: 8 March 2022).

More than a third of the pollen diagrams (40 %) are young; i.e. the base is palynologically dated to the Subatlantic bio-

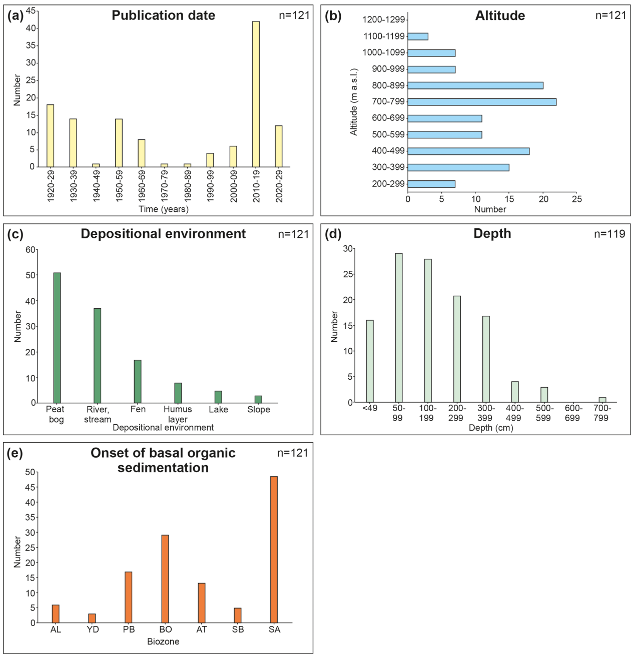

Figure 4. Metadata of pollen diagrams from the Erzgebirge. The respective data and further information are given in Tables 1 and S1. **(a)** Publication date, **(b)** altitude, **(c)** depositional environment, **(d)** depth, **(e)** and onset of basal organic sedimentation (AL, Allerød; YD, Younger Dryas; PB, Preboreal; BO, Boreal; AT, Atlantic; SB, Subboreal; SA, Subatlantic).

zone (ca. 2400–0 cal yr BP; Fig. 4e). The second most frequent onset of sedimentation, on the other hand, dates to the Boreal (ca. 10 640 to 9220 cal yr BP; 24 %), followed by the Preboreal (ca. 11 560 to 10 640 cal yr BP, 14 %) and Atlantic (ca. 9220–5660 cal yr BP, 11 %). Remarkably, 7 % of pollen diagrams already started in the Late Glacial, the oldest of which date to the Allerød (ca. 13 350–12 700 cal yr BP).

Micro-charcoal analysis, which is a powerful tool to reconstruct natural and anthropogenic fire dynamics (e.g. Bobek et al., 2019), has only been applied in 27 pollen diagrams (22 %), most of them of a young age with low depth (Conedera et al., 2009; Knapp et al., 2013).

4.2 Chronological control by radiocarbon data

Most pollen records from the Erzgebirge are poorly dated. So far only 118 radiocarbon dates from 43 pollen diagrams are available, with usually only one to three dates per record (Table S1). The majority of 78 profiles (64 %) has no independent age control; i.e. dating is solely based on palynostratigraphy. The latter is calibrated to supra-regional vegetation phenomena or, more recently, to regional historical events (such as the extensive clearing of mountain forests assumed for the 12th and 13th centuries CE; e.g. Hempel, 2009; Kenzler, 2012). Accordingly, the zonation suggested by Firbas (1949, 1952), which is based on the not unproblem-

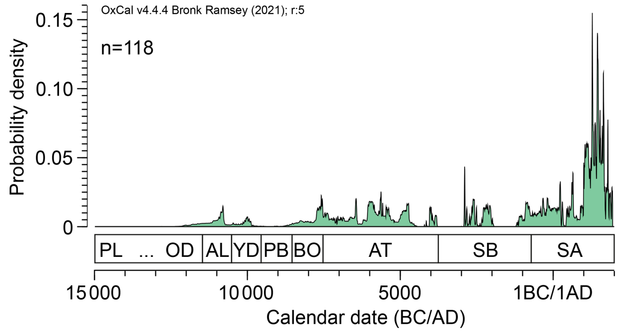

Figure 5. Temporal distribution of calibrated radiocarbon ages from pollen diagrams from the Erzgebirge using the OxCal programme (https://c14.arch.ox.ac.uk/oxcal.html, last access: 18 January 2022; Bronk Ramsey, 2017).

atic Blytt–Sernander scheme (Birks and Seppä, 2010), must also be used for the regional Holocene biozone stratigraphy (comprising terms such as Preboreal, for instance), which was used anyway in the older regional literature and is therefore necessary for a comparison.

The radiocarbon dates are from bulk peat (41 %), plant macro-remains (17 %), gyttja and organic detritus (15 %), wood (14 %), and charcoal (13 %). Most of the dates were obtained by accelerator mass spectrometry (AMS). The ages dominantly cluster in the Subatlantic biozone, followed by clustering in the Atlantic, Subboreal (5660 to 2400 cal yr BP), and Boreal (Fig. 5). Seven Late Glacial dates (Younger Dryas, 12 700–11 560 cal yr BP; Allerød) are particularly noteworthy, while only one date originates from the earliest Holocene (Preboreal).

On the Saxon side of Erzgebirge, the pollen diagrams with both the highest number of radiocarbon dates ($> n =$ five each) and a multi-millennial record are those of Georgenfelder Hochmoor (ID 57b in Fig. 1, 867 m a.s.l., nine radiocarbon dates; Stebich and Litt, 1997), Pfahlbergmoor (ID 43, 1017 m a.s.l., seven dates; Seifert-Eulen, 2016), and Mothäuser Heide (ID 1, 768 m a.s.l., six dates; Lange et al., 2005; Theuerkauf et al., 2007). For the Bohemian side, diagrams are available from Boží Dar (ID 23, 1015 m a.s.l., eight dates; Veron et al., 2014) and Komořanské jezero (ID 6d, 230 m a.s.l., six dates; Jankovská and Pokorný, 2013).

In addition, a general comment on the use of absolute chronological terms in this paper is that we deliberately do not use a uniform terminology here but one that is adapted to the context and thus to the usual application. When addressing the dating of pollen diagrams and Holocene vegetation phases, which is a natural–scientific data aspect, we refer to calibrated radiocarbon dates (cal yr BP). However, when contextualising prehistorical or historical anthropogenic developments, calendar years (years BCE/CE or centuries CE) are used, following common practice in the historical sciences.

4.3 Further palaeobotanical data sources from the region

In addition to pollen and archaeological–historical data, there are further natural–scientific data sources from the Erzgebirge that provide palaeobotanical information on Holocene forest and land-use history. Some findings from peat stratigraphy, anthracology, dendrochronology, and botanical macro-remain analysis, briefly outlined below, are largely data sources that have mainly been used regionally no earlier than the 2010s. Accordingly, in contrast to the pollen data and with a certain exception to subfossil wood and dendrochronology, there are no older datasets available.

Since the beginning of palynological and peat stratigraphical studies, special attention has been paid to "tree stump horizons" that have often been exposed or drilled in the raised bogs of Erzgebirge (Schreiber, 1921; Rudolph and Firbas, 1924; Frenzel, 1930; Schmeidl, 1940; Seifert-Eulen, 2016). This refers to subfossil tree remains found in situ (mostly stumps, rarely trunks), representing mostly *Pinus mugo*, *Picea*, and *Betula*. They occur at certain positions in the mire stratigraphy, usually as a single horizon, rarely as several superimposed horizons. In the early phase of regional mire research, i.e. in the first half of the 20th century CE, many peatlands were exposed by peat cuttings, which enabled an excellent investigation of the local stratigraphy and thus also the observation of these tree stump horizons in a frontal view. The peat horizon in which the tree remains were embedded was mostly heavily decomposed. By contrast, the peat below and above this horizon was much less decomposed. The palynostratigraphical dating of the tree stump horizons yielded different ages from the early Holocene to the late Holocene with a certain accumulation at the turn from Subboreal to Subatlantic (Frenzel, 1930). Already Rudolph and Firbas (1924) paralleled this striking change (i.e. hiatus) in the peat stratigraphy with the so-called *Grenzhorizont* ("border horizon") or, more recently, with the *Rekurrenzfläche* ("recurrence surface") or *Schwarztorf–Weißtorf-Kontakt* ("black peat–white peat contact"), representing a widespread peat marker horizon in northwestern Germany and beyond (Weber, 1926; Behre, 2008). Such horizons, indicating a temporary cessation of peat formation and afforestation, have also been detected in raised bogs in other low mountain ranges in central Europe, for instance in the Harz, Rhön, and Fichtelgebirge (Overbeck and Griéz, 1954; Firbas et al., 1958; Willutzki, 1962; Beug et al., 1999). Most of these were dated to the late Holocene and partially paralleled with the peatland stratigraphy in northwestern Germany and the Netherlands. In fact, the dates available from the northwestern German plain show a maximum age range from 2300 BCE to 700 CE with a data cluster between 800 BCE and 100 CE (Behre, 2008). This sequence of more and less decomposed peat layers is currently interpreted as mostly locally caused phases of weaker and stronger peat growth, respectively (Lang, 1994). Furthermore, in the peatlands of this lowland region there are numerous tree stump horizons under and in peat sequences that date back to the mid- and late Holocene (Achterberg et al., 2016). With regard to the state of knowledge in the Erzgebirge, it should be noted that neither dendrological and dendrochronological nor radiometric investigations have been carried out on these tree stump horizons. Botanical macro-remain, charcoal, and pedological data are also missing. As a result, their dating and genesis cannot be presented in detail at present, and a systematic reference to regional peatland development or even to the supra-regional climate development cannot be established thus far.

Recently, a so-called "forest-clearing horizon" with the preservation of subfossil wood as well as charcoal and wooden chips was discovered during a geoarchaeological re-evaluation of the abandoned medieval settlement site of Warnsdorf in the Tharandt Forest (ca. 360 m a.s.l., ID 91; Kaiser et al., 2020a; Fig. 1). A larger in situ root of *Pinus*, dating 997–1155 CE, was embedded in a peat layer covered by anthropogenic sediments. Additional pollen and plant macro-remain data from the peat together with the subfossil wood and sedimentological data allow for insights into the local vegetation and land-use history of this site during the High Medieval Period. Although the *Pinus* root exposed no clear-cutting marks, wooden chips from *Abies* in the same horizon indicate intentional tree cutting (Spehr, 2002). In general, *Pinus*, *Abies*, *Picea*, and *Betula* were documented as subfossil wood. In addition, *Fagus*, *Quercus*, and *Corylus* were detected in the local pollen record. Similar forest-clearing horizons could also be studied in the Harz and in the Bohemian–Moravian Highlands. This generally constitutes a new and promising geoarchaeological–palaeopedological feature for central Europe, documenting the medieval clearing of mountain forests by human exploitation (Kaiser et al., 2020a).

In the Erzgebirge, as in all other low mountain ranges and in the lowlands of central Europe (e.g. Ludemann, 2010; Schmidt et al., 2016; Rutkiewicz et al., 2019; Kaiser et al., 2020b; Raab et al., 2022), there are countless remains of historical charcoal production. Remains of so-called charcoal kilns or charcoal hearths are detectable as circular and thin accumulations of charcoal several metres in diameter. Small plateaus were usually dug into slopes for this purpose. Initial remote sensing investigations using lidar data showed spatial densities of 40–81 charcoal kilns per square kilometre for three test areas in the central Erzgebirge, which are comparable with data from other German mountains such as the Harz, Schwarzwald, and Kellerwald (Tolksdorf et al., 2020a). Since the 2010s, systematic anthracological investigations have been carried out in these charcoal kilns on both the Saxon and the Bohemian sides of the Erzgebirge. These include botanical determinations of the tree remains and their dating by radiocarbon analysis and dendrochronology (Tolksdorf et al., 2015; Kočár et al., 2018; Tolksdorf, 2018; Tolksdorf et al., 2020a; Neubauer, 2022). The ages range from the end of the 12th to the 18th centuries CE. Timber species determinations show a clear shift in taxa (from *Fagus* and *Abies* to *Picea* and pioneer deciduous tree species) and a reduction in timber diameters over this period (Tolksdorf et al., 2021).

Dendrochronological dating has been used regularly in the Erzgebirge for several decades, mostly in the context of studies on building history, archaeology, forest ecology, and dendro-geomorphology (e.g. Spitzer, 2010; Hoffmann and Heußner, 2013; Tolksdorf and Schröder, 2016; Vejpustková et al., 2017; Vilímek et al., 2018). In particular, the ubiquitous use of construction wood since the Middle Ages for ore mines, ore processing facilities, and water management facilities has subfossilised huge amounts of wood in the region. After their discovery, there is enormous potential here for palaeoecological investigations, which has already been used to some extent. For instance, from the archaeologically investigated medieval mines of Dippoldiswalde (375 m a.s.l.) and Niederpöbel (500 m a.s.l.) in the eastern Erzgebirge, around 3400 botanically determined timbers are available to date (Cappenberg et al., 2020). Most common taxa are *Abies* ($n = 2103$, 62 %), *Picea* ($n = 444$, 13 %), and *Fagus* ($n = 333$, 10 %), with a minor share also *Acer*, *Pinus*, *Quercus*, and *Ulmus* that occur (together $n = 520$, 15 %). Of these, the dendrochronological dates ($n = 1112$) show a total age interval from the 12th to the 13th century CE, cumulating in the middle of the latter. In addition to similarities, i.e. the usage preference of *Abies* at the beginning of local mining, differences at both locations are visible, i.e. a different role and dating of *Picea* and deciduous tree species.

A rather new data source for the Erzgebirge is macroremain analysis, which has increasingly become available in the last decade, resulting from (geo-)archaeological investigations (e.g. Kočár et al., 2018; Tolksdorf, 2018; Kaiser et al., 2021; Herbig, 2022). The preferably determined herb and shrub species supplement the knowledge on late Holocene vegetation structure in various ecological details. This applies above all in view of the local human impact, e.g. on the deforestation and establishment of a replacement vegetation. In addition, there is sometimes remarkable evidence on the regional use of plants, e.g. as food. In the course of local archaeological studies, remains of figs (*Ficus carica*) and grapes (*Vitis vinifera*) were found in Kovářská/Schmiedeberg in Bohemia (810 m a.s.l.; Kočár et al., 2018) and remains of figs, rice (*Oryza sativa*), and pepper (*Piper nigrum*) in Freiberg in Saxony (400 m a.s.l.; Schubert and Herbig, 2017). This late medieval to early modern evidence proves both that local elites were supplied with quite luxurious goods and that there were long-distance trade connections, sometimes as far as the Mediterranean region and beyond.

5 Outline of the Holocene vegetation history using pollen data

5.1 Methodological aspects

Pollen data cannot be interpreted directly in terms of past plant abundances because single taxa produce pollen in very different amounts, and different pollen types may be dispersed differently. As a result, taxa may be over-/underrepresented in the pollen record. Methods to account for that bias have become available over the past decades, e.g. REVEALS (Sugita, 2007a) and ROPES (Theuerkauf and Couwenberg, 2018) for pollen records from larger lakes and LOVE (Sugita, 2007b) and MARCO POLO (Mrotzek et al., 2017) for pollen records from small forest hollows. Hitherto, such methods have not been applied for the interpretation of pollen records from the Erzgebirge. Moreover, most of the methods require pollen productivity estimates (PPEs), which have not been available from this area to date.

All these methods are suited for the interpretation of a single pollen record. To interpret the larger number of pollen records from the Erzgebirge, we here apply the extended downscaling approach (EDA; Theuerkauf and Couwenberg, 2017; Abraham et al., 2023). This approach explores whether the distribution of plant taxa in the past has been determined by abiotic landscape patterns, e.g. the underlying soils, including site water and relief conditions. The EDA is a forward-modelling approach that determines the most likely vegetation composition with a given landscape pattern, e.g. represented by the soil pattern. We apply the EDA for four distinct pollen stratigraphic phases of the Holocene, which are also well distinguishable in the early pollen records (see Sect. 5.3): the *Corylus* phase, the *Picea* phase, the *Fagus–Picea* phase, and finally the *Abies–Fagus–Picea* phase. For each phase, we include raw pollen counts from 12 and 15 pollen records from higher altitudes, i.e. in between ca. 400 and 1000 m a.s.l. (Table S2). EDA was not applied to the Late Glacial and very early Holocene periods because in the Erzgebirge the number of records from these particular periods is too low and dating too uncertain. As most of the early records from the 1920s to 1960s do not include herbal pollen, EDA analysis only includes the tree taxa. PPEs are derived by applying ROPES with a pollen record from Lake Černé jezero in the Šumava Mountains (Carter et al., 2018). As a landscape pattern for Erzgebirge we use the soil pattern from the Soil Map of Germany on the scale 1 : 200 000 for the Saxonian part (https://www.boden.sachsen.de/, last access: 7 January 2022) and the European Soil Database for the Bohemian part (https://esdac.jrc.ec.europa.eu/content/european-soil-database-v20-vector-and-attribute-data, last access: 7 January 2022). For comparison of pollen diagrams, we, whenever raw counts were available, recalculated pollen percentage values based on an upland pollen sum (excluding pollen types attributable to taxa growing on peatlands, such as grass type or *Calluna*).

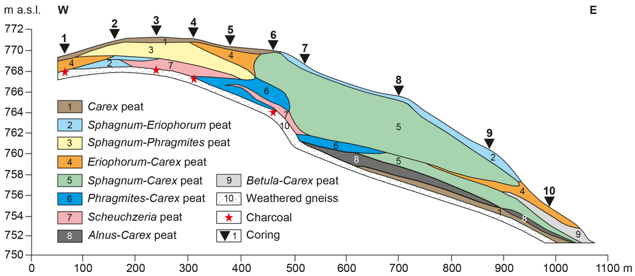

Figure 6. Cross-section through the Mothäuser Heide mire, central Erzgebirge (from Edom, et al., 2011, adapted).

5.2 Overview

The, so far, the best overview of the Holocene vegetation history of the higher altitudes of the Erzgebirge is provided by the pollen diagram Mothäuser Heide (ID 1, 768 m a.s.l.), which is also one of the best dated, long pollen records from the region (Lange et al., 2005; Theuerkauf et al., 2007; Edom et al., 2011; Figs. 1, 6, 7). For the early and mid-Holocene, the very early analysed, high-resolution pollen diagram Sebastiansberg (ID 29c, 842 m a.s.l.; Schmeidl, 1940; Fig. 1) is also useful, although limited to tree pollen. For the early Holocene, the pollen diagram Pfahlbergmoor (ID 43, 1017 m a.s.l.; Seifert-Eulen, 2016; Fig. 1) also provides a record of herb pollen.

The latter diagram shows that, like in the northern lowlands, *Pinus* and *Betula* were the first tree taxa present in the early Holocene (Firbas, 1952). *Corylus* was the first thermophilic, deciduous taxon that expanded in the early Holocene, soon followed by *Ulmus*, *Quercus*, *Tilia*, and finally *Alnus*. As radiocarbon dates from this early period are not available, it yet remains unknown whether the expansion of thermophilic taxa started at ca. 10 500 cal yr BP, as in the northern lowlands (Giesecke et al., 2011), or with some delay. This *Corylus*-dominated forest phase (see below for details) lasted for about 500–1000 years. The available pollen data are insufficient to evaluate whether the forests of that period were fully closed or if open spots remained. The Pfahlbergmoor diagram shows still clearly elevated pollen percentages of grass pollen during that period, which may indicate some degree of forest openness. However, the grass pollen may also originate from local wetland vegetation.

Forest composition in the Erzgebirge then changed at ca. 9000 cal yr BP due to the expansion of *Picea* (see *Picea* phase below), at ca. 6000 cal yr BP due to the expansion of *Fagus* (see *Fagus–Picea* phase below), and finally at ca. 4200 cal yr BP due to the expansion of *Abies* (see *Abies–Fagus–Picea* phase below; Fig. 7).

Despite the widespread historic evidence of forest clearance also at higher altitudes of the Erzgebirge for the last millennium (e.g. Kenzler, 2012; Tolksdorf, 2018), some long pollen records from larger peatlands in the high altitudes show no clear signal of increased forest openness. In the Mothäuser Heide diagram, for instance, pollen percentages of open indicators such as Poaceae, *Artemisia*, or *Plantago lanceolata* remain low. One possible explanation is that the youngest peat layers are missing due to earlier drainage of the peatland (see Sect. 6.4). Nonetheless, *Secale* pollen is continuously present in low percentages (0.5 %–1 %) in the top 1.5 m of the record comprising the last ca. 2000 years (Fig. 7). Whether these pollen finds indicate that local cereal cultivation in the mountains already started 2000 years ago or rather originated from distant transport from the adjacent southern lowlands, being only ca. 20 km away, remains unclear.

In general, the clearing and occupation period from around the late 12th to the 15th–16th centuries CE saw a drastic decrease in *Fagus* and *Abies*; an increase in non-arboreal pollen; and an increase in *Picea*, *Pinus*, and other pioneer tree species (Fig. 7). In the last ca. 300–400 years, many diagrams reflect very open landscape conditions, with a renewed forest increase in the last ca. 150 years.

A conceivable establishment of a summary pollen diagram and anthropogenic impact phases for the Erzgebirge, as published in the synthesis of many diagrams, for example, for the Šumava Mountains, Czech Republic, or the Auvergne Mountains (Miras et al., 2018; Kozáková et al., 2022) and the Morvan Mountains, both in France (Jouffroy-Bapicot et al., 2013), respectively, has failed so far due to the lack of digitally available palynological raw data (pollen counts) and well radiometrically dated diagrams.

5.3 Main Holocene vegetation phases of Erzgebirge

5.3.1 Vegetation phases

Betula–Pinus phase, ca. 11 600–10 200 cal yr BP

The pattern and timing of vegetation succession after the onset of the Holocene remain yet unclear because the first millennium of the Holocene is represented in very few, no, or poorly dated diagram sections only. The existing pollen records have been interpreted as the onset of the Holocene triggered immediate forest expansion in the Erzgebirge, starting with a short *Betula*-dominated phase and followed by a short *Pinus*-dominated phase. A basal radiocarbon date from the pollen diagram Pfahlbergmoor (ID 43, 1017 m a.s.l.; Seifert-Eulen, 2016; Fig. 1) may instead suggest that early Holocene forest expansion was delayed by at least several centuries. Moreover, pollen of open vegetation indicators, such as *Juniperus* and *Artemisia*, is still well present during the *Betula*- and *Pinus*-rich sub-phases. Hence, patches of open vegetation likely also existed during these sub-phases. Besides *Betula* and *Pinus*, further tree taxa that are poorly represented in the pollen records, such as *Populus* or *Sorbus*, may also have played some role.

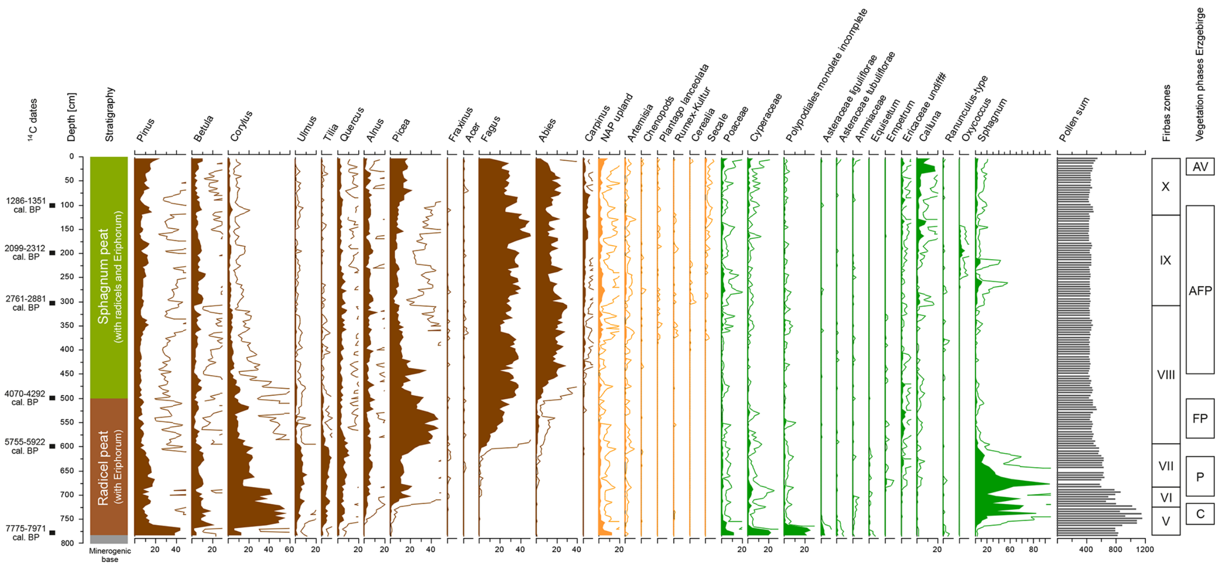

Figure 7. Typical pollen diagram from a mire in the montane ecological zone of the central part of the Erzgebirge: Mothäuser Heide (ID 1), 768 m a.s.l. (selected taxa; Lange et al., 2005; Theuerkauf et al., 2007, adapted). The units of the diagram axes below are percentages, except for the pollen sum, which shows counts. Pollen percentages have been calculated based on an upland pollen sum, including trees and shrubs (brown) and upland herbs (orange). The Firbas zones refer to Firbas (1949). Abbreviations for the vegetation phases of the Erzgebirge: C, *Corylus* phase; P, *Picea* phase; FP, *Fagus–Picea* phase; AFP, *Abies–Fagus–Picea* phase; AV, anthropogenic vegetation).

Corylus phase, ca. 10 200–9000 cal yr BP

In this phase, forests of the Erzgebirge were dominated by deciduous tree taxa. Altitudinal trends are not recognisable for this period (Fig. 8).

Picea phase, ca. 9000–6000 cal yr BP

Forest composition then changed around 9000 cal yr BP due to the expansion of *Picea* in the Erzgebirge. Still, the forests of the following *Picea* phase were dominated by deciduous tree taxa, i.e. mostly *Tilia*, *Ulmus*, *Quercus*, *Corylus*, and *Fraxinus*. The altitudinal gradient suggests that *Picea* was increasingly abundant in higher altitudes, while *Corylus* and *Quercus* were less abundant (Fig. 8).

Fagus–Picea phase, ca. 6000–4500 cal yr BP

At around 6000 cal yr BP, *Fagus* expanded in the Erzgebirge, while *Ulmus* and *Tilia* and later *Quercus* sharply declined. The decline in *Ulmus* likely corresponds to the mid-Holocene elm decline well known from sites across central and north-western Europe (Giesecke et al., 2017). The altitudinal gradients show that *Picea* was present in the highest altitudes of the mountains, whereas *Fagus* and other deciduous taxa were the most abundant in the lower and mid-altitudes (Fig. 8).

Abies–Fagus–Picea phase, ca. 4500–1000 cal yr BP

At around 4500 cal yr BP, forest composition again changed due to the expansion of *Abies*. Until about 1000 cal yr BP, *Abies* and *Fagus* became the dominating tree taxa in the Erzgebirge. *Picea* existed more frequently than before and was mainly limited to the highest altitudes (Fig. 8).

Anthropogenic vegetation, ca. 1000–0 cal yr BP

The past millennium is generally poorly represented in pollen records from the large Erzgebirge peatlands. Older pollen records mostly lack herbal pollen and hence are unsuited for exploring the role of anthropogenic vegetation. Younger records suffer from the decomposition of upper peat layers due to modern drainage. Hence, the past millennium is generally represented with a few samples in longer peat sequences only. Only the pollen diagram Kleiner Kranichsee shows a somewhat higher resolution (ID 44a, 927 m a.s.l.; Seifert-Eulen, 2016; Fig. 1). Moreover, due to the lack of radiocarbon dates, dating mostly relies on biostratigraphy. The widespread prominent increase in synanthropic pollen types, i.e. Cerealia, *Secale*, *Plantago lanceolata*, and *Rumex acetosella*, is attributed to the high medieval colonisation of that area in the late 12th to 13th centuries CE (e.g. Großer et al., 2006). Even in the highest altitudes of the Erzgebirge does the sum of synanthropic indicators arrive at about 10 % and the sum of all terrestrial open indicators (including grasses) at 30 %–50 %, indicating largely open conditions and widespread agricultural activity. At lower altitudes the sum of synanthropic pollen types arrives at about 20 %, indicating even more open vegetation and stronger agricultural activity.

While the increase in synanthropic pollen types indicates a decline in forest cover, changes in tree pollen composition

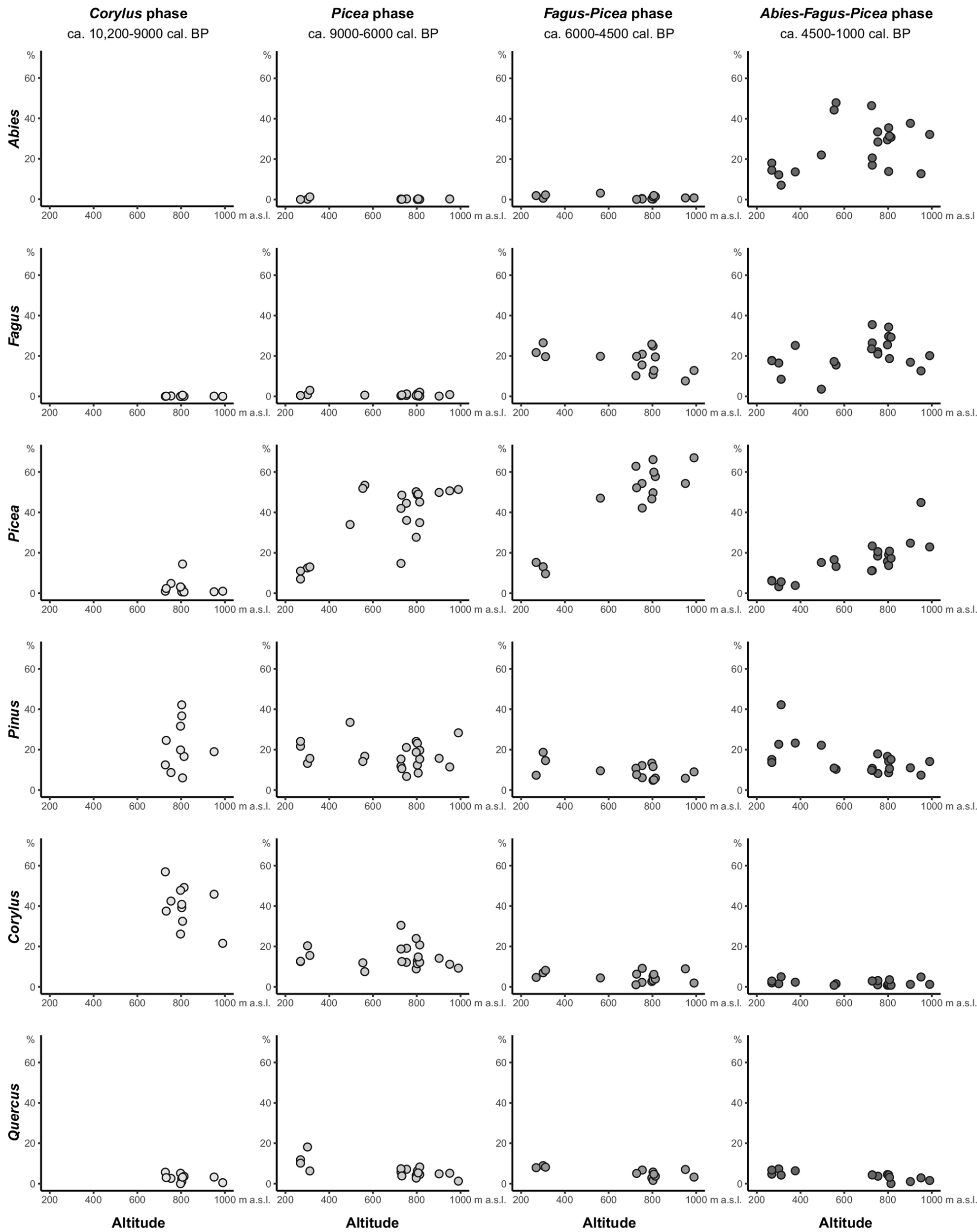

Figure 8. Pollen percentages of selected tree taxa versus altitude for four Holocene vegetation phases in the Erzgebirge.

indicate additional changes in forest composition. Clearly lower pollen percentages in *Fagus* and *Abies* and higher percentages in *Pinus* and *Picea* indicate a shift in overall forest composition towards *Pinus* and *Picea*. Whether, with overall declining forests, *Pinus* and *Picea* indeed expanded cannot be estimated with the data available. The increasing values of *Pinus* could possibly also partly be attributed to *Pinus mugo* on the peatlands in higher altitudes and widespread *Pinus sylvestris* plantation in lower altitudes since the late 18th century CE. The observation that *Abies* and *Fagus*, but not *Picea*, declined due to more intense land use possibly reflects that *Abies* and *Fagus* formerly occupied sites more suitable for land-use activities, i.e. better drained and climatically favourable sites.

5.3.2 EDA analysis

For the early Holocene *Corylus* phase, EDA analysis suggests that the forests on the widespread loamy soils were dominated by *Corylus*, *Tilia*, and *Ulmus*, whereas on the sandy soils *Corylus*, *Tilia*, and *Betula* were most abundant (Fig. 9). For the areas with debris-rich soils, a higher cover of *Fraxinus* is indicated. *Pinus* as the only coniferous taxon of that phase was probably mostly rare, covering only about 10 % of the main substrate types.

For the following *Picea* phase, EDA analysis indicates small differences in forest composition between sandy and loamy soils, with *Tilia* being somewhat more abundant on loamy soils (ca. 35 %) than on sandy soils (ca. 20 %; Fig. 9). Coniferous trees, mostly *Picea*, probably covered about one-third of the mountains. *Pinus* was also present, except on loamy soils.

For the *Fagus–Picea* phase, EDA analysis suggests that *Fagus* became the dominant tree taxon on sandy soils, possibly covering ca. 75 % of those areas (Fig. 9). Other deciduous tree taxa largely disappeared from these sites. *Picea* and *Pinus* played only a minor role. For loamy soils, a co-dominance of *Fagus* and *Picea* is indicated; other tree taxa were rare. EDA analysis indicates dominance of *Picea*, *Quercus*, *Corylus*, and *Tilia* on debris-rich soils; *Fagus* was likely rare here. For the rare sites with thicker loess substrate, first stands of *Abies* are also indicated.

For the *Abies–Fagus–Picea* phase, EDA analysis indicates co-dominance of *Fagus* and *Abies* on sandy and loamy soils, with a somewhat higher cover of *Fagus* on sandy soils and a somewhat higher cover of *Abies* on loamy soils (Fig. 9). Other deciduous taxa and *Picea* likely remained limited to other sites, i.e. debris-rich soils.

5.3.3 Local vegetation differentiation and conceptual summary

For the area around the Mothäuser Heide pollen diagram (ID 1; Fig. 1), the spatial distribution of the vegetation can be reconstructed with the help of the EDA analysis for four vegetation phases. The diagram itself is at 768 m a.s.l., while the surrounding area has an altitude range of ca. 620 to 800 m a.s.l. This area is characterised by a rather flat relief, loamy soil substrates at dry to wet sites, and peat at very wet sites. The current local climate parameters (1980–2010 period) show an annual average temperature of 4.9 °C and an annual precipitation of 937 mm (weather station Kühnhaide, 723 m a.s.l.; https://wetter-kühnhaide.de/, last access: 15 April 2022). The distribution of past vegetation is shown schematically (Fig. 10). Only those species for which clear connections with the respective site types were observed are shown. Occurrence of other species in small proportions (e.g. *Acer*) are likely. In general, there were clear changes in the vegetation over time on all site types, with the exception of the stream sites, which were initially dominated by *Corylus* and later by *Alnus* (Theuerkauf et al., 2007).

The outlines of the Holocene vegetation history described in the section above are presented as a conceptual pictorial model for a general, i.e. "normal zonal", site in the montane ecological zone in Fig. 11. All previous concepts for the phase structure of the Holocene vegetation history, including the new suggestion here, are listed in Table 2.

6 Discussion

6.1 General considerations

Despite a sometimes-high density of pollen diagrams in the landscapes of central Europe, regionally oriented diagram compilations and syntheses on the Holocene vegetation history are rare. A remarkably early example relates to Bohemia, where 130 pollen diagrams were compiled and evaluated already in the 1920s (Rudolph, 1928). More recent examples from central Europe include the Island of Rügen/Baltic Sea ($n = 40$; Lange et al., 1986), the Berlin area ($n = 73$; Behre et al., 1996), the eastern Alps and their forelands ($n = 301$; Wahlmüller, 1993), Hrubý Jeseník ($n = 16$; Dudová et al., 2018), Harz ($n = 37$; Beug et al., 1999), Schwarzwald ($n = 101$; Lang, 2005), Bayerischer Wald ($n = 22$; Stojakowits and Friedmann, 2019), the Northern Calcareous Alps of Germany and Austria ($n = 32$; Friedmann et al., 2022), Šumava ($n = 30$; Kozáková et al., 2022), and the entire territory of Bohemia and Moravia ($n = 40$; Bobek et al., 2019). Although some data in online repositories are available (e.g. https://epdweblog.org/, last access: 3 June 2022; https://www.pangaea.de/, last access: 3 June 2022; https://botany.natur.cuni.cz/palycz/, last access: 3 June 2022), these databases are usually incomplete for the regions and do not provide any synthetic analyses on the regional vegetation history "at the push of a button", so to speak. For the analysis of a specific region, the only option that remains is to compile the palynological data, including the accompanying radiocarbon data, as completely as possible and, if available, to open up further data sources such as macro-remain analyses, dendrochronological and anthracological analyses, or historical data on vegetation and land-use dynamics.

For the Erzgebirge so far 121 pollen diagrams have been produced. This is somewhat surprising at first, since even scholars familiar with the regional data material noted in the 2000s and 2010s that the regional palynological database, particularly new pollen diagrams, would be rather small (e.g. Lange et al., 2005; Sadovnik et al., 2013). This "astonishing growth" since then is certainly due to the fact that in this paper not only classical pollen diagrams were sought and found, but also pollen diagrams from a broad disciplinary perspective, including palynology, geology, geomorphology, archaeology, and peatland studies; this compilation was done often providing "unconventional" palynological data. Looking at the point in time when the diagrams were created, it becomes clear that despite an undoubted revival of regional palynology after 1989–1990 (53 % of the diagrams), there was already a broad base of older pollen diagrams before (47 % of the diagrams). However, it must be emphasised that many of the 121 diagrams are of little use for a well-elaborated vegetation history because (1) most of them were not independently dated by radiocarbon ages and can hardly be dated by pollen stratigraphy; (2) many published diagrams are of

Table 2. Late Pleistocene and Holocene forest vegetation phases in the Erzgebirge after different authors.

Chronology[1]	Chronology	Biozone		Palyno-zone	Rudolph and Firbas (1924)	Frenzel (1930)	Firbas (1952)	Hempel (2009)	Brízová (2014a)	This study
(Years BCE/CE)	(cal yr BP)			(Firbas, 1949)[2]						
750 BCE–2000 CE	1150–0	Subatlantic	Late	Xc	*Picea*	*Picea*	*(Pinus–)Picea*	Cleared and used forests	*Pinus–Betula(–Picea)* and synanthropic taxa	Anthropogenic vegetation
				Xb						
				Xa			*Fagus–Abies*	LMA[4]: *Quercus–Abies*, *Abies–Fagus*; UMA[5]: *Abies* (?)	*Abies–Fagus–Picea*	*Abies–Fagus–Picea*
	2400–1150		Early	IX	*Fagus–Abies*	*Fagus–Abies*				
3800–750	5660–2400	Subboreal		VIII	*Fagus–Picea*		*Picea–Fagus*	*Picea–Fagus*	*Picea–Fagus–Abies*	
7500–3800	7500–5660	Atlantic	Late	VII	*Quercus* mixed	*Picea*	*Picea–Quercus* mixed forest	LMA: *Quercus* mixed forest–*Picea*; UMA: *Picea*	*Picea–Quercus* mixed forest	*Fagus–Picea*
	9220–7500		Early	VI	Forest[3]-*Picea*	*Quercus* mixed forest–*Picea*	*Picea–Quercus* mixed forest	LMA: *Quercus* mixed forest; UMA: *Quercus* mixed forest–*Picea*	*Picea*	*Picea*
8500–7500	10 640–9220	Boreal	Late	Vb	*Corylus*	*Pinus–Corylus*	*Pinus–Corylus*	LMA: *Quercus* mixed forest–*Corylus*; UMA: *Corylus–Pinus–Betula*	*Pinus–Corylus*	*Corylus*
			Early	Va		*Pinus*		LMA: *Pinus*; UMA: *Pinus–Betula*		
9500–8500	11 560–10 640	Preboreal		IV	*Pinus* with *Betula* and *Salix*	*Betula–Pinus*	*Pinus*, *Pinus–Betula*	LMA: *Betula–Pinus*; UMA: *Betula–Pinus* or tundra	*Betula–Pinus*	*Betula–Pinus*
10 600–9500	12 700–11 560	Younger Dryas		III	–	–	–	Tundra	Tundra	–
11 400–10 600	13 350–12 700	Allerød		II	–	–	–	*Betula–Pinus*	Forest tundra	–
15 000–11 400	15 000–13 350	Pleniglacial to Older Dryas		Ia-c	–	–	–	Tundra	Tundra	–

[1] Correlation of chronology, biozone, and pollen zone is based on Giesecke et al. (2012, adapted). [2] Modified after Lang (1994). [3] Consisting of *Quercus*, *Tilia*, *Ulmus*, *Fraxinus*, and *Acer*. [4] LMA, lower mountain area (ca. 300–800 m a.s.l.). [5] UMA, upper mountain area (ca. 800–1200 m a.s.l.).

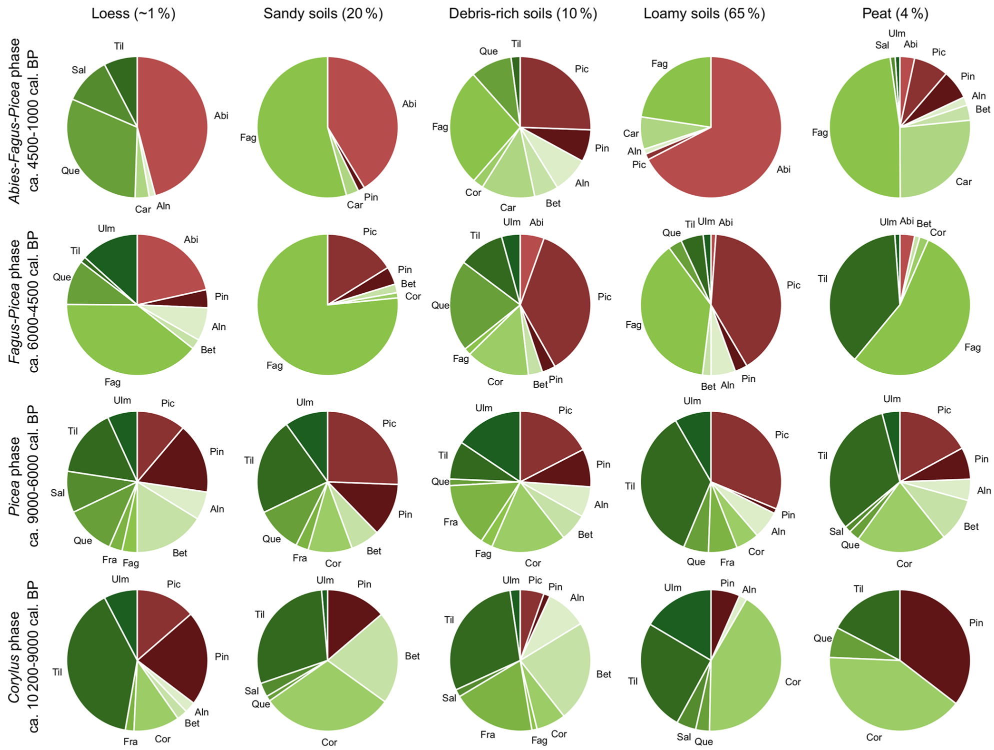

Figure 9. Results of the extended downscaling approach (EDA) analysis, showing the forest composition for typical soil sites for four Holocene vegetation phases in the Erzgebirge. The numbers behind the soil types above show their share in the region. Using the example of *Abies* during the *Abies–Fagus–Picea* phase, ca. 4500–1000 cal yr BP, it becomes clear what a strong influence the soil type has on the modelled forest composition. *Abies* dominates the loamy soils with 70 % and shows a much lower share with 45 % and 42 % at the sites with loess and sandy soils, respectively. *Abies* has a very low share of 5 % in peat soils and does not occur on debris-rich soils.

poor quality and incomplete, and the pollen counts are not available digitally; and (3) many diagrams are strongly influenced by local or aquatic pollen input.

The following Discussion section is largely based on the questions that we formulated in the introductory section. All in all, of course, this review is to be understood as an overview of the all material available on the Holocene vegetation history from a palynological perspective. Further questions on details of the regional forest history such as a fine differentiation of the local vegetation according to altitude, soil, water balance, and exposure; the possible reflection of natural disturbance events (e.g. storms, fires, biotic calamities); or the analysis of the long-term diversity of plant taxa in the regional mountain forests are, thus, reserved for future studies. These studies should then be done in conjunction with newly created, taxonomically as well as chronologically high-resolution pollen diagrams, including age control by radiocarbon dating.

Nevertheless, as can be seen from the larger text volume of Sect. 6.5 and 6.6, we would like to place a certain emphasis on the conditions in the Middle Ages and in the Early Modern Period. This can be explained by the reason for this review, i.e. by corresponding projects with a focus on this time. The natural forests of the medieval past could serve as a useful model for the necessary ecological forest conversion of the future (Piovesan et al., 2018; Morel and Nogué, 2019; Słowiński et al., 2019).

6.2 Critical reflection of the EDA results

We in this study for the first time applied EDA analysis in a larger mid-mountain range. Smaller mountain regions have already been investigated using EDA in the North Bohemian sandstone areas (Abraham et al., 2023). The primary goal was to explore major vegetation patterns in relation to soil conditions. Such patterns are indeed apparent, e.g. the higher cover of *Fagus* on sandy soils and the higher cover of first *Picea* and later *Abies* on loamy soils during the *Fagus–Picea* and the *Abies–Fagus–Picea* phase. However, in particular results for rarer taxa should not be over-interpreted because of limitations of the data available. We for each phase could include only 12–15 pollen records, whereas a number of 20 or more is suggested for robust results (Theuerkauf and Couwenberg, 2017). Moreover, most pollen records are characterised by low sample resolution and low pollen counts, which implies high error margins, particularly for rarer taxa and the rare soil types. Due to the often-lacking herbal pollen, we had to limit EDA analysis to tree taxa. This limitation is

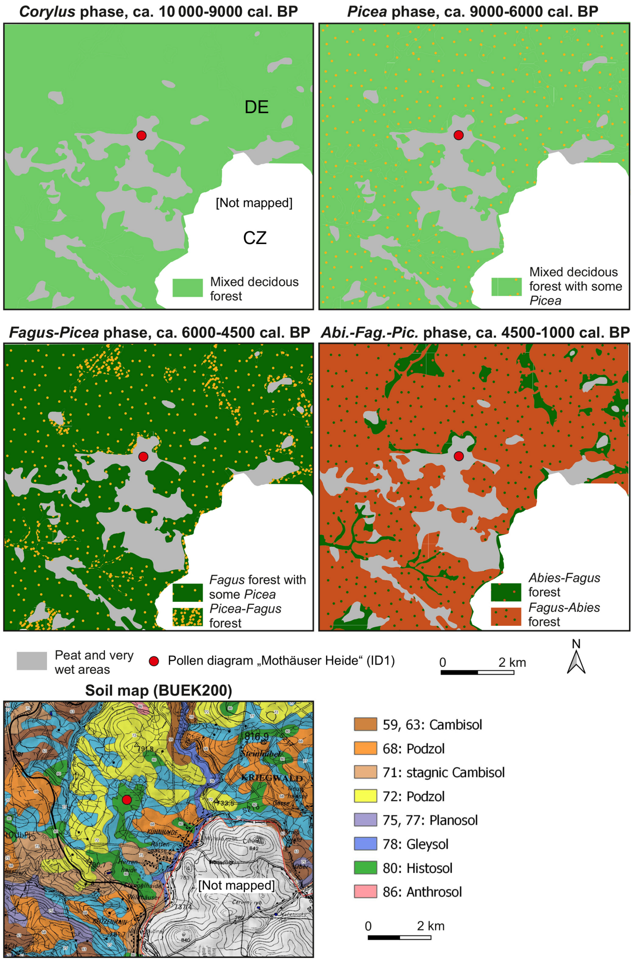

Figure 10. Palaeovegetation maps of the Mothäuser Heide mire for four Holocene vegetation phases based on the extended downscaling approach (EDA) analysis. The mixed deciduous forest in the 10 200–9000 cal yr BP phase was dominated by *Corylus*, *Tilia*, and *Ulmus*, while on the same sites in the 9000–6000 cal yr BP phase *Tilia*, *Ulmus*, *Quercus*, *Corylus*, and *Fraxinus* dominated, supplemented by *Picea*. Below is a soil map in the same section as the palaeovegetation maps above (Soil Map of Germany 1 : 200 000; BGR, modified).

the most relevant for the *Corylus* phase, when the vegetation of the Erzgebirge may still have been partly open. During the three later periods, patches of open vegetation were likely rare.

Previous syntheses on the Holocene vegetation history in the Erzgebirge (e.g. Rudolph and Firbas, 1924; Firbas, 1952; Hempel, 2009; Seifert-Eulen, 2016) have only marginally dealt with the potential dependence of palaeovegetation on soil patterns. Their focus was mostly on the larger-scale vegetation reconstruction as a function of altitude. An exception is the palynological research of Jacob (1956), who has already demonstrated a clear dependence of the palaeovegetation on the site pattern through a large number of pollen diagrams for the low-lying Tharandt Forest (ca. 190–460 m a.s.l.).

One key problem in all quantitative approaches, including EDA, for the interpretation of pollen records is the selection of a suitable pollen dispersal model. In the absence of other options, we have used a Lagrangian stochastic model adjusted for a lowland setting. Even though the northern part of the Erzgebirge is rather flat, this dispersal model is not ideal for the given mountain setting. Finally, our analysis has been limited to soil patterns, yet other environmental parameters are certainly relevant in the mountain region as well, namely the (micro-)relief. Including these parameters will be a worthwhile next step for palynological research, at least when more pollen data from the region become available.

6.3 Drivers of natural forest dynamics

The early Holocene forest expansion, including first the cold-adapted tree taxa *Betula* and *Pinus* and later the warm-adapted tree taxa *Corylus*, *Ulmus*, *Quercus*, *Tilia*, and *Alnus*, has been climatically triggered by the warming of the Holocene. As precise dating of early Holocene pollen records in the Erzgebirge is still lacking, it remains open whether the tree taxa expanded later than in the surrounding lowlands, i.e. whether the higher altitude caused some delay in warming.

Drivers of the later major changes in forest composition, i.e. formed by *Picea* (ca. 9000 cal yr BP), *Fagus* (ca. 6000 cal yr BP), and *Abies* (ca. 4500 cal yr BP), are less clear. All three events match the overall Holocene spread of these taxa across central Europe (Giesecke and Brewer, 2018), suggesting that differential expansion in the Erzgebirge is due to the more or less rapid Holocene expansion of these taxa and is not related to specific climatic events. This hypothesis might be tested by comparison of the exact timing of expansion in the western, central, and eastern Erzgebirge, thus comprising a distinct spatial gradient. *Fagus*, for example, expanded much earlier in the central European Šumava Mountains to the southwest (Kozáková et al., 2022) than in the Hrubý Jeseník Mountains to the east (Dudová et al., 2018), reflecting an eastward migration of this taxon. Hence, for the Erzgebirge one would expect that *Fagus* accordingly expanded from west to east. However, sample resolution and dating of the available pollen records are insufficient to prove such a trend at the moment.

Moreover, in the Mothäuser Heide (ID 1) record, the expansion of Fagus at ca. 5900–5800 cal yr BP appears synchronous to the decline of *Ulmus* and *Tilia*, which may point to four different explanations. First, under the assumption that the *Ulmus* decline in the Erzgebirge is analogous to the well-known *Ulmus* decline period in the lowlands of northwestern Europe (ca. 6350–5280 cal yr BP; Parker et al., 2002), i.e. has also been caused by a pathogen, the expansion of *Fagus* may have been triggered by the demise of *Ulmus*. Secondly, the synchronous *Ulmus* decline and *Fagus* expan-

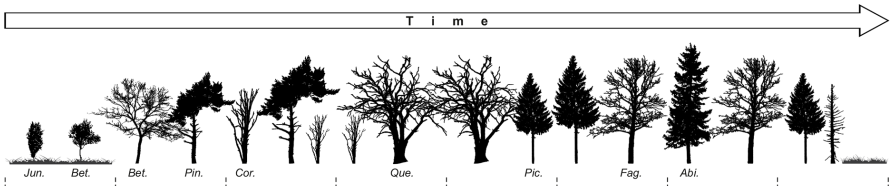

Chronology yrs BCE / CE	15 000 to 9500	9500 to 8500	8500 to 7500	7500 to 5700	5700 to 3800	3800 to 750	750 to 1150	1150 to 2000
Chronology yrs cal. BP	14 000 to 11 560	11 560 to 10 640	10 640 to 9220	9220 to 7500	7500 to 5660	5660 to 2400	2400 to 800	800 to 0
Biozone	Pleniglacial to Younger Dryas	Preboreal	Boreal	Early Atlantic	Late Atlantic	Subboreal	Early Subatlantic	Late Subatlantic
Palynozone after Firbas	Ia-c to III	IV	V	VI	VII	VIII	IX-Xa	Xb-c
Vegetation	prevailing tundra	*Betula-Pinus*	*Pinus-Corylus*	*Quercus* mixed forest	*Quercus* mixed forest-*Picea*	*Picea-Fagus*	*Abies-Fagus*	*Picea* and synanthropic taxa

Figure 11. Conceptual model of the late Pleistocene and Holocene forest vegetation development in the montane ecological zone of the Erzgebirge using a pictorial timeline. The trees shown symbolise the eponymous vegetation phases and do not reflect the complete mixing ratios of the tree taxa that were actually present (abbreviations for woody taxa: *Jun.*, *Juniperus communis*; *Bet.*, *Betula spec.*; *Pin.*, *Pinus sylvestris*; *Cor.*, *Corylus avellana*; *Que.*, *Quercus spec.*; *Pic.*, *Picea abies*; *Fag.*, *Fagus sylvestris*; *Abi.*, *Abies alba*).

sion are purely incidental. Thirdly, the decline of *Ulmus* (and *Tilia*) in the Erzgebirge has not been caused by a pathogen attack but by the expansion of *Fagus*, thus by species competition. Finally, the decline of *Ulmus* and the expansion of *Fagus* may have been triggered by the same event, such as climate fluctuation. Again, the available pollen records are insufficient to prove these above-mentioned hypotheses. Therefore, other possible natural disturbance factors that could also have had a strong impact on the regional forest vegetation in the past, such as insect outbreak, drought, storm, or fire (e.g. Kulakowski et al., 2017; Bobek et al., 2019; Schafstall et al., 2022), have not yet been evaluated for the study area.

Altitudinal analysis of the pollen records suggests that altitude had only limited effects on forest composition above 300–400 m a.s.l., except that during all times pollen proportions of *Picea* were the highest in the altitudes above ca. 1000 m a.s.l. (Fig. 8). *Picea* was likely always most abundant along the highest altitudes.

6.4 Prehistoric human impact

So far, there are only a few indications of an already premedieval anthropogenic influence on the mountain forests from the pollen diagrams available in the Erzgebirge. Some diagrams (e.g. Mothäuser Heide, ID 1) show the presence or even continuous curves of potential pasture and meadow indicators such as *Artemisia*, *Rumex*, and *Plantago* from around 2000 cal BCE at the earliest. Even cereal pollen occurs sporadically already before the High Medieval, i.e. before ca. 1150 CE. However, there are usually no previous or synchronous drastic declines in tree taxa or tree species shifts that would indicate corresponding forest clearings. Moreover, the low percentages of the synanthropic taxa (Mothäuser Heide, ID 1: 1.4 % maximum for the period 3000–1000 cal yr BP) do not rule out long-distance input from the surrounding low-lying areas, some of which, particularly in the Elbe/Labe River valley to the east, in the Lösshügelland to the north and in the Ohře Graben and the North Bohemian Basin to the south, have been intensively populated from the Neolithic onwards (Blažek et al., 1995; Christl and Simon, 1995; Kenzler, 2012). In general, there are no in-depth studies on recent pollen precipitation for the Erzgebirge that would allow for an assessment of the possible far-distance pollen transport even in (pre-)historic times. In particular, peat profiles at crest sites close to the steep southern slope of the mountain range have a potentially increased exposure to supra-regional pollen input. Corresponding studies in the Schwarzwald in SW Germany urge caution in the interpretation of those taxa, which occur in low percentages (Hölzer and Hölzer, 2014).

An interesting coincidence of synanthropic taxa (reflecting land use), heavy metal deposition (mining and metallurgy), and charcoal (fire) is shown in the pollen and geochemical data from the Kovářská bog at 870 m a.s.l. in the central Bohemian Erzgebirge (Bohdálková et al., 2018). Already from ca. 950 cal BCE has there been evidence of taxa that indicate grain cultivation, grazing/meadow management, and clearing of forests. Although these findings suggest local human activities in the mountains themselves during the Bronze Age, early Iron Age, and Roman Age, the corresponding archaeological findings from the immediate vicinity of the pollen diagram (up to ca. 5–10 km distance) are still missing.

This leads to the general question on the evidence of prehistoric anthropogenic activities in the study area, indicated by archaeological finds and place names. In the lower eastern Saxon Erzgebirge southeast of Freiberg, at an altitude of ca. 300 m a.s.l., both late Neolithic and Iron Age artefacts have been found (Kreienbrink et al., 2020). However, individual prehistoric finds, such as stone axes or metal objects, have been found at various locations throughout the mountains, including the crest area (Christl and Simon, 1995). In the neighbouring Vogtland area, however, up to at least about 400 m a.s.l. a larger number of Bronze Age sites, including evidence of synchronous metallurgy (Tolksdorf et al., 2019), exist. At the Erzgebirge historic Slavic place names usually occur below 300 m a.s.l. Only very occasionally is there evidence of place names at higher altitudes, such as the town name Zöblitz at 600 m a.s.l. in the central part (Wenzel, 2016). But the majority of historical place names are of German origin and date from the Middle Ages or Modern Period. Also, in the Bohemian Erzgebirge there have so far only been single prehistoric stray finds (Blažek et al., 1995). Kenzler (2012) summarises that there have been no permanent settlements in the mountains for the entire prehistory. According to the available records, the Erzgebirge were only visited for raw material extraction, hunting, and crossing. However, this interpretation can also be due to the state of research, as findings on prehistoric settlements or intensive use of other low mountain ranges in central Europe suggest (e.g. Rösch, 2013; Kozáková et al., 2015, 2022; Henkner et al., 2018; Dreslerová et al., 2020; Wiezik et al., 2022).

In view of the early human impact, the archaeological indications of Bronze Age tin placer mining around 2000–1300 cal BCE from the western and eastern Erzgebirge from altitudes of 900 and 740 m a.s.l., respectively, are particularly remarkable (Bartelheim and Niederschlag, 1997; Tolksdorf et al., 2020b). These mining and probably even metallurgic activities were inevitably associated with (ultra?)local forest clearings and also required transport routes, which have been at least partially free from vegetation. To date, however, there are no pollen diagrams near these early mining sites with a potential palynological record of these local dynamics. Available diagrams in greater distance to these sites (IDs 3, 4, 57b, 44a, 44b, 45; Fig. 1) show no pollen signals specifically for the period 2000–1300 cal BCE that would indicate deforestation or other anthropogenic activities in the area. However, geochemical and palynological evidence of local early mining in the Bronze Age, early Iron Age, and Roman Age is also available from the Bohemian Erzgebirge (Veron et al., 2014; Bohdálková et al., 2018). In summary, it is very likely that prehistoric mining in the Erzgebirge, which has only just initially been researched, led to local forest clearings and the development of replacement vegetation communities at certain sites and routes. Whether other local land-use activities also took place at least seasonally (e.g. grazing by transport animals and livestock, hunting, timber extraction, and honey production) can only be assumed analogous to other prehistoric and early medieval mountain areas in central Europe (e.g. Rösch, 2000; Valde-Nowak, 2013; Schreg, 2014; van der Knaap et al., 2020; Hrubý, 2021).

In addition, it should be mentioned that the Erzgebirge were already a transit area in the prehistory, specifically since the Neolithic, connecting today's central and northern Germany with the Bohemian Basin. Corresponding paths crossed the mountain crest area at various points (Hauswald and Simon, 1995; Ruttkowski, 2002; Kenzler, 2012). Along these routes and in local camps, the latter potentially necessary as rest stops for shelter, changing horses, and procuring food and fodder (Bell, 2020), the natural forest vegetation has certainly been anthropogenically modified.

6.5 Forest structure and human impact in the Middle Ages

Already the early palynological works on the Erzgebirge have suggested that before the high to late medieval clearings (late 12th to early 16th centuries CE), the montane zone was densely forested, mainly by *Fagus* and *Abies* with a certain amount of *Picea* (Rudolph and Firbas, 1924; Frenzel, 1930; Firbas, 1952; Jacob, 1956). Following that, *Picea* was more abundant or even dominant in the crest area. Locally, i.e. in the mires there, *Pinus mugo* likely played an important role.

For the low-lying Tharandt Forest (ca. 190–460 m a.s.l.) it could be shown, using a spatial approach based on a total of 22 pollen profiles (IDs 77–89, Fig. 1), which is unique for the study area thus far, that the tree species composition described above was much more spatially complex in detail (Jacob, 1956). Different locations here, i.e. differences in relief, exposure, substrate/soil, and water balance, led to a close-meshed pattern of different forest vegetation. Indeed, *Fagus* and *Abies* occurred extensively on slopes and plateaus. *Picea* grew in the floodplains of streams together with *Alnus glutinosa* and *Betula pubescens*. In addition, *Picea* occurred in further cool and damp to wet locations (steep northern slopes, ravines, swamps, and mires). *Pinus sylvestris*, *Quercus* species, and *Betula pendula* inhabited rocky outcrops, sandy soils, and sunny slopes. Based on the data available at this time, the distribution pattern of *Fraxinus excelsior*, *Ulmus* species, *Acer* species, and *Populus* species remains somewhat unclear. These tree species obviously did not play a significant role over a large area, but they were mixed in. *Corylus avellana* was common in bright places. The variance of shrubs was not determined. In addition to this site-related control of the tree species distribution, there were also dynamic biotic and abiotic effects, e.g. as a result of the life cycle of the trees, competition, or calamities (e.g. insect infestation, fire, relief instability/soil erosion; Leuschner and Ellenberg, 2017). Although the example of the Tharandt Forest, which has been very well examined palynologically, represents a forest lying low in the Erzgebirge, it can be assumed that a similarly complex spatial differentiation also applied to the higher-lying areas in the region. This is indicated by the record of current site-related tree species differences in near-natural forest protection areas on higher altitudes in that region (Sächsisches Staatsministerium für Umwelt und Landwirtschaft, 2008).

Already the early works indicate the end of a large-scale *Fagus* and *Abies* dominance and the formation of replacement vegetation in the 12th–13th centuries CE according to the still-valid basic outlines of the medieval settlement history in the region. The current dominance of *Picea* was interpreted as the result of natural reforestation after abandonment of intensive land use in the late Middle Ages and in modern times but above all of reforestation since the 18th century CE. This has been clearly proven both by older investigations and by more recent forest historical investigations (e.g. Kienitz, 1936; Nožička, 1962; Thomasius, 1994). However, the temporal resolution of the last ca. 1000 years in the older pollen diagrams was normally low, and the general focus was mostly on the entire Holocene, neglecting a detailed characterisation of the vegetation dynamics in the Middle Ages and afterwards.

Even from the more recently analysed pollen diagrams do only a few have a sufficiently large thickness of sediments originating from the last ca. 1000 years, i.e. enabling a higher temporal resolution, and an independent chronological control by radiocarbon dates. Of these, the diagram SPI-1, Spindelbach (ID 22, ca. 850 m a.s.l.; Houfková et al., 2019; Marešová, 2022; Fig. 1), located on the crest area of the Bohemian site of central Erzgebirge, is particularly suitable for characterising the local forest vegetation immediately before the start of the medieval clearing and the moment of deforestation, as well as the development of replacement vegetation. This alluvial–colluvial sequence is 82 cm thick and dated by four radiocarbon ages. The dominance of pollen from the climax tree species *Fagus* (max 15 %), *Abies* (max 12 %), and *Picea* (max 10 %), accompanied by a high amount of fern spores (max 40 %), indicates that the broader area around the sampling site was still forested at the beginning of the 14th century CE. The area was cleared around 1350 CE for the establishment of an agrarian settlement (called Spindelbach after written medieval sources), as reflected by a decrease in the sum of tree pollen to below 12 %, the increase in non-arboreal pollen up to 79 %, and the emergence of various synanthropic taxa. According to the pollen data, livestock breading and grain cultivation have been the main economic bases in the village area. Moreover, as at the same time five mining villages were established in an only 5 km radius around Spindelbach, human-induced deforestation likely affected the tree species composition even in the broader area. In the period about 1450–1480 CE, the village declined and finally was abandoned. Its desertion corresponded to an epoch of regional economic and demographic stagnation, overexploitation of the mountain forests, and an era of harmful weather events (Houfková et al., 2019), which are probably connected with the onset of the Little Ice Age. Immediately after abandonment, forest regeneration started again, reflected by a renewed increase in *Picea* (max 10 %), and together with *Betula* (max 20 %) formed a secondary forest. The sum of tree pollen soon reached a maximum of ca. 60 %. Even though *Picea* was restored by natural succession, *Fagus* and *Abies* never achieved their former abundance, attaining relative maxima of ca. 7 % and 2 %, respectively. In the mountains, *Picea* is generally considered a pioneer tree species that benefits from sites that have previously been cleared by humans, while the natural re-establishment of *Fagus* and *Abies* requires more sensitive conditions (e.g. close proximity to parent trees, microclimatic protection, shade; Ellenberg, 1996).

The reflection of the local deforestation of a largely still-native forest in the high-lying profile Spindelbach, which dates back to the second half of the 14th century CE, is quite late compared to the historically known medieval settlement and land-use history in the Erzgebirge at other sites (e.g. Blažek et al., 1995; Kenzler, 2012; Tolksdorf, 2018; Cappenberg et al., 2020). Forest clearing and subsequent agricultural or industrial activities (mining, metallurgy, glass, and charcoal production) can generally be expected at many other, but often much lower, locations since the second half of the 12th century CE (Fig. 12). For example, the start of silver mining in the eastern Erzgebirge at Freiberg (ca. 380 m a.s.l.) dates to the year 1168 CE (Wagenbreth and Wächtler, 1988), at Dippoldiswalde (ca. 375 m a.s.l.) to the last quarter of the 12th century CE (Schubert, 2017), and at Niederpöbel (ca. 530 m a.s.l.) to the period 1180–1240 CE (Cappenberg et al., 2020); fortifications and village settlements in the central Erzgebirge around Zöblitz (ca. 600 m a.s.l.) and in Ullersdorf (730 m a.s.l.) date from the late 12th to 13th centuries CE (Billig and Geupel, 1992; Tolksdorf et al., 2020a); and the Teufelsschloss castle in the western Erzgebirge near Eibenstock (ca. 650 m a.s.l.) dates to the late 12th century CE/around 1200 CE (Billig and Geupel, 1992).

This early settlement/land-use period, dated independently of history and archaeology records, and the, thus, inevitable forest-clearing phase of the late 12th to 13th century CE are also represented in several pollen diagrams (IDs 32–37; Fig. 1) obtained from medieval to modern stream valley sediments around the abandoned mining town Přísečnice/Preßnitz (ca. 720 m a.s.l.), located on the Bohemian side of the central Erzgebirge (Kočár et al., 2018). These diagrams show a somewhat earlier deforestation (13th century CE) caused by agriculture and mining in comparison to the nearby pollen diagram SPI-1, Spindelbach (ID 22), described above. Although the proportions of the main tree species vary significantly in these six diagrams, they are basically the same at the moment of local clearing, namely *Fagus*, *Abies*, and *Picea*. In some cases, there were not a complete clearing and agricultural or industrial use of the sites but only a forest thinning with an increase in *Picea* and a decrease in *Fagus* and *Abies*.

Thus, based on the current knowledge from all available pollen diagrams – although these are not always available in the "right" place, and targeted palynological transect studies are also still missing – it can be assumed that in the Erzgebirge from the submontane (ca. 300–500 m a.s.l.), via the montane (ca. 500–900 m a.s.l.) to the high-montane zone (ca. 900–1200 m a.s.l.), forests with *Fagus* and *Abies*, and to a minor degree *Picea*, existed until the high medieval clearing.

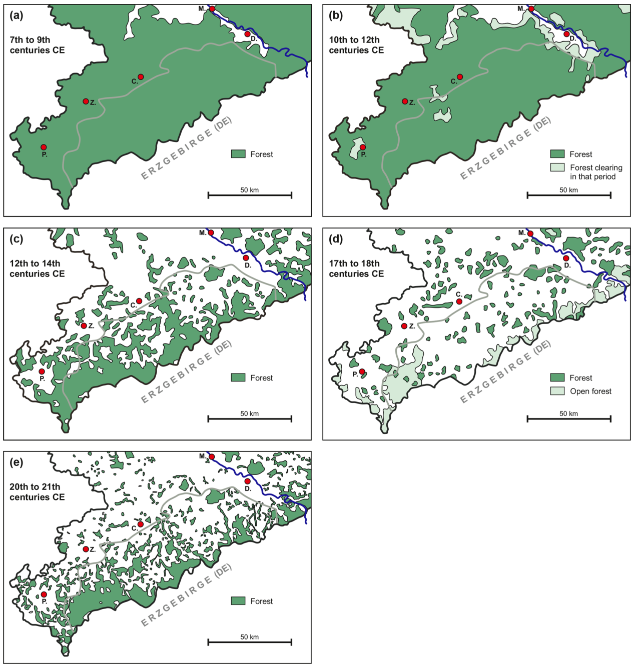

Figure 12. Historical forest cover dynamics of the Erzgebirge (Saxon part) and surroundings (spatial data: Hempel, 2009, modified). **(a)** The 7th to 9th centuries CE, **(b)** 10th to 12th centuries CE, **(c)** 12th to 14th centuries CE, **(d)** 17th to 18th centuries CE, and **(e)** 20th to 21st centuries CE.

Other tree species (e.g. *Acer*, *Ulmus*, *Pinus*, *Fraxinus*, *Alnus*) also grew in smaller proportions on average but with potentially greater local participation. In the 20th century CE, there were still mostly small-scale locations with *Fagus* and *Acer* in the upper reaches of the Erzgebirge, i.e. up to ca. 1000–1100 m a.s.l. (Heynert, 1964). Also, isolated occurrences of *Abies* were still reported in the 19th–20th centuries CE up to about 1000 m a.s.l. (Firbas, 1952). This means that these tree species of the former "hercynic mixed mountain forest" (Drude, 1902) had, from today's perspective, an almost unimaginable, much wider distribution up to the High Medieval than indicated by their current sparse distribution "in the endless spruce sea". Natural (mixed) *Picea* forests, however, regularly had a very small proportion at the highest altitudes (> ca. 900 m a.s.l.) and here in special locations such as wet sites or those with shallow soils as well as rocky cliffs and other sites with extreme conditions that restrict competition from other tree species (Heynert, 1964; Schmidt et al., 2002; Hempel, 2009).

Of course, for potential tree species distribution, in addition to anthropogenic processes, climatic developments during the Middle Ages and afterwards must also be considered. So far, however, there has been no regional climate reconstruction for the Erzgebirge for the last ca. 1000 years (Tolksdorf and Scharnweber, 2018). Therefore, only the quantitative reconstructions generally available for central Europe (e.g. Glaser, 2008; Büntgen et al., 2011; Luterbacher et al., 2016) can be transferred to this area. This applies to the Medieval Climate Anomaly (ca. 900–1200 CE, relatively warm) and Little Ice Age (ca. 1250–1700 CE, relatively cold) main thermal phases on the one hand and to exceptional dry (ca. 950–1700 CE, ca. 1490–1540 CE) and wet periods (ca. 1050–1150 CE, ca. 1600–1800 CE) on the other hand. At higher altitudes in particular, a combination of cooler and wetter conditions could potentially benefit *Picea* and disadvantage *Fagus* and *Abies*. However, historical sources show that the Erzgebirge was still suitable for the cultivation of robust field crops at the end of the Little Ice Age, even at higher altitudes. Although the upper zones of the Erzgebirge can generally be considered agriculturally unfavourable areas, cereals, potatoes, and garden fruits could be cultivated even in the rather cold 18th to 19th centuries CE (i.e. the very late part of the Little Ice Age) for subsistence economy up to the mountain crest area at around 1000 m a.s.l. (Sigismund, 1859). Even today, fields with grain, rape, and forage grass reach up to an altitude of ca. 950 m a.s.l., for example in Oberwiesenthal. Thus, the last ca. 1000 years in the Erzgebirge have most probably enabled the potential existence of the climatically more demanding *Fagus*, several other deciduous tree species, and *Abies* at all times and almost everywhere, except in mires and other extreme sites. Therefore the expansion of the climatically less demanding *Picea* in the Early Modern Period and afterwards, which can actually be determined in pollen diagrams and in historical sources, was a consequence of succession after repeated anthropogenic disturbance or direct planting and not of climatic cause (see from a central European perspective Seim et al., 2022).

The information given above shows that medieval vegetation dynamics have been studied in detail at least for some sites at different altitudes. For Saxony, Hempel (2009) presented a map of the "natural vegetation at around 1000 (−1200) CE" based on the state of knowledge on Holocene vegetation development available at that time (Fig. 13). It is based on geobotanical, palynological, archaeological, historical, and onomastic data. For the Erzgebirge this map shows along an altitudinal gradient *Abies*-dominated forests in the lower position; *Fagus*-dominated forests in the middle position; and *Picea*-dominated forests in the upper position, there together with large mire areas. In fact, these three tree species are mixed in different proportions, sometimes with a higher proportion of other trees (*Acer, Pinus*). Compared to the map of the potentially natural vegetation according to Schmidt et al. (2002; Fig. 3) – for a definition and discussion of both methodological concepts see, for example, Jaroslav (1998), Chiarucci et al. (2010), and Loidi et al. (2010) – in addition to similarities (*Picea* forests in the crest area, *Fagus* forests in the middle altitude), it is striking that *Abies*-dominated forests are mapped for the lowest mountain positions and for the northward-adjoining loess hill and glacial morainic landscape. The map of the potentially natural vegetation, however, shows *Quercus*–*Fagus* forests

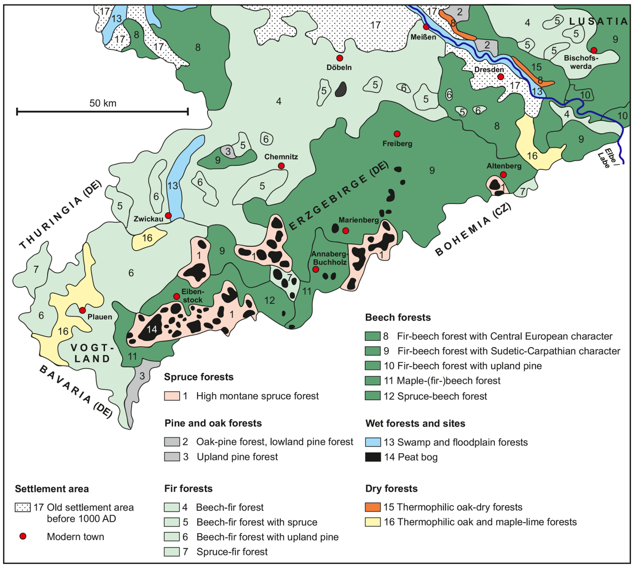

Figure 13. Reconstructed natural vegetation at around 1000 (−1200) CE for the Erzgebirge (Saxon part) and surroundings (spatial data: Hempel, 2009, modified).

or *Carpinus–Quercus* forests, as they also occur at least on a small scale in the present. This somewhat unusual "invasion" of the mountain tree *Abies* in the lowlands is explained by Hempel (2009) in terms of vegetation ecology: *Abies*, in the mountains with somewhat similar demands as *Fagus*, would be a more competitive tree species on the prevailing compacted and thus seasonally waterlogged (i.e. stagnant water) loess and morainic soils in the hills and lowlands near the mountains. Geobotanical, historical, onomastic, and to a lesser extent also pollen analytical arguments (e.g. Jacob, 1971) are provided for this. In general, however, this hypothesis still needs to be verified.

6.6 Modern forest dynamics

While at least some local pollen records cover the Middle Ages and the Early Modern Period, pollen data from the past ca. 300 years are largely missing. On the one hand, this has to do with the obviously little palynological interest in this period so far. On the other hand, younger peat layers were lost due to drainage and subsequent oxidation in almost all Erzgebirge mires. This means that the last few centuries often evade potential analysis in mires.

One of the few studies attempting to palynologically resolve the last few hundreds of years is the one from the Ocean Bog mire (ID 75, 900 m a.s.l.; Fig. 1) in the western part of the Erzgebirge in Bohemia (Novak et al., 2008). This pollen diagram, only 36 cm thick and dated using ^{210}Pb, has been interpreted to show a (near-)natural (or already regenerated?) forest at the end of the 17th/beginning of the 18th century CE, consisting of *Fagus*, *Abies*, and *Picea*, as well as other tree species (e.g. *Pinus*, *Betula*, *Alnus*). The sum of tree pollen in that time reached 90 %. In the first half of the 19th century CE there was a shift from a closed- to an open-canopy forest (arboreal pollen– AP – ca. 70 %) caused by local human impact. *Fagus* and *Abies* almost disappeared, and *Picea* increased sharply. The strongest open character was reached around the beginning of the 20th century CE (AP ca. 45 %). More recent events, such as the forest dieback in the second half of the 20th century CE (decreasing *Picea*), the emergence of invasive plant species (detection of *Ambrosia*), and local wetland regeneration (increasing *Sphagnum*) are also reflected very well in this diagram. This example underlines the potential of high-resolution pollen analysis of young peat layers in at least some Erzgebirge peatlands.

From the Early Modern Period, the proportion and diversity of synanthropic taxa increased significantly compared to the Middle Ages. Of course, the altitude must be considered here because the lower altitudes (< 500 m a.s.l.) are climatically more suitable than the upper altitudes (> 500 m a.s.l.) for diversified agriculture with a correspondingly richer use of cultivated plants. The sum of synanthropic taxa reaches up to ca. 10 % maximum in higher altitudes and 15 %–20 % maximum in the lower altitudes, respectively. In addition, there is a wider spectrum of palynologically proven plants (e.g. *Cannabis*, *Linum*). Forest management from the 18th century CE onwards (Thomasius, 1994) also left traces in the pollen precipitation. On the one hand, the proportions of *Picea* and *Pinus*, as tree species that are particularly intensively planted in the region, increased significantly (*Picea* max 67 %; *Pinus* max 50 %). On the other hand, single pollen from new tree species imported from other regions were often found (e.g. *Larix*, *Juglans*, *Pseudotsuga*, *Castanea*).

The settlement and industrial development in the Erzgebirge, particularly mining and metallurgy, caused a massive consumption of wood resources, especially from the turn of the 15th/16th centuries CE onwards. At the same time, the human population grew, many mining towns were founded, and more forest areas were cleared for agricultural use (e.g. Wilsdorf et al., 1960; Thomasius, 1994; Cembrzyński, 2019; Claire, 2022). This leads to a drastic reduction in the forest area up to the mountain crest. The minimum of the forest area was reconstructed for the late 17th to 18th centuries CE (Hempel, 2009; Fig. 12). During this time, the highest mountain top in the Saxon Erzgebirge, the Fichtelberg (1215 m a.s.l.), was also forest-free (Sächsisches Staatsministerium für Umwelt und Landwirtschaft, 2008). However, this development was neither temporally nor spatially homogeneous at the expense of the forest area. An economic crisis hit the region already as early as the 14th century CE (Derner et al., 2016), and the Thirty Years' War during the first half of the 17th century CE also led in phases to a decrease in the pressure of use and to a renewed increase in forest cover (Wetzel, 2010). In these phases, pioneer forests were able to develop again in areas formerly used for agriculture or industry, which was accompanied by an increase in, for example, *Picea* and *Betula* in pollen diagrams. Larger areas of forest were probably still present in the western Erzgebirge in the late Middle Ages (Hempel, 2009). From the 18th to the 20th century CE, government measures in particular led to a re-expansion of the forest areas in the entire region, in particular through the establishment of *Picea* monocultures (Fig. 12). Forest losses due to emission damages in the 1960s to 1990s, mainly in the crest region, have since been compensated for. On the Bohemian side alone ca. 40 000 ha was reforested (Šrámek et al., 2008).

However, the current and coming years' climate-change-related forest damages, especially at *Picea* (due to droughts and subsequent bark beetle infestation), could surpass anything documented from the 20th century CE in the Erzgebirge (Kupková et al., 2018; SMEKUL, 2020; Gdulová et al., 2021). This regional development fits into the dynamics for central Europe with a huge loss of *Picea* stands since the 2010s (e.g. Neumann et al., 2017; Bałazy et al., 2019; Schuldt et al., 2020). In Germany alone, the area with tremendous tree losses amounts to ca. 500 000 ha between 2018 and 2021, which corresponds to ca. 5 % of the German forest cover (DLR German Aerospace Center, 2022).

Efforts have been made in the Erzgebirge for decades to achieve ecological forest conversion, mainly including the conversion of *Picea* monocultures to mixed stands involving *Fagus*, other deciduous trees, *Abies*, and *Picea* (Eisenhauer and Sonnemann, 2009; Staatsbetrieb Sachsenforst, 2017). On the one hand, however, the speed of active forest conversion is currently not keeping pace with the dying of forest stands. On the other hand, a lack of mother trees for deciduous trees and *Abies* as well as excessive game populations slow down natural forest change (Fuchs et al., 2021). In the future, *Fagus*, other deciduous trees, and possibly also *Abies* in the Erzgebirge will probably benefit from the rising temperatures resulting from climate change and expand upwards. *Picea*, however, will probably continue to come under massive pressure to exist, especially due to drought stress and competition from other tree species, and will even disappear over large areas in the lower altitudes as a still-dominant tree (e.g. Kölling et al., 2007; Kašpar et al., 2021).

7 Conclusions

Understanding the status and anticipating possible future changes in central European mountain forests are facilitated by a systematic historical perspective. For the Erzgebirge, the review of available pollen records provides insights into the vegetation history both on a millennial scale (i.e. whole Holocene) and on a centennial scale (i.e. last centuries). The 121 pollen diagrams compiled for this represent an exceptionally high data density for a low mountain range in central Europe. On the one hand, this results from a remarkably long palynological research tradition since the 1920s. On the other hand, projects on environmental history in particular have led to a significant increase in pollen data since the 1990s. From the evaluation, analysis, and discussion of the regional data, we draw the following conclusions.

Although all pollen diagrams may help to reveal the presence/absence of the major tree taxa, only the more recent diagrams also ensure a resolution of the other taxa categories (i.e. rare trees, shrubs, herbs, grasses, spores). To date, only a few diagrams have chronological control by radiocarbon ages. This makes it necessary to create, in the future, more taxonomically and chronologically high-resolution as well as radiometrically well-dated pollen diagrams in the region, preferably along site sequences/toposequences using larger peatlands.

The six main regional vegetation phases identified for the Holocene (*Betula–Pinus* phase, *Corylus* phase, *Picea* phase, *Fagus–Picea* phase, *Abies–Fagus–Picea* phase, anthropogenic vegetation phase) largely correspond to existing older schemes for the Erzgebirge and other low mountain ranges in northern central Europe.

For four vegetation phases, clear differences in the proportion of the main tree taxa can be seen on the basis of the present analyses with regard to both the soil and the altitude. For example, in the *Abies–Fagus–Picea* phase (ca. 4500–1000 cal yr BP) on the prevailing loamy soils and up to about 1000 m a.s.l., *Abies* (max ca. 50 %) dominates followed by *Fagus* (max ca. 40 %). During most times pollen proportions of *Picea* were the highest in the highest altitudes, i.e. above ca. 1000 m a.s.l.

Some pollen diagrams located up to an altitude of ca. 900 m a.s.l. show the presence or even continuous curves of potential pasture and meadow indicators from around 2000 cal BCE at the earliest. Even cereal pollen occurs sporadically already before the High Medieval. However, these signals cannot (currently) be interpreted as unequivocal indicators of widespread prehistoric land use, since no supplementing studies on the influence of a potential long-distance pollen input are available from the area. However, archaeological and geochemical findings show that local mining and metallurgical activities took place even at higher altitudes in the Erzgebirge in the Bronze Age and the Iron Age.

The pollen records show that immediately before the extensive clearing in the High Middle Ages (12th/13th centuries CE) from the submontane (ca. 300–500 m a.s.l.), via the montane (ca. 500–900 m a.s.l.) to the high-montane zone (> ca. 900 m a.s.l.), mixed forests of *Fagus* and *Abies* with a certain proportion of *Picea* grew in most sites in the Erzgebirge. Other tree species (e.g. *Acer*, *Ulmus*, *Pinus*, *Fraxinus*, *Alnus*) also grew in smaller proportions on average but with potentially greater local participation. Natural (mixed) *Picea* forests, however, regularly had a very small proportion only at the highest altitudes (> ca. 900 m a.s.l.).

Despite the large number of pollen diagrams, the moment of local clearing (late 12th to mid-14th centuries CE) and the development of replacement vegetation has so far only been precisely dated and botanically reflected in detail in a few cases. Although the proportions of the main tree species vary significantly in these diagrams, they are basically the same at the moment of clearing, namely *Fagus*, *Abies*, and *Picea*. In some cases, there was not a complete clearing with following agricultural, settlement, or industrial use of the sites but only a forest thinning with an increase in *Picea* and a decrease in *Fagus* and *Abies*.

A few records make it clear that, despite modern disturbances in the geoarchives due to peat extraction, drainage, or overbuilding, there is a high palynological potential for in-depth research also into the more recent vegetation and environmental history of the region, i.e. covering the last ca. 300 years.

Data availability. Data relating to this paper can be found in the Supplement or are available from the corresponding author upon reasonable request.

Supplement. The supplement related to this article is available online at: https://doi.org/10.5194/egqsj-72-127-2023-supplement.

Author contributions. This study was designed by KK and MT. KK and MT wrote the paper; FH provided contributions. All authors read, commented on, and approved the paper.

Competing interests. The contact author has declared that none of the authors has any competing interests.

Disclaimer. Publisher's note: Copernicus Publications remains neutral with regard to jurisdictional claims in published maps and institutional affiliations.

Acknowledgements. The authors would like to thank Inge Eckert (Freiberg) for creating Fig. 1. To estimate PPEs from a mountainous area with the ROPES approach, Petr Kuneš (Prague) kindly provided pollen data from the Černé jezero pollen record (Šumava). We owe proofreading of a previous draft of the paper to Mary Teresa Lavin-Zimmer (Potsdam). We would like to thank Jutta Lechterbeck (Stavanger) and the anonymous reviewer for reviewing our paper. Furthermore, we would like to thank a really large number of German and Czech colleagues from the fields of botany, geosciences, archaeology, and forest sciences who with their findings, discussions, and inspirations made this review paper possible. With particular gratitude, we think of all those who have been researching the Holocene landscape history of the Erzgebirge with great dedication and success for over a 100 years. Our contribution is based on the solid foundation they have laid.

Financial support. Publication costs of the paper were supported within the funding programme Open-Access-Publikationskosten of the Deutsche Forschungsgemeinschaft (DFG) (grant no. 491075472).

The article processing charges for this open-access publication were covered by the Helmholtz Centre Potsdam – GFZ German Research Centre for Geosciences.

Review statement. This paper was edited by Ingmar Unkel and reviewed by Jutta Lechterbeck and one anonymous referee.

References

Abraham, V.: Palynological synthesis for the Czech Republic, Ph.D. thesis, Charles University in Prague, Faculty of Science, Department of Botany, 163 pp., 2014.

Abraham, V., Kuneš, P., Petr, L., Svitavská-Svobodová, H., Kozáková, R., Jamrichová, E., Švarcová, M. G., and Pokorný, P.: A pollen-based quantitative reconstruction of the Holocene vegetation updates a perspective on the natural vegetation in the Czech Republic and Slovakia, Preslia, 88, 409–434, https://www.preslia.cz/P164Abraham.pdf (last access: 25 April 2022), 2016.

Abraham, V., Man, M., Theuerkauf, M., Pokorný, P., Bobek, P., and Novák, J.: Spatially explicit, quantitative reconstruction of past vegetation based on pollen or charcoal data as a tool for autecology of trees, Landscape Ecol., 38, 1747–1763, https://doi.org/10.1007/s10980-023-01652-8, 2023.

Achterberg, I., Frechen, M., Bauerochse, A., Eckstein, J., and Leuschner, H. H.: The Göttingen tree-ring chronologies of peat-preserved oaks and pines from Northwest Germany, Z. Dtsch. Ges. Geowiss., 168, 9–19, https://doi.org/10.1127/zdgg/2016/0042, 2016.

Bałazy, R., Zasada, M., Ciesielski, M., Waraksa, P., and Zawiła-Niedźwiecki, T.: Forest dieback processes in the Central European Mountains in the context of terrain topography and selected stand attributes, For. Ecol. Manage., 435, 106–119, https://doi.org/10.1016/j.foreco.2018.12.052, 2019.

Bartelheim, M. and Niederschlag, E.: Ein Befund zur vorgeschichtlichen Zinngewinnung im Erzgebirge?, Archäologie Aktuell, 4, 60–66, 1997.

Bednářová, E., Böhm, A.-K., Feske, N., Gemballa, R., Hahn, A., Hájková, L., Hanel, M., Hoy, A., Krofta, K., Küchler, W., Kučera, J., Kyselý, J., Lippert, S.-A., Petzold, R., Schöder, L., Seják, J., Skalák, P., Štěpánek, P., Urban, A., Vizina, A., and Zahradníček, P.: Der Klimawandel im böhmisch-sächsischen Grenzraum, Změna klimatu v česko-saském pohraničí, Sächsisches Landesamt für Umwelt, Landwirtschaft und Geologie, Dresden, 140 pp., 2014.

Behre, K.-E.: Landschaftsgeschichte Norddeutschlands, Umwelt und Siedlung von der Steinzeit bis zur Gegenwart, Wachholtz, Neumünster, ISBN 3529024996, 300 pp., 2008.

Behre, K.-E., Brande, A., Küster, H., and Rösch, M.: Germany, in: Palaeoecological Events During the Last 15 000 Years: Regional Syntheses of Palaeoecological Studies of Lakes and Mires in Europe, edited by: Berglund, B. E., Birks, H. J. B., Ralska-Jasiewiczowa, M., and Wright, H. E., Wiley, Chichester, 507–551, ISBN 0471958409, 1996.

Bell, M.: Making one's way in the world: the footprints and trackways of prehistoric people, Oxbow Books, Oxford, https://doi.org/10.2307/j.ctv138wsp4, 2020.

Beug, H.-J.: Franz Firbas, 1902–1964, Taxon 14, 77–83, https://www.jstor.org/stable/1216456 (last access: 15 March 2022), 1965.

Beug, H.-J.: Zum Gedenken an Franz Firbas (1902-1964) anlässlich seines 100. Geburtstages, E&G Quaternary Sci. J., 52, 1–3, https://doi.org/10.3285/eg.52.1.01, 2003.

Beug, H.-J., Henrion, I., and Schmüser, A.: Landschaftsgeschichte im Hochharz, Die Entwicklung der Wälder und Moore seit dem Ende der letzten Eiszeit, Papierflieger, Clausthal-Zellerfeld, ISBN 3897202565, 454 pp., 1999.

Bičík, I. and Štěpánek, V.: Post-war changes of the land-use structure in Bohemia and Moravia: Case study Sudetenland, GeoJournal, 32, 253–259, https://doi.org/10.1007/BF01122117, 1994.

Billig, G. and Geupel, V.: Entwicklung, Form und Datierungen der Siedlungen in der Kammregion des Erzgebirges, Siedlungsforschung: Archäologie – Geschichte – Geographie, 10, 173–194, 1992.

Birks, H. J. B. and Seppä, H.: Late-Quaternary palaeoclimatic research in Fennoscandia – A historical review, Boreas, 39, 655–673, https://doi.org/10.1111/j.1502-3885.2010.00160.x, 2010.

Blažek, J., Černá, E., and Velímský, T.: Zur Siedlungsgeschichte der böhmischen Seite des Erzgebirges, Germania, 73, 463–479, https://doi.org/10.11588/ger.1995.92672, 1995.

Bobek, P., Svobodová-Svitavská, H., Pokorný, P., Šamonil, P., Kuneš, P., Kozáková, R., Abraham, V., Klinerová, T., Švarcová, M. G., Jamrichová, E., Krauseová, E., and Wild, J.: Divergent fire history trajectories in Central European temperate forests revealed a pronounced influence of broadleaved trees on fire dynamics, Quaternary Sci. Rev., 222, 105865, https://doi.org/10.1016/j.quascirev.2019.105865, 2019.

Bohdálková, L., Bohdálek, P., Břízová, E., Pacherová, P., and Kuběna, A. A.: Atmospheric metal pollution records in the Kovářská Bog (Czech Republic) as an indicator of anthropogenic activities over the last three millennia, Sci. Total Environ., 633, 857–874, https://doi.org/10.1016/j.scitotenv.2018.03.142, 2018.

Böhm, A. K.: Hochmoore im Erzgebirge – Untersuchungen zum Zustand und Stoffaustragsverhalten unterschiedlich degradierter Flächen, Ph.D. thesis, Technische Universität Dresden, 200 pp., 2006.

Bramer, H., Hendl, M., Marcinek, J., Nitz, B., Ruchholz, K., and Slobodda, S.: Physische Geographie. Mecklenburg-Vorpommern, Brandenburg, Sachsen-Anhalt, Sachsen, Thüringen, Hermann Haack, Gotha, ISBN 3730108859, 627 pp., 1991.

Brízová, E.: Reconstruction of the vegetational evolution of the Bozí Dar peat bog during Late Glacial and Holocene, Geolines, 2, p. 10, 1995.

Brízová, E.: Das Erzgebirge – Umwelt und Bergbau. in: Silberrausch und Berggeschrey, Archäologie des mittelalterlichen Bergbaus in Sachsen und Böhmen, edited by: Smolnik, R., Beier and Beran, Unterweißbach, 185–192, ISBN 3941171992, 2014a.

Brízová, E.: Erzgebirgische Moorgebiete als ein Archiv zum Studium der menschlichen Auswirkungen auf die Natur, in: ArchaeoMontan 2013. Krusna krajina – Erz(gebirgs)-landschaft – Ore Landscape. Internationale Fachtagung Kadaň 26. bis 28. September 2013, edited by: Smolnik, R., Arbeits- und Forschungsberichte zur sächsischen Bodendenkmalpflege Beiheft, 28, 199–207, Dresden, ISBN 978-3-943770-14-8, 2014b.

Bronk Ramsey, C.: Methods for summarizing radiocarbon datasets, Radiocarbon, 59, 1809–1833, https://doi.org/10.1017/RDC.2017.108, 2017.

Büntgen, U., Tegel, W., Nicolussi, K., McCormick, M., Frank, D., Trouet, V., Kaplan, J. O., Herzig, F., Heussner, K.-U., Wanner, H., Luterbacher, J., and Esper, J.: 2500 years of European climate variability and human susceptibility, Science, 331, 578–582, https://doi.org/10.1126/science.1197175, 2011.

Cappenberg, K., Schubert, M., and Hemker, C.: Landschaftsveränderungen in Montanregionen, Mindestens 900 Jahre "human impact" im Erzgebirge, Mitteilungen der Deutschen Gesellschaft für Archäologie des Mittelalters und der Neuzeit, 33, 179–192, https://doi.org/10.11588/dgamn.2020.0.77903, 2020.

Carter, V. A., Chiverrell, R. C., Clear, J. L., Kuosmanen, N., Moravcová, A., Svoboda, M., Svobodová-Svitavská, H., van Leeuwen, J. F. N., van der Knaap, W. O., and Kuneš, P.: Quantitative palynology informing conservation ecology in the Bohemian/Bavarian forests of Central Europe, Front. Plant Sci., 8, 2268, https://doi.org/10.3389/fpls.2017.02268, 2018.

Cembrzyński, P.: The ecology of mining, Human-environmental relations in the Medieval and Early Modern mining in Central Europe, Kwartalnik Historii Kultury Materialnej, 67, 17–39, https://doi.org/10.23858/KHKM67.2019.1.002, 2019.

Chiarucci, A., Araújo, M. B., Decocq, G., Beierkuhnlein, C., and Fernández-Palacios, J. M.: The concept of potential natural vegetation: an epitaph?, J. Veg. Sci., 21, 1172–1178, https://doi.org/10.1111/j.1654-1103.2010.01218.x, 2010.

Christl, A. and Simon, K.: Nutzung und Besiedlung des sächsischen Erzgebirges und des Vogtlandes bis zur deutschen Ostkolonisation, Germania, 73, 441–479, 1995.

Claire, S.: The Ore Mountains mining area in Bohemia: A reservoir of silver resources in Central Europe in the sixteenth century, Global Environ., 15, 47–70, https://doi.org/10.3197/ge.2022.150103, 2022.

Conedera, M., Tinner, W., Neff, C., Meurer, M., Dickens, F. A., and Krebs, F.: Reconstructing past fire regimes: methods, applications, and relevance to fire management and conservation, Quaternary Sci. Rev., 28, 555–576, https://doi.org/10.1016/j.quascirev.2008.11.005, 2009.

Derner, K. (Ed.): Středověké hornictvi a hutnictvi na Přisecnicku ve středním Krušnohoří. Mittelalterlicher Bergbau und Hüttenwesen in der Region Pressnitz im mittleren Erzgebirge, Veröffentlichungen des Landesamtes für Archäologie Sachsen, 68, Landesamt für Archäologie Sachsen, Dresden, ISBN 978-3-943770-40-7, 496 pp., 2018.

Derner, K., Hrubý, P., and Schubert, M.: Mittelalterliche Silberproduktion im wettinischen und premyslidischen Regierungsraum: Neue archäologische Untersuchungen, Der Anschnitt, Z. Kunst Kultur im Bergbau, 68, 216–241, 2016.

DLR German Aerospace Center: Concern about German forests. Satellite data reveal extensive losses in the forest inventory, 21 February 2022, https://www.dlr.de/content/en/articles/news/2022/01/20220221_concern-about-german-forests.html (last access: 30 December 2022), 2022.

Dreslerová, D., Kozáková, R., Metlička, M., Brychová, V., Bobek, P., Čišecký, Č., Demján, P., Lisá, L., Pokorná, A., Michálek, J., Strouhalová, B., and Trubač, J.: Seeking the meaning of a unique mountain site through a multidisciplinary approach. The Late La Tène site at Sklářské Valley, Šumava Mountains, Czech Republic, Quaternary Int., 542, 88–108, https://doi.org/10.1016/j.quaint.2020.03.013, 2020.

Drude, O.: Der Hercynische Florenbezirk. Grundzüge der Pflanzenverbreitung im mitteldeutschen Berg- und Hügellande vom Harz bis zur Rhön, bis zur Lausitz und dem Böhmer Walde, Pflanzenverbreitung in Mitteleuropa nördlich der Alpen No. 1, Verlag von Wilhelm Engelmann, Leipzig, 671 pp., 1902.

Dudová, L., Hájek, M., Petr, L., and Jankovská, V.: Holocene vegetation history of the Jeseníky Mts: Deepening elevational contrast in pollen assemblages since late prehistory, J. Veg. Sci., 29, 371–381, https://doi.org/10.1111/jvs.12612, 2018.

Edom, F., Dittrich, I., Keßler, K., Münch, A., Peters, R., Theuerkauf, M., and Wendel, D.: Klimatische Stabilität von Mittelgebirgsmooren. Auswirkungen des Klimawandels auf wasserabhängige Ökosysteme – Teilprojekt Erzgebirgsmoore, Schriftenreihe des LfULG, Heft 1/2011, Sächsisches Landesamt für Umwelt, Landwirtschaft und Geologie, Dresden, 1–80, 2011.

Eisenhauer, D. R. and Sonnemann, S.: Waldbaustrategien unter sich ändernden Umweltbedingungen – Leitbilder, Zielsystem und Waldentwicklungstypen, Waldökologie, Landschaftsforschung und Naturschutz, 8, 71–88, 2009.

Ellenberg, H.: Vegetation Mitteleuropas mit den Alpen in ökologischer, dynamischer und historischer Sicht, Ulmer, Stuttgart (5th Edition), ISBN 3800134284, 1095 pp., 1996.

Firbas, F.: Spät- und nacheiszeitliche Waldgeschichte Mitteleuropas nördlich der Alpen. Erster Band: Allgemeine Waldgeschichte, Gustav Fischer, Jena, 480 pp., 1949.

Firbas, F.: Spät- und nacheiszeitliche Waldgeschichte Mitteleuropas nördlich der Alpen. Zweiter Band: Waldgeschichte der einzelnen Landschaften, Gustav Fischer, Jena, 256 pp., 1952.

Firbas, F., Münnich, K. O., and Wittke, W.: C14-Datierungen zur Gliederung der nacheiszeitlichen Waldentwicklung und zum Alter von Rekurrenzflächen im Fichtelgebirge, Flora, 146, 512–520, 1958.

Frenzel, H.: Entwicklungsgeschichte der sächsischen Moore und Wälder seit der letzten Eiszeit auf Grund pollenanalytischer Untersuchungen, Abhandlungen des Sächsischen Geologischen Landesamts, 9, 1–119, 1930.

Friedmann, A., Stojakowits, P., and Korch, O.: History of vegetation and land-use change in the northern Calcareous Alps (Germany/Austria), in: Mountain Landscapes in Transition. Effects of Land Use and Climate Change, edited by: Schickhoff, U., Singh, R. B., Mal, S., Sustainable Development Goals Series, 601–612, https://doi.org/10.1007/978-3-030-70238-0_28, 2022.

Fuchs, Z., Vacek, Z., Vacek, S., and Gallo, J.: Effect of game browsing on natural regeneration of European beech (L.) forests in the Krušné hory Mts. (Czech Republic and Germany), Central European Forestry Journal, 67, 166–180, https://doi.org/10.2478/forj-2021-0008, 2021.

Gdulová, K., Marešová, J., Barták, V., Szostak, M., Cervenka, J., and Moudrý, V.: Use of TanDEM-X and SRTM-C data for detection of deforestation caused by bark beetle in central European mountains, Remote Sens., 13, 3042, https://doi.org/10.3390/rs13153042, 2021.

Giesecke, T. and Brewer, S.: Notes on the postglacial spread of abundant European tree taxa, Veg. Hist. Archaeobot., 27, 337–349, https://doi.org/10.1007/s00334-017-0640-0, 2018.

Giesecke, T., Bennett, K. D., Birks, H. J. B., Bjune, A. E., Bozilova, E., Feurdean, A., Finsinger, W., Froyd, C., Pokorný, P., Rösch, M., Seppä, H., Tonkov, S., Valsecchi, V., and Wolters, S.: The pace of Holocene vegetation change – testing for synchronous developments, Quaternary Sci. Rev., 30, 2805–2814, https://doi.org/10.1016/j.quascirev.2011.06.014, 2011.

Giesecke, T., Wolters, S., Jahns, S., and Brande, A.: Exploring Holocene changes in palynological richness in northern Europe – Did Postglacial immigration matter?, PLoS ONE, 7, e51624, https://doi.org/10.1371/journal.pone.0051624, 2012.

Giesecke, T., Brewer, S., Finsinger, W., Leydet, M., and Bradshaw, R. H.: Patterns and dynamics of European vegetation change over the last 15,000 years, J. Biogeogr., 44, 1441–1456, https://doi.org/10.1111/jbi.12974, 2017.

Glaser, R.: Klimageschichte Mitteleuropas: 1200 Jahre Wetter, Klima, Katastrophen, Wissenschaftliche Buchgesellschaft, Darmstadt, ISBN 3896786040, 277 pp., 2008.

Grober, U.: Sustainability: A Cultural History, Green Books, Totnes/Devon, ISBN 0857840452, 224 pp., 2012.

Gross, H.: Zwei bemerkenswerte begrabene Moorböden aus dem Gebiet von Hainichen in Sachsen, Berichte der Geologischen Gesellschaft, 3, 209–218, 1958.

Großer, K. H., Wolters, S., and Schaarschmidt, J.: Das Hochmoor bei Jahnsgrün im Erzgebirge, Naturschutzarbeit in Sachsen, 48, 41–52, 2006.

Grunewald, K. and Bastian, O.: Ecosystem assessment and management as key tools for sustainable landscape development: a case study of the Ore Mountains region in Central Europe, Ecol. Model., 295, 151–162, https://doi.org/10.1016/j.ecolmodel.2014.08.015, 2015.

Hahne, J.: Untersuchungen zur spät und postglazialen Vegetationsgeschichte im nordöstlichen Bayern (Bayerisches Vogtland, Fichtelgebirge, Steinwald), Flora, 187, 169–200, 1992.

Hansell, F.: Mineral extractive industries in the context of European world heritage cultural landscape conservation and management: The case study of the Erzgebirge/Krušnohoří mining region, in: 50 Years World Heritage Convention: Shared Responsibility – Conflict & Reconciliation, edited by: Albert, M. T., Bernecker, R., Cave, C., Prodan, A. C., and Ripp, M., Heritage Studies, Springer, Cham, 321–333, https://doi.org/10.1007/978-3-031-05660-4_25, 2022.

Hauswald, K. and Simon, K.: Der Kulmer Steig vor dem Mittelalter. Zu den ältesten sächsisch-böhmischen Verkehrswegen über das Osterzgebirge, Arbeits- und Forschungsberichte zur sächsischen Bodendenkmalpflege, 37, 9–98, 1995.

Heinrich, W. and Lange, E.: Ein Beitrag zur Kenntnis der Waldgeschichte des Thüringisch-Sächsischen Vogtlandes, Feddes Repertorium, 80, 437–462, 1969.

Hemker, C.: New insights on mining archaeology in the Erzgebirge (Ore Mountains), World of Mining – Surface & Underground, 70, 409–416, 2018.

Hempel, W.: Die Pflanzenwelt Sachsens von der Späteiszeit bis zur Gegenwart, Weissdorn-Verlag, Jena, ISBN 9783936055573, 248 pp., 2009.

Hengst, K.: Erzgebirge/Krušné hory im Spiegel der Sprache seit etwa 3000 Jahren. "Hercynia silva – Fergunna – Miriquidi – Böhmerwald – Erzgebirge". in: Erzgebirge – Heimat und domov. 8. Deutsch-Tschechischen Begegnungsseminar Gute Nachbarn –

Schlechte Nachbarn?, edited by: Mehnert, E. and Lang, P., Frankfurt am Main, 71–79, ISBN 3631550278, 2006.

Henkner, J., Ahlrichs, J., Fischer, E., Fuchs, M., Knopf, T., Rösch, M., Scholten, T., and Kühn, P.: Land use dynamics derived from colluvial deposits and bogs in the Black Forest, Germany, J. Plant Nutr. Soil Sci., 18, 240–260, https://doi.org/10.1002/jpln.201700249, 2018.

Herbig, C.: "O mensch zart, bedenck der blumen art". Pflanzliche Großreste aus archäologischen Befunden als Indizien für Ernährung, Landwirtschaft und Umwelt in mittelalterlichen Bergstädten im Erzgebirge, in: Leben und Tod in einer Bergstadt. Die Welterbe-Bestandteile Dippoldiswalde, Freiberg, Annaberg und Marienberg im Spiegel archäologischer, archäobotanischer und anthropologischer Studien, edited by: Smolnik, R., Veröffentlichungen des Landesamtes für Archäologie Sachsen, 78, Landesamt für Archäologie Sachsen, Dresden, 137–167, ISBN 978-3-943770-63-6, 2022.

Heynert, H.: Zur Ursprünglichkeit des Tannen-Höhenkiefernwaldes im westlichsten Sächsischen Erzgebirge und seinem Vorlande, Drudea, 1, 5–24, 1961.

Heynert, W.: Das Pflanzenleben des hohen Westerzgebirges. Ein Beitrag zur Geobotanik des Westerzgebirges, Theodor Steinkopff, Dresden and Leipzig, 141 pp., 1964.

Hoffmann, Y. and Heußner, K.-U.: Die Errichtung der romanischen Kirche zu Raschau und der Zeitpunkt der bäuerlichen Kolonisation im oberen Erzgebirge, Sächsische Heimatblätter, 59, 253–261, 2013.

Hölzer, A. and Hölzer, A.: Untersuchungen zum Rezentpollenniederschlag im Nordschwarzwald im Bereich der Hornisgrinde, standort.wald – Mitteilungen des Vereins für forstliche Standortskunde und Forstpflanzenzüchtung, 48, 63–76, 2014.

Houfková, P., Bešta, T., Bernardová, A., Vondrák, D., Pokorný, P., and Novák, J.: Holocene climatic events linked to environmental changes at Lake Komořany Basin, Czech Republic, The Holocene, 27, 1–14, https://doi.org/10.1177/0959683616683250, 2017.

Houfková, P., Horák, H., Pokorná, A., Bešta, T., Pravcová, I., Novák, J., and Klír, T.: The dynamics of a non-forested stand in the Krušné Mts.: the effect of a short-lived medieval village on the local environment, Veg. Hist. Archaeobot., 28, 607–621, https://doi.org/10.1007/s00334-019-00718-5, 2019.

Hrubý, P.: Erzbergbau und Edelmetallproduktion im böhmischen Königreich während des 13. Jhs. im Kontext der europäischen Montanarchäologie, Veröffentlichungen des Landesamtes für Archäologie Sachsen, 71, Landesamt für Archäologie Sachsen, Dresden, ISBN 978-3-943770-55-1, 248 pp., 2021.

Hrubý, P., Hejhal, P., Malý, K., Kočár, P., and Petr, L.: Centrální Českomoravská vrchovina na prahu vrcholného středověku: archeologie, geochemie a rozbory sedimentárních výplní niv, Masarykova Univerzita, Brno, ISBN 978-80-210-7126-1, 270 pp., 2014.

ICOMOS: International Council on Monuments and Sites: Advisory Body Evaluation. Erzgebirge/Krušnohoří (Germany/Czechia) No 1478, https://whc.unesco.org/en/list/1478/documents/ (last access: 27 January 2022), 2019.

Jacob, H.: Waldgeschichtliche Untersuchungen im Tharandter Gebiet, Feddes Repertorium Beiheft, 137, 183–275, 1956.

Jacob, H.: Pollenanalysen aus dem Gebiet des ehemaligen Göttwitzer Sees bei Mutzschen, Kr. Grimma. Ein Beitrag zur Entwicklung von Vegetation und Klima seit der Bronzezeit, Arbeits- und Forschungsberichte zur sächsischen Bodendenkmalpflege, 19, 159–175, 1971.

Jankovská, V.: Pollenanalysen der mittelalterlichen Ablagerungen in dem Moster Gebiet. Památky Archeologické, 86, 132–154, 1995.

Jankovská, V. and Pokorný, P.: Reevaluation of the palaeoenvironmental record of the former Komořanské jezero lake: Late-Glacial and Holocene palaeolimnology and vegetation development in north-western Bohemia, Czech Republic, Preslia, 85, 265–287, 2013.

Jankovská, V., Kunes, P., and van der Knaap, W. O.: Flaje-Kiefern (Krušné Hory Mountains): Late Glacial and Holocene vegetation development, Grana, 46, 214–216, https://doi.org/10.1080/00173130701526341, 2007.

Jaroslav, M.: Reconstructed natural versus potential natural vegetation in vegetation mapping-a discussion of concepts, Appl. Veg. Sci., 1, 173–176, https://doi.org/10.2307/1478946, 1998.

Jouffroy-Bapicot, I., Vannière, B., Gauthier, É., Richard, H., Monna, F., and Petit, C.: 7000 years of vegetation history and land-use changes in the Morvan Mountains (France): A regional synthesis, The Holocene, 23, 1888–1902, https://doi.org/10.1177/0959683613508161, 2013.

Kaiser, K., Hrubý, P., Tolksdorf, J. F., Alper, G., Herbig, C., Kočár, P., Petr, L., Schulz, L., and Heinrich, I.: Cut and covered: Subfossil trees in buried soils reflect medieval forest composition and exploitation of the central European uplands, Geoarchaeology, 35, 42–62, https://doi.org/10.1002/gea.21756, 2020a.

Kaiser, K., Schneider, T., Küster, M., Dietze, E., Fülling, A., Heinrich, S., Kappler, C., Nelle, O., Schult, M., Theuerkauf, M., Vogel, S., de Boer, A. M., Börner, A., Preusser, F., Schwabe, M., Ulrich, J., Wirner, M., and Bens, O.: Palaeosols and their cover sediments of a glacial landscape in northern central Europe: Spatial distribution, pedostratigraphy and evidence on landscape evolution, Catena, 193, 104647, https://doi.org/10.1016/j.catena.2020.104647, 2020b.

Kaiser, K., Tolksdorf, J. F., de Boer, A. M., Herbig, C., Hieke, F., Kasprzak, M., Kočár, P., Petr, L., Schubert, M., Schröder, F., Fülling, A., and Hemker, C.: Colluvial sediments originating from past land-use activities in the Erzgebirge Mountains, Central Europe: occurrence, properties and historic environmental implications, Archaeol. Anthropol. Sci., 13, 220, https://doi.org/10.1007/s12520-021-01469-z, 2021.

Kašpar, J., Tumajer, J., Šamonil, P., and Vašíčková, I.: Species-specific climate-growth interactions determine tree species dynamics in mixed Central European mountain forests, Environ. Res. Lett., 16, 034039, https://doi.org/10.1088/1748-9326/abd8fb, 2021.

Käubler, R.: Vergleichende Betrachtungen zu geomorphologischen Ergebnissen im höchsten Teil des Erzgebirges, Hercynia, 6, 109–114, 1969.

Kenzler, H.: Die hoch- und spätmittelalterliche Besiedlung des Erzgebirges: Strategien zur Kolonisation eines landwirtschaftlichen Ungunstraumes, Bamberger Schriften zur Archäologie des Mittelalters und der Neuzeit, 4. Habelt, Bonn, ISBN 978-3-7749-3742-0, 452 pp., 2012.

Kienitz, E.: Wandlung des Holzartenbildes im sächsischen Staatswalde seit dem 16. Jahrhundert, mit Ausblicken auf die Pollenanalyse (Forstinspektionsbezirke Eibenstock und

Grimma), Tharandter Forstliches Jahrbuch, 87, 285–326, 413–448, 459–523, 641–690, 747–799, 824–853, 1936.

Kleber, A., Terhorst, B., Bullmann, H., Hülle, D., Leopold, M., Müller, S., Raab, T., Sauer, D., Scholten, T., Dietze, M., Felix-Henningsen, P., Heinrich, J., Spies, E.-D., and Thiemeyer, H.: Subdued mountains of Central Europe, in: Mid-Latitude Slope Deposits (Cover Beds), edited by: Kleber, A. and Terhorst, B., Developments in Sedimentology, 66, Elsevier, Amsterdam, 9–93, https://doi.org/10.1016/B978-0-444-53118-6.00002-7, 2013.

Knapp, H., Robin, V., Kirleis, W., and Nelle, O.: Woodland history in the upper Harz Mountains revealed by kiln site, soil sediment and peat charcoal analyses, Quaternary Int., 289, 88–100, https://doi.org/10.1016/j.quaint.2012.03.040, 2013.

Knapp, H. D., Klaus, S., and Fähser, L.: Der Holzweg. Wald im Widerstreit der Interessen, Oekom, München, ISBN 978-3-96238-266-7, 480 pp., 2021.

Kočár, P., Petr, L., and Kočárová, R.: Vegetationswandel im Bergrevier Preßnitz. in: Mittelalterlicher Bergbau und Hüttenwesen in der Region Preßnitz im mittleren Erzgebirge. Středověké hornictvi a hutnictvi na Přisecnicku ve středním Krušnohoří, edited by: Derner, K., Veröffentlichungen des Landesamtes für Archäologie Sachsen, 68, Landesamt für Archäologie Sachsen, Dresden, 67–78, ISBN 978-3-943770-40-7, 2018.

Kölling, C., Zimmermann, L., and Walentowski, H.: Klimawandel: Was geschieht mit Buche und Fichte?, AFZ-Der Wald, 11/2007, 584–588, 2007.

Kozáková, R., Pokorný, P., Peša, V., Danielisová, A., Čuláková, K., and Svobodová, H. S.: Prehistoric human impact in the mountains of Bohemia. Do pollen and archaeological data support the traditional scenario of a prehistoric "wilderness"?, Rev. Palaeobot. Palynol., 220, 29–43, https://doi.org/10.1016/j.revpalbo.2015.04.008, 2015.

Kozáková, R., Bobek, P., Dreslerová, D., Abraham, V., and Svobodová-Svitavská, H.: The prehistory and early history of the Šumava Mountains (Czech Republic) as seen through anthropogenic pollen indicators and charcoal data, The Holocene, 31, 145–159, https://doi.org/10.1177/0959683620961484, 2022.

Kreienbrink, F., Döhlert-Albani, N., Conrad, M., Herbig, C., Martin, I., Schubert, M., Tinapp, C., Hößler, R., Johl, S., Krämer, U., Mauksch, K., Priske, C., and Stäuble, H.: Von der Großenhainer Pflege übers Elbtal ins Erzgebirge. Die Ausgrabungen an der EUGAL, Ausgrabungen in Sachsen, 7, 134–149, 2020.

Krutzsch, H.: Waldaufbau, Deutscher Bauernverlag, Berlin, 159 pp., 1952.

Kubíková, J.: Forest dieback in Czechoslovakia, Vegetatio, 93, 101–108, https://doi.org/10.1007/BF00033204, 1991.

Kulakowski, D., Seidl, R., Holeksa, J., Kuuluvainen, T., Nagel, T. A., Panayotov, M., Svoboda, M., Thorn, S., Vacchiano, G., Whitlock, C., Wohlgemuth, T., and Bebi, P.: A walk on the wild side: Disturbance dynamics and the conservation and management of European mountain forest ecosystems, For. Ecol. Manage., 388, 120–131, https://doi.org/10.1016/j.foreco.2016.07.037, 2017.

Kupková, L., Potůčková, M., Lhotáková, Z., and Albrechtová, J.: Forest cover and disturbance changes, and their driving forces: A case study in the Ore Mountains, Czechia, heavily affected by anthropogenic acidic pollution in the second half of the 20th century, Environ. Res. Lett., 13, 095008, https://doi.org/10.1088/1748-9326/aadd2c, 2018.

Küssner, R. and Mosandl, R.: Conceptions for converting the forests in the Ore Mts. into ecologically managed ecosystems. in: SO_2-pollution and forest decline in the Ore Mountains, edited by: Lomsky, B., Materna, J., and Pfanz, H., Forestry and Game Management Research Institute, Jiloviste-Strnady, Czech Republic, 326–342, 2002.

Landestalsperrenverwaltung des Freistaates Sachsen: Eine Zeitreise in die sächsische Wasserwirtschaft, Pirna, 2017.

Lang, G.: Quartäre Vegetationsgeschichte Europas, Fischer, Jena, ISBN 3334604055, 462 pp., 1994.

Lang, G.: Seen und Moore des Schwarzwaldes als Zeugen spätglazialen und holozänen Vegetationswandels. Stratigraphische, pollenanalytische und großrestanalytische Untersuchungen, Andrias, 16, Staatliches Museum für Naturkunde, Karlsruhe, 166 pp., 2005.

Lange, E. and Heinrich, W.: Floristische und vegetationskundliche Beobachtungen auf dem MTB Frankenberg/Sa. [5044], Hercynia, 7, 53–86, 1970.

Lange, E., Jeschke, L., and Knapp, H. D.: Ralswiek und Rügen. Landschaftsentwicklung und Siedlungsgeschichte der Ostseeinsel. Teil I Die Landschaftsgeschichte der Insel Rügen seit dem Spätglazial, Schriften zur Ur- und Frühgeschichte, 38, Akademie Verlag, Berlin, ISBN 311257463X, 194 pp., 1986.

Lange, E., Christl, A., and Joosten, H.: Ein Pollendiagramm aus der Mothäuser Heide im oberen Erzgebirge unweit des Grenzüberganges Reitzenhain, in: Kirche und geistiges Leben im Prozess des mittelalterlichen Landesausbaus in Ostthüringen/Westsachsen, edited by: Sachenbacher, P., Beiträge zur Frühgeschichte und zum Mittelalter Ostthüringens, 2, Beier & Beran, Langenweißbach, 153–169, ISBN 978-3-937517-04-9, 169 pp., 2005.

Lauterbach, K.: Vom Grenzwald zur Grenzlinie. Zur Entstehung der sächsisch-böhmischen Grenze, Sächsische Heimatblätter, 64, 104–108, https://doi.org/10.52410/shb.Bd.64.2018.H.2.S.104-108, 2018.

Loidi, J., del Arco, M., Pérez de Paz, P.L., Asensi, A., Díez Garretas, B., Costa, M., Díaz González, T., Fernández-González, F., Izco, J., Penas, Á., Rivas-Martínez, S., and Sánchez-Mata, D.: Understanding properly the 'potential natural vegetation' concept, J. Biogeogr. 37, 2209–2211, https://doi.org/10.1111/j.1365-2699.2010.02302.x, 2010.

Ludemann, T.: Past fuel wood exploitation and natural forest vegetation in the Black Forest, the Vosges and neighbouring regions in western Central Europe, Palaeogeogr. Palaeoclimatol. Palaeoecol., 291, 154–165, https://doi.org/10.1016/j.palaeo.2009.09.013, 2010.

Luterbacher, J., Werner, J. P., Smerdon, J. E., Fernández-Donado, L., González-Rouco, F. J., Barriopedro, D., Ljungqvist, F. C., Büntgen, U., Zorita, E., Wagner, S., Esper, J., McCarroll, D., Toreti, A., Frank, D., Jungclaus, J. H., Barriendos, M., Bertolin, C., Bothe, O., Brázdil, R., Camuffo, D., Dobrovolný, P., Gagen, M., García-Bustamante, E., Ge, Q., Gómez-Navarro, J. J., Guiot, J., Hao, Z., Hegerl, G. C., Holmgren, K., Klimenko, V. V., Martín-Chivelet, J., Pfister, C., Roberts, N., Schindler, A., Schurer, A., Solomina, O., von Gunten, L., Wahl, E., Wanner, H., Wetter, O., Xoplaki, E., Yuan, N., Zanchettin, D., Zhang, H., and Zerefos, C.: European summer temperatures since Roman times, Environ. Res. Lett., 11, 024001, https://doi.org/10.1088/1748-9326/11/2/024001, 2016.

Marešová, P.: Human impact as reflected in the pollen record, with a focus on the Middle Ages, Ph.D. thesis, Thesis Series, No. 7., University of South Bohemia, Faculty of Science, School of Doctoral Studies in Biological Sciences, České Budějovice, 167 pp., 2022.

Miras, Y., Mariani, M., Ledger, P., Mayoral, A., Chassiot, L., and Lavrieux, M.: Holocene vegetation dynamics and first land-cover estimates in the Auvergne Mountains (Massif Central, France): Key tools to landscape management, Interdisciplinaria Archaeologica – Natural Sciences in Archaeology, 9, 179–190, http://iansa.eu/papers/IANSA-2018-02-miras.html (last access: 20 January 2022), 2018.

Möller, A.: Der Dauerwaldgedanke – Sein Sinn und seine Bedeutung, in: Kommentierter Reprint 1990, edited by: Bode, W., Oberteuringen, Degreif Verlag, 1922.

Morel, A. C. and Nogué, S.: Combining contemporary and paleoecological perspectives for estimating forest resilience, Front. Forests Global Change, 2, 57, https://doi.org/10.3389/ffgc.2019.00057, 2019.

Mrotzek, A., Couwenberg, J., Theuerkauf, M., and Joosten, H.: MARCO POLO – A new and simple tool for pollen-based stand-scale vegetation reconstruction, The Holocene, 27, 321–330, https://doi.org/10.1177/0959683616660171, 2017.

Neubauer, G.: Rekonstruktion der Nutzungsgeschichte einer Waldfläche an der Sauschwemme bei Johanngeorgenstadt (Erzgebirgskreis) anhand der Untersuchung von Holzkohle aus historischen Meilern, MSc. thesis, Institut für Waldwachstum und Forstliche Informatik, Technische Universität Dresden, 99 pp., 2022.

Neumann, M., Mues, V., Moreno, A., Hasenauer, H., and Seidl, R.: Climate variability drives recent tree mortality in Europe, Global Chang. Biol., 23, 4788–4797, https://doi.org/10.1111/gcb.13724, 2017.

Novak, M., Brizova, E., Adamova, M., Erbanova, L., and Bottrell, S. H.: Accumulation of organic carbon over the past 150 years in five freshwater peatlands in western and central Europe, Sci. Total Environ., 390, 425–436, https://doi.org/10.1016/j.scitotenv.2007.10.011, 2008.

Nožička, J.: Proměnylesů a vývoj lesního hospodaření v Krusnohorí do r. 1848 [Die Änderung des Waldbestandes und die Entwicklung der Forstwirtschaft im Erzgebirge bis 1848], Rozprav y Československé Akademie Včd. flada matematických a přírodních véd, 72 (3), Praha, 113 pp., 1962.

Overbeck, F. and Griéz, I.: Mooruntersuchungen zur Rekurrenzflächenfrage und Siedlungsgeschichte in der Rhön, Flora, 141, 51–99, 1954.

Parker, A. G., Goudie, A. S., Anderson, D. E., Robinson, M. A., and Bonsall, C.: A review of the mid-Holocene elm decline in the British Isles, Prog. Phys. Geog., 26, 1–45, https://doi.org/10.1191/0309133302pp323ra, 2002.

Peschel, A. and Wetzel, M.: Naturraum Erzgebirge, in: Erzgebirge, edited by: Schattkowsky, M., Kulturlandschaften Sachsens Band 3, Edition Leipzig, Leipzig, 9–26, 2010.

Piekalski, J. (Ed.): Historyczny krajobraz kulturowy zachodnich Sudetów, Wstęp do badań. Instytut Archeologii Uniwersytetu Wrocławskiego, Wrocław, ISBN 978-83-614116-78-4, 724 pp., 2020.

Piovesan, G., Mercuri, A. M., and Mensing, S. A.: The potential of paleoecology for functional forest restoration planning: lessons from Late Holocene Italian pollen records, Plant Biosyst., 152, 508–514, https://doi.org/10.1080/11263504.2018.1435582, 2018.

Raab, T., Raab, A., Bonhage, A., Schneider, A., Hirsch, F., Birkhofer, K., Drohan, P., Wilmking, M., Kreyling, J., Malik, I., Wistuba, M., van der Maaten, E., van der Maaten-Theunissen, M., and Urich, T.: Do small landforms have large effects? A review on the legacies of pre-industrial charcoal burning, Geomorphology, 413, 108332, https://doi.org/10.1016/j.geomorph.2022.108332, 2022.

Rösch, M.: Land use and food production in Central Europe from the Neolithic to the Medieval period: Change of landscape, soils and agricultural systems according to archaeobotanical data, in: Economic archaeology: from structure to performance in European archaeology, edited by: Kerig, T. and Zimmermann, A., Habelt, Bonn, 109–127, 2013.

Rösch, M.: *Abies alba* and *Homo sapiens* in the Schwarzwald – a difficult story, Interdisciplinaria Archaeologica, 6, 47–62, http://iansa.eu/papers/IANSA-2015-01-roesch.pdf (last access: 13 March 2021), 2015.

Rösch, M.: Long-term human impact as registered in an upland pollen profile from the southern Black Forest, southwestern Germany, Veg. Hist. Archaeobot., 9, 205–218, https://doi.org/10.1007/BF01294635, 2000.

Rudolph, K.: Die bisherigen Ergebnisse der botanischen Mooruntersuchungen in Böhmen, Beihefte zum Botanischen Centralblatt, 45, Abt. II, 1–180, 1928.

Rudolph, K. and Firbas, F.: Pollenanalytische Untersuchungen böhmischer Moore (Vorläufige Mitteilung), Berichte der deutschen botanischen Gesellschaft, 40, 393–405, 1922.

Rudolph, K. and Firbas, F.: Paläofloristische und stratigraphische Untersuchungen böhmischer Moore. Die Hochmoore des Erzgebirges. Ein Beitrag zur postglazialen Waldgeschichte Böhmens, Beihefte zum Botanischen Centralblatt, 41, Abt. II, 1–162, 1924.

Rutkiewicz, P., Malik, I., Wistuba, M., and Osika, A.: High concentration of charcoal hearth remains as legacy of historical ferrous metallurgy in southern Poland, Quaternary Int., 512, 133–143, https://doi.org/10.1016/j.quaint.2019.04.015, 2019.

Ruttkowski, M.: Altstraßen im Erzgebirge. Archäologische Denkmalinventarisation Böhmischer Steige, Arbeits- und Forschungsberichte zur sächsischen Bodendenkmalpflege, 44, 264–297, 2002.

Sächsische Landesstiftung Natur und Umwelt: Praktischer Moorschutz im Naturpark Erzgebirge/Vogtland und Beispiele aus anderen Gebirgsregionen: Methoden, Probleme, Ausblick, Lausitzer Druck- und Verlagshaus, Bautzen, 93 pp., 2007.

Sächsisches Staatsministerium für Umwelt und Landwirtschaft: Naturschutzgebiete in Sachsen, Dresden, 720 pp., 2008.

Sadovnik, M., Csaplovics, E., and Heynowski, R.: Palaeoecology and geoinformatics for landscape archaeological monitoring in support of heritage documentation in the Ore Mountains, in: Proceedings International Conference Mining Cultural Landscape Krušnohory/Erzgebirge and its nomination for the UNESCO World Heritage List, National Technical Museum in Prague, 11–12 November 2013, 1–13, 2013.

Schafstall, N., Kuosmanen, N., Kuneš, P., Svobodová, H. S., Svitok, M., Chiverrell, R. C., Halsall, K., Fleischer, P., Knížek, M., and Clear, J. L.: Sub-fossil bark beetles as indicators of past disturbance events in temperate *Picea* *abies* mountain forests, Quaternary Sci. Rev., 275, 107289, https://doi.org/10.1016/j.quascirev.2021.107289, 2022.

Scheithauer, J. and Grunewald, K.: Saurer Regen und Waldsterben im ehemaligen Schwarzen Dreieck (Osterzgebirge), in: Ökologische Problemräume Deutschlands, edited by: Zepp, H., Wissenschaftliche Buchgesellschaft, Darmstadt, 111–132, 2007.

Schlöffel, M.: Die postglaziale Waldgeschichte der Lehmheide. Rekonstruktion spät- und postglazialer Umweltbedingungen an einem Torfprofil aus dem Erzgebirge, Arbeits- und Forschungsberichte zur sächsischen Bodendenkmalpflege 51/52, 9–27, 2011.

Schmeidl, H.: Beitrag zur Frage des Grenzhorizontes im Sebastiansberger Hochmoor, Beihefte zum Botanischen Centralblatt, 40, Abt. II, 493–524, 1940.

Schmidt, M., Mölder, A., Schönfelder, E., Engel, F., and Fortmann-Valtink, W.: Charcoal kiln sites, associated landscape attributes and historic forest conditions: DTM-based investigations in Hesse (Germany), For. Ecosyst., 3, 8, https://doi.org/10.1186/s40663-016-0067-6, 2016.

Schmidt, P. A.: Veränderung der Flora und Vegetation von Wäldern unter Immissionseinfluß, Forstwiss. Cent.bl., 112, 213–224, https://doi.org/10.1007/BF02742150, 1993.

Schmidt, P. A., Hempel, W., Denner, M., Döring, N., Gnüchtel, A., Walter, B., and Wendel, D.: Potentielle Natürliche Vegetation Sachsens mit Karte 1 : 200 000, Materialien zu Naturschutz und Landschaftspflege, 2002, Sächsisches Landesamt für Umwelt und Geologie, Radebeul, 230 pp., 2002.

Schreiber, H.: Die Moore und die Torfgewinnung im Erzgebirge, Arbeiten der deutschen Sektion des Landeskulturrates für Böhmen, 28, 1–45, 1921.

Schreg, R.: Uncultivated landscapes or wilderness? Early medieval land use in low mountain ranges and flood plains of Southern Germany, Eur. J. Post-Class. Archaeol., 4, 69–98, http://www.postclassical.it/PCA_vol.4_files/PCA4_Schreg.pdf (last access: 9 June 2021), 2014.

Schubert, M.: Archäologische und naturwissenschaftliche Untersuchungen in den mittelalterlichen Bergbaustädten Dippoldiswalde und Freiberg, Acta rerum naturalium, 21, 125–140, https://actarerumnaturalium.cz/wp-content/uploads/2019/12/archiv_2017-21_10.pdf (last access: 29 May 2022), 2017.

Schubert, M. and Herbig, C.: Buntmetallurgische Prozesse aus mittelalterlichen Bergbausiedlungen im internationalen Vergleich mit einem Ausblick auf die (exquisiten) Ernährungsgewohnheiten der Dippoldiswalder und Freiberger Bergleute, Mitteilungen der Deutschen Gesellschaft für Archäologie des Mittelalters und der Neuzeit, 30, 195–208, 2017.

Schuldt, B., Buras, A., Arend, M., Vitasse, Y., Beierkuhnlein, C., Damm, A., Gharun, M., Grams, T. E. E., Hauck, M., Hajek, P., Hartmann, H., Hiltbrunner, E., Hoch, G., Holloway-Phillips, M., Körner, C., Larysch, E., Lübbe, T., Nelson, D. B., Rammig, A., Rigling, A., Rose, L., Ruehr, N., Schumann, K., Weiser, F., Werner, C., Wohlgemuth, T., Zang, C. S., and Kahmen, A.: A first assessment of the impact of the extreme 2018 summer drought on Central European forests, Basic Appl. Ecol., 45, 86–103, https://doi.org/10.1016/j.baae.2020.04.003, 2020.

Schwabenicky, W.: Der mittelalterliche Silberbergbau im Erzgebirgsvorland und im westlichen Erzgebirge unter besonderer Berücksichtigung der Ausgrabungen in der wüsten Bergstadt Bleiberg bei Frankenberg, Verlag Klaus Gumnior, Chemnitz, ISBN 3937386203, 258 pp., 2009.

Sebastian, U.: Die Geologie des Erzgebirges, Springer Spektrum, Berlin-Heidelberg, ISBN 3827429765, 279 pp., 2013.

Segers-Glocke, C. and Witthöft, H. (Eds.): Aspects of mining and smelting in the upper Harz Mountains (up to the 13th/14th century) – In the early times of a developing European culture and economy, Sachüberlieferung und Geschichte, 33, Scripta Mercaturae Verlag, St. Katharinen, ISBN 978-3-89590-101-0, 168 pp., 2000.

Seifert-Eulen, M.: Die Moore des Erzgebirges und seiner Nordabdachung, Vegetationsgeschichte ausgewählter Moore, Geoprofil, 14, 4–78, 2016.

Seim, A., Marquer, L., Bisson, U., Hofmann, J., Herzig, F., Kontic, R., Lechterbeck, J., Muigg, B., Neyses-Eiden, M., Rzepecki, A., Rösch, M., Walder, F., Weidemüller, J., and Tegel, W.: Historical spruce abundance in Central Europe: A combined dendrochronological and palynological approach, Front. Ecol. Evol., 10, 909453, https://doi.org/10.3389/fevo.2022.909453, 2022.

Sigismund, B.: Lebensbilder vom Sächsischen Erzgebirge, Lorck, Leipzig, 136 pp., 1859.

Slobodda, S.: Entstehung, Nutzungsgeschichte, Pflege- und Entwicklungsgrundsätze für erzgebirgische Hochmoore, in: Ökologie und Schutz der Hochmoore im Erzgebirge, edited by: Sächsische Akademie für Natur und Umwelt, Dresden, 10–30, 1998.

Słowiński, M., Lamentowicz, M., Łuców, D., Barabach, J., Brykała, D., Tyszkowski, S., Pieńczewska, A., Śnieszko, Z., Dietze, E., Jażdżewski, K., Obremska, M., Ott, F., Brauer, A., and Marcisz, K.: Paleoecological and historical data as an important tool in ecosystem management, J. Environ. Manage., 236, 755–768, https://doi.org/10.1016/j.jenvman.2019.02.002, 2019.

SMEKUL – Sächsisches Staatsministerium für Energie, Klimaschutz, Umwelt und Landwirtschaft (Ed.): Waldzustandsbericht 2020, Dresden, 63 pp., 2020.

Spehr, R.: Die Wüstung Warnsdorf im Tharandter Wald, Mitteilungen des Freiberger Altertumsvereines 91, 5–62, 2002.

Spitzer, J. M.: Dendrochronologische Untersuchungen von Jahrringbreiten an *Pinus rotundata* in der Mothhäuser Haide, Diploma thesis, Institut für Allgemeine Ökologie und Umweltschutz, Technische Universität Dresden, 78 pp., 2010.

Šrámek, V., Slodičák, M., Lomský, B., Balcar, V., Kulhavý, J., Hadaš, P., Pulkráb, K., Šišák, L., Pěnička, L., and Sloup, M.: The Ore Mountains: Will successive recovery of forests from lethal disease be successful?, Mt. Res. Dev., 28, 216–221, https://doi.org/10.1659/mrd.1040, 2008.

Staatsbetrieb Sachsenforst (Ed.): Exkursionsführer zur AFSV-Jahrestagung 2017. Standortswandel und Waldumbau im Oberen Erzgebirge, Pirna, 119 pp., 2017.

Stebich, M. and Litt, T.: Das Georgenfelder Hochmoor – ein Archiv für Vegetations-, Siedlungs- und Bergbaugeschichte, Leipziger Geowissenschaften, 5, 209–216, 1997.

Stojakowits, P. and Friedmann, A.: Anthropogene Einflussnahme in den Hochlagen des Bayerischen Waldes. Aussagen aufgrund der bisherigen Pollenanalysen, Fines Transire, 28, 175–185, 2019.

Suda, T.: Historie vegetace Chebské pánve ze sedimentárního záznamu lokality SOOS, Diploma thesis, Univerzita Karlova v Praze, Prague, 65 pp., 2012.

Sugita, S.: Theory of quantitative reconstruction of vegetation I: pollen from large sites REVEALS regional vegetation composition, The Holocene, 17, 229–241, https://doi.org/10.1177/0959683607075837, 2007a.

Sugita, S.: Theory of quantitative reconstruction of vegetation II: all you need is LOVE, The Holocene, 17, 243–257, https://doi.org/10.1177/0959683607075838, 2007b.

Theuerkauf, M. and Couwenberg, J.: The extended downscaling approach: A new R-tool for pollen-based reconstruction of vegetation patterns, The Holocene, 27, 1252–1258, https://doi.org/10.1177/095968361668325, 2017.

Theuerkauf, M. and Couwenberg, J.: ROPES reveals past land cover and PPEs from single pollen records, Front. Earth Sci., 6, 14, https://doi.org/10.3389/feart.2018.00014, 2018.

Theuerkauf, M., Haberl, A., Wulf, K., Joosten, H., and DUENE e.V. Greifswald: Holozäner Vegetationswandel im Einzugsgebiet der Mothhäuser Haide/Erzgebirge, Unpublished project report as part of the LfUG project "Auswirkungen des Klimawandels auf wasserabhängige Ökosysteme", University of Greifswald, 55 pp., 2007.

Thomasius, H.: The influence of mining in the Saxon Erzgebirge on woods and forestry up to the beginning of the 19th century, GeoJournal, 32, 103–125, https://doi.org/10.1007/BF00812496, 1994.

Tolksdorf, J. F. (Ed.): Mittelalterlicher Bergbau und Umwelt im Erzgebirge. Eine interdisziplinäre Untersuchung, Veröffentlichungen des Landesamtes für Archäologie Sachsen, 67, Landesamt für Archäologie Sachsen, Dresden, ISBN 3943770370, 213 pp., 2018.

Tolksdorf, J. F. and Scharnweber, T.: Holzfunde als mehrdimensionale Quelle zur Rekonstruktion von Wirtschaft und Landschaft. in: Mittelalterlicher Bergbau und Umwelt im Erzgebirge. Eine interdisziplinäre Untersuchung, edited by: Tolksdorf, J. F., Veröffentlichungen des Landesamtes für Archäologie Sachsen, 67, Landesamt für Archäologie Sachsen, Dresden, 37–56, ISBN 3943770370, 2018.

Tolksdorf, J. F. and Schröder, F.: Rekonstruktion von Holznutzung und Landschaftsgeschichte in einer mittelalterlichen Bergbaulandschaft bei Niederpöbel. Interdisziplinärer Ansatz und methodische Abwägungen, Mitteilungen der Deutschen Gesellschaft für Archäologie des Mittelalters und der Neuzeit, 29, 175–184, 2016.

Tolksdorf, J. F., Elburg, R., Schröder, F., Knapp, H., Herbig, C., Westphal, T., Schneider, B., Fülling, A., and Hemker, C.: Forest exploitation for charcoal production and timber since the 12th century in an intact medieval mining site in the Niederpöbel Valley (Erzgebirge, Eastern Germany), J. Archaeol. Sci. Rep., 4, 487–500, https://doi.org/10.1016/j.jasrep.2015.10.018, 2015.

Tolksdorf, J. F., Kaiser, K., and Bertuch, M.: Stand der Untersuchungen zur Landschaftsgeschichte. in: Mittelalterlicher Bergbau und Umwelt im Erzgebirge. Eine interdisziplinäre Untersuchung, edited by: Tolksdorf, J. F., Veröffentlichungen des Landesamtes für Archäologie Sachsen, 67, Landesamt für Archäologie Sachsen, Dresden, 30–33, ISBN 3943770370, 2018.

Tolksdorf, J. F., Hemker, C., and Schubert, M.: Bronzezeitlicher Zinnseifenbergbau bei Schellerhau im östlichen Erzgebirge, Sachsen, Der Anschnitt, 71, 223–233, 2019.

Tolksdorf, J. F., Kaiser, K., Petr, L., Herbig, C., Kočár, P., Heinrich, S., Wilke, F. D. H., Theuerkauf, M., Fülling, A., Schubert, M., Schröder, F., Křivánek, R., Schulz, L., Bonhage, A., and Hemker, C.: Past human impact in a mountain forest: geoarchaeology of a medieval glass production and charcoal hearth site in the Erzgebirge, Germany, Reg. Environ. Chang., 20, 71, https://doi.org/10.1007/s10113-020-01638-1, 2020a.

Tolksdorf, J. F., Schröder, F., Petr, L., Herbig, C., Kaiser, K., Kočár, P., Fülling, A., Heinrich, S., Hönig, H., and Hemker, C.: Evidence for Bronze Age and Medieval tin placer mining in the Erzgebirge mountains, Saxony (Germany), Geoarchaeology, 35, 198–216, https://doi.org/10.1002/gea.21763, 2020b.

Tolksdorf, J. F., Schubert, M., Schröder, F., Bertuch, M., and Heinrichsen, A.: Meilerplätze im Erzgebirge – Erfassung mittels LiDAR und Einbeziehung dieser Quellengattung in der Montanarchäologie, in: Beiträge zur Landnutzungsgeschichte in der Niederlausitz und im Erzgebirge, edited by: Hirsch, F., Raab, A. and Raab, Geopedology and Landscape Development Research Series (GeoRS), 10, 82–91, Brandenburgische Technische Universität, Cottbus, https://doi.org/10.26127/BTUOpen-5388, 2021.

Valde-Nowak, P.: Short settled Neolithic sites in the Mountains – Economy or religious practice? Case studies from the Polish Carpathians and German Mid-Mountains, in: Economic Archaeology: From Structure to Performance in European Archaeology, edited by: Kerig, T. and Zimmermann, A., Habelt, Bonn, 215–225, 2013.

van der Knaap, W. O., van Leeuwen, J. F. N., Fahse, L., Szidat, S., Studer, T., Baumann, J., Heurich, M., and Tinner, W.: Vegetation and disturbance history of the Bavarian Forest National Park, Germany, Veget. Hist. Archaeobot., 29, 277–295, https://doi.org/10.1007/s00334-019-00742-5, 2020.

Vejpustková, M., Čihák, T., Samusevich, A., Zeidler, A., Novotný, R., and Šrámek, V.: Interactive effect of extreme climatic event and pollution load on growth and wood anatomy of spruce, Trees, 31, 575–586, https://doi.org/10.1007/s00468-016-1491-5, 2017.

Veron, A., Novak, M., Brizova, E., and Stepanova, M.: Environmental imprints of climate changes and anthropogenic activities in the Ore Mountains of Bohemia (Central Europe) since 13 cal. kyr BP, The Holocene, 24, 919–931, https://doi.org/10.1177/0959683614534746, 2014.

Vilímek, V. and Raška, P.: The Krušné Hory Mts. – The Longest Mountain Range of the Czech Republic, in: Landscapes and Landforms of the Czech Republic, edited by: Pánek, T. and Hradecký, J., World Geomorphological Landscapes, Springer, Berlin, 113–122, https://doi.org/10.1007/978-3-319-27537-6_10, 2016.

Vilímek, V., Fantucci, R., and Stemberk, J.: Dendrogeomorphological investigations of slope deformation on Salesius Hill in the Krušné Hory Mts, In: Landslides. Proceedings of the First European Conference on Landslides, Prague, Czech Republic, 24–26 June 2002, edited by: Rybář, J., Stemberk, J., and Wagner, P., Routledge, London, 321–326, 2018.

Vlach, V., Matouskova, M., and Ledvinka, O.: Impacts of regional climate change on hydrological drought characteristics in headwaters of the Ore Mountains, River Res. Appl., 37, 919–930, https://doi.org/10.1002/rra.3818, 2021.

von Carlowitz, H. C. and von Rohr, J. B.: Sylvicultura Oeconomica (reprint of the 2nd edition from 1732), Kessel, Remagen-Oberwinter, ISBN 978-3-941300-19-4, 69 pp., 2012.

Wagenbreth, O. and Wächtler, E. (Eds.): Der Freiberger Bergbau. Technische Denkmale und Geschichte, Springer Spektrum, Berlin & Heidelberg, ISBN 978-3-662-44763-5, 385 pp., 1988.

Wahlmüller, N.: Palynologische Forschung in den Ostalpen und ihren vorgelagerten Gebieten, Berichte des Naturwissenschaftlich-medizinischen Vereins in Innsbruck, 80, 81–95, 1993.

Weber, C. A.: Grenzhorizont und Klimaschwankungen, Abhandlungen des Naturwissenschaftlichen Vereins zu Bremen, 26, 98–106, 1926.

Wendel, D.: Autogene Regenerationserscheinungen in erzgebirgischen Moorwäldern und deren Bedeutung für Schutz und Entwicklung der Moore, Ph.D. thesis, Technische Universität Dresden, 233 pp., 2010.

Wenzel, W.: Slawische Namen im Erzgebirge mit besonderer Berücksichtigung des Raumes um Limbach-Oberfrohna, Sächsische Heimatblätter, 62, 214–217, https://journals.qucosa.de/shb/article/view/98 (last access: 8 October 2021), 2016.

Wetzel, M.: Das Erzgebirge im Wandel der Geschichte. in: Erzgebirge, edited by: Schattkowsky, M., Kulturlandschaften Sachsens 3, Edition Leipzig, Leipzig, 27–72, 2010.

Wiezik, M., Jamrichová, E., Máliš, F., Beláňová, E., Hrivnák, R., Hájek, M., and Hájková, P.: Transformation of West-Carpathian primeval woodlands into high-altitude grasslands from as early as the Bronze Age, Veget. Hist. Archaeobot., 1–6, https://doi.org/10.1007/s00334-022-00896-9, 2022.

Willutzki, H.: Zur Waldgeschichte und Vermoorung sowie über Rekurrenzflächen im Oberharz, Nova Acta Leopoldina NF, 25, 1–52, 1962.

Wilsdorf, H., Herrmann, W., and Löffler, K.: Bergbau, Wald, Flöße: Untersuchungen zur Geschichte der Flößerei im Dienste des Montanwesens und zum montanen Transportproblem, Freiberger Forschungshefte, 28, Akademie-Verlag, Berlin, 360 pp., 1960.

Zelinka, V., Zacharová, J., and Skaloš, J.: Analysis of spatiotemporal changes of agricultural land after the Second World War in Czechia, Sci. Rep., 11, 1–15, https://doi.org/10.1038/s41598-021-91946-1, 2021.

Zimmermann, F., Lux, H., Maenhaut, W., Matschullat, J., Plessow, K., Reuter, F., and Wienhaus, O.: A review of air pollution and atmospheric deposition dynamics in southern Saxony, Germany, Central Europe, Atmos. Environ., 37, 671–691, https://doi.org/10.1016/S1352-2310(02)00829-4, 2003.

Zinke, P.: Nutzungsgeschichte, Zustand und Revitalisierung der Moore im Erzgebirge, Telma, 32, 267–280, https://doi.org/10.23689/fidgeo-2884, 2002.

E&G Quaternary Sci. J., 72, 163–184, 2023
https://doi.org/10.5194/egqsj-72-163-2023

Open Access E&G Quaternary Science Journal

Research article

What do dust sinks tell us about their sources and past environmental dynamics? A case study for oxygen isotope stages 3–2 in the Middle Rhine Valley, Germany

Mathias Vinnepand[1], Peter Fischer[1], Ulrich Hambach[2,3], Olaf Jöris[4], Carol-Ann Craig[5], Christian Zeeden[6], Barry Thornton[5], Thomas Tütken[7], Charlotte Prud'homme[8], Philipp Schulte[9], Olivier Moine[10], Kathryn E. Fitzsimmons[11], Christian Laag[12,13], Frank Lehmkuhl[9], Wolfgang Schirmer[14], and Andreas Vött[1]

[1]Natural Hazard Research and Geoarchaeology, Institute for Geography, Johannes Gutenberg-Universität Mainz, 55099 Mainz, Germany
[2]BayCEER and Chair of Geomorphology, University of Bayreuth, 95440 Bayreuth, Germany
[3]Emil Racovita Institute of Speleology (ERIS), Romanian Academy, Cluj-Napoca branch, Clinicilor 5, 400006 Cluj-Napoca, Romania
[4]MONREPOS Archaeological Research Centre and Museum for Human Behavioural Evolution, Leibniz-Zentrum für Archäologie, 56567 Neuwied, Germany
[5]Environmental and Biogeochemical Sciences Group, The James Hutton Institute, Aberdeen, AB15 8QH, Scotland, UK
[6]Rock Physics and Borehole Geophysics, LIAG – Leibniz Institute for Applied Geophysics, 30655 Hanover, Germany
[7]Applied and Analytical Paleontology, Institute of Geosciences, Johannes Gutenberg-Universität Mainz, 55099 Mainz, Germany
[8]Institute of Earth Surface Dynamics, University of Lausanne, 1015 Lausanne, Switzerland
[9]Chair in Physical Geography and Geoecology, Department of Geography, RWTH Aachen, 52056 Aachen, Germany
[10]Laboratoire de Géographie Physique, UMR 8591 CNRS Université Paris 1 UPEC, Thiais 94320, France
[11]Department of Geosciences, University of Tübingen, 72076 Tübingen, Germany
[12]Department of Research and Development, Nolte Geoservices GmbH, 48301 Nottuln, Germany
[13]Institut de Physique du Globe de Paris, CNRS, Université Paris Cité, 75238 Paris, France
[14]independent researcher: Wolkenstein 24, 91320 Wolkenstein, Germany

Correspondence: Mathias Vinnepand (mavinnep@uni-mainz.de) and Peter Fischer (p.fischer@geo.uni-mainz.de)

Relevant dates: Received: 24 May 2022 – Revised: 13 June 2023 – Accepted: 20 June 2023 – Published: 4 August 2023

How to cite: Vinnepand, M., Fischer, P., Hambach, U., Jöris, O., Craig, C.-A., Zeeden, C., Thornton, B., Tütken, T., Prud'homme, C., Schulte, P., Moine, O., Fitzsimmons, K. E., Laag, C., Lehmkuhl, F., Schirmer, W., and Vött, A.: What do dust sinks tell us about their sources and past environmental dynamics? A case study for oxygen isotope stages 3–2 in the Middle Rhine Valley, Germany, E&G Quaternary Sci. J., 72, 163–184, https://doi.org/10.5194/egqsj-72-163-2023, 2023.

Abstract: The study of geological archives of dust is of great relevance as they are directly linked to past atmospheric circulation and bear the potential to reconstruct dust provenance and flux relative to climate changes. Among the dust sinks, loess–palaeosol sequences (LPSs) represent the only continental and non-aquatic archives that are predominantly built up by dust deposits close to source areas, providing detailed information on Quaternary climatic and terrestrial environmental changes. Upper Pleistocene LPSs of western central Europe have been investigated in great detail showing their linkage to millennial-scale northern hemispheric climate oscillations, but comprehensive data on dust composition and potential source–sink relationships as well as inferred past atmospheric circulation patterns for this region are still fragmentary.

Here, we present an integrative approach that systematically combines sedimentological, rock magnetic, and bulk geochemical data, as well as information on Sr and Nd isotope composition, enabling a synthetic interpretation of LPS formation. We focus on the Schwalbenberg RP1 profile in the Middle Rhine Valley in Germany and integrate our data into a robust age model that has recently been established based on high-resolution radiocarbon dating of earthworm calcite granules. We show that Schwalbenberg RP1 is subdivided into a lower section corresponding to late oxygen isotope stage 3 (OIS; ∼ 40–30 ka) and an upper section dating into the Last Glacial Maximum (LGM; ∼ 24–22 ka), separated by a major stratigraphic unconformity. Sedimentological proxies of wind dynamics (*U* ratio) and pedogenesis (finest clay) of the lower section attest to comparable and largely synchronous patterns of northern hemispheric climatic changes supporting the overall synchronicity of climatic changes in and around the North Atlantic region. The anisotropy of magnetic susceptibility (AMS) reveals a clear correlation between finer grain size and increasing AMS foliation within interstadials, possibly owing to continuous accumulation of dust during pedogenic phases. Such a clear negative correlation has so far not been described for any LPS on stadial–interstadial scales.

Distinct shifts in several proxy data supported by changes in isotope composition ($^{87}Sr/^{86}Sr$ and εNd) within the lower section are interpreted as changes in provenance and decreasing weathering simultaneously with an overall cooling and aridification towards the end of OIS 3 (after ∼ 35 ka) and enhanced wind activity with significant input of coarse-grained material recycled from local sources related to increased landscape instability (after ∼ 31.5 ka). We find that environmental conditions within the upper section, most likely dominated by local to regional environmental signals, significantly differ from those in the lower section. In addition, AMS-based reconstructions of near-surface wind trends may indicate the influence of north-easterly winds beside the overall dominance of westerlies. The integrative approach contributes to a more comprehensive understanding of LPS formation including changes in dust composition and associated circulation patterns during Quaternary climate changes.

Kurzfassung: Die Untersuchung geologischer Staubarchive ist von großer Bedeutung, da diese unmittelbar mit der atmosphärischen Zirkulation verknüpft sind und somit das Potenzial besitzen, sowohl Änderungen in der Staub-Herkunft als auch im Staubfluss in Verbindung mit Klimaänderungen zu rekonstruieren. Löss-Paläosol-Sequenzen (LPS) stellen in diesem Zusammenhang die einzigen kontinentalen nicht-aquatischen Archive dar, die sich aus Staubablagerungen bilden, die in relativer Nähe ihrer Liefergebiete liegen. Sie liefern zudem detaillierte Informationen über klimatische und terrestrische Umweltveränderungen im Quartär, die sich in Proxy-Daten der Staubzusammensetzung und der syn- und postsedimentären Veränderung widerspiegeln. Zwar belegen detaillierte Untersuchungen von LPS im westlichen Mitteleuropa direkte Verknüpfungen mit den jungpleistozänen Klimaschwankungen der nördlichen Hemisphäre, jedoch sind umfassende Daten zur Staubzusammensetzung und zur Kopplung von Staubquellen und -senken sowie zu den abgeleiteten atmosphärischen Zirkulationsmustern in der Region immer noch lückenhaft.

Unter Anwendung eines integrativen Ansatzes, der systematisch sedimentologische, gesteinsmagnetische und geochemische Daten kombiniert und durch Daten zur Isotopenzusammensetzung ergänzt wird, ist eine synthetische Interpretation der Bildung von LPS, hier am Beispiel des Profils RP1 am Schwalbenberg im Mittelrheintal, möglich. Wir verbinden unsere Daten mit einem detaillierten und robusten Altersmodell, das kürzlich auf der Grundlage hochauflösender Radiokohlenstoffdatierungen an Regenwurmkalziten (sog. Earthworm Calcite Granules, ECG) publiziert wurde. Auf Basis dieses Altersmodells kann gezeigt werden, dass das Profil RP1 in zwei Abschnitte, die durch eine deutliche Diskordanz getrennt sind, gegliedert wird. Der liegende Abschnitt entspricht dabei dem späten Sauerstoff-Isotopenstadium (OIS) 3 (∼ 40–30 ka), während der hangende Abschnitt in das Letztglaziale Maximum (LGM) datiert (∼ 24–22 ka). Für den liegenden Abschnitt zeigen die sedimentologischen Proxy-Daten (*U* Ratio, feinster Ton) vergleichbare und weitgehend synchrone Muster zwischen dem Schwalbenberg und Daten aus grönländischen Eisbohrkernen (NGRIP) und unterstützten somit die Annahme einer Synchronität von Klimaänderungen in und um den Nordatlantik.

Die Anisotropie der Magnetischen Suszeptibilität (AMS) zeigt in Interstadialen eine klare Korrelation kleinerer Korngrößen mit zunehmender AMS-Foliation, die möglicherweise auf kontinuierliche Staubakkumulation während der Pedogenese zurückzuführen ist. Ein solch klarer Zusammenhang wurde für LPS mit stadial–interstadialer Auflösung bisher nicht beschrieben.

Im liegenden Abschnitt von Profil RP1 am Schwalbenberg wird eine Abkühlung und Aridifizierung im späten OIS 3 (nach ~ 35 ka) durch signifikante Änderungen in verschiedenen Proxy-Daten und der Isotopenzusammensetzung ($^{87}Sr/^{86}Sr$ und εNd) deutlich, die auf unterschiedliche Staubquellen und abnehmende Verwitterung hindeuten. Zusätzlich führt eine erhöhte Instabilität der Landschaft in Richtung des LGM (nach ~ 31,5 ka) zu verstärkter Windaktivität und dem Eintrag grobkörnigen Materials, das aus lokalen Quellen recycelt wurde.

Die Proxy-Daten des hangenden Abschnitts deuten auf Umweltbedingungen hin, die sich signifikant von jenen des Liegenden unterscheiden und vermutlich durch lokale bis regionale Einflüsse dominiert werden. AMS-basierte Rekonstruktionen der oberflächennahen Windtrends lassen neben der Dominanz von Westwinden auf einen phasenweisen Einfluss von Winden aus nordöstlicher Richtung schließen. Insgesamt sehen wir den vorgestellten integrativen Ansatz als einen wichtigen Beitrag zum besseren Verständnis der Bildung von LPS, welche die Veränderungen der Staubzusammensetzung und damit verbundener Zirkulationsmuster im Zuge quartärer Klimaänderungen besser beleuchtet.

1 Introduction

The production of mineral dust, its aeolian transport, and its deposition are important processes of the Earth–atmosphere system affecting the global radiative balance, changing the hydroclimate, and providing nutrients to both terrestrial and marine ecosystems (Muhs, 2013; Knippertz and Stuut, 2014; Marx et al., 2018). In order to understand potential links between dust flux and climate changes during the Quaternary, the study of geological archives of dust is of great relevance, as these are directly linked to past atmospheric circulation (Schaffernicht et al., 2020). As such they bear the potential to reconstruct dust provenance and dust flux relative to Quaternary climate changes whose proxies are frequently recorded in some of these archives (e.g. Mahowald et al., 2006; Újvári et al., 2016).

While ice, marine, and lake records are prominent Quaternary palaeoenvironmental and palaeoclimatic archives also tracing variations in atmospheric dustiness (e.g. Rasmussen et al., 2014; Sirocko et al., 2016; Kämpf et al., 2022), loess–palaeosol sequences (LPSs) represent the only continental and non-aquatic archive that is predominantly built up by dust deposits close to source areas (Muhs, 2013). They are thus providing detailed information on terrestrial palaeoenvironmental and palaeoclimatic change including dust composition and post-sedimentary alteration (e.g. Újvári et al., 2012; Schaetzl et al., 2018).

In western and central Europe, enhanced dust deposition during Upper Pleistocene stadial periods has been largely ascribed to increased fine particle production through glacial grinding activity, frost shattering, and entrainment of silty material from alluvial plains; glacial outwash plains; endorheic basins; and exposed continental shelves (Frechen et al., 2003; Antoine et al., 2009; Smalley et al., 2009; Lehmkuhl et al., 2021; Pötter et al., 2021). In combination with gustier winds related to steepened meridional temperature gradients during stadial periods (McGee et al., 2010), the increased dustiness is reflected in peak dust accumulation especially during oxygen isotope stage (OIS) 2 along the western European loess belt (e.g. Frechen et al., 2003; Újvári et al., 2017; Fischer et al., 2021; Schmidt et al., 2021). This pattern is also observed in regional aquatic archives, such as maar lakes (e.g. Seelos et al., 2009; Fuhrmann et al., 2021) and supra-regional archives, such as Greenland ice cores (e.g. Rasmussen et al., 2014; Újvári et al., 2022).

In recent times, Upper Pleistocene key LPSs in western Europe have been investigated in great detail showing their linkage to northern hemispheric glacial–interglacial and millennial-timescale climate oscillations (e.g. Rousseau et al., 2007; Moine et al., 2017; Fischer et al., 2021; Prud'homme et al., 2022), but comprehensive data on dust composition and potential source–sink relationships as well as inferred palaeo-wind directions for this region are still scarce (e.g. Taylor et al., 2014; Schatz et al., 2015).

With this study we aim to contribute to a better understanding of dust provenance and past environmental dynamics using different methodological tools to investigate dust composition and to discuss potential source–sink relationships during late OIS 3 (~ 40–30 ka) and parts of OIS 2 (~ 24–22 ka) in western central Europe. Over the last few years, we were able to show that the Schwalbenberg LPSs in the Middle Rhine Valley in Germany resolve the last glacial cycle in exceptional temporal detail (Fischer et al., 2021; Vinnepand et al., 2022), proving previous studies that suggested a linkage with the last glacial millennial-scale climate oscillations recorded in Greenland ice cores (Schirmer, 2000, 2011). Here, we focus on the 5.6 m deep section RP1, exposed at the southern edge of the Schwalbenberg. The RP1 profile was studied in detail by Fischer et al. (2021). Beside quantitative climate reconstructions based on the study of oxygen and carbon isotopes of earthworm calcite granules (ECGs), Bayesian age modelling based on radiocarbon dating of ECGs was used to establish a robust and reliable age model of the Schwalbenberg RP1 LPS (Prud'homme et al., 2022). Here, we use high-resolution sedimentological, rock magnetic, and bulk geochemical data to characterize dust composition along the stratigraphy. In addition, isotope geochemical measurements ($^{143}Nd/^{144}Nd$ and $^{87}Sr/^{86}Sr$) were conducted at lower resolution.

The *U* ratio, defined as the ratio of coarse versus medium plus fine silt, is employed to reconstruct wind dynamics and potential processes of sediment reworking (Vandenberghe et al., 1985; Vandenberghe, 2013). In addition, the finest clay content mostly reflects pedogenically formed clay (Schulte and Lehmkuhl, 2018) but potentially also dust components that have travelled longer distances (e.g. Muhs, 2013).

Beside such sedimentological data, the magnetic susceptibility evolved to an essential stratigraphic tool in the investigation of LPSs. As shown for many sites in Eurasia, magnetic susceptibility increases in palaeosols (magnetic enhancement), while relatively unaltered loess shows lower values. In contrast, lower magnetic susceptibility in palaeosols compared to loess is explained by the wind-vigour model (e.g. Evans and Heller, 2001); by waterlogging causing dissolution of iron minerals, which is mainly observed in loess affected by periglacial conditions (e.g. Taylor et al., 2014; Fischer et al., 2019); or by high amounts of primary magnetically enhanced sediments and their weathering products (von Suchodoletz et al., 2009; Obreht et al., 2016). In addition to low field bulk magnetic susceptibility (hereafter MS) the frequency-dependent magnetic susceptibility (hereafter MS_{fd}) is a qualitative parameter that allows us to determine the relative amount of newly formed ultrafine magnetic particles in the course of (incipient) pedogenesis (e.g. Buggle et al., 2014; Bradák et al., 2021). In the context of the reconstruction of past circulation patterns, the anisotropy of magnetic susceptibility (AMS) can additionally be utilized, which potentially reflects near-surface wind directions, if the primary magnetic fabric is preserved (Hrouda, 2007; Zhang et al., 2010; Taylor and Lagroix, 2015; Zeeden and Hambach, 2021).

In addition to these physical parameters, the bulk element composition is frequently employed to identify potential provenance shifts and sediment recycling as well as weathering intensity (cf. Buggle et al., 2011; Klasen et al., 2015; Profe et al., 2016; Vinnepand et al., 2022). In combination with Sr and Nd isotope geochemistry, which is a common tool in provenance studies (Grousset and Biscaye, 1989, 2005), potential changes in dust sources as well as secondary alteration of isotope signals may be detected in LPSs. While $^{143}Nd/^{144}Nd$ is a well-established provenance proxy that is strongly resistant to surface processes (e.g. weathering) (Goldstein and Jacobsen, 1988; Meyer et al., 2009; Grousset and Biscaye, 2005), $^{87}Sr/^{86}Sr$ might be prone to grain size effects (Feng et al., 2009) and to alteration through weathering (e.g. Clauer and Chaudhuri, 1995), potentially limiting a straightforward interpretation in terms of changing dust sources.

The systematic combination of these physical and geochemical proxy data opens the perspective for a comprehensive interpretation of LPS formation in the Middle Rhine Valley in Germany. Employing such an integrative approach, we aim to detect significant shifts in dust composition and discuss potential causes against the background of palaeoenvironmental and palaeoclimatic oscillations during the time period investigated.

2 Regional setting and stratigraphy

The Schwalbenberg site in the Middle Rhine Valley is located in the centre of the Rhenish Massif (Germany; 50.562378° N, 7.240425° E; −90–135 m a.s.l. – above sea level; Fig. 1). Up to 30 m thick Upper Pleistocene LPSs drape the lower middle terrace 1 (LMT 1) of the penultimate glaciation (cf. Boenigk and Frechen, 2006) and at least two further, older terrace levels of the Rhine, overall resolving Atlantic-driven Upper Pleistocene climate oscillations in more detail than any other terrestrial archive in the region described so far (Fischer et al., 2021). Nowadays, the area is characterized rather by a maritime climate influence (mean annual temperature: 10.2 °C; mean annual precipitation: 643 mm; Deutscher Wetterdienst, 2023), with low-air-pressure systems predominantly entering the area from the Atlantic to the west (Prud'homme et al., 2022).

During the Upper Pleistocene the site was situated between the glaciated Alps in the south; the Fennoscandian (FIS) and British–Irish ice sheets (BIIS) in the north, which reached their maximum extents during the Last Glacial Maximum (LGM) (e.g. Lambeck et al., 2014); and the – at this time – dried out plains of the English Channel westward and north-westward (Fig. 1), all of which are considered important dust-producing and dust source areas for LPSs in western and central European periglacial realms (Antoine et al., 2009; Lehmkuhl et al., 2021; Baykal et al., 2022). In addition, the alluvial plains of – over long periods – braided river systems, here the Rhine and its tributaries, are assumed to represent major regional dust sources during stadial phases (e.g. Schatz et al., 2015; Rousseau et al., 2018).

Furthermore, the Rhenish Massif itself experienced intensive frost-weathering in the most severe cold periods of the Pleistocene and intensive sediment relocation under cold and humid conditions, forming Pleistocene periglacial slope deposits (PPSDs) (Sauer and Felix-Henningsen, 2006), rep-

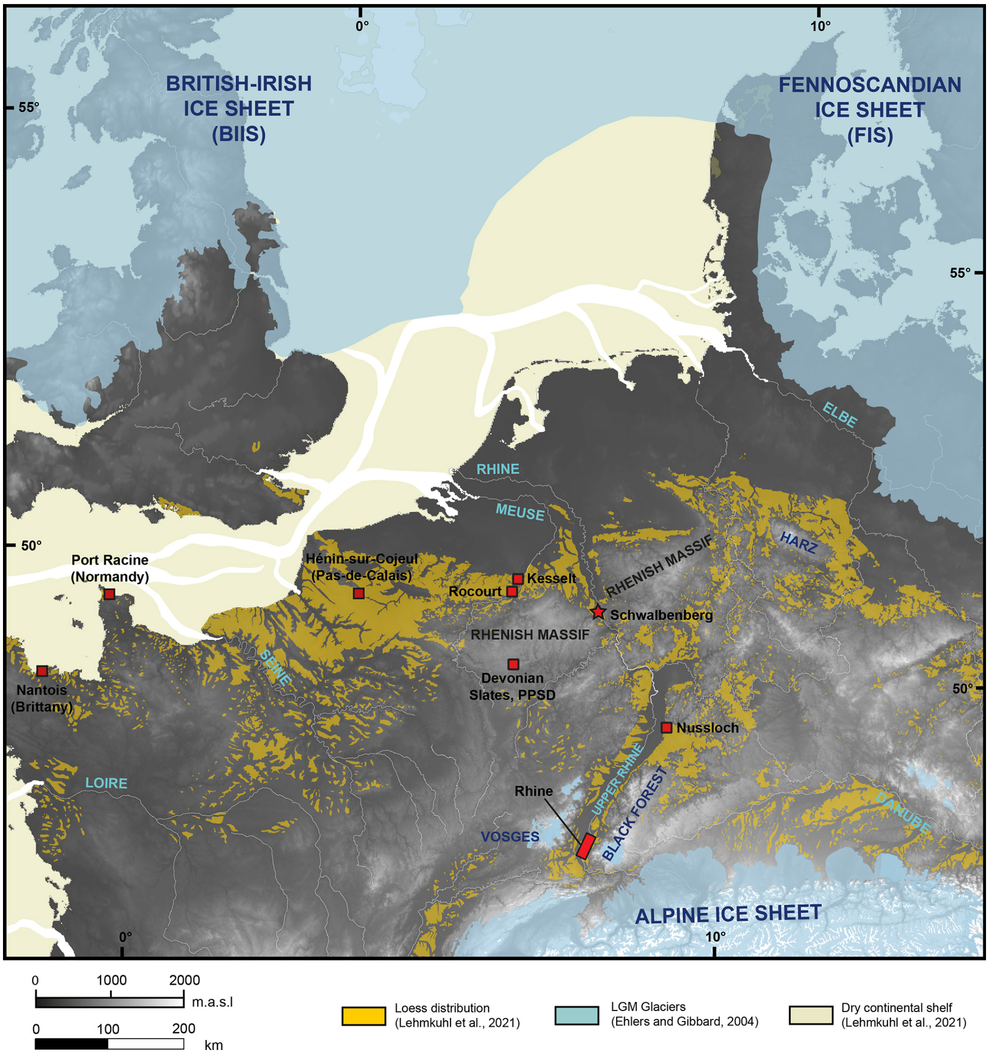

Figure 1. Map based on the digital elevation model (GLOBE 1.0) showing western central Europe during the Last Glacial Maximum (LGM, centred at ∼ 22 ka); the location of the Schwalbenberg site in the Middle Rhine Valley, Germany; and selected key sites (see text for explanation). The Schwalbenberg site is located between the Alpine ice sheet in the south and the Fennoscandian and British–Irish ice sheets in the north.

resenting potential subordinated local dust sources (Janus, 1988; Römer et al., 2016).

During the Upper Pleistocene, the Schwalbenberg site was located close to the alluvial plains of the braided systems of the rivers Ahr and Rhine, reflecting possible sources of mineral dust of local to regional origin. The comparably small Ahr River catchment (6.63 $m^3 s^{-1}$ mean annual discharge; Ministry for Environment RLP, 2021) is located in the northern parts of the Eifel area where Devonian rocks (mostly schistose clayey silt- and sandstones and subordinated limestones) are predominant (Meschede, 2018; Fig. 2). In contrast, the Rhine catchment until the mouth of the Ahr (2010 $m^3 s^{-1}$ mean annual discharge ∼ 20 km south of Schwalbenberg; International commission for the hydrology of the Rhine basin, 2021) includes the north-western Alps and the Upper Rhine Graben (with small tributaries draining parts of the Vosges, Black Forest, and Odenwald), as well as its main tributaries with the rivers Neckar (draining parts of the Swabian Alb, Triassic Keuperbergland (Keuper Uplands), Black Forest, and Odenwald), Main (draining the Fichtel Mountains, Franconian Alb, and several other Franconian uplands), Lahn (draining the Rhenish Massif), Nahe (draining predominantly the Saar–Nahe basin), and Mosel (draining parts of the Vosges, the easternmost Paris Basin, and the Rhenish Massif) (Meyer and Stets, 1996; Fig. 2).

In this study, we focus on the 5.60 m thick RP1 profile located at the southern fringe of the Schwalbenberg facing the Ahr valley (Figs. 3, 4). The profile was described and subdivided into 21 stratigraphic units (SUs), correlated to superordinate stratigraphic units (SSUs) D, E, and F within the gen-

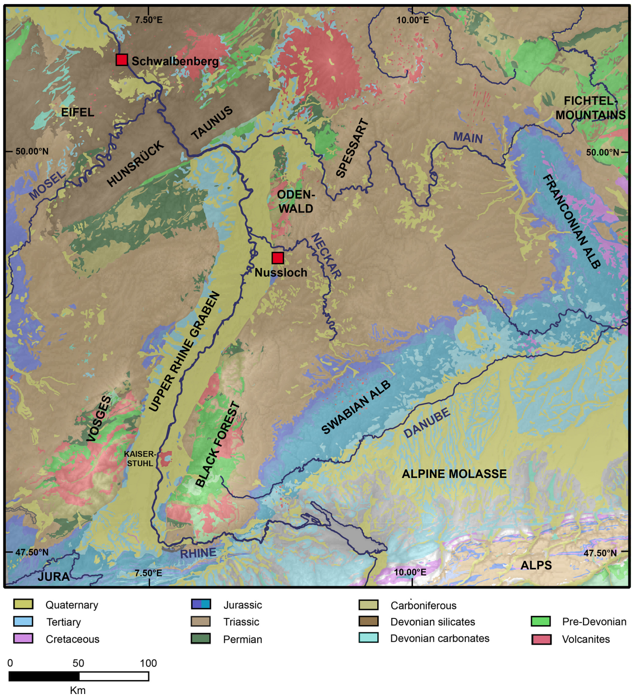

Figure 2. Geological map showing the main geological units of the Rhine catchment up to the Lower Rhine Embayment (Federal Institute for Geosciences and Natural Resources Germany, 2022). Calcareous rocks and sediments dominate the Rhine catchment in the northern Alps and the Molasse basin. The flanks of the Upper Rhine Graben include volcanites and metamorphic pre-Devonian rocks as well as Triassic siliciclastics and carbonates. The Rhenish Massif is dominated by Devonian slates and sandstones, and subordinated Devonian limestones occur.

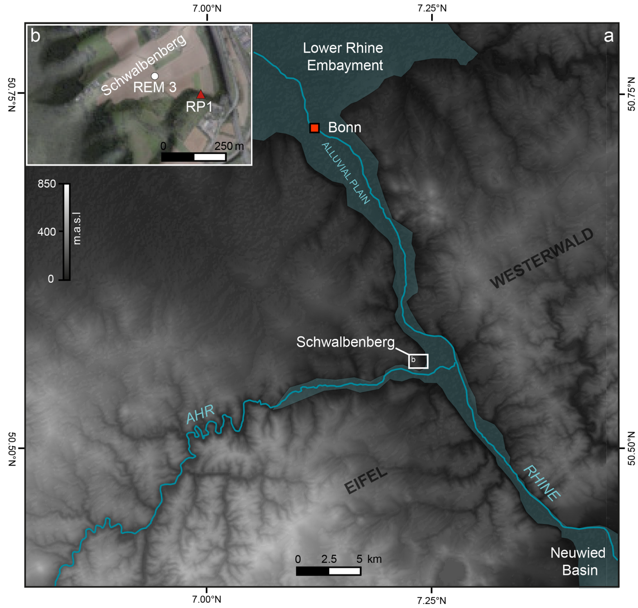

Figure 3. (a) Map of the Lower Middle Rhine Valley in western central Germany based on the digital elevation model (DEM based on SRTM 30 data by USGS (2022). The Schwalbenberg site is located north-west of the confluence of the Rhine and the Ahr. These river systems are the most important source areas of mineral dust. **(b)** The inset map (BingMaps, 2021) shows the position of the REM 3 key LPSs and the RP1 section (cf. Fischer et al., 2021; Prud'homme et al., 2022).

eral Schwalbenberg stratigraphic model (Fischer et al., 2021; see Table 1). The SSUs were defined by lithology and by the classification of palaeosols according to the IUSS Working Group WRB (Schad et al., 2015).

High-resolution radiocarbon dating on ECGs confirm that the lower section of the sequence covers late OIS 3, which is characterized by the formation of Calcaric Cambisols at Schwalbenberg correlated to Greenland Interstadials (GIs) 8–6 (cf. Fischer et al., 2021; Prud'homme et al., 2022). The Calcaric Cambisols of SUs 2–6 build a soil complex, whilst the uppermost Calcaric Cambisol (SU 8), correlated to GI 6, is clearly separated from the previous one by a loess layer (SU 7).

Based on the RP1 age model (Prud'homme et al., 2022), the Gelic Gleysol of SU 11 covers the transition from GI 5.2 to Greenland Stadial (GS) 5.2. A formation during milder climate conditions during GI 5.2 is likely. The next loess layer of SU 12 is truncated due to erosion prior to accumulation of the upper section represented by SSU F.

SSU F above the unconformity (base of SU 13) contains reworked loess, loess, and weakly developed Gelic Gleysols correlated to OIS 2 between ∼ 24 000 and 21 900 cal BP (see Sect. 3.5).

3 Materials and methods

Continuous sampling in 2 cm intervals was performed for grain size, bulk geochemical, and rock magnetic analyses including the determination of the anisotropy of magnetic susceptibility (AMS). However, the latter was conducted for every second sample (see Sect. 3.3). In addition, we collected 30 samples with 5 cm sampling width for Sr and Nd isotope analyses according to stratigraphy (see Fig. 4 for sample distribution, sampling intervals are given in Table S2).

3.1 Laser granulometry

We analysed the grain size of samples from the Schwalbenberg RP1 profile to calculate the U ratio and finest clay proportion. The U ratio is defined as the ratio of coarse versus medium and fine silt (Vandenberghe et al., 1985; Újvári et al., 2016) and is used to discriminate between sediments that were transported by dynamic and relatively strong winds (high U ratio) and those transported by weaker winds (low U ratio) (Vandenberghe et al., 1997). The finest clay proportion (fCl < 0.2 µm) mainly reflects post-depositional

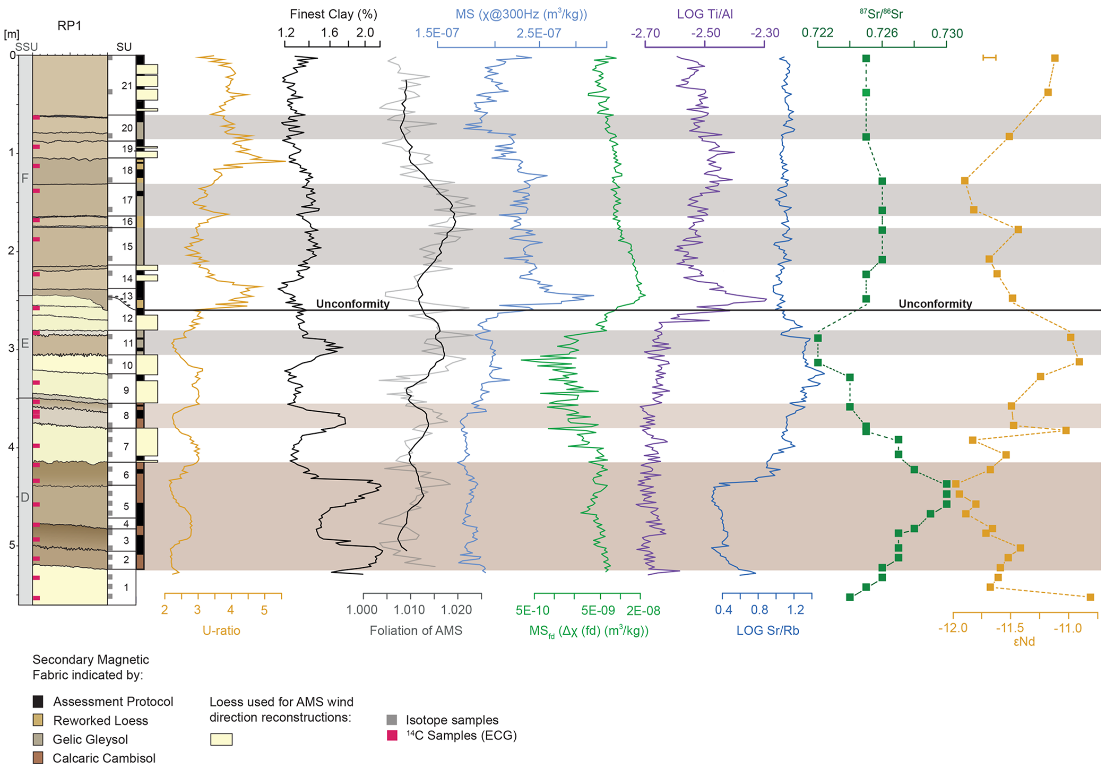

Figure 4. From left to right: stratigraphic log of profile RP1 and positions of ECG samples used for radiocarbon dating (modified after Prud'homme et al., 2022; radiocarbon ages are given in Table 1). SSUs and SUs are given according to Fischer et al. (2021); log depicting secondary magnetic fabric and loess layers used for AMS-based reconstruction of near-surface wind directions following the statistical assessment (see Supplement for details); grain size data: U ratio and finest clay; magnetic fabric and environmental magnetism: foliation of the AMS, MS (χ @300 Hz), and MS_{fd} ($\Delta\chi$(fd)); geochemical data: log Ti/Al and log Sr/Rb; isotope geochemistry: $^{87}Sr/^{86}Sr$ and εNd. Sr and Nd isotope sampling positions are indicated by grey squares next to the stratigraphic log of SUs, and 2σ for internal basalt standard measurements (reproducibility) is below the size of the sample symbols for $^{87}Sr/^{86}Sr$ but exceeds these for εNd (see scale in the data plot). For the calculation, statistics and uncertainty of AMS data, and details on sample reproducibility of isotope measurements, we refer the reader to the Supplement.

grain size reduction by chemical weathering (Schulte and Lehmkuhl, 2018).

We undertook granulometry using a laser diffraction particle size analyser (LS 13 320 PIDS, Beckman Coulter) to analyse non-decalcified samples (cf. Schulte et al., 2016). Sample pre-treatment involved removal of organic carbon by 0.70 mL 20 % H_2O_2 and dispersion with 25 mL of $Na_4P_2O_7$ at 0.1 mol L^{-1} for 12 h (Jones, 2003; Blott et al., 2004). Quadrupole measurements using two different concentrations ensured high precision. Through data processing, we applied the Mie theory (fluid RI: 1.33; sample RI: 1.55; imaginary RI: 0.1; Jones, 2003; Ozer et al., 2010).

3.2 Bulk geochemistry

We integrated the Ti/Al ratio as a provenance indicator, as both elements are relatively immobile and their ratio is not significantly affected by weathering or pedogenesis (e.g. Zech et al., 2008; Sheldon and Tabor, 2009). In addition, we complementarily use the Sr/Rb ratio as an indicator of weathering intensity based on the assumption that Sr shows an analogous behaviour to Ca being easily soluble and mobile in the course of weathering, while Rb behaves relatively immobile under moderate weathering conditions due to strong adsorption to clay minerals (e.g. Buggle et al., 2011). We are aware of the fact that the initial Sr/Rb ratio is maybe partly masked by the dynamics of carbonate-bound Sr in the course of secondary carbonate precipitation (e.g. Buggle et al., 2011; Profe et al., 2016), the latter effect being detailed by Vinnepand et al. (2020) for the Schwalbenberg LPS.

We determined element composition with a polarization energy dispersive X-ray fluorescence (EDP-XRF) spectrometer (Spectro Xepos, Spectro) onto pressed sample pellets (bulk sediments < 2 mm) (see Vinnepand et al., 2022). Measurements were performed in duplicates to ensure data quality (measurements were excluded in the case when duplicates exceeded 3σ). We used the decadic logarithm (log ratios) of element ratios for data symmetry and to overcome the closed sum constraint (Weltje et al., 2015; Profe et al., 2016). For

Table 1. Subdivision of the RP1 profile into superordinate stratigraphic units (SSUs) F, E, and D (lower (older) SSUs are not exposed at RP1) and stratigraphic units (SUs) and their corresponding lithological and pedological interpretation (see Fischer et al., 2021, for further details). The ages were published by Prud'homme et al. (2022) based on radiocarbon dating applied to 22 ECG samples, and the calibration was based on IntCal20 (Reimer et al., 2020). The Greenland events are shown according to the INTIMATE event stratigraphy (Rasmussen et al., 2014). The radiocarbon ages have been integrated into Bayesian age modelling (Prud'homme et al., 2022) using the Bacon software (Blaauw and Christeny, 2011). The age model is integrated into Fig. 6 in the Discussion section.

Profile RP1	SSU	SU	Lithology/pedology	Age (cal BP) min–max (2σ)	Greenland events
Upper section	F	21	Loess	–	
	F	20	Gelic Gleysol	21 426–22 150	GS 2.1a
	F	19	Loess	22 327–22 500	GS 2.1a
	F	18	Reworked loess	22 424–22 652	GS 2.1a
	F	17	Gelic Gleysol	22 557–22 846	GS 2.1a
	F	16	Reworked loess	22 793–23 073	GS 2.1a
	F	15	Gelic Gleysol	23 079–23 663	GI 2.2
	F	14	Loess	23 863–24 619	GS 3
Unconformity (base of SU 13)	F	13	Reworked loess	–	–
Lower section	E	12	Loess	30 199–30 970	GS 5.2/GI 5.1
	E	11	Gelic Gleysol	31 128–32 018	GI 5.2/GS 5.2
	E	10	Loess	–	GI 5.2/GS 5.2
	E	9	Loess (partly laminated)	31 862–33 931	GS 6/GI 5.2
	E	9	Loess (partly laminated)	32 562–33 412	GI 6/GS 6
	E	9	Loess (partly laminated)	32 922–33 614	GI 6/GS 6
	D	8	Calcaric Cambisol	33 077–33 703	GI 6
	D	7	Loess	33 728–34 310	GS 7
		6		34 749–34 153	GI 7/GS 7
	D	6		35 134–34 453	GI 7/GS 7
	D	5	Soil complex (Calcaric	34 879–35 675	GI 7
	D	4	Cambisols, SU 2–6)	35 298–36 380	GS 8
	D	3		36 406–37 473	GI 8
	D	2		36 826–38 129	GI 8
	D	1	Loess	37 374–38 873	GS 9
	D	1	Loess	38 162–39 963	GS 9

integrating the element concentrations of Sr and Nd in the context of mixing equations (cf. Faure and Mensing, 2005), we applied XRF measurements to the same samples used for isotopic measurements (see Sect. 3.4).

3.3 Magnetic susceptibility and anisotropy of magnetic susceptibility

Since the 1980s environmental magnetic parameters have been recognized as fundamental palaeoclimate proxies for Eurasian LPSs, and low field magnetic susceptibility (MS) was established as a stratigraphic tool, facilitating correlations between terrestrial deposits and the marine record. The latter is based on stratigraphic oxygen isotope data for oceanic foraminifera, which in turn is a proxy for global ice volume (e.g. Evans and Heller, 2003; Liu et al., 2012). The frequency dependency of magnetic susceptibility (MS_{fd}), also expressed as the absolute difference of χ @300 Hz and χ @3000 (Hz χ @300 Hz–χ @3000 Hz $= \Delta\chi$), provides information on magnetic grain size spectra and may allow for the assignment of magnetic enhancement to soil formation processes to wind vigour effects and depletion due to hydromorphy in comparison to the low field MS (Forster et al., 1994; Bradák et al., 2021).

Furthermore, MS in LPS deposits has one additional application. Directional measurements of MS on oriented samples are used for fabric analyses. The AMS (anisotropy of magnetic susceptibility) method is an established structural indicator even in unconsolidated geological materials (Bradák et al., 2020). Magnetic fabric can be correctly approximated by a second-order symmetric tensor and fabric magnitude (i.e. degree of anisotropy) and fabric shape (i.e. prolate or oblate). Additionally, the orientation of principal axes of AMS ellipsoids (K_{MAX}, K_{INT}, K_{MIN}) can be used for fabric characterization and quantification (Hrouda, 2007).

In order to study the natural physical properties of the undisturbed sedimentological fabric, we collected oriented samples (cube edge lengths 2 cm, hence 8 cm^3 sample volume) exhibiting a ~ 2.1 cm vertical spacing of their centres (Zeeden et al., 2015; Zeeden and Hambach, 2021). The volume MS was measured using a susceptibility bridge (VFSM; Magnon, Germany) at AC fields of $300\,\mathrm{A\,m^{-1}}$ at 300 and 3000 Hz, respectively. Subsequently, the resulting values were mass normalized and given as mass-specific MS (χ) (cf. Buggle et al., 2014; Zeeden et al., 2018). Every second sample (~ 4.2 cm stratigraphic resolution) was subject to AMS measurements using a MFK1-FA kappabridge (AGICO) in a $400\,\mathrm{A\,m^{-1}}$ and 976 Hz alternating field and a rotator. We visualized the results of AMS measurements as a magnetic susceptibility ellipsoid with three orthogonal principal axes: the maximum axis (K_{MAX}), the intermediate axis (K_{INT}), and the minimal axis (K_{MIN}) by using the Anisoft v. 5.0.18 software supplied by AGICO. The magnetic susceptibility ellipsoid defines the overall magnetic fabric of a rock sample, reflecting the statistically preferred orientation of mineral grains. In this study, we employed the most common anisotropy parameters that are used to investigate the nature of magnetic fabrics in LPS, i.e. lineation (L) and foliation (F) describing the shaped and oblateness of an AMS ellipsoid, respectively. The data are presented in rose diagrams of K_{MAX} and stereoplots displaying the full spatial orientation of K_{MAX}, K_{INT}, and K_{MIN}. The applied assessment protocol (see Fig. 4) and associated statistical analyses are detailed in the Supplement.

3.4 Strontium and neodymium isotope geochemistry

The original Sr and Nd isotope compositions of igneous rocks represent fingerprints for their petrogenesis (e.g. preferential partitioning of incompatible Nd and Rb into the melt and compatible Sm and Sr into the solid residue during magmatic differentiation) and age (radioactive decay of ^{87}Rb to ^{87}Sr and ^{147}Sm to ^{143}Nd) (DePaolo and Wasserburg, 1976; Goldstein et al., 1984; Grousset and Biscaye, 1989). This leads to characteristic $^{143}\mathrm{Nd}/^{144}\mathrm{Nd}$ (εNd) and $^{87}\mathrm{Sr}/^{86}\mathrm{Sr}$ isotope signatures in crustal and mantle rocks, with felsic rocks having high $^{87}\mathrm{Sr}/^{86}\mathrm{Sr}$ and low $^{143}\mathrm{Nd}/^{144}\mathrm{Nd}$ (εNd) and the inverse for mafic (mantle-derived) rocks (εNd represents the original measured $^{143}\mathrm{Nd}/^{144}\mathrm{Nd}$ normalized to the chondritic uniform reservoir 0.512638 (CHUR, $t=0$) (Faure and Mensing, 2005) following the equation

$$\varepsilon\mathrm{Nd} = (^{144/143\mathrm{Nd}}\mathrm{sample}/^{144/143\mathrm{Nd}}\mathrm{CHUR} - 1) \times 10\,000. \quad (1)$$

Older rocks of similar mineralogical composition have more radiogenic $^{87}\mathrm{Sr}/^{86}\mathrm{Sr}$ and εNd due to prolonged radioactive decay. Sediments forming through physical weathering of crustal rocks inherit the isotope composition of their bedrock (Goldstein and Jacobsen, 1988, 1987). The Sr isotope composition in a dust sink may differ from the source due to mineral sorting e.g. during (aeolian) transport (Újvári et al., 2012), and selective depletion of Sr-bearing minerals during chemical weathering (e.g. Drouet et al., 2007). Hence, more soluble Sr-rich minerals such as carbonates may change the original $^{87}\mathrm{Sr}/^{86}\mathrm{Sr}$ bulk sediment composition. In contrast, εNd is strongly resistant to surface weathering and grain size sorting effects (Meyer et al., 2009; Újvári et al., 2012; Wang et al., 2007; Zhu et al., 2021), still reflecting the original or rather unchanged source rock composition. Prior to sample digestion, we dissolved pedogenic calcites while preserving clay minerals (0.5 M acetic acid) (Újvári et al., 2012). For sample digestion, we used 6 mL of 48 % HF (AR grade) and 1 mL of trace grade 68 % HNO_3 and heated the mixture at 150 °C in Teflon bombs. Purified Sr and Nd fractions were used to determine $^{143}\mathrm{Nd}/^{144}\mathrm{Nd}$ and $^{87}\mathrm{Sr}/^{86}\mathrm{Sr}$ using an Isotopix Phoenix TIMS (thermal ionization mass spectrometer) device through multi-dynamic analyses. For quality control, we ran the NIST SRM 987 reference material ($^{87}\mathrm{Sr}/^{86}\mathrm{Sr} = 0.710255 \pm 0.000013$ at 2σ, $n=5$) for Sr and the JNdi-1 reference material ($^{143}\mathrm{Nd}/^{144}\mathrm{Nd} = 0.512103 \pm 0.000004$ at 2σ, $n=7$) for Nd. The average standard error for 100 ratios of data for each of the samples is 0.000011 for $^{87}\mathrm{Sr}//^{86}\mathrm{Sr}$ and 0.000002 ± 2 SE for $^{143}\mathrm{Nd}/^{144}\mathrm{Nd}$ (for more information on sample preparation, purification, and quality control, please see Supplement).

3.5 Age modelling

Prud'homme et al. (2022) constrained the time span of a distinct unconformity at the base of SU 13 as a ~ 5–6 kyr hiatus spanning 30 970–30 199 to 24 619–23 863 cal BP, based on the closest radiocarbon ages below and above the unconformity, respectively (see Table 1). Quantitative climate reconstructions and the age model presented in Prud'homme et al. (2022) were related to the stratigraphical positions of the ECG samples chosen for either stable isotope analyses or radiocarbon dating, whereof no samples were taken from SU 13 and the lower part of SU 14 (both SUs located above the unconformity). Here, we performed continuous sampling in 2 cm intervals for grain size, bulk geochemical, and rock magnetic analyses. Thus, we produced a continuous analytical data set along a discontinuous age model. To account for this, we also integrated the stratigraphic information as described by Fischer et al. (2021). Based on their litho- and pedostratigraphic model, the erosional phase causing the hiatus in section RP1 must have taken place with or shortly after the deposition of the Eltville tephra. This tephra, whose average age is around 24.3 ka (Zens et al., 2017; Förster et al., 2020), is an important stratigraphic marker found in many western European LPSs (e.g. Meijs et al., 1983). We then re-calculated the age model with 2 cm intervals using the Bacon software (Blaauw and Christeny, 2011) and the IntCal20 calibration curve (Reimer et al., 2020). For the profile section from 260 cm (base of SU 13 = unconformity) to 222 cm below surface (position of the first radiocarbon sample above the unconformity), we assume a continuous age decrease with depth, ranging from 24 300 to 23 945 cal BP.

With regard to our interpretation of the proxy data plotted against the age model (Fig. 6), we are aware that age uncer-

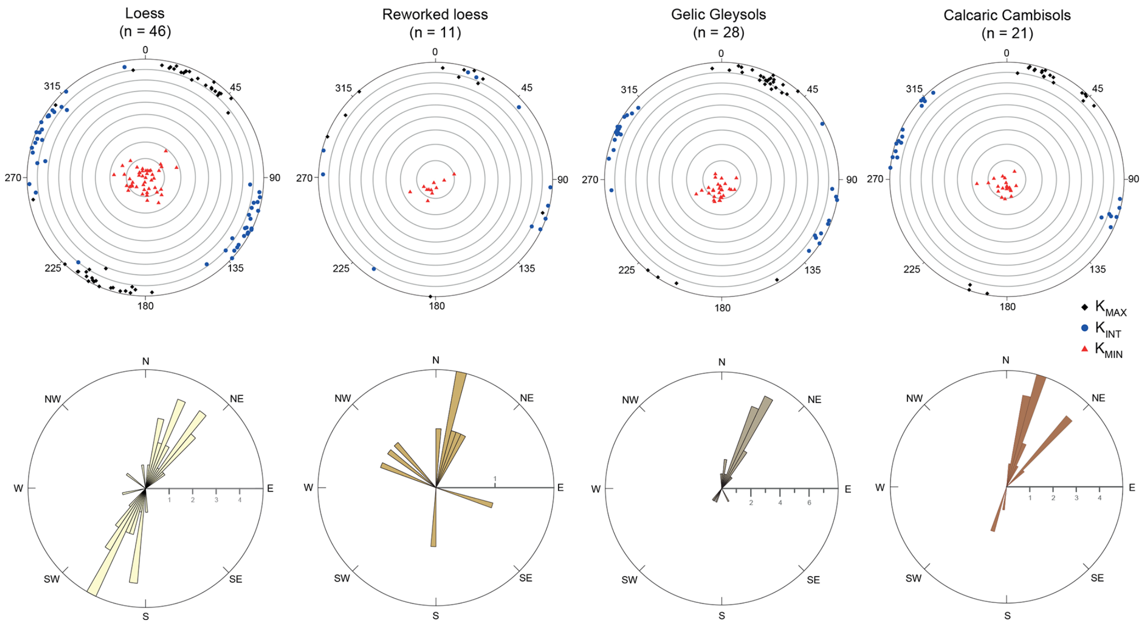

Figure 5. Stereoplots showing the full spatial orientation of K_{MAX}, K_{INT}, and K_{MIN} and rose diagrams of the lineations for all samples that passed the criteria as outlined (Fig. 4 and Sect. S1 in the Supplement) and the subsets for loess, reworked loess, Gelic Gleysols, and Calcaric Cambisols. See Figs. S1 and S2 for a comparison of all samples for each sediment type.

tainties occur both in the radiocarbon-based age model and in the INTIMATE (INTegration of Ice-core, MArine and TErrestrial records) event stratigraphy. In the latter, for instance, the maximal counting error for GI 5.2 is 1024 years (Rasmussen et al., 2014) and thus in a similar range as the errors in the underlying Bacon age model.

4 Results

4.1 Down-profile variation in selected proxy data

A clear subdivision of the RP1 profile is visible in all selected proxies. Based on significant sedimentological changes in the stratigraphical succession, a lower section (SUs 1–12) reaching to the unconformity and an upper section above the unconformity (SUs 13–21) are distinguished (Fig. 4). The U ratio shows maxima in the loess layers (SUs 7, 9, 10, 12) and in the middle of the basal soil complex (SUs 1–6), while the finest clay shows an inverse behaviour with distinct maxima in all well-developed palaeosols. Above the unconformity, the variations in clay content are significantly lower, showing a minimum at the transition from SU 13 to 14 and weak maxima in the Gelic Gleysols of SUs 15 and 17. In contrast, the U ratio shows higher and significant variations with absolute maxima in SUs 13 and 18 and weak minima in the Gelic Gleysols (SUs 15 and 17). Throughout the profile and especially below the unconformity, minima in the U ratio and maxima in the finest clay correspond to increased foliation values.

The MS shows low variations in the entire lower part, with a slight decrease from the base to the midst of SU 8, followed by slight increases towards the midst of SU 11 from where it slightly decreases again. Obviously, palaeosols and loess layers are not clearly differentiated. The $\mathrm{MS_{fd}}$ shows an overall decrease from the base to SU 11, with increased amplitudes above SU 6 and an inverse trend compared to the MS from the top of SU 8 to SU 11. In the top part of SU 11, the values significantly increase towards the unconformity. In SU 13 both MS and $\mathrm{MS_{fd}}$ reach maximum values, whereof the MS forms a distinct peak. Above, the MS shows minima in SUs 15, 17, and 20, where intensive hydromorphic staining has been observed. Another maximum is observed at the base of the reworked loess of SU 18, while the $\mathrm{MS_{fd}}$ is continuously decreasing towards the top of the sequence. Log Ti/Al shows minor variations throughout the lower section, with slightly increasing values on top of the Calcaric Cambisol of SU 8. As described for the MS and $\mathrm{MS_{fd}}$, also log Ti/Al increases towards the unconformity and above, again forming a distinct maximum in SU 13. Generally lowered values are observed until the top of SU 17 and above SU 19, with higher values in between. Log Sr/Rb shows the lowest values in the well-developed palaeosols of the basal soil complex. From the top of SU 5 the values increase, before they newly decrease from the top of SU 11 towards the unconformity. Remarkably, the MS and log Sr/Rb show a high correlation from SU 7 to SU 11. Above the unconformity, log Sr/Rb shows no significant variations. Both the $^{87}\mathrm{Sr}/^{86}\mathrm{Sr}$ ratio and εNd cover a relative restricted range from 0.722 to 0.730 and from −10.77 to −11.98, respectively. The $^{87}Sr/^{86}Sr$ ratio increases from the base until SU 6. In contrast, apart from the lowermost sample εNd follows this trend until SU 3 but turns into the opposite trend thereafter, reaching the absolute minimum at the base of SU 6, accompanied by the absolute maximum of $^{87}Sr/^{86}Sr$. Towards the unconformity, both $^{87}Sr/^{86}Sr$ and εNd show an inverse behaviour with decreasing $^{87}Sr/^{86}Sr$ and increasing εNd values. Above the unconformity, throughout the upper section only minor variations in $^{87}Sr/^{86}Sr$ occur. In contrast, εNd overall decreases towards the base of SU 18, apart from one peak at the top of SU 16. From the base of SU 18 it increases again until the top of the sequence, thus being decoupled from $^{87}Sr/^{86}Sr$ in the upper part of the sequence.

To sum up, all proxy records indicate not only significantly differing characteristics below and above the unconformity but also a clear change starting in the upper part of the Gelic Gleysol of SU 11.

4.2 Magnetic fabric

Overall, the preferential direction of the lineation of all samples that passed the assessment protocol (see Fig. 4, Sect. S1) is SSW to NNE (Fig. 5). This is also true for datasets comprising all samples (Figs. S1, 2). All stereoplots show a horizontal plain defined by K_{MAX}, K_{INT}, and K_{MIN} plotting perpendicular to this plain and close to the vertical axis. It should be noted that the principal axes of the AMS ellipsoids and the resulting lineations are linears and not vectors, as they do not indicate a distinct direction but only an alignment. For example, an NE-pointing trend in the rose diagrams is equivalent to a SW trend and vice versa, as the diagram is to be read point-symmetrically. In the rose diagrams of lineation and stereoplots, the loess units indicate clear populations (~ 15 to $\sim 45°$ and ~ 195 to $\sim 225°$) aligned $\sim$ NE-SW. However, reworked loess exhibits a second subordinate direction perpendicular to the main direction ($\sim$ NNE–SSW), possibly reflecting multiple water-runoff and sediment reworking effects (cf. Tarling and Hrouda, 1993). The Gelic Gleysols show a clear dominance of NNE–SSW lineations, and the Calcaric Cambisols show a preferential trend of lineations scattering between NNE–NE and SSW–SW. Further information on the AMS results is given in the Supplement.

5 Discussion

5.1 Stratigraphic interpretation of proxy data

In order to comprehensively discuss our results, all Schwalbenberg RP1 proxy data were plotted against the radiocarbon-derived Bayesian age model (Fig. 6) accomplished by sedimentation rate and precipitation quantification (Prud'homme et al., 2022). Schwalbenberg RP1 is subdivided into a lower section that covers the period from the end of GS 9 until the end of GS 5.2 ($\sim$ 39 200–30 800 cal BP) and an upper section covering the last third of GS 3 until GS 2.1 ($\sim$ 24 300–21 900 cal BP). In the lower section, well-developed palaeosols and loess layers particularly resolve the period from GIs 8–5.2 and corresponding GSs, respectively. Ranging between 2 and 3, the U ratio shows values typical for central European LPSs, with lower values during interstadials related to reduced wind activity and higher values during stadials indicating gustier winds (e.g. Vandenberghe, 2013; Kämpf et al., 2022).

The basal soil complex (SUs 2–6) contains well-developed Calcaric Cambisol horizons depicted by two distinct clay peaks and lowest Sr/Rb values, attesting intensive weathering and pedogenesis. In this context, the increase in $^{87}Sr/^{86}Sr$ is unlikely to predominantly reflect provenance changes due to its susceptibility to weathering impacts (cf. Clauer and Chauduri, 1995), while the distinct shift in εNd might be related to a dust source signal (see Sect. S4).

The first clay maximum is followed by an increase in the U ratio and a distinct peak in the sedimentation rate, corresponding to the second half of GI 8. After a short decline, the Schwalbenberg sedimentation rate increases in tandem with elevated dust probabilities in the nearby Eifel maar lakes (Eifel Laminated Sediment Archive, ELSA, dust probability; Seelos et al., 2009), indicating continuous dust input until the beginning of GI 5.2. This pattern diverges from the trend recorded in the North Greenland Ice Core Project (NGRIP), where high Ca^{2+} values relate to GSs and distinct minima to GIs. This difference supports the idea of an accretionary character of the Schwalbenberg LPSs in general and the palaeosols in particular, as described by Vinnepand et al. (2020) and Fischer et al. (2021).

After GI 7, clay contents in RP1generally decrease but still peak within the palaeosols of GI 6 (Calcaric Cambisol) and GI 5.2 (Gelic Gleysol). The U ratio follows exactly the opposite trend, showing overall coarsening. Hence, this indicates enhanced wind activity from GS 7 onwards, with clear maxima during GSs and reduction during GIs, respectively.

The MS_{fd} shows overall decreasing values from SU 1 up to the base of SU 11, indicating a continuous reduction in fine magnetic particles. As MS is contemporaneously increasing (Fig. 4), we assume that this opposite trend is related to a domination of wind vigour over pedogenesis (e.g. Evans and Heller, 2001). This is also supported by high U ratio values especially in loess layers (SUs 9 and 10) and a strong increase in log Sr/Rb, indicating reduced weathering and input of primary carbonates at the same time (see Vinnepand et al., 2020; Fischer et al., 2021).

Log Ti/Al, which is interpreted to relate to provenance (Zech et al., 2008; Profe et al., 2016), shows only minor fluctuations in the entire lower section until SU 12. In contrast, significant decreases in $^{87}Sr/^{86}Sr$ and increases in εNd are observed within GS 7 (top of SU 6 and SU 7) towards GI 6 (SU 8) and GS 6 (on top of SU 8) towards GI 5.2 (SU 11), respectively.

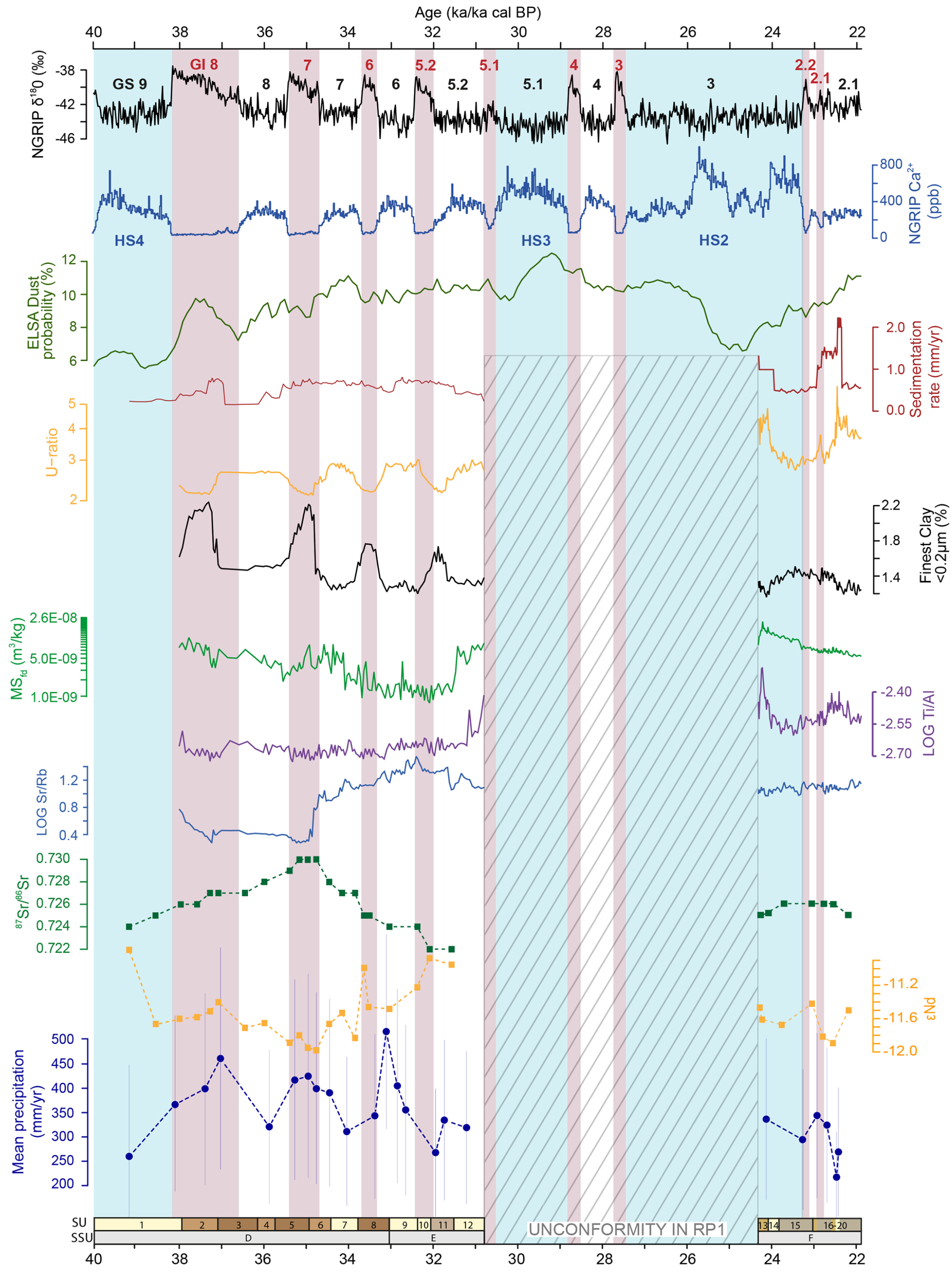

Figure 6. Comparison of selected proxy data from Schwalbenberg RP1, compared with the NGRIP event stratigraphy, with δ^{18}O and Ca^{2+} according to Rasmussen et al. (2014), and ELSA dust probability according to Seelos et al. (2009). Greenland Interstadials (GIs 8 to 2.1) are numbered in red and Greenland Stadials (GSs) in black, and Heinrich Stadials (HS4 to HS2) according to Reutenauer et al. (2015) are highlighted in light blue. Originally given as ages in years before 2000, the chronological scale has been shifted by 50 years to allow for direct comparisons with the calibrated radiocarbon scale given in calibrated years before CE 1950 (cal BP). Chronostratigraphy and sedimentation rates from Schwalbenberg are based on Bayesian age–depth modelling of the radiocarbon dated sequence using IntCal20 (cf. Prud'homme et al., 2022). U ratio, finest clay, frequency dependence of magnetic susceptibility MS_{fd} ($\Delta\chi$(fd)), log Ti/Al, and log SR/Rb are based on a continuous 2 cm sampling interval. ^{87}Sr/^{86}Sr and εNd are based on 35 samples along the profile (see Fig. 4). Mean annual precipitation estimates are based on the δ^{13}C values of ECGs (Prud'homme et al., 2022). SUs and SSUs according to Fischer et al. (2021). All data are given in Tables ST1 and ST2 in the Supplement.

These trends are likely to be related to a provenance change (see Sect. 5.2) that was contemporary with a strong decrease in reconstructed precipitation values.

During the following GS 5.2 a significant shift occurred. This was characterized by increased input of fine magnetic particles in accordance with a distinct increase in log Ti/Al and enhanced wind dynamics as indicated by the U ratio. In combination with the observed isotopic signals, this indicates severe changes in palaeoenvironmental conditions (see Sect. 5.3).

Above the unconformity, which we constrain to a hiatus of up to 6.5 kyr (between 30 800 and 24 300 cal BP), completely different characteristics are observed in both the stratigraphic record and the proxy data. We interpret the maxima in the U ratio, MS, and MS_{fd} as well as in log Ti/Al in SU 13 as the result of sediment relocation and recycling involving re-deposition of the Eltville tephra. The latter contains detrital volcanogenic magnetic Ti–Fe oxides which show frequently an oxidized rim of maghemite resulting from low-temperature oxidation upon incorporation into sediment. This oxidation process leads to particle-internal fining causing increasing superparamagnetic behaviour similar to pedogenic neo-formation. Here, it is limited to the maghemized shell consisting of ultrafine domains in the superparamagnetic single-domain (SD) range and therefore significantly increases the MS (e.g. Liu et al., 2012; Zhang et al., 2021). The highest sedimentation rates are in accordance with input of coarser material as indicated by the highest U ratio values. ELSA dust probability is also indicating increased dustiness, which is – for this time interval – not observed in NGRIP Ca^{2+}. The finest clay at RP1 is slightly increased where the U ratio forms a minimum related to the weakly developed Gelic Gleysols. After the distinct maximum, the MS_{fd} shows a continuous decrease. While log Sr/Rb and $^{87}Sr/^{86}Sr$ show almost no variations, log Ti/Al is increasing contemporarily with fluctuating εNd during GS 2, for which the lowest precipitation value is reconstructed. Overall, the stratigraphy and related proxy data and the comparison to NGRIP indicate that above the unconformity the dominance of local to regional effects caused the major changes.

5.2 Isotope geochemistry and AMS-derived near-surface wind trends: identification of dust source–sink relationships?

Potential shifts in dust provenance from the OIS 3 to OIS 2 transition have been reported based on bulk geochemistry and luminescence sensitivity for different Schwalbenberg LPSs (Klasen et al., 2015; Profe et al., 2016; Fitzsimmons et al., 2021; Vinnepand et al., 2022). These studies indicate that sediment recycling within local source areas as well as changes in wind direction may have caused the different signals. Here, we add information on isotopic composition and AMS-derived near-surface wind trends for Schwalbenberg RP1. We compare Sr and Nd isotope data from different potential dust source areas in western Europe (Fig. 7a). As stated before (see Sects. 4.1, 5.1), the variations in εNd are restricted to a narrow range, and significant shifts in $^{87}Sr/^{86}Sr$ in the lower section of the sequence may be related to enhanced in situ weathering. Against this background, caution is required in interpreting the presented data, but, nevertheless, our combination of proxies allows for some substantial contributions to the discussion of dust source-to-sink relationships. This is especially true as data on dust provenance based on precisely dated LPSs are still rather scarce, with Schwalbenberg RP1 representing one of the best dated LPSs of the wider region (Prud'homme et al., 2022).

Overall, the relatively coarse character of the silt and the regional geographic setting of the Schwalbenberg at the confluence of the rivers Ahr and Rhine in the centre of the Rhenish Massif (Fig. 1) suggest dominating local to regional dust components in most parts of the RP1 profile. Figure 7 shows that the Schwalbenberg Sr and Nd isotope data generally plot along a gradient between the recent suspended sediment load of the Upper Rhine (Tricca et al., 1999) and Devonian slates from the Rhenish Massif (Moragues-Quiroga et al., 2017). Hence, both the Rhine catchment and the Rhenish Massif can be assumed as potential silt source areas. In addition, both mixing hyperbolas between Eifel volcanites and the Devonian slates and the Siebengebirge and Westerwald volcanites and the Devonian slates indicate a certain amount of these volcanites to the Schwalbenberg LPSs. This might also be reflected in the relatively high Nd concentrations at Schwalbenberg (mean: 68.48 ppm; $n = 30$) in comparison to the Rhine suspended sediment load (11.1 ppm; Tricca et al., 1999), the Devonian slates of the Rhenish Massif (mean: 44.39 ppm; $n = 5$; Moragues-Quiroga et al., 2017), and regional Pleistocene periglacial slope deposits (mean = 44.64 ppm; $n = 3$; Moragues-Quiroga et al., 2017). As reference, leucite basalt and phonolite andesites typically have high Nd concentrations around 81 ppm (Faure and Mensing, 2005).

In contrast to Schwalbenberg, the LPS key sections of Nussloch (Figs. 1, 7), located approx. 200 km south-southeast on the eastern bank of the Upper Rhine, appear to be dominated by dust input from the alluvial plain of the Rhine River and other local sources (Schatz et al., 2015).

For other LPSs like Kesselt and Rocourt, both situated in Belgium at the north-western edge of the Rhenish Massif (Fig. 1), Sr and Nd isotope values of sediments that were deposited within the LGM (Gallet et al., 1998) indicate an important role of the Rhenish Massif as an additional local dust source besides the Rhine system. Similar findings were also reported for OIS 2 loess within the southern part of the Lower Rhine Embayment and the north-western edge of the Rhenish Massif (northern edge of the Eifel area) by Janus (1988). In that study a systematic increase in heavy minerals indicative of short-distance transport from the Eifel and Rhenish Massif sediment source towards LPSs located north-west of Schwalbenberg was observed, next to heavy minerals indica-

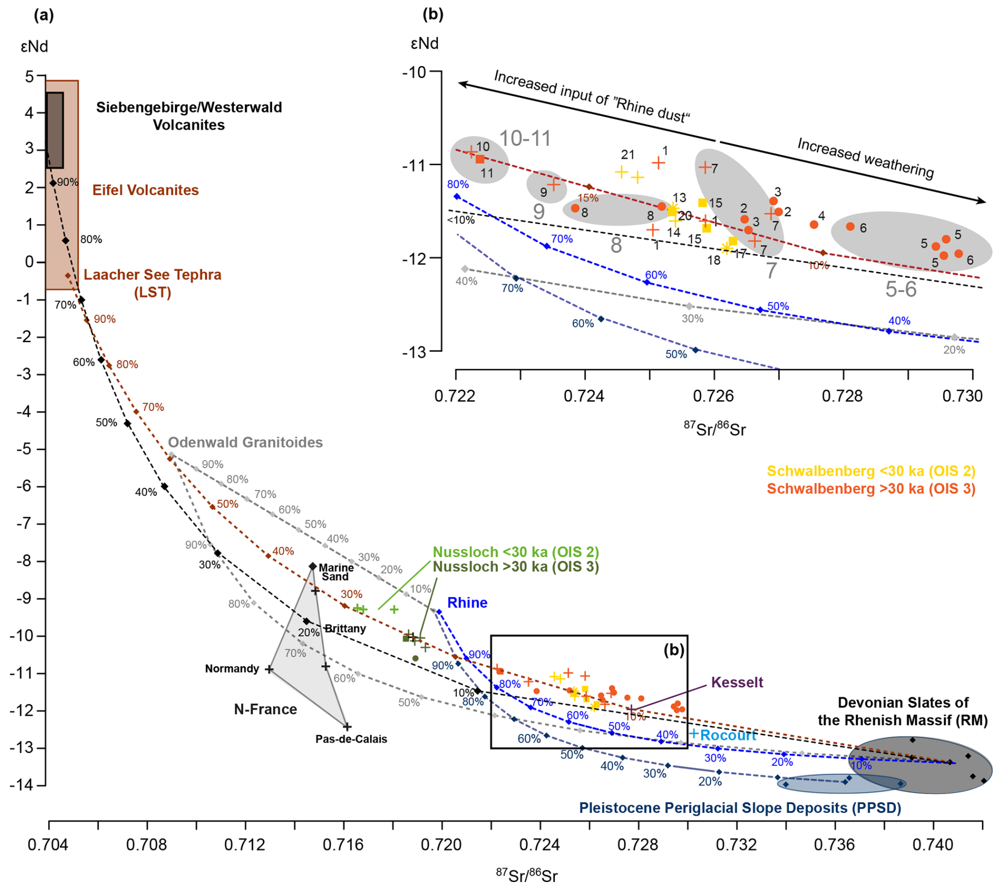

Figure 7. **(a)** εNd and $^{87}Sr/^{86}Sr$ of reference samples from different sites in western central Europe in comparison to Schwalbenberg RP1. Mixing hyperbolas indicate the possible mixing of two endmembers (in percentage) considering their Sr and Nd element concentrations and their respective isotope values (cf. Faure and Mensing, 2005; all data are presented in Table ST3 in the Supplement) and were calculated for mixtures between different endmembers (Devonian slate saprolite of the Rhenish Massif as continental crust endmember (grey; Moragues-Quiroga et al., 2017), Rhine suspended sediment load (blue; Tricca et al., 1999), Odenwald granitoids (light grey; Siebel et al., 2012), Siebengebirge and Westerwald volcanites (black; Schubert et al., 2015), Laacher See tephra and Eifel volcanites (red, as mantle-representing endmember; Wörner et al., 1985; note that Förster et al. (2020) showed that the Eltville tephra found at Schwalbenberg originated from an earlier eruption of the Laacher See volcano at 24.3 ka), northern France (Gallet et al., 1998), and Pleistocene periglacial slope deposits (PPSDs) in the Rhenish Massif (Moragues-Quiroga et al., 2017)). Our plot suggests that the Schwalbenberg LPSs are dominated by sediments from the Rhine valley as also described for Nussloch (Schatz et al., 2015). Compared to the latter, the isotope composition of the Kesselt and Rocourt LPSs (Gallet et al., 1998) (see Fig. 1) and the Schwalbenberg LPSs indicate a higher amount of dust originating from Devonian slates of the Rhenish Massif and/or PPSDs overlying the Devonian rocks. In addition, mantle-derived material from the Eifel and from the Siebengebirge and Westerwald potentially contributes to the dust deposited at Schwalbenberg. Odenwald granitoids may reflect a contribution via small Rhine tributaries. **(b)** Detail of plot **(a)** (see inset): the grey numbers refer to SUs, and the grey ellipses highlight that the samples above SU 7 up to SU 11 may reflect an enhanced contribution of sediments from the Rhine towards the end of OIS 3. In contrast, SUs below SU 7 down to SU 5, correlating to matured Calcaric Cambisols from the basal soil complex of the RP1 profile, plot offsite towards more radiogenic Sr isotope values, indicating enhanced weathering. Symbology: loess (+), reworked loess (∗), Gelic Gleysols (■), and Calcaric Cambisols (•).

tive of Rhine terraces and small Eifel riverbeds dissecting the Rhine terraces as the main source areas.

Although the data shown in Fig. 7 indicate general differences in dust provenance, we have to keep in mind that (i) the variations in Schwalbenberg RP1 Sr isotope composition are certainly also influenced by in situ pedogenesis (see Fig. 7b, especially within SUs 5 and 6 where the strongest weathering is observed); (ii) the reference data for the suspended sediment load from the southernmost part of the Upper Rhine River (south of the Kaiserstuhl; see Fig. 1) mainly reflect material originating from Miocene marine sediments of the Alpine Molasse (Buhl et al., 1991), thus not including important Rhine tributaries located further north (e.g. the rivers Main, Nahe, Lahn, and Mosel); (iii) also non-alpine provenance spectra contribute considerably to the Pleistocene and recent sediment budged of the Upper Rhine (Preusser et al., 2021; Hülscher et al., 2018); and (iv) sediments from the Rhine catchment most likely experienced several cycles of grain size reduction, sorting, and mixing within the alluvial plain and fluvial transport prior to its deposition at the Schwalbenberg LPSs. Such processes occurring in the alluvial plains of river systems have recently been discussed by Pötter et al. (2021) for LPSs from the Lower Danube and by Baykal et al. (2022) for LPSs from the northern fringe of the European loess belt in the context of dust provenance.

Despite the given limitations a clear change in isotope composition after GI 7 (top of SU 6 and SU 7) and after GI 6 (SU 8) up to GS 5.2 (top SU 11) is indicated by slightly increasing εNd and decreasing $^{87}Sr/^{86}Sr$ values, pointing to enhanced input of dust being more comparable to the Rhine suspended load (see Fig. 7b). This trend is accompanied by a reduction of fine magnetic particles (decreasing MS_{fd}), reduced weathering (increasing log Sr/Rb), and gustier winds indicated by a dominance of wind vigour (inverse behaviour of MS and MS_{fd}) and high U ratio values (see Sect. 5.1).

Throughout the upper section of RP1 both isotope ratios do not show typical inverse trends (Fig. 6). This may be due to sediment sorting and reworking as observed within the RP1 upper section, which may have biased the Sr isotope composition. Nevertheless, slightly varying εNd values in combination with significant variations in log Ti/Al might reflect increased dust input from local to regional sources of the Rhenish Massif. In combination with the AMS-based reconstruction of SSW–NNE near-surface wind trends (Figs. 4, 8), we assume that the alluvial plains of the rivers Rhine and Ahr most likely are the dominating local sediment sources for the investigated part of the Schwalbenberg LPS.

Based on our AMS data, however, we cannot decide whether the near-surface winds came from SSW or NNE, but wind regime statistics for the Schwalbenberg site in the valley setting indicate an overall dominance of westerly and south-westerly winds during the LGM and recent times (Prud'homme et al., 2022).

In addition to these large alluvial sources, exposed fine-grained rocks (e.g. in the incised upper Ahr valley), alluvial plains of small creeks, abandoned river terraces, and widespread Pleistocene periglacial slope deposits (PPSDs) may also have played an important role in silt production. Furthermore, recycling of loess deposits may have contributed an additional dust component into the LPS (cf. Mroczek, 2013).

Overall, the obtained data on dust provenance and near-surface wind trends point to dominating local dust sources that were associated with gustier winds with predominant SSW–NNE wind directions in stadial phases, while interstadials may have been characterized by a significant dust component from more distant sources. In this context, we found a significant negative relationship between the AMS foliation (F) and the U ratio in SUs 5, 7, and 8 (see Fig. S4), whereof SU 5 correlates to GI 7 and SU 8 to GI 6 (Fig. 6). This may indicate that fine to medium silt particles establish

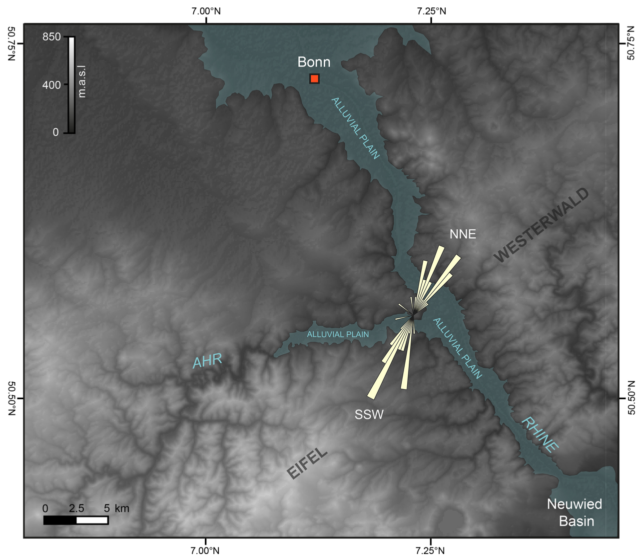

Figure 8. DEM-based map (SRTM 30; USGS 2022) showing reconstructed near-surface wind trends for the Schwalbenberg site and possible short distance entrainment areas for mineral dust. The SSW–NNE wind trend estimates are only based on AMS measurements of loess samples (beige rose diagram), which passed the assessment protocol for primary magnetic fabric (see Fig. 4) that is described in Sects. 3.3 and S1. For AMS stereoplots and rose diagrams please see Fig. 5.

the AMS signal within these interstadials, possibly owing to the continuous accumulation of dust during soil formation resulting in accretionary palaeosols (Fischer et al., 2021; Vinnepand et al., 2022). To our knowledge, such a clear correlation between finer grain sizes and increasing foliation has been so far not described in any LPS on stadial–interstadial scales (cf. Bradák et al., 2021). However, Zhang et al. (2010) proposed a model in which more frequent summer precipitation during relative mild climatic periods (interglacials and interstadials) led to an improved settling of anisotropic grains (e.g. micas and clay minerals), causing the overall increased AMS foliation. In contrast, most loess units throughout RP1 and weakly developed Gelic Gleysols in the upper section (SUs 15, 17, 20) show a positive linear relationship between F and the U ratio, indicating that coarse silt particles play a major role for the AMS signal in these units that were related to gustier winds and input of short-travelled dust.

5.3 Palaeoenvironmental and palaeoclimatic implications

Millennial- to centennial-scale synchronicity between the Schwalbenberg LPSs and the NGRIP $\delta^{18}O$ record was proposed based on litho- and pedostratigraphic evidence combined with organic carbon contents (Fischer et al., 2021), further attested by radiocarbon dating and a quantitative climate reconstruction based on the investigation of ECGs (Prud'homme et al., 2022). Here we observe very largely synchronous patterns between NGRIP $\delta^{18}O$ and Ca^{2+} and the Schwalbenberg sedimentological proxies (U ratio, finest clay), further supporting the close synchronicity of western European and North Atlantic climate changes. In addition, we present proxy data allowing for further characterization of the dust deposited within the Schwalbenberg LPSs and comprehensive palaeoenvironmental reconstructions based on magnetic fabric, environmental magnetism, bulk geochemistry, and isotope composition.

The lower section of the Schwalbenberg RP1 profile covers in high resolution the period from the end of GS 9 (contemporary with Heinrich Stadial 4) to the end of GS 5.2 (Fig. 6). In the wider region this period is characterized by a distinct opening of the landscape as suggested by a landscape evolution model of the Eifel area that is based on multi-method approaches applied to ELSA (Sirocko et al., 2016). This model documents the transition from boreal forested environments (landscape evolution zone (LEZ) 7, onset ∼ 49 years b2k) to steppe-like open environments (LEZ 6, ∼ 36.4–28.45 years b2k), which is interpreted as the environmental reaction due to a longer cooling trend accompanied by increased aridity in the Rhenish Massif at roughly the time of the OIS 3 to OIS 2 transition. At Schwalbenberg this cooling trend is, on the one hand, reflected in decreasing intensities of soil formation from the lower soil complex (SUs 2–6, covering GI 8 and 7) towards the Calcaric Cambisol correlated to GI 6 (SU 8) and the Gelic Gleysol correlated to GI 5 (SU 11) (cf. Vinnepand et al., 2020; Fischer et al., 2021). On the other hand, overall increasing U ratio values and the reduction of fine magnetic particles as indicated by decreasing MS_{fd} values point towards an enhancement of wind activity and increasing dryness simultaneously with reduced sediment recycling until mid-GS 5.2 at ∼ 31 500 cal BP. The latter is also supported by reduced weathering intensity following GI 7, as evidenced in a slightly increasing log Sr/Rb ratio accompanied by a distinct decrease in $^{87}Sr/^{86}Sr$ and an increase in εNd. This can be interpreted in terms of an enhanced input of dust that carries an isotope signal comparable to that of the Rhine's suspended load (Fig. 7b). This trend coincides with distinct aridification, climate cooling, and grain coarsening observed in some LPSs along the Rhine during late OIS 3 (Prud'homme et al., 2018; Vinnepand et al., 2020) and might be related to intensified periglacial conditions in the local silt sources and enhanced glacial grinding activity and sediment availability in front of the advancing Alpine ice sheet and the Rhine Glacier in particular (Ivy-Ochs et al., 2008).

For the interstadial periods we are able to reconstruct reduced but still pronounced dust deposition at the Schwalbenberg LPSs (Fischer et al., 2021; Prud'homme et al., 2022). Vegetation cover and moister conditions as suggested by Prud'homme et al. (2022) especially for GIs 8–6 for Schwalbenberg favour (reduced) dust deposition rather than its entrainment (see Újvári et al., 2016). In addition, intensified syn-sedimentary soil formation in interstadials, especially during GI 8 and GI 7, leads to the production of clay minerals in the course of silicate weathering, hampering the entrainment of particles due to strong cohesion and adhesion forces (cf. Újvári et al., 2016). As discussed before, we observed an inverse correlation of the U ratio and the AMS foliation but a positive correlation of the finest clay and the foliation within the Calcaric Cambisols of the lower section of RP1 (see Sect. S1). This could point, beside secondary grain size reduction in the course of pedogenesis, to an input of finer-grained (potentially long-distant) aeolian material during interstadials, which might be also visible in described shifts in εNd (see Sect. 5.2).

At Schwalbenberg we observe a further distinct shift around 31 500 cal BP associated with increased wind activity and in particular significantly enhanced sediment recycling reflected by a distinct shift in MS_{fd} and a potential provenance shift indicated by log Ti/Al (Fig. 6). On a regional scale, the same period is characterized by increased flood activity in the Eifel area (Sirocko et al., 2016) possibly related to enhanced seasonal landscape instability caused by a reduced vegetation cover and associated sediment relocation. On a supra-regional scale, the advancing Fennoscandian (FIS) and British–Irish ice sheets (BIIS) correlating with the onset of the LGM (Lambeck et al., 2014), with some moderate ice marginal retreats during HS3 (Toucanne et al., 2015), and the further advancing Rhine Glacier (Ivy-Ochs et al., 2008) played an important role in dust production and circulation patterns in western, central, and eastern Europe (Schaffernicht et al., 2020). Simultaneously, a significant increase in the sedimentation rate occurred at Nussloch (Prud'homme et al., 2022), whereas in northern France the first genuine loess unit originates only from the following stadial GS 5.1 (Antoine et al., 2014). Associated with overall cooler and drier conditions over western and central Europe during the LGM, evidence is provided for cyclones that were capable of triggering enhanced dustiness related to higher wind speeds (Pinto and Ludwig, 2020). This is in agreement with the assumption of strong NW winds especially between 34 and 17 ka, resulting in local input of coarse aeolian material, high sedimentation rates, and the SE-trending "greda" morphology at Nussloch (Antoine et al., 2009).

At Schwalbenberg RP1, however, on top of the distinct unconformity that is related to local channel formation and sediment relocation, which may have reworked and included the Eltville tephra (Fischer et al., 2021), different proxies pinpoint environmental conditions that were significantly different from the preceding ones that were most likely dominated by local to regional signals.

Sediment relocation reflected within SU 13 was followed by reduced wind activity, input of finer-grained sediments, and reduced sedimentation rates until ∼ 22 900 cal BP, roughly coinciding with the later part of LEZ 5 in the Eifel area that represents the transition from steppe to tundra-like environments (Sirocko et al., 2016).

After 22 900 cal BP, the sedimentation rate and U ratio reach the highest values throughout the entire RP1 profile, indicating increased dustiness but also potential sediment reworking processes. Enhanced dustiness is, however, also reflected in the REM 3 LPS (cf. Fischer et al., 2021; Fig. 3) and the ELSA dust probability (Fig. 6) associated with the development of the polar desert of LEZ 4 in the Eifel area (Sirocko et al., 2016) but is decoupled from NGRIP Ca^{2+}, which shows a clear minimum after 23 300 BP.

Further evidence for local to regional dust transport is provided by heavy mineral analyses of the Dehner Maar, where increased dust activity and a shift from predominantly westerly to strong easterly winds is reported for the period from 23 until 20 ka (Römer et al., 2016). In this context, the AMS-based reconstruction of near-surface wind trends at Schwalbenberg RP1 may point to periods with significant north-easterly winds during overall dominating western wind directions (Prud'homme et al., 2022). This would be in agreement with dust-cycle simulations for the LGM, showing that beside westerlies and embedded cyclones persistent easterlies associated with anticyclonic flow may have also played a significant role for dust deposition. These would have resulted in westward-running dust plumes and associated high dust accumulation rates in the North German plain including adjacent regions (Pinto and Ludwig, 2020; Schaffernicht et al., 2020).

6 Conclusions

We present an integrative approach that systematically combines physical and geochemical proxies, enabling a synthetic interpretation of LPS formation in western central Europe. We focus on the Schwalbenberg RP1 LPS that is exposed north-west of the confluence of the Ahr and Rhine rivers in the centre of the Rhenish Massif. We integrate our data into a robust and reliable age model that has been established based on high-resolution dating of ECGs. We show that Schwalbenberg RP1 is subdivided into a lower section and an upper section that are separated by a major stratigraphic unconformity. Whereas the lower section corresponds to late OIS 3 ($\sim$ 39 200–30 800 cal BP; end of GS 9 until GS 5.2), the upper section dates into the LGM ($\sim$ 24 300–21 900 cal BP; end of GS 3 until GS 2.1).

In general, we could confirm the assumption of syn-sedimentary soil formation during interstadials, give evidence for provenance changes with overall dominating local to regional dust sources, and confirm the close temporal linkages to other climate archives in the North Atlantic region, which we have highlighted in earlier studies.

Based on our synthetic approach we can draw the following, more specific conclusions:

- In combination with the established age model, the sedimentological proxies of the lower section at Schwalbenberg RP1 attest to – to a certain degree – similar and largely synchronous patterns of northern hemispheric climatic changes as evidenced in NGRIP $\delta^{18}O$ and Ca^{2+}, supporting the overall synchronicity of climatic changes in and around the North Atlantic region.

- A significant negative relationship between the AMS foliation and the U ratio found in interstadial palaeosols and intercalated stadial loess layers, respectively, may indicate that fine to medium silt particles increase the foliation. This could possibly reflect the continuous accumulation of fine dust during soil formation and the simultaneous increase in precipitation, causing improved alignment of sediment grains into the bedding plain. To our knowledge, such a clear correlation between finer grain size and increasing foliation has so far not been described for any LPS for stadial–interstadial cycles, i.e. on millennial to centennial timescales.

- A distinct shift towards increased input of "Rhine dust" and reduced weathering intensity occurs simultaneously with an overall cooling and aridification trend in Europe towards the end of OIS 3.

- A further distinct shift visible in all proxy data around 31 500 cal BP, interpreted in terms of enhanced wind activity with significant input of coarse-grained material recycled from local sources, is possibly related to increased landscape instability when tundra-like conditions – probably associated with deep seasonal or even permafrost – developed towards the LGM.

- The proxies within the upper section pinpoint environmental conditions that were significantly different from those in the lower section, which were most likely dominated by more local to regional signals and high sedimentation rates.

- AMS-based reconstructions of near-surface wind trends may indicate the influence of north-easterly winds beside the overall dominance of westerlies and embedded cyclones, causing high dust accumulation rates.

Overall, by integrating our approach in the study of LPSs over a broader geographic area, we see the opportunity for a more comprehensive understanding of LPS formation including changes in dust composition and associated circulation patterns during Quaternary climate changes.

Data availability. All raw data are available in the tables of the Supplement with this publication.

Supplement. The supplement related to this article is available online at: https://doi.org/10.5194/egqsj-72-163-2023-supplement.

Author contributions. This study was designed by PF, UH, MV, and CZ. Fieldwork and sampling was done by PF, UH, OM, MV, and the TerraClime team. Granulometric and bulk geochemical analyses were performed by FL and PS at RWTH Aachen University. The Sr and Nd isotope analyses were conducted by CC at the James Hutton Institute in Aberdeen, Scotland. Interpretation and manuscript writing were executed by MV and PF, with the contribution of all other authors. Research funds were raised by KF, PF, and AV (see below).

Competing interests. At least one of the (co-)authors is a member of the editorial board of *E&G Quaternary Science Journal*. The peer-review process was guided by an independent editor, and the authors do not have any other competing interests to declare.

Disclaimer. Publisher's note: Copernicus Publications remains neutral with regard to jurisdictional claims in published maps and institutional affiliations.

Special issue statement. This article is part of the special issue "Quaternary research from and inspired by the first virtual DEUQUA conference". It is a result of the vDEUQUA2021 online conference in September/October 2021.

Acknowledgements. This articles contributes to the TerraClime project (project number 337232800) funded by the German Research Foundation (DFG). We greatly appreciate the extensive fieldwork conducted by the whole TerraClime Team and associates, namely Kristina Reetz (JGU Mainz), Alexandra Nimmrichter (JGU Mainz), and Aileen Klinger (JGU Mainz). We would like to thank the two reviewers for constructive comments that helped to significantly improve the manuscript.

Financial support. This research has been supported by the Deutsche Forschungsgemeinschaft (grant no. 337232800).

This open-access publication was funded by Johannes Gutenberg University Mainz.

Review statement. This paper was edited by Hans von Suchodoletz and reviewed by two anonymous referees.

References

Antoine, P., Rousseau, D.-D., Moine, O., Kunesch, S., Hatté, C., Lang, A., Tissoux, H., and Zöller, L.: Rapid and cyclic aeolian deposition during the Last Glacial in European loess: a high-resolution record from Nussloch, Germany, Quaternary Sci. Rev., 28, 2955–2973, https://doi.org/10.1016/j.quascirev.2009.08.001, 2009.

Antoine, P., Goval, E., Jamet, G., Coutard, S., Moine, O., Hérisson, D., Auguste, P., Guérin, G., Lagroix, F., Schmidt, E., Robert, V., Debenham, N., Meszner, S., and Bahain, J. J.: The upper pleistocene loess sequences of havrincourt (Pas-de-Calais, France). Stratigraphy, palaeoenvironments, geochronology and human occupations, Quaternaire, 25, 321–368, https://doi.org/10.4000/quaternaire.7278, 2014.

Baykal, Y., Stevens, T., Bateman, M. D., Pfaff, K., Sechi, D., Banak, A., Šuica, S., Zhang, H., and Nie, J.: Eurasian Ice Sheet derived meltwater pulses and their role in driving atmospheric dust activity: Late Quaternary loess sources in SE England, Quaternary Sci. Rev., 296, 107804, https://doi.org/10.1016/j.quascirev.2022.107804, 2022.

Blaauw, M. and Christeny, J. A.: Flexible paleoclimate age-depth models using an autoregressive gamma process, Bayesian Anal., 6, 457–474, https://doi.org/10.1214/11-BA618, 2011.

Blott, S. J., Croft, D. J., Pye, K., Saye, S. E., and Wilson, H. E.: Particle size analysis by laser diffraction, Geological Society, London, Special Publications, 232, 63–73, https://doi.org/10.1144/GSL.SP.2004.232.01.08, 2004.

Boenigk, W. and Frechen, M.: The Pliocene and Quaternary fluvial archives of the Rhine system, Quaternary Sci. Rev., 25, 550–574, https://doi.org/10.1016/j.quascirev.2005.01.018, 2006.

Bradák, B., Seto, Y., Chadima, M., Kovács, J., Tanos, P., Újvári, G., and Hyodo, M.: Magnetic fabric of loess and its significance in Pleistocene environment reconstructions, Earth-Sci. Rev., 210, 103385, https://doi.org/10.1016/j.earscirev.2020.103385, 2020.

Bradák, B., Seto, Y., Stevens, T., Újvári, G., Fehér, K., and Költringer, C.: Magnetic susceptibility in the European Loess Belt: New and existing models of magnetic enhancement in loess, Palaeogeogr. Palaeocl., 569, 110329, https://doi.org/10.1016/j.palaeo.2021.110329, 2021.

Buggle, B., Glaser, B., Hambach, U., Gerasimenko, N., and Marković, S.: An evaluation of geochemical weathering indices in loess-paleosol studies, Quaternary Int., 240, 12–21, https://doi.org/10.1016/j.quaint.2010.07.019, 2011.

Buggle, B., Hambach, U., Müller, K., Zöller, L., Marković, S. B., and Glaser, B.: Iron mineralogical proxies and quaternary climate change in SE-european loess-paleosol sequences, Catena, 117, 4–22, https://doi.org/10.1016/j.catena.2013.06.012, 2014.

Buhl, D., Neuser, R. D., Richter, D. K., Riedel, D., Roberts, B., Strauss, H., and Veizer, J.: Nature and nurture: Environmental isotope story of the River Rhine, Naturwissenschaften, 78, 337–346, https://doi.org/10.1007/BF01131605, 1991.

Clauer, N. and Chaudhuri, S.: Clays in Crustal Environments, Springer, Berlin, Heidelberg, https://doi.org/10.1007/978-3-642-79085-0, 1995.

DePaolo, D. J. and Wasserburg, G. J.: Nd isotopic variations and petrogenetic models, Geophys. Res. Lett., 3, 249–252, https://doi.org/10.1029/GL003i005p00249, 1976.

Deutscher Wetterdienst: Deutscher Wetterdienst (German Meteorological Service): https://www.dwd.de/DE/leistungen/klimadatendeutschland/klimadatendeutschland.html, (last access: 2 March 2022), 2023.

Drouet, Th., Herbauts, J., Gruber, W., and Demaiffe, D.: Natural strontium isotope composition as a tracer of weathering patterns and of exchangeable calcium sources in acid leached soils developed on loess of central Belgium, Eur. J. Soil Sci., 58, 302–319, https://doi.org/10.1111/j.1365-2389.2006.00840.x, 2007.

Evans, M. E. and Heller, F.: Magnetism of loess/palaeosol sequences: recent developments, Earth-Sci. Rev., 54, 129–144, https://doi.org/10.1016/S0012-8252(01)00044-7, 2001.

Evans, M. E. and Heller, F.: Environmental Magnetism: Principles and Applications of Enviromagnetics, Elsevier, Amsterdam, 318 pp., ISBN 978-0-122-43851-6, 2003.

Faure, G. and Mensing, T. M.: Principles and applications, John Wiley & Sons, Inc, New York, ISBN 978-0-471-38437-3, 2005.

Federal Institute for Geosciences and Natural Resources Germany: Federal Institute for Geosciences and Natural Resources Germany, https://www.bgr.bund.de/DE/Home/homepage_node.html, last access: 23 March 2022.

Feng, J.-L., Zhu, L.-P., Zhen, X.-L., and Hu, Z.-G.: Grain size effect on Sr and Nd isotopic compositions in eolian dust: implications for tracing dust provenance and Nd model age, Geochem. J., 43, 123–131, https://doi.org/10.2343/geochemj.1.0007, 2009.

Fischer, P., Hambach, U., Klasen, N., Schulte, P., Zeeden, C., Steininger, F., Lehmkuhl, F., Gerlach, R., and Radtke, U.: Landscape instability at the end of MIS 3 in western Central Europe: evidence from a multi proxy study on a Loess-Palaeosol-Sequence from the eastern Lower Rhine Embayment, Germany, Quaternary Int., 502, 119–136, https://doi.org/10.1016/j.quaint.2017.09.008, 2019.

Fischer, P., Jöris, O., Fitzsimmons, K. E., Vinnepand, M., Prud'homme, C., Schulte, P., Hatté, C., Hambach, U., Lindauer, S., Zeeden, C., Peric, Z., Lehmkuhl, F., Wunderlich, T., Wilken, D., Schirmer, W., and Vött, A.: Millennial-scale terrestrial ecosystem responses to Upper Pleistocene climatic changes: 4D-reconstruction of the Schwalbenberg Loess-Palaeosol-Sequence (Middle Rhine Valley, Germany), CATENA, 196, 104913, https://doi.org/10.1016/j.catena.2020.104913, 2021.

Fitzsimmons, K. E., Perić, Z., Nowatzki, M., Lindauer, S., Vinnepand, M., Prud'homme, C., Dave, A. K., Vött, A., and Fischer, P.: Luminescence Sensitivity of Rhine Valley Loess: Indicators of Source Variability?, Quaternary, 5, 1, https://doi.org/10.3390/quat5010001, 2021.

Förster, M. W., Zemlitskaya, A., Otter, L. M., Buhre, S., and Sirocko, F.: Late Pleistocene Eifel eruptions: insights from clinopyroxene and glass geochemistry of tephra layers from Eifel Laminated Sediment Archive sediment cores, J. Quaternary Sci., 35, 186–198, https://doi.org/10.1002/jqs.3134, 2020.

Forster, Th., Evans, M. E., and Heller, F.: The frequency dependence of low field susceptibility in loess sediments, Geophys. J. Int., 118, 636–642, https://doi.org/10.1111/j.1365-246X.1994.tb03990.x, 1994.

Frechen, M., Oches, E., and Kohlfeld, K.: Loess in Europe – mass accumulation rates during the Last Glacial Period, Quaternary Sci. Rev., 22, 1835–1857, https://doi.org/10.1016/S0277-3791(03)00183-5, 2003.

Fuhrmann, F., Seelos, K., and Sirocko, F.: Eolian sedimentation in central European Auel dry maar from 60 to 13 ka, Quaternary Res., 101, 4-12, https://doi.org/10.1017/qua.2020.81, 2021.

Gallet, S., Jahn, B., Van Vliet Lanoë, B., Dia, A., and Rossello, E.: Loess geochemistry and its implications for particle origin and composition of the upper continental crust, Earth Planet. Sci. Lett., 156, 157–172, https://doi.org/10.1016/S0012-821X(97)00218-5, 1998.

Goldstein, S. J. and Jacobsen, S. B.: The Nd and Sr isotopic systematics of river-water dissolved material: Implications for the sources of Nd and Sr in seawater, Chem. Geol.: Isotope Geoscience section, 66, 245–272, https://doi.org/10.1016/0168-9622(87)90045-5, 1987.

Goldstein, S. J. and Jacobsen, S. B.: Nd and Sr isotopic systematics of river water suspended material: implications for crustal evolution, Earth Planet. Sci. Lett., 87, 249–265, https://doi.org/10.1016/0012-821X(88)90013-1, 1988.

Goldstein, S. L., O'Nions, R. K., and Hamilton, P. J.: A Sm-Nd isotopic study of atmospheric dusts and particulates from major river systems, Earth Planet. Sci. Lett., 70, 221–236, https://doi.org/10.1016/0012-821X(84)90007-4, 1984.

Grousset, F. E. and Biscaye, P. E.: Nd and Sr Isotopes as Tracers of Wind Transport: Atlantic Aerosols and Surface Sediments, in: Paleoclimatology and Paleometeorology: Modern and Past Patterns of Global Atmospheric Transport, edited by: Leinen, M. and Sarnthein, M., Springer Netherlands, Dordrecht, 385–400, https://doi.org/10.1007/978-94-009-0995-3_16, 1989.

Grousset, F. E. and Biscaye, P. E.: Tracing dust sources and transport patterns using Sr, Nd and Pb isotopes, Chem. Geol., 222, 149–167, https://doi.org/10.1016/J.CHEMGEO.2005.05.006, 2005.

Hrouda, F.: Anisotropy of magnetic susceptibility of rocks in the Rayleigh Law region: Modelling errors arising from linear fit to non-linear data, Studia Geophyssica et Geodaetica, 51, 423–438, https://doi.org/10.1007/s11200-007-0024-5, 2007.

Hülscher, J., Bahlburg, H., and Pfänder, J.: New geochemical results indicate a non-alpine provenance for the Alpine Spectrum (epidote, garnet, hornblende) in quaternary Upper Rhine sediment, Sediment. Geol., 375, 134–144, https://doi.org/10.1016/j.sedgeo.2018.02.010, 2018.

Ivy-Ochs, S., Kerschner, H., Reuther, A., Preusser, F., Heine, K., Maisch, M., Kubik, P. W., and Schlüchter, C.: Chronology of the last glacial cycle in the European Alps, J. Quaternary Sci., 23, 559–573, https://doi.org/10.1002/jqs.1202, 2008.

Janus, U.: Löss der südlichen niederrheinischen Bucht, Kölner Geographische Arbeiten, 49, ISSN 0454-1294. 1988.

Jones, R. M.: Particle size analysis by laser diffraction: ISO 13320, standard operating procedures, and Mie theory, American Laboratory, Corpus ID 221270121, 2003.

Kämpf, L., Rius, D., Duprat-Oualid, F., Crouzet, C., and Millet, L.: Evidence for wind patterns and associated landscape response in Western Europe between 46 and 16 ka cal. BP, Quaternary Sci. Rev., 298, 107846, https://doi.org/10.1016/j.quascirev.2022.107846, 2022.

Klasen, N., Fischer, P., Lehmkuhl, F., and Hilgers, A.: Luminescence dating of loess deposits from the Remagen-Schwalbenberg site, Western Germany, Geochronometria, 42, 67–77, https://doi.org/10.1515/geochr-2015-0008, 2015.

Knippertz, P. and Stuut, J.-B. W. (Eds.): Mineral Dust, Springer Netherlands, Dordrecht, https://doi.org/10.1007/978-94-017-8978-3, 2014.

Lambeck, K., Rouby, H., Purcell, A., Sun, Y., and Sambridge, M.: Sea level and global ice volumes from the Last Glacial Maximum to the Holocene, P. Natl. Acad. Sci. USA, 111, 15296–15303, https://doi.org/10.1073/pnas.1411762111, 2014.

Lehmkuhl, F., Nett, J. J., Pötter, S., Schulte, P., Sprafke, T., Jary, Z., Antoine, P., Wacha, L., Wolf, D., Zerboni, A., Hošek, J., Marković, S. B., Obreht, I., Sümegi, P., Veres, D., Zeeden, C., Boemke, B., Schaubert, V., Viehweger, J., and Hambach, U.: Loess landscapes of Europe – Mapping, geomorphology, and zonal differentiation, Earth-Sci. Rev., 215, 103496, https://doi.org/10.1016/j.earscirev.2020.103496, 2021.

Liu, Q., Roberts, A. P., Larrasoaña, J. C., Banerjee, S. K., Guyodo, Y., Tauxe, L., and Oldfield, F.: Environmental magnetism: Principles and applications, Rev. Geophys., 50, RG4002, https://doi.org/10.1029/2012RG000393, 2012.

Mahowald, N. M., Muhs, D. R., Levis, S., Rasch, P. J., Yoshioka, M., Zender, C. S., and Luo, C.: Change in atmospheric mineral aerosols in response to climate: Last glacial period, preindustrial, modern, and doubled carbon dioxide climates, J. Geophys. Res.-Atmos., 111, D10202, https://doi.org/10.1029/2005JD006653, 2006.

Marx, S. K., Kamber, B. S., McGowan, H. A., Petherick, L. M., McTainsh, G. H., Stromsoe, N., Hooper, J. N., and May, J.-H.: Palaeo-dust records: A window to understanding past environments, Global Planet. Change, 165, 13–43, https://doi.org/10.1016/j.gloplacha.2018.03.001, 2018.

McGee, D., Broecker, W. S., and Winckler, G.: Gustiness: The driver of glacial dustiness?, Quaternary Sci. Rev., 29, 2340–2350, https://doi.org/10.1016/j.quascirev.2010.06.009, 2010.

Meijs, E., Mücher, H., Ouwerkerk, G., Romein, A., and Stoltenberg, H.: Evidence of Presence of the Eltville Tuff Layer in Dutsch and Belgian Limbourg and the Consequences for the Loess Stratigraphy, E&G Quaternary Sci. J., 33, 59–78, https://doi.org/10.3285/eg.33.1.06, 1983.

Meschede, M.: Geologie Deutschlands: ein prozessorientierter Ansatz, Springer Spektrum, Berlin, 252 pp., ISBN 978-3662452974, 2018.

Meyer, R., Nicoll, G. R., Hertogen, J., Troll, V. R., Ellam, R. M., and Emeleus, C. H.: Trace element and isotope constraints on crustal anatexis by upwelling mantle melts in the North Atlantic Igneous Province: an example from the Isle of Rum, NW Scotland, Geol. Magazine, 146, 382–399, https://doi.org/10.1017/S0016756809006244, 2009.

Meyer, W. and Stets, J.: Das Rheintal zwischen Bingen und Bonn, Borntraeger, Berlin, 386 pp., ISBN 978-3-443-15069-3, 1996.

Moine, O., Antoine, P., Hatté, C., Landais, A., Mathieu, J., Prud'homme, C., and Rousseau, D. D.: The impact of Last Glacial climate variability in west-European loess revealed by radiocarbon dating of fossil earthworm granules, P. Natl. Acad. Sci. USA, 114, 209–214, https://doi.org/10.1073/pnas.1614751114, 2017.

Moragues-Quiroga, C., Juilleret, J., Gourdol, L., Pelt, E., Perrone, T., Aubert, A., Morvan, G., Chabaux, F., Legout, A., Stille, P., and Hissler, C.: Genesis and evolution of regoliths: Evidence from trace and major elements and Sr-Nd-Pb-U isotopes, CATENA, 149, 185–198, https://doi.org/10.1016/j.catena.2016.09.015, 2017.

Mroczek, P.: Recycled loesses – A micromorphological approach to the determination of local source areas of Weichselian loess, Quaternary Int., 296, 241–250, https://doi.org/10.1016/j.quaint.2013.02.040, 2013.

Muhs, D. R.: The geologic records of dust in the quaternary, Aeolian Res., 9, 3–48, https://doi.org/10.1016/j.aeolia.2012.08.001, 2013.

Obreht, I., Zeeden, C., Hambach, U., Veres, D., Marković, S. B., Bösken, J., Svirčev, Z., Bačević, N., Gavrilov, M. B., and Lehmkuhl, F.: Tracing the influence of Mediterranean climate on Southeastern Europe during the past 350,000 years, Sci. Rep., 6, 36334, https://doi.org/10.1038/srep36334, 2016.

Ozer, M., Orhan, M., and Isik, N. S.: Effect of Particle Optical Properties on Size Distribution of Soils Obtained by Laser Diffraction, Environ. Eng. Geosci., 16, 163–173, https://doi.org/10.2113/gseegeosci.16.2.163, 2010.

Pinto, J. G. and Ludwig, P.: Extratropical cyclones over the North Atlantic and western Europe during the Last Glacial Maximum and implications for proxy interpretation, Clim. Past, 16, 611–626, https://doi.org/10.5194/cp-16-611-2020, 2020.

Pötter, S., Veres, D., Baykal, Y., Nett, J. J., Schulte, P., Hambach, U., and Lehmkuhl, F.: Disentangling Sedimentary Pathways for the Pleniglacial Lower Danube Loess Based on Geochemical Signatures, Front. Earth Sci., 9, 600010, https://doi.org/10.3389/feart.2021.600010, 2021.

Preusser, F., Büschelberger, M., Kemna, H. A., Miocic, J., Mueller, D., and May, J.-H.: Exploring possible links between Quaternary aggradation in the Upper Rhine Graben and the glaciation history of northern Switzerland, Int. J. Earth Sci. (Geol. Rundsch), 110, 1827–1846, https://doi.org/10.1007/s00531-021-02043-7, 2021.

Profe, J., Zolitschka, B., Schirmer, W., Frechen, M., and Ohlendorf, C.: Geochemistry unravels MIS 3/2 paleoenvironmental dynamics at the loess–paleosol sequence Schwalbenberg II, Germany, Palaeogeogr. Palaeoclim. Palaeoecol., 459, 537–551, https://doi.org/10.1016/j.palaeo.2016.07.022, 2016.

Prud'homme, C., Lécuyer, C., Antoine, P., Hatté, C., Moine, O., Fourel, F., Amiot, R., Martineau, F., and Rousseau, D.-D.: δ 13 C signal of earthworm calcite granules: A new proxy for palaeoprecipitation reconstructions during the Last Glacial in western Europe, Quaternary Sci. Rev., 179, 158–166, https://doi.org/10.1016/j.quascirev.2017.11.017, 2018.

Prud'homme, C., Fischer, P., Jöris, O., Gromov, S., Vinnepand, M., Hatté, C., Vonhof, H., Moine, O., Vött, A., and Fitzsimmons, K. E.: Millennial-timescale quantitative estimates of climate dynamics in central Europe from earthworm calcite granules in loess deposits, Commun. Earth Environ., 3, 1–14, https://doi.org/10.1038/s43247-022-00595-3, 2022.

Rasmussen, S. O., Bigler, M., Blockley, S. P., Blunier, T., Buchardt, S. L., Clausen, H. B., Cvijanovic, I., Dahl-Jensen, D., Johnsen, S. J., Fischer, H., Gkinis, V., Guillevic, M., Hoek, W. Z., Lowe, J. J., Pedro, J. B., Popp, T., Seierstad, I. K., Steffensen, J. P., Svensson, A. M., Vallelonga, P., Vinther, B. M., Walker, M. J. C., Wheatley, J. J., and Winstrup, M.: A stratigraphic framework for abrupt climatic changes during the Last Glacial period based on three synchronized Greenland ice-core records: refining and extending the INTIMATE event stratigraphy, Quaternary Sci. Rev., 106, 14–28, https://doi.org/10.1016/j.quascirev.2014.09.007, 2014.

Reimer, P. J., Austin, W. E. N., Bard, E., Bayliss, A., Blackwell, P. G., Bronk Ramsey, C., Butzin, M., Cheng, H., Edwards, R. L., Friedrich, M., Grootes, P. M., Guilderson, T. P., Hajdas, I., Heaton, T. J., Hogg, A. G., Hughen, K. A., Kromer, B., Manning, S. W., Muscheler, R., Palmer, J. G., Pearson, C., Van Der Plicht, J., Reimer, R. W., Richards, D. A., Scott, E. M., Southon, J. R., Turney, C. S. M., Wacker, L., Adolphi, F., Büntgen, U., Capano, M., Fahrni, S. M., Fogtmann-Schulz, A., Friedrich, R., Köhler, P., Kudsk, S., Miyake, F., Olsen, J., Reinig, F., Sakamoto, M., Sookdeo, A., and Talamo, S.: The IntCal20 Northern Hemisphere Radiocarbon Age Calibration Curve (0–55 cal kBP), Radiocarbon, 62, 725–757, https://doi.org/10.1017/RDC.2020.41, 2020.

Reutenauer, C., Landais, A., Blunier, T., Bréant, C., Kageyama, M., Woillez, M.-N., Risi, C., Mariotti, V., and Braconnot, P.: Quantifying molecular oxygen isotope variations during a Heinrich stadial, Clim. Past, 11, 1527–1551, https://doi.org/10.5194/cp-11-1527-2015, 2015.

Römer, W., Lehmkuhl, F., and Sirocko, F.: Late Pleistocene aeolian dust provenances and wind direction changes reconstructed by heavy mineral analysis of the sediments of the Dehner dry maar (Eifel, Germany), Global Planet. Change, 147, 25–39, https://doi.org/10.1016/j.gloplacha.2016.10.012, 2016.

Rousseau, D. D., Sima, A., Antoine, P., Hatté, C., Lang, A., and Zöller, L.: Link between European and North Atlantic abrupt climate changes over the last glaciation, Geophys. Res. Lett., 34, L22713, https://doi.org/10.1029/2007GL031716, 2007.

Rousseau, D.-D., Derbyshire, E., Antoine, P., and Hatté, C.: European Loess Records, Reference Module in Earth Systems and Environmental Sciences, Elsevier, Amsterdam, https://doi.org/10.1016/b978-0-12-409548-9.11136-4, 2018.

Sauer, D. and Felix-Henningsen, P.: Saprolite, soils, and sediments in the Rhenish Massif as records of climate and landscape history, Quaternary Int., 156–157, 4–12, https://doi.org/10.1016/j.quaint.2006.05.001, 2006.

Schad, P., Van Huyssteen, M., Anjos, L., Gaistordo, C., Deckers, J., Dondeyne, S., Eberhardt, E., Gerasimova, M., Harms, B., Jones, A., Krasilnikov, P., Reinsch, T., Vargas, T., and Zhang, G.: World reference base for soil resources 2014 International soil classification system for naming soils and creating legends for soil maps, 3rd Ed., edited by: Peter Schad, Cornie van Huyssteen, Erika Michéli, FAO, Rome (Italy), ISBN 978-92-5-108369-7, 2015.

Schaetzl, R. J., Bettis, E. A., Crouvi, O., Fitzsimmons, K. E., Grimley, D. A., Hambach, U., Lehmkuhl, F., Marković, S. B., Mason, J. A., Owczarek, P., Roberts, H. M., Rousseau, D.-D., Stevens, T., Vandenberghe, J., Zárate, M., Veres, D., Yang, S., Zech, M., Conroy, J. L., Dave, A. K., Faust, D., Hao, Q., Obreht, I., Prud'homme, C., Smalley, I., Tripaldi, A., Zeeden, C., and Zech, R.: Approaches and challenges to the study of loess – Introduction to the LoessFest Special Issue, Quaternary Res., 89, 563–618, https://doi.org/10.1017/qua.2018.15, 2018.

Schaffernicht, E. J., Ludwig, P., and Shao, Y.: Linkage between dust cycle and loess of the Last Glacial Maximum in Europe, Atmos. Chem. Phys., 20, 4969–4986, https://doi.org/10.5194/acp-20-4969-2020, 2020.

Schatz, A.-K., Qi, Y., Siebel, W., Wu, J., and Zöller, L.: Tracking potential source areas of Central European loess: examples from Tokaj (HU), Nussloch (D) and Grub (AT), Open Geosci., 7, 678–7, https://doi.org/10.1515/geo-2015-0048, 2015.

Schirmer, W.: Eine Klimakurve des Oberpleistozäns aus dem rheinischen Löss, E&G Quaternary Sci. J., 50, 25–49, https://doi.org/10.3285/eg.50.1.02, 2000.

Schirmer, W.: Rhine loess at Schwalbenberg II — MIS 4 and 3, E&G Quaternary Sci. J., 61, 32–47, https://doi.org/10.3285/eg.61.1.03, 2011.

Schmidt, C., Zeeden, C., Krauß, L., Lehmkuhl, F., and Zöller, L.: A chronological and palaeoenvironmental re-evaluation of two loess-palaeosol records in the northern Harz foreland, Germany, based on innovative modelling tools, Boreas, 50, 746–763, https://doi.org/10.1111/bor.12510, 2021.

Schubert, S., Jung, S., Pfänder, J. A., Hauff, F., and Garbe-Schönberg, D.: Petrogenesis of Tertiary continental intraplate lavas between Siebengebirge and Westerwald, Germany: Constraints from trace element systematics and Nd, Sr and Pb isotopes, J. Volcanol. Geotherm. Res., 305, 84–99, https://doi.org/10.1016/J.JVOLGEORES.2015.08.023, 2015.

Schulte, P. and Lehmkuhl, F.: The difference of two laser diffraction patterns as an indicator for post-depositional grain size reduction in loess-paleosol sequences, Palaeogeogr. Palaeoclim. Palaeoecol., 509, 126–136, https://doi.org/10.1016/j.palaeo.2017.02.022, 2018.

Schulte, P., Lehmkuhl, F., Steininger, F., Loibl, D., Lockot, G., Protze, J., Fischer, P., and Stauch, G.: Influence of HCl pretreatment and organo-mineral complexes on laser diffraction measurement of loess–paleosol-sequences, CATENA, 137, 392–405, https://doi.org/10.1016/j.catena.2015.10.015, 2016.

Seelos, K., Sirocko, F., and Dietrich, S.: A continuous high-resolution dust record for the reconstruction of wind systems in central Europe (Eifel, Western Germany) over the past 133 ka, Geophys. Res. Lett., 36, L2072, https://doi.org/10.1029/2009GL039716, 2009.

Sheldon, N. D. and Tabor, N. J.: Quantitative paleoenvironmental and paleoclimatic reconstruction using paleosols, Earth-Sci. Rev., 95, 1–52, https://doi.org/10.1016/j.earscirev.2009.03.004, 2009.

Siebel, W., Eroğlu, S., Shang, C. K., and Rohrmüller, J.: Zircon geochronology, elemental and Sr-Nd isotope geochemistry of two Variscan granitoids from the Odenwald-Spessart crystalline complex (mid-German crystalline rise), Mineral. Petrol., 105, 187–200, https://doi.org/10.1007/s00710-012-0200-3, 2012.

Sirocko, F., Knapp, H., Dreher, F., Förster, M. W., Albert, J., Brunck, H., Veres, D., Dietrich, S., Zech, M., Hambach, U., Röhner, M., Rudert, S., Schwibus, K., Adams, C., and Sigl, P.: The ELSA-Vegetation-Stack: Reconstruction of Landscape Evolution Zones (LEZ) from laminated Eifel maar sediments of the last 60,000 years, Global Planet. Change, 142, 108–135, https://doi.org/10.1016/j.gloplacha.2016.03.005, 2016.

Smalley, I., O'Hara-Dhand, K., Wint, J., Machalett, B., Jary, Z., and Jefferson, I.: Rivers and loess: The significance of long river transportation in the complex event-sequence approach to loess deposit formation, Quaternary Int., 198, 7–18, https://doi.org/10.1016/j.quaint.2008.06.009, 2009.

Tarling, D. H. and Hrouda, F.: The Magnetic Anisotropy of Rocks, Chapman & Hall, London, 1993.

Taylor, S. N. and Lagroix, F.: Magnetic anisotropy reveals the depositional and postdepositional history of a loess-paleosol sequence at Nussloch (Germany): AMS of the Nussloch Loess-Paleosol Sequence, J. Geophys. Res.-Solid Earth, 120, 2859–2876, https://doi.org/10.1002/2014JB011803, 2015.

Taylor, S. N., Lagroix, F., Rousseau, D. D., and Antoine, P.: Mineral magnetic characterization of the upper pleniglacial nussloch loess sequence (Germany): An insight into local environmental processes, Geophys. J. Int., 199, 1463–1480, https://doi.org/10.1093/gji/ggu331, 2014.

Toucanne, S., Soulet, G., Freslon, N., Jacinto, R. S., Dennielou, B., Zaragosi, S., Eynaud, F., Bourillet, J.-F., and Bayon, G.: Millennial-scale fluctuations of the European Ice Sheet at the end of the last glacial, and their potential impact on global climate, Quaternary Sci. Rev., 123, 113–133, 2015.

Tricca, A., Stille, P., Steinmann, M., Kiefel, B., Samuel, J., and Eikenberg, J.: Rare earth elements and Sr and Nd isotopic compositions of dissolved and suspended loads from small river systems in the Vosges mountains (France), the river Rhine and groundwater, Chem. Geol., 160, 139–158, https://doi.org/10.1016/S0009-2541(99)00065-0, 1999.

Újvári, G., Varga, A., Ramos, F. C., Kovács, J., Németh, T., and Stevens, T.: Evaluating the use of clay mineralogy, Sr–Nd isotopes and zircon U–Pb ages in tracking dust provenance: An example from loess of the Carpathian Basin, Chem. Geol., 304–305, 83–96, https://doi.org/10.1016/j.chemgeo.2012.02.007, 2012.

Újvári, G., Kok, J. F., Varga, G., and Kovács, J.: The physics of wind-blown loess: Implications for grain size proxy interpretations in Quaternary paleoclimate studies, Earth-Sci. Rev., 154, 247–278, https://doi.org/10.1016/j.earscirev.2016.01.006, 2016.

Újvári, G., Stevens, T., Molnár, M., Demény, A., Lambert, F., Varga, G., Jull, A. J. T., Páll-Gergely, B., Buylaert, J.-P., and Kovács, J.: Coupled European and Greenland last glacial dust activity driven by North Atlantic climate, P. Natl. Acad. Sci. USA, 114, E10632–E10638, https://doi.org/10.1073/pnas.1712651114, 2017.

Újvári, G., Klötzli, U., Stevens, T., Svensson, A., Ludwig, P., Vennemann, T., Gier, S., Horschinegg, M., Palcsu, L., Hippler, D., Kovács, J., Di Biagio, C., and Formenti, P.: Greenland Ice Core Record of Last Glacial Dust Sources and Atmospheric Circulation, J. Geophys. Res.-Atmos., 127, e2022JD036597, https://doi.org/10.1029/2022JD036597, 2022.

Vandenberghe, J.: Grain size of fine-grained windblown sediment: A powerful proxy for process identification, Earth-Sci. Rev., 121, 18–30, https://doi.org/10.1016/j.earscirev.2013.03.001, 2013.

Vandenberghe, J., Mücher, H., Roebroeks, W., and Gemke, D.: Lithostratigraphy and palaeoenvironment of the Pleistocene deposits at Maastricht-Belvédère, southern Limburg, the Netherlands, Analecta Praehistorica Leidensia 18-Maastricht-Belvédère: Stratigraphy, palaeoenvironment and archaeology of the middle and late pleistocene deposits, Analecta Praehist. Leiden, 18, 7–18, 1985.

Vandenberghe, J., Zhisheng, A., Nugteren, G., Huayu, L., and Van Huissteden, K.: New absolute time scale for the Quaternary climate in the Chinese Loess region by grain-size analysis, Geology, 25, 35–38, https://doi.org/10.1130/0091-7613(1997)025<0035:NATSFT>2.3.CO;2, 1997.

Vinnepand, M., Fischer, P., Fitzsimmons, K., Thornton, B., Fiedler, S., and Vött, A.: Combining Inorganic and Organic Carbon Stable Isotope Signatures in the Schwalbenberg Loess-Palaeosol-Sequence Near Remagen (Middle Rhine Valley, Germany), Front. Earth Sci., 8, 276, https://doi.org/10.3389/feart.2020.00276, 2020.

Vinnepand, M., Fischer, P., Jöris, O., Hambach, U., Zeeden, C., Schulte, P., Fitzsimmons, K. E., Prud'homme, C., Perić, Z., Schirmer, W., Lehmkuhl, F., Fiedler, S., and Vött, A., Decoding geochemical signals of the Schwalbenberg Loess-Palaeosol-Sequences – A key to Upper Pleistocene ecosystem responses to climate changes in western Central Europe, Catena, 212, 106076, https://doi.org/10.1016/j.catena.2022.106076, 2022.

von Suchodoletz, H., Kühn, P., Hambach, U., Dietze, M., Zöller, L., and Faust, D.: Loess-like and palaeosol sediments from Lanzarote (Canary Islands/Spain) – Indicators of palaeoenvironmental change during the Late Quaternary, Palaeogeogr. Palaeoclimatol. Palaeoecol., 278, 71–87, https://doi.org/10.1016/j.palaeo.2009.03.019, 2009.

Wang, Y.-X., Yang, J.-D., Chen, J., Zhang, K.-J., and Rao, W.-B.: The Sr and Nd isotopic variations of the Chinese Loess Plateau during the past 7 Ma: Implications for the East Asian winter monsoon and source areas of loess, Palaeogeogr. Palaeoclimatol. Palaeoecol., 249, 351–361, https://doi.org/10.1016/j.palaeo.2007.02.010, 2007.

Weltje, G. J., Bloemsma, M. R., Tjallingii, R., Heslop, D., Röhl, U., and Croudace, I. W.: Prediction of Geochemical Composition from XRF Core Scanner Data: A New Multivariate Approach Including Automatic Selection of Calibration Samples and Quantification of Uncertainties, in: Micro-XRF Studies of Sediment Cores: Applications of a non-destructive tool for the environmental sciences, edited by: Croudace, I. W. and Rothwell, R. G., Springer Netherlands, Dordrecht, 507–534, https://doi.org/10.1007/978-94-017-9849-5_21, 2015.

Wörner, G., Staudigel, H., and Zindler, A.: Isotopic constraints on open system evolution of the Laacher See magma chamber (Eifel, West Germany), Earth Planet. Sci. Lett., 75, 37–49, https://doi.org/10.1016/0012-821X(85)90048-2, 1985.

Zech, M., Zech, R., Zech, W., Glaser, B., Brodowski, S., and Amelung, W.: Characterisation and palaeoclimate of a loess-like permafrost palaeosol sequence in NE Siberia, Geoderma, 143, 281–295, https://doi.org/10.1016/j.geoderma.2007.11.012, 2008.

Zeeden, C. and Hambach, U.: Magnetic Susceptibility Properties of Loess From the Willendorf Archaeological Site: Implications for the Syn/Post-Depositional Interpretation of Magnetic Fabric, Front. Earth Sci., 8, 599491, https://doi.org/10.3389/feart.2020.599491, 2021.

Zeeden, C., Hambach, U., and Händel, M.: Loess magnetic fabric of the Krems-Wachtberg archaeological site, Quaternary Int., 372, 188–194, https://doi.org/10.1016/j.quaint.2014.11.001, 2015.

Zeeden, C., Hambach, U., Obreht, I., Hao, Q., Abels, H. A., Veres, D., Lehmkuhl, F., Gavrilov, M. B., and Marković, S. B.: Patterns and timing of loess-paleosol transitions in Eurasia: Constraints for paleoclimate studies, Global Planet. Change, 162, 1-7, https://doi.org/10.1016/j.gloplacha.2017.12.021, 2018.

Zens, J., Zeeden, C., Römer, W., Fuchs, M., Klasen, N., and Lehmkuhl, F.: The Eltville Tephra (Western Europe) age revised: Integrating stratigraphic and dating information from different Last Glacial loess localities, Palaeogeogr. Palaeoclimatol. Palaeoecol., 466, 240–251, https://doi.org/10.1016/j.palaeo.2016.11.033, 2017.

Zhang, Q., Appel, E., Stanjek, H., Byrne, J. M., Berthold, C., Sorwat, J., Rösler, W., and Seemann, T.: Humidity related magnetite alteration in an experimental setup, Geophys. J. Int., 224, 69–85, https://doi.org/10.1093/gji/ggaa394, 2021.

Zhang, R., Kravchinsky, V. A., Zhu, R., and Yue, L.: Paleomonsoon route reconstruction along a W–E transect in the Chinese Loess Plateau using the anisotropy of magnetic susceptibility: Summer monsoon model, Earth Planet. Sci. Lett., 299, 436–446, https://doi.org/10.1016/j.epsl.2010.09.026, 2010.

Zhu, X., Liu, L., Wang, X., and Ji, J.: The Sr-Nd isotope geochemical tracing of Xiashu Loess and its implications for the material transport mechanism of the Yangtze River, CATENA, 203, 105335, https://doi.org/10.1016/j.catena.2021.105335, 2021.

E&G Quaternary Sci. J., 72, 185–187, 2023
https://doi.org/10.5194/egqsj-72-185-2023

Open Access E&G Quaternary Science Journal

Preface

Preface: Quaternary research from and inspired by the first virtual DEUQUA conference

Julia Meister[1], Hans von Suchodoletz[2], and Christian Zeeden[3]

[1]Institute of Geography and Geology, University of Würzburg, 97074 Würzburg, Germany
[2]Institute of Geography, University of Leipzig, 04103 Leipzig, Germany
[3]Rock Physics and Borehole Geophysics, Leibniz Institute for Applied Geophysics, 30655 Hanover, Germany

Correspondence: Julia Meister (julia.meister@uni-wuerzburg.de)

Relevant dates: Published: 9 August 2023

How to cite: Meister, J., von Suchodoletz, H., and Zeeden, C.: Preface: Quaternary research from and inspired by the first virtual DEUQUA conference, E&G Quaternary Sci. J., 72, 185–187, https://doi.org/10.5194/egqsj-72-185-2023, 2023.

1 The vDEUQUA2021 online conference

The global Covid-19 pandemic, which began in 2020 and did not abate until 2022, had not only a major impact on the lives of millions of people, but also a noticeable impact on science (Jack and Glover, 2021; Schadeberg et al., 2022). In this context, as with numerous other conferences, the regular meeting of the German Quaternary Association (DEUQUA) had to be postponed from 2020 to 2022, so in early 2021 the following question arose: "do we want to live for 4 years without intensive exchange on Quaternary science issues?" To fill this gap, a team of eight Quaternary scientists at different career stages from different research institutions organized the virtual "vDEUQUA2021" meeting from 29 to 30 September 2021. Supported by DEUQUA and the scientific platform Sciencesconf as well as the University of Würzburg, it was possible to organize this meeting via the online platforms Gather and Zoom. The online format limited classical face-to-face exchange but at the same time enabled an unprecedented international DEUQUA conference with more than 180 participants from 21 countries, with a share of more than 50 % early-career scientists. This led to intensive exchange and networking within a much broader Quaternary community than at previous on-site DEUQUA meetings.

The very interdisciplinary conference program and the high number of contributions impressively demonstrated the strong interest in Quaternary science and the high demand for scientific exchange despite – or especially because of – the exceptional pandemic situation. This may be explained by (i) the key role that Quaternary science plays in determining the pre-industrial background of the dramatic current climatic, geomorphological and geoecological changes due to strongly increased human activity ("the past is the key to the future"; Woodroffe and Murray-Wallace, 2012; McCaroll, 2015) and (ii) the rapid methodical developments within this field that are permanently expanding the possibilities of approaching climate and environmental archives in novel ways, as well as of addressing new research questions, requiring intensive and rapid scientific exchange and feedback (Banerji et al., 2022; Britton et al., 2022). Accordingly, these recent developments are also reflected in the 12 articles of this conference volume, which deal with pre-industrial climatic, geomorphological and geoecological changes as well as with methodological developments.

2 The contributions to this volume

Vinnepand et al. (2023) study paleoenvironmental changes at the Schwalbenberg RP1 loess–paleosol sequence in the Middle Rhine Valley in Germany between $\sim$40 and 22 ka using a multi-method approach. Their results confirm the assumption of synsedimentary soil formation during interstadials, show loess provenance changes with overall dominating local to regional dust sources and confirm the close temporal linkages of their proxies to those in other paleoclimate archives in the North Atlantic region.

Tinapp et al. (2023) report on valley development of the Elbe Valley near Dresden during the last ∼ 15 kyr. Their study links sedimentation, soil formation and archeology in the area. Sedimentologically, they find that a Preboreal clayey sedimentation phase is followed by two fine sandy sedimentation phases before Holocene clayey sedimentation occurs. Of particular interest is the finding that during a longer period between the Atlantic and Subboreal the Lower Weichsel Terrace was used for settlement by the Linear Pottery culture. Thereafter flooding led to sparser (Bronze Age) or absent settlements on the lower terrace.

Pötter et al. (2023) reconstruct a wetland environment for a late Middle to Upper Pleniglacial (approx. 30–20 ka) loess sequence in western Germany. They find that the investigated section was influenced by periodical flooding, leading to marshy conditions and a stressed ecosystem. Overall, the results show that the landscape of the study area was much more fragmented during this time than previously thought.

Hardt et al. (2023) investigate the geomorphological and geological characteristics of the archeological sites Hawelti–Melazo and their surroundings in northern Ethiopia by performing sedimentological analyses, as well as direct (luminescence) and indirect (radiocarbon) sediment dating. They were able to reconstruct the paleoenvironmental conditions in the late Quaternary, which they integrated into the wider context of Tigray.

Schwahn et al. (2023) investigate the loess sequence of Köndringen in the Upper Rhine Graben using a multi-method approach including the measurement of color, grain size, organic matter and carbonate content. The analyses reveal that the sequence comprises several fossil soils and layers of reworked soil material. According to luminescence dating, it reaches back more than 500 000 years.

Ullmann et al. (2022) highlight the application of a freely available tool for Google Earth Engine. The software allows cloud-free satellite images to be processed. They show processing examples for the Nile Delta (Egypt) and how remote sensing images are used to find indications of buried landforms, such as former river branches of the Nile.

Liu et al. (2022) present an isotope geochemical study on mammoth tooth enamel from the Upper Rhine Graben. Their work is both methodological and applied. While methodological aspects of obtaining ideal samples are discussed, their study also reports high-resolution paleoenvironmental records of likely sub-seasonal resolution.

Engel et al. (2022) investigate the late-glacial Bergstraßenneckar, a former course of the Neckar River in the Upper Rhine Graben in southwest Germany, by sediment cores and geophysical measurements. They were able to reconstruct the shift from a running river to silting-up meanders that took place about 11 000 to 10 500 years ago.

Abdulkarim et al. (2022) analyze the patterns and provenance of paleochannels in the French Upper Rhine alluvial plain. They find at least five paleochannel groups which can be distinguished. Assessing their timing and sedimentology will shed further light on the paleochannel evolution of the area.

Schulze et al. (2022) study a Late Weichselian loess–paleosol sequence in the southern Upper Rhine Graben in southwestern Germany using a multi-method approach. They found drier conditions in the southern compared with the northern Upper Rhine Graben, and they confirm an earlier start of massive loess accumulation compared with the arrival of glaciers in the foreland of the Alps.

Kirchner et al. (2022) evaluate recent soil agro-potential and search for evidence of prehistoric and historic land use by applying a pedo-geomorphological approach in the surroundings of Munigua, a small Roman city in the ancient province of Hispania Baetica (SW Spain). The available evidence of Roman agricultural use in the Munigua area suggests that the city's economy was by no means solely focused on mining.

Labahn et al. (2022) measure $\delta^{18}O$ of plant-derived lipids in a loess–paleosol sequence in Serbia over the last glacial–interglacial cycle, a method that was recently proposed as a paleoclimatic/paleohydrologic proxy. They obtained enough bulk lipids for analysis, demonstrating the general applicability of this method to loess–paleosol sequences. Furthermore, systematically higher values in paleosols compared with loess layers were observed. However, short-term climatic fluctuations could not be recognized, which requires further research.

Disclaimer. Publisher's note: Copernicus Publications remains neutral with regard to jurisdictional claims in published maps and institutional affiliations.

Acknowledgements. We warmly thank all the authors and reviewers who contributed to or supported this special issue during the challenging Covid-19 period. We are very grateful to Chief Editor Christopher Lüthgens for his assistance in creating this special issue.

Financial support. This open-access publication was funded by Julius-Maximilians-Universität Würzburg.

References

Abdulkarim, M., Chapkanski, S., Ertlen, D., Mahmood, H., Obioha, E., Preusser, F., Rambeau, C., Salomon, F., Schiemann, M., and Schmitt, L.: Morpho-sedimentary characteristics of Holocene paleochannels in the Upper Rhine alluvial plain, France, E&G Quaternary Sci. J., 71, 191–212, https://doi.org/10.5194/egqsj-71-191-2022, 2022.

Banerji, U. S., Goswami, V., and Joshi, K. B.: Quaternary dating and instrumental development: An overview, J. Asian Earth Sci., X 7, 100091, https://doi.org/10.1016/j.jaesx.2022.100091, 2022.

Britton, K., Crowley, B. E., Bataille, C. P., Miller, J. H., and Wooller, M. J.: Editorial: A Golden Age for Strontium Isotope Research? Current Advances in Paleoecological and Archaeological Research, Front. Ecol. Evolut., 9, 820295, https://doi.org/10.3389/fevo.2021.820295, 2022.

Engel, M., Henselowsky, F., Roth, F., Kadereit, A., Herzog, M., Hecht, S., Lindauer, S., Bubenzer, O., and Schukraft, G.: Fluvial activity of the late-glacial to Holocene "Bergstraßenneckar" in the Upper Rhine Graben near Heidelberg, Germany – first results, E&G Quaternary Sci. J., 71, 213–226, https://doi.org/10.5194/egqsj-71-213-2022, 2022.

Hardt, J., Nir, N., Lüthgens, C., Menn, T. M., and Schütt, B.: Palaeoenvironmental research at Hawelti–Melazo (Tigray, northern Ethiopia) – insights from sedimentological and geomorphological analyses, E&G Quaternary Sci. J., 72, 37–55, https://doi.org/10.5194/egqsj-72-37-2023, 2023.

Jack, T., and Glover, A.: Online conferencing in the midst of COVID-19: an "already existing experiment" in academic internationalization without air travel, Sustainability: Science, Practice and Policy, 17, 292–304, https://doi.org/10.1080/15487733.2021.1946297, 2021.

Kirchner, A., Herrmann, N., Matras, P., Müller, I., Meister, J., and Schattner, T. G.: A pedo-geomorphological view on land use and its potential in the surroundings of the ancient Hispano-Roman city Munigua (Seville, SW Spain), E&G Quaternary Sci. J., 71, 123–143, https://doi.org/10.5194/egqsj-71-123-2022, 2022.

Labahn, J., Bittner, L., Hirschmann, P., Roettig, C.-B., Burghardt, D., Glaser, B., Marković, S. B., and Zech, M.: ^{18}O analyses of bulk lipids as novel paleoclimate tool in loess research – a pilot study, E&G Quaternary Sci. J., 71, 83–90, https://doi.org/10.5194/egqsj-71-83-2022, 2022.

Liu, Z., Prendergast, A., Drysdale, R., and May, J.-H.: Comparison of bulk and sequential sampling methodologies on mammoth tooth enamel and their implications in paleoenvironmental reconstructions, E&G Quaternary Sci. J., 71, 227–241, https://doi.org/10.5194/egqsj-71-227-2022, 2022.

McCaroll, D.: 'Study the past, if you would divine the future': a retrospective on measuring and understanding Quaternary climate change, J. Quaternary Sci., 30, 154–187, https://doi.org/10.1002/jqs.2775, 2015.

Pötter, S., Seeger, K., Richter, C., Brill, D., Knaak, M., Lehmkuhl, F., and Schulte, P.: Pleniglacial dynamics in an oceanic central European loess landscape, E&G Quaternary Sci. J., 72, 77–94, https://doi.org/10.5194/egqsj-72-77-2023, 2023.

Schadeberg, A., Ford, E., Wieczorek, A.M., Gammage, L.C., López-Acosta, M., Buselic, I., Turk Dermastia, T., Fontela, M., Galobart, C., Llopis Monferrer, N., Lubósny, M., Piarulli, S., and Suaria, G.: Productivity, pressure, and new perspectives: impacts of the COVID-19 pandemic on marine early-career researchers, ICES J. Mar. Sci., 79, 2298–2310, https://doi.org/10.1093/icesjms/fsac167, 2022.

Schulze, T., Schwahn, L., Fülling, A., Zeeden, C., Preusser, F., and Sprafke, T.: Investigating the loess–palaeosol sequence of Bahlingen-Schönenberg (Kaiserstuhl), southwestern Germany, using a multi-methodological approach, E&G Quaternary Sci. J., 71, 145–162, https://doi.org/10.5194/egqsj-71-145-2022, 2022.

Schwahn, L., Schulze, T., Fülling, A., Zeeden, C., Preusser, F., and Sprafke, T.: Multi-method study of the Middle Pleistocene loess–palaeosol sequence of Köndringen, SW Germany, E&G Quaternary Sci. J., 72, 1–21, https://doi.org/10.5194/egqsj-72-1-2023, 2023.

Tinapp, C., Selzer, J., Döhlert-Albani, N., Fischer, B., Heinrich, S., Herbig, C., Kreienbrink, F., Lauer, T., Schneider, B., and Stäuble, H.: Late Weichselian–Holocene valley development of the Elbe valley near Dresden – linking sedimentation, soil formation and archaeology, E&G Quaternary Sci. J., 72, 95–111, https://doi.org/10.5194/egqsj-72-95-2023, 2023.

Ullmann, T., Möller, E., Baumhauer, R., Lange-Athinodorou, E., and Meister, J.: A new Google Earth Engine tool for spaceborne detection of buried palaeogeographical features – examples from the Nile Delta (Egypt), E&G Quaternary Sci. J., 71, 243–247, https://doi.org/10.5194/egqsj-71-243-2022, 2022.

Vinnepand, M., Fischer, P., Hambach, U., Jöris, O., Craig, C.-A., Zeeden, C., Thornton, B., Tütken, T., Prud'homme, C., Schulte, P., Moine, O., Fitzsimmons, K. E., Laag, C., Lehmkuhl, F., Schirmer, W., and Vött, A.: What do dust sinks tell us about their sources and past environmental dynamics? A case study for oxygen isotope stages 3–2 in the Middle Rhine Valley, Germany, E&G Quaternary Sci. J., 72, 163–184, https://doi.org/10.5194/egqsj-72-163-2023, 2023.

Woodroffe, C. D. and Murray-Wallace, C. V.: Sea-level rise and coastal change: the past as a guide to the future, Quaternary Sci. Rev., 54, 4–11, https://doi.org/10.1016/j.quascirev.2012.05.009, 2012.

E&G Quaternary Sci. J., 72, 189–201, 2023
https://doi.org/10.5194/egqsj-72-189-2023

Open Access E&G Quaternary Science Journal

Research article

Subglacial hydrology from high-resolution ice-flow simulations of the Rhine Glacier during the Last Glacial Maximum: a proxy for glacial erosion

Denis Cohen[1,2], Guillaume Jouvet[3,4], Thomas Zwinger[5], Angela Landgraf[6], and Urs H. Fischer[6]

[1]Department of Earth and Environmental Science, New Mexico Tech, Socorro, New Mexico, USA
[2]CoSci LLC, Orlando, Florida, USA
[3]Department of Geography, University of Zurich, Zurich, Switzerland
[4]Institute of Earth Surface Dynamics, University of Lausanne, Lausanne, Switzerland
[5]CSC – IT Center for Science Ltd., Espoo, Finland
[6]Nagra, Wettingen, Switzerland

Correspondence: Denis Cohen (denis.cohen@cosci-llc.com)

Relevant dates: Received: 7 November 2022 – Revised: 11 April 2023 – Accepted: 3 July 2023 – Published: 21 August 2023

How to cite: Cohen, D., Jouvet, G., Zwinger, T., Landgraf, A., and Fischer, U. H.: Subglacial hydrology from high-resolution ice-flow simulations of the Rhine Glacier during the Last Glacial Maximum: a proxy for glacial erosion, E&G Quaternary Sci. J., 72, 189–201, https://doi.org/10.5194/egqsj-72-189-2023, 2023.

Abstract: At the Last Glacial Maximum (LGM), the Rhine Glacier complex (Rhine and Linth glaciers) formed large piedmont lobes extending north into the Swiss and German Alpine forelands. Numerous overdeepened valleys there were formed by repeated glaciations. A characteristic of these overdeepened valleys is their location close to the LGM ice margin, away from the Alps. Numerical models of ice flow of the Rhine Glacier indicate a poor fit between the sliding distance, a proxy for glacial erosion, and the location of these overdeepenings. Calculations of the hydraulic potential based on the computed time-dependent ice surface elevations of the Rhine Glacier lobe obtained from a high-resolution thermo-mechanically coupled Stokes flow model are used to estimate the location of subglacial water drainage routes. Results indicate that the subglacial water discharge is high and focused along glacial valleys and overdeepenings when water pressure is equal to the ice overburden pressure. These conditions are necessary for subglacial water to remove basal sediments, expose fresh bedrock, and favor further erosion by quarrying and abrasion. Knowledge of the location of paleo-subglacial water drainage routes may be useful to understand patterns of subglacial erosion beneath paleo-ice masses that do not otherwise relate to the sliding of ice. Comparison of the erosion pattern from subglacial meltwater with those from quarrying and abrasion shows the importance of subglacial water flow in the formation of distal overdeepenings in the Swiss lowlands.

Kurzfassung: Während des letzteiszeitlichen Maximums (LGM) kam es zur Bildung von grossen Vorlandloben des Rheingletschersystems (Rhein- und Linthgletscher), die sich nordwärts in das Schweizer und deutsche Alpenvorland erstreckten. Durch wiederholte Vergletscherungen wurden dort zahlreiche übertiefte Täler ausgeschürft. Ein Merkmal dieser übertieften Tälern ist deren Lage in der Nähe des LGM-

Eisrands weit weg von den Alpen. Jedoch zeigen numerische Modellierungen des Eisfliessens des Rheingletschers eine schlechte Übereinstimmung der Gleitdistanz, Proxyindikator für glaziale Erosion, mit der Lage dieser Übertiefungen. Deshalb werden Berechnungen des hydraulischen Potenzials basierend auf zeitabhängigen Höhen der Eisoberfläche der Rheingletscherlobe, welche von einem hoch aufgelösten thermo-mechanisch gekoppelten Modell für Stoke'sches Fliessen resultieren, benutzt, um die Lage der Entwässerungsrouten unter dem Eis abzuschätzen. Die Resultate deuten darauf hin, dass der subglaziale Wasserabfluss gross ist und entlang glazialen Tälern und Übertiefungen geführt wird, wenn der Wasserdruck dem Eisüberlagerungsdruck entspricht. Dies sind notwendige Bedingungen, unter denen basale Sedimente wegtransportiert werden und frischer Fels freigelegt wird, um weitere glaziale Erosion zu begünstigen. Somit ist die Kenntnis der Lage von subglazialen Paläo-Entwässerungsrouten nützlich, um die Erosionsmuster unter Paläo-Gletschern zu verstehen, die nicht mit der Gleitbewegung des Eises in Verbindung gebracht werden können. Ein Vergleich der durch subglaziale Schmelzwässer erzeugten Erosionsmuster mit jenen, die durch direkte Gletschererosion entstanden sind, zeigt die Wichtigkeit der subglazialen Schmelzwasserflüsse für die Entstehung von Übertiefungen im alpenfernen Schweizer Vorland auf.

1 Introduction

At the Last Glacial Maximum (LGM), the Rhine Glacier complex (Cohen et al., 2018), combining the Rhine and Linth glaciers, descended well into the Swiss and German Alpine forelands, forming two large piedmont lobes. The Rhine Glacier lobe covered present-day Lake Constance and land to the north in southern Germany, and the Linth Glacier lobe advanced beyond the city of Zurich, Switzerland. Repeated glaciations since the Middle–Late Pleistocene (Preusser et al., 2011; Ellwanger et al., 2011) have carved numerous landforms in the Alps such as deep alpine valleys with prominent horns and ridges. In the forelands, the passage of glaciers left numerous imprints on the landscape such as terminal moraines, outwash deposits, and erratics (e.g., Schlüchter, 1988, 2004; Keller and Krayss, 2005a; Preusser et al., 2007; Beckenbach et al., 2014; Gaar et al., 2019); drumlin fields (Kamleitner, 2022); tunnel valleys (Reber and Schlunegger, 2016); and overdeepened valleys now filled with sediments such as the Thur, the Glatt, and the Aare valleys (e.g., Preusser et al., 2011; Dehnert et al., 2012; Dürst Stucki and Schlunegger, 2013) or with water such as Lake Constance and Lake Zurich. A surprising characteristic of these overdeepenings along these valleys is their proximity to the terminal position of past glacial maxima in a region where one would expect that the erosive power of ice, often associated with the rate of sliding at the base (e.g., Hallet, 1981; Humphrey and Raymond, 1994; MacGregor et al., 2000; Koppes et al., 2015; Herman et al., 2015), would be smaller in comparison to that of large alpine valleys where ice fluxes and sliding speeds are higher. The existence of these overdeepenings in a distal-foreland setting thus remains puzzling.

Previous models of ice flow of the Rhine Glacier (Cohen and Jouvet, 2017; Haeberli et al., 2020; Fischer et al., 2021; Seguinot and Delaney, 2021) indicate that the sliding distance, a proxy for glacial erosion based on the time-integrated sliding speed, or a power of it, during the advance and retreat of the Rhine Glacier lobe into the foreland, does not correlate well with the location of existing overdeepenings (Fig. 1) owing to the short time period over which ice covered these distal forelands. More recent work by Egholm (2022) using a landscape evolution model indicates that the formation of distal overdeepenings is possible if the rock material is significantly weaker there than the material in the Alpine massif. The model of Egholm (2022) used empirical parametrizations of abrasion and quarrying (Ugelvig et al., 2018) that were fitted against theoretical models (Hallet, 1981; Iverson, 2012). Egholm (2022)'s results, however, were mostly obtained using a steady-state climate model in which ice occupation time over the Swiss Alpine foreland was artificially long, in contrast with the geomorphic record for the Rhine Glacier (e.g., Keller and Krayss, 2005b) that suggests a maximum extent lasting a couple of thousand of years. This dilemma begs the question as to what other subglacial glaciological process could have contributed to the erosion of the northern Alpine forelands and the formation of these distal overdeepenings.

Several authors have noted the importance of subglacial water in glacial erosion (see review by Alley et al., 2019). Erosion by quarrying (Hooke, 1981; Iverson, 1991; Alley et al., 1999), whereby blocks of rock are plucked from the glacier bed by the moving ice, depends on subglacial water pressure fluctuations. Field experiments (Cohen et al., 2006) and models of quarrying (Iverson, 1991, 2012; Hallet, 1996; Beaud et al., 2014; Ugelvig et al., 2018) have shown a link between fluctuations in water pressure and the rate of opening of pre-existing bedrock cracks and fractures. Furthermore, large-scale investigations of the erosive power of glaciers (Koppes et al., 2015) indicate that temperate basal conditions, which imply the presence of subglacial water, are indicative of higher erosion rates, particularly at middle to high latitudes where seasonal and diurnal temperature variations are high and thus increase the possibility of significant water pressure fluctuations. Subglacial water is also key to the removal of sediments eroded and deposited at the base of glaciers (e.g., Hallet, 1996) that would otherwise blanket the bedrock, preventing any erosion process from occurring (Alley et al., 2019). Indeed, freeze-on conditions along the adverse slope of overdeepenings inhibit subglacial water flow and sediment removal, leading to decrease in erosion there (e.g., Hooke, 1991; Alley et al., 2003; Werder, 2016). Thus, subglacial water plays an important role in the erosive power of glaciers.

Lacking a clear link between sliding ice (or motion) and observed locations of overdeepenings in the Swiss Alpine forelands underneath the paleo-Rhine Glacier and paleo-Linth Glacier lobes, we seek to find whether subglacial water drainage distribution under the paleo-Rhine Glacier complex could help us understand the location of these overdeepenings. Our approach uses the numerical ice-flow model described in Cohen et al. (2018) but with a new climate signal to drive the ice model and a finer horizontal discretization to better resolve the ice flow. Calculated ice surface elevation, together with basal topography, allows us to compute the hydraulic potential and hydraulic head and the associated flow accumulation area during the course of advance and retreat of the Rhine Glacier around the LGM. Time integration of the flow accumulation area yields a metric for glacial erosion by subglacial water to test against the positions of observed overdeepenings. The underlying assumption in this analysis is that larger values of the time-integrated flow accumulation area indicate zones with significant subglacial water flow, which, over seasonal and annual timescales, have high potential for subglacial water fluxes that would enhance sediment removal and increase glacial erosion. We then compare patterns of relative erosion by quarrying, abrasion, and subglacial water flow to show the importance of subglacial water in the formation of distal overdeepenings in the Swiss lowlands.

The remainder of this paper is divided into three parts. Section 2 presents the methodology to compute the time-integrated flow accumulation area and the erosion by quarrying, abrasion, and subglacial water; Sect. 3 discusses the source of the data used for the computation; finally, Sect. 4 reports results and discusses them.

2 Methods

Subglacial water flow paths are calculated using the method described in Chu et al. (2016) (see also Arnold et al., 1998; Willis et al., 2012; Livingstone et al., 2013) and used in several studies to estimate subglacial water drainage locations in Greenland and Antarctica (e.g., Le Brocq et al., 2009; see also references in Chu et al., 2016) and in paleo-ice masses such as the Fennoscandian Ice Sheet (e.g., Shackleton et al., 2018). More sophisticated models of subglacial hydrology (e.g., GlaDS; Werder et al., 2013) coupled to ice-flow models (e.g., Gagliardini and Werder, 2018, with Elmer/Ice) are too computationally expensive to be applied to the long timescales and the large complex topography of the paleo-Rhine Glacier system.

Water flows down the hydraulic potential gradient, and the water flux, Q, can be calculated as (Shreve, 1972)

$$Q = -k \nabla \phi, \tag{1}$$

where k is the hydraulic conductivity of the subglacial water system and ϕ is the hydraulic potential, defined as

$$\phi = \rho_\mathrm{w} g Z_\mathrm{b} + p_\mathrm{w}. \tag{2}$$

Here $\rho_\mathrm{w} = 1000\,\mathrm{kg\,m^{-3}}$ is the density of water (constant), $g = 9.81\,\mathrm{m\,s^{-2}}$ is the acceleration due to gravity, Z_b is the elevation of the basal surface (glacier bed topography), and p_w is the water pressure. In glaciological applications, the water pressure at the bottom of the ice is often not known. In paleo-glaciological applications, no subglacial water pressure data exist, so it is often not computed (e.g., Cohen et al., 2018). Here we assume that the water pressure at the bed of the glacier is a fraction of the ice overburden pressure; i.e.,

$$p_\mathrm{w} = f\, p_\mathrm{i}, \tag{3}$$

where f is known as the flotation factor and

$$p_\mathrm{i} = \rho_\mathrm{i}\, g\, H, \tag{4}$$

with $\rho_\mathrm{i} = 917\,\mathrm{kg\,m^{-3}}$ being the ice density (constant) and H the ice thickness (variable). Substituting Eqs. (3) and (4) into Eq. (2) yields

$$\phi = \rho_\mathrm{w} g Z_\mathrm{b} + f \rho_\mathrm{i}\, g\, H, \tag{5}$$

where the hydraulic potential now only depends on the basal surface topography and the ice thickness. As an alternative we can use the hydraulic head, h, defined as

$$h = Z_\mathrm{b} + f \frac{\rho_\mathrm{i}}{\rho_\mathrm{w}} H. \tag{6}$$

The value of the flotation factor f depends on the basal water pressure. When water pressure equals ice overburden pressure, $f = 1$. Values greater than 1 are observed during times of intense surface melt that bring water through crevasses and moulins directly to the bed of the glacier (Meierbachtol et al., 2013; Wright et al., 2016). Since our ice-flow model (Cohen et al., 2018) does not simulate subglacial water pressures and given the uncertainties in both the basal surface during the last glacial cycle and estimates of the ice surface, we assume spatially fixed values of f over the entire glacier system and compute the hydraulic potential for three cases – $f = 0.6$, $f = 1$, and $f = 1.1$ – to study the effects of water pressure on subglacial water drainage paths. Low values of f imply

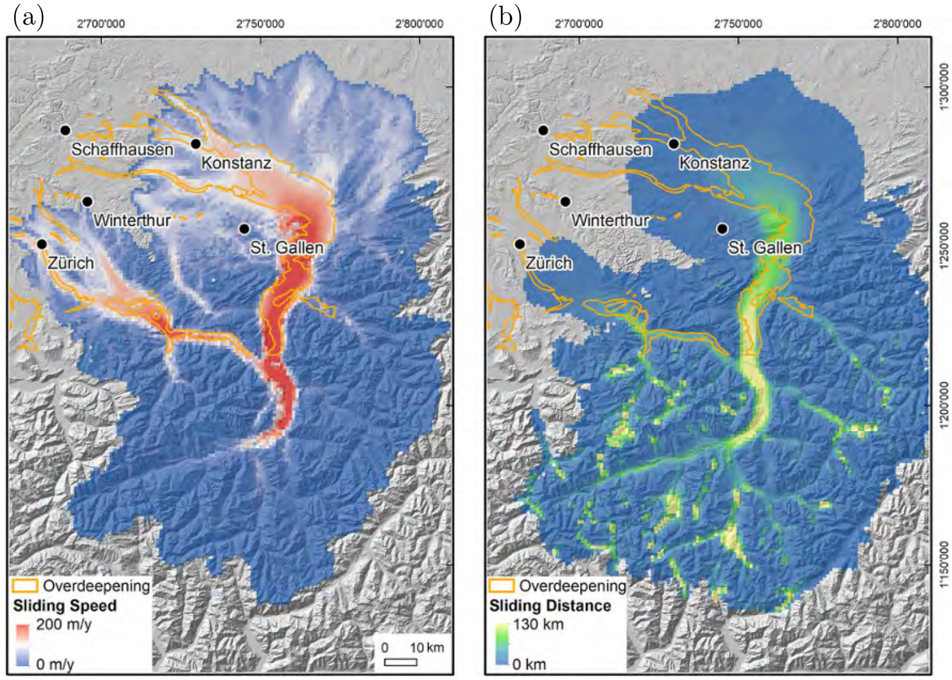

Figure 1. Map of **(a)** sliding speed and **(b)** sliding distance calculated by integrating the sliding speed over the advance and the retreat of the Rhine Glacier system during the last glacial cycle (see Cohen, 2017; Cohen and Jouvet, 2017; and Cohen et al., 2018, for details). The location of overdeepenings is indicated in orange. Reproduced from Fischer et al. (2021).

that basal topography dominates, while higher values emphasize the ice surface topography (see Eq. 6).

The subglacial water drainage paths can be obtained by computing the upstream accumulation area at each of the cells of the raster of the hydraulic head (Flowers and Clarke, 1999; Fischer et al., 2005; Chu et al., 2016; Pitcher et al., 2016) using the D_∞ algorithm of Tarboton (1997) to compute flow directions. Water drainage flow paths are continuous paths with high values of upstream accumulation areas.

On the long timescales over which erosion occurs (on the order of thousands of years), the ice thickness (H in Eq. 6) evolves with advances and retreats of the glacier. To include these transient effects, we compute the subglacial water flow paths at each available time step for the ice surface (every 10 years) and integrate the computed upstream accumulation area over time to obtain a time-integrated view of subglacial water drainage paths.

Estimates of erosion by subglacial water flow are calculated using the method of Kirkham et al. (2022) based on a model of subglacial channel erosion by Carter et al. (2017). Here we only compute the erosive component (see Kirkham et al., 2022, Eq. 3),

$$\dot{E}_\mathrm{s} = K_1 \left(\frac{\nu_\mathrm{s}}{\alpha_\mathrm{cc}}\right)\left(\frac{\max\left(\tau_\mathrm{cc}-\tau_k, 0\right)}{g\left(\rho_\mathrm{s}-\rho_\mathrm{w}\right) D_{15}}\right)^{3/2}, \tag{7}$$

where

$$\tau_\mathrm{cc} = 0.125\, f_\mathrm{cc}\, \rho_\mathrm{w}\, u_\mathrm{c}^2, \tag{8}$$

$$\tau_k = 0.025\, D_{15}\, g\left(\rho_\mathrm{s}-\rho_\mathrm{w}\right), \tag{9}$$

$$\nu_\mathrm{s} = D_{15}^2 \frac{\left(\rho_\mathrm{s}-\rho_\mathrm{w}\right) g}{9\mu_\mathrm{w}}. \tag{10}$$

Here τ_cc is the channel shear stress, τ_k is the critical shear stress, ν_s is the mean sediment velocity, u_c is the water velocity in the channel, $f_\mathrm{cc} = 0.07\,\mathrm{m}^{-2/3}\,\mathrm{s}^{-2}$ denotes the channel roughness parameters, $\rho_\mathrm{s} = 2600\,\mathrm{kg\,m}^{-3}$ is the solid density of sediment grains, $D_{15} = 0.1\,\mathrm{mm}$ is the 15th-percentile grain size, and $\mu_\mathrm{w} = 1.78 \times 10^{-3}\,\mathrm{Pa\,s}$ is the viscosity of water. The water flow velocity in the channel, u_c, is computed from the flow accumulation area weighted by the available meltwater at each cell, which is estimated by summing the surface melt rate and the basal melt rate. The meltwater is then scaled by multiplying it by the grid cell area divided by the cross-sectional area of the channel, assumed to be 30 m wide and 2 m deep, to obtain the channel water velocity. Although changing the channel size would affect the relationship between τ_cc and τ_k and thus where erosion occurs, it does not affect the overall results of erosion patterns as our calculations are meant to only look at erosion patterns and not calculate erosion magnitudes. The surface melt rate is calculated in the ablation area of the glacier and is proportional to the number of positive degree days (PDDs) (Hock, 2003). It is assumed to be zero in the accumulation area. The basal melt rate is computed from the geothermal heat flux map of Medici and Rybach (1995). Frictional heat generated by ice sliding over the substrate is an order of magnitude smaller than either surface or basal melt and is thus neglected.

To compare patterns of subglacial erosion due to ice motion, we also estimate erosion by quarrying, $\dot{E}_\mathrm{q}$, and abrasion, $\dot{E}_\mathrm{a}$, given, respectively, by (see Ugelvig et al., 2016, 2018)

$$\dot{E}_\mathrm{q} = K_\mathrm{q}\ p_\mathrm{e}^3 v_\mathrm{s}, \tag{11}$$

$$\dot{E}_\mathrm{a} = K_\mathrm{a}\ v_\mathrm{s}^2, \tag{12}$$

where $p_\mathrm{e} = p_\mathrm{w} - p_\mathrm{i}$ is the effective pressure, v_s is the glacier sliding speed, and K_q and K_a are constants.

All erosion rates are time-integrated to yield a total erosion over the course of the advance and retreat of the glacier during the LGM. Because of uncertainties in model and parameter values, a direct comparison between quarrying, abrasion, and subglacial meltwater erosion is not possible. Instead, these quantities are used to look at relative patterns of erosion by normalizing them. This makes the exact values of the parameters K_1 (Eq. 7) and K_q and K_a (Eqs. 11 and 12, respectively) irrelevant.

3 Data

Only two surfaces are required to compute the hydraulic potential and subglacial water flow paths: the basal surface (Z_b in Eq. 6) and the ice surface from which the ice thickness, H, can be obtained (see Eq. 6). The ice surface is computed from ice-flow simulations of the paleo-Rhine Glacier complex around the LGM using Elmer/Ice, an open-source, finite-element multi-physics Fortran code (Gagliardini et al., 2013; Ruokolainen et al., 2020). Elmer/Ice computes the transient three-dimensional ice velocities, temperatures, and pressures as well as the elevation of the ice surface based on fully coupled thermo-mechanical equations by solving the non-linear Stokes flow equation together with the heat equation and the mass balance equation at the ice surface (see Cohen et al., 2018, for details). The mass balance is based on the positive-degree-day model (Hock, 2003) that computes ice melt as a function of air temperature. PDDs are computed using the method of Calov and Greve (2005) over month-long intervals using factors of 8 and 3 mm °C^{-1} d^{-1} for ice and snow, respectively. Air temperature and precipitation are obtained by linear interpolation using a glacial-index (GI) approach (Sutter et al., 2019) between LGM and pre-industrial (PI) climate states. The GI follows the δ^{18}O signal of the Antarctica EPICA ice core (Jouzel et al., 2007), rescaled to between 0 (no ice, PI) and 1 (maximum ice volume at the LGM). The LGM climate state provides 2 km resolution maps of the temperature and precipitation over the entire Alps computed from a regional climate model by dynamical downscaling of a global Earth system model (see details in Velasquez et al., 2020, 2022; Russo et al., 2022; Buzan et al., 2023).

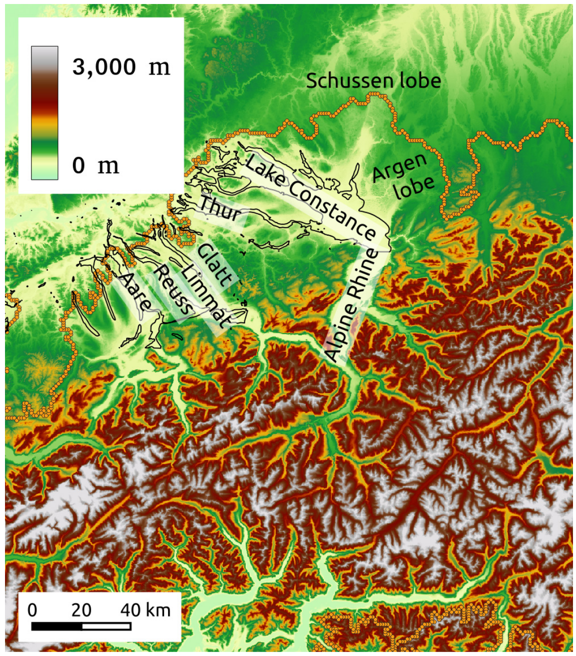

Figure 2. Basal topography with outline of overdeepened basins in black and extent of ice at the LGM with orange circles (Ehlers and Gibbard, 2008).

3.1 Basal surface

The basal surface is the present-day topography minus the computed ice thickness of major present-day glaciers using the model of Farinotti et al. (2019). It remains unchanged during the ice-flow simulation. Figure 2 shows the basal topography used in the model simulation.

3.2 Ice surface

The ice surface evolves with time during the advance of the Rhine Glacier towards its maximum LGM position and during its retreat. Figure 3 shows three ice surface elevations at 27 ka, at 22.9 ka (LGM), and at 14.2 ka. Ice surface elevations are available every 10 years from 27 to 14.2 ka.

3.3 Calculation of hydraulic potential and flow accumulation area

The hydraulic potential is first calculated on the unstructured triangular mesh of the Elmer/Ice finite-element model at every time step (every 10 years). Resolution in the mesh ranges from 800 to 1100 m, with increased resolution in areas of steeper slope gradients. The nodal values of the hydraulic potential are then linearly interpolated to a uniform raster at a resolution of 500 m. The calculation of the flow accumulation area is performed on the hydraulic potential using the open toolbox SAGA (System for Automated Geoscientific Analyses; Conrad et al., 2015) and summed over time to compute the time-integrated values.

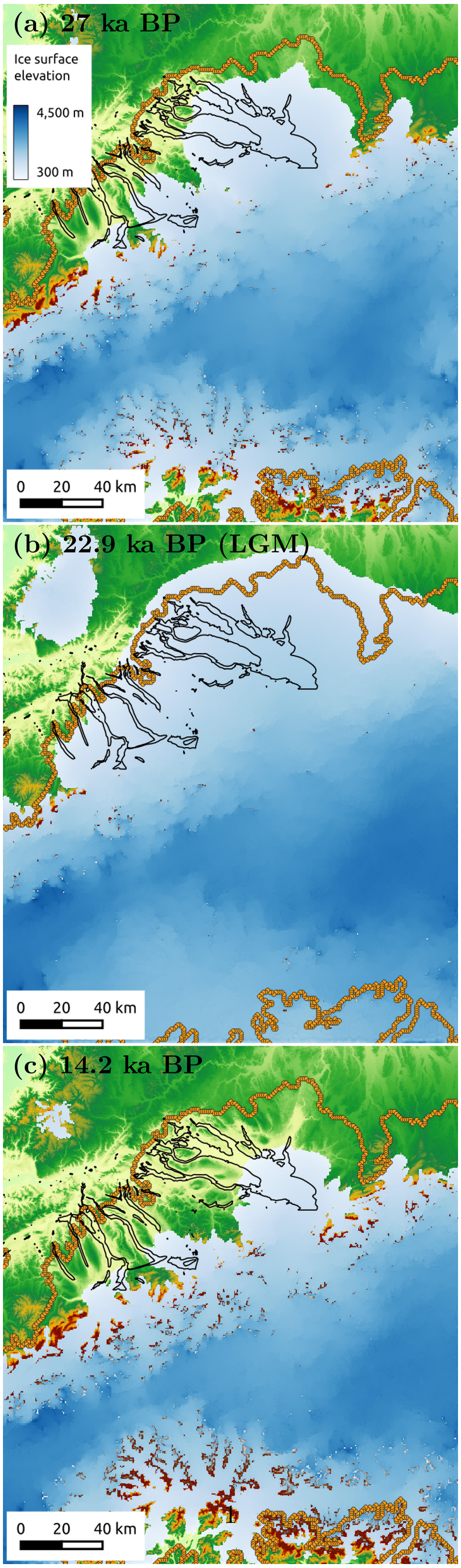

Figure 3. Ice surface elevation in blue at **(a)** 27 ka (start of simulation), **(b)** 22.9 ka (LGM), and **(c)** 14.2 ka (end of simulation). LGM ice extent is shown with orange circles (Ehlers and Gibbard, 2008).

4 Results and discussion

Figure 4 shows the subglacial water drainage routes based on the flow accumulation area of the hydraulic potential (or hydraulic head) at three different times for flotation values of $f = 0.6$ (Fig. 4, left panels), $f = 1.0$ (Fig. 4, center panels), and $f = 1.1$ (Fig. 4, right panels).

The flow accumulation area can be understood as a proxy for subglacial water flux that passes through a specific drainage channel because water flux to the glacier is an increasing function of the upstream flow accumulation area.

When $f = 0.6$ (Fig. 4, left panels), subglacial water drainages are mostly concentrated in the Alpine Rhein Valley in the Alps, in Lake Constance, and along major valleys in the forelands such as the drainage of Lake Zurich. Drainages are constrained by basal topography, following valley morphology. Lake Constance (a zone of constant elevation), where the Alpine Rhein Glacier flows, concentrates a significant flux of subglacial water according to the model. Water exits the Rhine Glacier lobe to the north via existing valleys in the German Alpine foreland, following the Überlingen branch of present-day Lake Constance. In the Swiss Alpine foreland, water drains out of Lake Constance via the Untersee and also by connecting to the Thur Valley, which coincides with an overdeepening there. In the Linth Glacier lobe, subglacial water also flows along Lake Zurich and the Limmat and Glatt valleys, where two overdeepenings are located (Preusser et al., 2010; Buechi et al., 2018). The Reuss and Aare overdeepenings are also pathways for subglacial water drainages further to the west. The drainage pattern does not change significantly with time (see Fig. 4a, c, e) except at $t = 14.2$ ka when the ice has retreated halfway out of Lake Constance and completely out of the distal overdeepenings in the Swiss forelands.

The drainage pattern is significantly different when $f = 1.0$ (Fig. 4, center panels), equivalent to zero effective pressure at the base. Water now drains out of the Lake Constance basin to the north in many concentrated flow channels, such as the Schussen Valley, against an adverse bedrock slope (see basal topography in Fig. 2) and where a few overdeepenings have been noted (Ellwanger et al., 2011). Subglacial flow is also more important along many valleys in the foreland, both in the Rhine Glacier (e.g., Thur) and in the Linth Glacier (e.g., Reuss) lobes. Because of higher water pressure, the hydraulic potential gradient conforms less to the basal (or bed) topography, and subglacial water moves more along the gradient determined by the slope of the glacier surface; subglacial water paths no longer follow topographic lows.

At a yet higher flotation value ($f = 1.1$, Fig. 4, right panels), when water pressure exceeds ice overburden pressure, subglacial drainages out of the Alpine Rhine are also diverted to the north across Lake Constance and then ascending the bedrock slope north of it. Water drainage, however, occurs over many more subglacial channels that fan out radially from the Lake Constance basin. Because of the high wa-

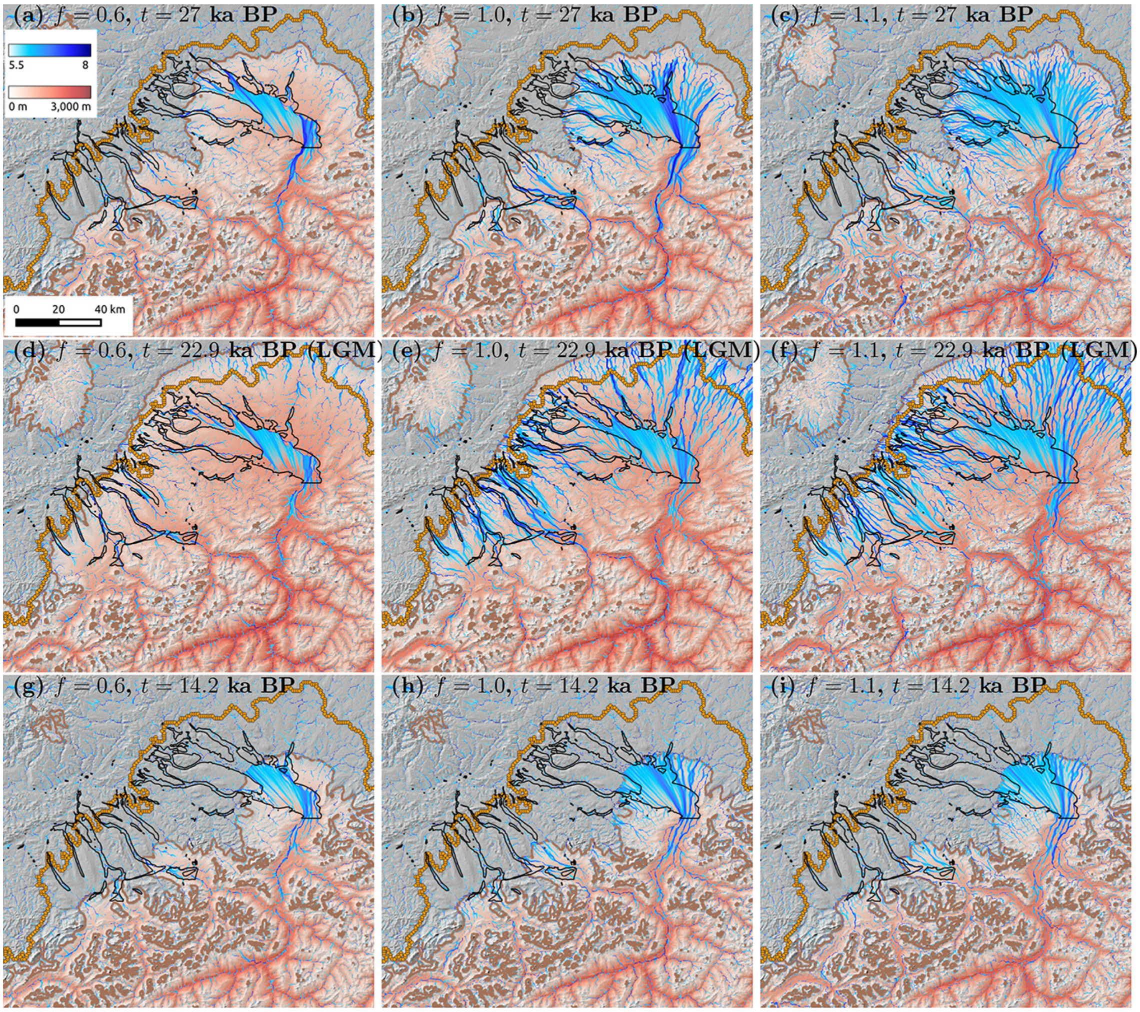

Figure 4. The $\log_{10}$ of computed flow accumulation area (in m^2) in blue at three different times – **(a, b, c)** 27 ka, **(d, e, f)** 22.9 ka (LGM), and **(g, h, i)** 14.2 ka – based on the hydraulic potential for a flotation factor of **(a, d, g)** $f = 0.6$, **(b, e, h)** $f = 1.0$, and **(c, f, i)** $f = 1.1$. Hillshade topography and ice thickness in red shades at the times indicated are shown in the background. Actual LGM ice extent is shown with orange circles. Modeled ice extent is shown with a brown line. Black outlines indicate locations of overdeepenings.

ter pressures, drainages are no longer constrained by basal topography and can move from one valley to the next over topographic high points such as from the Thur to the Lower Rhine overdeepenings out of the Untersee. High flotation values cause water drainage paths to cut across valleys and overdeepenings, such as, for example, in the Thur Valley, in the Rhine Glacier lobe, and in the Reuss and Linth lobes. In the Alps, water drainage paths are no longer constrained to the valley centers but meander on the sides of the valley and along the valley walls (contrast Fig. 4d and f), even cutting across mountain ranges during retreat (see Fig. 4i).

Basal conditions where the value of flotation is equal to 1 or greater are unlikely to occur over the entire glacier basal surface and for significant lengths of time. High basal water pressure arising from increased surface melting would promote the development of an efficient drainage system that would tend to reduce basal water pressure (e.g., Bartholomaus et al., 2008; Sundal et al., 2011; Andrews et al., 2014). These basal conditions, despite their limited duration, could have the potential to produce significant changes in the basal geomorphology, for example, because of substantial increases in the capacity of subglacial water streams to transport sediments and in their ability to further erode bedrock by processes of abrasion and quarrying associated with both larger fluctuations in basal water pressure and increased basal sliding speed (e.g., van de Wal et al., 2008; Schoof, 2010; Bartholomew et al., 2010; Hewitt, 2013).

The time integration of subglacial water flow paths over the 12.8 kyr of the simulation covering advance and retreat of the Rhine Glacier around the LGM is shown in Fig. 5 for the three values of flotation: $f = 0.6$, 1, and 1.1.

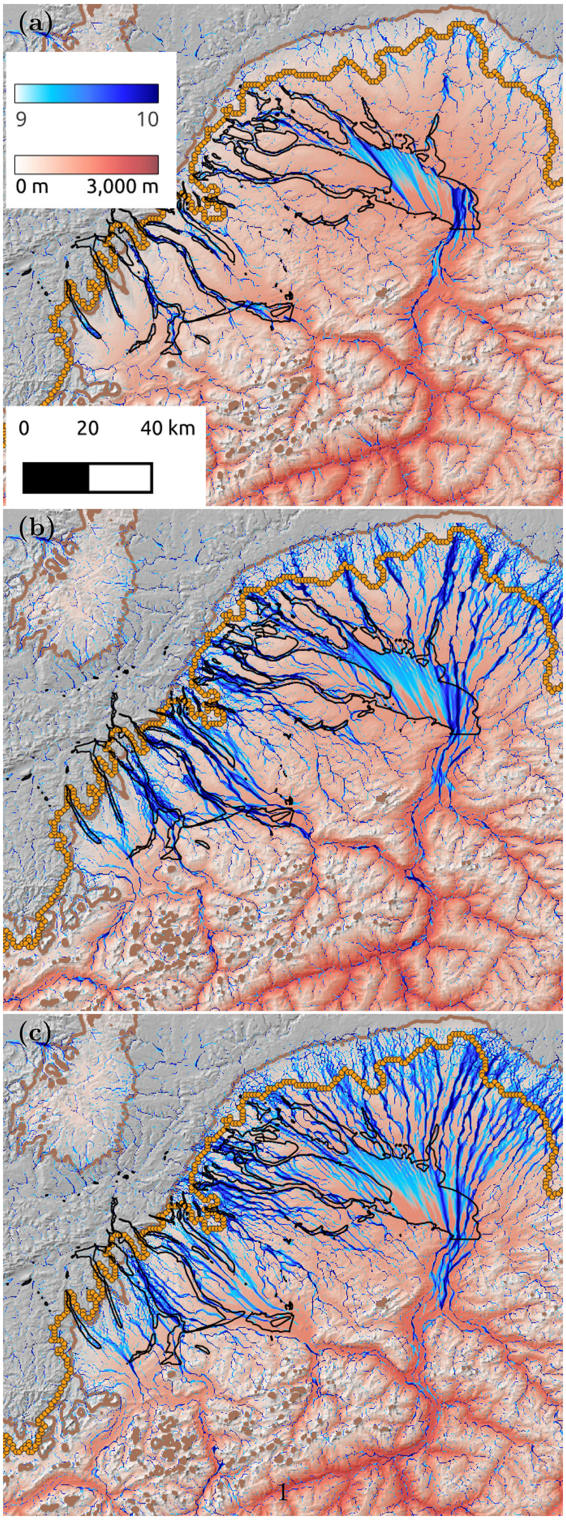

Figure 5. The $\log_{10}$ of the time-integrated flow accumulation area (in m^2) over 12.8 kyr (in blue) for **(a)** $f = 0.6$, **(b)** $f = 1$, and $f = 1.1$ with hillshade topography and ice thickness at the LGM (red colors) in the background. LGM ice extent is shown with orange circles. Model ice extent is shown with a brown line. Black outlines indicate location of overdeepenings.

Clear differences exist between a moderate flotation value ($f = 0.6$) and flotation values with zero effective pressure ($f = 1$) or where water pressure exceeds ice overburden pressure ($f = 1.1$). Although high water pressures in excess of hydrostatic pressure have been noted in both Alpine (e.g., Flowers and Clarke, 1999) and Greenland (e.g., Banwell et al., 2013; Lindbäck et al., 2015) settings and may be occurring in overdeepenings (Lawson et al., 1998), they may not be representative of long-timescale average values in large areas of the Rhine Glacier lobe. Subglacial water flow drainages with high water pressure bypass some topographic relief, producing near-straight channels that cut across relief, such as in the northern part of the Rhine Glacier lobe. These high-water-pressure subglacial drainage paths also cut across overdeepenings in the Thur, Glatt, and Limmat overdeepenings in the Rhine Glacier and Linth Glacier lobes. A value of f equal to unity yields the closest match with the actual mapping of overdeepenings, although many overdeepenings are also well matched for $f = 0.6$, particularly in the Linth Glacier lobe and the lower Thur Valley. Overdeepened regions north of Lake Constance require higher flotation values to be occupied by a subglacial water drainage path. When water pressure exceeds ice overburden pressure such as when $f = 1.1$, subglacial drainages are too distributed and no longer only conform to valleys, a situation that may occur during periods of significant melt (such as during retreat) but is likely not representative of the situation over longer timescales.

High values of the time-integrated flow accumulation area represent drainage pathways with large fluxes of water. Many of these high-discharge zones correspond to several locations of overdeepenings such as the Schussen, Thur, Limmat, Reuss, and Aare overdeepened valleys. In the Aare Valley, a tunnel valley system has been identified beneath the city of Bern (Dürst Stucki and Schlunegger, 2013; Reber and Schlunegger, 2016) with a branching pattern that resembles the pattern observed in our simulation. The presence of this tunnel valley system has been associated with an area of high water pressure. Our simulation also indicates that a flotation value of 1 is necessary for significant subglacial water drainage to occur in this area.

Figure 6 shows patterns of erosion for quarrying, abrasion, and subglacial water flow. All values of erosion have been scaled to between 0 and 1 by dividing the computed values by their respective maximum value. All erosion types have been time-integrated over the course of the advance and retreat of the ice during the LGM.

A clear difference in the erosion pattern emerges between erosion due to ice motion (quarrying and abrasion) and erosion due to subglacial meltwater flow. Erosion by ice motion is greatest at the base of alpine valleys where sliding is fastest and where the ice occupation time is longest. Limited durations of ice cover and lower sliding speeds near the margin limit erosion by ice motion there. Erosion by quarrying (Fig. 6a) shows more variability in the Rhine, Linth, and

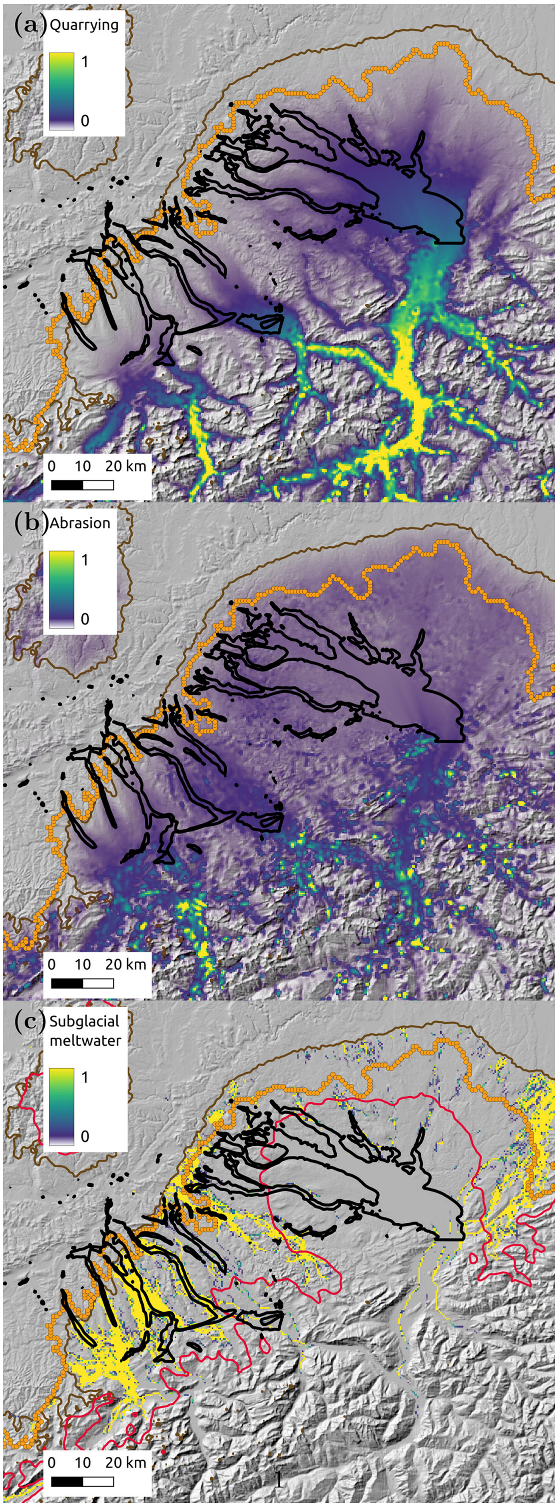

Figure 6. Normalized erosion by **(a)** quarrying, **(b)** abrasion, and **(c)** subglacial meltwater flow. Background shows hillshade topography. LGM margin is shown with orange circles; modeled maximum LGM extent is shown with a brown curve. Black curves indicate areas of overdeepenings. The red curve in **(c)** is the equilibrium line at the LGM separating accumulation (south) from ablation (north) in the Alps.

Reuss lobes owing to its cubic dependence on the ice thickness via the effective pressure term (see Eq. 11). Any variation in ice thickness along or across overdeepenings amplifies erosion by quarrying, resulting in a significant change in the total amount of quarrying in these areas. In contrast, erosion by abrasion (Fig. 6b), which only depends on the square of the sliding speed (see Eq. 11), is more uniform in these lobes. Erosion by subglacial meltwater flow (Fig. 6c) is significantly different: it is almost entirely focused near the ice margin, particularly to the northwest in the Reuss and Linth lobes, the Thur Valley, and the Argen lobe (see Fig. 2). This is due to the large available surface melt in these areas that have larger ablation areas. This is visible by comparing, for example, the position of the equilibrium line (Fig. 6c, red line) to the LGM margin (Fig. 6c, brown line). In the northwestern lobes and in the northeastern part of the Rhine lobe, the area for available surface meltwater is significantly larger then in the main Rhine lobe, explaining why most erosion by subglacial meltwater occurs preferentially there. Also, channel shear stress is more likely to exceed critical shear stress in areas where subglacial channel velocity is higher (see u_c in Eq. 8), which occurs where more surface melt is available and thus increases the potential for erosion by subglacial meltwater.

The different erosion patterns due to ice motion and subglacial meltwater suggest that the existence of distal-foreland overdeepenings in the Swiss lowlands is driven, at least in part, by erosion by subglacial meltwater. Furthermore, high water flux during high-water-pressure events along these valleys and the associated fluctuations in water pressure in the channels could have increased the rate of glacial erosion by quarrying (e.g., Cohen et al., 2006), a dependence that is not included in the simple quarrying erosion law in Eq. (11). This may have been further enhanced by pre-existing rock weaknesses due, for example, to a higher density of joints or faulting (e.g., Dühnforth et al., 2010; Hooyer et al., 2012) such as is found in the Lake Constance area (Fabbri et al., 2021). The patterns of subglacial water drainage paths computed from numerical simulations of ice flow and ice surface elevation indicate a possible link between the subglacial water flux and the existence of overdeepenings. The location of these overdeepenings suggests that these overdeepenings are controlled, in part, by higher rock erodibility in these areas, which, during glacial times, were preferentially excavated by the combined effects of water and ice.

5 Conclusions

We present a model of subglacial water drainages underneath the Rhine Glacier during the advance and retreat around the LGM. The model is based on high-resolution ice surfaces obtained from a numerical ice-flow model. The model computes ice velocities and ice surface elevations using a thermomechanical Stokes flow model coupled to a high-resolution regional climate model to give the most plausible representation of the Rhine Glacier during its advance and retreat around the LGM. The hydraulic potential (or head) calculated from transient elevations of the ice surface together with the basal topography yields a map of subglacial water flux during the LGM. Results of the calculation show that subglacial water drainage is strongly constrained by topography for low values of water pressure (small flotation factor), focusing water flow in valleys in the foreland. When water pressure equals ice overburden pressure (flotation value equal to 1), the subglacial drainages coincide with regions of intense glacial erosion as observed by numerous overdeepenings there. When water pressure exceeds ice overburden pressure and flotation is greater than 1, the pattern of subglacial drainages changes to straighter channels that bypass valleys, mountain ranges, and overdeepened basins. This suggests that the maximum potential for glacial erosion by subglacial water channels is obtained when water pressure underneath the Rhine Glacier and Linth Glacier lobes were, on average, close to the ice overburden pressure. These conditions favor high water flow volumes and maximize the potential for subglacial water fluctuations needed for enhanced erosion by ice and water. Finally, comparison of the erosion pattern from subglacial meltwater with those from quarrying and abrasion shows the importance of subglacial water channels in the formation of distal overdeepenings in the Swiss lowlands.

Code availability. The software package Elmer FEM version 9 which contains Elmer/Ice can be downloaded via Zenodo, https://doi.org/10.5281/zenodo.7892181 (Ruokolainen et al., 2023).

Data availability. Data are not publicly available as part of the climate data were obtained from another group (references cited in text) and they have not been made available publicly as of now. Other data sources are not publicly available as they were obtained from Nagra.

Author contributions. The research was conceived by DC, UHF, and AL. The ice-flow modeling was performed by DC with help from TZ and GJ. DC carried out hydrological modeling and interpretation. DC wrote the paper with inputs from all co-authors.

Competing interests. The contact author has declared that none of the authors has any competing interests.

Disclaimer. Publisher's note: Copernicus Publications remains neutral with regard to jurisdictional claims in published maps and institutional affiliations.

Special issue statement. This article is part of the special issue "Subglacial erosional landforms and their relevance for the long-term safety of a radioactive waste repository". It is the result of a virtual workshop held in December 2021.

Financial support. This research has been supported by the National Cooperative for the Disposal of Radioactive Waste (Nagra, grant no. 20632).

Review statement. This paper was edited by Sonja Breuer and reviewed by Meike Bagge and Anders Damsgaard.

References

Alley, R. B., Strasser, J. C., Lawson, D. E., Evenson, E. B., and Larson, G. J.: Glaciological and geological implications of basal-ice accretion in overdeepenings, Geol. S. Am. S., 337, 1–9, https://doi.org/10.1130/0-8137-2337-X.1, 1999.

Alley, R. B., Lawson, D. E., Evenson, E. B., and Larson, G. J.: Sediment, glaciohydraulic supercooling, and fast glacier flow, Ann. Glaciol., 36, 135–141, https://doi.org/10.3189/172756403781816121, 2003.

Alley, R. B., Cuffey, K. M., and Zoet, L. K.: Glacial erosion: status and outlook, Ann. Glaciol., 60, 1–13, https://doi.org/10.1017/aog.2019.38, 2019.

Andrews, L. C., Catania, G. A., Hoffman, M. J., Gulley, J. D., Lüthi, M. P., Ryser, C., Hawley, R. L., and Neumann, T. A.: Direct observations of evolving subglacial drainage beneath the Greenland Ice Sheet, Nature, 514, 80–83, https://doi.org/10.1038/nature13796, 2014.

Arnold, N., Richards, K., Willis, I., and Sharp, M.: Initial results from a distributed, physically based model of glacier hydrology, Hydrol. Process., 12, 191–219, https://doi.org/10.1002/(SICI)1099-1085(199802)12:2<191::AID-HYP571>3.0.CO;2-C, 1998.

Banwell, A. F., Willis, I. C., and Arnold, N. S.: Modeling subglacial water routing at Paakitsoq, W Greenland, J. Geophys. Res.-Earth Surf., 118, 1282–1295, https://doi.org/10.1002/jgrf.20093, 2013.

Bartholomaus, T. C., Anderson, R. S., and Anderson, S. P.: Response of glacier basal motion to transient water storage, Nat. Geosci., 1, 33–37, https://doi.org/10.1038/ngeo.2007.52, 2008.

Bartholomew, I., Nienow, P., Mair, D., Hubbard, A., King, M. A., and Sole, A.: Seasonal evolution of subglacial drainage and acceleration in a Greenland outlet glacier, Nat. Geosci., 3, 408–411, https://doi.org/10.1038/ngeo863, 2010.

Beaud, F., Flowers, G. E., and Pimentel, S.: Seasonal-scale abrasion and quarrying patterns from a two-dimensional ice-flow model coupled to distributed and channelized subglacial drainage, Geomorphology, 219, 176–191, https://doi.org/10.1016/j.geomorph.2014.04.036, 2014.

Beckenbach, E., Müller, T., Seyfried, H., and Simon, T.: Potential of a high-resolution DTM with large spatial coverage for visualization, identification and interpretation of young (Würmiam) glacial geomorphology – a case study from Oberschwaben (southern Germany), Quaternary Science Journal, 63, 107–129, https://doi.org/10.3285/eg.63.2.01, 2014.

Buechi, M. W., Graf, H. R., Haldimann, P., Lowick, S. E., and Anselmetti, F. S.: Multiple Quaternary erosion and infill cycles in overdeepened basins of the northern Alpine foreland, Swiss J. Geosci., 111, 133–167, https://doi.org/10.1007/s00015-017-0289-9, 2018.

Buzan, J. R., Russo, E., Kim, W. M., and Raible, C. C.: Winter sensitivity of glacial states to orbits and ice sheet heights in CESM1.2, EGUsphere [preprint], https://doi.org/10.5194/egusphere-2023-324, 2023.

Calov, R. and Greve, R.: Correspondence: A semi-analytical solution for the positive degree-day model with stochastic temperature variations, J. Glaciol, 51, 173–175, 2005.

Carter, S. P., Fricker, H. A., and Siegfried, M. R.: Antarctic subglacial lakes drain through sediment-floored canals: theory and model testing on real and idealized domains, The Cryosphere, 11, 381–405, https://doi.org/10.5194/tc-11-381-2017, 2017.

Chu, W., Creyts, T. T., and Bell, R. E.: Rerouting of subglacial water flow between neighboring glaciers in West Greenland, J. Geophys. Res.-Earth Surf., 121, 925–938, https://doi.org/10.1002/2015JF003705, 2016.

Cohen, D.: Numerical Reconstruction of the Rhine Glacier at the Last Glacial Maximum, Tech. rep., Nagra Arbeitsbericht NAB 17–25,, 2017.

Cohen, D. and Jouvet, G.: Transient Simulations of the Rhine Glacier over the Last Glacial Cycle, Tech. rep., Nagra Arbeitsbericht NAB 17–47, 2017.

Cohen, D., Hooyer, T. S., Iverson, N. R., Thomason, J. F., and Jackson, M.: Role of transient water pressure in quarrying: A subglacial experiment using acoustic emissions, J. Geophys. Res.-Earth Surf., 111, F03006, https://doi.org/10.1029/2005JF000439, 2006.

Cohen, D., Gillet-Chaulet, F., Haeberli, W., Machguth, H., and Fischer, U. H.: Numerical reconstructions of the flow and basal conditions of the Rhine glacier, European Central Alps, at the Last Glacial Maximum, The Cryosphere, 12, 2515–2544, https://doi.org/10.5194/tc-12-2515-2018, 2018.

Conrad, O., Bechtel, B., Bock, M., Dietrich, H., Fischer, E., Gerlitz, L., Wehberg, J., Wichmann, V., and Böhner, J.: System for Automated Geoscientific Analyses (SAGA) v. 2.1.4, Geosci. Model Dev., 8, 1991–2007, https://doi.org/10.5194/gmd-8-1991-2015, 2015.

Dehnert, A., Lowick, S. E., Preusser, F., Anselmetti, F. S., Drescher-Schneider, R., Graf, H. R., Heller, F., Horstmeyer, H., Kemna, H. A., Nowaczyk, N. R., Züger, A., and Furrer, H.: Evolution of an overdeepened trough in the northern Alpine Foreland at Niederweningen, Switzerland, Quaternary Sci. Rev., 34, 127–145, https://doi.org/10.1016/j.quascirev.2011.12.015, 2012.

Dühnforth, M., Anderson, R. S., Ward, D., and Stock, G. M.: Bedrock fracture control of glacial erosion processes and rates, Geology, 38, 423–426, https://doi.org/10.1130/G30576.1, 2010.

Dürst Stucki, M. and Schlunegger, F.: Identification of erosional mechanisms during past glaciations based on a bedrock surface model of the central European Alps, Earth Planet. Sci. Lett., 384, 57–70, 2013.

Egholm, D.: Controls on Overdeepening Formation in a Distal Foreland Setting, Tech. rep., Nagra Arbeitsbericht NAB 22-17, 2022.

Ehlers, J. and Gibbard, P.: Extent and chronology of Quaternary glaciation, Episodes, 31, 211–218, 2008.

Ellwanger, D., Wielandt-Schuster, U., Franz, M., and Simon, T.: The Quaternary of the southwest German Alpine Foreland (Bodensee–Oberschwaben, Baden-Württemberg, Southwest Germany), Quaternary Sci. J., 60, 306–328, 2011.

Fabbri, S., Affentranger, C., Krastel, S., Lindhorst, K., Wessels, M., Madritsch, H., Allenbach, R., Herwegh, M., Heuberger, S., Wielandt-Schuster, U., Pomella, H., Schwestermann, T., and Anselmetti, F.: Active Faulting in Lake Constance (Austria, Germany, Switzerland) Unraveled by Multi-Vintage Reflection Seismic Data, Front. Earth Sci., 9, https://doi.org/10.3389/feart.2021.670532, 2021.

Farinotti, D., Huss, M., Fürst, J. J., Landmann, J., Machguth, H., Maussion, F., and Pandit, A.: A consensus estimate for the ice thickness distribution of all glaciers on Earth, Nat. Geosci., 12, 168–173, https://doi.org/10.1038/s41561-019-0300-3, 2019.

Fischer, U. H., Braun, A., Bauder, A., and Flowers, G. E.: Changes in geometry and subglacial drainage derived from digital elevation models: Unteraargletscher, Switzerland, 1927–97, Ann. Glaciol., 40, 20–24, https://doi.org/10.3189/172756405781813528, 2005.

Fischer, U. H., Bebiolka, A., Brandefelt, J., Cohen, D., Harper, J., Hirschorn, S., Jensen, M., Kennell, L., Liakka, J., Näslund, J.-O., Normani, S., Stück, H., and Weitkamp, A.: Chapter 11 – Radioactive waste under conditions of future ice ages, in: Snow and Ice-Related Hazards, Risks, and Disasters (Second Edition), edited by: Haeberli, W. and Whiteman, C., Hazards and Disasters Series, 323–375, Elsevier, 2nd Edn., https://doi.org/10.1016/B978-0-12-817129-5.00005-6, 2021.

Flowers, G. E. and Clarke, G. K. C.: Surface and bed topography of Trapridge Glacier, Yukon Territory, Canada: digital elevation models and derived hydraulic geometry, J. Glaciol., 45, 165–174, https://doi.org/10.3189/S0022143000003142, 1999.

Gaar, D., Graf, H. R., and Preusser, F.: New chronological constraints on the timing of Late Pleistocene glacier advances in northern Switzerland, E&G Quaternary Sci. J., 68, 53–73, https://doi.org/10.5194/egqsj-68-53-2019, 2019.

Gagliardini, O. and Werder, M. A.: Influence of increasing surface melt over decadal timescales on land-terminating Greenland-type outlet glaciers, J. Glaciol., 64, 700–710, https://doi.org/10.1017/jog.2018.59, 2018.

Gagliardini, O., Zwinger, T., Gillet-Chaulet, F., Durand, G., Favier, L., de Fleurian, B., Greve, R., Malinen, M., Martín, C., Råback, P., Ruokolainen, J., Sacchettini, M., Schäfer, M., Seddik, H., and Thies, J.: Capabilities and performance of Elmer/Ice, a new-generation ice sheet model, Geosci. Model Dev., 6, 1299–1318, https://doi.org/10.5194/gmd-6-1299-2013, 2013.

Haeberli, W., Fischer, U. H., Cohen, D., and Schnellmann, M.: Radioaktive Abfälle und Eiszeiten in der Schweiz: Können Gletscher und Permafrost zukünftiger Eiszeiten die langfristige Sicherheit der geplanten Lager beeinflussen?, Wasser Energie Luft, 112, 261–269, 2020.

Hallet, B.: Glacial Abrasion and Sliding: their Dependence on the Debris Concentration in Basal Ice, Ann. Glaciol., 2, 23–28, https://doi.org/10.3189/172756481794352487, 1981.

Hallet, B.: Glacial quarrying: a simple theoretical model, Ann. Glaciol., 22, 1–8, https://doi.org/10.3189/1996AoG22-1-1-8, 1996.

Herman, F., Beyssac, O., Brughelli, M., Lane, S. N., Leprince, S., Adatte, T., Lin, J. Y. Y., Avouac, J.-P., and Cox,

S. C.: Erosion by an Alpine glacier, Science, 350, 193–195, https://doi.org/10.1126/science.aab2386, 2015.

Hewitt, I. J.: Seasonal changes in ice sheet motion due to melt water lubrication, Earth Planet. Sci. Lett., 371–372, 16–25, https://doi.org/10.1016/j.epsl.2013.04.022, 2013.

Hock, R.: Temperature index melt modelling in mountain areas, J. Hydrol., 282, 104–115, 2003.

Hooke, R.: Flow law for polycrystalline ice in glaciers: comparison of theoretical predictions, laboratory data, and field measurements, Rev. Geophys. Space. Phys., 19, 664–672, 1981.

Hooke, R. L.: Positive feedbacks associated with erosion of glacial cirques and overdeepenings, GSA Bulletin, 103, 1104, https://doi.org/10.1130/0016-7606(1991)103<1104:PFAWEO>2.3.CO;2, 1991.

Hooyer, T. S., Cohen, D., and Iverson, N. R.: Control of glacial quarrying by bedrock joints, Geomorphology, 153, 91–101, https://doi.org/10.1016/j.geomorph.2012.02.012, 2012.

Humphrey, N. F. and Raymond, C. F.: Hydrology, erosion and sediment production in a surging glacier: Variegated Glacier, Alaska, 1982–83, J. Glaciol., 40, 539–552, https://doi.org/10.3189/S0022143000012429, 1994.

Iverson, N. R.: Morphology of glacial striae: Implications for abrasion of glacier beds and fault surfaces, GSA Bulletin, 103, 1308–1316, https://doi.org/10.1130/0016-7606(1991)103<1308:MOGSIF>2.3.CO;2, 1991.

Iverson, N. R.: A theory of glacial quarrying for landscape evolution models, Geology, 40, 679–682, https://doi.org/10.1130/G33079.1, 2012.

Jouzel, J., Masson-Delmotte, V., Cattani, O., Dreyfus, G., Falourd, S., Hoffmann, G., Minster, B., Nouet, J., Barnola, J.-M., Chappellaz, J., Fischer, H., Gallet, J. C., Johnsen, S., Leuenberger, M., Loulergue, L., Luethi, D., Oerter, H., Parrenin, F., Raisbeck, G., Raynaud, D., Schilt, A., Schwander, J., Selmo, E., Souchez, R., Spahni, R., Stauffer, B., Steffensen, J. P., Stenni, B., Stocker, T. F., Tison, J. L., Werner, M., and Wolff, E. W.: Orbital and millennial Antarctic climate variability over the past 800 000 years, Science, 317, 793–796, 2007.

Kamleitner, S.: Reconstructing the evolution and dynamics of Central Alpine glaciers during the Last Glacial Maximum on the basis of their geomorphological footprints and cosmogenic nuclide surface exposure dating, PhD thesis, University of Zürich, 186 pp., https://doi.org/10.3929/ethz-b-000579564, 2022.

Keller, O. and Krayss, E.: Der Rhein-Linth-Gletscher im letzten Hochglazial. 1. Teil: Einleitung; Aufbau und Abschmelzen des Rhein-Linth-Gletschers im Oberen Würm, Vierteljahrsschrift der Naturforschenden Gesellschaft in Zürich, 150, 19–32, 2005a.

Keller, O. and Krayss, E.: Der Rhein-Linth-Gletscher im letzten Hochglazial. 2. Teil: Datierung und Modelle der Rhein-Linth-Vergletscherung. Klima-Rekonstruktionen, Vierteljahrsschrift der Naturforschenden Gesellschaft in Zürich, 150, 69–85, 2005b.

Kirkham, J. D., Hogan, K. A., Larter, R. D., Arnold, N. S., Ely, J. C., Clark, C. D., Self, E., Games, K., Huuse, M., Stewart, M. A., Ottesen, D., and Dowdeswell, J. A.: Tunnel valley formation beneath deglaciating mid-latitude ice sheets: Observations and modelling, Quaternary Sci. Rev., 107680, https://doi.org/10.1016/j.quascirev.2022.107680, in press, 2022.

Koppes, M., Hallet, B., Rignot, E., Mouginot, J., Wellner, J. S., and Boldt, K.: Observed latitudinal variations in erosion as a function of glacier dynamics, Nature, 526, 100–103, https://doi.org/10.1038/nature15385, 2015.

Lawson, D. E., Strasse r, J. C., Evenson, E. B., Alley, R. B., Larson, G. J., and Arcone, S. A.: Glaciohydraulic supercooling: a freeze-on mechanism to create stratified, debris-rich basal ice: I. Field evidence, J. Glaciol., 44, 547–562, https://doi.org/10.3189/S0022143000002069, 1998.

Le Brocq, A., Payne, A., Siegert, M., and Alley, R.: A subglacial water-flow model for West Antarctica, J. Glaciol., 55, 879–888, https://doi.org/10.3189/002214309790152564, 2009.

Lindbäck, K., Pettersson, R., Hubbard, A. L., Doyle, S. H., van As, D., Mikkelsen, A. B., and Fitzpatrick, A. A.: Subglacial water drainage, storage, and piracy beneath the Greenland ice sheet, Geophys. Res. Lett., 42, 7606–7614, https://doi.org/10.1002/2015GL065393, 2015.

Livingstone, S. J., Clark, C. D., Woodward, J., and Kingslake, J.: Potential subglacial lake locations and meltwater drainage pathways beneath the Antarctic and Greenland ice sheets, The Cryosphere, 7, 1721–1740, https://doi.org/10.5194/tc-7-1721-2013, 2013.

MacGregor, K. R., Anderson, R., Anderson, S., and Waddington, E.: Numerical simulations of glacial-valley longitudinal profile evolution, Geology, 28, 1031–1034, 2000.

Medici, F. and Rybach, L.: Geothermal Map of Switzerland 1995 (Heat Flow Density), Tech. Rep. 30, Swiss Geophysical Commission, 1995.

Meierbachtol, T., Harper, J., and Humphrey, N.: Basal Drainage System Response to Increasing Surface Melt on the Greenland Ice Sheet, Science, 341, 777–779, https://doi.org/10.1126/science.1235905, 2013.

Pitcher, L. H., Smith, L. C., Gleason, C. J., and Yang, K.: CryoSheds: a GIS modeling framework for delineating land-ice watersheds for the Greenland Ice Sheet, GISci. Remote Sens., 53, 707–722, https://doi.org/10.1080/15481603.2016.1230084, 2016.

Preusser, F., Blei, A., Graf, H., and Schlüchter, C.: Luminescence dating of Würmian (Weichselian) proglacial sediments from Switzerland: methodological aspects and stratigraphical conclusions, Boreas, 36, 130–142, https://doi.org/10.1111/j.1502-3885.2007.tb01187.x, 2007.

Preusser, F., Reitner, J., and Schlüchter, C.: Distribution, geometry, age and origin of overdeepened valleys and basins in the Alps and their foreland, Swiss J. Geosci., 103, 407–426, https://doi.org/10.1007/s00015-010-0044-y, 2010.

Preusser, F., Graf, H. R., Keller, O., Krayss, E., and Schlüchter, C.: Quaternary glaciation history of northern Switzerland, E&G Quaternary Sci. J., 60, 21, https://doi.org/10.3285/eg.60.2-3.06, 2011.

Reber, R. and Schlunegger, F.: Unravelling the moisture sources of the Alpine glaciers using tunnel valleys as constraints, Terra Nova, 28, 202–211, https://doi.org/10.1111/ter.12211, 2016.

Ruokolainen, J., Malinen, M., Råback, P., Zwinger, T., Pursula, A., and Byckling, M.: ElmerSolver Manual, Tech. Rep. Online, CSC – IT Center for Science, https://www.nic.funet.fi/pub/sci/physics/elmer/doc/ElmerSolverManual.pdf (last access: 9 August 2023), 2020.

Ruokolainen, J., Malinen, M., Råback, P., Zwinger, T., Takala, E., Kataja, J., Gillet-Chaulet, F., Ilvonen, S., Gladstone, R., Byckling, M., Chekki, M., Gong, C., Ponomarev, P., van Dongen, E., Robertsen, F., Wheel, I., Cook, S., t7saeki, luzpaz, and Rich_B. : ElmerCSC/elmerfem: Elmer 9.0 (release-9.0), Zenodo [code], https://doi.org/10.5281/zenodo.7892181, 2023.

Russo, E., Fallah, B., Ludwig, P., Karremann, M., and Raible, C. C.: The long-standing dilemma of European summer temperatures at the mid-Holocene and other considerations on learning from the past for the future using a regional climate model, Clim. Past, 18, 895–909, https://doi.org/10.5194/cp-18-895-2022, 2022.

Schlüchter, C.: A non-classical summary of the Quaternary stratigraphy in the Northern Alpine Foreland of Switzerland, Bulletin de la Société neuchâteloise de Géographie, 32, 143–157, 1988.

Schlüchter, C.: The Swiss glacial record – A schematic summary, in: Quaternary Glaciations Extent and ChronologyPart I: Europe, edited by: Ehlers, J. and Gibbard, P., Vol. 2, Part 1 of: Developments in Quaternary Sciences, 413–418, Elsevier, https://doi.org/10.1016/S1571-0866(04)80092-7, 2004.

Schoof, C.: Ice sheet acceleration driven by melt supply variability, Nature, 468, 803–806, 2010.

Seguinot, J. and Delaney, I.: Last-glacial-cycle glacier erosion potential in the Alps, Earth Surf. Dynam., 9, 923–935, 2021.

Shackleton, C., Patton, H., Hubbard, A., Winsborrow, M., Kingslake, J., Esteves, M., Andreassen, K., and Greenwood, S. L.: Subglacial water storage and drainage beneath the Fennoscandian and Barents Sea ice sheets, Quaternary Sci. Rev., 201, 13–28, https://doi.org/10.1016/j.quascirev.2018.10.007, 2018.

Shreve, R.: Movement of water in glaciers, J. Glaciol, 11, 205–214, 1972.

Sundal, A. V., Shepherd, A., Nienow, P., Hanna, E., Palmer, S., and Huybrechts, P.: Melt-induced speed-up of Greenland ice sheet offset by efficient subglacial drainage, Nature, 469, 521–524, https://doi.org/10.1038/nature09740, 2011.

Sutter, J., Fischer, H., Grosfeld, K., Karlsson, N. B., Kleiner, T., Van Liefferinge, B., and Eisen, O.: Modelling the Antarctic Ice Sheet across the mid-Pleistocene transition – implications for Oldest Ice, The Cryosphere, 13, 2023–2041, https://doi.org/10.5194/tc-13-2023-2019, 2019.

Tarboton, D. G.: A new method for the determination of flow directions and upslope areas in grid digital elevation models, Water Resour. Res., 33, 309–319, https://doi.org/10.1029/96WR03137, 1997.

Ugelvig, S. V., Egholm, D. L., and Iverson, N. R.: Glacial landscape evolution by subglacial quarrying: A multiscale computational approach, J. Geophys. Res.-Earth Surf., 121, 2042–2068, https://doi.org/10.1002/2016JF003960, 2016.

Ugelvig, S. V., Egholm, D. L., Anderson, R. S., and Iverson, N. R.: Glacial Erosion Driven by Variations in Meltwater Drainage, J. Geophys. Res.-Earth Surf., 123, 2863–2877, https://doi.org/10.1029/2018JF004680, 2018.

van de Wal, R. S. W., Boot, W., van den Broeke, M. R., Smeets, C. J. P. P., Reijmer, C. H., Donker, J. J. A., and Oerlemans, J.: Large and Rapid Melt-Induced Velocity Changes in the Ablation Zone of the Greenland Ice Sheet, Science, 321, 111–113, https://doi.org/10.1126/science.1158540, 2008.

Velasquez, P., Messmer, M., and Raible, C. C.: A new bias-correction method for precipitation over complex terrain suitable for different climate states: a case study using WRF (version 3.8.1), Geosci. Model Dev., 13, 5007–5027, https://doi.org/10.5194/gmd-13-5007-2020, 2020.

Velasquez, P., Messmer, M., and Raible, C. C.: The role of ice-sheet topography in the Alpine hydro-climate at glacial times, Clim. Past, 18, 1579–1600, https://doi.org/10.5194/cp-18-1579-2022, 2022.

Werder, M., Hewitt, I., Schoof, C., and Flowers, G.: Modeling channelized and distributed subglacial drainage in two dimensions, J Geophys. Res.-Earth Surf., 118, 2140–2158, 2013.

Werder, M. A.: The hydrology of subglacial overdeepenings: A new supercooling threshold formula, Geophys. Res. Lett., 43, 2045–2052, https://doi.org/10.1002/2015GL067542, 2016.

Willis, I. C., Fitzsimmons, C. D., Melvold, K., Andreassen, L. M., and Giesen, R. H.: Structure, morphology and water flux of a subglacial drainage system, Midtdalsbreen, Norway, Hydrol. Process., 26, 3810–3829, https://doi.org/10.1002/hyp.8431, 2012.

Wright, P. J., Harper, J. T., Humphrey, N. F., and Meierbachtol, T. W.: Measured basal water pressure variability of the western Greenland Ice Sheet: Implications for hydraulic potential, J. Geophys. Res.-Earth Surf., 121, 1134–1147, https://doi.org/10.1002/2016JF003819, 2016.

E&G Quaternary Sci. J., 72, 203–218, 2023
https://doi.org/10.5194/egqsj-72-203-2023

Open Access E&G Quaternary Science Journal

Research article

The loess landscapes of the Lower Rhine Embayment as (geo-)archeological archives – insights and challenges from a geomorphological and sedimentological perspective

Frank Lehmkuhl, Philipp Schulte, Wolfgang Römer, and Stephan Pötter

Department of Geography, RWTH Aachen University, Wüllnerstr. 5b, 52056 Aachen, Germany

Correspondence: Frank Lehmkuhl (flehmkuhl@geo.rwth-aachen.de)

Relevant dates: Received: 16 February 2023 – Revised: 12 June 2023 – Accepted: 1 August 2023 – Published: 5 September 2023

How to cite: Lehmkuhl, F., Schulte, P., Römer, W., and Pötter, S.: The loess landscapes of the Lower Rhine Embayment as (geo-)archeological archives – insights and challenges from a geomorphological and sedimentological perspective, E&G Quaternary Sci. J., 72, 203–218, https://doi.org/10.5194/egqsj-72-203-2023, 2023.

Abstract: Archeological and geoscientific research in loess landscapes remains challenging due to erosional discordances and the relocation of sediments by fluvial erosion and slope wash. The Lower Rhine Embayment (LRE) can serve as a blueprint for archeological and paleoenvironmental research in loess landscapes of Central Europe. The accumulation of wind-blown dust; paleosols developed therein; and the archeological artifacts preserved in loess, colluvial or alluvial sediments are evidence of the Pleistocene and Holocene dynamics of the landscape. Geomorphologic processes in different and specific relief positions must be considered different processes that transform and relocate sediments and archeological remains. Besides aeolian accumulation, erosion and deflation have also transformed the landscape of the LRE. These include fluvial slope wash, gully formation, colluviation, and periglacial processes such as solifluction, cryoturbation and the formation of ice wedge pseudomorphs. In addition, other post-depositional processes, including weathering and soil formation, modify the sedimentary record. In light of the landscape evolution from more hilly landscapes to the flat, agriculturally used terrain we see today, we highlight the relevance and importance of different geomorphological and soil processes including their impacts and challenges for archeological and geoscientific studies.

Kurzfassung: Archäologische und geowissenschaftliche Forschung ist in Lösslandschaften aufgrund von Erosionsdiskordanzen und der Verlagerung von Sedimenten durch fluviale Erosion bis heute eine Herausforderung. Die Niederrheinische Bucht kann als Blaupause für die archäologische und paläoökologische Forschung in mitteleuropäischen Lösslandschaften dienen. Die Akkumulation von Staub, darin entwickelte Paläoböden sowie archäologische Artefakte, welche im Löss und den korrelaten Sedimenten wie Kolluvien und Auenlehmen erhalten geblieben sind, liefern wichtige Hinweise für die pleistozäne und holozäne Landschaftsdynamik. All diese Indizien können helfen, die Paläoumweltbedingungen früherer Siedlungen zu verstehen. Die verschiedenen geomorphologischen Prozesse und deren spezifische Reliefposition müssen berücksichtigt werden, da Lösssedimente und darin enthaltene archäologische Artefakte durch diese Prozesse umgewandelt und verlagert werden können. Neben der äolischen Akkumulation haben auch Erosion und Deflation die

Landschaft der Niederrheinischen Bucht verändert. Dies sind insbesondere fluviale Hangabspülungen, Erosionsgullies, Kolluvien und periglaziale Prozesse wie Solifluktion, Kryoturbation und die Bildung von Eiskeilpseudomorphosen. Darüber hinaus führen Prozesse nach der Ablagerung, einschließlich Verwitterung und Bodenbildung, zu Veränderungen in den Sedimentarchiven. Vor dem Hintergrund der Landschaftsentwicklung von vorwiegend hügeligen Landschaften hin zum flachen, landwirtschaftlich genutzten Gelände, wie wir es heute vorfinden, beleuchten wir die Relevanz und Bedeutung verschiedener geomorphologischer und bodenkundlicher Prozesse sowie deren Auswirkungen und Herausforderungen für archäologische und geowissenschaftliche Untersuchungen und Studien.

Dedication. Dedicated to Prof. J. Richter on the occasion of his retirement.

1 Introduction

In the last few decades, interest in geoarcheology among geoscientists has grown, leading to increased collaboration between archeologists and geoscientists in loess research (Chu and Nett, 2021). Pioneering studies in the 1980s and 1990s inter alia integrated stratigraphic, sedimentological and archeological data from the southern Limburg (the Netherlands) to reconstruct Middle to Late Pleistocene environments and human behavior (van Kolfschoten and Roebroeks, 1985; Vandenberghe et al., 1993). Although geoarcheology always aimed at the involvement of expertise by specialists from both scientific branches, the implementations of geoscientific data in archeological contexts changed throughout time. Sedimentary archives changed, in the view of (geo-)archeologists, from the inanimate bed of archeological finds to a part of the habitat of our ancestors, influencing their cultural evolution and behavior (see Chu and Nett, 2021, and references therein).

Generally, the bonds between loess research and Paleolithic archeology are tight. This is due to the relatively high number of archeological find spots in European loess regions in comparison to other archives of terrestrial sediments. This abundance is related to several anthropogenic and natural factors (e.g., Boemke et al., 2022). Loess landscapes in Central Europe are linked to Pleistocene steppic or tundra biomes (Lehmkuhl et al., 2021), which were important habitats for hunter–gatherer subsistence. These environments were most likely ideal hunting grounds and supplied early modern humans with enough nutrition through droves of large mammals (Sirocko et al., 2016). Given its aeolian origin and rapid accumulation of dust, loess provides favorable conditions for a good preservation of open-air sites such as the famous sites of Krems-Wachtberg (Einwögerer et al., 2006) and Willendorf in Austria (Nigst et al., 2014), Dolní Věstonice in Czechia (Formicola et al., 2001), and Rheindahlen in the Lower Rhine Embayment (LRE) (Bosinski, 1966). These sites are preserved due to their thick loess cover, which protected the archeological inventory from atmospheric influences and relocation processes.

In the early 2000s, archeologists and geoscientists from the University of Cologne and the RWTH Aachen University started to collaborate. This resulted in several joint projects such as the CRC 806 "Our Way to Europe" between 2009 and 2021 focusing especially on the last glacial cycle (e.g., Fischer et al., 2021, 2019, 2017; Lehmkuhl et al., 2018, 2016; Zens et al., 2018). Joint work, especially on Holocene reworked colluvial and alluvial sequences with a (geo-)archeological focus, provides further results on the changes in geomorphic processes, sedimentation and soil development. The latter processes were caused and intensified by the changes in land use by agriculture societies since the Neolithic period. Several geoarcheological projects, including PhD monographs, have focused on Holocene colluvial and alluvial sediments in the LRE as part of these projects (e.g., Gerz, 2017; Protze, 2014; Schmidt-Wygasch, 2011; Schulz, 2007).

Loess in Western and Central Europe formed mainly during cold stages of the Pleistocene. Loess consists of windblown dust which was trapped by topographical barriers (Antoine et al., 2016; Lehmkuhl et al., 2016) or by the vegetation cover (Zech et al., 2012). Post-depositional processes, summarized under the term loessification (Pécsi, 1990), lead to the unique characteristics of loess, such as the high porosity, the vertical stability when dry or the high fertility of soils developing on loess (Sprafke and Obreht, 2016). Colder and drier periods during glacials and stadials enabled dust accumulation, while soil formation resulting from chemical weathering occurred during the warmer and wetter intervals such as interglacials and interstadials. The cyclicity of the environmental conditions in the Pleistocene led to alterations of loess layers and paleosols, so-called loess–paleosol sequences (LPSs). Therefore, loess deposits are valuable archives for climate and landscape evolution in the Pleistocene (Antoine et al., 2009). The characteristics of LPSs record local to regional imprints of global climatic fluctuations (Obreht et al., 2017).

However, the preservation of loess and the conservation of potential archeological findings embedded in loess depend strongly on the geomorphological setting (Antoine et al., 2016; Lehmkuhl et al., 2016). The high erodibility of loess may lead to large hiatuses and differences in the local stratigraphy (Fenn et al., 2020; Obreht et al., 2015; Steup and

Fuchs, 2017). In humid climates, where precipitation mainly occurs as rain, LPSs are prone to relocation and reworking, as well as soil formation processes. During the Pleistocene, the landscapes in Central and Eastern Europe were additionally shaped by periglacial processes, such as cryoturbation or solifluction and also by aeolian deflation (Antoine et al., 2016; Lehmkuhl et al., 2021; Zens et al., 2018). These processes can also affect the archeological assemblage. Within the last few years, there has been an increasing interest in archeological open-air sites lacking stratigraphic integrity, especially in loess landscapes (Chu et al., 2019; Fitzsimmons et al., 2020), as they help to improve our knowledge about Paleolithic occupation patterns.

The Lower Rhine Embayment (LRE) is an important study area for Pleistocene environmental dynamics and human behavior in Central Europe. As a typical part of the oceanic-influenced northern European loess belt, the LRE has been subjected to numerous geomorphological, stratigraphic and archeological research activities within the last decades (e.g., Fischer et al., 2017; Geilenbrügge, 2010; Gerlach, 2006; Kels, 2007; Lehmkuhl et al., 2021, 2016; Meurers-Balke et al., 1999; Pötter et al., 2023; Schirmer, 2016; Zimmermann, 2012; Zimmermann et al., 2005). Loess and geoarcheological research benefited from numerous excavations resulting from past and ongoing quarrying activities in clay, marl and loess pits; in brickyards; and from the large opencast lignite mining at Hambach, Inden and Garzweiler (Fig. 1).

The landscape of the LRE is strongly affected by human impact. Since the Neolithic, anthropogenic activity has transformed the landscape by agricultural and various infrastructural measures. Human interferences accelerated markedly from the Industrial Revolution onwards and were in particular enhanced by mining activities. Early mining and quarrying activities in the LRE include the development of marl and clay pits and brickyards. Since the 20th century, opencast lignite mining has been carried out. These exposures provide insights into the structure and stratigraphy of loess sections, as well as evidence for and findings of human occupation. The density of archeological findings in loess landscapes is strongly biased by these anthropogenic factors. On the one hand, the construction of infrastructure or settlements, as well as mining activity, increases the number of finds due to excavating activity (Boemke et al., 2022; Gerlach, 2006). On the other hand, these activities potentially destroy archeological open-air sites. However, archeological artifacts may be undetectable and inaccessible under thick loess cover, even with geophysical prospection methods (Scharl et al., 2021).

The objective of this study is to review and cast light on the sedimentary history of loess in the LRE, including Pleistocene accumulation, relocation processes and Holocene soil erosion. This includes processes which could be summarized as site formation processes (see Waters and Kuehn, 1996). The study is based on five selected LPSs from various geomorphological settings and discusses climatic and anthropogenic influences which have affected these deposits during the Holocene. Challenges and perspectives for geoarcheological research in the LRE are highlighted based on the site formation processes derived from a review of published research as well as our own research.

2 Study area

The Lower Rhine Embayment (LRE) is situated in North Rhine-Westphalia, Germany, in the northern foreland of the Rhenish massif (Fig. 1). The LRE is part of the western European rift system (Ahorner, 1962; Lehmkuhl et al., 2016; Schirmer, 2003, 1990). It is a tectonic fracture zone dominated by relative subsidence with tectonic graben, horsts and half-horst structures. In the south, the LRE is bordered by the Eifel Mountains with elevations up to more than 600 m a.s.l. (above sea level). To the north, the LRE opens towards the North German Plain and Westphalian lowlands, with elevations from ~ 160 m a.s.l. in the south to less than 40 m a.s.l. in the north. The flat topography is interrupted by fluvial valleys and horst structures with elevations of more than 200 m a.s.l. (Boenigk and Frechen, 2006). Northwest- to southeast-striking normal faults are dominant and divide the LRE into several blocks with different rates of vertical movement and lateral tilting (Ahorner, 1962). The highest subsidence occurs in the eastern part of the major geological blocks (Ahorner, 1962; Klostermann, 1992). High subsidence favored high sedimentation rates of Pleistocene deposits, which mainly consist of fluvial and aeolian sediments overlying Paleogene to Neogene sands (Klostermann, 1992). However, tectonic structures appear to be of subordinate importance for the distribution of aeolian deposits. Instead, there is a strong differentiation in grain size from northwest to southeast at the northern margin of the northern European loess belt (Lehmkuhl et al., 2021). Quaternary fluvial deposits are derived from the river systems of Meuse and Rhine, whereas the aeolian deposits can be differentiated in vast loess covers in the south, thinner loess towards the north, and sandy loess and aeolian sand to the northwest (Fig. 1; Lehmkuhl et al., 2018). The thickness of loess deposits overlying older bedrock and Pleistocene terraces depends on the geomorphological and tectonic setting. The larger rivers incised in Early and Middle Quaternary deposits, and in these valleys Late Quaternary fluvial, colluvial and alluvial deposits were accumulated.

The LRE is part of the northern European loess belt, which extends from western France through Belgium, Germany and Poland to Ukraine and Russia. This region preserves the most diversified pedosedimentary records in Europe (Lehmkuhl et al., 2021, 2016). The variability in the environmental conditions during the Pleistocene influenced the deposits of the LRE. The deposits exhibit a complex stratigraphy with erosional unconformities and permafrost features such as ice wedge pseudomorphs or cryoturbation features, as well as thermokarst erosional features. Within recent years, several authors published updated stratigraphic frameworks for the Lower Rhine loess (Fischer et al., 2019; Lehmkuhl et al., 2016; Schirmer, 2016; Zens et al., 2018). These studies include detailed descriptions of single stratigraphic units, their most important properties and characteristics, and their supposed chronostratigraphic position (Fig. 2). The most recent research activities have concentrated on the neighboring LPS of Remagen–Schwalbenberg south of the LRE. This LPS is situated on the lower middle terrace of the Rhine River (LMT1 after Boenigk and Frechen, 2006; Fischer et al., 2021). New results provided one of the most spectacular high-resolution and well-dated loess cores of Central Europe (Fischer et al., 2021; Vinnepand et al., 2022). An overview of the most recent stratigraphic approaches and key marker horizons for the European loess and the LRE for the last glacial cycle is published in Lehmkuhl et al. (2016, 2021).

Recent annual precipitation in the LRE varies between 800 mm in the western part to 650 mm in the southeastern area in the rain shadow of the Eifel Mountains (Nilson, 2006). Whereas the mountainous areas are covered with forest, the nearby flat and mainly loess-covered areas have been dominated by agricultural use since the Neolithic (Zimmermann, 2012). Holocene climatic conditions enhanced weathering and pedogenic processes, mainly decalcification, clay formation and clay translocation. As a result of weathering and soil formation processes loess sediments were transformed into different soil types, ranging from initial calcic Regolsols towards Cambisols and Luvisols. Intense agricultural activity causes high soil erosion and consequently relocation of soils and sediments.

3 Selected sites and their geomorphological and sedimentological setting in the LRE

The Lower Rhine Embayment shows clear differences in the occurrence and properties of LPSs in relation to the (meso-)relief. Loess sequences in plateau-like positions, which are flat to undulating interfluve areas, tend to be shorter, shallower and more affected by erosion than sections in depressions, in paleochannels, on gentle inclined straight slopes and on slope toes. The latter are often covered by reworked sediments of older paleosols redeposited as heterogeneous, finely laminated colluvium (Lehmkuhl et al., 2016; Schirmer, 2016, and references therein). In order to demonstrate the different effects of the relocation and soil formation processes on the LPS as a function of the geomorphological setting, we selected five sites: these are Garzweiler, Rheindahlen, Sandgewand fault, Siersdorf and Elsbach Valley. Previously published stratigraphic data are re-evaluated and discussed in the context of the landscape dynamics of the LRE.

The long LPS exposed in the opencast lignite mine of *Garzweiler* (Fig. 3a) shows a typical Pleistocene stratigraphy of the LRE. Older deposits, dating back to the Middle Pleistocene, are usually decalcified and relatively dense. The younger, Late Pleistocene loess deposits show varying carbonate contents, mainly governed by weathering processes and leaching. In addition, fluvial erosion is displayed by gullies and small trough-shaped valleys. For a detailed analysis of the architecture and stratigraphy of the Garzweiler LPS, see Kels (2007).

The *Rheindahlen* LPS (Fig. 3b) is exposed in a former brickyard near the city of Mönchengladbach (Fig. 1). This sequence is a crucial archive for the LRE, as it additionally hosts some of the oldest stratified Middle Paleolithic artifacts in the LRE (Bosinski, 1966). The stratigraphy is condensed due to erosional processes. The plateau-like setting favored the preservation of Weichselian, Saalian and Elsterian loess sediments and interglacial and interstadial paleosols (Klostermann and Thissen, 1995).

Thin loess and periglacial cover beds were exposed at the *Sandgewand fault* (Fig. 3c) close to Eschweiler in the course of the construction of a pipeline. Here, the loess cover is very thin (less than 1 m) or in many cases absent. Pleniglacial silty sediments, including ice wedge pseudomorphs that cut through them, are adjacent in the upslope plateau setting. (Fig. 4a). Exposures along the slope of the Sandgewand fault (Fig. 4b) show alternating layers of shallow periglacial cover beds (debris layers) and weathered thin silty sediments in the following sequence from the base to the toe of the slope. The weathered debris of the Paleozoic basement of the exposure is covered by pebbles and gravels, possibly corresponding to the main terrace of the Early Pleistocene. There is a cover layer of solifluction debris (30 to 40 cm thick) with a hook-shaped form downslope from the Sandgewand fault. This downfaulted material is covered by thin silty sediments (30 to 10 cm) and a second periglacial debris layer (40 to 20 cm). Along the whole trench Holocene colluvial deposits and disturbed surfaces form the top of the sequence.

The *Siersdorf* LPS (Fig. 3d) shows the situation of a paleochannel incised into an old Pleistocene terrace (Knaak et al., 2021; Pötter et al., 2023). This channel was filled up during the Middle to early Upper Pleniglacial. After aeolian dust was trapped in a wet environment characterized by swampy conditions, loess and soil sediments were deposited by short-range fluvial relocation. The Upper Pleniglacial shows a rather typical sequence of marker horizons, such as the so-called Eben Zone (Fig. 2). Larger ice wedge pseudomorphs and frost crevasses extend from the Brabant loess into the upper part of the Hesbaye loess, indicating a cold and dry climate at the end of the last glacial cycle. The laminated Hesbaye loess contains also smaller ice wedge pseudomorphs.

The sequence exposed in the *Elsbach Valley* (Fig. 3e) provides a complex stratigraphy resulting from the superimposition of different Pleistocene and Holocene processes. This exposure was opened up and later completely removed by Garzweiler opencast mining. The trough-shaped valley head showed a sequence with several fluvial channels filled

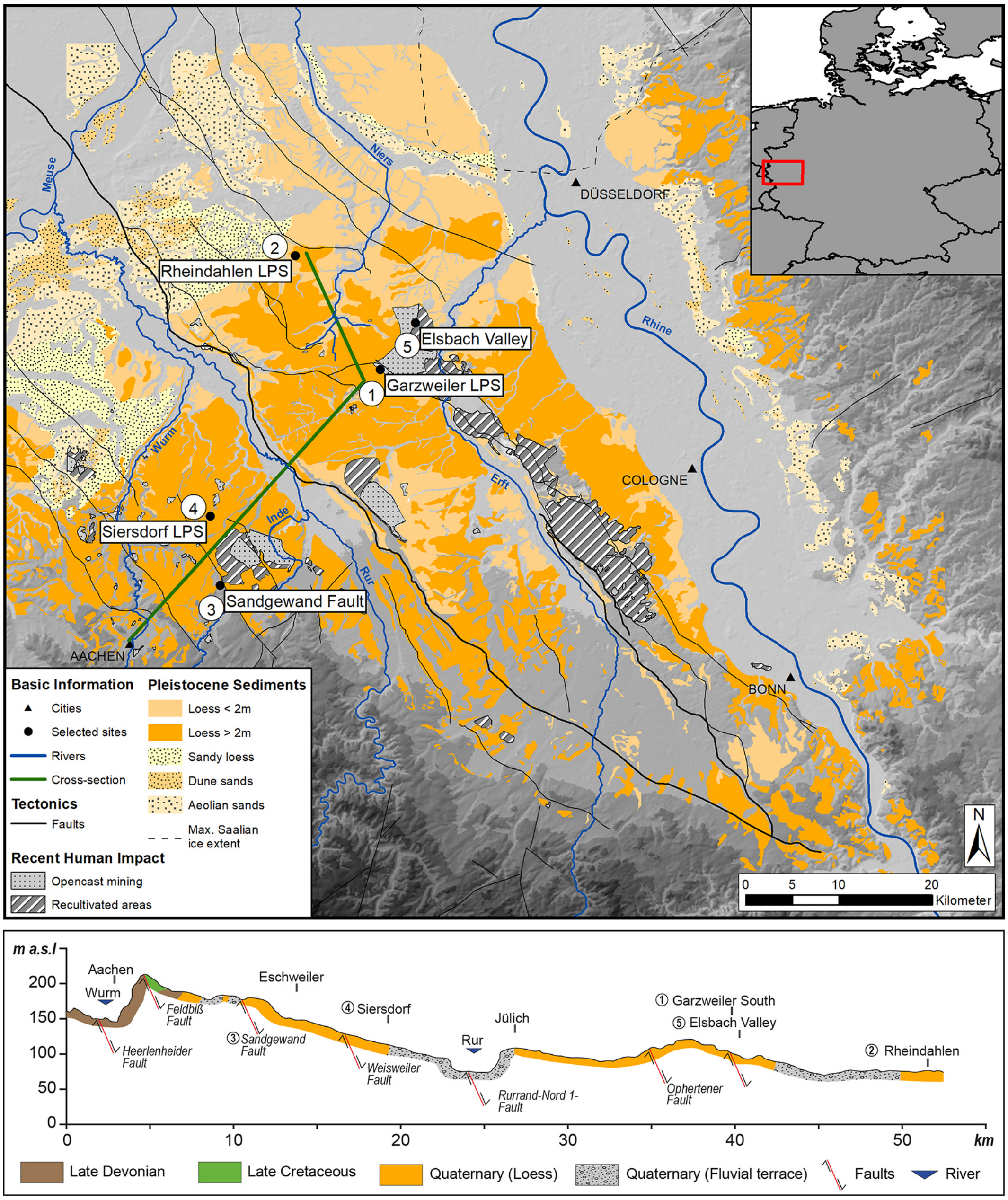

Figure 1. Map with distribution of aeolian sediments in the Lower Rhine Embayment (modified after Lehmkuhl et al., 2016). The cross section shows the surface geology and fault lines. The five selected sites are examples for different geomorphological settings. Map and geological data based on the geological survey maps at 1 : 100 000 (Geological Survey of North Rhine-Westphalia, 2013) and the geological survey maps at 1 : 200 000 (Federal Institute for Geosciences and Natural Resources, 2002).

with aeolian and fluvial sediments. The loess deposit is dissected by numerous paleochannels that were filled with relocated Saalian sediments. These sediments are covered with small remnants of the Eemian soil on top. Based on a stratigraphic evaluation, it was eroded during the Lower Pleniglacial or Middle Pleniglacial. The completely missing Middle Pleniglacial reflects the "normal case" of the LRE. The Upper Pleniglacial is well preserved, and the Eben unconformity follows the paleochannel and eroded older sediments again in the middle part of the section (Lehmkuhl et al., 2016). During the Holocene the trough-shaped valley head was completely filled with more than 7 m of colluvial sediments, thereby reducing the relative relief and causing a flattening of the landscape. The processes were triggered and enhanced by climatic shifts but mainly by soil erosion and

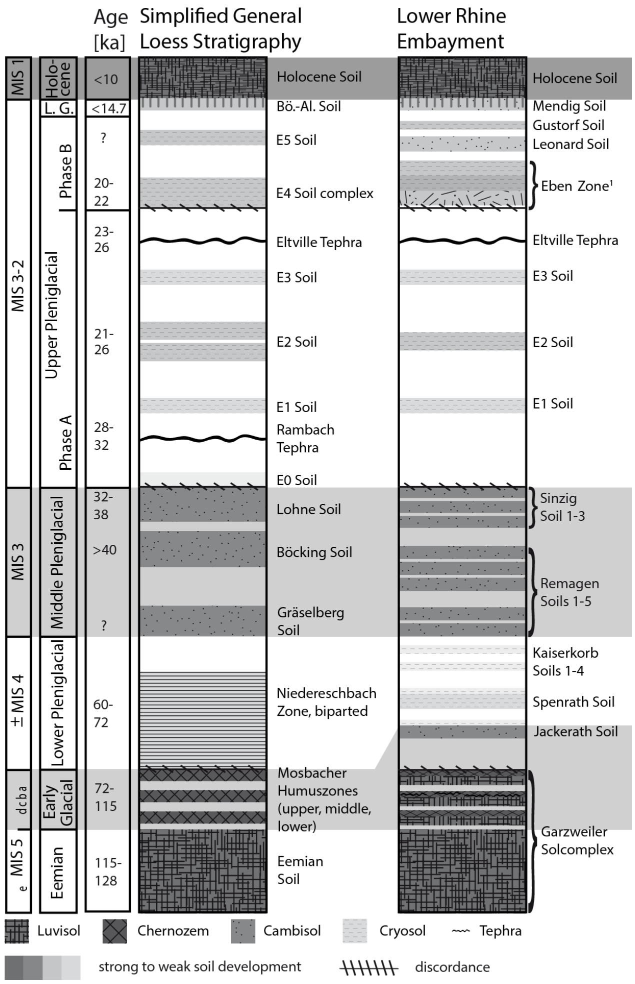

Figure 2. Simplified western European loess stratigraphy and comparison with the local stratigraphy of the LRE (Lehmkuhl et al., 2016, modified). The Eben Zone contains the Kesselt Layer, Belmen and Elfgen soils (cf. Schirmer, 2016). The Loess stratigraphy is named according to the pedostratigraphic notation of Antoine et al. (2009, 2013). The Marine Isotopic Stages (MISs) are mentioned as an additional large-scale climatic orientation (without exact temporal correspondence for the LRE).

colluvation due to anthropogenic land use change and agriculture.

4 Pleistocene and Holocene processes in the Lower Rhine Embayment

Different landscape settings and related sediment sequences provide insights concerning the relation between typical geomorphological processes and the correlated sediment stratigraphy. The analysis of Pleistocene LPSs and Holocene colluvial and alluvial sediments enables the reconstruction of the paleoenvironmental evolution from the Middle Pleistocene onwards (Fig. 2).

4.1 Pleistocene settings, environments and processes

Loess landscapes are formed by a multitude of geomorphological and sedimentological processes. This so-called sedimentary history of loess is influenced not only by processes within the landscape itself, but also by processes in source regions for detrital material (Pötter, 2021). The most important sedimentological process in loess landscapes is dust accumulation (Pye, 1995, 1984), mostly on topographic barriers (Antoine et al., 2016; Leger, 1990; Lehmkuhl et al., 2016) or vegetation (Zech et al., 2012), so-called loessification (Sprafke and Obreht, 2016). However, post-depositional processes strongly shaped these landscapes during the Pleistocene and Holocene. These processes include

- erosion and relocation due to fluvial processes (slope wash during the Pleistocene and slope wash and gully erosion in the Holocene)
- permafrost-related processes including ice wedge pseudomorphs
- solifluction and freezing–thawing processes including periglacial wash denudation
- aeolian sedimentation and deflation in later times
- soil formation during interglacials and interstadials.

In the following, we will evaluate the effect of these processes in the various geomorphological settings.

4.1.1 Geomorphological setting and Pleistocene processes

Lehmkuhl et al. (2016) defined four main geomorphological positions for LPSs in the LRE (Table 1): plateau-like areas, flat to undulating interfluve areas and flat-topped loess-covered fluvial terrace remnants, which are here named plateaus, slopes, slope toes, depressions and erosional channels. The most important factors affecting the characteristics of loess deposits are slope wash and hillslope processes, the slope aspect, dust accumulation and deflation, cryogenic processes, and solution and other processes of soil formation.

The geomorphologic setting has strongly influenced the processes in the Pleistocene. Table 1 summarizes the different processes and intensities of processes associated with the topographic settings. Loess, which is formed on a plateau-like position, is rarely eroded by slope wash due to the low gradients. However, deflation can play an important role in these positions, resulting in shorter, shallower and more condensed sequences. Deflation in plateau situations and interfluve areas often leads to erosional hiatuses. Additionally, these sequences are often affected by frost and desiccation cracks (see examples in Lehmkuhl, 2016). LPSs in slope positions are affected by intense erosion and relocation processes (Table 1). Slope wash during the Pleistocene was most

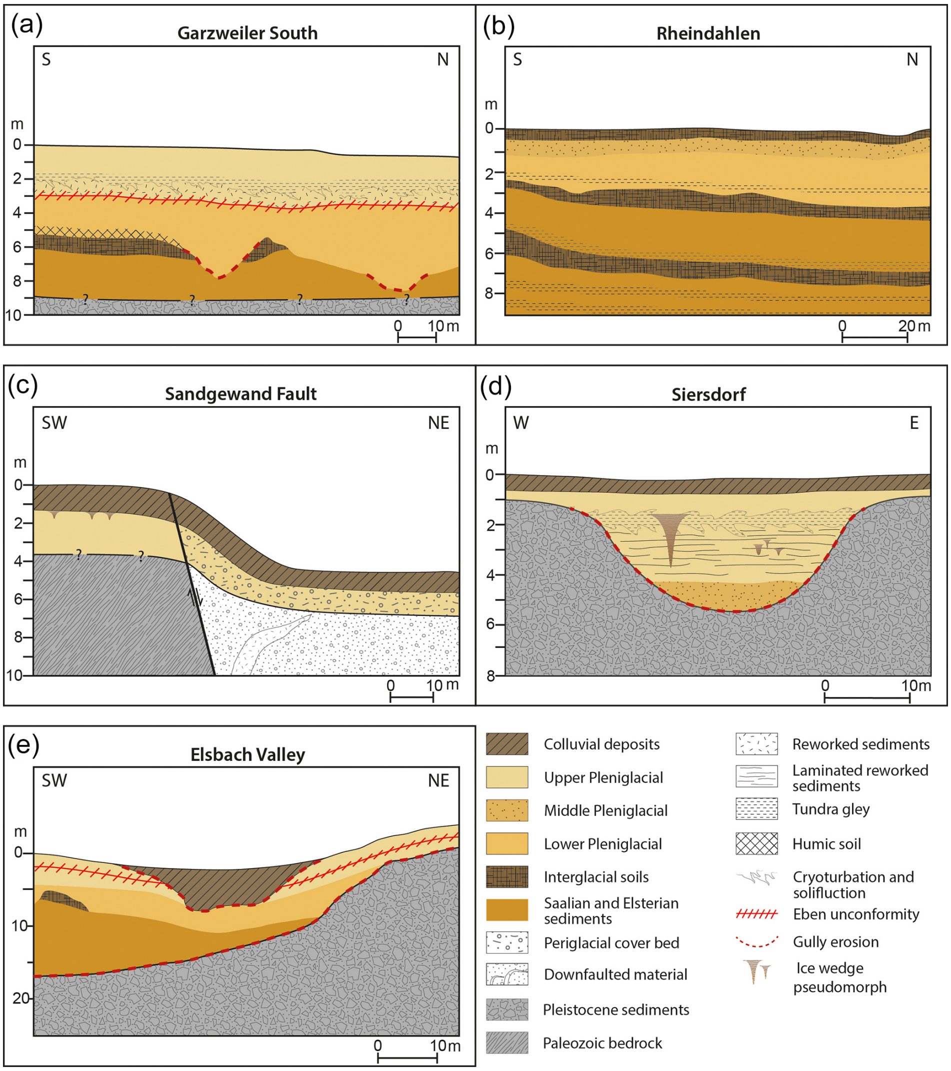

Figure 3. Selected key sites. Further explanations are given in the text; for locations see Fig. 1.

likely related to nivation, i.e., snow accumulation and thawing. During large parts of the Pleistocene periglacial conditions in the LRE resulted in solifluction as a denudative slope process. Bedrock areas favored the formation of periglacial cover beds. Solifluction starts at slope gradients as low as 2° (see French, 2017, and references therein) and can give rise to marked unconformities in the LPS. Especially the LRE, as a humid loess landscape region (cf. Lehmkuhl et al., 2016, 2021), was prone to intense relocation processes on slopes such as solifluction. Therefore, depressions and slope toes are mainly composed of relocated loess instead of pure aeolian deposits. For example, the Eben unconformity and the following Kesselt Layer provide evidence for slope erosion and denudation resulting in a hiatus and for drier periods in ice wedge pseudomorphs (Fig. 5). Most studied loess sequences are, however, situated either on slope toes or in depressions and filled paleochannels. As dust on slope toes is often accumulated on the leeward topographic barrier of the valley (east-facing slope), the asymmetric valleys of the periglacial loess belt favored the accumulation of loess (Antoine et al., 2016; Lehmkuhl et al., 2021, 2016). The importance of topographical barriers and depressions in loess formation was highlighted by several authors (Antoine et al., 2016; Leger, 1990; Lehmkuhl et al., 2021, 2016; Mason et al., 1999; Muhs, 2013). The slope aspect also reveals that dust was mainly deposited on eastern (lee) sites. Very often asymmetric (periglacial) valleys strengthened this process. The formation of loess has been affected by soil processes and colluviation in depressions and at slope toes.

4.1.2 Middle Pleistocene deposits and processes

Middle Pleistocene loess deposits are rarely found in the LRE. Most (pedo-)sedimentary features of pre-Saalian age, i.e., older than Marine Isotope Stage (MIS) 6, are only pre-

Table 1. Processes in loess landscapes in relation to the relief. The impact of different processes according to the position of loess sections from weak (−), medium (±), strong (+) to very strong (++). Modified according to Lehmkuhl et al. (2016).

	A: Plateau	B: Slope	C: Slope toe	D: Depressions and erosional channels
1: Slope wash and hill slope processes	−	++	+	−
2: Deflation	++	−	−	−
3: Slope aspect (west–east/north–south)	−	++	+	−
4: Sedimentation	±	−	+	++
5: Cryogenic features				
(a) Frost cracks	+	−	−	−
(b) Ablation and solifluction	−	++	+	−
6: Decalcification and solution	±	+	+	±
7: Intensity of soil development	±	−	+	++

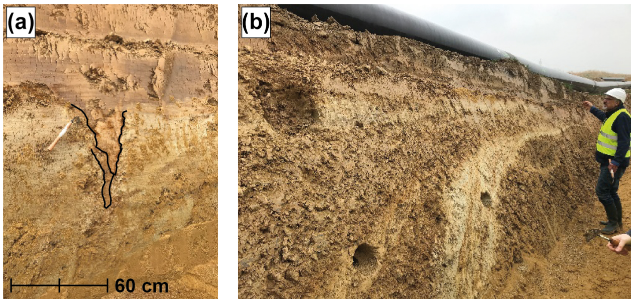

Figure 4. Exposures in a trench close to the Sandgewand fault near Eschweiler (Figs. 1 and 3c) during pipeline construction. **(a)** Pleniglacial silty sediments including ice wedge pseudomorphs in the upslope plateau setting. **(b)** Slope position near the fault. A hook-shaped sequence of alternating layers of two shallow periglacial cover beds (debris layers) interbedded and topped by weathered thin silty sediments covers the weathered debris of the Paleozoic basement. In both images, Holocene colluvial deposits and disturbed surfaces form the top of the sequences (Photos: Frank Lehmkuhl, 2020).

served in specific geomorphological situations. Type localities for pre-Saalian loess in the LRE are, e.g., the Rheindahlen and Erkelenz LPSs (Schirmer, 2002). In adjacent regions in southern Limburg in the Netherlands and Belgium, the Kesselt–Op de Schans and Hezerwater LPSs provide chronostratigraphic sequences reaching back up to MIS 12 (Meijs, 2002; Meijs et al., 2013; van Baelen, 2017; Vanmonfort et al., 1998). Although in special situations Middle Pleistocene deposits may account for up to 25 % of the sedimentary budget (Kels and Schirmer, 2011), the relatively poor preservation of Middle Pleistocene loess in the LRE is due to several factors. Firstly, the paleogeography of the European loess belt changed substantially throughout the Pleistocene. During the Elsterian glaciation, vast proglacial lakes in northern Central Europe reduced the size of important potential deflation areas. These areas could not serve as dust sources (Lehmkuhl et al., 2021). Secondly, the depositional milieu of aeolian sediments in the European loess belt shifted southwards due to the greater extent of the Middle Pleistocene continental ice sheets compared to the Late Pleistocene ones. During the Saalian glaciation, e.g., the ice extent reached the LRE, with margins near the city of Düsseldorf (Fig. 1, extent modified according to Ehlers et al., 2011). Aeolian cover sands and sand dunes were formed in the vicinity of the ice sheets, comparable to the Late Pleistocene European sand belt, and loess deposits developed to the south (southwest) (Kalińska-Nartiša et al., 2015; Lehmkuhl et al., 2016; Zeeberg, 1998). Thirdly, the Middle Pleistocene loess deposits of the LRE were strongly affected by erosion, reworking, relocation and re-deposition during later stages. The vastest extent of Pleistocene continental ice sheets occurred during the penultimate glacial (MIS 6; Ehlers et al., 2011). During the glacial advances, older loess deposits were reworked and eroded. In contrast, in the Late Pleistocene, the margin of the continental ice sheets was further north, and the LRE was under the influence of permafrost (Andrieux et al., 2016; Lehmkuhl et al., 2021; Vandenberghe et al., 2014), which contributed to a reworking of the loess deposits (see Sect. 4.1.3).

The Middle Pleistocene loess deposits of neighboring southern Limburg show characteristic features related to the paleogeography. According to van Baelen (2017) and Meijs et al. (2013), Kesselt–Op de Schans exhibits a local chronostratigraphic sequence which can be attributed to MIS 8 and 9. Due to the vicinity of the continental ice sheets, these deposits can be characterized as sandy loess. Loess deposits in the LRE associated with the Saalian glacial period are relatively homogenous when compared stratigraphically with Late Glacial loess (see Sect. 4.1.3). The deposits mainly consist of solifluidal and colluvial loess packages. The onset of Saalian loess formation took place after an extensive landscape reorganization with almost complete erosion of older loess deposits, associated with the so-called Wetterau discordance (Schirmer, 2002). The Saalian sequences in the LRE

Figure 5. The Eben Zone including the Kesselt Layer in the valley head of the Elsbach creek. The ice wedge pseudomorphs disturb the horizon of the underlying Eben unconformity. Photo: Frank Lehmkuhl.

and adjacent regions generally show relatively high contents of fine sand, indicating a nearby source area, such as the glaciofluvial outwash plains of the Drenthe stadial ice sheets (Lehmkuhl et al., 2017).

The oldest loess sequences related to the penultimate Saalian glacial cycle in the LRE are found in the Garzweiler lignite mine (e.g., Kels, 2007) and in Rheindahlen. Additionally, Middle Paleolithic archeological findings were reported, for example, from the nearby region near Maastricht, the Netherlands; in Hezerwater at Veldwezelt (Vanmonfort et al., 1998); and in the brickyard quarry Kesselt–Op de Schans. Inden-Altdorf in the LRE revealed the first open-site habitation features with associated hearths and stone tools for the Middle Paleolithic in Central Europe (Pawlik and Thissen, 2017). These sites are ideally located as they provide access to fluvial gravel of the old Meuse River terraces, which contain a large number of flint pebbles as a high-quality raw material source of flint. For the Middle Paleolithic site of Inden-Altdorf unfortunately the geomorphological setting, sedimentation and the dating methods of the site are not described in detail. Pawlik and Thissen (2017) stated that this site dates to an earlier phase of MIS 5, between ca. 120–100 ka and the time of early Neanderthals in Europe.

4.1.3 Late Pleistocene deposits and processes

The Late Pleistocene and especially the last glacial period are imprinted in the LRE as a highly complex pedostratigraphic succession (see Fig. 2; Antoine et al., 2016; Lehmkuhl et al., 2021, 2016). This complex stratigraphy is, e.g., due to large erosional gaps which were formed during climatic transitions. Therefore, complete Late Pleistocene loess archives are rare (Lehmkuhl et al., 2016; Zens et al., 2018). After the Eemian interglacial, Chernozem-like humic soils were formed under steppe-like environmental conditions. This was followed by a transition to colder and more continental conditions, which are reflected in the respective loess stratigraphy (e.g., Haesaerts et al., 2016; Schirmer, 2016; Semmel, 1998). The first phases of the last glacial cycle are characterized by redeposited finely laminated sediments, while the loess packages contain several thin and weakly developed tundra gleys and humic soils (Zens et al., 2018). The most recent loess layer in this subdomain contains two sedimentary facies: the niveo-aeolian (cold-humid) and the homogenous loess (cold-arid). They were termed Hesbaye and Brabant loess in Belgium and the Lower Rhine Embayment (e.g., Haesaerts et al., 2016; Schirmer, 2016) and can be also observed in northern France (Antoine et al., 2016).

As mentioned above, the LRE was affected by a variety of geomorphological processes (Table 1). These processes were mainly governed by the prevalence of periglacial conditions combined with the more oceanic climate of the LRE. Compared to loess domains further east with a more continental climate, permafrost features such as ice wedge pseudomorphs prevail (Jary, 2009).

In the lowlands of the LRE, between the Rur and Rhine rivers, there are large loess plateaus (flat to undulating interfluve areas). The loess often covers Pleistocene river terraces, as in the case of the Rheindahlen (Bosinski, 1966) or parts of the Garzweiler LPS (Kels, 2007). Slope processes such as solifluction are subordinate in plateau environments (Table 1). However, LPSs in such settings can be affected by other processes triggered or enhanced by periglacial conditions. Frost crack formation or cryoturbation are important post-depositional alteration processes in plateau environments, influencing pedofeatures formed in situ such as clay cutanes (Martin Kehl, personal communication, December 2022).

Solifluction was one of the dominant processes in slope positions (Table 1). This is evident in parts of the long section of the Garzweiler LPS or the Elsbach Valley with a gradient of more than 2°. In addition, the location at the Sandgewand fault exposure near Eschweiler provides evidence for strong downslope movements of thin layers of loess derivates and debris of periglacial cover beds, indicating wet and cold conditions (Figs. 3, 4). At the slope position the sedimentary sequences were reworked twice by solifluction, probably during the Pleniglacial and, again, during the Younger Dryas.

Depressions and (dry) valleys are specific settings which act as sediment sinks for aeolian dust and reworked sediments. This is indicated in the Siersdorf LPS. In this LPS the Middle to Upper Pleniglacial sequence developed in an incised channel of a Middle Pleistocene river terrace (Pötter et al., 2023). Depressions and paleochannels influence not only sedimentary processes, but also (micro-)hydroclimatic conditions. In Siersdorf, the channel setting favored the development of wet, swampy conditions, with periodic semi-terrestrial conditions during the late Middle Pleniglacial. After this episode, however, the channel acted as a sink for relocated soil sediments, which were deposited in the early Upper Pleniglacial. Subsequently, aeolian accumulation resumed producing a typical Upper Pleniglacial succession, including the Eben Zone and unaltered, high-glacial loess (Pötter et al., 2023).

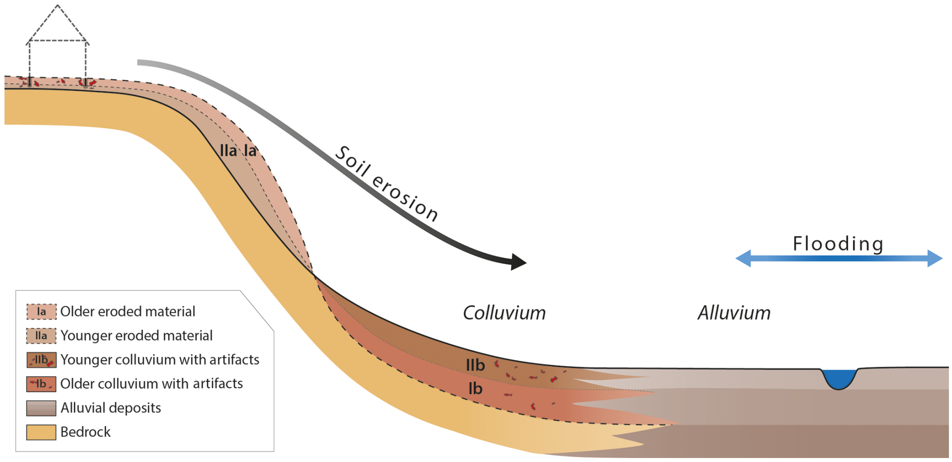

Figure 6. Simplified sketch of the acceleration of soil erosion and the development of colluvium due to the onset of agriculture since the Neolithic Revolution and Metal Ages. This soil erosion also enhanced floodplain sediments (alluvium). Archeological finds are relocated and buried under colluvial sediments. Redrawn and modified according to Gerlach (2006).

4.2 Holocene morphodynamics and human interferences

Since the Late Pleistocene (Bolling–Allerød oscillation), rapid warming has resulted in a denser vegetation cover and in soil development. This warm period was interrupted by the cooling event of the Younger Dryas. Due to the dense vegetation cover since the beginning of the Holocene, the rates of geomorphologic processes on the land surface in Central Europe were reduced and the morphodynamic activity was weaker as compared to the Pleistocene. Natural Holocene processes are characterized by soil development and in generally moderate fluvial erosion and accumulation, especially in the floodplains.

Human societies have interfered with the landscapes and soils by different agricultural practices and land use changes, especially since the onset of agriculture in the Neolithic period. The effects of land use on highly erodible loess were often associated with severe soil erosion including the development of gullies and colluvial accumulations. At the same time soil erosion resulted in an increased sediment supply to the rivers, thereby enhancing the accumulation of floodplain and alluvial deposits (Fig. 6). These deposits often serve as indications for climate or land use change. As a consequence of the increasing agricultural land use since the Neolithic Revolution, soil erosion was associated with the development of colluvial deposits at foot slopes. In particular colluviation was enhanced during the Metal Ages and the Middle Ages. An additional consequence was that archeological remains and finds were destroyed, relocated and buried under colluvial sediments.

In the Lower Rhine Embayment, as in other parts of Central Europe, there are several main periods of colluvial deposition or colluviation. Increased colluviation occurred during the Metal Ages, Roman times, medieval times and modern times (see Table 2). Four main periods associated with alluvial and floodplain deposition can be distinguished (see Table 2). The depositional periods of colluvial sedimentation can be distinguished using an interdisciplinary approach including granulometric, geochemical and archeological methods (Protze, 2014).

Especially during the Metal Ages and High Middle Ages erosion is clearly detectable. In the woodlands the production of charcoal and firewood, as well as grazing activities, led to a strong deforestation. In addition, the development of mining and related industries in the 15th to 16th centuries, as well as the increase in these activities in the 19th century, resulted in a high contamination of floodplain deposits. Different periods of minor soil erosion can be distinguished since medieval times. Socioeconomic effects and the increase in grassland resulted in a reduction in soil erosion (Nilson, 2006; Schmidt-Wygasch, 2011).

The floodplain or overbank sediments, consisting mainly of silty material, were deposited on the valley floors near rivers and alluvial systems. Below these silty deposits, coarser Pleistocene deposits are composed mainly of gravels interspersed with sandy layers and sandy lenses. As silty accumulations are less resistant to erosion they are often removed during floods. Deposits in abandoned channels, gullies or depressions are usually better preserved than plain accumulations. Particularly overbank deposits are often associated with human activity and can preserve important paleogeographical information (Kalicki, 2000).

Schmidt-Wygasch (2011) demonstrated for the lower reaches of the Inde River in the LRE that the first overbank deposits above the Pleistocene gravel layer of the lower terrace were accumulated in the Late Glacial and the Preboreal periods (A and B in Table 2). These loamy deposits resulted from land cover change at the transition from the Pleistocene to Holocene, which was associated with a change from braided river systems to meandering rivers incising into more cohesive material. There apparent lack of floodplain sedimentation in the early Holocene and Neolithic Age (Atlantic period) was associated with widespread soil development. The lack of floodplain sedimentation and soil formation is an indication of low soil erosion and therefore low sedimentation.

The first period characterized by enhanced soil erosion started in the Bronze Age (Subboreal) with the onset of more intensive land use. The clearance and agriculture supported the sediment transport to the rivers and floodplains and the accumulation of overbank deposits. Beginning with this time Schmidt-Wygasch (2011) distinguished four periods of widespread accumulations of overbank or floodplain deposits (I–IV in Table 1): (I) the beginning of agriculture since Neolithic times and enhanced land use during the Metal Ages, (II) the enhanced impact of agriculture and soil erosion in Bronze Age times, (III) the period of maximum soil erosion in the medieval times including the first acceleration in the beginning of the 19th century, and (IV) modern times since the middle of the 19th century including the Great Acceleration after World War II with modern agriculture and channelized rivers and creeks. All periods of enhanced soil erosion are human induced and resulted from land cover change by agriculture (anthropogenic origin). The maximum accumulation of floodplain deposits occurred in periods II and III. Figure 7 shows the accumulation of floodplain sediments in the lower reaches of the Inde River above a layer with Roman roof tiles (tegula) above abandoned river channels. This indicates more than 2 m of floodplain aggradation during the last 2000 years of such a small river in loess landscapes. Since the end of the 19th century the rivers were straightened and river banks were increasingly protected by embankments (Wolf et al., 2021). These changes were associated with a more concentrated and enhanced discharge, which in turn, resulted in reduced accumulation rates on the floodplains. Concerning the human interferences in river systems since the end of the 19th century, Wolf et al. (2021) were able to distinguish several periods of land use change and river (water) management.

5 Implications for archeological research in loess landscapes

Loess is one of the main terrestrial archives of Pleistocene landscapes and environments and therefore has an important connection to the preservation and interpretation of Paleolithic sites (Chu and Nett, 2021). These authors summarized the current trends and future directions in Pleistocene geoarcheology of European loess. They stated that loess records are unique insofar as they can address broad-scale spatiotemporal changes, but they can also provide windows into brief moments in time.

Figure 7. Exposure in the fore field of the lignite mining in the floodplain deposits of the (old) Inde River. Roman archeological layer with roof tiles (tegula) was buried by more than 2 m of overbank deposits. Beyond the people two small river channels are visible. Within the first small step wooden posts as fortification against lateral erosion were found. In the background the loess-covered middle terrace with a Roman villa rustica on top is situated. Photo: Frank Lehmkuhl (2008).

The low-energy deposition of Late Pleistocene loess-forming dust is known to finely preserve archeological sites with minimal spatial redistribution that can often be refitted to an impressive degree (Roebroeks et al., 1997; Vallin et al., 2001) and are even occasionally suitable for use-wear and residue analyses (Pawlik and Thissen, 2017; Sano, 2012; Wilczyński et al., 2020). Loess records are also excellent repositories of faunal prey, fire features, pits, habitation structures and early hominid burials that provide singular insights into local hominid behavioral patterns (see Chu and Nett, 2021, and references therein). The thickness and temporal resolution of the loess cover vary depending on the relief position. In the LRE this is related to the distribution of different tectonic blocks, the Pleistocene terraces and the distribution of bedrock. The sequences are often incomplete in their temporal resolution due to erosional discordances.

Fault scarps and terrace edges have been smoothed by geomorphic processes, such as solifluction and slope wash. As shown by Lehmkuhl et al. (2015) the depth of the Eemian Rocourt soil complex varies between 1 and 5 m below the surface.

Toward the north and west the aeolian deposits coarsen to sandy loess and sand. The coarsening is a function of the northern loess margin and the distribution of Neogene and Paleogene sands and the proximity of the formerly braided Meuse River system in the west which acted as additional local sand sources. During the maximum extent of the ice sheets in the penultimate glacial cycle (see the extent of the Saalian ice in Fig. 1), the ice margin extended much further south and consequently the loess facies is much coarser. All

Table 2. Time of accumulation of the overbank deposits. Adapted and modified from Schmidt-Wygasch (2011).

Period	Time of accumulation	
Period A	Late Glacial, Preboreal (till 7000 BCE)	Natural alluvial deposits in former braided rivers (mainly in channels)
Period B	Mesolithic Age (7000 till 6000 BCE)	
Period I	Bronze Age (1500/1600 till 800 BCE): *oldest* overbank deposits	Alluvial deposits resulting from soil erosion due to agricultural periods
Period II	Late Bronze Age and Iron Age till medieval times (750 BCE till 1200/1300 CE): *old* overbank deposits	
Period III	High Middle Ages till modern times (1300/1400 CE till the 19th century): *young* overbank deposits	
Period IV	Modern times (since mid of the 19th century): *youngest* overbank deposits, industrialization straightened the rivers	

of the older deposits may have been subjected to reworking and repositioning during later periods. Middle Pleistocene loess can be found in the LRE just in a few places, especially in depressions and on higher terraces.

The complex response of the geomorphic process system continued through the Holocene and was amplified by human interferences, resulting in soil erosion and in the deposition of colluvial and alluvial sequences. These processes destroyed upslope archeological remains but preserved several sequences with valuable information on human occupation and land use change at the slope toe and in depressions.

The study of the Pleistocene and Holocene geomorphologic dynamics in the different relief settings provides for geoscientists and archeologists an analytical tool for reconstructing the settlement, the environment and the landscape evolution. The analysis of the different intensities of erosion, relocation, redeposition and transformation processes with respect to the different temporal and spatial scales remains a challenging task in loess research. In addition, loess deposits have undergone post-depositional alterations such as weathering, bioturbation and pedogenesis that obscure anthropogenic evidence. Understanding the relationship between relief position and geomorphic processes enables a more comprehensive analysis of the complex stratigraphy of the LPSs and of sedimentary environments which are related to the (paleo-)relief. Understanding these relationships will allow the consideration of environmental differences in relation to relief position in archeological studies. Therefore, loess research requires interdisciplinary research, especially between archeologists and geomorphologists.

6 Conclusions

Loess is a valuable archive for archeological findings and provides evidence of the paleoenvironmental setting of human settlements. In addition, the timing of human occupation and the paleoclimate evolution can be disentangled through the analysis of LPSs. Marker layers and different dating techniques help to constrain the timing. Landscapes in the northern European loess belt and especially in humid periglacial environments not only have been shaped by the formation of widespread loess deposits during the Middle and Late Pleistocene but have also been subjected to reworking processes by periglacial and fluvial processes. In addition, active tectonics since the Pleistocene have influenced the thickness and preservation of loess in the LRE. During periods of less intensive land use in the early Holocene, soils developed on more or less stable land surfaces. As loess landscapes provide very fertile soils, they are among the first regions to undergo Neolithic agriculture. However, with the onset of agriculture and changes in land use, soil erosion caused enormous sediment relocations and relief changes. Colluvial and alluvial sediments resulting from soil erosion provide an additional archive of landscape evolution. They contain archeological findings from the Neolithic period onwards. All these different geomorphological processes have contributed to smoothing of the more pronounced paleo-relief of the LRE. The flat landscape we find today is the result of the natural and human-enhanced geomorphic processes that must be considered in loess and archeological research.

Data availability. All data are provided in the tables and figures of this paper and are available upon request to the corresponding author.

Author contributions. FL: conceptualization, supervision, writing and design of the original draft, funding acquisition. PS: validation, writing original draft, visualization. WR: validation, writing original draft, data curation. SP: validation, writing original draft, data curation.

All authors contributed to the discussion and interpretation of the results and reviewed and edited the manuscript.

Competing interests. The contact author has declared that none of the authors has any competing interests.

Disclaimer. Publisher's note: Copernicus Publications remains neutral with regard to jurisdictional claims in published maps and institutional affiliations.

Acknowledgements. We would like to thank Max Formen and Viktor Schaubert for their help with the figures. Discussions with numerous colleagues from loess research, geology and archeology, especially during the joint research in the frame of the CRC 806 "Our Way to Europe" and with Renate Gerlach and Jürgen Richter, are acknowledged.

Financial support. This open-access publication was funded by the RWTH Aachen University.

Review statement. This paper was edited by Christopher Lüthgens and reviewed by Ludwig Zoeller and one anonymous referee.

References

Ahorner, L.: Untersuchungen zur quartären Bruchtektonik der Niederrheinischen Bucht, E&G Quaternary Sci. J., 13, 24–105, https://doi.org/10.3285/eg.13.1.04, 1962.

Andrieux, E., Bertran, P., and Saito, K.: Spatial analysis of the French Pleistocene permafrost by a GIS database: French Pleistocene permafrost database, Permafrost Periglac., 27, 17–30, https://doi.org/10.1002/ppp.1856, 2016.

Antoine, P., Rousseau, D.-D., Moine, O., Kunesch, S., Hatté, C., Lang, A., Tissoux, H., and Zöller, L.: Rapid and cyclic aeolian deposition during the Last Glacial in European loess: a high-resolution record from Nussloch, Germany, Quaternary Sci. Rev., 28, 2955–2973, https://doi.org/10.1016/j.quascirev.2009.08.001, 2009.

Antoine, P., Rousseau, D.-D., Degeai, J.-P., Moine, O., Lagroix, F., Kreutzer, S., Fuchs, M., Hatté, C., Gauthier, C., Svoboda, J., and Lisá, L.: High-resolution record of the environmental response to climatic variations during the Last Interglacial–Glacial cycle in Central Europe: the loess-palaeosol sequence of Dolní Věstonice (Czech Republic), Quaternary Sci. Rev., 67, 17–38, https://doi.org/10.1016/j.quascirev.2013.01.014, 2013.

Antoine, P., Coutard, S., Guerin, G., Deschodt, L., Goval, E., Locht, J.-L., and Paris, C.: Upper Pleistocene loess-palaeosol records from Northern France in the European context: Environmental background and dating of the Middle Palaeolithic, Quaternary Int., 411, 4–24, https://doi.org/10.1016/j.quaint.2015.11.036, 2016.

Boemke, B., Einwögerer, T., Händel, M., and Lehmkuhl, F.: Upper Palaeolithic site probability in Lower Austria – a geoarchaeological multi-factor approach, J. Maps, 1–9, https://doi.org/10.1080/17445647.2021.2009926, 2022.

Boenigk, W. and Frechen, M.: The Pliocene and Quaternary fluvial archives of the Rhine system, Quaternary Sci. Rev., 25, 550–574, https://doi.org/10.1016/j.quascirev.2005.01.018, 2006.

Bosinski, G.: Der paläolithische Fundplatz Rheindahlen, Ziegelei Dreesen-Westwand, Bonner Jahrbücher, 318–343 Seiten, https://doi.org/10.11588/BJB.1965.0.73843, 1966.

Chu, W. and Nett, J. J.: The past in dust: current trends and future directions in Pleistocene geoarcheology of European loess, J. Quaternary Sci., 36, 1279–1292, https://doi.org/10.1002/jqs.3388, 2021.

Chu, W., Pötter, S., Doboş, A., Albert, T., Klasen, N., Ciornei, A., Bösken, J. J., and Schulte, P.: Geoarchaeology and geochronology of the Upper Palaeolithic site of Temere?ti Dealu Vinii, Banat, Romania: Site formation processes and human activity of an open-air locality, Quartär, 66, 111–134, https://doi.org/10.7485/QU66_5, 2019.

Ehlers, J., Gibbard, P. L., and Hughes, P. D.: Quaternary Glaciations – Extent and Chronology, Elsevier, Amsterdam, 1126 pp., 77–101, 2011.

Einwögerer, T., Friesinger, H., Händel, M., Neugebauer-Maresch, C., Simon, U., and Teschler-Nicola, M.: Upper Palaeolithic infant burials, Nature, 444, 285–285, https://doi.org/10.1038/444285a, 2006.

Federal Institute for Geosciences and Natural Resources © 2002. General Geological Map of Germany 1 : 200,000 (GUEK200) – CC 5502 Cologne. Hannover.

Fenn, K., Durcan, J. A., Thomas, D. S. G., Millar, I. L., and Marković, S. B.: Re-analysis of late Quaternary dust mass accumulation rates in Serbia using new luminescence chronology for loess–palaeosol sequence at Surduk, Borea, 49, 634–652, https://doi.org/10.1111/bor.12445, 2020.

Fischer, P., Hambach, U., Klasen, N., Schulte, P., Zeeden, C., Steininger, F., Lehmkuhl, F., Gerlach, R., and Radtke, U.: Landscape instability at the end of MIS 3 in western Central Europe: evidence from a multi proxy study on a Loess-Palaeosol-Sequence from the eastern Lower Rhine Embayment, Germany, Quaternary Int., 502, Part A, 119–136, https://doi.org/10.1016/j.quaint.2017.09.008, 2017.

Fischer, P., Hambach, U., Klasen, N., Schulte, P., Zeeden, C., Steininger, F., Lehmkuhl, F., Gerlach, R., and Radtke, U.: Landscape instability at the end of MIS 3 in western Central Europe: evidence from a multi proxy study on a Loess-Palaeosol-Sequence from the eastern Lower Rhine Embayment, Germany, Quaternary Int., 502, 119–136, https://doi.org/10.1016/j.quaint.2017.09.008, 2019.

Fischer, P., Jöris, O., Fitzsimmons, K. E., Vinnepand, M., Prud'homme, C., Schulte, P., Hatté, C., Hambach, U., Lindauer, S., Zeeden, C., Peric, Z., Lehmkuhl, F., Wunderlich, T., Wilken, D., Schirmer, W., and Vött, A.: Millennial-scale terrestrial ecosystem responses to Upper Pleistocene climatic changes: 4D-reconstruction of the Schwalbenberg Loess-Palaeosol-Sequence (Middle Rhine Valley, Germany), CATENA, 196, 104913, https://doi.org/10.1016/j.catena.2020.104913, 2021.

Fitzsimmons, K. E., Doboş, A., Probst, M., and Iovita, R.: Thinking Outside the Box at Open-Air Archeological Contexts: Examples From Loess Landscapes in Southeast Romania, Front. Earth Sci., 8, 561207, https://doi.org/10.3389/feart.2020.561207, 2020.

Formicola, V., Pontrandolfi, A., and Svoboda, J.: The Upper Paleolithic triple burial of Dolni Vestonice: Pathology and funerary behavior, Am. J. Phys. Anthropol., 115, 372–379, https://doi.org/10.1002/ajpa.1093, 2001.

French, H. M.: The periglacial environment, Fourth Edn., Wiley, Blackwell, Hoboken, NJ, 1 pp., https://doi.org/10.1002/9781118684931, 2017.

Geilenbrügge, U.: Ausgrabungen und Forschungen zu den Metallzeiten im rheinischen Braunkohlenrevier, in: Materialien zur Bodendenkmalpflege, Braunkohlenarchäologie im Rheinland, vol. 21, edited by: Kunow, J., 53–58, 2010.

Gerlach, R.: Holozän: Die Umgestaltung der Landschaft durch den Menschen seit dem Neolithikum, in: Urgeschichte im Rheinland, edited by: Kunow, J. and Wegner, H., Köln, 87–98, 190 pp. 2006.

Gerz, J.: Prähistorische Mensch-Umwelt-Interaktionen im Spiegel von Kolluvien und Befundböden in zwei Löss-Altsiedellandschaften mit unterschiedlicher Boden- und Kulturgeschichte (Schwarzerderegion bei Halle/Saale und Parabraunerderegion Niederrheinische Bucht), Köln, https://kups.ub.uni-koeln.de/7529/ (last access: August 2023), 2017.

Haesaerts, P., Damblon, F., Gerasimenko, N., Spagna, P., and Pirson, S.: The Late Pleistocene loess-palaeosol sequence of Middle Belgium, Quaternary Int., 411, 25–43, https://doi.org/10.1016/j.quaint.2016.02.012, 2016.

Jary, Z.: Periglacial markers within the Late Pleistocene loess–palaeosol sequences in Poland and Western Ukraine, Quaternary Int., 198, 124–135, https://doi.org/10.1016/j.quaint.2008.01.008, 2009.

Kalicki, T.: Grain size of the overbank deposits as carriers of paleogeographical information, Quaternary Int., 72, 107–114, https://doi.org/10.1016/S1040-6182(00)00026-4, 2000.

Kalińska-Nartiša, E., Thiel, C., Nartišs, M., Buylaert, J.-P., and Murray, A. S.: Age and sedimentary record of inland eolian sediments in Lithuania, NE European Sand Belt, Quaternary Res., 84, 82–95, https://doi.org/10.1016/j.yqres.2015.04.001, 2015.

Kels, H.: Bau und Bilanzierung der Lössdecke am westlichen Niederrhein, https://docserv.uni-duesseldorf.de/servlets/DocumentServlet?id=3628 (last access: August 2023), 2007.

Kels, H. and Schirmer, W.: Relation of loess units and prehistoric ind density in the Garzweiler open-cast mine, Lower Rhine, E&G Quaternary Sci. J., 59, 59–65, https://doi.org/10.3285/eg.59.1-2.05, 2011.

Klostermann, J.: Das Quartär der Niederrheinischen Bucht, Geologisches Landesamt Nordrhein-Westfalen, Krefeld, 1–200, 1992.

Klostermann, J. and Thissen, J.: Die stratigraphische Stellung des Lößprofils von Mönchengladbach-Rheindahlen (Niederrhein), E&G Quaternary Sci. J., 45, 42–58, https://doi.org/10.3285/eg.45.1.05, 1995.

Knaak, M., Becker, S., Steffens, W., Mustereit, B., Hartkopf-Fröder, C., Prinz, L., Stichling, S., Schulte, P., and Lehmkuhl, F.: Boden des Jahres 2021 – ein Lössprofil auf der Aldenhovener Lössplatte, in: Archäologie im Rheinland 2020, Nünnerich-Asmus, Oppenheim, ISBN 978-3-96176-162-3, 2021.

Leger, M.: Loess landforms, Quaternary Int., 7–8, 53–61, https://doi.org/10.1016/1040-6182(90)90038-6, 1990.

Lehmkuhl, F.: Modern and past periglacial features in Central Asia and their implication for paleoclimate reconstructions, Prog. Phys. Geog.: Earth and Environment, 40, 369–391, https://doi.org/10.1177/0309133315615778, 2016.

Lehmkuhl, F., Wirtz, S., Falk, D., and Kels, H.: Geowissenschaftliche Untersuchungen zur Landschaftsentwicklung im Tagebau Garzweiler – LANU-Projekt 2012–2014, in: Archäologie im Rheinland 2014, edited by: Kunow, J. and Trier, M., Theiss Verlag, Stuttgart, 64–66, ISBN 978-3-8062-3214-1, 2015.

Lehmkuhl, F., Zens, J., Krauß, L., Schulte, P., and Kels, H.: Loess-paleosol sequences at the northern European loess belt in Germany: Distribution, geomorphology and stratigraphy, Quaternary Sci. Rev., 153, 11–30, https://doi.org/10.1016/j.quascirev.2016.10.008, 2016.

Lehmkuhl, F., Schulte, P., and Zens, J.: Sedimentological investigation of the stratigraphic sequence., in: The Lower to Middle Palaeolithic Transition in Northwestern Europe: Evidence from Kesselt-Op de Schans, Leuven University Press, 70–76, ISBN 9789462700987, 2017.

Lehmkuhl, F., Pötter, S., Pauligk, A., and Bösken, J.: Loess and other Quaternary sediments in Germany, J. Maps, 14, 330–340, https://doi.org/10.1080/17445647.2018.1473817, 2018.

Lehmkuhl, F., Nett, J. J., Pötter, S., Schulte, P., Sprafke, T., Jary, Z., Antoine, P., Wacha, L., Wolf, D., Zerboni, A., Hošek, J., Marković, S. B., Obreht, I., Sümegi, P., Veres, D., Zeeden, C., Boemke, B., Schaubert, V., Viehweger, J., and Hambach, U.: Loess landscapes of Europe – Mapping, geomorphology, and zonal differentiation, Earth-Sci. Rev., 215, 103496, https://doi.org/10.1016/j.earscirev.2020.103496, 2021.

Mason, J. A., Nater, E. A., Zanner, C. W., and Bell, J. C.: A new model of topographic effects on the distribution of loess, Geomorphology, 28, 223–236, https://doi.org/10.1016/S0169-555X(98)00112-3, 1999.

Meijs, E. P. M.: Loess stratigraphy in Dutch and Belgian Limburg, E&G Quaternary Sci. J., 51, 115–131, https://doi.org/10.3285/eg.51.1.08, 2002.

Meijs, E. P. M., van Peer, P., and de Warrimont, J. P. L. M. N.: Geomorphologic context and proposed chronostratigraphic position of Lower Palaeolithic artefacts from the Op de Schans pit near Kesselt (Belgium) to the west of Maastricht, Neth. J. Geosci., 91, 137–157, https://doi.org/10.1017/S0016774600001554, 2013.

Meurers-Balke, J., Kalis, A. J., Gerlach, R., and Jürgens, A.: Landschafts-und Siedlungsgeschichte des Rheinlandes, in: Knörzer K, editor. PflanzenSpuren. Archäobotanik im Rheinland: Agrarlandschaft und Nutzpflanzen im Wandel der Zeiten. Köln, Bonn: Rheinland-Verlag, Kommission bei R. Habelt, 11–66, 1999.

Muhs, D. R.: 11.9 Loess and its Geomorphic, Stratigraphic, and Paleoclimatic Significance in the Quaternary, in: Treatise on Geomorphology, Elsevier, 149–183, https://doi.org/10.1016/B978-0-12-374739-6.00302-X, 2013.

Nigst, P. R., Haesaerts, P., Damblon, F., Frank-Fellner, C., Mallol, C., Viola, B., Götzinger, M., Niven, L., Trnka, G., and Hublin, J.-J.: Early modern human settlement of Europe north of the Alps occurred 43,500 years ago in a cold steppe-type environment, P. Natl. Acad. Sci. USA, 111, 14394–14399, https://doi.org/10.1073/pnas.1412201111, 2014.

Nilson, E.: Räumlich-strukturelle und zeitlich-dynamische Aspekte des Landnutzungswandels im Dreiländereck Belgien-Niederlande-Deutschland: eine Analyse mittels eines multitemporalen, multifaktoriellen und grenzübergreifenden Geographischen Informationssystems, Publikationsserver der RWTH Aachen University, http://darwin.bth.rwth-aachen.de/opus3/volltexte/2006/1612/ (last access: August 2023), 2006.

Obreht, I., Zeeden, C., Schulte, P., Hambach, U., Eckmeier, E., Timar-Gabor, A., and Lehmkuhl, F.: Aeolian dynamics at the Orlovat loess–paleosol sequence, northern Serbia, based on detailed textural and geochemical evidence, Aeolian Res., 18, 69–81, https://doi.org/10.1016/j.aeolia.2015.06.004, 2015.

Obreht, I., Hambach, U., Veres, D., Zeeden, C., Bösken, J., Stevens, T., Marković, S. B., Klasen, N., Brill, D., Burow, C., and Lehmkuhl, F.: Shift of large-scale atmospheric systems over Europe during late MIS 3 and implications for Modern Human dispersal, Sci. Rep., 7, 5848, https://doi.org/10.1038/s41598-017-06285-x, 2017.

Pawlik, A. and Thissen, J.: Traceological analysis of “unusual” wear traces on lithic artefacts from the Middle Palaeolithic site Inden-Altdorf and the functional context of the site, Quaternary Int., 427, 104–127, https://doi.org/10.1016/j.quaint.2015.11.125, 2017.

Pécsi, M.: Loess is not just the accumulation of dust, Quaternary Int., 7, 1–21, 1990.

Pötter, S.: The sedimentary history of loess: sources, deposition, and reworking of aeolian sediments as indicators for palaeoenvironmental changes in the Danube Basin, PhD Thesis, RWTH Aachen University, Aachen, 231 pp., https://doi.org/10.18154/RWTH-2021-05739, 2021.

Pötter, S., Seeger, K., Richter, C., Brill, D., Knaak, M., Lehmkuhl, F., and Schulte, P.: Pleniglacial dynamics in an oceanic central European loess landscape, E&G Quaternary Sci. J., 72, 77–94, https://doi.org/10.5194/egqsj-72-77-2023, 2023.

Protze, J.: Eine Mensch gemachte Landschaft“ – Diachrone, geochemische und sedimentologische Untersuchungen an anthropogen beeinflussten Sedimenten und Böden der Niederrheinischen Lössbörde, Aachen, 2014.

Pye, K.: Loess, Prog. Phys. Geog.: Earth and Environment, 8, 176–217, https://doi.org/10.1177/030913338400800202, 1984.

Pye, K.: The nature, origin and accumulation of loess, Quaternary Sci. Rev., 14, 653–667, https://doi.org/10.1016/0277-3791(95)00047-X, 1995.

Roebroeks, W., Kolen, J., Van Poecke, M., and Van gijn, A.: “Site J”: an early Weichselian (Middle Palaeolithic) flint scatter at Maastricht-Belvedere, The Netherlands, pal, 9, 143–172, https://doi.org/10.3406/pal.1997.1231, 1997.

Sano, K.: Functional variability in the Magdalenian of northwestern Europe: A lithic microwear analysis of the Gönnersdorf K-II assemblage, Quaternary Int., 272–273, 264–274, https://doi.org/10.1016/j.quaint.2012.02.057, 2012.

Scharl, S., Amelung, W., Bömke, B., Gerlach, R., Lauer, F., Lehmkuhl, F., Lehndorf, E., Maier, M., Schmidt, I., Szya, S., and Zimmermann, A.: Human-environment interaction, in: The Journey of Modern Humans from Africa to Europe, edited by: Litt, T., Richter, J., and Schäbitz, F., Culture-Environmental Interaction and Mobility, 175–203, 2021.

Schirmer, W.: Schwalbenberg südlich Remagen, Rheingeschichte zwischen Mosel und Maas.–deuqua-Führer, 1, 105–108, ISBN 3926963042, 1990.

Schirmer, W.: Compendium of the Rhein loess sequence, Terra Nostra, 10, 8–23, 2002.

Schirmer, W.: Die Eben-Zone im Oberwürmlöss zwischen Maas und Rhein, in: Landschaftsgeschichte im Europäischen Rheinland, Vol. 4, edited by: Schirmer, W., LIT Verlag, Münster, 351–416, 2003.

Schirmer, W.: Late Pleistocene loess of the Lower Rhine, Quaternary Int., 411, 44–61, https://doi.org/10.1016/j.quaint.2016.01.034, 2016.

Schmidt-Wygasch, C.: Neue Untersuchungen zur holozänen Genese des Unterlaufs der Inde - Chronostratigraphische Differenzierung der Auelehme unter besonderer Berücksichtigung der Montangeschichte der Voreifel, Aachen, PhD thesis, https://publications.rwth-aachen.de/record/459435/files/3842.pdf (last access: August 2023), 2011.

Schulz, W.: Die Kolluvien der westlichen Kölner Bucht – Gliederung, Entstehungszeit und geomorphologische Bedeutung, PhD thesis http://nbn-resolving.de/urn:nbn:de:hbz:38-19656 (last access: August 2023), 2007.

Semmel, A.: Zur paläopedologischen Grundgliederung des älteren Würmlösses in Mitteleuropa, Mitteilungen deutscher bodenkundlichen Gesellschaft, 88, 449–452, 1998.

Sirocko, F., Knapp, H., Dreher, F., Förster, M. W., Albert, J., Brunck, H., Veres, D., Dietrich, S., Zech, M., Hambach, U., Röhner, M., Rudert, S., Schwibus, K., Adams, C., and Sigl, P.: The ELSA-Vegetation-Stack: Reconstruction of Landscape Evolution Zones (LEZ) from laminated Eifel maar sediments of the last 60,000years, Global Planet. Change, 142, 108–135, https://doi.org/10.1016/j.gloplacha.2016.03.005, 2016.

Sprafke, T. and Obreht, I.: Loess: Rock, sediment or soil – What is missing for its definition?, Quaternary Int., 399, 198–207, https://doi.org/10.1016/j.quaint.2015.03.033, 2016.

Steup, R. and Fuchs, M.: The loess sequence at Münzenberg (Wetterau/Germany): A reinterpretation based on new luminescence dating results, Zeitschrift für Geomorphologie, Supplementary Issues, 61, 101–120, https://doi.org/10.1127/zfg_suppl/2016/0408, 2017.

Vallin, L., Masson, B., and Caspar, J.-P.: Taphonomy at Hermies, France: A Mousterian Knapping Site in a Loessic Context, J. Field Archaeol., 28, 419–436, https://doi.org/10.1179/jfa.2001.28.3-4.419, 2001.

van Baelen, A.: The Lower to Middle Palaeolithic Transition in Northwestern Europe: Evidence from Kesselt-Op de Schans, 01 Edn., Leuven University Press, Leuven, Belgium, 242 pp., ISBN 9789462700987, 2017.

Vandenberghe, J., Roebroeks, W., and van Kolfschoten, T.: Maastricht-Belvédère: stratigraphy, palaeoenvironment and archaeology of the Middle and Late Pleistocene deposits. Part II, Mededelingen Rijks Geologische Dienst, 47, 1–91, 1993.

Vandenberghe, J., French, H. M., Gorbunov, A., Marchenko, S., Velichko, A. A., Jin, H., Cui, Z., Zhang, T., and Wan, X.: The Last Permafrost Maximum (LPM) map of the Northern Hemisphere: permafrost extent and mean annual air temperatures, 25-17 ka BP: The Last Permafrost Maximum (LPM) map of the Northern Hemisphere, Boreas, 43, 652–666, https://doi.org/10.1111/bor.12070, 2014.

van Kolfschoten, T. and Roebroeks, W.: Maastricht-Belvédère: stratigraphy, palaeoenvironment and archaeology of the Middle and Late Pleistocene deposits, Mededelingen Rijks Geologische Dienst, 39, 1–121, 1985.

Vanmonfort, B., Vermeersch, P. M., Groenendijk, A. J., Meijs, E., De Warrimont, J.-P., and Gullentops, F.: The middle palaeolithic site of Hezerwater at Veldwezelt, Belgian Limburg, Notae Praehistoricae, 18, 5–11, 1998.

Vinnepand, M., Fischer, P., Jöris, O., Hambach, U., Zeeden, C., Schulte, P., Fitzsimmons, K. E., Prud'homme, C., Perić, Z., Schirmer, W., Lehmkuhl, F., Fiedler, S., and Vött, A.: Decoding geochemical signals of the Schwalbenberg Loess-Palaeosol-Sequences — A key to Upper Pleistocene ecosystem responses to climate changes in western Central Europe, CATENA, 212, 106076, https://doi.org/10.1016/j.catena.2022.106076, 2022.

Waters, M. R. and Kuehn, D. D.: The geoarchaeology of place: The effect of geological processes on the preservation and interpretation of the archaeological record, Am. Antiquity, 61, 483–497, 1996.

Wilczyński, J., Žaár, O., Nemergut, A., Kufel-Diakowska, B., Hoyo, M. M., Mroczek, P., Páll-Gergely, B., Oberc, T., and Lengyel, G.: The Upper Palaeolithic at Trenčianske Bohuslavice, Western Carpathians, Slovakia, J. Field Archaeol., 45, 270–292, https://doi.org/10.1080/00934690.2020.1733334, 2020.

Wolf, S., Esser, V., Schüttrumpf, H., and Lehmkuhl, F.: Influence of 200 years of water resource management on a typical central European river. Does industrialization straighten a river?, Environ. Sci. Eur., 33, 15, https://doi.org/10.1186/s12302-021-00460-8, 2021.

Zech, M., Rass, S., Buggle, B., Löscher, M., and Zöller, L.: Reconstruction of the late Quaternary paleoenvironments of the Nussloch loess paleosol sequence, Germany, using n-alkane biomarkers, Quaternary Res., 78, 226–235, https://doi.org/10.1016/j.yqres.2012.05.006, 2012.

Zeeberg, J.: The European sand belt in eastern Europe – and comparison of Late Glacial dune orientation with GCM simulation results, Boreas, 27, 127–139, https://doi.org/10.1111/j.1502-3885.1998.tb00873.x, 1998.

Zens, J., Schulte, P., Klasen, N., Krauß, L., Pirson, S., Burow, C., Brill, D., Eckmeier, E., Kels, H., Zeeden, C., Spagna, P., and Lehmkuhl, F.: OSL chronologies of paleoenvironmental dynamics recorded by loess-paleosol sequences from Europe: Case studies from the Rhine-Meuse area and the Neckar Basin, Palaeogeogr. Palaeocl., 509, 105–125, https://doi.org/10.1016/j.palaeo.2017.07.019, 2018.

Zimmermann, A.: Cultural cycles in Central Europe during the Holocene, Quaternary Int., 274, 251–258, https://doi.org/10.1016/j.quaint.2012.05.014, 2012.

Zimmermann, A., Meurers-Balke, J., and Kalis, A. J.: Das Neolithikum im Rheinland: Die Ausbreitung des Neolithikums und das Verhältnis der frühen Bauern zu den spätmesolithischen Sammlerinnen und Jägern, Bonner Jahrbücher, 1–63, 2005.

E&G Quaternary Sci. J., 72, 219–234, 2023
https://doi.org/10.5194/egqsj-72-219-2023

Open Access E&G Quaternary Science Journal

Research article

A 1100-year multi-proxy palaeoenvironmental record from Lake Höglwörth, Bavaria, Germany

Sudip Acharya[1], Maximilian Prochnow[1], Thomas Kasper[2], Linda Langhans[1], Peter Frenzel[3], Paul Strobel[1], Marcel Bliedtner[1], Gerhard Daut[1], Christopher Berndt[2], Sönke Szidat[4,5], Gary Salazar[4,5], Antje Schwalb[6], and Roland Zech[1]

[1]Institute of Geography, Friedrich Schiller University Jena, 07743 Jena, Germany
[2]Institute for Geography and Geology, University of Greifswald, 17489 Greifswald, Germany
[3]Institute of Geosciences, Friedrich Schiller University Jena, 07743 Jena, Germany
[4]Department of Chemistry, Biochemistry and Pharmaceutical Sciences, University of Bern, Bern, Switzerland
[5]Oeschger Centre for Climate Change Research, University of Bern, Bern, Switzerland
[6]Institute of Geosystems and Bioindication, Technische Universität Braunschweig, 38106 Braunschweig, Germany

Correspondence: Sudip Acharya (sudip.acharya@uni-jena.de)

Relevant dates: Received: 21 March 2023 – Revised: 4 September 2023 – Accepted: 28 September 2023 – Published: 14 November 2023

How to cite: Acharya, S., Prochnow, M., Kasper, T., Langhans, L., Frenzel, P., Strobel, P., Bliedtner, M., Daut, G., Berndt, C., Szidat, S., Salazar, G., Schwalb, A., and Zech, R.: A 1100-year multi-proxy palaeoenvironmental record from Lake Höglwörth, Bavaria, Germany, E&G Quaternary Sci. J., 72, 219–234, https://doi.org/10.5194/egqsj-72-219-2023, 2023.

Abstract: Anthropogenic activities have exerted strong influence on ecosystems worldwide, particularly since 1950 CE. The local impact of past human activities often started much earlier and deserves detailed study. Here, we present an environmental record from a 278 cm long sedimentary core from Lake Höglwörth (Bavaria, Germany). Sedimentological and geochemical parameters indicate that the organic-rich bottom sediments of the record consist of peat that formed prior to 870^{+140}_{-160} CE, when lake sediments started to accumulate. After 870^{+140}_{-160} CE, distinct shifts in lithology, elemental composition, and the biological record are visible and are interpreted to result from the construction of a monastery on the lake peninsula in 1125 CE and/or the damming of the lake. From 1120 ± 120 to 1240^{+110}_{-120} CE, the lake environment was relatively stable. This period was followed by enhanced deforestation that led to a more open landscape and soil erosion, visible in increased allochthonous input from 1240^{+110}_{-120} to 1380^{+90}_{-110} CE. This was accompanied by high aquatic productivity and bottom or interstitial water anoxia from 1310^{+100}_{-120} to 1470^{+90}_{-100} CE, possibly triggered by increased nutrient availability. Enhanced allochthonous input and a substantial shift in the aquatic community can be assigned to the construction of a flour mill and related rerouting of a small creek in 1701 CE. High aquatic productivity and bottom or interstitial water anoxia after 1960 ± 10 CE correspond to recent eutrophication resulting from accelerated local anthropogenic activities. The sedimentary record from Lake Höglwörth exemplarily demonstrates that anthropogenic activities have had substantial environmental impacts on aquatic environments during the past millennium.

Kurzfassung: Anthropogene Aktivitäten haben insbesondere seit dem Jahr 1950 CE weltweit einen starken Einfluss auf Ökosysteme. Jedoch hatten menschliche Aktivitäten oft schon viel früher Auswirkungen auf Ökosysteme und verdienen eine detaillierte Untersuchung. Hier präsentieren wir sedimentologische, geochemische und paläontologische Ergebnisse eines 278 cm langen Sedimentbohrkerns aus dem Höglwörther See (Bayern, Deutschland), der die letzten 1100 Jahre abdeckt. Sedimentologische und geochemische Parameter deuten darauf hin, dass die unteren organikreichen Sedimente aus Torf bestehen, der sich vor etwa 870^{+140}_{-160} CE bildete, bevor sich die Seesedimente ablagerten. Nach 870^{+140}_{-160} CE sind deutliche Änderungen in der Lithologie, der Elementkomposition und der biologischen Zusammensetzung zu erkennen, die auf den Bau des Klosters Höglwörth auf der Halbinsel des Sees um 1125 CE und/oder eine Aufstauung des Sees zurückzuführen sind. Von 1120 ± 120 bis 1240^{+110}_{-120} CE war die Ökologie des Sees relativ stabil. Danach folgte eine verstärkte Entwaldung, die zu einer offeneren Landschaft und stärkerer Bodenerosion führte, was durch erhöhten allochthonen Eintrag von etwa 1240^{+110}_{-120} to 1380^{+90}_{-110} CE sichtbar ist. Dies führte zu einer hohen aquatischen Produktivität und Anoxie des Hypolimnions von etwa 1310^{+100}_{-120} to 1470^{+90}_{-100} CE – möglicherweise ausgelöst durch eine erhöhte Nährstoffverfügbarkeit. Der Bau einer Getreidemühle und die damit verbundene Umleitung eines kleinen Baches im Jahr 1701 CE führten zu einem verstärkten allochthonen Eintrag und einer erheblichen Veränderung der aquatischen Gesellschaft. Die hohe aquatische Produktivität und die Anoxie des Hypolimnions nach 1960 ± 10 CE zeigen die rezente Eutrophierung, die auf verstärkte lokale anthropogene Aktivitäten zurückzuführen ist. Die Sedimente des Höglwörther Sees zeigen somit beispielhaft, dass anthropogene Aktivitäten während des letzten Jahrtausends erhebliche Auswirkungen auf aquatische Ökosysteme gehabt haben.

1 Introduction

Abrupt shifts in ecosystems all over the globe during the past decades are related to human activities and are in stark contrast with ranges of the natural variability evident at least during the Holocene (Steffen et al., 2015). To define this marked shift in Earth's environment, the term "Anthropocene" has been suggested for a new geological era, which is proposed to have started around 1950 CE and has prompted intense scientific and societal debate (Waters and Turner, 2022; Crutzen and Stoermer, 2021; Lewis and Maslin, 2015). However, the onset of human impact often occurred much earlier, both locally and regionally (Ruddiman et al., 2020; Waters et al., 2016), and requires more detailed, local palaeoenvironmental studies.

Bavaria is a region significantly impacted by humans as far back as the early medieval period (∼ 1000 CE) (Bauer and Bauer, 1993) with increased settlements and agricultural activities (Gilck and Poschlod, 2020; Klein Goldewijk et al., 2011). The shift in land cultivation practices from subsistence agriculture with livestock and crop production to cattle grazing for meat and dairy production during the medieval period led to the establishment of pastureland (Enters et al., 2008, 2006). This is documented in lacustrine records as a decrease in tree pollen and an intensification of soil erosion due to the widespread land use (Dotterweich, 2003). A significant decrease in population during the late medieval period (from 1300 to 1450 CE) and beyond can be attributed to military conflicts, epidemic plagues, and cooler climate conditions associated with the Little Ice Age and led to the abandonment of numerous villages and settlements (Küster, 2020; Franz, 2019; Enters et al., 2006; Jäger, 1958). These results are supported by findings of archeological excavations and historical documents from the region (Blei, 2011; Waldner, 1983). An increase in human impacts such as nutrient loading, excessive use of fertilizers, and changes in land use/land cover has led to a substantial alteration in aquatic ecosystems, including the loss of biodiversity, eutrophication, and anoxia over the past few decades (Enters et al., 2006; Alefs and Müller, 1999). Although these significant human activities have been documented, it remains unclear if and how the human activities during the past millennium impacted the natural ecosystem in the region. Also, the available palaeoenvironmental records are mainly derived from large lakes (Rösch et al., 2021; Schubert et al., 2020; Lauterbach et al., 2011; Richard, 1996), which capture regional signals and exhibit different environmental responses compared to small lakes that record local signals (Adrian et al., 2009; Enters et al., 2006).

Here, we present a study from Lake Höglwörth, a small, eutrophic lake situated in south-eastern Bavaria, Germany (Wasserwirtschaftsamt Traunstein, 2018). The lake has undergone severe ecological alternation (algal production and anoxia) over the past decades (Fam and Kerstin, 2018; Wasserwirtschaftsamt Traunstein, 2018). A 278 cm long sediment record from Lake Höglwörth was analysed using sedimentological, geochemical, and biological methods. Specifically, our study aims to investigate (1) whether the recent algal production and anoxia in the lake did occur in the past and (2) whether and how past human activities affected the lithological, geochemical, and biological environment of Lake Höglwörth over the past millennium.

2 Methodology

2.1 Site description

Lake Höglwörth (47.81° N, 12.84° E; 531 m above sea level; Fig. 1) is a small (surface area 0.14 km^2), irregularly shaped, and eutrophic lake, located in a paraglacial meltwater channel that formed during the Last Glacial Maximum when the Salzach Glacier forced drainage along its ice margin in a north-western direction at the northern forelands of the European Alps in south-eastern Bavaria, Germany. Postglacial landslide and mudflow deposits of still unknown age (presumably during the Middle to Late Holocene) are present north-west of the lake and are thought to be responsible for blocking the valley and former damming of the lake as seen in lidar imagery (Landesamt für Digitalisierung, 2022). Today, the lake has a maximum water depth of 6 m; has an average depth of 3.1 m (for a description of bathymetry, please refer to the Supplement); and is fed by three small creeks, i.e. Höglwörther Schornbach, Höglwörther Seebach, and Moosgraben. Lake Höglwörth is drained by the Rauschbach. The lake has a catchment area of 2.3 km^2, and it is geologically characterized by deposits of the last glacial period and patches of Cretaceous to Eocene bedrock (Glückert, 1974). Cambisols and Luvisols are the most common catchment soil types, whereas Stagnosols and Gleysols have developed in the surrounding valleys (Landesamt für Digitalisierung, 2022).

On the peninsula of the lake, an Augustinian monastery is located, constructed in 1125 CE (Brugger et al., 2008). On the western side of the lake, a flour mill is situated, built in 1701 CE by diverting the Höglwörther Seebach into the lake (Brugger et al., 2008); consequently the catchment of the lake has enlarged since. The mill was torn down in 1922 CE.

At the meteorological station in Piding, ∼ 10 km southeast of Lake Höglwörth, mean annual precipitation (1991 to 2020) is 1340 mm. Mean annual temperature is 9.2 °C, with a temperature maximum during summer (June–July 18.5 °C) and a temperature minimum during winter (January–February −0.2 °C) (DWD Climate Data Center, 2020).

2.2 Sediment coring, core processing, and dating

Sediment cores were retrieved from Lake Höglwörth in 2019 from a water depth of 4.7 m (Figs. 1 and S2 in the Supplement). For the uppermost (∼ 1 m) sediment section, a UWITEC gravity corer with a diameter of 90 mm was used, while longer sediment cores with a diameter of 63 mm were retrieved in overlapping core sections (2 m each), using a platform-based UWITEC piston coring system. Cores were split, photographed, and lithologically described at the laboratory of the Physical Geography Department of the Friedrich Schiller University Jena. Lithological marker layers within the core sections were used to establish a continuous sediment sequence with a total length of 278 cm (Fig. S2).

In cooperation with the Laboratory for the Analysis of Radiocarbon (LARA), University of Bern, Switzerland, ^{14}C ages were obtained from eight macrofossil samples and one bulk organic matter sample (Table 1) (Salazar et al., 2015; Szidat et al., 2014), using a Mini Carbon Dating System (MICADAS) accelerator mass spectrometer (AMS) coupled online to an Elementar analyser (Ruff et al., 2010). Prior to radiocarbon analysis, samples were treated with ∼ 4 % HCl at 60 °C for 8 h to remove carbonates. Ages obtained from LARA were calibrated using the online version of the software Calib 8.2 (Stuiver and Reimer, 1993), combined with the IntCal20 calibration dataset (Reimer et al., 2020) and the bomb peak Northern Hemisphere 1 calibration dataset (Hua et al., 2013), particularly for the ^{14}C age at 8 cm depth. Additionally, the upper 40 cm sediment of core was analysed for ^{137}Cs activity at Technische Universität Dresden, Germany. Final age–depth modelling was carried out with the help of the software package rbacon 2.4.3 (Blaauw and Christen, 2011).

2.3 Lithology and geochemical analysis

Non-destructive X-ray fluorescence (XRF) scanning was carried out with an ITRAX XRF core scanner at the Geomorphology and Polar Research Group (GEOPOLAR), University of Bremen, Germany. Single halves of core segments were scanned at 5 mm intervals using a molybdenum tube (Mo) as the X-ray source operating at 30 kV voltage, 50 mA current, and an exposure time of 5 s. In order to eliminate sediment matrix effects (i.e. interferences with water content, surface roughness, and grain size variations), raw elemental counts were normalized by logarithmic transformation and are given as centred log ratios (Ramisch et al., 2018; Weltje et al., 2015). XRF scanning produced reliable counts (elements with counts $>$ 100 and mean square errors $<$ 2) for titanium (Ti), iron (Fe), manganese (Mn), strontium (Sr), calcium (Ca), and potassium (K). The degree of incoherent scattering (inc) and coherent scattering (coh) is used to calculate the inc / coh ratio, which is a proxy for organic matter content (Fortin et al., 2013; Guyard et al., 2007). Magnetic susceptibility was determined at 2 mm resolution, using a Bartington MS2E surface scanning sensor (Bartington Instruments Ltd., Witney, UK).

Grain size and elemental analyses were conducted on 1 cm sediment slices collected at an interval of 12 cm. For grain size analyses, ∼ 0.2 g of dry sediment was treated with H_2O_2 (∼ 10 % and ∼ 30 %) and ∼ 30 % HCl to remove organic matter and carbonates. Grain size measurements were performed using an LS 13 320 Laser Diffraction Particle Size

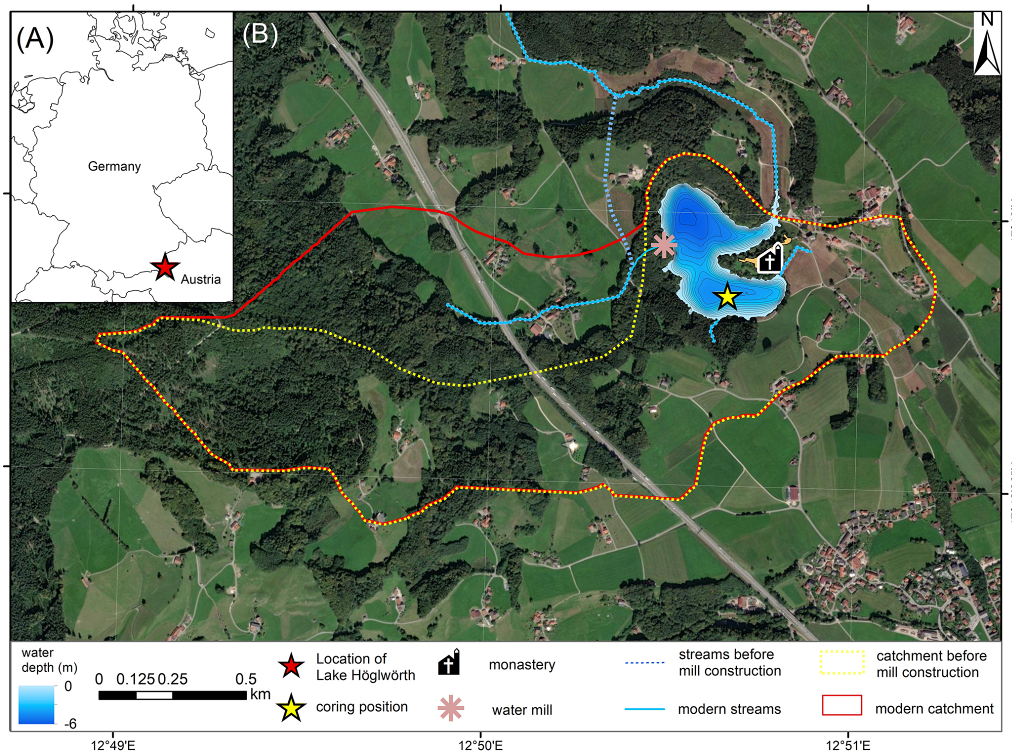

Figure 1. **(a)** Overview of the study area. Red star shows the location of Lake Höglwörth. **(b)** Image of Lake Höglwörth and its modern catchment indicated by red line (modified from © Google Earth, 2022). Blue line indicates the streams. Dashed yellow and blue lines indicate the catchment and streams, respectively, before mill construction. The coring position is indicated by a yellow star.

Analyzer (Beckman Coulter, Brea, CA, USA). Samples were measured with the aqueous liquid module in several 60 s cycles until a reproducible signal was obtained. The "Fraunhofer" optical model of light scattering was used for computing grain size distribution. Further statistical calculations were done with a modified version of the software GRADISTAT 4.2 (Blott and Pye, 2001).

Approximately 20 mg of the freeze-dried sediments ($-50\,°C$, >72 h) was packed into tin capsules for the measurement of total carbon (TC), total nitrogen (TN), and isotopic composition of bulk nitrogen ($\delta^{15}N$). The total organic carbon (TOC) and isotopic composition of bulk organic carbon ($\delta^{13}C$) were measured on decalcified sediment samples, treated with $\sim 4\,\%$ HCl at 60 °C for 8 h, and washed with deionized water until reaching pH neutrality. Carbonate content was calculated as $CaCO_3$ from the difference between TC and TOC, and the C/N ratio was calculated as the molar ratio. The measurements were carried out using an elemental analyser (vario EL cube) coupled to an isotope ratio mass spectrometer (IRMS, isoprime precisION; both devices from Elementar, Langenselbold, Germany). The precision was checked by co-analysing L-Prolin, EDTA, and USGS6 with known isotopic composition. The analytical uncertainty for these standards was $< 0.1\,‰$ for both $\delta^{15}N$ and $\delta^{13}C$. The isotopic values of ^{15}N and ^{13}C are expressed in delta notation ($\delta^{15}N$, $\delta^{13}C$) against air and Vienna Pee Dee Belemnite (V-PDB), respectively.

2.4 Biological analysis

Sediment samples of 2–3 cm thickness and a volume of 16 to 47 mL each were stirred with deionized water in an overhead-shaker for 1 to 5 h and sieved for organic and inorganic macrofossils over mesh sizes of 1 mm and 200 µm, respectively. Because samples below 238 cm depth could not be disintegrated, H_2O_2 (5 %) was added, but disintegration was insufficient, allowing a rough identification of the main sediment components only. After sieving, residues were washed with deionized water and dried at $\sim 50\,°C$. All macrofossils from the 1 mm sieve were identified to the lowest possible taxonomic level. Dried smaller sieve residues served for the picking of specific microfossils. Ostracods, testate amoebae and statoblasts of bryozoans were documented on the species level, while counting of the other remnants (ephippia of Cladocera, oospores of Charophyta, glochidia of Bivalvia, eggs of uncertain origin, remains of fishes such as vertebra and scales, oribatid mites, and charcoal) was on the group level only. Relative abundance data for Ostracoda, testate amoebae, and statoblasts rely on complete counts of all specimens, but usually only up to 300 per group within the samples were counted. All taxa were photographed with the help

Table 1. The ^{14}C calculation parameters, conventional radiocarbon ages, and 2σ calibrated ages for the sediment core from Lake Höglwörth. Calibrations were performed using IntCal20.

Lab code	Core ID	Core depth (cm)	Composite depth (cm)	Material	Carbon mass (µg)	$F^{14}C$	u	$\delta^{13}C$ (‰)	Conventional ^{14}C age (BP)	Median cal age and 2σ uncertainty (cal BP)	Median cal age and 2σ uncertainty (CE)
BE-16110.1.1	HGW19_5	8	8	macrofossil	253	1.0573	0.0108	−27.2	−448 ± 82	−57 ± 12	2007 ± 12
BE-16109.1.1	HGW19_6_1	51	67	macrofossil	75	0.9548	0.0084	−26.5	372 ± 71	411 ± 72	1539 ± 72
BE-16108.1.1	HGW19_7_1	28	92	macrofossil	181	0.9674	0.0097	−26.6	266 ± 81	308 ± 135	1642 ± 135
BE-16107.1.1	HGW19_6_2	23	116	macrofossil	187	0.9558	0.0098	−26.8	363 ± 83	402 ± 87	1548 ± 87
BE-16106.1.1	HGW19_6_2	47	140	macrofossil	24	0.9108	0.0116	−26.0	750 ± 102	695 ± 91	1255 ± 91
BE-16105.1.1	HGW19_7_2	49	188	macrofossil	24	0.9055	0.0118	−24.6	798 ± 104	735 ± 94	1215 ± 94
BE-16104.1.1	HGW19_6_3	25	224	macrofossil	114	0.8644	0.0085	−23.2	1170 ± 79	1091 ± 91	859 ± 91
BE-16103.1.1	HGW19_6_3	89	276	bulk peat	208	0.6601	0.0078	−23.5	3336 ± 95	3574 ± 116	−1624 ± 116

of a Keyence VHX-6000 digital microscope. Additionally, remains of other molluscs, insects such as weevils, and plants such as fruits and seeds were documented (Table S1 in the Supplement). Identification and autecological interpretation of microfossils rely on Meisch (2000) and Fuhrmann (2012) for Ostracoda, Schönborn (1966) and Scott et al. (2001) for testate amoebae, Glöer (2015) for aquatic molluscs, Klausnitzer (2019) for bryozoan statoblasts (Frenzel, 2019), and datasets available on the Smithsonian Institution's National Museum of Natural History (https://naturalhistory.si.edu/, last access: 4 October 2021) for other groups in a more general way.

3 Results and interpretation

3.1 Lithology and dating

The sediment record from Lake Höglwörth shows four different lithological units (Figs. 2–4), which are derived from changes in sediment colour, texture, and properties: Unit A (from 278 to 238 cm) consists of overall dark-brown-to black-coloured sediments with high organic carbon and sand contents, as well as low carbonate and low clay contents (Figs. 3 and 4). Greyish sand deposits were observed in several depths throughout Unit A. A sharp boundary in lithology and sediment colour is present at 238 cm depth and marks a transition from Unit A to Unit B. The sediments in Unit B (from 238 to 196 cm) are light reddish at the bottom and grey-coloured at the top. Unit B has lower sand but higher clay contents compared to Unit A, and silt is the dominant grain size. Silt contents remain very high (> 70 %) in Unit C (from 196 to 88 cm). Sediment colour changes distinctly at 196 cm, ranging from grey to black colour in a mottled pattern. The change from dark grey to light grey sediments at 88 cm marks the transition to Unit D (from 88 cm to the top). Brownish colours occur at 60 cm, whereas the top part of the core reveals brighter sediments (Fig. 2).

The ^{14}C ages from the Lake Höglwörth sediment core are shown in Table 1. The calibrated median ^{14}C ages range from 1620 ± 120 BCE at 276 cm, to 2007 ± 12 CE at 8 cm. The majority of the ^{14}C ages from the Lake Höglwörth sediment core are in stratigraphic order (Fig. 2; Table 1). Only one sample at 67 cm depth shows an age reversal; however its error range overlaps with the age range of the sample at 92 cm depth (Fig. 2).

The ^{137}Cs activity shows two peaks at 14 and 26 cm (Fig. 2). The first peak at 14 cm likely reflects the fallout from the 1986 CE Chernobyl accident, while the second peak at 26 cm likely reflects the fallout from the weapon testing in 1963 CE (Sirocko et al., 2013; Appleby et al., 1991; Appleby and Oldfield, 1978).

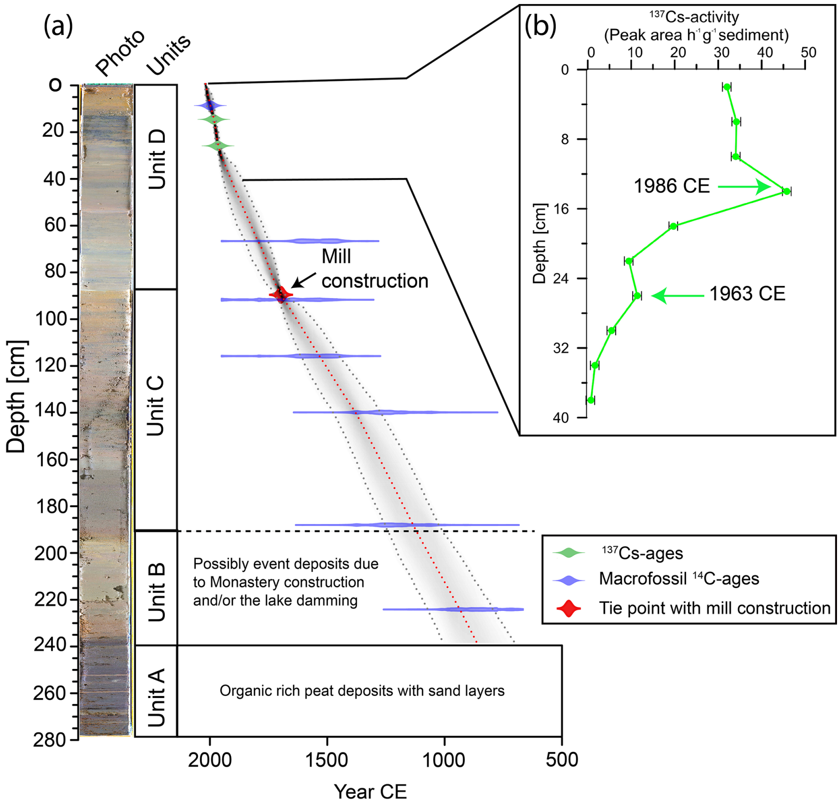

Figure 2. **(a)** Photo of the sediment core from Lake Höglwörth, units, and bacon age–depth model (Blaauw and Christen, 2011). The age–depth model is based on the tie point of mill construction at 1701 CE, indicated by a red symbol, calibrated radiocarbon ages are displayed as probability density functions of the 2σ distributions indicated by a blue symbol, and ^{137}Cs ages are shown in green. **(b)** The ^{137}Cs activity (peak area h^{-1} g^{-1} sediment).

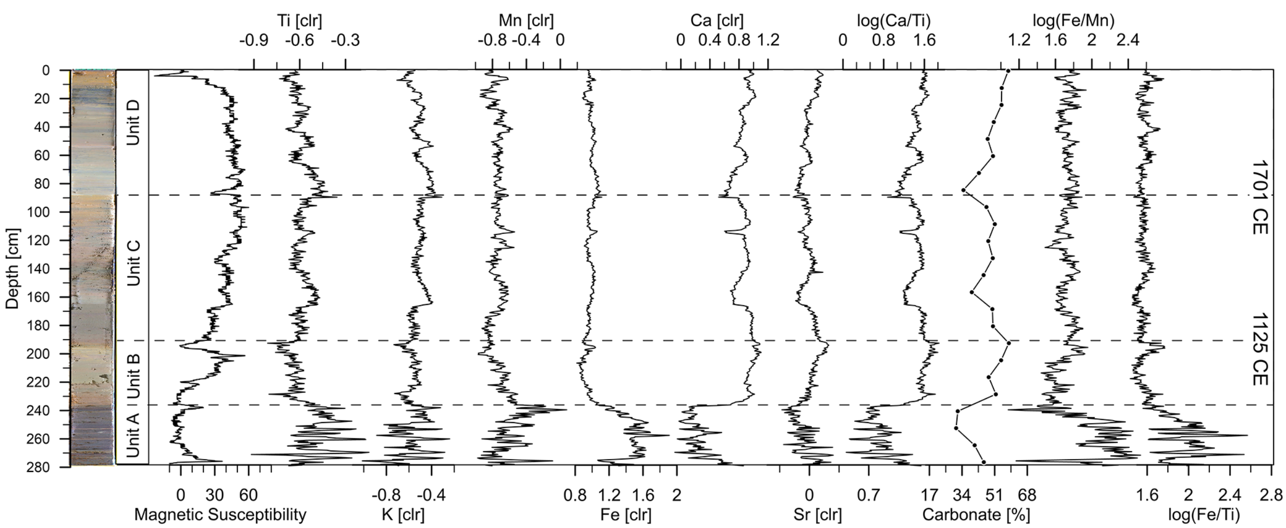

Figure 3. Variations in magnetic susceptibility and selected elements as well as carbonate content [%] along the depth profile at Lake Höglwörth. Elemental data are shown as centred log ratios (clr).

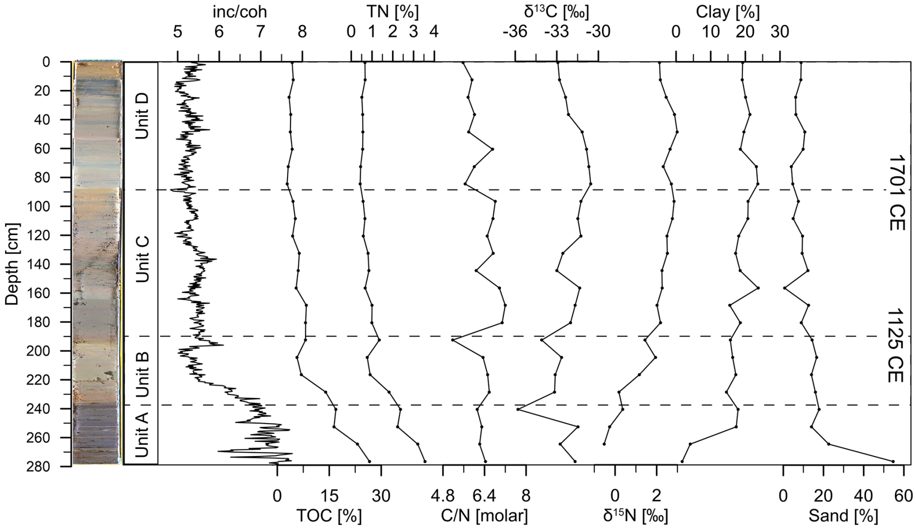

Figure 4. Variations in inc / coh, total organic carbon (TOC), total nitrogen (TN), the molar ratio of TOC [%] and TN [%] (C/N [molar]), and the bulk isotopic composition of organic carbon δ^{13}C and nitrogen δ^{15}N [‰] as well as sand [%] and clay [%] contents along the depth profile of Lake Höglwörth.

3.2 Geochemical analysis

Magnetic susceptibility values are low in Unit A and the lower part of Unit B. The upper part of Unit B reveals the maximum magnetic susceptibility of the entire record. After a significant drop at the transition from Unit B to Unit C, values remain on a quite constant high level with only minor fluctuations up to 20 cm composite depth. However, one minimum stands out at 88 cm depth, marking the transition to Unit D (Fig. 3). A trend towards lower values characterizes the top part of the core. The XRF analysis shows several changes in elemental records, associated with lithological changes (Fig. 3). Ti and K as proxies for allochthonous minerogenic input and catchment erosion (Strobel et al., 2021; Boes et al., 2011; Kastner et al., 2010) yield mostly the same pattern throughout the record, with high dynamic variability in Unit A but rather small variability in the following units. Ca and Sr show an opposite pattern compared to Ti and K. Ca and Sr are often linked to authigenic carbonate precipitation, e.g. due to enhanced lake productivity and/or evaporation (Kasper et al., 2012). The log(Ca/Ti) ratio can thus be used as a proxy for lake productivity versus minerogenic input. The very similar pattern of the log(Ca/Ti) ratio and $CaCO_3$ of our record corroborates this interpretation (Fig. 3). Mn and Fe follow a very similar pattern with decreasing trends from Unit A towards Unit B, followed by persistently lower values. The log(Fe/Mn) ratio was proposed as a proxy for redox conditions due to the higher solubility of Mn in a reducing environment relative to Fe (Makri et al., 2021; Żarczyński et al., 2019). Higher values thus indicate a stratified water column or reducing conditions. The log(Fe/Mn) ratio might well be influenced by other processes such as diagenesis and detrital input (Makri et al., 2021). As during anoxia and when diagenetic processes are dominant within the sediments, both the Fe and the Mn are dissolved, while Ti remains a stable component (Aufgebauer et al., 2012; Boes et al., 2011). This would significantly alter the log(Fe/Ti) ratio compared to the log(Fe/Mn) ratio. Since this is not the case and both the ratios follow very similar trends, the effects of diagenesis and detrital input on the redox conditions derived from the log(Fe/Mn) ratio are supposed to be negligible in Lake Höglwörth (Evans et al., 2020; Kylander et al., 2013). Additionally, reconstructed anoxia based on log(Fe/Mn) is corroborated by the biological record discussed below. Despite the shift from Unit A to Unit B, log(Fe/Mn) ratios show only small changes.

TOC values range between 2.8 % and 26.6 %, exhibit the highest values in Unit A, and decrease towards Unit D. The inc / coh ratio shows a quite similar pattern to TOC and thus can be used as a proxy for organic matter as well (Fortin et al., 2013; Guyard et al., 2007). TN values range from 3.5 % to 0.4 % and follow the pattern of TOC in the entire record (Fig. 4). The C/N ratio ranges from 5.1 to 7.1 with an average value of 6.3, indicating that organic matter is primarily derived from autochthonous sources (Meyers, 2003). δ^{13}C ranges from −34.1 ‰ to −30.5 ‰ and shows a pattern similar to the C/N ratio (Fig. 4), implying organic matter is mainly authigenically derived. δ^{15}N values vary between −0.2 ‰ and 3.0 ‰ and show an increasing trend from the bottom towards the top of the record.

3.3 Biological remains

Analysis of biological remains from the sediment core documents at least 30 different taxa from the sediment core (Fig. S4a–b, Table S1). Species level identification was achieved for Mollusca, Ostracoda, and Bryozoa. Other fossils encountered were oribatid mites, ephippia of cladocerans, beetle remains, fruits and seeds of angiosperm plants, oospores of charophytes, and fragments of mosses. Most taxa are aquatic, but there are a considerable number of terrestrial taxa as well.

Fossil remains are very rare in Unit A, suggesting unfavourable conditions for their preservation. Higher abundances in other units indicate better preservation. Broad maxima are visible in Units B and C for most taxa, suggesting higher deposition of fossil remains in these units. Glochidia do not appear before the upper part of Unit C and flourish in Unit D, whereas charophytes and *Hippuris* are abundant in Units B and C and disappear in Unit D.

Oribatid mites are highly abundant in Units B and C, whereas their abundance decreased in the earlier portion of Unit D. Ephippia are highly abundant in Unit B, but abundances decrease afterwards to the top.

Fish remains in the sediment show a broad maximum in the middle of Unit B, suggesting the start of and a substantial increase in the fish population in Lake Höglwörth with a short-lived breakdown at the limit to Unit C (Fig. 5).

Schoenoplectus is abundant in Units B and D but scarce in Unit C. Bryozoan statoblasts are relatively stable in Unit C, whereas they show a steady increase in the upper part of Unit D. Charcoal is very rare in Unit A, abundances are high in Units B and C, and they decrease throughout Unit D (Fig. 5).

Dominant ostracod species are *Cypridopsis vidua* and *Candona candida* (Fig. 6a). Swimming ostracod species such as *Cypridopsis vidua* can avoid the oxygen deficiency of the bottom water by swimming in between macrophytes and are often found in highly productive waterbodies (Meisch, 2000). Their abundance is high at the middle of Unit C and in the later portion of Unit D. *Cypria ophtalmica* reaches high abundances in Units B and D but is almost absent from Unit C. *Limnocythere inopinata*, *Sarscypridopsis aculeata*, and *Cyclocypris* sp. are rare and restricted to the younger half of the core. In contrast, *Darwinula stevensoni*, known to live on mud in waterbodies such as fishponds (Meisch, 2000), is frequent in the older part of the core and vanishes in Unit D.

Testate amoebae can be found in the younger three units of the core in high abundances (Fig. 6b). There is a change recognizable from dominating *Difflugia oblonga* in basal Units C and B to prevailing *Difflugia corona* above in Unit D. *Difflugia urceolata* is a species that prefers cooler waters and can tolerate low oxygen contents as well (Scott et al., 2001). *Difflugia urceolata* and *Difflugia bidens* are rare but typical of Unit D.

Bryozoan statoblasts and most of the other fossil remains are missing from Unit A (Figs. 4–6). The dominating taxon is *Plumatella* spp., comprising the species *Plumatella casmiana*, *Plumatella geimermassardi*, and *Plumatella repens*, which are hard to discriminate based on badly preserved fossil material. Bryozoan statoblasts show highest abundances in Unit C and steadily increase in the upper part of Unit D (Fig. 5). The rarer species *Plumatella fruticosa* and *Cristatella mucedo* replace each other over the record: the former is typical of Units B and C, whereas the latter species is abundant in Unit B and the youngest part of the core. The zebra mussel *Dreissena polymorpha* appears in the upper 25 cm of the sediment core.

4 Discussion

4.1 Chronostratigraphy

Unit A is characterized by organic-rich, low clay, and high sand contents and rare fossils. The calibrated ^{14}C age in this unit is substantially higher (> 2400 years) than the samples from other units, suggesting a very low accumulation rate or a discontinuous accumulation of the deposits (depositional gaps and/or erosion events). The lithological, geochemical, and biological records show a distinctly different depositional environment in Unit A compared to the other units. A local small wetland, peat, or a floodplain of a small creek with the presence of sedges and reeds is assumed. Since peat or floodplain deposits with presumably discontinuous character were not the primary focus of this study, the ^{14}C age at 276 cm was excluded from age–depth modelling. For Units B to D, an age–depth model was calculated where during the first iteration, only the ^{137}Cs and ^{14}C ages were considered (Fig. S3). This reveals that the record roughly covers the last 1100 years. At 88 cm depth, where a distinct shift in lithology and ecological species as well as minerogenic input occurred, an age of 1650^{+80}_{-120} CE is obtained. Considering the error range, this shift in the lacustrine environment matches the time frame of the flour mill construction and diversion of the input channel in 1701 CE. Therefore, we refined our chronology in a second iteration and included this age as a tie point for the final age–depth model (Fig. 2). It should be noted that the ^{14}C age at 67 cm shows a slightly older age in both iterations, probably due to the input of older carbon as a result of enhanced minerogenic input after the channel diversion. However, this is still within the 2σ uncertainty range of the age–depth model (Fig. 2).

4.2 Stages of lake evolution

4.2.1 Pre-lake deposits prior to 870^{+140}_{-160} CE

The lowermost part of the sediment record represents most probably the pre-lake valley floor or a former wetland area (floodplain of the creek), with peat forming prior to the modern Lake Höglwörth. Authigenic carbonate precipitation was not favourable in this phase, as suggested by low contents of $CaCO_3$ and log(Ca/Ti) ratios. Furthermore, the presence of preserved plant macro-remains and high log(Fe/Mn) ratios indicate anoxia that is typical in swamp/fen/peat bog environments. Several sandy layers suggest occasionally occurring flash-flooding events. Two peaks of charcoal suggest

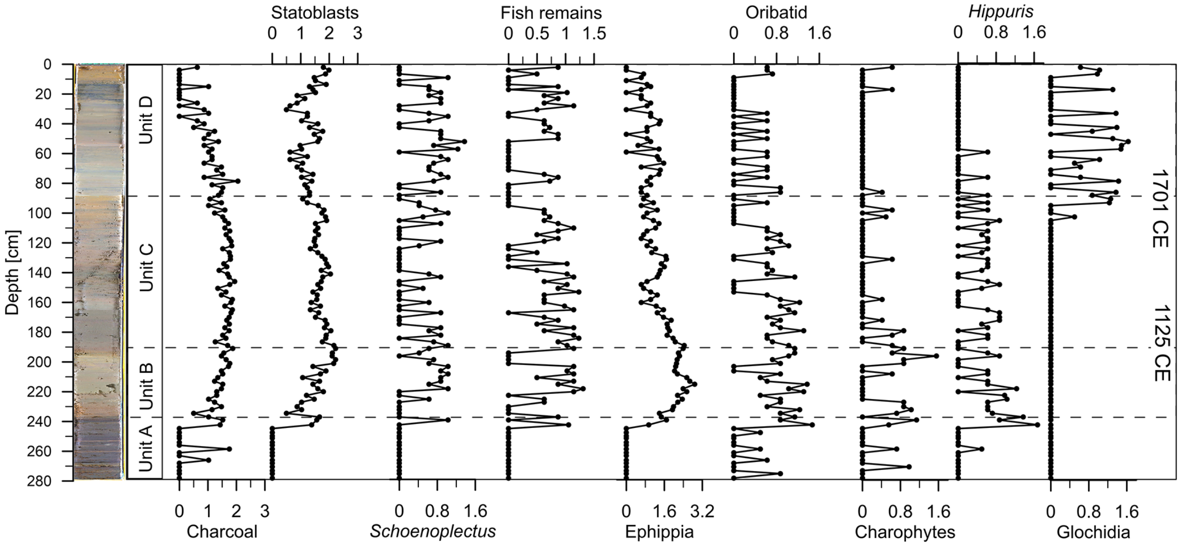

Figure 5. Quantity of charcoal, statoblasts of freshwater bryozoans, *Schoenoplectus*, fish remains, ephippia of cladocerans, oribatid mites, charophyte oospores, *Hippuris*, and glochidia of unionid bivalves (log(individual species $(x)+1$) / 100 mL) along core depth.

rare fire events in the area. The dominance of oribatid mites, with some rare findings of charophytes, implies a terrestrial or semi-aquatic habitat with dense vegetation and the presence of smaller waterbodies at this location (Frenzel, 2019).

4.2.2 From 870^{+140}_{-160} to 1120 ± 120 CE

An abrupt change from high organic peat-like deposits to more silty deposits suggests increasing water levels that established a lacustrine environment after 870^{+140}_{-160} CE (Figs. 3–6). Fossils become much more abundant and diverse during this phase, and remains of many groups appear for the first time (e.g. statoblasts of bryozoans, *Schoenoplectus*, fish remains) or increase dramatically (e.g. *Hippuris*, oribatid mites). High counts of Cladocera, *Difflugia oblonga*, statoblasts, and ostracods such as *Candona candida* and *Darwinula stevensoni* characterize Lake Höglwörth as a shallow and macrophyte-rich waterbody (Fuhrmann, 2012; Meisch, 2000). In general, high abundances of ostracods suggest high aquatic production (Ruiz et al., 2013), which is further supported by increased carbonate precipitation. Decreasing TOC and TN values document a shift in nutrients, which is further supported by increasing δ^{15}N and δ^{13}C values (Meyers, 2003). Finer-grained sediments, a decrease in submerged macrophytes after 870^{+140}_{-160} CE, and a substantial increase in fish remains around 1000^{+130}_{-140} CE points towards a slowly rising water level. A distinct increase in charcoal abundance infers increasing fire events in the lake catchment (Fig. 5).

The monastery Höglwörth on the lake peninsula was constructed in 1125 CE (Bauer and Bauer, 1993). During the construction phase, the peninsula was probably enlarged by soil material previously extracted from an artificial ditch around the construction area (Landesamt für Digitalisierung, 2022). In addition, the lake was probably dammed, but whether this was done before or during the construction of the monastery and when these activities happened are not known. Therefore, we cannot rule out that the sediments that accumulated between 870^{+140}_{-160} and 1120 ± 120 CE result, at least partly, from these construction activities and/or the damming.

4.2.3 From 1120 ± 120 to 1701 CE

Human activities in the lake catchment increased during this stage, as indicated by the charcoal content that likely reflects high levels of firewood burning (Whitlock and Larsen, 2001; Fig. 5). This is contemporaneous with an increase in human activities in the region (Gilck and Poschlod, 2020; Enters et al., 2006).

Decreasing abundance of statoblasts, ephippia, and charophytes, as well as lower diversity in ostracods and testate amoebae and increasing δ^{13}C and δ^{15}N values, points to an increased trophic state of the lake (Figs. 4–6; Poikane et al., 2018; Torres et al., 2012; Hartikainen et al., 2009).

In 1120 ± 120 CE, enhanced flux of minerogenic material (Ti, K) was probably caused by the monastery construction in 1125 CE and would very likely have increased aquatic productivity (Haas et al., 2019). A further increase in minerogenic input from 1240^{+110}_{-120} to 1380^{+90}_{-110} CE associated with higher clay contents as well as increased values for magnetic susceptibility (Dearing et al., 1996) suggests increased soil erosion in the catchment of the lake (Fig. 3). This coincides with the massive medieval deforestation in Bavaria during the 13th century as a result of a growing population and increasing agropastoral activities (Gilck and Poschlod, 2020;

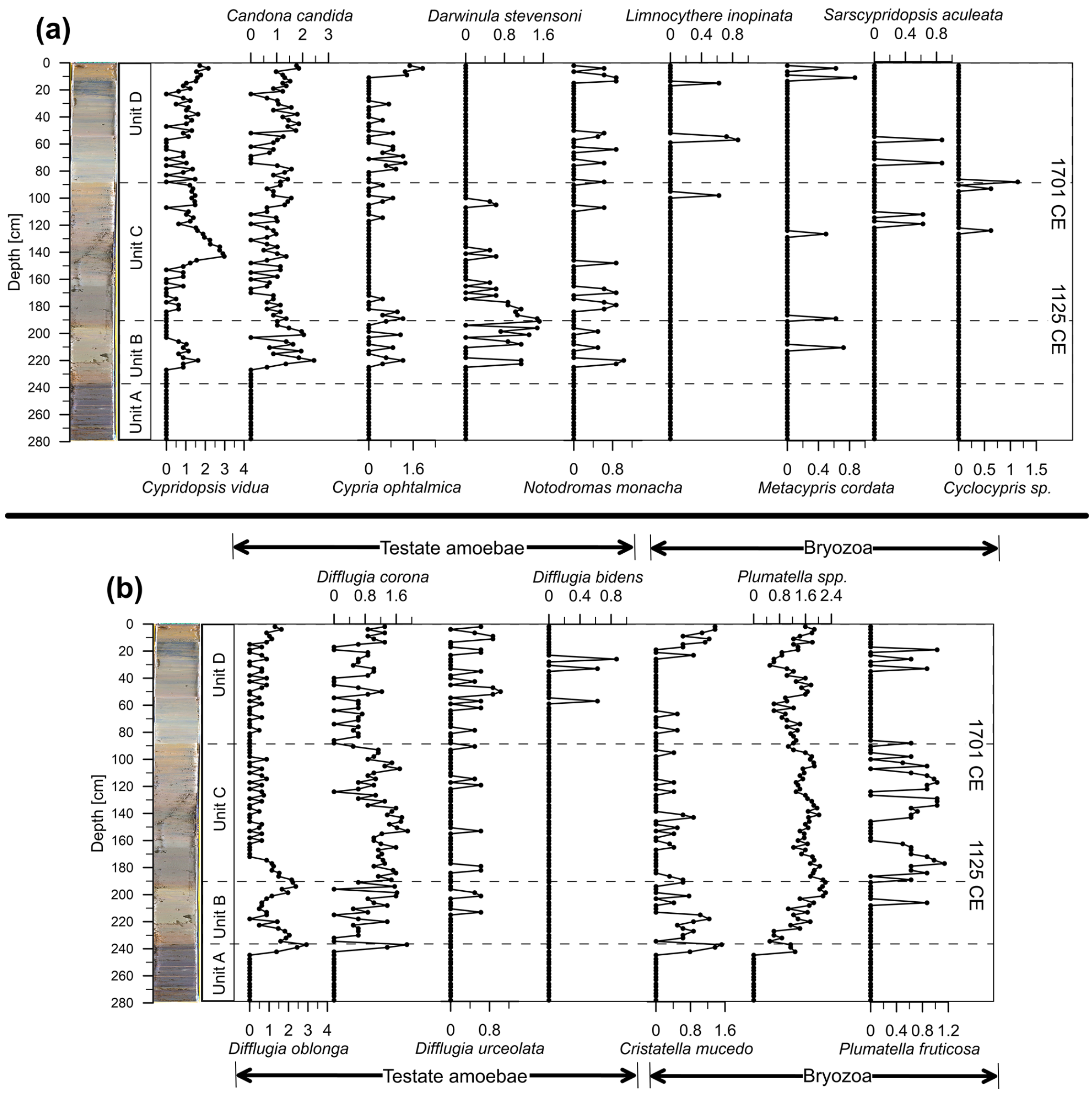

Figure 6. **(a)** Distribution of ostracods and **(b)** testate amoebae and bryozoan statoblasts within the core from Lake Höglwörth. Ostracoda, testate amoebae, and Bryozoa abundances are given as abundance for 100 mL of sediment and are log-transformed [$\log(x+1)$].

van der Knaap et al., 2019; Enters et al., 2008). However, enhanced terrestrial input could also be related to a series of extreme precipitation and flood events such as the St Mary Magdalene flood in 1342/1343 (Bauch, 2019; Reinhardt-Imjela et al., 2018). During almost the same time (from 1310^{+100}_{-120} to 1470^{+90}_{-100} CE), anoxia occurred, as reflected by higher log(Fe/Mn) ratios and the abundance of *Cypridopsis vidua* and *Difflugia urceolata* because these species can avoid oxygen deficiency by swimming in between macrophytes (Fig. 7; Scott et al., 2001; Meisch, 2000). As the lake is relatively shallow and water might be seasonally mixed, the anoxia could mainly have occurred at the bottom of or in the interstitial water (Fam and Kerstin, 2018). In combination with bottom or interstitial water anoxia, abundances of ostracods as well as charophytes and pronounced calcite precipitation indicate overall enhanced aquatic productivity. Therefore, deforestation probably led to higher allochthonous input, which likely caused increased nutrient delivery. Similar processes were reported from other sites such as Lake Salęt in Poland, where anthropogenic activities during the medieval period led to stronger soil erosion and higher productivity (Gąsiorowski et al., 2021). Lacustrine carbonate precipitation (log(Ca/Ti) ratios, $CaCO_3$) is not only affected by biological productivity, but also driven by temperature and thus higher evaporation (Kasper et al., 2012; Mueller et al., 2009; Brown et al., 2007). Considering the chronological uncertainties, carbonate precipitation increased in Lake Höglwörth during periods of higher temperatures during the

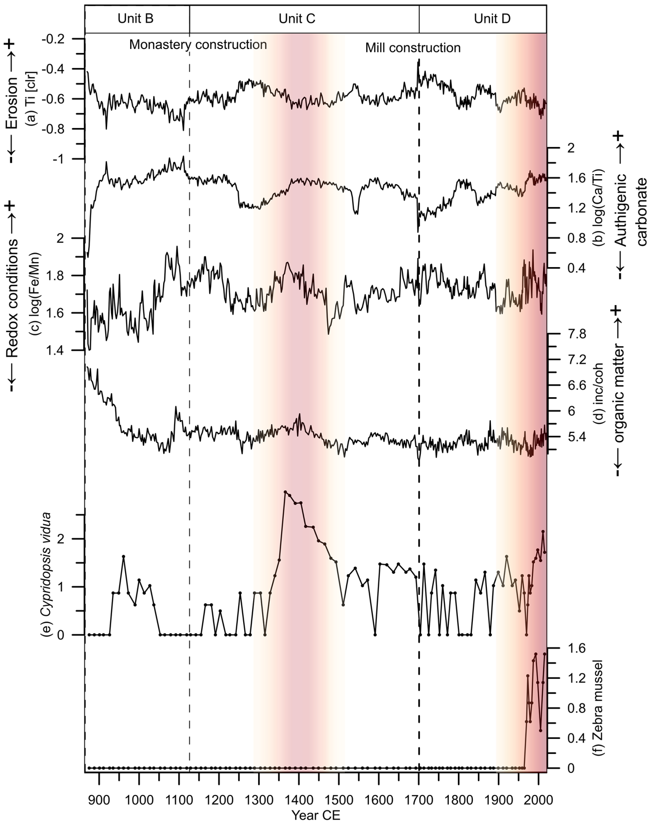

Figure 7. Distribution of selected environmental proxies for the core from Lake Höglwörth. **(a)** The Ti centred log ratio (Ti [clr]) represents the minerogenic input; **(b)** log(Ca/Ti) indicates the authigenic carbonate precipitation; **(c)** log(Fe/Mn) reflects redox conditions; **(d)** inc / coh refers to organic matter deposition. **(e, f)** Absolute abundance ($\log(x+1)\,100\,\mathrm{mL}^{-1}$) of *Cypridopsis vidua* and zebra mussels, respectively. Red shading indicates the periods with prevailing bottom or interstitial water anoxia in the lake as inferred from high log(Fe/Mn) and abundance of *Cypridopsis vidua* as well as other species mentioned in the text.

past millennium for Europe (PAGES 2k Consortium, 2013). Hence, increased biological production and higher temperatures might have been responsible for the authigenic carbonate precipitation in our record. The presence of glochidia, which are larval stages of unionid bivalves that live as parasites on fishes (Glöer, 2015), reflect the fact that abundant fish lived in Lake Höglwörth after 1620^{+50}_{-80} CE. Their dominance within the uppermost, youngest part of the record might have been driven by fish aquaculture as practised by many monastery societies (Brugger et al., 2008).

4.2.4 From 1701 to 2019 CE

High allochthonous input and a substantial shift in aquatic communities (e.g. disappearance of *Plumatella fruticosa*, *Hippuris*, *Darwinula stevensoni*, and charophytes and appearance of glochidia) around 1701 CE coincided with the construction of a flour mill and the related rerouting of the Höglwörther Seebach (Figs. 3–7; Gałczyńska et al., 2019; Melzer, 1999). An increased influx of water and minerogenic input, associated with the mill construction, might have affected lake water turbidity, water chemistry, and/or mixing regimens, consequently changing the aquatic fauna (Bhateria and Jain, 2016; Nilsson and Renöfält, 2008; Bunn and Arthington, 2002). Additionally, the production of the mill might have discharged wastewater into Lake Höglwörth, causing enrichment in nutrients such as N and P.

Enhanced carbonate precipitation is documented from 1800^{+50}_{-40} to 2019 CE (Fig. 7). This was accompanied by a reduced minerogenic input and thus perhaps caused by increased primary productivity in the lake, leading to epilimnetic carbonate precipitation (Sun et al., 2019; Balci et al., 2018). Additionally, the post-industrial revolution rise in global temperature may have led to increased lake evaporation and thus enhanced carbonate precipitation (DWD Climate Data Center, 2023; IPCC, 2021; DWD Climate Data Center, 2020). The high abundance of *Difflugia urceolata* and *Cypridopsis vidua* after 1850^{+40}_{-50} CE point towards anoxia in the lake (Fig. 7). The high abundance of the testate amoebae *Difflugia urceolata* and the appearance of *Difflugia bidens* after 1850^{+40}_{-50} CE suggest a higher trophic state, possibly due to increased nutrient input from anthropogenic activities. This is corroborated by decreasing δ^{15}N and δ^{13}C values.

After around the 1960s, Lake Höglwörth was affected by eutrophication due to increased agriculture activities and the associated input of nutrients as inferred from decreasing δ^{15}N values. This is in line with increased anthropogenic activities globally and the start of the industrial revolution in the region (Steffen et al., 2015; De Vries, 1994). Eutrophication is common for lakes in Bavaria (Enters et al., 2006; Bayrisches Landesamt, 1996) and central Europe (Bartram et al., 2002). The zebra mussel *Dreissena polymorpha*, a neozoon, an invasive species, and native to lakes in Russia and Ukraine, appeared in Lake Höglwörth around 1960 ± 10 CE (Fig. 7; Neumann and Jenner, 1992). This is contemporaneous with its spread to alpine lakes (Minchin et al., 2002; Binder, 1965).

5 Conclusion

This study analysed a sediment core from Lake Höglwörth for lithology, geochemistry, and biology to investigate the palaeoenvironmental conditions and anthropogenic impact on a lacustrine system. Our findings suggest that a wetland environment (peat formation) existed prior to 870^{+140}_{-160} CE, when the lake sediment started to accumulate. Distinct shifts in sedimentology, elemental composition, and the biological record from 870^{+140}_{-160} to 1120 ± 120 CE are attributed to the construction of the monastery in 1125 CE and/or damming of the lake. Our record documents increased allochthonous input from 1240^{+110}_{-120} to 1380^{+90}_{-110} CE related to enhanced soil erosion. Prevailing bottom or interstitial water anoxia from 1310^{+100}_{-120} to 1470^{+90}_{-100} CE can be related to higher nutrient input as a consequence of enhanced anthropogenic activities such as deforestation. A shift in the sedimentological and biological record at 1701 CE is possibly caused by the diversion of a small creek necessary for the operation of a newly built mill. Channel diversion increased the allochthonous input into the lake and had a significant impact on aquatic communities. Overall, this study shows that past human activities during the last millennium have had a significant impact on the lithological, geochemical, and biological environment, causing algal blooms and anoxia in Lake Höglwörth repeatedly during the last millennium prior to recent decades. Also, this study demonstrates that dam construction can have severe impacts on aquatic ecosystems. Lakes have undergone significant environmental changes in the past for various reasons, and understanding the causes and impacts of these changes can be valuable for predicting future ecological pathways as well as for restoration efforts.

Data availability. The data presented in this paper can be found as an Excel dataset in the Supplement of this paper.

Supplement. The supplement related to this article is available online at: https://doi.org/10.5194/egqsj-72-219-2023-supplement.

Author contributions. SA: conceptualization, formal analysis, investigation, discussions, writing (original draft, review and editing); MP: investigation, discussions, writing (review and editing); TK: fieldwork, writing (review and editing); LL: biological analyses and documentation, writing of a biological draft, writing (review and editing); PF: conceptualization and supervision of biological work, taxonomic identification, biological interpretation, co-writing of a biological draft, writing (review and editing); PS: conceptualization, investigation, discussions, fieldwork, writing (review and editing); MB: conceptualization, discussions, writing (review and editing); GD: fieldwork, writing (review and editing); CB: sample preparation, taxonomic identification, writing (review and editing); SS: writing (review and editing); GS: writing (review and editing); AS: funding acquisition, discussions, writing (review and editing); RZ: conceptualization, fieldwork, discussions, supervision, writing (review and editing).

Competing interests. The contact author has declared that none of the authors has any competing interests.

Acknowledgements. This study was funded by the German Research Foundation (DFG) via the International Research Training Group "Geo-ecosystems in Transition on the Tibetan Plateau (TransTiP)" (DFG grant 317513741/GRK 2309). We acknowledge support by the German Research Foundation, project no. 512648189, and the Open Access Publication Fund of the Thueringer Universitaets- und Landesbibliothek Jena. Maximilian Prochnow gratefully acknowledges the support of a fellowship from the state of Thuringia (Landesgraduiertenstipendium 2022). The authors want to thank Julian Struck (Friedrich Schiller University Jena) for contributions during discussions and help with lab work. Rafael Stiens is acknowledged for performing the XRF scanning at the University of Bremen. Jana Löhrlein, Theresa Henning, Moritz Mäding, and Josefin Sperling are thanked for their support in the laboratory. We thank associate editor Elisabeth Dietze and the two reviewers for their valuable and helpful comments that improved this paper.

Financial support. This research has been supported by the German Research Foundation (DFG, grant no. 317513741/GRK 2309). Article processing charges were supported by the German Research Foundation (project no. 512648189) and the Open Access Publication Fund of the Thueringer Universitaets- und Landesbibliothek Jena.

Review statement. This paper was edited by Elisabeth Dietze and reviewed by Christoph Mayr and one anonymous referee.

References

Adrian, R., O'Reilly, C. M., Zagarese, H., Baines, S. B., Hessen, D. O., Keller, W., Livingstone, D. M., Sommaruga, R., Straile, D., Van Donk, E., Weyhenmeyer, G. A., and Winder, M.: Lakes as sentinels of climate change, Limnol. Oceanogr., 54, 2283–2297, https://doi.org/10.4319/lo.2009.54.6_part_2.2283, 2009.

Alefs, J. and Müller, J.: Differences in the eutrophication dynamics of Ammersee and Starnberger See (Southern Germany), reflected by the diatom succession in varve-dated sediments, J. Paleolimnol., 21, 395–407, 1999.

Appleby, P. G. and Oldfield, F.: The calculation of lead-210 dates assuming a constant rate of supply of unsupported ^{210}Pb to the sediment, Catena, 5, 1–8, https://doi.org/10.1016/S0341-8162(78)80002-2, 1978.

Appleby, P. G., Richardson, N., and Nolan, P. J.: ^{241}Am dating of lake sediments, Hydrobiologia, 214, 35–42, https://doi.org/10.1007/BF00050929, 1991.

Aufgebauer, A., Panagiatopoulos, K., Wagner, B., Schaebitz, F., Viehberg, F. A., Vogel, H., Zanchetta, G., Sulpizio, R., Leng, M. J., and Damaschke, M.: Climate and environmental change over the last 17 ka recorded in sediments from Lake Prespa (Albania/F.Y.R. of Macedonia/Greece), Quatern. Int., 274, 122–135, https://doi.org/10.1016/j.quaint.2012.02.015, 2012.

Balci, N., Demirel, C., Akcer Ön, S., Gültekin, A. H., and Kurt, M. A.: Evaluating abiotic and microbial factors on carbonate precipitation in Lake Acigöl, a hypersaline lake in Southwestern Turkey, Quatern. Int., 486, 116–128, https://doi.org/10.1016/j.quaint.2017.12.046, 2018.

Bartram, J., Thyssen, N., and Gowers, A.: Water and health in Europe: a joint report from the European Environment Agency and the WHO Regional Office for Europe, WHO Regional Office for Europe, WHO Regional Publications European Series No. 93, ISBN 9289013605, 2002.

Bauch, M.: Die Magdalenenflut 1342 am Schnittpunkt von Umwelt- und Infrastrukturgeschichte: Ein compound event als Taktgeber für mittelalterliche Infrastrukturentwicklung und Daseinsvorsorge, NTM. Zeitschrift für Geschichte der Wissenschaften, Technik und Medizin, 27, 273–309, https://doi.org/10.1007/s00048-019-00221-y, 2019.

Bauer, H. and Bauer, A.: Klöster in Bayern: eine Kunst-und Kulturgeschichte der Klöster in Oberbayern, Niederbayern und der Oberpfalz, CH Beck, ISBN 3406377548, 1993.

Bayrisches Landesamt: Kostenbewußte Abwasserentsorgung, in: Informationsberichte des Bayrischen Landesamtes für Wasserwirtschaft, Bayrisches Landesamt für Wasserwirtschaft, Heft 2/96, 1996.

Bhateria, R. and Jain, D.: Water quality assessment of lake water: a review, Sustainable Water Resources Management, 2, 161–173, https://doi.org/10.1007/s40899-015-0014-7, 2016.

Binder, E.: Un mollusque envahissant, la Dreissena polymorpha, Musee de Geneve, 54, 2–4, 1965.

Blaauw, M. and Christen, J. A.: Flexible Paleoclimate Age-Depth Models Using an Autoregressive Gamma Process, Bayesian Anal., 6, 457–474, https://doi.org/10.1214/ba/1339616472, 2011.

Blei, J.: Die Saline Bad Reichenhall–Überlegungen zu herrschaftlichen Besitzverhältnissen und Handelsmechanismen von der Römerzeit bis zu den Bajuwaren, edited by: Herz, P., Schmid, P., and Stoll, O., Ökonomie und Politik, Facetten europäischer Geschichte im Imperium Romanum und dem frühen Mittelalter, RiU, 5, 151–170, 2011.

Blott, S. J. and Pye, K.: GRADISTAT: a grain size distribution and statistics package for the analysis of unconsolidated sediments, Earth Surf. Proc. Land., 26, 1237–1248, https://doi.org/10.1002/esp.261, 2001.

Boes, X., Rydberg, J., Martinez-Cortizas, A., Bindler, R., and Renberg, I.: Evaluation of conservative lithogenic elements (Ti, Zr, Al, and Rb) to study anthropogenic element enrichments in lake sediments, J. Paleolimnol., 46, 75–87, https://doi.org/10.1007/s10933-011-9515-z, 2011.

Brown, E. T., Johnson, T. C., Scholz, C. A., Cohen, A. S., and King, J. W.: Abrupt change in tropical African climate linked to the bipolar seesaw over the past 55,000 years, Geophys. Res. Lett., 34, L20702, https://doi.org/10.1029/2007gl031240, 2007.

Brugger, W., Dopsch, H., and Wild, J.: Höglwörth, Das Augustiner-Chorherrenstift mit den Pfarreien Anger und Piding, Verein Freunde der Salzburger Geschichte, ISBN 9783902582034, 2008.

Bunn, S. E. and Arthington, A. H.: Basic principles and ecological consequences of altered flow regimes for aquatic biodiversity, Environ. Manage., 30, 492–507, https://doi.org/10.1007/s00267-002-2737-0, 2002.

Crutzen, P. J. and Stoermer, E. F.: The "Anthropocene"(2000), in: Paul J. Crutzen and the Anthropocene: A New Epoch in Earth's History. The Anthropocene: Politik–Economics–Society–Science, edited bu: Benner, S., Lax, G., Crutzen, P. J., Pöschl, U., Lelieveld, J., and Brauch, H. G., Springer, Cham, https://doi.org/10.1007/978-3-030-82202-6_2, 2021.

Dearing, J. A., Dann, R., Hay, K., Lees, J., Loveland, P., Maher, B. A., and O'grady, K.: Frequency-dependent susceptibility measurements of environmental materials, Geophys. J. Int., 124, 228–240, https://doi.org/10.1111/j.1365-246X.1996.tb06366.x, 1996.

De Vries, J.: The industrial revolution and the industrious revolution, J Econ. Hist., 54, 249–270, https://doi.org/10.1017/S0022050700014467, 1994.

Dotterweich, M.: Land Use and Soil Erosion in northern Bavaria during the last 5000 Years, in: Long Term Hillslope and Fluvial System Modelling, Springer, 201–229, https://doi.org/10.1007/3-540-36606-7_11, 2003.

DWD Climate Data Center: Hohenpeißenberg Jahresmittel der Temperatur 1781–2022, https://www.dwd.de/DE/forschung/atmosphaerenbeob/zusammensetzung_atmosphaere/hohenpeissenberg/bild/lange_tempreihe.html (last access: 6 February 2023), 2023.

DWD Climate Data Center: Recent and historical dataset: Monthly means of precipitation totals, monthly mean air temperature and highest daily maximum temperature of a month for station Piding (CDC-ID 7424), DWD Climate Data Center [dataset], https://opendata.dwd.de/climate_environment/CDC/observations_germany/climate/multi_annual/mean_91-20/ (last access: 16 September 2022), 2020.

Enters, D., Lucke, A., and Zolitschka, B.: Effects of land-use change on deposition and composition of organic matter in Frickenhauser See, northern Bavaria, Germany, Sci. Total Environ., 369, 178–187, https://doi.org/10.1016/j.scitotenv.2006.05.020, 2006.

Enters, D., Dörfler, W., and Zolitschka, B.: Historical soil erosion and land-use change during the last two millennia recorded in lake sediments of Frickenhauser See, northern Bavaria, central Germany, The Holocene, 18, 243–254, https://doi.org/10.1177/0959683607086762, 2008.

Evans, G., Augustinus, P., Gadd, P., Zawadzki, A., Ditchfield, A., and Hopkins, J.: A multi-proxy paleoenvironmental interpretation spanning the last glacial cycle (ca. 117 ± 8.5 ka BP) from a lake sediment stratigraphy from Lake Kai Iwi, Northland, New Zealand, J. Paleolimnol., 65, 101–122, https://doi.org/10.1007/s10933-020-00151-z, 2020.

Fam, C. and Kerstin, W.: Gewässerökologische Untersuchung des Höglwörther Sees, Gesellschaft für Landschaftsökologie, Gewässerbiologie & Umweltplanung mbH, 2018.

Fortin, D., Francus, P., Gebhardt, A. C., Hahn, A., Kliem, P., Lisé-Pronovost, A., Roychowdhury, R., Labrie, J., and St-Onge, G.: Destructive and non-destructive density determination: method comparison and evaluation from the Laguna Potrok Aike sedimentary record, Quaternary Sci. Rev., 71, 147–153, https://doi.org/10.1016/j.quascirev.2012.08.024, 2013.

Franz, G.: Der dreissigjährige Krieg und das deutsche Volk, De Gruyter Oldenbourg, https://doi.org/10.1515/9783110509328, 2019.

Frenzel, P.: Fossils of the southern Baltic Sea as palaeoenvironmental indicators in multi-proxy studies, Quatern. Int., 511, 6–21, https://doi.org/10.1016/j.quaint.2018.09.014, 2019.

Fuhrmann, R.: Atlas quartärer und rezenter Ostrakoden Mitteldeutschlands, Altenburger Naturwissenschaftliche Forschungen 15, Naturkundliches Museum Mauritianum Altenburg, 1–320, 2012.

Gałczyńska, M., Milke, J., Gamrat, R., and Stoltman, M.: Common mare's tail (*Hippuris Vulgaris* L.) in the assessment of water status and their phytoremediation, Folia Pomeranae Universitatis Technologiae Stetinensis Agricultura, Alimentaria, Piscaria et Zootechnica, 348, 57–70, https://doi.org/10.21005/aapz2019.49.1.06, 2019.

Gąsiorowski, M., Sienkiewicz, E., Ciołko, U., Kaucha, K., Kupryjanowicz, M., and Szal, M.: Cultural eutrophication of a Central European lowland lake from the Bronze Age to the present recorded in diatom and Cladocera remains, Catena, 204, 105404, https://doi.org/10.1016/j.catena.2021.105404, 2021.

Gilck, F. and Poschlod, P.: The history of human land use activities in the Northern Alps since the Neolithic Age. A reconstruction of vegetation and fire history in the Mangfall Mountains (Bavaria, Germany), The Holocene, 31, 579–591, https://doi.org/10.1177/0959683620981701, 2020.

Glöer, P.: Süßwassermollusken – ein Bestimmungsschlüssel für die Muscheln und Schnecken im Süßwasser der Bundesrepublik Deutschland, Deutscher Jugendbund für Naturbeobachtung, Augsburg, ISBN 9783923376025, 2015.

Glückert, G.: On Pleistocene glaciations in the German Alpine foreland, Bull. Geol. Soc. Finl., 46, 117–131, 1974.

Guyard, H., Chapron, E., St-Onge, G., Anselmetti, F. S., Arnaud, F., Magand, O., Francus, P., and Mélières, M.-A.: High-altitude varve records of abrupt environmental changes and mining activity over the last 4000 years in the Western French Alps (Lake Bramant, Grandes Rousses Massif), Quaternary Sci. Rev., 26, 2644–2660, https://doi.org/10.1016/j.quascirev.2007.07.007, 2007.

Haas, M., Baumann, F., Castella, D., Haghipour, N., Reusch, A., Strasser, M., Eglinton, T. I., and Dubois, N.: Roman-driven cultural eutrophication of Lake Murten, Switzerland, Earth Planet. Sc. Lett., 505, 110–117, https://doi.org/10.1016/j.epsl.2018.10.027, 2019.

Hartikainen, H., Johnes, P., Moncrieff, C., and Okamura, B.: Bryozoan populations reflect nutrient enrichment and productivity gradients in rivers, Freshwater Biol., 54, 2320–2334, https://doi.org/10.1111/j.1365-2427.2009.02262.x, 2009.

Hua, Q., Barbetti, M., and Rakowski, A. Z.: Atmospheric Radiocarbon for the Period 1950–2010, Radiocarbon, 55, 2059–2072, https://doi.org/10.2458/azu_js_rc.v55i2.16177, 2013.

IPCC: Climate Change 2021: The Physical Science Basis. Contribution of Working Group I to the Sixth Assessment Report of the Intergovernmental Panel on Climate Change, edited by: Masson-Delmotte, V., Zhai, P., Pirani, A., Connors, S. L., Péan, C., Berger, S., Caud, N., Chen, Y., Goldfarb, L., Gomis, M. I., Huang, M., Leitzell, K., Lonnoy, E., Matthews, J. B. R., Maycock, T. K., Waterfield, T., Yelekçi, O., Yu, R., and Zhou, B., Cambridge University Press, Cambridge, United Kingdom and New York, NY, USA, 2391 pp,, https://doi.org/10.1017/9781009157896, 2021.

Jäger, H.: Entwicklungsperioden agrarer Siedlungsgebiete im mittleren Westdeutschland seit dem frühen 13. Jahrhundert, Würzb. Geogr. Arb., 6, 1–136, 1958.

Kasper, T., Haberzettl, T., Doberschütz, S., Daut, G., Wang, J., Zhu, L., Nowaczyk, N., and Mäusbacher, R.: Indian Ocean Summer Monsoon (IOSM)-dynamics within the past 4 ka recorded in the sediments of Lake Nam Co, central Tibetan Plateau (China), Quaternary. Sci. Rev., 39, 73–85, https://doi.org/10.1016/j.quascirev.2012.02.011, 2012.

Kastner, S., Ohlendorf, C., Haberzettl, T., Lücke, A., Mayr, C., Maidana, N. I., Schäbitz, F., and Zolitschka, B.: Southern hemispheric westerlies control the spatial distribution of modern sediments in Laguna Potrok Aike, Argentina, J. Paleolimnol., 44, 887–902, https://doi.org/10.1007/s10933-010-9462-0, 2010.

Klausnitzer, B.: Stresemann – Exkursionsfauna von Deutschland – Bd. 1 Wirbellose (ohne Insekten), 9. Aufl., Springer Verlag, Berlin, 735 pp., ISBN 3662553538,, 2019.

Klein Goldewijk, K., Beusen, A., Van Drecht, G., and De Vos, M.: The HYDE 3.1 spatially explicit database of human-induced global land-use change over the past 12,000 years, Global Ecol. Biogeogr., 20, 73–86, https://doi.org/10.1111/j.1466-8238.2010.00587.x, 2011.

Küster, H.: Die Alpen: Geschichte einer Landschaft, CH Beck, ISBN 9783406748288, 2020.

Kylander, M. E., Klaminder, J., Wohlfarth, B., and Löwemark, L.: Geochemical responses to paleoclimatic changes in southern Sweden since the late glacial: the Hässeldala Port lake sediment record, J. Paleolimnol., 50, 57–70, https://doi.org/10.1007/s10933-013-9704-z, 2013.

Landesamt für Digitalisierung: Breitband und Vermessung, https://geoportal.bayern.de/bayernatlas/?zoom=12&lang=de&topic=ba&bgLayer=historisch&E=787743.03&catalogNodes=11 (last access: 23 June 2022), 2022.

Lauterbach, S., Brauer, A., Andersen, N., Danielopol, D. L., Dulski, P., Hüls, M., Milecka, K., Namiotko, T., Obremska, M., and Von Grafenstein, U.: Environmental responses to Lateglacial climatic fluctuations recorded in the sediments of pre-Alpine Lake Mondsee (northeastern Alps), J. Quaternary Sci., 26, 253–267, https://doi.org/10.1002/jqs.1448, 2011.

Lewis, S. L. and Maslin, M. A.: Defining the anthropocene, Nature, 519, 171–180, https://doi.org/10.1038/nature14258, 2015.

Makri, S., Wienhues, G., Bigalke, M., Gilli, A., Rey, F., Tinner, W., Vogel, H., and Grosjean, M.: Variations of sedimentary Fe and Mn fractions under changing lake mixing regimes, oxygenation and land surface processes during Lateglacial and Holocene times, Sci. Total Environ., 755, 143418, https://doi.org/10.1016/j.scitotenv.2020.143418, 2021.

Meisch, C.: Freshwater Ostracoda of western and central Europe, Sußwasserfauna von Mitteleuropa, 8/3, ISBN 9783827410016, 522 pp., 2000.

Melzer, A.: Aquatic macrophytes as tools for lake management, Hydrobiologia, 398, 182–190, https://doi.org/10.1023/A:1017001703033, 1999.

Meyers, P. A.: Applications of organic geochemistry to paleolimnological reconstructions: a summary of examples from the Laurentian Great Lakes, Org. Geochem., 34, 261–289, https://doi.org/10.1016/S0146-6380(02)00168-7, 2003.

Minchin, D., Lucy, F., and Sullivan, M.: Zebra Mussel: Impacts and Spread, in: Invasive Aquatic Species of Europe. Distribution, Impacts and Management, edited by: Leppäkoski, E., Gollasch, S., and Olenin, S., Springer, Dordrecht, 135–146, https://doi.org/10.1007/978-94-015-9956-6_15, 2002.

Mueller, A. D., Islebe, G. A., Hillesheim, M. B., Grzesik, D. A., Anselmetti, F. S., Ariztegui, D., Brenner, M., Curtis, J. H., Hodell, D. A., and Venz, K. A.: Climate drying and associated forest decline in the lowlands of northern Guatemala during the late Holocene, Quaternary Res., 71, 133–141, https://doi.org/10.1016/j.yqres.2008.10.002, 2009.

Neumann, D. and Jenner, H. A.: The zebra mussel *Dreissena polymorpha*: Ecology, Biological Monitoring and First Applications in the Water Quality Management, Schweizerbart science publishers, Stuttgart, ISBN 978-3-510-53002-1, 1992.

Nilsson, C. and Renöfält, B. M.: Linking Flow Regime and Water Quality in Rivers a Challenge to Adaptive Catchment Management, Ecol. Soc., 13, 18 pp., 2008.

PAGES 2k Consortium: Continental-scale temperature variability during the past two millennia, Nat. Geosci., 6, 339–346, https://doi.org/10.1038/ngeo1797, 2013.

Poikane, S., Portielje, R., Denys, L., Elferts, D., Kelly, M., Kolada, A., Maemets, H., Phillips, G., Sondergaard, M., Willby, N., and van den Berg, M. S.: Macrophyte assessment in European lakes: Diverse approaches but convergent views of 'good' ecological status, Ecol. Indic., 94, 185–197, https://doi.org/10.1016/j.ecolind.2018.06.056, 2018.

Ramisch, A., Tjallingii, R., Hartmann, K., Diekmann, B., and Brauer, A.: Echo of the Younger Dryas in Holocene Lake Sediments on the Tibetan Plateau, Geophys. Res. Lett., 45, 11154–11163, https://doi.org/10.1029/2018gl080225, 2018.

Reimer, P. J., Austin, W. E. N., Bard, E., Bayliss, A., Blackwell, P. G., Bronk Ramsey, C., Butzin, M., Cheng, H., Edwards, R. L., Friedrich, M., Grootes, P. M., Guilderson, T. P., Hajdas, I., Heaton, T. J., Hogg, A. G., Hughen, K. A., Kromer, B., Manning, S. W., Muscheler, R., Palmer, J. G., Pearson, C., van der Plicht, J., Reimer, R. W., Richards, D. A., Scott, E. M., Southon, J. R., Turney, C. S. M., Wacker, L., Adolphi, F., Büntgen, U., Capano, M., Fahrni, S. M., Fogtmann-Schulz, A., Friedrich, R., Köhler, P., Kudsk, S., Miyake, F., Olsen, J., Reinig, F., Sakamoto, M., Sookdeo, A., and Talamo, S.: The IntCal20 Northern Hemisphere Radiocarbon Age Calibration Curve (0–55 cal kBP), Radiocarbon, 62, 725–757, https://doi.org/10.1017/rdc.2020.41, 2020.

Reinhardt-Imjela, C., Imjela, R., Bölscher, J., and Schulte, A.: The impact of late medieval deforestation and 20th century forest decline on extreme flood magnitudes in the Ore Mountains (Southeastern Germany), Quatern. Int., 475, 42–53, https://doi.org/10.1016/j.quaint.2017.12.010, 2018.

Richard, V.: Paläolimnologische und vegetationsgeschichtliche Untersuchungen an Sedimenten aus Fuschlsee und Chiemsee (Salzburg und Bayern) [A study of the paleolimnology and vegetation history of sediments from lakes Fuschlsee and Chiemsee (Austria and Germany)], Schweizerbart Science Publishers, Stuttgart, Germany, ISBN 978-3-443-64182-5, 1996.

Rösch, M., Friedmann, A., Rieckhoff, S., Stojakowits, P., and Sudhaus, D.: A Late Würmian and Holocene pollen profile from Tüttensee, Upper Bavaria, as evidence of 15 Millennia of landscape history in the Chiemsee glacier region, Acta Palaeobotanica, 61, 136–147, https://doi.org/10.35535/acpa-2021-0008, 2021.

Ruddiman, W. F., He, F., Vavrus, S. J., and Kutzbach, J. E.: The early anthropogenic hypothesis: A review, Quaternary Sci. Rev., 240, 106386, https://doi.org/10.1016/j.quascirev.2020.106386, 2020.

Ruff, M., Fahrni, S., Gäggeler, H. W., Hajdas, I., Suter, M., Synal, H. A., Szidat, S., and Wacker, L.: On-line Radiocarbon Measurements of Small Samples Using Elemental Analyzer and MICADAS Gas Ion Source, Radiocarbon, 52, 1645–1656, https://doi.org/10.1017/s003382220005637x, 2010.

Ruiz, F., Abad, M., Bodergat, A. M., Carbonel, P., Rodríguez-Lázaro, J., González-Regalado, M. L., Toscano, A., García, E. X., and Prenda, J.: Freshwater ostracods as environmental tracers, Int. J. Environ. Sci. Te., 10, 1115–1128, https://doi.org/10.1007/s13762-013-0249-5, 2013.

Salazar, G., Zhang, Y. L., Agrios, K., and Szidat, S.: Development of a method for fast and automatic radiocarbon measurement of aerosol samples by online coupling of an elemental analyzer with a MICADAS AMS, Nuclear Instruments and Methods in Physics Research Section B: Beam Interactions with Materials and Atoms, 361, 163–167, https://doi.org/10.1016/j.nimb.2015.03.051, 2015.

Schönborn, W.: Beschalte Amöben:(Testacea), Ziemsen, Wittenberg-Lutherstadt, 1966.

Schubert, A., Lauterbach, S., Leipe, C., Scholz, V., Brauer, A., and Tarasov, P. E.: Anthropogenic and climate controls on vegetation changes between 1500 BCE and 500 CE reconstructed from a high-resolution pollen record from varved sediments of Lake Mondsee, Austria, Palaeogeogr. Palaeocl., 559, 109976, https://doi.org/10.1016/j.palaeo.2020.109976, 2020.

Scott, D. B., Medioli, F. S., and Schafer, E. T.: Monitoring in coastal environments using foraminifera and thecamoebian indicators, Cambridge University Press, ISBN 0-521-56173-6, 2001.

Sirocko, F., Dietrich, S., Veres, D., Grootes, P. M., Schaber-Mohr, K., Seelos, K., Nadeau, M.-J., Kromer, B., Rothacker, L., Röhner, M., Krbetschek, M., Appleby, P., Hambach, U., Rolf, C., Sudo, M., and Grim, S.: Multi-proxy dating of Holocene maar lakes and Pleistocene dry maar sediments in the Eifel, Germany, Quaternary Sci. Rev., 62, 56–76, https://doi.org/10.1016/j.quascirev.2012.09.011, 2013.

Steffen, W., Broadgate, W., Deutsch, L., Gaffney, O., and Ludwig, C.: The trajectory of the Anthropocene: The Great Acceleration, The Anthropocene Review, 2, 81–98, https://doi.org/10.1177/2053019614564785, 2015.

Strobel, P., Struck, J., Zech, R., and Bliedtner, M.: The spatial distribution of sedimentary compounds and their environmental implications in surface sediments of Lake Khar Nuur (Mongolian Altai), Earth Surf. Proc. Land., 46, 611–625, https://doi.org/10.1002/esp.5049, 2021.

Stuiver, M. and Reimer, P. J.: Extended ^{14}C data base and revised CALIB 3.0 ^{14}C age calibration program, Radiocarbon, 35, 215–230, 1993.

Sun, D., He, Y., Wu, J., Liu, W., and Sun, Y.: Hydrological and Ecological Controls on Autochthonous Carbonate Deposition in Lake Systems: A Case Study From Lake Wuliangsu and the Global Perspective, Geophys. Res. Lett., 46, 6583–6593, https://doi.org/10.1029/2019gl082224, 2019.

Szidat, S., Salazar, G. A., Vogel, E., Battaglia, M., Wacker, L., Synal, H.-A., and Türler, A.: ^{14}C analysis and sample preparation at the new Bern Laboratory for the Analysis of Radiocarbon with AMS (LARA), Radiocarbon, 56, 561–566, https://doi.org/10.2458/56.17457, 2014.

Torres, I. C., Inglett, P. W., Brenner, M., Kenney, W. F., and Ramesh Reddy, K.: Stable isotope ($\delta^{13}C$ and $\delta^{15}N$) values of sediment organic matter in subtropical lakes of different trophic status, J. Paleolimnol., 47, 693–706, https://doi.org/10.1007/s10933-012-9593-6, 2012.

van der Knaap, W. O., van Leeuwen, J. F. N., Fahse, L., Szidat, S., Studer, T., Baumann, J., Heurich, M., and Tinner, W.: Vegetation and disturbance history of the Bavarian Forest National Park, Germany, Veg. Hist. Archaeobot., 29, 277–295, https://doi.org/10.1007/s00334-019-00742-5, 2019.

Waldner, W.: Salt Mining and Trading in the Berchtesgaden and Salzburg Area, in: Mineral Deposits of the Alps and of the Alpine Epoch in Europe, edited by: Schneider, H. J., Special Publication No. 3 of the Society for Geology Applied to Mineral Deposits, 3, Springer, Berlin, Heidelberg, https://doi.org/10.1007/978-3-642-68988-8_1, 1983.

Wasserwirtschaftsamt Traunstein: Höglwörther See: https://www.wwa-ts.bayern.de/fluesse_seen/gewaesserportraits/hoeglwoerther_see/index.htm (last access: 25 August 2022), 2018.

Waters, C. N. and Turner, S. D.: Defining the onset of the Anthropocene, Science, 378, 706–708, https://doi.org/10.1126/science.ade2310, 2022.

Waters, C. N., Zalasiewicz, J., Summerhayes, C., Barnosky, A. D., Poirier, C., Galuszka, A., Cearreta, A., Edgeworth, M., Ellis, E. C., Ellis, M., Jeandel, C., Leinfelder, R., McNeill, J. R., Richter, D., Steffen, W., Syvitski, J., Vidas, D., Wagreich, M., Williams, M., Zhisheng, A., Grinevald, J., Odada, E., Oreskes, N., and Wolfe, A. P.: The Anthropocene is functionally and stratigraphically distinct from the Holocene, Science, 351, aad2622, https://doi.org/10.1126/science.aad2622, 2016.

Weltje, G. J., Bloemsma, M. R., Tjallingii, R., Heslop, D., Röhl, U., and Croudace, I. W.: Prediction of Geochemical Composition from XRF Core Scanner Data: A New Multivariate Approach Including Automatic Selection of Calibration Samples and Quantification of Uncertainties, in: Micro-XRF Studies of Sediment Cores: Applications of a non-destructive tool for the environmental sciences, edited by: Croudace, I. W. and Rothwell, R. G., Springer Netherlands, Dordrecht, 507–534, https://doi.org/10.1007/978-94-017-9849-5_21, 2015.

Whitlock, C. and Larsen, C.: Charcoal as a fire proxy, in: Tracking Environmental Change Using Lake Sediments, in: Developments in Paleoenvironmental Research, edited by: Smol, J. P., Birks, H. J. B., Last, W. M., Bradley, R. S., and Alverson, K., Springer, Dordrecht, 3, 75–97, https://doi.org/10.1007/0-306-47668-1_5, 2001.

Żarczyński, M., Wacnik, A., and Tylmann, W.: Tracing lake mixing and oxygenation regime using the Fe/Mn ratio in varved sediments: 2000 year-long record of human-induced changes from Lake Żabińskie (NE Poland), Sci. Total Environ., 657, 585–596, https://doi.org/10.1016/j.scitotenv.2018.12.078, 2019.

E&G Quaternary Sci. J., 72, 235–237, 2023
https://doi.org/10.5194/egqsj-72-235-2023

Open Access E&G Quaternary Science Journal

Thesis abstract

Geometry, chronology and dynamics of the last Pleistocene glaciation of the Black Forest

Felix Martin Hofmann

Institute of Earth and Environmental Sciences, University of Freiburg, 79104 Freiburg, Germany

Correspondence: Felix Martin Hofmann (felix.martin.hofmann@geologie.uni-freiburg.de)

Relevant dates: Received: 4 September 2023 – Revised: 9 October 2023 – Accepted: 25 October 2023 – Published: 4 December 2023

How to cite: Hofmann, F. M.: Geometry, chronology and dynamics of the last Pleistocene glaciation of the Black Forest, E&G Quaternary Sci. J., 72, 235–237, https://doi.org/10.5194/egqsj-72-235-2023, 2023.

Supervisor: Frank Preusser (University of Freiburg)
Co-supervisor: Stefan Hergarten (University of Freiburg)
Dissertation online: https://doi.org/10.6094/UNIFR/241069

Atmospheric circulation patterns over Europe during the Late Pleistocene remain insufficiently understood. One of the central questions in this debate is whether humid airflow from the Mediterranean Sea triggered the marine oxygen isotope stage-2 maximum advance of glaciers (at around 26–24 ka) in the European Alps that had their main accumulation area south of the main weather divide in this mountain range. If this southerly airflow hypothesis is correct, the southern Black Forest (southern Germany) would have been in a leeward position with respect to the Alps and little precipitation would have been available for ice build-up. Therefore, it is likely that the four interconnected ice caps in this region reached their Late Pleistocene maximum extent asynchronously with the glaciers in the Alps. As an age determination of the last glaciation maximum in the southern Black Forest is still pending, this assumption cannot yet be verified. The general trend towards warmer climatic conditions during the last glacial termination was punctuated by rapid drops in temperature, leading to successive periods of ice-marginal stability and moraine formation in the Variscan ranges of central Europe. Precipitation patterns in central Europe during this period remain largely elusive. Precipitation reconstructions with data from former glaciers can fill this gap, but they require additional data on the evolution of glaciers in the Variscan ranges in central Europe. This particularly applies to the southern Black Forest, where ice-marginal landforms have hitherto not been directly dated. This study addresses these issues by reconstructing the last glaciation of this region.

Digital elevation models (DEMs) derived from light detection and ranging data (xy resolution: 1 m) were first systematically used to map glacial landforms in the southern Black Forest. The results were confirmed during extensive field surveys. Geomorphological mapping in the region NW of the highest summit of the Black Forest, Feldberg (1493 m above sea level (a.s.l.)), revealed that some previously described moraines must be rejected, whereas other moraines were mapped for the first time. These findings underline that thorough geomorphological investigations are always needed prior to the application of dating methods (Hofmann et al., 2020).

Large boulders on moraines and erratic boulders were selected for ^{10}Be cosmic-ray exposure (CRE) dating. As numerous sampling sites lay in heavily forested areas, topographic shielding factors were determined with DEMs following Li (2018) and the guidelines of Hofmann (2022). According to preliminary CRE ages of erratic boulders and moraine boulders SE of Feldberg, glacier retreat from the Late Pleistocene maximum position may have been underway by ~ 21 ka at the latest. This working hypothesis needs to be confirmed with additional data. In the region NW of Feldberg (Fig. 1), the timing of this glacial phase re-

Published by Copernicus Publications on behalf of the Deutsche Quartärvereinigung (DEUQUA) e.V.

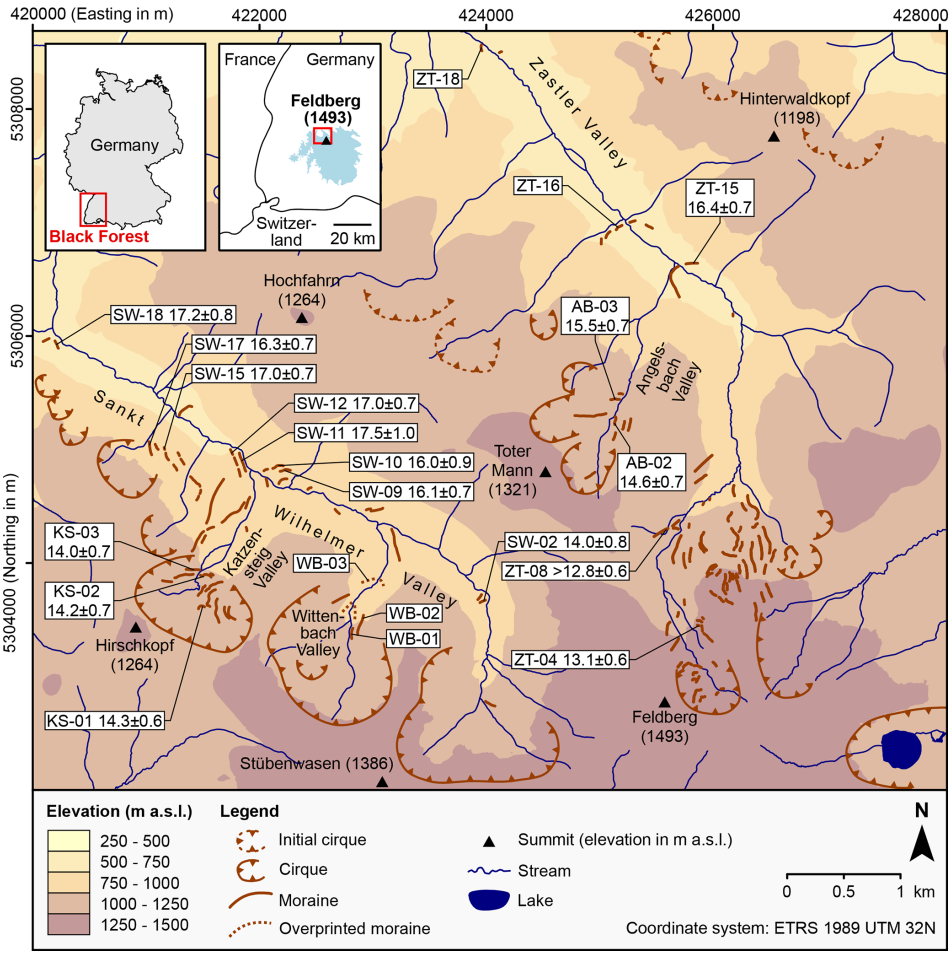

Figure 1. Glacial landforms in the region NW of Feldberg (Hofmann et al., 2020, 2022, 2023). CRE ages of moraines and external uncertainties (Hofmann et al., 2022, 2023) are given in thousands of years (ka) before 2010 CE and ka, respectively. The inset maps show the location of the Black Forest and the Late Pleistocene maximum ice extent (light-blue polygon) according to Hemmerle et al. (2016).

mains currently unknown. The presumably oldest moraines in the Zastler Valley were devoid of suitable boulders for dating (Fig. 1). In the neighbouring Sankt Wilhelmer Valley, moraines at the Late Pleistocene maximum position have probably not been preserved. CRE ages of moraines NE of Feldberg cluster around 17–16, 15–14 and 13 ka, indicating three distinct periods of successive ice-marginal stability during the last deglaciation (Fig. 1; Hofmann et al., 2022, 2023).

Reconstructing DEMs of glacier surfaces and equilibrium line altitudes (ELAs) revealed that, during the period of valley glaciation in the region NW of Feldberg (by 17–16 ka at the latest), the ELAs varied between 1140 and 1160 m a.s.l. During the subsequent period of cirque glaciation (no later than 15–14 ka), the ELAs of glaciers ranged from 1150 to 1210 m a.s.l. with no clear spatial trend across the studied valleys. Varying sizes of snow drift and avalanche catchments of glaciers explain the best spatial variations in ELAs. Due to the strong effect of these processes on ELAs and large errors in the precipitation–temperature equation used, additional work is needed for realistic and more precise estimates of annual precipitation (Hofmann et al., 2022, 2023).

This study allowed for reconstructing the Late Pleistocene glacial history of the southern Black Forest in unprecedented detail. The high potential for climate reconstructions warrants further studies in this region. They should particularly focus on obtaining additional data on the Late Pleistocene glaciation maximum and on extracting a climatic signal from ELAs of glaciers.

Data availability. For the data supporting this study, see the thesis (Hofmann, 2023), Hofmann (2022), and Hofmann et al. (2020, 2022, 2023). For rivers and lakes in Fig. 1, see LUBW (2022a) and LUBW (2022b), respectively.

Competing interests. The author has declared that there are no competing interests.

Disclaimer. Publisher's note: Copernicus Publications remains neutral with regard to jurisdictional claims made in the text, published maps, institutional affiliations, or any other geographical representation in this paper. While Copernicus Publications makes every effort to include appropriate place names, the final responsibility lies with the authors.

Special issue statement. This article is part of the special issue "Quaternary research in times of change – inspired by INQUA Roma 2023". It is a result of the INQUA conference, Rome, Italy, 14–20 July 2023.

Acknowledgements. The author thanks the reviewer, Stefan Winkler, for his comments that resulted in improvements to the manuscript.

Financial support. This research has been supported by the Deutsche Forschungsgemeinschaft (grant nos. 426333515 and 516126018) and the Studienstiftung des Deutschen Volkes.

The article processing charge was funded by the Quaternary scientific community, as represented by the host institution of *EGQSJ*, the German Quaternary Association (DEUQUA).

Review statement. This paper was edited by Gilles Rixhon and reviewed by Stefan Winkler.

References

Hemmerle, H., May, J.-H., and Preusser, F.: Übersicht über die pleistozänen Vergletscherungen des Schwarzwaldes, Ber. Naturf. Ges. Freiburg i. Br., 106, 31–67, 2016.

Hofmann, F. M.: Technical note: Evaluating a geographical information system (GIS)-based approach for determining topographic shielding factors in cosmic-ray exposure dating, Geochronology, 4, 691–712, https://doi.org/10.5194/gchron-4-691-2022, 2022.

Hofmann, F. M.: Geometry, Chronology and Dynamics of the last Pleistocene glaciation of the Black Forest, Dissertation, Faculty of Environment and Natural Resources, University of Freiburg, Germany, https://doi.org/10.6094/UNIFR/241069, 2023.

Hofmann, F. M., Rauscher, F., McCreary, W., Bischoff, J.-P., and Preusser, F.: Revisiting Late Pleistocene glacier dynamics northwest of the Feldberg, southern Black Forest, Germany, E&G Quaternary Sci. J., 69, 61–87, https://doi.org/10.5194/egqsj-69-61-2020, 2020.

Hofmann, F. M., Preusser, F., Schimmelpfennig, I., Léanni, L., and ASTER Team: Late Pleistocene glaciation history of the southern Black Forest, Germany: ^{10}Be cosmic-ray exposure dating and equilibrium line altitude reconstructions in Sankt Wilhelmer Tal, J. Quaternary Sci., 37, 688–706, https://doi.org/10.1002/jqs.3407, 2022.

Hofmann, F. M., Steiner, M., Hergarten, S., ASTER Team, and Preusser, F.: Limitations of precipitation reconstructions using equilibrium line altitudes exemplified for former glaciers in the Southern Black Forest, Central Europe, Quaternary Res., 1–25, https://doi.org/10.1017/qua.2023.53, 2023.

Li, Y.-K.: Determining topographic shielding from digital elevation models for cosmogenic nuclide analysis: a GIS model for discrete sample sites, J. Mt. Sci., 15, 939–947, https://doi.org/10.1007/s11629-018-4895-4, 2018.

LUBW (Landesanstalt für Umwelt Baden-Württemberg): Fließgewässer (AWGN) [data set], https://rips-datenlink.lubw.de/UDO_download/Fliessgewaessernetz.zip (last access: 30 November 2023), 2022a.

LUBW: Stehendes Gewässer (AWGN) [data set], https://rips-datenlink.lubw.de/UDO_download/StehendeGewaesser.zip (last access: 30 November 2023), 2022b

CONTENTS

https://www.eg-quaternary-science-journal.net/

ISSN 0424-7116